1-1-2017

Design, Synthesis And Biological Evaluation Of Histone Deacetylase (hdac) Inhibitors: Saha (vorinostat) Analogs And Biaryl Indolyl Benzamide Inhibitors Display Isoform Selectivity

Ahmed Negmeldin
Wayne State University,

DESIGN, SYNTHESIS AND BIOLOGICAL EVALUATION OF HISTONE DEACETYLASE (HDAC) INHIBITORS: SAHA (VORINOSTAT) ANALOGS AND BIARYL INDOLYL BENZAMIDE INHIBITORS DISPLAY ISOFORM SELECTIVITY

by

AHMED THABET NEGMELDIN

DISSERTATION

Submitted to the Graduate School of

Wayne State University,

Detroit, Michigan

in partial fulfillment of the requirements

for the degree of

DOCTOR OF PHILOSOPHY

2017

MAJOR: CHEMISTRY (Organic)

Approved By:

_____

Advisor Date

_____

_____

_____

DEDICATION

To my beloved mother, father, wife and children,

The most important people in my life

ACKNOWLEDGEMENTS

I would like to sincerely thank my supervisor Dr. Mary Kay H. Pflum for her continuous support, encouragement, valuable guidance, and patience given throughout the period of this work. During the last five years, I learned a lot of scientific, writing, presentation and mentoring skills from her. She is an amazing and outstanding mentor. I would like also to convey my gratitude to the committee members, Dr. Jeremy J. Kodanko, Dr. Young-Hoon Ahn, and Dr. Steven M. Firestine. I want to thank them for their valuable time, constructive comments and useful suggestions.

My special thanks to all the lab members with whom I've worked together over the past few years in the Pflum lab, Geetha Padige, Danusha Nalawansha, Alexander Stark, Inosha Gomes, Satish Garre, Todd Faner, Thilani Anthony, Ahmed Fouda, Maheeka Embogama, Pavithra Dehigama, Cyprien Nanah, Nuan Acharige, Aparni Kaushalya, Vindya Mudiyanselage, and Michael Moussa. I had a great, wonderful, and an unforgettable time in the Pflum lab with you all.

I want also to thank all the Lumigen Instrument Center staff and the Chemistry Department administrative staff for their support.

I would like to thank my mother, father for their efforts, support and encouragement. Without their support, my success wouldn't have been possible. Last but not least, my gratitude goes to my wife for her great support, continuous support and encouragement through these years. Thank you for taking care of everything during this long journey.

TABLE OF CONTENTS

LIST OF TABLES

LIST OF FIGURES

LIST OF SCHEMES

CHAPTER 1 - INTRODUCTION

Some of the text in this chapter was reprinted or modified from: Negmeldin, A. T.; Padige, G.; Bieliauskas, A. V.; Pflum, M. K. H., Structural Requirements of HDAC Inhibitors: SAHA Analogues Modified at the C2 Position Display HDAC6/8 Selectivity, *ACS Medicinal Chemistry Letters* **2017**, 8 (3), 281-286; Bieliauskas, A. V.; Weerasinghe, S. V. W.; Negmeldin, A. T.; Pflum, M. K. H., Structural requirements of histone deacetylase inhibitors: SAHA analogs modified on the hydroxamic acid, *Arch. Pharm. (Weinheim, Ger.)* **2016,** *349*, 373-382; and Negmeldin, A. T. and Pflum, M. K. H., The structural requirements of histone deacetylase inhibitors: SAHA analogs modified at the C4 position display dual HDAC6/HDAC8 selectivity, *European Journal of Medicinal Chemistry* (Submitted)

1.1. Epigenetic mechanism and gene expression

The chromosome is an important X-shaped cellular structure that carry all the hereditary genetic information of the organism (genome) in the form of genes. In eukaryotes, the chromosome is a highly condensed structure of long chromatin fiber, which is a complex that consists of multiple nucleosome units (Figure 1.1). DNA double strand (blue strand) that carries genetic information is wrapped around histone proteins forming each nucleosome unit (Figure 1.1).[1-2] The compactness of the nucleosome structure is affected by different epigenetic modifications, which by its turn affects DNA accessibility.[2]

Epigenetic modifications play an essential role in regulation of gene transcription, DNA repair, DNA replication, and cell growth through mechanisms independent of structure of DNA.[3-4] Several epigenetic changes are known to date, such as DNA methylation and histone tail modifications. Post-translational modifications of histone proteins are among the major dynamic epigenetic changes that regulate DNA expression and replication. Several post-translational covalent modifications of histone proteins are known, such as acetylation, methylation, phosphorylation, and ubiquitination (Figures 1.1 and 1.2A).[4-5] Acetylation is

controlled by two main classes of enzymes, histone acetyltransferases (writers) and histone deacetylases (erasers)(Figure 1.1).[2]

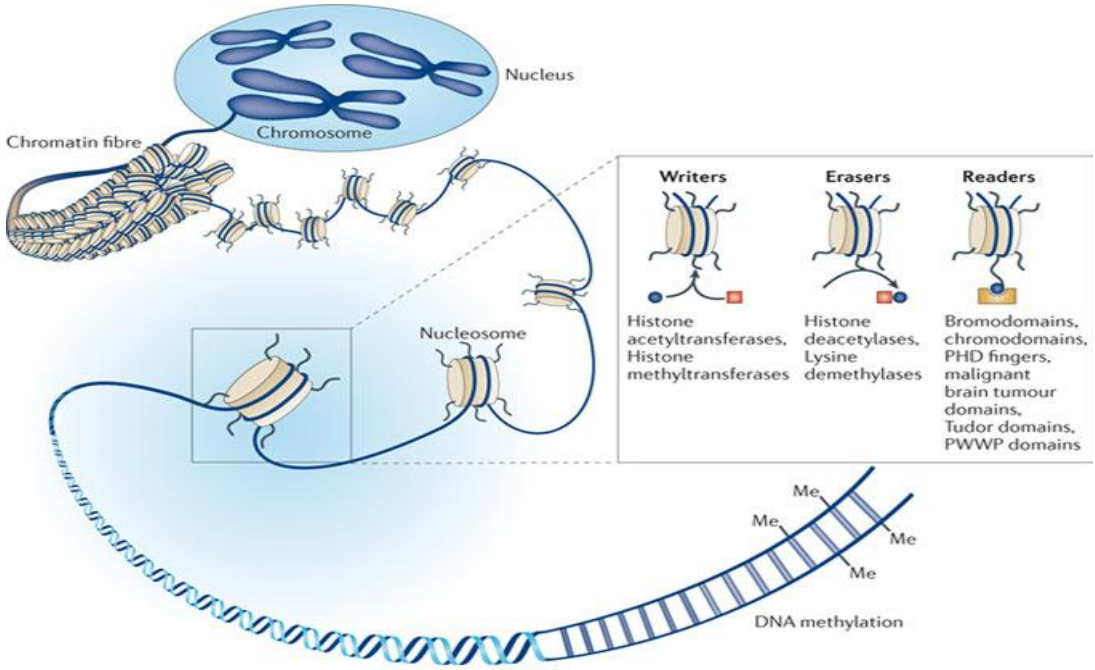

Figure 1.1. Chromosome structure showing the chromatin fiber and the nucleosome unit with the wrapping of DNA around histone proteins.[2] Post-translational modifications of Histone *N*-terminal residues are governed by several enzymes including, histone acetyltransferases and histone methyltransferases (readers), histone deacetylases and lysine demethylases (erasers). *Reused with permission from nature publishing group (see Appendix E).*

1.2. Regulation of transcription by Histone Deacetylase (HDAC) Proteins

Histone Deacetylase (HDAC) proteins play an essential role in the regulation of transcription in a balanced process with histone acetyl transferases (Figures 1.2A and 1.2B). DNA double strands are tightly wrapped around histone proteins due to the electrostatic interaction between the positively charged free amines of lysine side chains that are abundant in the histone protein *N*-terminal tails, and the negatively charged DNA backbone (Figures 1.2A and 1.2C). As a result of the tight interaction, DNA double strands are inaccessible to transcription factors in this state and

transcription is repressed (Figure 1.2A). Upon acetylation of the ε-amino group on the side chains of lysine amino acids with histone acetyl transferases (HATs), the compact structure will become loosened due to the acetylation of the amine groups and loss of the electrostatic interaction. In the acetylated state, the nucleosomal DNA will be accessible to transcription factors and will become transcriptionally active (Figures 1.2B and 1.2C). Several other key enzymes are involved in activation of transcription such as, lysine methyltransferases and lysine demethylases (Figure 1.2B). On the other hand, HDAC proteins catalyze deacetylation of acetylated lysine residues, which will turn off transcription (Figure 1.2A and 1.2C).[6] In addition, deubiquitination, methylation and demethylation of specific lysine amino acid residues can also lead to repression of transcription (Figure 1.2A). The overall acetylation levels and the dynamic balance of both acetylation and deacetylation reactions regulate gene expression as part of several post translational modifications to histone tails of nucleosome units.[4-6]

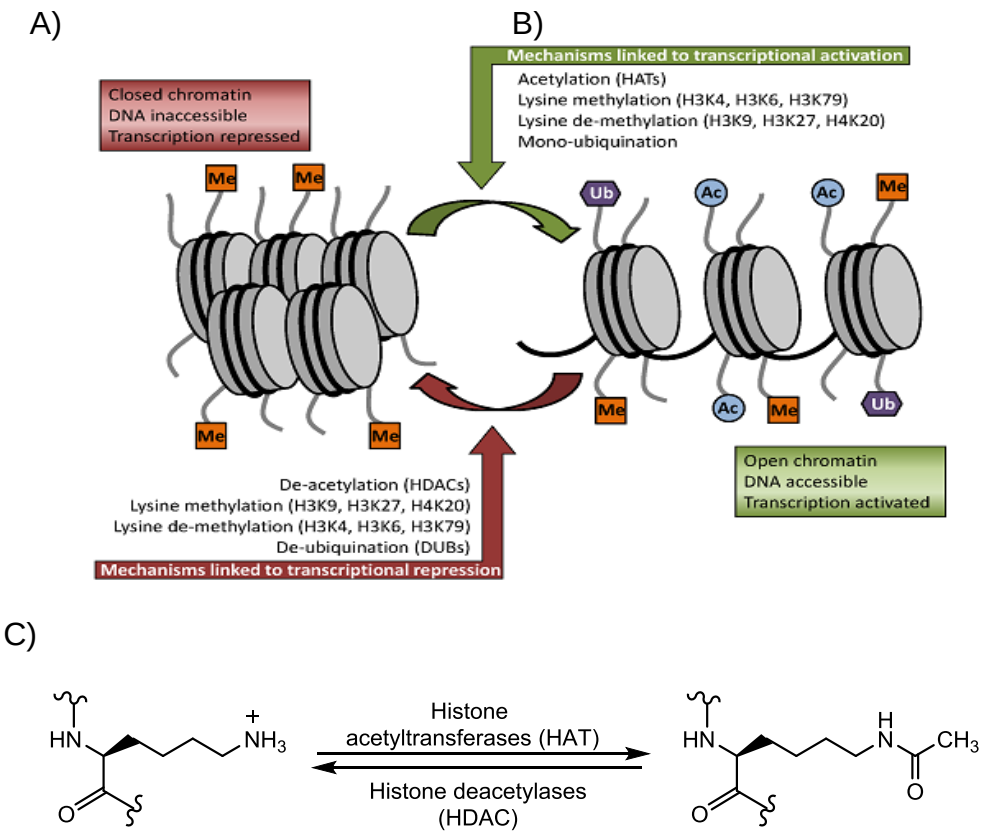

Figure 1.2. Role of histone deacetylase (HDAC) proteins in regulation of transcription. A) The wrapping of double stranded DNA around histone proteins, makes the DNA inaccessible to transcription factors.[5] B) Acetylation, methylation, demethylation, or ubiquitination of lysine residues loosens the histone structure, making the DNA accessible to transcription factors.[5] C) Lysine residue acetylation with histone acetyltransferase and deacetylation with histone deacetylase (HDAC). *Reused from open access article that permits unrestricted use or reproduction with proper citation (see Appendix E).*

1.3. Classification of HDAC proteins

The HDAC family contains 18 different proteins (Figure 1.3), which are grouped into four classes according to phylogenetic analysis (homology with yeast HDAC proteins), size, cellular localization, and number of catalytic active sites.[7] Eleven of them are metal-dependent, while the rest are NAD^+ dependent. The metal-dependent HDAC proteins are classified into classes I, II, and IV, while class III are

NAD^+ dependent.[7] The eleven metal-dependent HDAC proteins are the focus of this work.

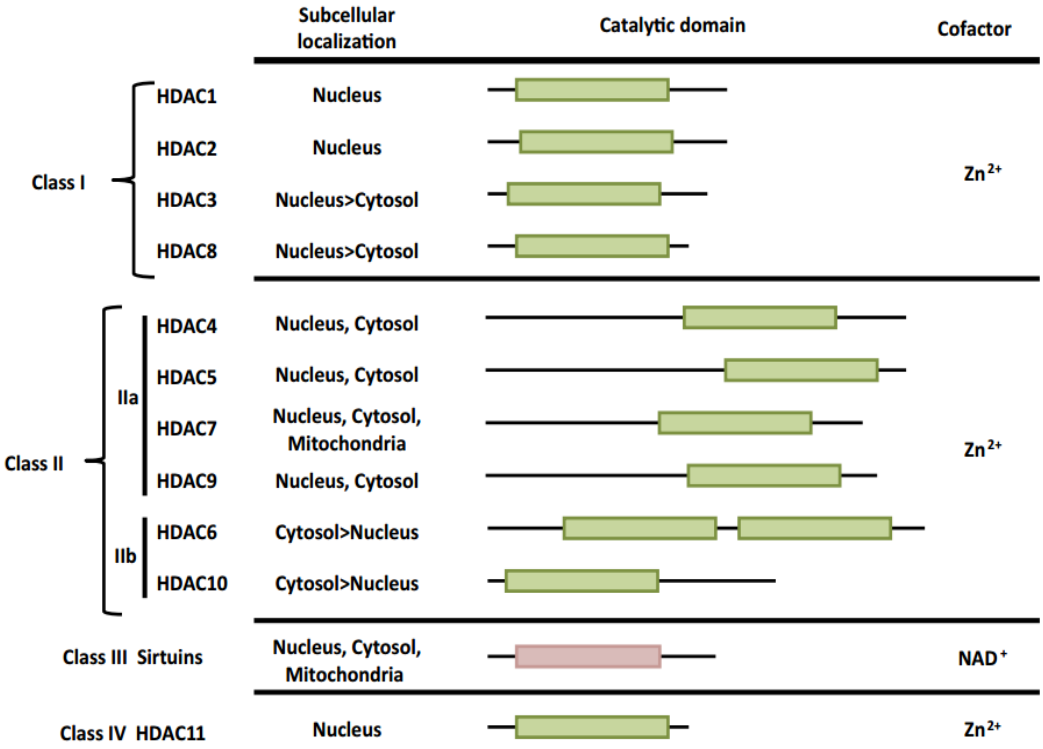

Figure 1.3. Classification of HDAC proteins into metal dependent and NAD^+ dependent, and the classification of the metal dependent into three classes.[8] *Reused with permission from Elsevier Ltd. (see Appendix E).*

Class I HDAC proteins include HDAC1, HDAC2, HDAC3, and HDAC8 (Figure 1.3), which are relatively smaller proteins (377-488 amino acids) compared to class II HDACs and are predominantly nuclear enzyme.[8-9] Both HDAC3 and HDAC8 can shuttle between the nucleus and the cytoplasm. HDAC1, 2, 3, and 8 are grouped in the same class due to homology to yeast RPD3, ubiquitous expression in almost all cell lines and tissues, and their key role in cell survival and proliferation (Figure 1.3).[9]

Class II HDAC proteins are relatively large proteins (669-1215 amino acids), have sequence similarity with yeast HDA1, and maintain the ability to shuttle between the cytoplasm and nucleus.[9-10] Class II HDACs are further divided into two

subclasses, class IIa and IIb. Class IIa includes HDAC4, HDAC5, HDAC7, and HDAC9 (Figure 1.3).[9] On the other hand, class IIb includes HDAC6 and HDAC10, which are mainly cytoplasmic and contain two catalytic domains. HDAC11 is a unique member of the HDAC family with a size of 347 residues and a sequence similarity to both classes I and II.[8-9, 11]

1.4. Catalysis mechanism of HDAC proteins

All HDAC enzymes have high sequence similarity in their active sites.[12] For the deacetylation reaction, several essential amino acids are important for catalysis. For example, based on the HDAC6 crystal structure, the zinc atom, histidine 573 (H573), histidine 574 (H574), and tyrosine 745 (Y745) have a crucial role in the deacetylation mechanism (Figure 1.4).[13-14] The metal ion and the three amino acids are conserved in most of the HDAC isoforms. The exception is class IIa enzymes, in which only the metal ion and two histidine amino acids are maintained. [13-23] The mechanism of deacetylation is believed to be similar among all of the HDAC isoforms, with differences in catalytic efficiency between them.[24-26] The crystal structure of the HDAC6 catalytic domain 2 (CD2) was recently reported with several snapshots showing all the key mechanistic steps in catalysis (Figure 1.4).[14] First, a water molecule (red sphere in Figure 1.4a) was chelated (red dashed line) with the zinc atom (grey sphere) and hydrogen bonded with the two histidine amino acids residue (black dashed lines with H573 and H574) (Figure 1.4a). In the same snapshot, an empty space between the chelated water molecule and Y745 is shown and is proposed to be where a substrate fits in the binding site. In order to study the binding of the substrate α-tubulin K40 peptide (orange structure in Figure 1.4b), Y745 was mutated to phenylalanine (Y745F) to prevent catalysis and capture the

HDAC6-substrate interaction. The second crystallographic snapshot showed the enzyme substrate-complex with the carbonyl of the ε-acetyl lysine coordinated to the metal ion without displacing the coordinated water molecule (Figure 1.4b). Next, H574, which is known to act as a general acid during catalysis, was mutated to alanine (H574A) in order to capture the enzyme during the transition state (Figure 1.4c). The snapshot showed a tetrahedral intermediate, indicating that H573 acted as a general base to deprotonate the water molecule. Nucleophilic attack by the deprotonated water molecule on the substrate carbonyl formed the tetrahedral intermediate in the active site, which was stabilized by both the zinc atom and Y745 (Figure 1.4c). Finally, the tetrahedral intermediate collapsed and yielded the free ε-lysine side chain of the substrate (not obtained in the crystal structure), and an acetate anion that was observed and stabilized by the metal ion, H573, H574, and Y745 (Figure 1.4d).

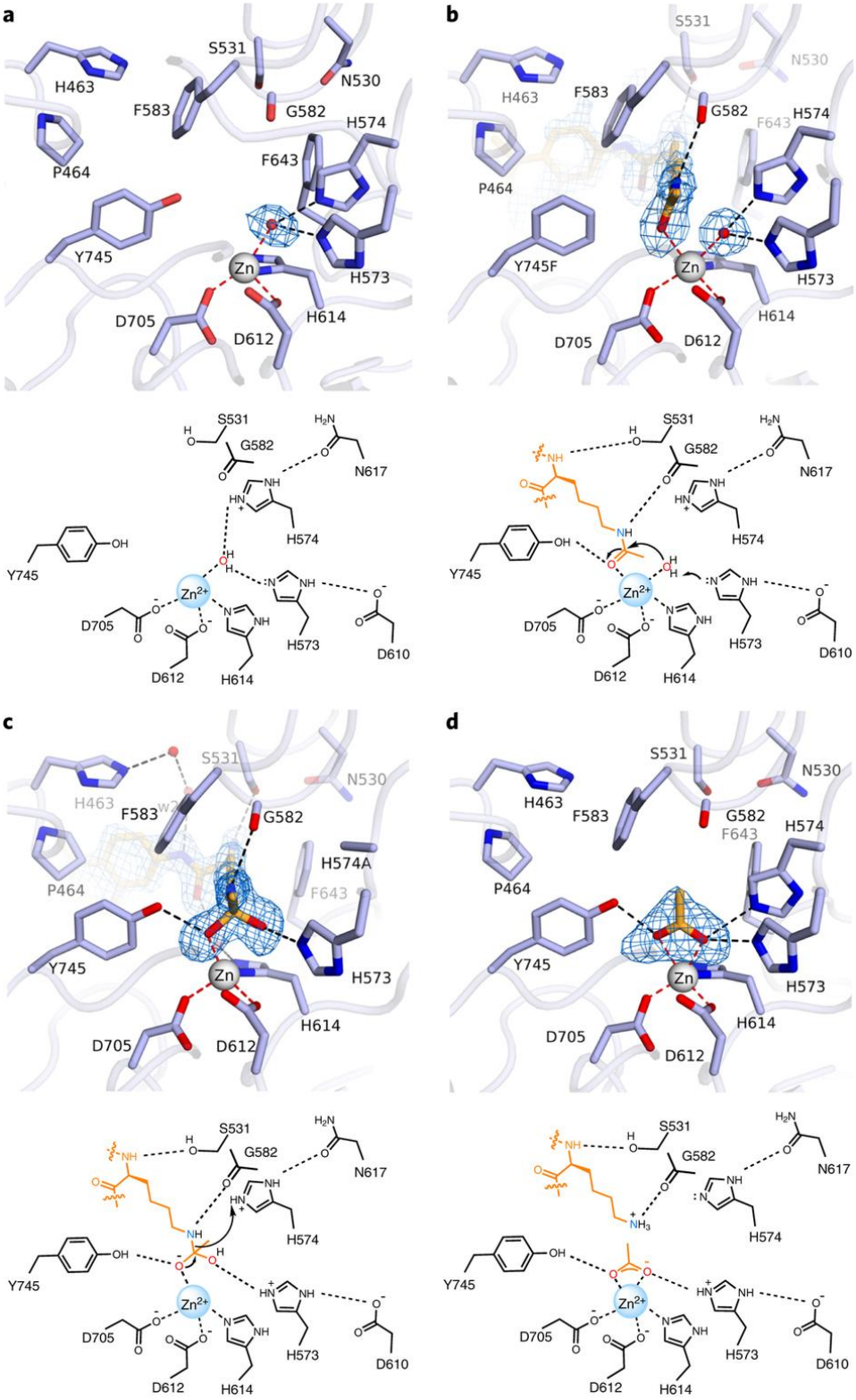

Figure 1.4. Snapshots of the HDAC6 catalytic domain 2 during catalysis with the corresponding proposed reaction shown below each snapshot. See text for complete explanation of images.[14] *Reused with permission from nature publishing group (see Appendix E).*

1.5. HDAC proteins and cancers

HDAC proteins regulate the expression of several cancer-related proteins involved in cell signaling, transcription, and tumor suppression through the deacetylation of nucleosomal histone proteins.[27-30] Mutations of HDAC proteins in cancer are rare, while aberrant or overexpression of HDAC proteins is common with many types of cancers.[9] Overexpression of HDAC proteins results in unregulated transcription and aberrant protein activity and function, which is linked to several diseases, including cancer.[28] HDAC proteins are also implicated in several other diseases, such as asthma and schizophrenia.[31-32] The aberrant expression of HDAC proteins in many cancers leads to poor expression of tumor suppressor proteins that are normally expressed in normal cells.[33]

Several reports have shown aberrant expression of individual HDAC isoforms in different types of cancers. HDAC1 was overexpressed in lung,[34] ovarian,[35] gastric,[36] prostate,[37] breast,[38] and colon cancers.[39] HDAC2 was overexpressed in colorectal and gastric cancers.[40] HDAC8 was highly expressed in neuroblastoma patients, leading to cancer progression and poor survival rates.[41] In addition, HDAC8 inhibition showed promising results in T-cell lymphoma and leukemia.[42] Class II HDAC6 was overexpressed in oral squamous cell carcinoma and ovarian cancer.[43-44] In addition, HDAC6 is implicated in several non-epigenetic cancer-related intracellular functions.[45-46] Overexpression of both HDAC6 and HDAC8 was linked to breast cancer metastasis and invasion.[47]

1.6. Anti-tumor activity of HDAC inhibitors

Due to their key role in cancer, HDAC proteins have emerged as interesting targets for cancer treatment, and several anti-cancer agents targeting HDAC

proteins have been developed.[6, 48-52] HDAC inhibitors, such as SAHA were found to decrease the sizes of lung, stomach, pancreas, mouth, ovaries, breast, and prostate tumors in mouse models.[31, 53-54] The effect of HDAC inhibitors on the acetylation states of both histone and non-histone substrates can lead to cell signaling dysregulation, transcription and expression changes, and protein degradation. Through these effects on tumor cells, HDAC inhibitors can reduce proliferation, migration, and angiogenesis, enhance differentiation and immunogenicity, and promote apoptosis (Figure 1.5).[50, 55-56] More specifically, HDAC inhibitors exhibited the ability to cause cancer cells differentiation, inhibition of the cell cycle, and induction of apoptosis.[55, 57-60] Several studies showed that treatment of cancer cells with HDAC inhibitors induced cell cycle arrest in the G1 or G2 phases (Figure 1.5a and 1.5b). Subsequent cancer cell differentiation might be observed after cell cycle arrest in G1 phase (Figure 1.5b).[61-62] Another crucial antitumor mechanism of HDAC inhibitors is based on apoptosis, where cancer cells that pass by the G1 cycle arrest can duplicate their DNA and get arrested at the G2 phase, where accumulated DNA and hyperacetylated histones lead to apoptosis (Figure 1.5a).[61-62] Several known HDAC inhibitors cause cancer cell apoptosis.[58, 63-66] HDAC inhibitors have the same effect on acetylation levels in both normal and cancer cells, but unlike cancer cells, normal cells can undergo a G2 checkpoint after the cell cycle arrest and survive after treatment (Figure 1.5). [61, 63, 65-66]

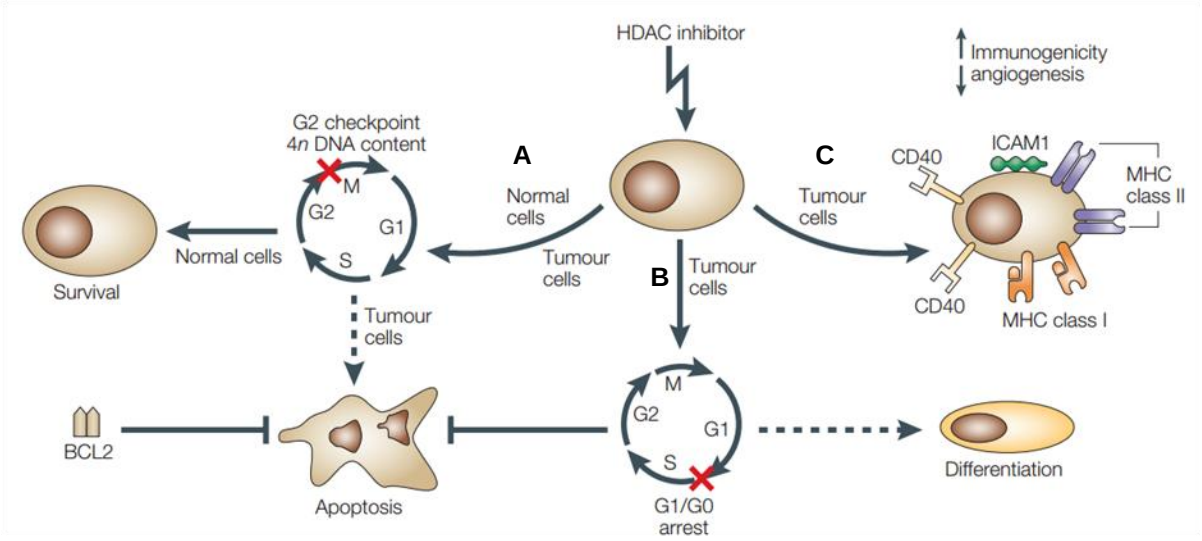

Figure 1.5. Effect of HDAC inhibitors on cancer and normal cells.[55] A)HDAC inhibitor induced G2 cell cycle arrest, and subsequent apoptosis. B) HDAC inhibitor induced G1 cell cycle arrest and cancer cell differentiation. C) HDAC inhibitor effect on enhancement of immunogenicity of cancer cells and reduction of angiogenesis. *Reused with permission from nature publishing group (see Appendix E).*

In addition to the main two mechanisms mentioned above, HDAC inhibitors have other indirect secondary effects on cancer cells. HDAC inhibitors can enhance cancer cells immunogenicity by induction of transcription of several extracellular proteins, receptors, and complexes (Figure 1.5c). Among these extracellular proteins are major histocompatibility complex (MHC) proteins, activation molecules (CD40, CD80, and CD86), and intercellular adhesion molecule (ICAM1). The increased expression of these proteins and receptors can augment the recognition and activity of the immune system against cancer cells (Figure 1.5c).[67-70]

1.7. FDA approved HDAC inhibitors

Several HDAC inhibitors have been approved by the FDA for treatment of cancer.[50] SAHA (suberoylamide hydroxamic acid, Vorinostat, Zolinza™) was approved in 2006 for treatment of cutaneous T-cell lymphoma (Figure 1.6).[49, 71-72] Romidepsin (FK-228, Istodax™) was approved in 2009 for treatment of cutaneous

T-cell lymphoma and in 2011 for treatment of peripheral T-cell lymphoma.[48, 73] In the last three years, two more HDAC inhibitors gained FDA approval for cancer treatment. Belinostat (PXD101, Belodaq™) was FDA-approved in 2014 for treatment of relapsed or refractory peripheral T-cell lymphoma (Figure 1.6).[51, 74] More recently Panobinostat (LBH-589, Farydak™) was approved in 2015 for treatment of multiple myeloma (Figure 1.6).[52, 75] Several other HDAC inhibitors are currently in clinical trials as anti-cancer candidates.[33, 76]

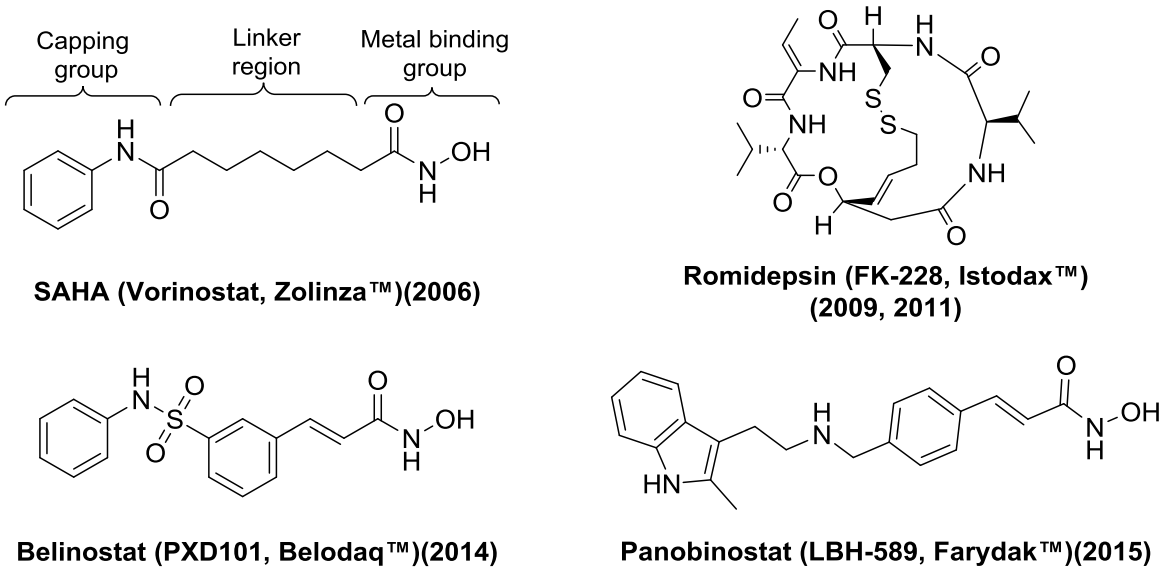

Figure 1.6. FDA approved HDAC inhibitors for treatment of cancer, with year of approval in parenthesis.

Most HDAC inhibitors share a common pharmacophore that is essential for binding and inhibition. The pharmacophore is composed of three important structural regions: the metal binding group, the linker region, and the capping group (Figure 1.6, see SAHA).[25] Three of the FDA approved drugs (SAHA, Belinostat and Panobinostat) have a hydroxamic acid moiety as the metal binding group and an aromatic ring system as the capping group. SAHA has a saturated six carbons

linker, while Belinostat and Panobinostat have unsaturated linkers with an aromatic rings. Romidepsin is a bicyclic depsipeptide prodrug that releases a thiol metal binding group upon reductive cleavage of the disulfide bond (Figure 1.6).

Despite the successes of HDAC inhibitors in cancer treatment, they manifest side effects in patients, including gastrointestinal symptoms, bone marrow suppression, fatigue, cardiac arrhythmia, nausea, dehydration, thrombocytopenia, and anorexia.[77-80] One hypothesis accounting for the observed side effects is the poor selectivity of the clinically tested HDAC inhibitors; most compounds inhibit all or many of the eleven HDAC isoforms (Table 1.1, see first four entries).[12, 78] For example, the FDA approved drugs, including SAHA, inhibit most or all the eleven metal-dependent HDAC isoforms (Table 1.1). In addition, the non-selectivity of the FDA approved drugs limits their use as biological tools to probe HDAC function in cancer biology.

Table 1.1. IC_{50} values of the FDA-approved drugs and some selective HDAC inhibitors discussed in text.[a]

Compound	HDAC isoforms and the corresponding IC_{50} values (nM)										
	1	2	3	4	5	6	7	8	9	10	11
SAHA[78, 81-82]	68	164	48	101	ND	90	104	1534	107	58	35
Romidepsin[83]	40	50	–	510	–	14,000	–	–	–	–	–
Belinostat[78]	41	125	30	115	–	82	67	216	128	–	–
Panobinostat[78]	3	3	4	12	–	61	14	248	3	–	–
Entinostat[78]	181	1,155	2,311	>10,000	–	>10,000	>10,000	>10,000	505	–	–
Apicidin[78]	>10,000	120	43	>10,000	–	>10,000	>10,000	575	>10,000	–	–
Cpd-60[84]	7	49	10,000	>10,000	>10000	>10,000	>10,000	>10,000	–	–	–
RGFP-966[85]	>15,000	>15,000	80	>15,000	>15,000	>15,000	>15,000	>15,000	>15,000	>15,000	>15,000
Tubastatin[86]	16,400	>30,000	>30,000	>30,000	>30,000	15	>30,000	854	>30,000	>30,000	>30,000
PCI-34051[87]	4,000	>50,000	>50,000	–	–	2,900	–	10	–	13,000	–
VAHA[88]	560,000	680,000	340,000	170,000	37,000	16,000	99,000	39,000	91,000	–	–
BRD-73954[89]	12,000	9,000	23,000	>33,000	>33,000	36	13,000	120	>33,000	–	–
Aminotetralin 32[90]	6,310	>100,000	>100,000	>100,000	>100,000	50	30,800	80	>35,000	>100,000	>100,000
acylhydrazone analog 3f[91]	>3,000	>3,000	–	–	–	27	–	130	–	–	–

[a] Values in table were collected from literature. "ND" not determined. "–" no data available.

1.8. Isoform selective HDAC inhibitors

While isoform selective inhibitors would be valuable on the bench top and in the clinic, only a few highly selective compounds have been identified (Figure 1.7 and Table 1.1). For example, entinostat (KHK2375, SNDX-275, formerly MS-275) is a benzamide inhibitor currently in phase II clinical trials and is selective for class I HDAC proteins with 4- to 400-fold selectivity for HDAC1, 2, and 3 over the other isoforms.[62, 78, 92] Apicidin is a cyclic peptide fungal metabolite that inhibits HDAC proteins with 17-230-fold selectivity towards class I HDAC2, 3, and 8.[78] Cpd-60 is another benzamide inhibitor that displayed at least 204-fold selectivity for HDAC1

and HDAC2 over HDAC3.[84] RGFP966 belongs to the benzamide HDAC inhibitors and showed more than 188-fold selectivity for HDAC3 over the other isoforms (Figure 1.7 and Table 1.1).[76] Tubastatin, which was developed as an HDAC6-selective inhibitor, demonstrated 87-fold or 1000-fold selectivity for HDAC6 over HDAC1, 2, and 3 according to different reports.[86, 93] Finally, PCI-34051 is a hydroxamic acid based HDAC8 selective inhibitor that was developed in 2008 and exhibited at least 290-fold selectivity for HDAC8 over HDAC1, 2, 3, 6, and 10 (Figure 1.7 and Table 1.1). [87]

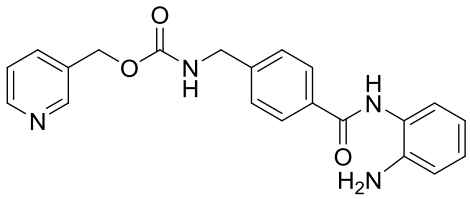

Entinostat (MS-275)
(HDAC1, 2, 3 selective)

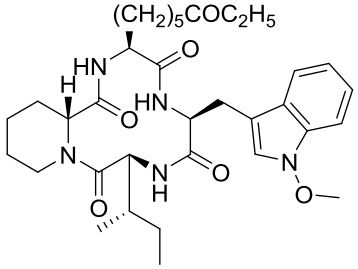

Apicidin
(HDAC2, 3, 8 selective)

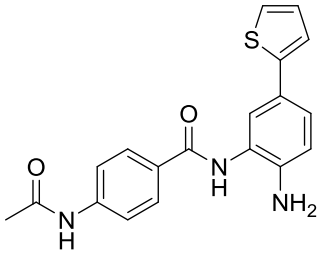

Cpd-60
(HDAC1/2 selective)

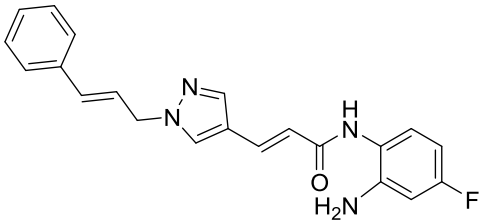

RGFP-966
(HDAC3 selective)

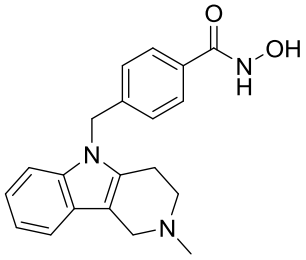

Tubastatin
(HDAC6 selective)

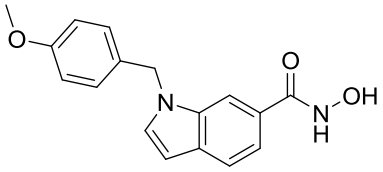

PCI-34051
(HDAC8 selective)

Figure 1.7. Chemical structures of some isoform selective HDAC inhibitors discussed in the text.

1.9. Dual HDAC6/HDAC8 selective HDAC inhibitors

HDAC inhibitors that target one or two HDAC isoforms will be valuable for development of new drugs with possibly fewer side effects than the non-selective inhibitors.[94-97] More specifically, recent reports suggested that inhibition of both HDAC6 and HDAC8 can have several possible synergistic therapeutic applications in the treatment of various cancers.[89-91] In addition, dual inhibition of HDAC6 and HDAC8 might have potential application in breast cancer angiogenesis and metastasis.[42, 89] Recently, several dual HDAC6/8 selective inhibitors have been developed (Figure 1.8).[88-91]

In 2011, Haggarty and co-workers developed valpropylhydroxamic acid (VAHA), which showed modest selectivity for HDAC6 and HDAC8, but with weak potency (16 and 39 μM) (Figure 1.8 and Table 1.1).[88] Two years later in 2013, Holson and co-workers reported the first dual HDAC6/HDAC8 selective inhibitor BRD-73954 (Figure 1.8).[89] The dual inhibitor BRD-73954 demonstrated high fold selectivity towards HDAC6 and 8 (at least 75-fold) over the other metal dependent HDAC proteins, with IC_{50} values of 36 and 120 nM with HDAC6 and HDAC8, respectively (Table 1.1).[89] In 2014, Tang et al. reported Aminotetralin 32 as another dual HDAC6/8 selective inhibitor (Figure 1.8). The compound exhibited at least 79-fold selectivity to HDAC6 and 8, and IC_{50} values in the range of 50-80 nM against HDAC and HDAC8 (Table 1.1).[90] Recently, another group reported the dual selective inhibitor *N*-acylhydrazone analog 3f (Figure 1.8), with IC_{50} values of 27 and 130 nM with HDAC6 and 8, and at least 23-fold dual selectivity.[91] The development of highly selective and potent dual HDAC6/HDAC8 selective inhibitors can possibly

enhance the efficacy of anti-cancer drugs compared to the current non-selective drugs. Moreover, selective HDAC inhibitors will be useful as chemical tools to study cancer-related HDAC cell biology.

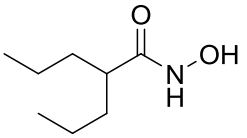

Valpropylhydroxamic acid (VAHA)

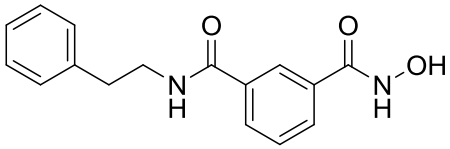

BRD-73954

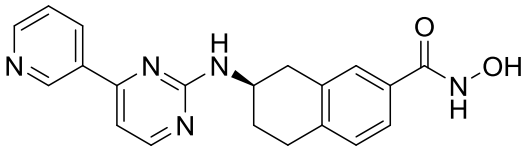

Aminotetralin 32

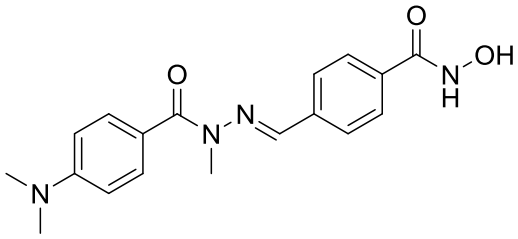

***N*-acylhydrazone analog 3f**

Figure 1.8. Chemical structures of dual HDAC6/HDAC8 selective HDAC inhibitors discussed in the text.

1.10. Binding of HDAC inhibitors to HDAC active sites

Most of HDAC inhibitors have three common important binding interaction regions (discussed in section 1.7), which are a capping group, a linker, and a metal binding group (Figure 1.9A). In all the metal-dependent HDAC proteins, these three regions form several essential interactions with the active site. As an example, SAHA docked into the active site of the HDAC1 crystal structure shows three significant binding interactions (Figure 1.9B).[98] First, the hydroxamic acid (the metal binding group) interacts with the metal binding region with five key interactions for inhibition of the enzyme (Figure 1.9C). The carbonyl group of the hydroxamic acid moiety chelates with the metal ion in the binding site with two electrostatic interactions, in addition to three hydrogen bonding interactions of the hydroxamic

acid group with H140, H141, and Y303 amino acids of the active site (Figure 1.9B and C). Moreover, the non-polar six carbons linker of SAHA interacts with the hydrophobic side chains of the amino acids lining the 11 Å channel (Figures 1.9A and 1.9B). Finally, the anilinamide capping group interacts with the solvent exposed region (Figures 1.9A and 1.9B). Another important part of the active site is the 14 Å channel, which is located at the bottom of the active site and helps in acetate escape (Figure 1.9B).[98]

HDAC inhibitors bind similarly to all the HDAC isoforms, with few variations with different HDAC isoforms active sites that impart isoform selectivity. Most of the metal-dependent HDAC crystal structures have been revealed, including HDAC1, HDAC2, HDAC3, HDAC4, HDAC7, and HDAC8 crystal structures [15, 19-21, 99-100], along with homology models of the other HDAC isoforms [22-23]. Recently, several crystal structures of both catalytic domains of HDAC6 were reported (see section 1.4).[13, 101] All crystal structures have the three common binding interaction regions, with high similarity in both sequence and binding site shape. Some of the isoforms lack the 14 Å channel (Figure 1.9B), including HDAC6 and HDAC8. On the other hand, several HDAC isoforms have a relatively wide 14 Å channel, such as HDAC1 and HDAC2, while others have a 14 Å channel with a constriction, like HDAC3.

When comparing the 11 Å channel (Figure 1.9B), HDAC6 and HDAC8 have a wider and shorter active site entrance (11 Å channel) than HDAC1, HDAC2, and HDAC3, which helped to develop several HDAC6 or HDAC8 selective inhibitors, or dual HDAC6/HDAC8 selective inhibitors. The high similarity in the binding site of both HDAC1 and HDAC2 is a challenge to rationally design and develop a selective

inhibitor to either HDAC1 or HDAC2. The availability of crystal structures for HDAC isoforms helped in developing isoform selective HDAC inhibitors, as well as in explaining the selectivity of several isoform selective HDAC inhibitors.

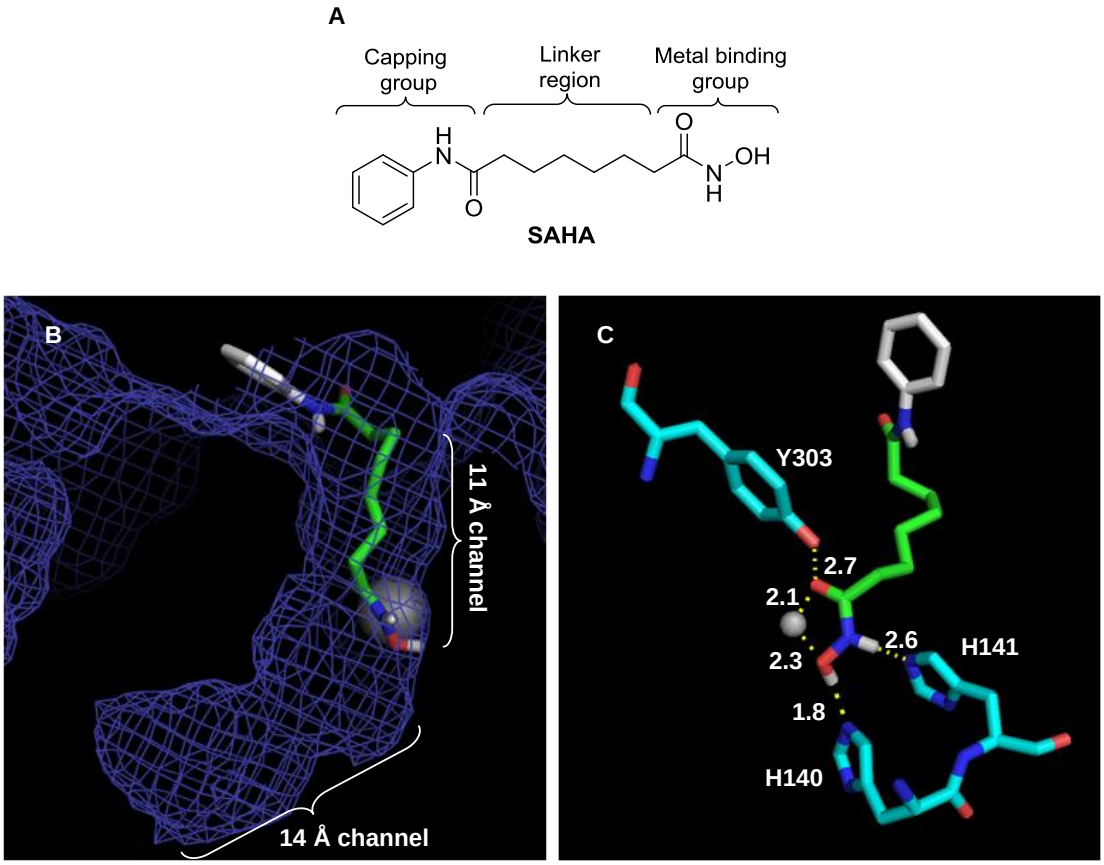

Figure 1.9. The important structural pharmacophore of HDAC inhibitors and binding to HDAC active sites. A) Structure of SAHA showing key pharmacophoric binding groups for HDAC inhibition. B and C) Binding of SAHA to HDAC1 crystal structure (deep blue mesh; PDB: 4BKX). Binding distances between the hydroxamic acid atoms and active site residues (numbered in figure) or the metal are displayed in Angstroms. The metal ion (Zn^{2+}) is represented as a grey sphere. Color-coded SAHA (C=green/white; O=red; N=blue, H=white).

1.11. Thesis Projects

While some selective compounds have been reported, identifying additional strictly isoform-selective HDAC inhibitors remains a challenge, especially for the isoforms for which no selective inhibitor has been identified, such as HDAC1.

Selective inhibitors can be used as a biological tools to elucidate the function of each isoform in the development and progression of cancer. In addition, isoform selective HDAC inhibitors will be valuable for the design and development of new promising drugs with less side effects. Moreover, modification of pan-inhibitors currently used in clinic can possibly improve their selectivity and reduce their clinical side effects.

Because most of the reported SAHA derivatives focus on modification of the capping group or metal binding group (Figure 1.9A). We are interested in our lab to modify the linker or the metal binding group with different groups.[102-105] Previously, our lab published several derivatives modified at C2, C3, C6 and the nitrogen atom of the metal binding group (Figure 1.10). Some of these derivatives showed isoform selectivity.[103-105] The C3-ethyl SAHA analog showed a modest preference for HDAC6 over HDAC1 and HDAC3.[104] Among the C6-modified SAHA analogs, C6-*t*-butly SAHA displayed a modest selectivity for HDAC1 and 6 compared to HDAC3.[105] In addition, several of the C7-modified SAHA analogs showed selectivity patterns to different isoforms, but with low fold selectivity.[106] More interestingly, one of the C7-SAHA analogs exhibited greater potency than SAHA both *in vitro* and with different cancer cell lines.

C2-modified SAHA analogs (Figure 1.6) were also generated and showed μM potency with HeLa cell lysates, but no selectivity assessment was performed.[103] In **Chapter 2**, the HDAC isoform selectivity of C2-SAHA analogs, including IC_{50} values, were assessed. *In cellulo* testing has also been performed, and docking studies were used to explain the observed selectivity of some of the C2-SAHA analogs. Enantioselective syntheses of both enantiomers of the most interesting derivative

were performed, and both of the pure enantiomers were screened for potency and selectivity.

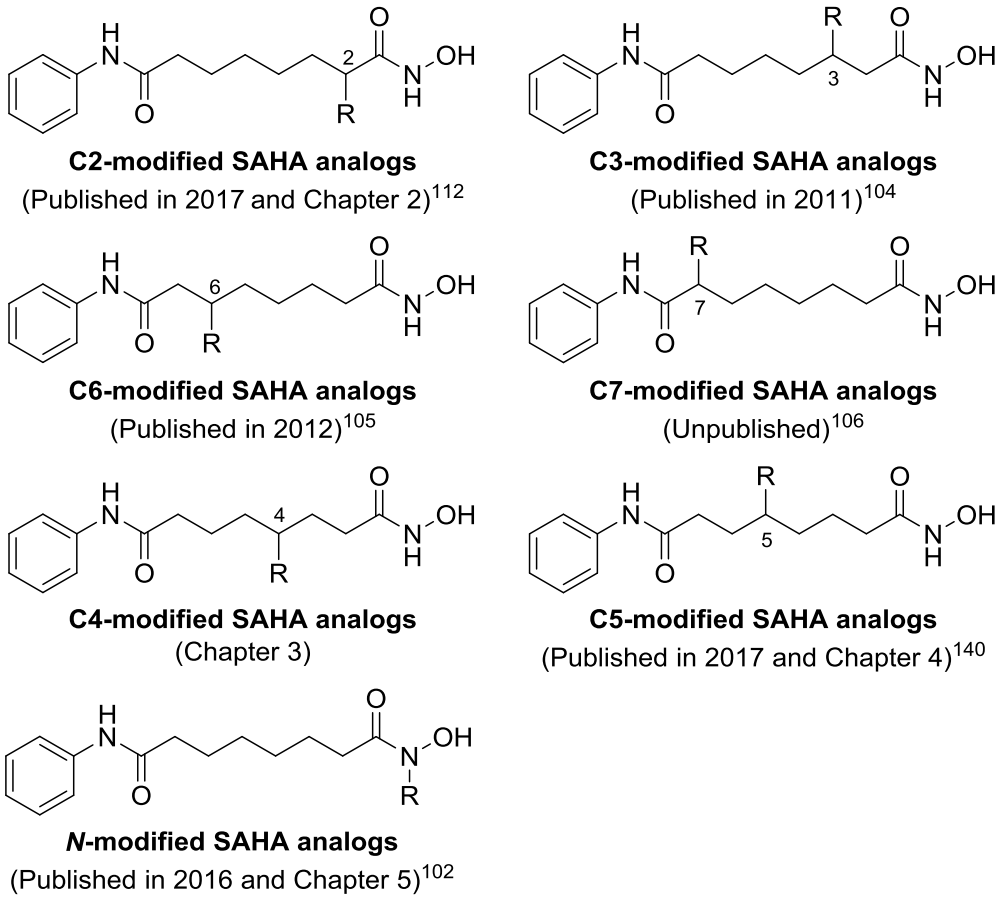

Figure 1.10. Chemical structures of SAHA analogs modified in the linker region and at the hydroxamic acid moiety created in the Pflum lab.

Chapters 3 and 4 discuss the synthesis of new SAHA derivatives substituted at the C4 and C5 positions of the linker region (Figure 1.10). The substituents chosen have different sizes and electronic properties to fit into active site of different HDAC isoforms (Figure 1.9) and to test the effect of these substituents on activity and/or selectivity. The newly synthesized derivatives were tested for their activity *in vitro* against HeLa cell lysates, as well as their selectivity with different HDAC isoforms. *In cellulo* testing was also done.

In **Chapter 5**, docking studies for previously synthesized and screened SAHA analogs modified at the hydroxamic acid moiety was performed. The docking studies suggested an explanation based on the analogs structures and the crystal structures of HDAC1 and HDAC3 the source of the observed HDAC1 preference, as well as the lower potency of the *N*-SAHA analogs compared to SAHA. Finally, **Chapter 6** focuses on the development of an HDAC1 selective inhibitor in order to use it as a biological tool and understand the HDAC1 related cancer biology. The design, synthesis, and screening of several biaryl indolyl benzamide derivatives as possible HDAC1-selective inhibitors are described in Chapter 6.

CHAPTER 2 - *IN VITRO* AND *IN CELLULO* SCREENING, ENANTIOSELECTIVE SYNTHESIS, AND DOCKING OF C2-MODIFIED SAHA ANALOGS

Some of the text in this chapter was reprinted or modified from: Negmeldin, A. T.; Padige, G.; Bieliauskas, A. V.; Pflum, M. K. H., Structural Requirements of HDAC Inhibitors: SAHA Analogues Modified at the C2 Position Display HDAC6/8 Selectivity, *ACS Medicinal Chemistry Letters* **2017**, 8 (3), 281-286; and Padige, G.; Negmeldin, A. T.; Pflum, M. K. H., Development of an ELISA-Based HDAC Activity Assay for Characterization of Isoform-Selective Inhibitors, *Journal of Biomolecular Screening* **2015**, 20 (10), 1277-1285)

2.1. Rationale for synthesis and screening of C2-modified SAHA analogs

Towards development of selective HDAC inhibitors, we previously created SAHA analogs containing substituents in the linker region between the hydroxamic acid and the anilide ends (Figure 1.6). A C3-modified SAHA analog showed modest preference for HDAC6, while C6-modified SAHA analogs displayed selectivity for HDAC1 and 6 compared to HDAC3.[103-105] In addition, modifying the amine of the hydroxamic acid reduced potency, but enhanced preference for HDAC1.[102] C2-modified SAHA analogs (Figure 2.1) were also generated by Dr. Anton Bieliauskas and screened with HeLa cell lysates by Dr. Sujith Weerasinghe (Scheme 2.1), and showed µM potency with HeLa cell lysates (Table 2.1) But no selectivity assessment was performed.[103] Because HeLa cell lysates contain all HDAC isoforms, the observed lower potency of the C2-SAHA analogs against HeLa cell lysates (Table 2.1) suggests that they might be selective for some isoforms over the others compared to SAHA.

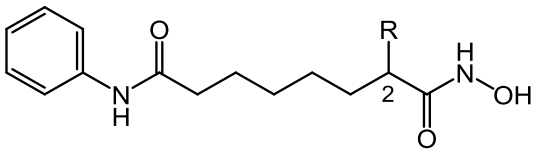

C_2-modified SAHA analogs

R = methyl (**1a**), ethyl (**1b**), *n*-propyl (**1c**), *n*-butyl (**1d**), allyl (**1e**), propargyl (**1f**), benzyl (**1g**), *n*-penyl (**1h**), *n*-hexyl (**1i**)

Figure 2.1. Chemical structures of C2-modified SAHA analogs (**1a**-**1i**).

Scheme 2.1. Synthesis of C2-modified SAHA analogs performed by Dr. Anton Bieliauskas [103]

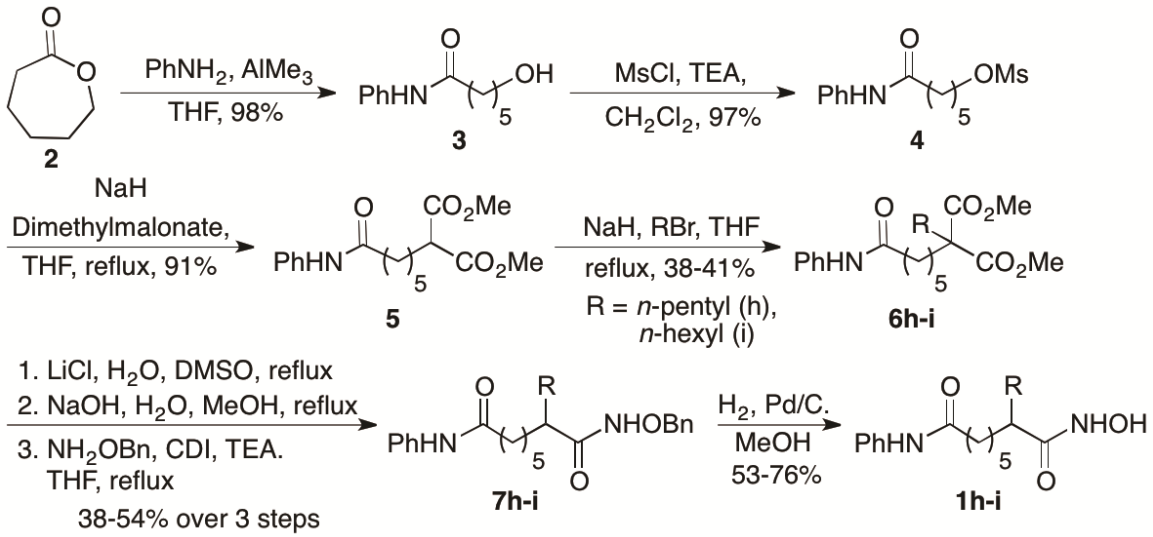

Table 2.1. IC_{50} values for SAHA, and C2-modified SAHA analogs (**1a-g**) with HeLa cell lysates.[a]

Compound	R	IC_{50} (μM)
SAHA		0.090 ± 0.004
1a	methyl	134 ± 6
1b	ethyl	449 ± 17
1c	*n*-propyl	154 ± 7
1d	*n*-butyl	72 ± 6
1e	allyl	144 ± 9
1f	propargyl	87 ± 5
1g	benzyl	226 ± 11

[a] Mean IC_{50} value and standard error of at least three independent trials are shown. Data provided by Dr. Sujith Weerasinghe.[103]

We report here a selectivity assessment of C2-modified SAHA analogs both *in vitro* and *in cellulo*. Modification at the C2 position led to reduced potency but enhanced selectivity compared to SAHA, with preference for HDAC6 and 8 over HDAC1, 2, and 3. Enantioselective syntheses of both enantiomers of the most

selective analog were also performed, with subsequent screening. Docking studies provided a structural rationale for the observed HDAC6/8 selectivity. The observed fold selectivities for some of the analogs were higher compared to known dual HDAC6/8 selective inhibitors (see section 1.9), but with submicro molar to micromolar IC_{50} values. HDAC6/8 dual inhibitors can be used as biological tools to study breast cancer metastasis.[89, 107] In addition, SAHA analogs reported here are useful lead compounds for further development of pharmacological agents and anti-cancer drug targeting HDAC6 and 8.

2.2. *In vitro* screening of C2-modified SAHA analogs

Herein we used the recently developed ELISA-based HDAC activity assay to screen the C2-modified SAHA analogs against mammalian-derived HDAC1, HDAC2, HDAC3, and HDAC6.[93, 108] The ELISA-based HDAC activity assay was developed in our lab primarily by Dr. Geetha Padige for screening and identification of isoform selective HDAC inhibitors. The assay relies on the use of mammalian cell expressed HDAC proteins, which is more biologically relevant than the widely used assays that use baclovirus-expressed recombinant HDAC proteins.[78] In addition, compared to other methods that use mammalian cell-expressed HDAC proteins, the ELISA-based HDAC activity assay is a robust and highly reproducible assay with much lower error rates.[93, 109-110] The assay is modeled after the classic ELISA, in which antibodies are used to immobilize proteins from mammalian cell extract onto a plate. In the ELISA-based HDAC activity assay, polystyrene high-binding or secondary antibody–coated 96-well plates were incubated with a primary HDAC antibody (Figure 2.2.A), followed by HeLa cell lysates to immunoprecipitate the respective HDAC isoform (Figure 2.2.B). Once the desired HDAC isoform was

affixed onto the plate, deacetylase activity was tested using commercially available HDAC Glo I/II assay, which produces a highly stable and sensitive chemiluminescent signal after reaction with the HDAC enzyme (Figure 2.2.C).[93, 111] Screening of HDAC inhibitors involved incubation of compounds with the affixed HDAC protein and monitoring the deacetylase activity remaining in the form of reduced chemiluminescent signal (Figure 2.2.C).[93, 108]

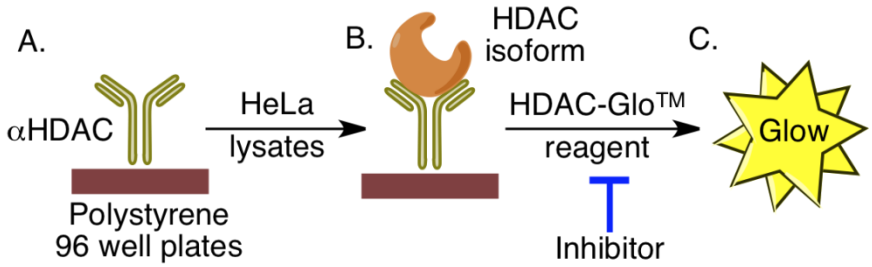

Figure 2.2. Principle of the ELISA based HDAC activity assay. A) Secondary antibody-coated or high binding polystyrene 96 well plates were incubated with primary HDAC antibody (αHDAC) to immobilize the antibody to the well, followed by washing. B) Incubation with HeLa cell lysates affixed to the well the specific HDAC isoform recognized by the immobilized antibody, followed by washing. C) Addition of the HDAC-Glo™ substrate and developer to the active HDAC isoform affixed to the well generated a quantifiable chemiluminescent signal (yellow star). Inclusion of an HDAC inhibitor in the reaction reduced the deacetylation activity of the affixed HDAC enzyme, resulting in a lower chemiluminescent signal.[93] *Reused with permission from SAGE publishing group.*

SAHA and analogs **1a-f** were tested by Dr. Geetha Padige[108, 112], while analogs **1g-i** were tested in this work.[112] As an initial test of selectivity, the potency of each C2-modified SAHA derivative was tested with HDAC1, 2, 3, and 6 at single concentrations of either 5 or 10 μM using the ELISA-based HDAC activity assay. All analogs (**1a-i**) displayed some selectivity for HDAC6 compared to HDAC1, HDAC2, and HDAC3 (Figure 2.3). Among them, the C2-benzyl (**1g**), C2-*n*-pentyl (**1h**), and C2-*n*-hexyl (**1i**) analogs showed the greatest difference in inhibitory activity comparing HDAC6 to HDAC1, HDAC2, and HDAC3. In contrast, the C2-methyl

SAHA analog was least selective, with similar activity against all the four HDAC isoforms tested (Figure 2.3).[112]

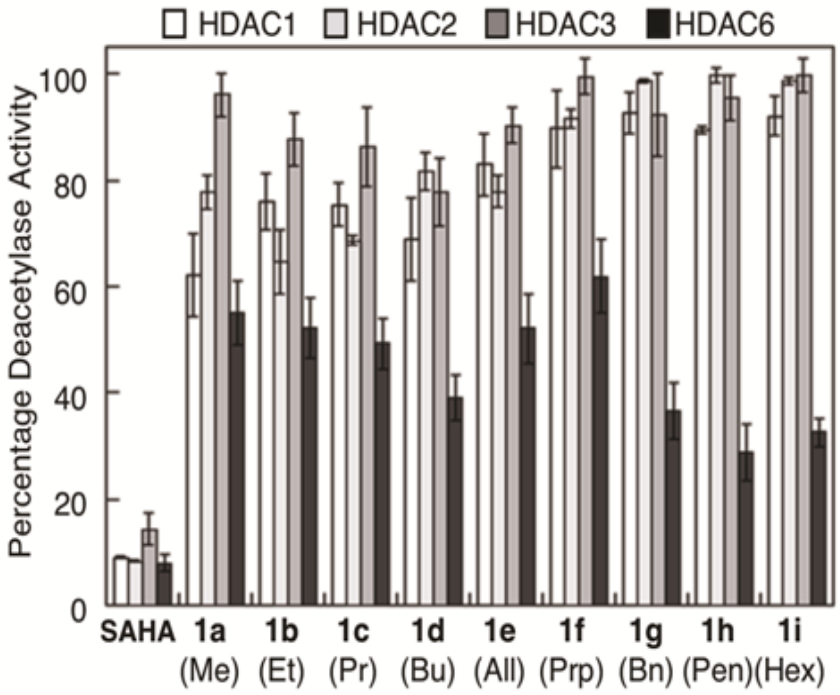

Figure 2.3. Isoform selectivity screening of SAHA and C2-modifed SAHA analogs (**1a-i**) against HDAC1, 2, 3, and 6 using the ELISA-based HDAC activity assay. [93] All analogs were tested at 5 μM concentration, except for 1d, which was tested at 10 μM. SAHA was tested at 1 μM.[93] Mean percent deacetylase activities from a minimum of three independent trials with standard errors were plotted (Table A.1). The substituent below each compound number corresponds to the R group in C2-modified SAHA (Table 2.1). Data for analogs **1a-f** was provided by Dr. Geetha Padige.[112]

To further assess selectivity, IC_{50} values for the most selective compounds in the initial screen, compounds **1g-i**, were determined with HDAC1, 2, 3, 6, and 8 (Table 2.2). HDAC8 was also tested due to its similar active site compared to HDAC6.[13] As controls, the IC_{50} values of both SAHA and tubastatin were included. As expected, SAHA displayed similar IC_{50} values with HDAC1-6, but 5-fold reduced activity with HDAC8, which is consistent with prior reports (see Table 1.1).[78, 113] Tubastatin showed at least 87-fold selectivity for HDAC6 over class I HDAC1, 2, and

3, but only 10-fold selectivity versus HDAC8.[93] Interestingly, the C2-modified SAHA analogs showed selectivity for HDAC6 and HDAC8, with IC_{50} values in the sub-micromolar to micromolar range (0.6-2.0 μM, Table 2.2). The C2-benzyl **1g** and C2-*n*-pentyl **1h** analogs displayed 33 to 92-fold selectivity for HDAC6 and HDAC8 over the Class I isoforms (Tables 2.2, A.4, and A.5, and Figures A.31 and A.32). The most selective compound, C2-*n*-hexyl SAHA **1i** displayed 49- to 300-fold selectivity for HDAC6 and HDAC8 compared to the class I isoforms (Tables 2.2 and A.6 and Figure A.33).

Table 2.2. IC_{50} values for SAHA, tubastatin, SAHA analogs **1g-1i** against HDAC1, 2, 3, 6 and 8.[a]

Compound	IC_{50} values (μM)				
	HDAC1	HDAC2	HDAC3	HDAC6	HDAC8
SAHA	0.033 ± 0.001	0.096 ± 0.01	0.020 ± 0.001	0.033 ± 0.003	0.54 ± 0.01
Tubastatin	2.7 ± 0.2	3.9 ± 0.4	2.9 ± 0.5	0.031 ± 0.004	0.33 ± 0.01
1g (benzyl)	84 ± 6	110 ± 10	91 ± 4	1.5 ± 0.2	1.2 ± 0.1
1h (pentyl)	48 ± 2	58 ± 2	43 ± 2	0.85 ± 0.05	1.3 ± 0.1
1i (hexyl)	180 ± 20	180 ± 30	98 ± 10	0.60 ± 0.05	2.0 ± 0.1
(*S*)-1i (hexyl)	330 ± 30	580 ± 30	530 ± 50	ND	3.1 ± 0.1
(*R*)-1i (hexyl)	ND	ND	ND	ND	0.71 ± 0.01

[a] Mean IC_{50} value and standard error of at least two independent trials are shown (Figures A.29-A.35 and Tables A.2-A.8).

It is notable that the selectivity of C2-*n*-hexyl SAHA **1i** for HDAC6 (>163-fold) is elevated compared to tubastatin (>87-fold), while showing 20-fold less potency than tubastatin (0.60 vs. 0.031 μM IC_{50} values). The conclusion is that C2-substituents impart selectivity by discriminating against HDAC1, HDAC2, and HDAC3.

2.3. *In cellulo* selectivity testing

To assess the HDAC6 selectivities of the analogs in a biologically relevant context, C2-benzyl (**1g**), C2-*n*-pentyl (**1h**), and C2-*n*-hexyl (**1i**) SAHA were tested for their abilities to increase the acetylation levels of HDAC substrates. Acetylated-α-tubulin (AcTub) was monitored as a known substrate of HDAC6, whereas acetylated-histone H3 (AcH3) was observed as a substrate for HDAC1, 2, and 3. U937 myeloid leukemia cells were used in these cellular HDAC6 selectivity studies. HDAC6 is overexpressed in several acute myeloid leukemia (AML) cell lines, suggesting that HDAC6 is a promising target for development of anti-leukemic drugs.[114] SAHA or the analogs were incubated with U937 cells before lysis and western blot analysis of protein acetylation. As expected, SAHA increased the acetylation levels of both α-tubulin and histone H3 (Figure 2.4a, lane 2, AcH3 and AcTub), consistent with its broad inhibition. In contrast, the HDAC6 selective inhibitor tubastatin affected only α-tubulin acetylation (Figure 2.4a, lane 3, AcTub). Similar to tubastatin, the three analogs **1h-i** increased acetylation levels of α-tubulin to a greater level than histone H3 (Figure 2.4a, lanes 4-6, AcH3). Quantification confirmed that **1h-i** significantly increased acetylation of α-tubulin compared to DMSO, but not acetyl histone H3 levels (Figure 2.4b and Table A.9). In addition, the C2-*n*-hexyl analog **1i** promoted a dose-dependent increase in acetylation of α-tubulin (Figure 2.4c, lanes 2-7, AcTub), but not histone H3 (Figure 2.4c, lanes 2-7, AcH3), compared to the DMSO control (Figure 2.4c, lane 1). The HDAC6-dependent acetylation of tubulin observed *in cellulo* is consistent with the HDAC6 selectivity observed *in vitro* (Table 2.2 and Figure 2.3).

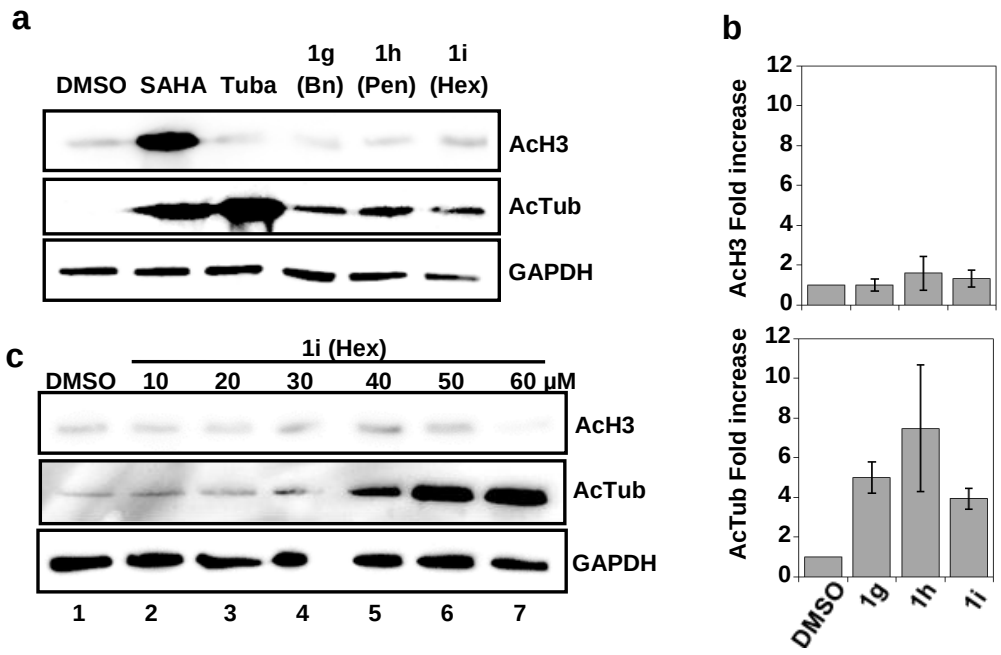

Figure 2.4. Cell-based selectivity testing of the C2-modified SAHA analogs. U937 cells were treated with (a) DMSO (1%), SAHA (2 µM), tubastatin (2 µM), C2-benzyl SAHA (**1g**, 30 µM), C2-*n*-pentyl SAHA (**1h**, 30 µM), C2-*n*-hexyl SAHA (**1i**, 30 µM), or (c) increasing concentrations of C2-*n*-hexyl SAHA analog (**1i**, 10-60 µM) before lysis, SDS-PAGE separation, and western blot analysis of acetyl-histone H3 (AcH3) and acetyl-α-tubulin (AcTub). GAPDH was a load control. Repetitive trials are shown in Figures A.36 and A.37. (b) Fold increase in AcH3 or AcTub after quantification of bands intensity from part a, with mean fold increase from four independent trials and standard error (Table A.9).

2.4. *In vitro* cell growth inhibition

To test the anti-cytotoxic properties of the HDAC6-selective inhibitors, analogs **1g-i** were tested in cell-based cytotoxicity assays using leukemia cell lines.[114] First, the analogs were tested with the Jurkat cell line (T-cell lymphoma derived cancer cell line) at 1 and 10 µM concentrations using an MTT assay (Figure 2.5, Table A.10). SAHA was also tested as a control. All compounds showed reduced cytotoxicity compared to the SAHA (Figure 2.5). Of the analogs, C2-*n*-hexyl SAHA (**1i**) showed the greatest cytotoxic effect, with only 47% viability at 10 µM concentration.

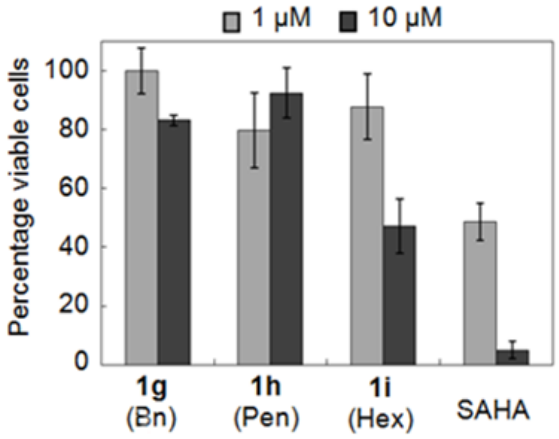

Figure 2.5. Cytotoxicity screening of **1g**, **1h**, **1i**, and SAHA with Jurkat cells. Inihbitors were tested at 1 and 10 μM concentrations using MTT assay. Mean percent viability from at least three independent trials with standard error were plotted (Table A.10).

To further assess cytotoxicity, both SAHA and the most potent analog **1i** were tested to determine EC_{50} values against three leukemia cancer cell lines: Jurkat, AML MOLM-13 (Acute myeloid leukemia cell line), and U937 cells. SAHA showed potent cytotoxicity, with EC_{50} values of 0.72, 1.2, and 0.88 μM with Jurkat, AML MOLM-13, and U937 cell lines, respectively (Table 2.3). The observed EC_{50} values are consistent with previous reports.[115-117] The high potency of SAHA may be due to its non-selectivity, as well as the high inhibitory activity against class I HDAC1, 2, and 3. The C2-*n*-hexyl SAHA analog **1i** showed roughly 10-fold reduced cytotoxicity compared to SAHA, with EC_{50} values of 11.8, 10.5, and 13.8 μM with Jurkat, AML MOLM-13, and U937 cell lines, respectively (Table 2.3). The reduced cytotoxicity is consistent with the 18-fold reduction in potency against HDAC6 compared to SAHA (Table 2.2). In addition, the selectivity for HDAC6 and 8 over HDAC1, 2, and 3 might also contribute to the lower cytotoxicity.

Table 2.3. EC_{50} values for SAHA and C2-*n*-hexyl (**1i**) SAHA analog against Jurkat, AML MOLM-13, and U937 cells using MTT assay.[a]

Compound	Cellular EC_{50} values (μM)		
	Jurkat	AML MOLM-13	U937
SAHA	0.72 ± 0.13	1.2 ± 0.06	0.88 ± 0.13
1i (hexyl)	11.8 ± 2.2	10.5 ± 3.1	13.8 ± 1.7

[a] Mean EC_{50} value and standard error of at least three independent trials are shown (Figures A.38 and A39, and Tables A.11 and A12).

2.5. Enantioselective Synthesis and Screening of (*R*)- and (*S*)-C2-*n*-hexyl SAHA

C2-*n*-hexyl SAHA (**1i**) contains a stereocenter at the 2 position, and the compounds tested to this point were racemic mixtures. To test the selectivity of each enantiomer, an enantioselective synthesis of C2-*n*-hexyl SAHA (**1i**) was employed using Evans chiral auxiliary **8** and octanoyl chloride (Schemes 2.2 and 2.3). Allyl bromide was added to the resulting amide **9** to generate chiral compound ***(R)*-10** from auxiliary **(*R*)-8** (Scheme 2.2) or **(*S*)-10** from auxiliary **(*S*)-8** (Scheme 2.3). After olefin metathesis with Grubbs' second-generation catalyst[118] and removal of the auxiliary, the olefin was reduced to generate **(*S*)-11** and **(*R*)-11**. Finally, coupling with hydroxylamine generated the two enantiomers of C2-*n*-hexyl SAHA, **(*S*)-1i** or **(*R*)-1i** in 95 and 92% ee, respectively (Figures A.26-A.28).

Scheme 2.2. Enantioselective synthesis of (*S*)-C2-*n*-hexyl SAHA **(*S*)-1i**

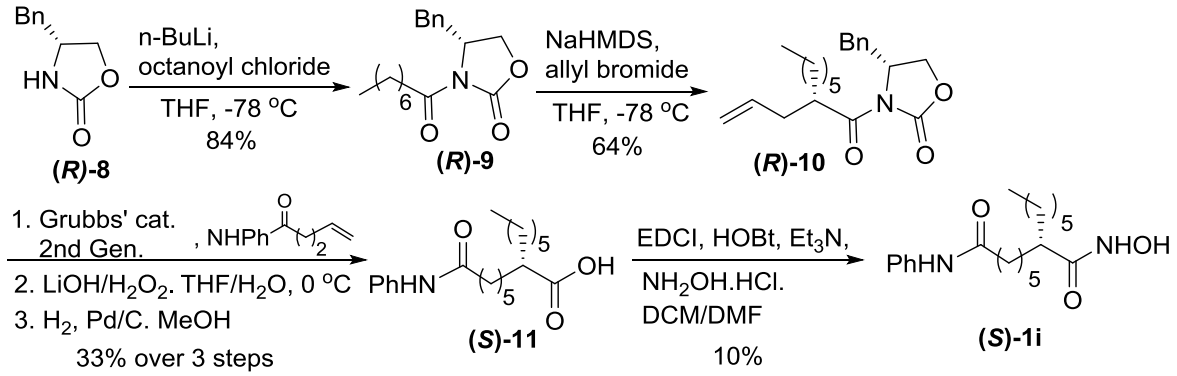

Scheme 2.3. Enantioselective synthesis of (*R*)-C2-*n*-hexyl SAHA **(*R*)-1i**

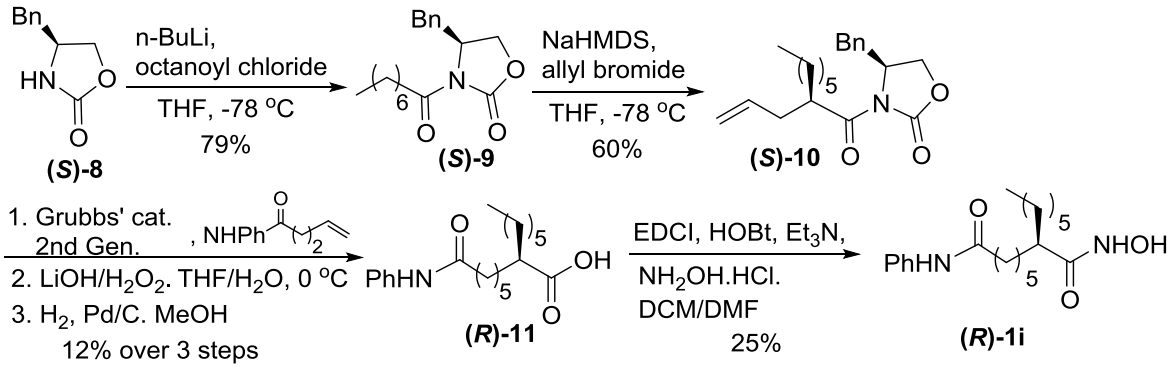

With the two C2-*n*-hexyl SAHA enantiomers in hand, IC_{50} values were determined (Table 2.2). As expected, both enantiomers displayed low micromolar to submicromolar potency with HDAC8 (3.1±0.1 or 0.71±0.01 μM), similar to racemic **1i** (2.0±0.1). The data suggested that **(*R*)-1i** is more potent than **(*S*)-1i**, although only by 4-fold. The **(*S*)-1i** enantiomer was further tested for selectivity against HDAC 1, 2, and 3. **(*S*)-1i** displayed 106- to 187-fold selectivity for HDAC8, which is greater than that observed with racemic **1i** (49- to 300-fold). In total, studies with the enantiomers of C2-*n*-hexyl SAHA indicated that both are low micromolar to submicromolar potency HDAC8 inhibitors, with the expected HDAC8 selectivity compared to HDAC1, 2, and 3.

2.6. Docking Studies with HDAC2 and HDAC6 crystal structures

To rationalize the HDAC6/8 selectivity of the C2-*n*-hexyl SAHA (**1i**) analog, we performed docking analysis using the AutoDock 4.2 program.[119] Both enantiomers of the analog were docked into the recently published HDAC6 crystal structure (pdb:5EEM)[101] and both displayed similar binding interactions (Figure 2.6), consistent with the similar IC_{50} values observed experimentally. For example, the hydroxamic acid was positioned in bonding distance (1.9-2.9 Å) of three active site

residues (H573, H574, and Y745) and the catalytic zinc atom in HDAC6 active site (Figures 2.6A and E). For comparison, docking of the parent SAHA compound with HDAC6 showed similar distances between the hydroxamic acid and the active site (1.6-2.4 Å, Figure 2.7A). To explore the HDAC6 selectivity, compound **1i** was also docked into the HDAC2 crystal structure (pdb ID: 3MAX).[19] In contrast to the bonding distances observed with HDAC6, elongated distances between the hydroxamic acid group and H145 (5.7-5.9 Å), H146 (3.8 Å), and Y308 (3.0-5.5 Å) were observed (Figures 2.6B and F). Metal binding was also weakened with longer bond distances (3.5-4.7 Å, Figures 2.6B and F). One possibility accounting for the weak binding with HDAC2 is that the bulky C2-*n*-hexyl substituent cannot favorably fit into the relatively narrow catalytic active channel of HDAC2.[86] Consistent with this possibility, superimposition of the docked poses of compound **1i** and SAHA with HDAC2 showed that the C2-*n*-hexyl substituent is positioned towards the solvent exposed surface of the active site, which consequently places the hydroxamic acid distant from the metal (Figure 2.6D and H). In contrast, the relatively wide catalytic pocket in HDAC6 allowed compound **1i** and SAHA to similarly position the hydroxamic acid within bonding distances of the catalytic metal and nearby residues (Figure 2.6C and G).

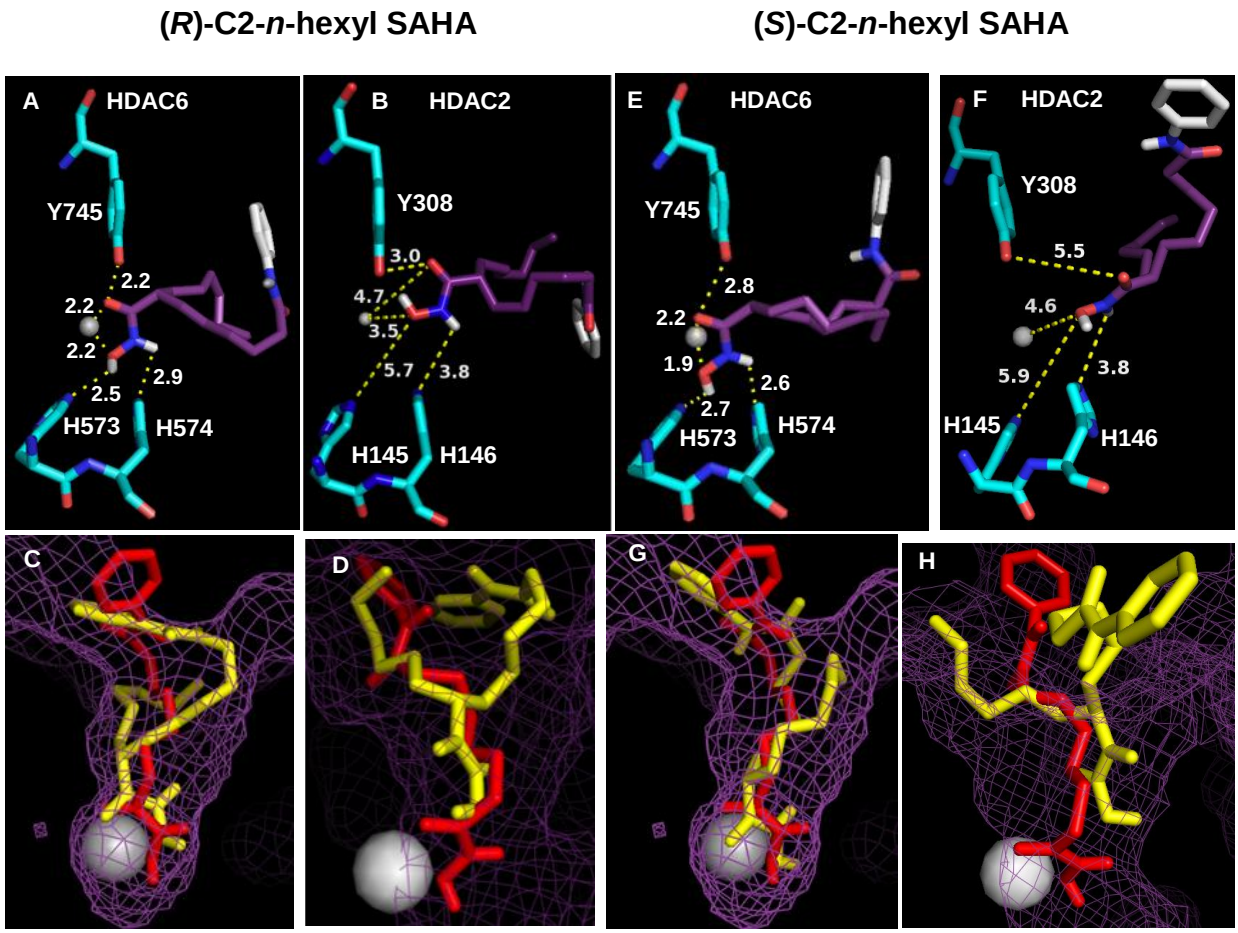

Figure 2.6. Docked poses of (*R*)-C2-hexyl SAHA (**A-D**) and (*S*)-C2-hexyl SAHA (**E-H**) in the crystal structures of HDAC6 and HDAC2 using Autodock 4.2**.** Binding distances in HDAC6 (**A**, **E**) and HDAC2 (**B**, **F**) between the hydroxamic acid atoms and active site residues (numbered in figure) or the metal are displayed in Angstroms. The atomic radius of the metal (Zn^{2+}) was set at 0.5 Å for clarity. Atom color-coding: C2-*n*-hexyl SAHA (C=purple/white; O=red; N=blue; H=White); amino acids (C=deep teal; O=red, N=blue); Zn^{2+} metal ion (grey sphere). **C**,**D** and **G**,**H**) Superimposition of SAHA (red) and (*R*) or (*S*) C2-*n*-hexyl SAHA **1i** (yellow) in the crystal structure of HDAC6 (**C**, **G**) and crystal structure of HDAC2 (**D**, **H**), with the metal ion (Zn^{2+}) represented as a grey sphere (1.35 Å radius). Notice that the metal sphere is in close proximity to the hydroxamic acid end of both SAHA and the analogs in the HDAC6 structures. In contrast, the analogs are positioned farther from the metal sphere than SAHA in the HDAC2 crystal structure, consistent with the poor potency observed.

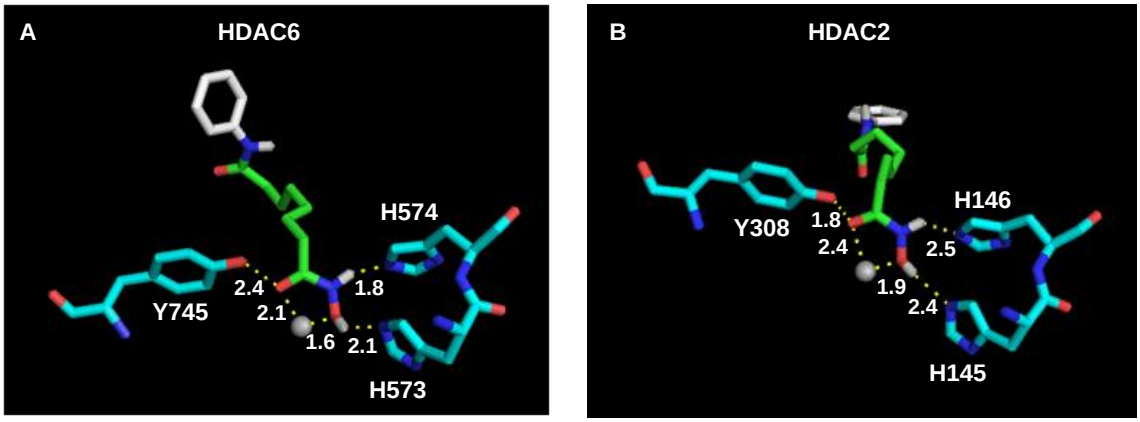

Figure 2.7. Docking poses of SAHA in the HDAC6 **(A)** and HDAC2 crystal structures **(B)** using Autodock 4.2. Binding distances between the hydroxamic acid atoms and active site residues (numbered in figure) or the metal are displayed in Angstroms. The atomic radii of the metals were set at 0.5 Å for clarity. Color-coded SAHA (C=green/white; O=red; N=blue; H=White) and amino acid residues (C=deep teal; O=red, N=blue); Zn^{2+} metal ion (grey sphere).

Because all HDAC isoforms show high conservation among their active site residues,[98, 120] previous studies suggested that the shape of the active sites might explain the HDAC6 selectivity of reported compounds.[22] In particular, HDAC6 maintains a wider active site entrance compared to the class I isoforms.[86] In previous work, HDAC6-selective inhibitors were generated by replacing the solvent-exposed anilide group of SAHA with bulky aryl groups.[86, 121-122] In addition, compounds with an aryl group attached directly adjacent to the hydroxamic acid demonstrated HDAC6 selectivity.[123] For example, tubastatin is a highly HDAC6-selective inhibitor that displays a series of bulky aryl groups near the hydroxamic acid.[86] Based on these prior studies, one hypothesis accounting for the selectivity of the C2-modified SAHA analogs is that the bulky substituent adjacent to the hydroxamic acid takes advantage of the wider active site entrance of HDAC6. In fact, the docking studies with C2-n-hexyl SAHA **1i** suggest that the wide active site entrance of HDAC6 accommodates the C2 substituents (Figures 2.6A, C, E, and G),

whereas the narrow channel of HDAC2 does not (Figures 2.6B, D, F, and H). In total, the determination that C2-modified SAHA analogs are HDAC6-selective inhibitors confirms prior structural analysis suggesting that HDAC6 maintains a wide active site entrance.

In conclusion, we report the synthesis and screening of several SAHA analogs substituted at the C2 position. C2-modified SAHA analogs displayed selectivity for HDAC6 and HDAC8 over HDAC1, 2, and 3. The highest selectivity observed was with C2-*n*-hexyl SAHA analog **1i**, which displayed 49- to 300-fold selectivity for HDAC6 and 8 over HDAC1, 2, and 3. Importantly, the selectivity of C2-*n*-hexyl SAHA is elevated compared to the widely used HDAC6-selective inhibitor, tubastatin. Cell-based selectivity testing of analogs **1g-i** reproduced the selectivity observed *in vitro*. The dual HDAC6/8 selective C2-modified SAHA analogs reported in this work can be useful as lead compounds to develop pharmacological tools and anti-cancer drugs targeting HDAC6 and HDAC8. More generally, these studies with SAHA analogs suggest that modifying known drugs can significantly improve their properties.

2.7. Experimental Procedures

2.7.1. Materials and instrumentation

Unless otherwise noted, chemicals were purchased from Sigma-Aldrich, Acros Organics, or Fisher Scientific. “Iron-free” glassware was prepared by rinsing glassware with 5 M HCl acid twice followed by washing with distilled de-ionized water. “Iron-free” silica gel was prepared by washing with 5M aqueous HCl, followed by washing with distilled de-ionized water until colorless, and subsequently drying under air or in the oven at 80°C. Flash chromatography was carried out using 60 Å,

230-400 mesh silica gel (Fisher Scientific). NMR spectra were taken on a Varian or Agilent 400, 500 or 600 MHz instruments. ^{1}HNMR spectra showed NMR solvents peaks at 3.3 ppm (for CD_3OD) and at 4.9 ppm (for trace amounts of water in NMR solvent), while ^{13}CNMR spectra showed NMR solvent peaks at 77 (for $CDCl_3$) or at 47 (for CD_3OD).[124] Infra red (IR) spectra were taken on Perkin Elmer Spectrum Two ATR-FTIR. Low resolution mass spectra (LRMS) were taken on Waters ZQ LC-SQMS, while high resolution mass spectra (HRMS) spectra were taken on a Waters LCT-MS premier TOF. HPLC analysis to assess the purity of final compounds was performed with a Waters 1525 Binary HPLC pump and Waters 2998 Photodiode Array detector. The separation was performed on a reverse phase HPLC analytical column (YMC America, 250 x 4.6 mmI.D, 4µm, 8 nm) using a gradient of 90% to 10% of buffer A over 30 minutes (buffer A = 0.1% HPLC grade trifluoroacetic acid (TFA) in water; buffer B = HPLC grade acetonitrile) at a flow rate of 1.0 mL/min at room temperature. Purity of the synthesized final compounds is indicated for each compound in the synthesis procedure. The enantiomeric excess (% ee) discussed in text was determined with the same HPLC system but with chiral analytical column (Chiracel OD-H, 250 x 4.6 mmI.D), eluting with 10% isopropanol in hexanes at a flow rate of 0.5 mL/min at room temperature. Optical rotations were measured in Perkin Elmer 341 Polarimeter.

2.7.2. Synthesis procedures for (*S*)-1i and *(R)*-1i

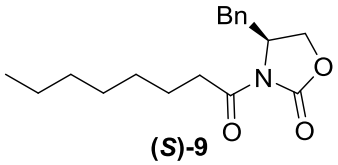

(*S*)-9

Synthesis of (*S*)-4-benzyl-3-octanoyloxazolidin-2-one ((*S*)-9). The compound was synthesized according to the reported procedure.[125] Briefly, **(S)-8** (1.44 g, 8.15 mmol) was dissolved in dry THF (25 mL) followed by the addition of butyl lithium (3.26 mL of 2.5 M solution, 8.16 mmol) drop wise under argon at -78°C. The reaction was stirred at that temperature for 10 minutes, then octanoyl chloride (1.53 mL, 8.96 mmol) was added drop wise. Stirring was continued for 30 minutes at -78°C, then the reaction temperature was gradually raised to room temperature over 30 minutes. The reaction was diluted with saturated solution of ammonium chloride (30 mL). THF was evaporated at reduced pressure and the reaction was extracted with ethyl acetate (2 x 30 mL). The organic extracts were then evaporated and the product was purified by flash silica-gel chromatography (5-10% ethyl acetate in hexanes) which yielded the product **(S)-9** (1.95 g, 79%). ^{1}HNMR (400 MHz, $CDCl_3$) δ (ppm): 0.88 (t, 3H), 1.34 (m, 8H), 1.68 (m, 2H), 2.75 (dd, 2H), 2.93 (m, 2H), 3.29 (dd, 1H), 4.18 (m, 2H), 4.66 (m, 1H), 7.21 (d, 2H), 7.27 (m, 1H), 7.33 (t, 2H); ^{13}CNMR (100 MHz, $CDCl_3$) δ (ppm): 14.09, 22.62, 24.26, 29.06, 29.09, 31.69, 35.54, 37.92, 55.15, 66.14, 127.33, 128.95, 129.42, 135.33, 153.46, 173.46. LRMS (LC-SQMS, **m/z**); found: [M+H], 304.04, calculated for $C_{18}H_{26}NO_3$, 304.18, found: [M+Na], 326.01, calculated for $C_{18}H_{25}NO_3Na$, 326.17. The spectral data for the synthesized compound was consistent with the reported data in literature.[125]

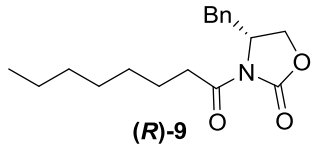

(*R*)-9

Synthesis of (*R*)-4-benzyl-3-octanoyloxazolidin-2-one ((*R*)-9). The procedure for **(S)-9** was followed, but yielding 2.18 g (84% yield) from **(R)-8** (1.5 g, 8.47 mmol). ^{1}HNMR (400 MHz, $CDCl_3$) δ (ppm): 0.90 (t, 3H), 1.30 (m, 8H), 1.68 (m, 2H), 2.76 (dd, 2H), 2.91 (m, 2H), 3.29 (dd, 1H), 4.16 (m, 2H), 4.66 (m, 1H), 7.2 (d, 2H), 7.27 (m, 1H), 7.33 (t, 2H); ^{13}CNMR (100 MHz, $CDCl_3$) δ (ppm): 14.1, 22.62, 24.26, 29.06, 29.09, 31.69, 35.54, 37.92, 55.15, 66.14, 127.32, 128.94, 129.42, 135.33, 153.46, 173.44. LRMS (LC-SQMS, **m/z**); found: [M+H], 304.08, calculated for $C_{18}H_{26}NO_3$, 304.18, found: [M+Na], 325.99, calculated for $C_{18}H_{25}NO_3Na$, 326.17. The spectral data for the synthesized compound was consistent with the reported data in literature. [125]

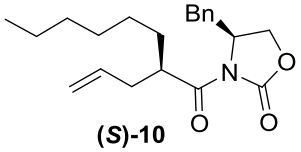

(*S*)-10

Synthesis of (*S*)-3-((*R*)-2-allyloctanoyl)-4-benzyloxazolidin-2-one ((*S*)-10). To compound **(S)-9** (1.95 g, 6.43 mmol) was added dry THF (25 mL) followed by reduction of the temperature to -78°C. NaHMDS (3.53 mL of 2 M solution, 7.07 mmol) was added drop wise under Argon and the reaction was stirred at -78°C for 1 hour. Allyl bromide (1.65 mL, 19.28 mmol) was then added drop wise, and the reaction was stirred at -78°C for 45 minutes, then the temperature was increased gradually to 0°C and stirring was continued for 1 hour at 0°C. The reaction was then quenched with saturated ammonium chloride solution (30 mL) and was left to stir at

room temperature for 15 minutes. The reaction was concentrated under reduced pressure, and the aqueous layer was extracted with ethyl acetate (3 x 30 mL). The extracts were evaporated and the product was purified by Flash silica-gel chromatography (3% ethyl acetate in hexanes) which yielded the product **(S)-10** (1.32 g, 60%). ^{1}HNMR (400 MHz, $CDCl_3$) δ (ppm): 0.87 (t, 3H), 1.27 (m, 8H), 1.49 (m, 1H), 1.7 (m, 1H), 2.32 (m, 1H), 2.47 (m, 1H), 2.65 (dd, 1H), 3.31 (dd, 1H), 3.91 (m, 1H), 4.16 (m, 2H), 4.66 (m, 1H), 5.05 (dd, 2H), 5.82 (m, 1H), 7.26 (m, 5H); ^{13}CNMR (100 MHz, $CDCl_3$) δ (ppm): 14.06, 22.58, 27.21, 29.34, 31.58, 31.66, 36.81, 38.11, 42.32, 55.53, 65.90, 117.09, 127.29, 128.93, 129.42, 135.33, 135.46, 153.16, 176.15. LRMS (LC-SQMS, **m/z**); found: [M+H], 344.04, calculated for $C_{21}H_{30}NO_3$, 344.21, found: [M+Na], 365.99, calculated for $C_{21}H_{29}NO_3Na$, 366.20. $[\alpha]_D^{23}$ = +74.5 (*c* .76, CH_2Cl_2).

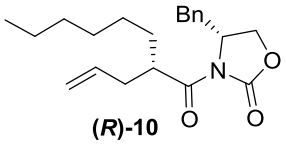

(***R***)-10

Synthesis of (*R*)-3-((*S*)-2-allyloctanoyl)-4-benzyloxazolidin-2-one ((*R*)-10). The procedure for **(S)-10** was followed, but yielding 1.56 g (64% yield) from **(R)-9** (2.15 g, 7.08 mmol). ^{1}HNMR (400 MHz, $CDCl_3$) δ (ppm): 0.87 (t, 3H), 1.27 (m, 8H), 1.49 (m, 1H), 1.72 (m, 1H), 2.32 (m, 1H), 2.45 (m, 1H), 2.66 (dd, 1H), 3.29 (dd, 1H), 3.91 (m, 1H), 4.15 (m, 2H), 4.68 (m, 1H), 5.06 (m, 2H), 5.82 (m, 1H), 7.27 (m, 5H); ^{13}CNMR (100 MHz, $CDCl_3$) δ (ppm): 14.06, 22.58, 27.20, 29.34, 31.58, 31.66, 36.80, 38.11, 42.32, 55.53, 65.89, 117.09, 127.29, 128.93, 129.41, 135.32, 135.46, 153.15, 176.15. LRMS (LC-SQMS, **m/z**); found: [M+H], 344.02, calculated for $C_{21}H_{30}NO_3$,

344.21, found: [M+Na], 366.02, calculated for $C_{21}H_{29}NO_3Na$, 366.20. $[\alpha]_D^{23}$ = −70.7 (*c* 0.49, CH_2Cl_2).

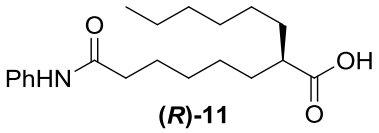

(*R*)-11

Synthesis of (*R*)-2-hexyl-8-oxo-8-(phenylamino)octanoic acid ((*R*)-11). To a solution of **(S)-10** (1.32 g, 3.84 mmol) in DCM (30 mL) was added *N*-phenylpent-4-enamide (2.69 g, 15.36 mmol) and Grubbs' second-generation catalyst (261 mg, 8 mol%). The reaction was heated at 50°C for 12 hours. The solvent was evaporated. Flash silica-gel chromatography (1:6 to 1:4 ethyl acetate in hexanes) which yielded the alkene intermediate (904 mg, 48%). The intermediate was used in the following reaction with no characterization.

The intermediate alkene (451 mg, 0.92 mmol) was dissolved in a mixture of THF (20 mL) and water (5 mL). Hydrogen peroxide (0.42 mL of 30% solution, 3.68 mmol) was added at 0°C, followed by lithium hydroxide monohydrate (78 mg, 1.86 mmol) dissolved in 3 mL water. The reaction was stirred at 0°C for 6 hours, then sodium sulfite (1 g) in 7 mL water was added. The reaction was stirred for additional 15 minutes at room temperature. The reaction was diluted with 10% HCl to pH 2, and then extracted with ethyl acetate (2 x 40 mL). The extracts were evaporated and the crude product was used in the next reaction.

The crude product was dissolved in methanol (15 mL), then 20% Pd/C was added (22 mg, 10% w/w). Air was replaced with argon (x3) then with hydrogen gas (3x). The reaction was left to stir under hydrogen overnight. The reaction was then filtered and the product was purified by Flash silica-gel chromatography (1:6 to 1:2

ethyl acetate in hexanes) which yielded the product **(R)-11** (212 mg, 69% over 2 steps). ^{1}HNMR (400 MHz, $CDCl_3$) δ (ppm): 0.87 (t, 3H), 1.28 (m, 14H), 1.68 (m ,4H), 2.32 (m, 3H), 7.08 (t, 1H), 7.27 (m, 2H), 7.52 (m, 3H); ^{13}CNMR (100 MHz, $CDCl_3$) δ (ppm): 14.06, 22.59, 25.42, 26.98, 27.34, 28.95, 29.20, 31.65, 31.88, 32.31, 37.14, 45.49, 119.91, 124.22, 128.95, 137.91, 171.66, 182.08. LRMS (LC-SQMS, **m/z**); found: [M+H], 334.16, calculated for $C_{20}H_{32}NO_3$, 334.23, found: [M+Na], 355.99, calculated for $C_{20}H_{31}NO_3Na$, 356.22, found: [M-H], 332.22, calculated for $C_{20}H_{30}NO_3$, 332.23.

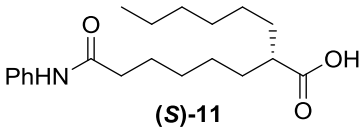

(***S***)-11

Synthesis of (*S*)-2-hexyl-8-oxo-8-(phenylamino)octanoic acid ((*S*)-11). The procedure for **(R)-11** was followed, but yielding 922 mg (43% yield) for the cross metathesis reaction from **(R)-10** (1.5 g, 4.4 mmol), and then 174 mg (28% over 2 steps) of **(S)-11**. ^{1}HNMR (400 MHz, $CDCl_3$) δ (ppm): 0.87 (t, 3H), 1.43 (m, 14H), 1.64 (m ,4H), 2.33 (m, 3H), 7.09 (t, 1H), 7.30 (m, 3H), 7.51 (d, 2H); ^{13}CNMR (100 MHz, $CDCl_3$) δ (ppm): 14.06, 22.59, 25.39, 26.97, 27.33, 28.94, 29.19, 31.64, 31.96, 32.29, 37.55, 45.39, 119.92, 124.22, 128.97, 137.91, 171.47, 181.79. LRMS (LC-SQMS, **m/z**); found: [M-H], 332.13, calculated for $C_{20}H_{30}NO_3$, 332.23.

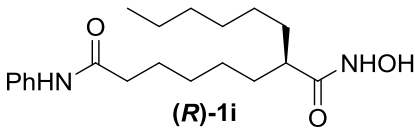

(***R***)-1i

Synthesis of (*R*)-2-hexyl-*N*^{1}-hydroxy-*N*^{8}-phenyloctanediamide ((*R*)-1i). In an acid washed flask, carboxylic acid **(*R*)-11** (295 mg, 0.87 mmol) was dissolved in

dry DCM (20 mL), followed by the addition of triethyl amine (247 uL, 1.77 mmol), HOBt (204 mg, 1.33 mmol) and EDCI HCl (272 mg, 1.42 mmol). The reaction was stirred for 1 hour, then triethyl amine (618 uL, 4.43 mmol), hydroxyl amine HCl (308 mg, 4.43 mmol) and DMF (5 mL) were added. The reaction was stirred overnight. The reaction was then concentrated under reduced pressure, diluted with distilled deionized water, and extracted with ethyl acetate (2 x 30 mL). The product was purified by Flash silica-gel chromatography (2% methanol in DCM, then 1:8 to 1:4 acetone in DCM) which yielded the product **(*R*)-1i** (30 mg, 10%). ^{1}HNMR (400 MHz, CD_3OD) δ (ppm): 0.89 (t, 3H), 1.35 (m, 14H), 1.67 (m, 4H), 2.02 (m, 1H), 2.35 (t, 2H), 7.07 (t, 1H), 7.28 (t, 2H), 7.52 (d, 2H); ^{13}CNMR (100 MHz, CD_3OD) δ (ppm): 13.00, 22.23, 25.34, 26.83, 27.14, 28.75, 28.94, 31.50, 32.28, 32.48, 36.43, 43.58, 119.84, 123.70, 128.34, 138.46, 173.24, 173.98; HRMS (Waters LCT-MS premier TOF, *m*/*z*): found [M+Na], 371.2313, calculated for $C_{20}H_{32}N_2O_3Na$, 371.2311. $[\alpha]_D^{23}$ = –1.74 (*c* 0.3, EtOH). Chiral HPLC: 92% ee.

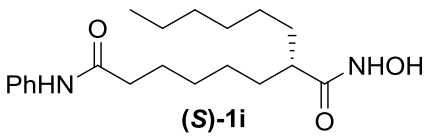

(*S*)-1i

Synthesis of (*S*)-2-hexyl-*N*^{1}-hydroxy-*N*^{8}-phenyloctanediamide ((*S*)-1i). The procedure for **(*R*)-1i** was followed, but yielding 30 mg (25% yield) from **(*S*)-11** (116 mg 0.35 mmol). ^{1}HNMR (400 MHz, CD_3OD) δ (ppm): 0.88 (t, 3H), 1.34 (m, 14H), 1.64 (m, 4H), 2.02 (m, 1H), 2.35 (t, 2H), 7.07 (t, 1H), 7.28 (t, 2H), 7.53 (d, 2H); ^{13}CNMR (100 MHz, CD_3OD) δ (ppm): 13.02, 22.24, 25.35, 26.84, 27.15, 28.76, 28.95, 31.51, 32.29, 32.49, 36.44, 43.58, 119.85, 123.71,128.35, 138.46, 173.24, 173.98; HRMS (Waters LCT-MS premier TOF, *m*/*z*): found [M+Na], 371.2320,

calculated for $C_{20}H_{32}N_2O_3Na$, 371.2311. $[\alpha]_D^{23}$ = +1.45 (*c* 0.9, EtOH). Chiral HPLC: 95% ee.

2.7.3. Procedures for biological screening

2.7.3.1. HeLa cell lysis

HeLa-S3 cells (purchased from Biovest Inc.) were lysed in lysis buffer (1×10^9 cells in 10 mL lysis buffer; 50mM Tris-HCl, pH 8.0, 10% glycerol, 150 mM NaCl, 0.5% Triton X-100) containing Calbiochem protease inhibitor cocktail set V with rotation at 4 °C for 30 min. Cell debris was removed by centrifugation at 12000 rpm at 4 °C for 30 min. Protein concentration of the supernatant was determined using Bio-Rad protein assay (BioRad, Bradford reagent).

2.7.3.2. Inhibitors testing with HDAC isoforms

Screening with HDAC1, 2, 3, and 6 was performed according to the reported procedure.[93] Briefly, individual wells of a high binding polystyrene 96-well white opaque plate (Thermo Scientific) were incubated in binding buffer (100 µL; 0.2M carbonate/0.2M bicarbonate buffer, pH 9.4) containing primary HDAC1 antibody (Sigma Aldrich, H3284, 100µL of 10µg/mL), primary HDAC2 antibody (Sigma Aldrich, H3159, 100µL of 10µg/mL), or primary HDAC6 antibody (Sigma Aldrich, SAB1404771, 100µL of 2µg/mL) with rocking (3 rpm) for 1 hr at room temperature, or at 4°C overnight with no rocking. For HDAC3 with compounds **1g-i,** primary HDAC3 antibody (Sigma Aldrich, H3034, 100µL of 25µg/mL) was used following the same procedure described above. But in the case of HDAC3 with all other compounds, wells of a secondary antibody coated 96-well white opaque plate (G-Biosciences) were incubated with primary HDAC3 antibody (Sigma Aldrich, H3034,

100µL of 1µg/mL) in TBST buffer (50 mM Tris-HCl, 150 mM NaCl, pH 7.4, 0.05% (v/v) Tween-20) containing 0.1% (w/v) bovine serum albumin (BSA, Jackson Immunoresearch) at 4°C overnight without rocking. For all reactions, unbound antibody was removed by washing quickly three times with TBST buffer (300 µL), followed by a fourth wash with TBST (300 µL) with 5 minutes incubation and rocking (3 rpm) at room temperature. In the case of high binding polystyrene plates containing HDAC1, 2, 3, or 6 antibodies, the unbound regions of the well were blocked with 5% non-fat dry milk in TBST buffer (300 µL) for 1 hr at room temperature with rocking (3 rpm). Because the secondary antibody coated plates containing HDAC3 were pre-blocked by the manufacturer, no additional blocking step was included.

To affix HDAC enzyme to the plate, HeLa cell lysates (100µL of 100µg/mL for HDAC1, 2, and 3 and 100µL of 1 mg/mL for HDAC6 in TBST buffer containing 0.1 % (w/v) non-fat dry milk) were added to each well and incubated for 1 h at 4°C without rocking, followed by washing with TBST, as described previously. For HDAC3 with compounds **1g-i** only, HeLa cell lysates (100µL of 1 mg/mL in TBST buffer containing 0.1 % (w/v) non-fat dry milk) were used, followed by incubation and washing as described earlier. Inhibitors in DMSO (1 µL) were mixed with HDAC-Glo™ buffer (24 µL), then added to the plate and incubated for 15 min at room temperature without rocking. An uninhibited control reaction was also included that contained DMSO (1 µL) in HDAC-Glo™ buffer (24 µL). Finally, deacetylase activity was measured using the HDAC-Glo™ assay kit (Promega) as per the manufacturer's protocol. Specifically, the HDAC-Glo™ substrate (1 mL) and

developer (1 µL) were first premixed, then to monitor deacetylase activity, the HDAC-Glo™ reagents (25µL) were added to each well (50 µL total volume) and incubated for 30-45 min at room temperature without rocking. The deacetylase activity was measured as luminescent signal using a GeniosPlus Fluorimeter (Tecan) at optimal gain. The concentrations of inhibitors reported in the single dose screen and dose-dependent studies are final concentrations after addition of HDAC-Glo™ reagent. For the single concentration screen, the percent deacetylase activity remaining was calculated by dividing the signal with inhibitor by the signal without inhibitor (DMSO negative control reaction), and then multiplying by 100. For dose-dependent reactions to determine IC_{50}, the luminescent signal was first background corrected with the signal from a negative control reaction where the HDAC antibody was absent in the initial antibody binding step before the percent deacetylase activity was calculated. The mean percent deacetylase activity along with standard error of three independent trials is reported.

Inhibitory activity with HDAC8 with all compounds was measured using the following procedure. In a half area 96-well plate, HDAC8 (75 ng, BPS Bioscience) was incubated in HDAC-Glo™ buffer (39 µL) with small molecule in DMSO (1 µL), or DMSO alone (1 µL) as a control, for 15 minutes at room temperature. HDAC-Glo™ reagent (10 µL) was added to each reaction and incubated for 15-30 min at room temperature. Luminescent signal was measured at 25-30 minutes after adding the substrate reagent using a GeniosPlus Fluorimeter (Tecan) at optimal gain. To determine IC_{50}, the luminescent signal was first background corrected with the signal from a background control reaction where no HDAC8 enzyme was added.

IC_{50} values were calculated by fitting the percent deacetylase activity remaining as a function of inhibitor concentration to a sigmoidal dose-response curve ($y = 100/(1+(x/IC_{50})^z)$, where y = percent deacetylase activity and x = inhibitor concentration) using non-linear regression with KaleidaGraph 4.1.3 software.

2.7.3.3. *In cellulo* target and selectivity validation

U937 cells were grown in RPMI media supplemented with 10% fetal calf serum and 1% penicillin/streptomycin under humidified conditions (37 °C, 5% CO_2). Cells were added (10^6 cells/well) to a 12 well flat bottom cell culture plate (Corning™ Costar™) in RPMI-1640 (with or with no phenol red) media, supplemented with 10% fetal calf serum and 1% penicillin/streptomycin (990 µL final volume). The cells were treated with DMSO (10 µL) or the small molecule in DMSO (10 µL), and incubated for 18 hours under humidified conditions (37 °C, 5% CO_2). The cells were then washed once with cold PBS (500 µL) and lysed with lysis buffer (20 µL) containing 1X protease inhibitor for 30 minutes at 0°C. The total protein concentration in the supernatant was then quantified using the Bradford assay kit (Bio-Rad) with BSA as the standard.

2.7.3.4. Sodium Dodecyl Sulfate-Polyacrylamide Gel Electrophoresis (SDS-PAGE)

In order to separate proteins, equal quantities of proteins from lysates prepared in section 2.7.3.3 were mixed with BME (2-mercapto ethanol, 10% of the final volume) and SDS loading buffer (50 mM Tris-Cl [pH 6.8], 100 mM DTT, 2% SDS, 0.1% bromophenol blue, and 10% glycerol) before the proteins were denatured at 95 °C for 3 minutes. The proteins in each sample were separated by

16% SDS-polyacrylamide gel electrophoresis (SDS-PAGE). SDS-PAGE gels were prepared according to the reported procedure.[126]

2.7.3.5. Western blotting and visualization of proteins levels

To detect and visualize proteins bands, proteins on the SDS-PAGE gel were transferred to PVDF membrane (Immobilon P, Millipore). The membrane was blocked with 5% (w/v) nonfat milk in TBST buffer at room temperature for 1 h. The blocked membrane was incubated with a primary antibody (anti-GAPDH (Cell Signaling, 5174P); anti-Acetyl-α-tubulin(Lys40) (Cell Signaling, 5335P), or anti-Acetyl-histone H3(Lys9) (Cell Signaling, 9649P)) at a 1:1000 dilution in TBST buffer at 4 °C overnight. Finally, the membrane was incubated with HRP-conjugated goat anti-rabbit secondary antibody (Cell signaling, 7074S; 7:10000 dilution) at room temperature for 1 h. HRP activity was detected using an enhanced chemiluminescence light-based detection substrate, SuperSignal West Dura Extended Duration Substrate (ThermoFisher Scientific, 34075) and Alpha Innotech FluorChem imaging system. The western blots were quantified using AlphaView FluorChem 3.2.2 program.

2.7.3.6. *In vitro* cell growth inhibition

Jurkat, AML-MOLM-13, or U937 cells were grown in RPMI media supplemented with 10% fetal calf serum and 1% penicillin/streptomycin under humidified conditions (37°C, 5% CO_2). Cells were seeded in 96-well cell culture plates with a density of $4x10^4$ cells in 99 µL of media composed of RPMI-1640 (no phenol red), supplemented with 10% fetal calf serum and 1% penicillin/streptomycin. The cells were treated with 1 µM or 10 µM single concentrations or serial dilution (2-fold) of compounds **1g-i** in DMSO (1 µL). DMSO only was used in the no inhibitor control. A

negative control was also included where no cells were added. The plate was incubated for 44 hours at 37 °C in humid 5% CO_2 atmosphere. A solution of 3-(4,5-dimethylthiazol-2-yl)-2,5-diphenyltetrazolium bromide (MTT, 10 µL of 5 mg/mL in DPBS buffer (HyClone™ Dulbecco's Phosphate Buffered Saline)) was added to each well. The cells were incubated for another 4 h at 37 °C in humid 5% CO_2 atmosphere for development to take place. The resulting purple formazan crystals were dissolved by addition of DMSO (150 µL), and the absorbance was measured at 595 nm using a GeniosPlus Fluorimeter (Tecan). For all wells containing inhibitor, the signal was background corrected with the signal from a negative control reaction (media and MTT only) before the percent viable cells was calculated. The percent viable cells was calculated by dividing the absorbance with inhibitor by the absorbance without inhibitor (DMSO, cells, and MTT). The assay was performed at least three independent times. For the single concentrations experiment, the mean percent viable cells along with standard error of three independent trials is reported in Figure 2.5. EC_{50} values were calculated by fitting the percent viable cells as a function of inhibitor concentration to a sigmoidal dose-response curve ($y = 100/(1+(x/EC_{50})^z)$, where y = percent viable cells and x = inhibitor concentration) using non-linear regression with KaleidaGraph 4.1.3 software (Table 2.3).

2.7.4. Docking procedure

The AutoDock 4.2 program[119, 127] was used to perform the docking calculations. The HDAC2 crystal structure was downloaded from the protein data bank (pdb ID: 3MAX).[128] The PyMOL program was used to delete two chains and remove water molecules, metal ions (calcium and sodium), and the cocrystallized ligand in the active site from the crystal structure; only the zinc atoms remained. For HDAC2, a

grid box of size 60 X 60 X 60 $Å^3$ with a spacing of 0.375 Å and centered at (69.643, 30.937, -0.989) was used. HDAC6 crystal structure was downloaded from protein databank. (pdb: 5EEM).[101] PyMOL program was used to manually delete potassium and sodium ions, and all water molecules. A grid box of size 42 X 44 X 40 $Å^3$ with a spacing of 0.375 Å and centered at (7.000, 17.000, -22.000) was used. For both HDAC2 and HDAC6, AutoDockTools-1.5.4[119] was used to add all polar hydrogen atoms, compute Gasteiger charges, merge all nonpolar hydrogen, and generate pdbqt files. The charge of the zinc atom was manually changed from zero to +2. The map type was set by choosing the ligand and then AutoGrid 4.2 was used to pre-calculate and generate the grid map files required for the docking calculations. All the docked compounds were drawn in ChemBioDraw Ultra 12.0, and Chem 3D Pro 12.0 was used to run MM2 job for energy minimization. Then AutoDockTools-1.5.4 program was used to choose torsions, compute Gasteiger charges, and generate the pdbqt files. All acyclic bonds were made rotatable, except the amide bonds. The generated pdbqt files for the enzymes were set as a rigid macromolecule and the genetic algorithm search parameters were set to 100 GA runs for each ligand with a population size of 150, a maximum number of 2.5 x 10^5 energy evaluations, a maximum number of 2.7 x 10^4 generations, a mutation rate of 0.2 and a crossover rate of 0.8. The docking parameters were set to default. All output DLG files were converted to pdbqt format and the results were visualized in PyMOL. Among the 100 docked poses generated, the ones shown in Figures 2.5 and 2.6 displayed optimal distances between the hydroxamic acid group of the inhibitor and the catalytic metal of the protein.

CHAPTER 3 - SYNTHESIS, BIOLOGICAL EVALUATION AND DOCKING OF SAHA DERIVATIVES SUBSTITUTED AT C4 POSITION

Some of the text in this chapter was reprinted or modified from: Negmeldin, A. T. and Pflum, M. K. H., The structural requirements of histone deacetylase inhibitors: SAHA analogs modified at the C4 position display dual HDAC6/HDAC8 selectivity. *European Journal of Medicinal Chemistry* (*Submitted*)

3.1. Rationale for synthesis of C4-modified SAHA analogs

After we observed a promising dual HDAC6/HDAC8 selectivity with some of the C2-modified SAHA analogs, we extended the modifications to the fourth carbon of the linker of SAHA in order to explore the effect on both potency and isoform selectivity (Figure 3.1). In this chapter, several new SAHA derivatives substituted in the linker region at the C4 position were synthesized and screened (Figure 3.1). The substituents chosen have different sizes to fit into the active sites of different HDAC isoforms (Figure 3.1). Similar to the C2-modified SAHA analogs, several C4-SAHA analogs showed substantial improvement in selectivity towards HDAC6 and HDAC8 over HDAC1, 2, and 3, but with a modest reduction in potency, compared to SAHA. Enantioselective syntheses of both enantiomers of the most interesting analog were performed and the pure enantiomers were tested for potency and selectivity. Docking studies provided a structural rationale for the HDAC6 selectivity. This study along with the previous studies discussed in this thesis emphasize that modification of the SAHA linker region can enhance isoform selectivity with different effects on potency.

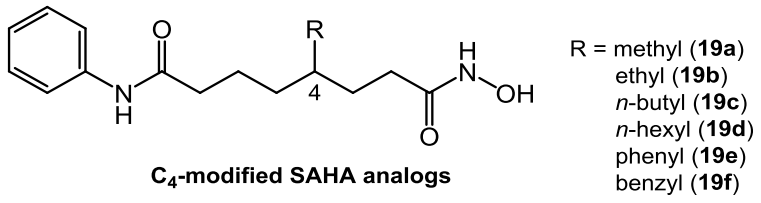

Figure 3.1. Chemical structures of C4-modified SAHA analogs (**19a**-**f**).

3.2. Synthesis of C4-substituted SAHA derivatives

Synthesis of the C4-SAHA analogs started from a cross metathesis reaction of methyl-4-pentenoate **12** with crotonaldehyde **13** using Grubbs' second-generation catalyst to afford the α,β-unsaturated aldehyde **14** (Scheme 3.1). Different substituents were appended to **14** via 1,4-addition using organolithium cuprates, followed by Horner–Wadsworth–Emmons reaction with benzyl phosphonoacetate to give the unsaturated benzyl esters **16a-f**. Reduction and hydrogenolysis of **16a-f** gave free acids **17a-f**, which were coupled with aniline to afford **18a-f**. Intermediates **18a-f** were reacted with hydroxylamine to afford the C4-substituted SAHA derivatives **19a-f** as racemic mixtures.

Scheme 3.1. Synthesis of C4-SAHA analogs (**19a-f**).

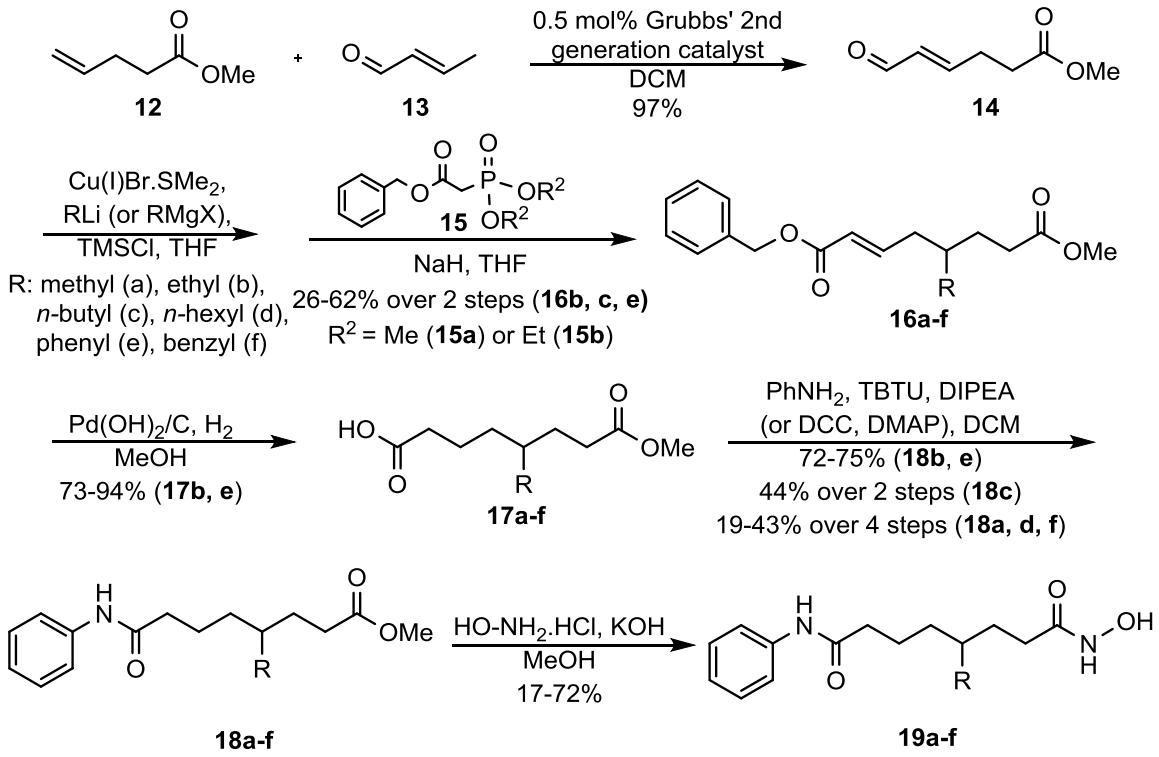

3.3. *In vitro* screening of C4-modified SAHA analogs

The analogs were tested for global HDAC inhibition with HeLa cell lysates as the source of all HDAC proteins (Table 3.1). HDAC activity was measured using the commercially available HDAC-Glo™ I/II substrate (Promega) (see section 2.2). The results of the screening showed that all of the synthesized derivatives were less potent than SAHA (Table 3.1 and B.1, and Figure B.140). The most potent derivative was C4-methyl SAHA (**19a**), which showed an IC_{50} value of 3.3 µM. Compared to the parent molecule SAHA, C4-methyl SAHA is 18-fold less potent than SAHA, while the rest of the analogs showed 78- to 344-fold reduction in potency. Because HeLa cell lysates contain all HDAC isoforms, the poor potency of the C4-SAHA analogs suggests that they may be selective for some HDAC isoforms, similar to prior C2-modified SAHA analogs (see sections 2.1 and 2.2).

Table 3.1. IC_{50} values for SAHA and C4-SAHA analogs (**19a-19f**) with HeLa cell lysates.[a]

Compound	R	IC_{50} (µM)
SAHA		0.20 ± 0.02
19a	methyl	3.3 ± 0.1
19b	ethyl	14 ± 1
19c	*n*-butyl	53 ± 2
19d	*n*-hexyl	60 ± 1
19e	phenyl	65 ± 6
19f	benzyl	62 ± 1

[a] Mean IC_{50} value and standard error of at least three independent trials are shown (Figure B.140 and Table B.1).

To assess selectivity, an initial screen was performed with analogs **19a-f** and the parent molecule SAHA at a single concentration against HDAC1, 2, 3, and 6 using the recently developed ELISA-based HDAC activity assay (see section 2.2).[93]

SAHA, as expected, showed no selectivity among HDAC1, 2, 3, and 6, inhibiting their activity to a similar extent (Figure 3.2). Interestingly, all C4-SAHA analogs (**19a-f**) displayed more potent inhibition against HDAC6 compared to HDAC1, HDAC2, and HDAC3 (Figure 3.2 and Table B.2). The analogs that showed the greatest difference in potency with HDAC6 versus the other isoforms were C4-*n*-butyl (**19c**) and C4-benzyl (**19f**). Among the analogs, the C4-methyl SAHA analog (**19a**) showed the smallest difference in potency comparing HDAC6 to HDAC1 and HDAC3 (Figure 3.2 and Table B.2). This single concentration screen suggested that C4-modification on the SAHA structure results in selectivity for HDAC6.

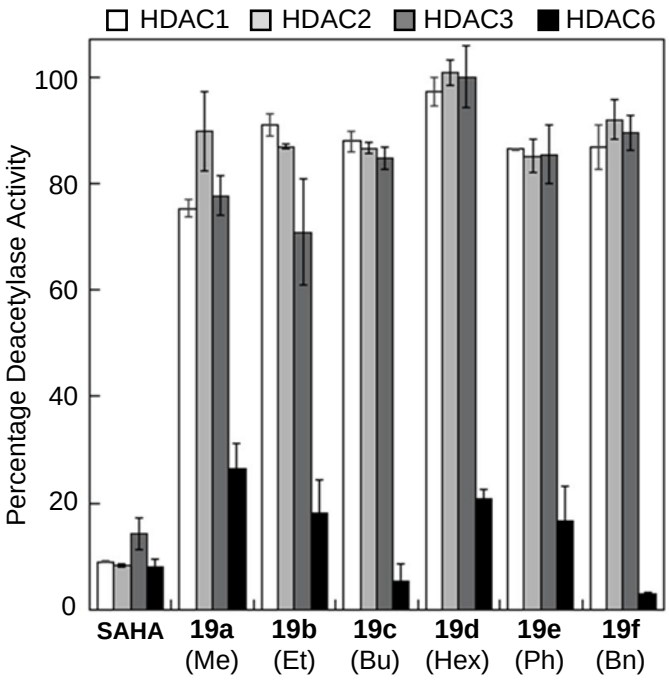

Figure 3.2. *In vitro* isoform selectivity screening of C4-modified SAHA analogs (**19a-f**) against HDAC1, HDAC2, HDAC3, and HDAC6 using the ELISA-based HDAC activity assay. Analogs **19a-f** were tested at 0.75, 0.75, 2.5, 1.25, 2.5, and 5 μM final concentration, respectively. SAHA was tested at 1 μM concentration.[93] Mean percent deacetylase activities from a minimum of two independent trials with standard errors were plotted (Table B.2).

To further assess selectivity, IC_{50} values for derivatives **19b-f** were determined with HDAC1, HDAC2, HDAC3, HDAC6, and HDAC8 isoforms (Table 3.2). In addition, the non-selective parent molecule SAHA, and the HDAC6-selective inhibitor tubastatin, were tested as control compounds (Table 3.2).[93] The non-selective inhibitor SAHA showed similar IC_{50} values with HDAC1, 2, 3, 6, and 8, which is expected for a non-selective inhibitor.[93] The HDAC6-selective inhibitor tubastatin displayed 87- to 130-fold selectivity for HDAC6 over HDACs 1, 2, and 3, and 11-fold selectivity for HDAC6 over HDAC8.[93, 112] Interestingly, the analogs **19b-f** had similar IC_{50} values compared to SAHA with HDAC6 and HDAC8, which were in the 57 to 290 nM range (Tables 3.2 and B.10). Moreover, analogs **19b-f** showed 28- to 740-fold selectivity for both HDAC6 and HDAC8 over HDAC1, 2, and 3. The C4-ethyl SAHA (**19b**) and C4-phenyl SAHA (**19e**) displayed the lowest selectivity among the analogs, with at least 28- and 38-fold selectivities for HDAC6 and 8 over HDAC1, 2, and 3 (Tables 3.2 and B.10). Modifying SAHA at the C4 position with long alkyl or bulky groups (*n*-butyl, *n*-hexyl, and benzyl groups in analogs **19c**, **19d**, and **19f**) led to substantial enhancement of selectivity with at least 170-fold selectivity for HDAC6 and 8 over HDAC1, 2, and 3 isoforms (Tables 3.2 and B.10). In addition, the modifications in analogs **19c**, **19d**, and **19f** led to modest reductions in HDAC6 potency (2.5 to 3-fold reduced), but more potent inhibition of HDAC8 (7- to 9.5-fold increased) compared to SAHA (Table 3.2).

In terms of structure-activity relationship (SAR) analysis, modifying SAHA at the C4 position with long alkyl substituents led to enhanced selectivity; the C4-hexyl **19d** analog with the longest alkyl chain demonstrated elevated selectivity (210- to

480-fold) compared to the C4-butyl **19c** analog (170- to 310-fold), which were both more selective that the C4-ethyl analog **19b** with the smallest alkyl chain (28- and 46-fold, Tables 3.2 and B.10). The length of the substituent also influenced the selectivities of the analogs with aryl groups at the C4 position; the lack of a methylene in C4-phenyl analog **19e** led to decreased selectivity (38- to 350-fold) compared to the C4-benzyl analog **19f (**210- to 740-fold). The reduced selectivity of C4-phenyl analog **19e** was due to both decreased potency against HDAC8 (290 nM) and greater potency with HDAC1 and 2 (11 and 12 μM) compared to C4-benzyl analog **19f** (57 nM, 29 μM, and 32 μM IC50 values with HDAC1, 2, and 8, Table 3.2). In total, the SAR analysis indicated that longer substituents at the C4 position led to greater HDAC6/8 selectivity.

Table 3.2. IC_{50} values for SAHA, tubastatin, SAHA analogs **19b-19f**, and pure enantiomers of the C4-benzyl SAHA **(*R*)-19f** and **(*S*)-19f** against HDAC1, 2, 3, 6 and 8.[a]

Compound	IC_{50} values (nM)[a]				
	HDAC1	HDAC2	HDAC3	HDAC6	HDAC8
SAHA[b]	33 ± 1	96 ± 10	20 ± 1	33 ± 3	540 ± 10
Tubastatin[b]	2,700 ± 200	3,900 ± 400	2,900 ± 500	31 ± 4	330 ± 10
19b (ethyl)	4,400 ± 300	4,900 ± 400	6,000 ± 1200	160 ± 10	130 ± 3
19c (*n*-butyl)	15,000 ± 1000	18,000 ± 2000	23,000 ± 3000	88 ± 7	74 ± 2
19d (*n*-hexyl)	35,000 ± 1000	38,000 ± 3000	30,000 ± 3000	140 ± 10	79 ± 3
19e (phenyl)	11,000 ± 1000	12,000 ± 1000	23,000 ± 2000	110 ± 10	290 ± 20
19f (benzyl)	29,000 ± 1000	32,000 ± 2000	42,000 ± 4000	140 ± 10	57 ± 2
(*R*)-19f	25,000 ± 2000	36,000 ± 3000	27,000 ± 2000	48 ± 8	27 ± 2
(*S*)-19f	40,000 ± 1000	51,000 ± 1000	37,000 ± 2000	95 ± 9	150 ± 10

[a] Mean IC_{50} value and standard error of at least three independent trials are shown (Figures B.141-B.147 and Tables B.3-B.9). [b] Previously reported IC_{50} values using the same assay procedure.[93, 112]

Compared to previously reported selective inhibitors, the observed HDAC6 selectivities with the analogs **19c**, **19d**, and **19f** were higher (at least 170-, and 210-fold) than the selectivity observed with the HDAC6 selective inhibitor tubastatin (at least 87-fold) (Table B.10). Moreover, **19c**, **19d**, and **19f** showed comparable selectivities (at least 200-, 380-, and 510-fold) relative to the HDAC8 selective inhibitor PCI-34051 (at least 400-fold).[87] Interestingly, C4-benzyl analog **19f** showed higher dual HDAC6/8 selectivity (at least 210- and 510-fold) than the known HDAC6/8 dual selective inhibitor BRD-73954 (at least 75-, and 250-fold selectivity to HDAC6, and 8 over HDAC1, 2, and 3).[89]

3.4. *In cellulo* selectivity testing

To further assess the observed HDAC6 selectivity *in cellulo*, C4-benzyl (**19f**) SAHA analog was tested for selectivity to inhibit HDAC6 over HDAC1, HDAC2, and HDAC3 in cells. The inhibition of HDAC6 was monitored by detecting the levels of its known substrate acetyl-α-tubulin (AcTub), whereas Class I HDAC proteins (HDAC1, 2, and 3) inhibition was monitored through the levels of their known substrate acetyl-histone H3 (AcH3). SAHA or the analogs **19c**, **19d**, or **19f** were incubated with U397 leukemia cells before lysis and western blot analysis of protein acetylation. As expected, SAHA showed an increase in the levels of both acetyl-α-tubulin and acetyl-histone H3 (Figure 3.3, lane 2), which is consistent with its non-selective inhibition of HDAC1, 2, 3, and 6 isoforms. In contrast, C4-benzyl (**19f**) showed a dose-dependent selective increase in levels of acetyl-α-tubulin (Figure 3.3, lanes 3-5, AcTub) over the levels of acetyl histone H3 (Figure 3.3, lanes 3-5, AcH3), compared to the DMSO control (Figure 3.3, lane 1). The observed HDAC6 selectivity

in cells is consistent with the selectivity observed in the *in vitro* screening (Table 3.2 and Figure 3.2).

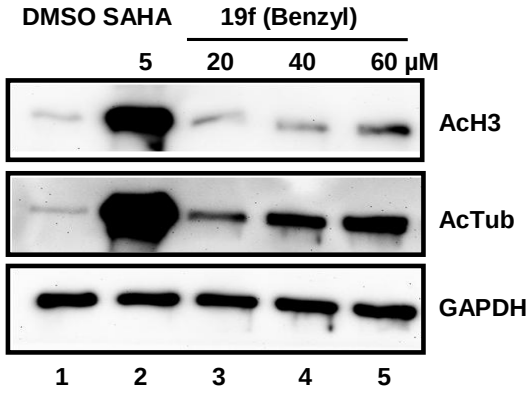

Figure 3.3. Cell based selectivity testing of the C4-benzyl SAHA analog **19f**. Western blots analysis of acetyl-histone H3 (AcH3) and acetyl-α-tubulin (AcTub) after treatment with SAHA or the C4-modified SAHA analogs. U937 cells were treated with DMSO (1%), SAHA (5 µM), or increasing concentrations of C4-benzyl SAHA (**19f**) analog (20-60 µM), before lysis, SDS-PAGE separation, transfer to a PVDF membrane, and western analysis with AcH3 or AcTub antibodies. GAPDH levels in the samples were also probed as a gel load control. A DMSO control sample was included for comparison to inhibitor treated samples. Repetitive trials are shown in Figure B.148.

3.5. *In vitro* cancer cell growth inhibition

To assess the cytotoxic effect of the HDAC6/8 selective inhibitors in cancer cells, SAHA derivatives **19c**, **19d**, and **19f** were tested with the leukemia cell lines U937 and Jurkat due to the prominent role of HDAC6 in leukemia.[114] To assess cytotoxicity, the EC_{50} values of SAHA and the three analogs **19c**, **19d**, and **19f** were determined with U937 cell line.[114] SAHA showed an EC_{50} value of 0.88 µM (Table 3.3), which is consistent with the cytotoxicity previously reported.[117] The non-selective inhibition of SAHA to all the HDAC proteins likely contributes to its high cytotoxicity. The C4-*n*-butyl (**19c**), C4-*n*-hexyl (**19d**), and C4-benzyl (**19f**) SAHA analogs displayed 34, 16, and 28 µM EC_{50} values with the U937 cell line, respectively (Table 3.3). Compared to SAHA, the analogs were 18- to 39-fold less

cytotoxic. To confirm the cytotoxicity study in U937 cells, SAHA and the analogs were also tested for cytotoxicity with the Jurkat cell line. The analogs showed reduced cytotoxicity compared to SAHA (Figure B.152, Table B.12), consistent with the study in U937 cells. The reduced cytotoxicity of the analogs in U937 and Jurkat cells compared to SAHA might be due to their selectivity toward HDAC6 and 8. Consistent with this hypothesis, similar lower cytotoxicities compared to the non-selective inhibitor SAHA were also observed with HDAC6 and dual HDAC6/8-selective inhibitors in previous reports.[91, 129-130]

Table 3.3. EC_{50} values of SAHA and C4-butyl, C4-hexyl and C4-benzyl SAHA analogs with U937 cells.[a]

Compound	EC_{50} (μM)
SAHA	0.88 ± 0.13
19c (*n*-butyl)	34 ± 2
19d (*n*-hexyl)	16 ± 3
19f (benzyl)	28 ± 7

[a]Mean EC_{50} value and standard error of at least three independent trials are shown. Data in table is associated with Figures B.149-B.151 and Table B.11.

3.6. Enantioselective synthesis and screening of (*R*)- and (*S*)-C4-benzyl SAHA analog (19f).

Since all analogs were synthesized and screened as racemic mixtures, enantioselective syntheses were performed to test the selectivity of both enantiomers of the most selective C4-benzyl SAHA analog (Schemes 3.2-3.4). The asymmetric synthesis was carried out utilizing Evan's oxazolidinone chiral auxiliary **(*R*)-8** to synthesize both enantiomers.[131] To synthesize the **(*RS*)-21** intermediate, 4-pentenoyl chloride was reacted with the chiral auxiliary **(*R*)-8** using *n*-butyllithium, which yielded pentenoyl oxazolidinone intermediate **(*R*)-20** (Scheme 3.2A).

Enantioselective addition of a benzyl group to **(*R*)-20** was achieved via a reaction with benzyl bromide, which gave **(*RS*)-21**. A similar procedure was employed to synthesize **(*RR*)-21** (Scheme 3.2B), but starting with 3-phenylpropanoyl chloride and the same chiral auxiliary **(*R*)-8**, followed by enantioselective addition of the allyl group using allyl bromide that gave **(*RR*)-21**. Both diastereomers were obtained in high diastereomeric ratios (dr), which were assessed from the ^{1}HNMR spectra of both diastereomers (99:1 dr for **(*RS*)-21**, and 97:3 dr for **(*RR*)-21** (see Figures B.78 and B.85). To remove the chiral auxiliary, each diastereomer was subjected to lithium aluminum hydride at 0°C, which produced alcohols **(*S*)-22** and **(*R*)-22** from **(*RS*)-21** and **(*RR*)-21**, respectively (Scheme 3.2). In order to assess the optical purity and the enantiomeric excess (ee) of the alcohol intermediates **(*S*)-22** and **(*R*)-22**, Mosher esters of both alcohols were synthesized by coupling each alcohol with (R)-(+)-α-Methoxy-α-trifluoromethylphenylacetic acid **(*R*)-MTPA** using EDCI and DMAP (Scheme B.1).[132] Analysis of the ^{1}HNMR spectra (obtained with 600 MHz instrument) showed that both Mosher esters were observed in high diastereomeric ratios (99:1 dr for **(*S*)-22-(*R*)-MTPA**, and 98:2 dr for **(*R*)-22-(*R*)-MTPA**, Figures B.93, B.94, B.99 and B.100), which implies that the alcohol intermediates **(*S*)-22** and **(*R*)-22** were obtained in high enantiomeric ratios (98% ee for **(*S*)-22** and 96% ee **(*R*)-22**).

Scheme 3.2. Enantioselective synthesis of intermediate alcohols **(*S*)-22** (Part A) and **(*R*)-22** (Part B)

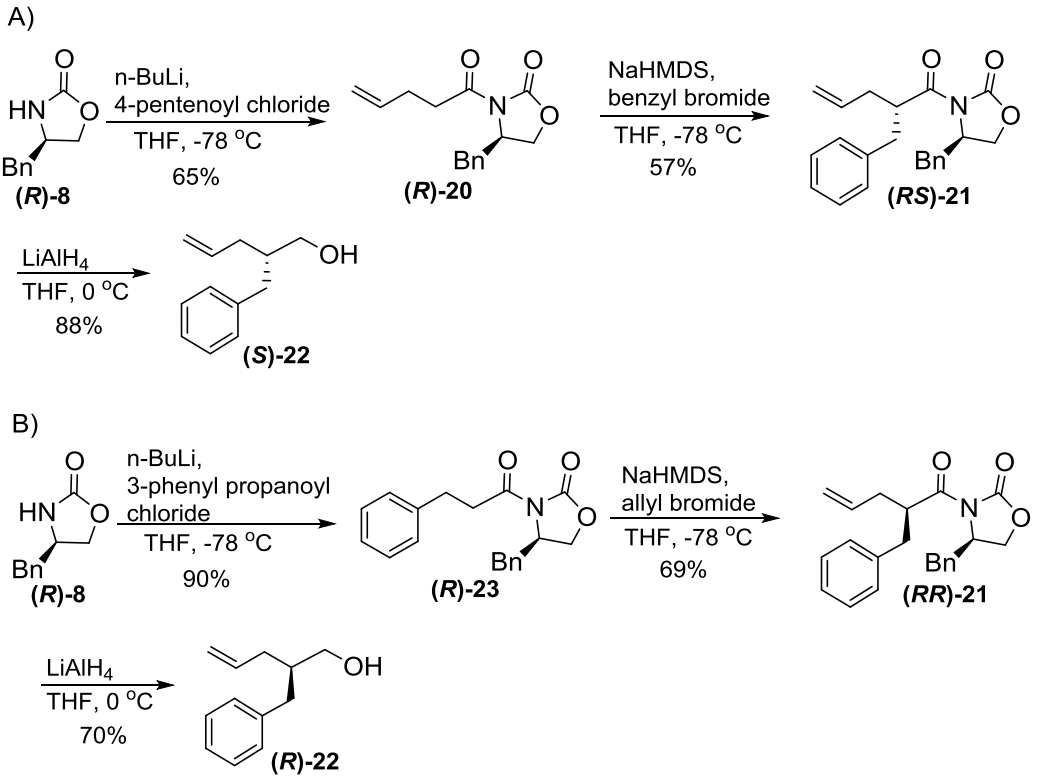

To synthesize the enantiopure C4-benzyl SAHA analogs **(*R*)-19f** and **(*S*)-19f,** both alcohols **(*S*)-22** and **(*R*)-22** were then converted to the methanesulfonate esters, followed by substitution with dimethyl malonate to give diesters **(*R*)-24** and **(*S*)-24**, respectively (Schemes 3.3 and 3.4). Krapcho decarboxylation afforded methyl ester intermediates **(*S*)-25** and **(*R*)-25**. Cross metathesis of the methyl esters with *N*-phenyl acrylamide **26** using Grubbs' second-generation catalyst afforded ester amides **(*S*)-27** and **(*R*)-27**.[118] Finally, reduction, followed by substitution with hydroxyl amine, gave both enantiomers of C4-benzyl SAHA analog, **(*R*)-19f** and **(*S*)-19f**.

Scheme 3.3. Synthesis of (*R*)-C4-benzyl SAHA analog **(*R*)-19f**

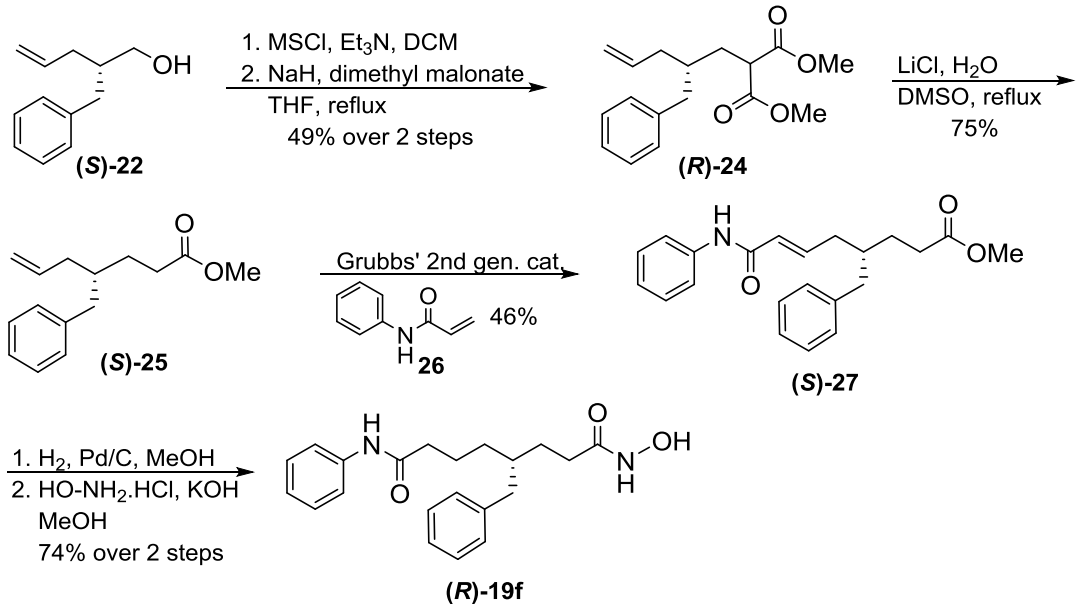

Scheme 3.4. Synthesis of (*S*)-C4-benzyl SAHA analog **(*S*)-19f**

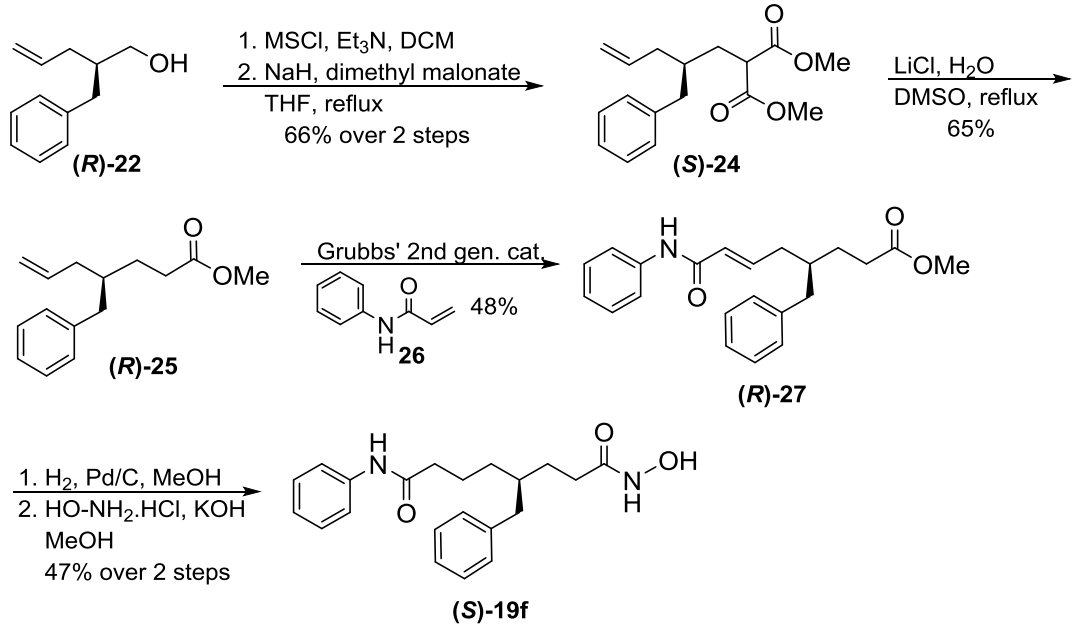

To assess the selectivity of each enantiomer, IC_{50} values of both the (*R*)-C4-benzyl SAHA **(*R*)-19f** and the (*S*)-C4-benzyl SAHA **(*S*)-19f** were determined with HDAC1, 2, 3, 6, and 8 (Table 3.2). Similar to the racemic mixture, both enantiomers showed dual HDAC6/HDAC8 selectivity. (*R*)-C4-benzy SAHA **(*R*)-19f** exhibited more

potent inhibition against HDAC6 and HDAC8 compared to the (*S*)-C4-benzyl SAHA **(*S*)-19f**, with IC_{50} values of 48 and 27 nM for **(*R*)-19f** and 95 and 150 nM for **(*S*)-19f** (Table 3.2). In addition, **(*R*)-19f** showed greater fold preference for HDAC6 and 8 over HDAC1, 2, and 3 (520- to 1300-fold) compared to the racemic mixture (210- to 740-fold). In contrast, **(*S*)-19f** showed lower fold selectivities (240- to 540-fold) compared to both **(*R*)-19f** and the racemic mixture (Tables 3.2 and B.10). *In vitro* screening revealed that both (*R*)-C4-benzyl SAHA and (*S*)-C4-benzyl SAHA are highly selective to HDAC6 and 8 over HDAC1, 2, and 3, with nanomolar potency. However **(*R*)-19f** was more potent and selective than **(*S*)-19f** (Tables 3.2 and B.10).

3.7. Docking Studies

Docking studies for both enantiomers of the C4-benzyl SAHA (**19f**) were performed using the AutoDock 4.2 and Autodock tools programs[119, 127] in order to explain the observed selectivity. The recently reported crystal structures of HDAC6 (PDB: 5G0H)[13] and HDAC3 (PDB: 4A69)[100] were used in these studies. SAHA, the parent molecule, was docked in both crystal structures as a validation step for the docking procedure and for comparison (Figure 3.5). With HDAC6, both enantiomers of the C4-benzyl SAHA were positioned similar to SAHA, as expected, with the hydroxamic acid moiety near the catalytic metal, the linker region in the 11 Å channel, and the anilide group in the solvent exposed region. In addition, the hydroxamic acid groups bound within 1.9-2.7 Å of the active site residues (H573, H574, and Y745) and the active site catalytic zinc atom (Figures 3.4A and 3.4C), similar to that of the parent molecule SAHA (1.7-2.7 Å) (Figure 3.5A). Docking with the HDAC6 crystal structure was consistent with the high binding affinity of C4-benzyl SAHA and SAHA (Table 3.2). Superimposition of each enantiomer and SAHA

showed a similar binding and positioning of the hydroxamic acid moiety (Figures 3.4E and 3.4G).

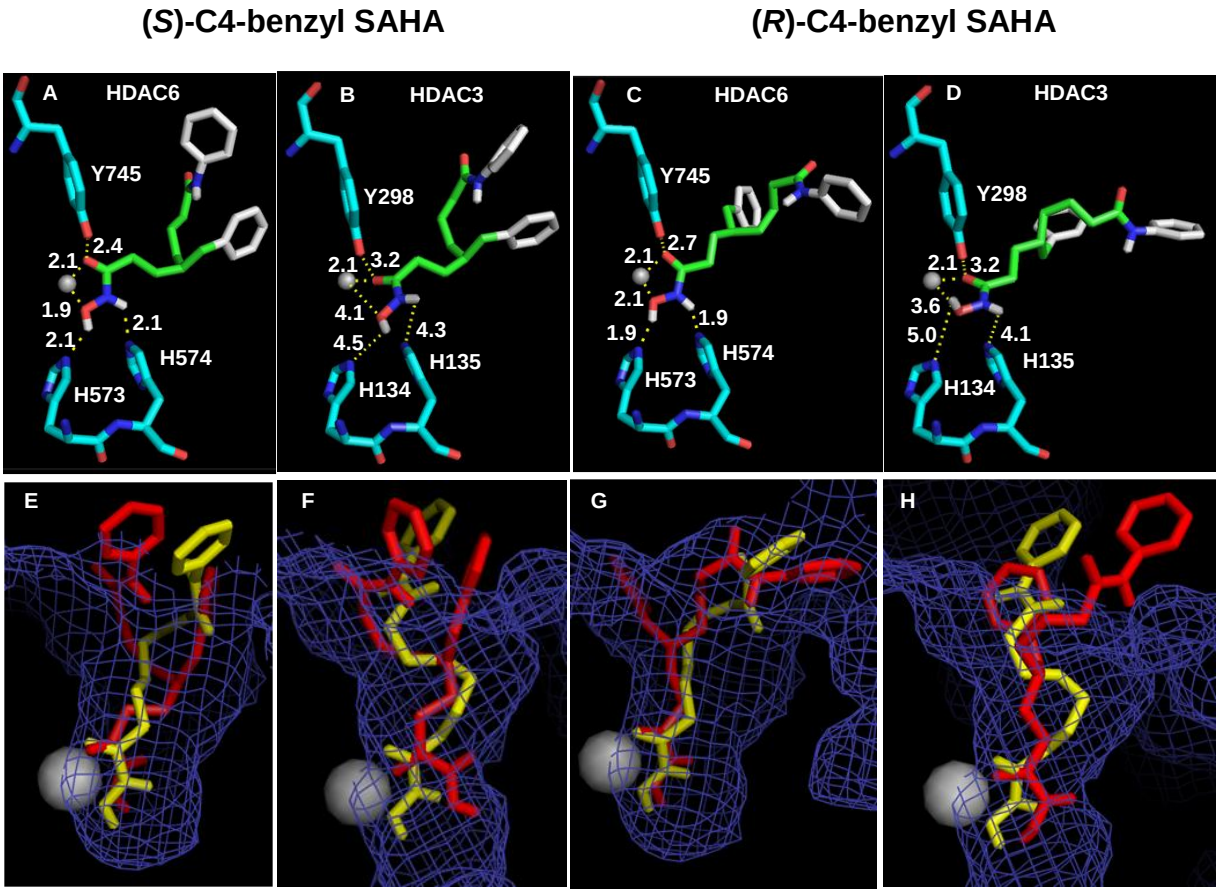

Figure 3.4. Docked pose of (*S*)-C4-benzyl SAHA (**A, B, E, F**) and (*R*)-C4-benzyl SAHA (**C, D, G, H**) in the crystal structures of HDAC6 (PDB: 5G0H) and HDAC3 (PDB: 4A69). Binding distances in HDAC6 (**A,C**) or HDAC3 (**B,D**) between the hydroxamic acid atoms and active site residues (numbered in figure) or the metal are displayed in Angstroms. The atomic radius of the metal (Zn^{2+}) was set at 0.6 Å for clarity. Atom color-coding: C4-benzyl SAHA **19f** (C=purple/white; O=red; N=blue; H=White); amino acids (C=deep teal; O=red, N=blue); Zn^{2+} metal ion (grey sphere). **E**,**G** and **F**,**H**) Shown is the superimposition of SAHA (yellow) and (*S*)- or (*R*)-C4-benzyl SAHA **19f** (red) in the crystal structures of HDAC6 (**E, G**) and HDAC3 (**F, H**), with the metal ion (Zn^{2+}) represented as a grey sphere (1.39 Å radius).

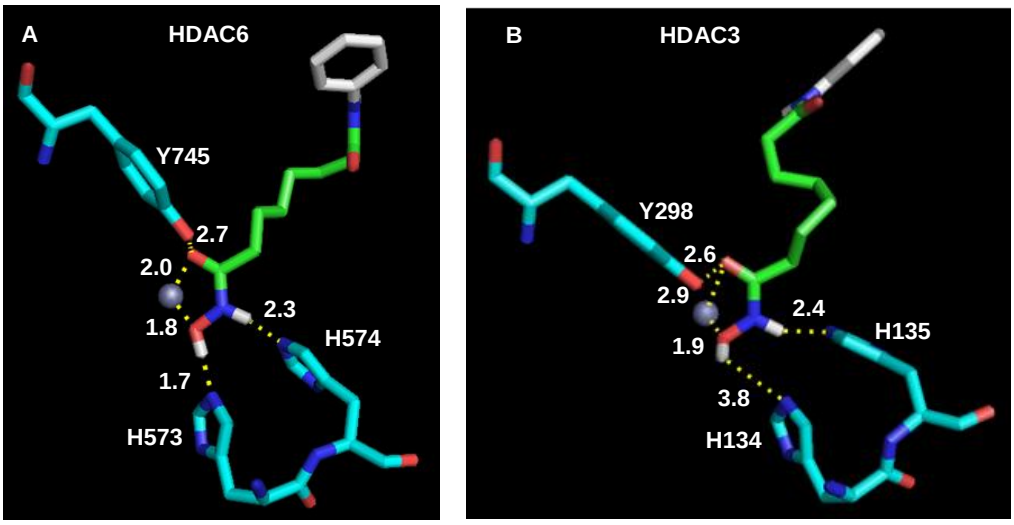

Figure 3.5. Docking poses of SAHA in the crystal structures of HDAC6 (PDB: 5G0H) (A) and HDAC3 (PDB: 4A69) (B). Binding distances between the hydroxamic acid atoms and active site residues (numbered in figure) or the metal are displayed in Angstroms. The atomic radii of the metals were set at 0.6 Å for clarity. Color-coded SAHA (C=green/white; O=red; N=blue; H=White) and amino acid residues (C=deep teal; O=red, N=blue); Zn^{2+} metal ion (grey sphere).

To explain the observed selectivity, **(*R*)-19f** and **(*S*)-19f** were also docked into the HDAC3 crystal structure. Longer and weaker binding interactions (2.1-5.0 Å) were observed with HDAC3 (Figures 3.4B and 3.4D) compared with HDAC6 (1.9-2.7 Å). Superimposition of both enantiomers with SAHA showed a shift in the position of the hydroxamic acid moieties away from the metal binding region compared to SAHA (Figure 3.4F and 3.4H). The docking analysis suggests that the presence of a bulky substituent on the C4 position weakens binding to HDAC3 due to steric clashes with the relatively narrow and long 11Å channel of HDAC3 (Figures 3.6B, see white and blue arrows), which placed the hydroxamic acid moiety away from the metal binding region (Figures 3.4B, 3.4D and 3.6B). On the other hand, HDAC6 maintains a wider and shorter V-shaped 11Å channel (Figure 3.6A, see white and blue arrows), which can accommodate relatively large C4 substituents with no effect

on binding of the hydroxamic acid group to the metal binding region (Figures 3.4A, 3.4C and 3.6A).

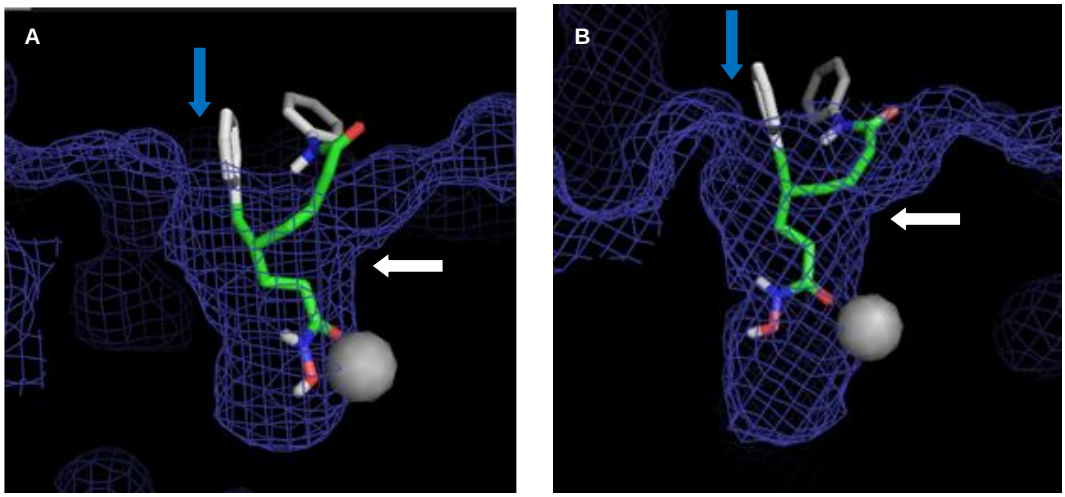

Figure 3.6. Docked poses of (*R*)-C4-benzyl SAHA **(*R*)-19f** in the crystal structures of HDAC6 (**A**) HDAC3 (**B**). The white arrows show the difference in the width of the active site entrances discussed in text (11 Å channel). The blue arrow in part A show how the benzyl group can be accommodated in HDAC6 active site with no effect on binding of the hydroxamic acid group In part B the benzyl group sterically interact with the relatively narrow 11 Å channel, which positioned the hydroxamic acid group distant from the metal (see blue arrow). The binding site for both HDAC6 and HDAC3 are shown as deep blue mesh. Atom color-coding: (*R*)-C4-benzyl SAHA (C=green/white; O=red; N=blue; H=white).

Recent studies reporting the HDAC6 crystal structure and prior docking studies demonstrated that HDAC6 maintain a wider and shorter 11Å channel compared to HDAC1, 2, and 3.[13, 86] In previous work, compounds with bulky aryl or cyclic groups in the linker region near the hydroxamic acid group had restricted access to the active site due to steric clash with the relatively narrower 11Å channel, which placed the metal binding group distant from the catalytic metal for weaker or no binding of the inhibitor.[13] In contrast, HDAC6 active site allowed such inhibitors to reach the metal binding region in the active, which led to preferential inhibition of HDAC6 over HDAC1, 2, and 3. In other recent reports, the presence of a bicyclic

linker or phenyl linker displayed dual HDAC6 and HDAC8 selectivity.[89-91] Moreover, valpropylhydroxamic acid with a propyl substituent showed selectivity to HDAC6 and 8, but with micromolar potency and low fold selectivity (only 9-17-fold selectivity against with HDAC1, 2, and 3).[88] SAHA analogs with a hexyl or benzyl substituent at the C2 linker also demonstrated dual HDAC6 HDAC8 selectivity.[112] Based on these reports and the docking studies, one possibility that accounts for selectivity is that substituting the C4 of SAHA linker with different groups can be accommodated in the relatively wider and shorter V-shaped 11Å cavity of HDAC6 active site (Figures 3.4A, 3.4C, 3.4E, 3.4G, and 3.6A), but not the narrower and relatively longer 11Å cavity of HDAC1, HDAC2, and HDAC3 (Figures 3.4B, 3.4D, 3.4F, and 3.4H). In addition, the size of the substituent plays a critical role in the selectivity. For example, analogs bearing smaller substituents (as methyl or ethyl in **19a** or **19b**) demonstrated lower selectivity compared to analogs comprising bulkier substituents (as butyl, hexyl, phenyl, and benzyl **19c-19f**) (Figure 3.2 and Table 3.2). In total, the docking results confirmed the previously reported structural analyses suggesting that the wider HDAC6 active site entrance is the source of selectivity.

In conclusion, SAHA analogs modified at the C4 position of the linker were synthesized and screened. The C4-SAHA analogs showed up to 1300-fold dual selectivity for HDAC6 and HDAC8 over HDAC1, HDAC2, and HDAC3. The best analogs were C4-*n*-butyl SAHA (**19c**) and C4-benzyl SAHA (**19f**). C4-*n*-butyl SAHA (**19c**), which showed 170- to 310-fold selectivity for HDAC6 and 8 compared to HDAC1, 2, and 3, with 88 and 74 nM IC_{50} with HDAC6 and HDAC8, respectively. C4-benzyl SAHA (**19f**) showed the highest fold selectivity with 210- to 740-fold

selectivity for HDAC6 and 8 compared to HDAC1, 2, and 3, and 140 and 57 nM IC_{50} with HDAC6 and HDAC8. Interestingly, the fold selectivity of C4-butyl and C4-benzyl SAHA analogs were higher than the recently reported dual HDAC6/8 selective inhibitors (at least 23-, 75-, and 79-fold).[89-91] Furthermore, *in cellulo* testing of C4-benzyl analog showed consistency with the *in vitro* screening. Enantioselective synthesis and screening of both enantiomers of the C4-benzyl SAHA revealed that (*R*)-C4-benzyl SAHA is more potent and selective than the (*S*) enantiomer, with 48 and 27 nM IC_{50} with HDAC6 and HDAC8, and 520- to 1300-fold selectivity for HDAC6 and 8 over HDAC1, 2, and 3. The dual HDAC6/HDAC8 selective C4-SAHA analogs reported in this work have the potential to be useful pharmacological tools for biomedical research and lead compounds for anti-cancer drug development. More generally, these studies with SAHA analogs suggest that modifying current drugs can significantly improve their properties.

3.8. Experimental Procedures

3.8.1. Materials and instrumentation

Details were provided in Section 2.7.1 of Chapter 2. Enantiomeric excess (ee%) was calculated in this chapter based on the NMR spectra of Mosher's esters of intermediate alcohols (Section 3.6).

3.8.2. Synthesis procedure

3.8.2.1. Synthesis procedures for 19a-19f

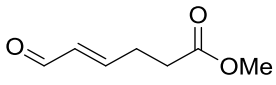

Synthesis of methyl (*E*)-6-oxohex-4-enoate (14): The compound was synthesized according to the reported procedure, with the use of a different

catalyst.[133] Briefly, in a flame dried 2-neck 100 mL flask, purged with argon, Grubbs' second generation catalyst (26.65 mg, 0.0314 mmol, 0.5 mol%) was dissolved in dry dichloromethane (20 mL). Crotonaldehyde **13** (2.6 mL, 31.38 mmol) and methyl pent-4-enoate **12** (0.78 mL, 6.28 mmol) were added, and the reaction was stirred with reflux for 3.5 hours under argon. The reaction was then cooled to room temperature, concentrated, and purified by silica gel flash chromatography (ethyl acetate:hexanes 1:4) to afford aldehyde **14** as an orange oily product (97%). The spectral data for the synthesized compound was consistent with the reported data in literature.[133]

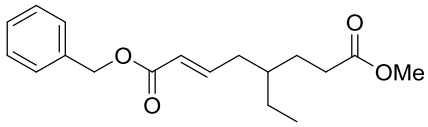

Synthesis of 1-benzyl 8-methyl (*E*)-5-ethyloct-2-enedioate (16b): In a 200 mL, 2-neck flame dried flask, copper(I)bromide dimethyl sulfide (2.17 g, 10.56 mmol) was dissolved in dry THF (20 mL). Air was purged with argon, and then the temperature was reduced to -15°C. Ethyllithium (12.35 mL of a 1.7M solution in dibutyl ether, 756 mg, 21.0 mmol) was added drop wise with stirring and the mixture was allowed to stir for additional 20 minutes at -15°C. The temperature was then reduced to -78°, followed by drop wise addition of chlorotrimethylsilane (3.44 g, 31.66 mmol) and methyl pent-4-enoate **14** (500 mg, 3.52 mmol). The reaction was stirred for 5 hours at -78°C. The reaction was then quenched by addition of a saturated ammonium chloride:ammonia solution (1:1) portion wise until the reaction color turned blue. The organic layer was collected, and the aqueous layer was extracted with ethyl acetate (3 x 30 mL). The combined

organic layers were dried over anhydrous Na_2SO_4, filtered, and rotavaped to an oily crude product, which was used in the next reaction without purification.

In a 200 mL 2-neck flame dried flask, air was purged with argon, NaH (169 mg of 60% NaH in mineral oil, 7.04 mmol) was dissolved in dry THF (20 mL). The reaction was then cooled to 0°C and benzyl diethyl phosphonoacetate 1**5b** (1.80 mL, 7.04 mmol) was added drop wise with stirring. The reaction was allowed to stir for 15 minutes at 0°C, then the crude product from the previous reaction was added. The reaction was stirred for another 30 minutes at 0°C, followed by stirring for 90 minutes at room temperature. The reaction was quenched with a saturated ammonium chloride solution (20 mL). The organic layer was collected, and the aqueous layer was extracted with ethyl acetate (3 x 25 mL). The combined organic layers were dried over anhydrous $MgSO_4$, filtered, and concentrated. The product was purified by flash silica gel chromatography (ethyl acetate:hexanes 1:9) to afford **16b** (375 mg, 35% over two steps). ^{1}HNMR (400 MHz, CD_3OD) δ (ppm): 0.86-0.90 (t, *J* = 7.2 Hz, 3H), 1.28-1.34 (m, 2H), 1.47 (m, 1H), 1.55-1.61 (m, 2H), 2.18-2.22 (m, 2H), 2.30-2.34 (t, *J* = 7.2 Hz, 2H), 3.63 (s, 3H), 5.15 (s, 2H), 5.89-5.93 (d, *J* = 16 Hz, 1H), 6.92-6.98 (m, 1H), 7.29-7.35 (m, 4H). ^{13}CNMR (100 MHz, CD_3OD) δ (ppm): 9.69, 25.31, 27.86, 30.79, 35.24, 35.33, 38.07, 50.66, 65.69, 122.02, 127.80 (2C), 128.15, 136.28, 148.47, 166.31, 174.4. IR: 2957, 2931, 2875, 1723, 1655, 1437 cm^{-1}. LRMS (ESI, m/z): calculated for $[M+H]^+$ $C_{18}H_{24}O_4H^+$, 305.2, found 305.2; calculated for $[M+Na]^+$ $C_{18}H_{24}O_4Na^+$, 327.2, found 327.1.

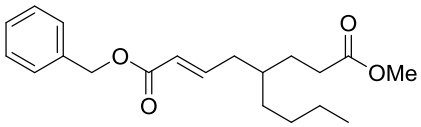

Synthesis of 1-benzyl 8-methyl (*E*)-5-ethyloct-2-enedioate (16c): The procedure was similar to that of **16b** except the following reagents were used: copper(I)bromide dimethyl sulfide (4.34 g, 21.10 mmol), *n*-butyllithium (16.86 ml of a 2.5 M solution in hexanes, 2.7 g, 42.2 mmol), chlorotrimethylsilane (6.87 g, 63.3 mmol), methyl pent-4-enoate **14** (1 g, 7.03 mmol), NaH (478 mg of 60% NaH in mineral oil, 11.95 mmol) and benzyl diethyl phosphonoacetate **14b** (3.42 g, 11.95 mmol). The reaction was left to stir at room temperature for 10 hours. The product was purified by flash silica gel chromatography (5% ethyl acetate in hexanes) to afford **16c** (602 mg, 26% over two steps). ^{1}HNMR (400 MHz, CD_3OD) δ (ppm): 0.91 (t, *J* = 6.8 Hz, 3H), 1.29 (m 7H), 1.58 (m, 3H), 2.22 (t, *J* = 6.0 Hz, 2H), 2.33 (t, *J* = 7.2 Hz, 2H), 3.63 (s, 3H), 5.16 (s, 2H), 5.91 (d, *J* = 15.2 Hz, 1H), 6.97 (dt, 1H), 7.34 (m, 4H). ^{13}CNMR (100 MHz, CD_3OD) δ (ppm): 12.96, 22.05, 28.35, 28.38, 30.78, 32.60, 35.77, 36.51, 50.64, 65.68, 122.01, 127.76 (2C), 128.12, 136.29, 148.47, 166.33, 174.44. IR: 3057, 3033, 2954, 2928, 2860, 1720, 1654, 1456, 1436 cm^{-1}. LRMS (ESI, m/z): calculated for $[M+Na]^+$ $C_{20}H_{28}O_4Na^+$, 355.19, found 355.16.

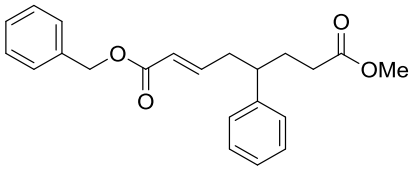

Synthesis of 1-benzyl 8-methyl (*E*)-5-phenyloct-2-enedioate (16e): The procedure was similar to that of **16b** except the following reagents were used: copper(I)bromide dimethyl sulfide (4.61 g, 22.40 mmol), phenyllithium (22.4 ml of a

2M in dibutyl ether, 44.8 mmol), chlorotrimethylsilane (8.53 mL, 76.24 mol), methyl pent-4-enoate **14** (1.06 g, 7.49 mmol), NaH (0.51 g of 60% NaH in mineral oil, 12.70 mmol) and benzyl dimethyl phosphonoacetate **15a** (2.67 mL, 12.70 mmol). The reaction was heated to reflux for 1 hour 45 minutes. The product was purified by column chromatography (diethyl ether:petroleum ether 1:6 to 1:4) to afford **16e** as an orange yellow oil (1.64 g, 62% over two steps). ^{1}HNMR (400 MHz, $CDCl_3$): 1.87 (m, 1H), 2.05 (m, 1H), 2.15 (m, 2H), 2.53 (t, *J* = 7.6 Hz, 2H), 2.67 (m, 1H), 3.61 (s, 3H), 5.14 (s, 2H), 5.82 (d, *J* = 15.2 Hz, 1H), 6.88 (dt, *J* = 15.6 Hz, and 7.2 Hz, 1H), 7.12 (d, *J* = 7.6 Hz, 2H), 7.22 (m, 1H), 7.37 (m. 7H). ^{13}CNMR (100 MHz, $CDCl_3$): 30.94, 31.96, 39.61, 44.50, 51.56, 66.05, 115.33, 120.33, 126.81, 127.53, 128.15, 128.53, 128.71, 136.04, 142.81, 147.45, 166.19, 173.82. IR: 3063, 3030, 2951, 1718, 1654, 1495, 1454, 1437 cm^{-1}. LRMS (ESI, m/z): calculated for $[M+H]^+$ $C_{22}H_{24}O_4H^+$, 353.2; found 353.4; calculated for $[M+Na]^+$ $C_{22}H_{24}O_4Na^+$, 375.2; found 375.3.

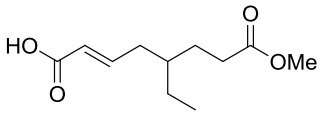

Synthesis of 8-methoxy-5-ethyl-8-oxooctanoic acid (17b): In a 50 mL flask, **16b** (375 mg, 1.2 mmol) was dissolved in MeOH (20 mL), then $Pd(OH)_2$ (87 mg of 20 wt. % $Pd(OH)_2$ on carbon, 0.12 mmol) was added. The air inside the flask was purged with argon (three times), then with hydrogen gas (three times). The reaction was stirred under hydrogen for 4 hours. The reaction was filtered through a celite plug, and the solvent was evaporated. The product was purified by silica gel flash chromatography (ethyl acetate:hexanes 1:1.5) to afford **17b** (299 mg, 94%); ^{1}HNMR (400 MHz, CD_3OD) δ (ppm): 0.84 (t, *J* = 7.2 Hz, 3H), 1.28 (m, 5H), 1.60 (m,

4H), 2.30 (m, 4H)**,** 3.66 (s, 3H) 11.40 (br s, 1H). ^{13}CNMR (100 MHz, CD_3OD) δ (ppm): 10.58, 21.69, 25.28, 28.00, 31.47, 32.11, 34.27, 38.12, 51.55, 174.52, 179.89. IR: 2956, 2930, 2873, 1738, 1709, 1614, 1459, 1439 cm^{-1}. LRMS (ESI, m/z): calculated for $[M+Na]^+$ $C_{11}H_{20}O_4Na^+$, 239.1, found 239.2.

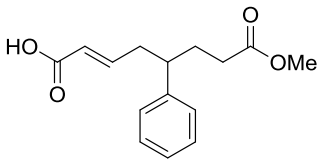

Synthesis of 8-methoxy-8-oxo-5-phenyloctanoic acid (17e): The procedure was similar to that of **17b** except the following reagents were used: **16e** (1.40 g, 3.98 mmol), $Pd(OH)_2$ (1.12 g of 20 wt. % $Pd(OH)_2$ on carbon, 1.59 mmol). The product was purified by column chromatography (ethyl acetate:petroleum ether 1:6 then 1:3) to afford **17e** (764 mg, 73%); ^{1}HNMR (400 MHz, CD_3OD): 1.40 (m, 2H), 1.63 (m, 2H), 1.80 (m, 1H), 1.98 (m, 1H), 2.10 (m, 2H), 2.20 (m, 2H), 2.54 (m, 1H), 3.60 (s, 3H), 7.17 (m, 3H), 7.28 (m, 2H); ^{13}CNMR (100 MHz, $CDCl_3$): 22.30, 31.80, 32.20, 33.95, 35.90, 45.15, 51.80, 126.40, 127.50, 128.30, 143.95, 174.30, 179.90. IR: 3028, 2948, 1734, 1705, 1603, 1494, 1453, 1437 cm^{-1}. LRMS (ESI, m/z): calculated for $[M+H]^+$ $C_{15}H_{20}O_4H^+$, 265.1; found 265.4; calculated for $[M+Na]^+$ $C_{15}H_{20}O_4Na^+$, 287.1; found 287.4.

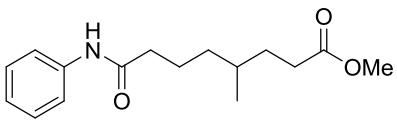

Synthesis of methyl 4-methyl-8-oxo-8-(phenylamino)octanoate (18a): The procedure was similar to **16b** except the following: copper(I)bromide dimethyl sulfide complex (2.26 g, 10.98 mmol), dry THF (40 mL), methyllithium (13.7 ml of a

1.6M solution in diethyl ether, 482 mg, 21.9 mmol), chlorotrimethylsilane (3.58 g, 32.94 mmol), methyl pent-4-enoate **14** (520 mg, 3.66 mmol). NaH (293 mg of 60% NaH in mineral oil, 7.32 mmol), dry THF (20 mL), benzyl diethyl phosphonoacetate **15b** (2.10 g, 7.32 mmol). The reaction was stirred for 3.5 hours. The product was used in the next step without purification.

The procedure was similar to **17b** except the following: Crude **16a** from prior step, MeOH (20 mL) and $Pd(OH)_2$ (413 mg of 20 wt. % $Pd(OH)_2$ on carbon, 0.59 mmol). The reaction was stirred under hydrogen for 3.5 hours. The reaction was filtered through a celite plug, and the solvent was evaporated. The crude product was used in the following reaction.

The crude product **17a** was dissolved in acetonitrile (10 mL), followed by addition of DIPEA (946 mg, 7.32 mmol) and TBTU (1.76 g, 5.49 mmol), and the reaction was left to stir for 20 minutes. Aniline (0.51 g, 5.49 mmol) was added, and the reaction was left to stir for 4.5 hours. The reaction was quenched with 10% aqueous HCl (20 mL). The aqueous layer was extracted with ethyl acetate (4 x 20 mL). The combined organic extracts were washed with a saturated $NaHCO_3$ (10 mL) and then dried over anhydrous Na_2SO_4, filtered, and evaporated. The product was purified by silica flash chromatography (ethyl acetate:hexanes 1:4) to afford **18a** (434 mg, 43% over four steps). ^{1}HNMR (400 MHz, CD_3OD) δ (ppm): 0.90 (d, *J* = 6.4 Hz, 3H), 1.21 (m, 1H), 1.43 (m, 3H), 1.74 (m, 3H), 2.67 (m, 4H), 3.63 (s, 3H), 7.06 (t, *J* = 7.6 Hz, 1H), 7.28 (t, *J* = 8.4 Hz, 2H), 7.53 (d, *J* = 8.8 Hz, 2H). ^{13}CNMR (100 MHz, CD_3OD) δ (ppm): 18.15, 22.90, 31.13, 31.50, 31.98, 35.79, 36.71, 50.61, 119.83, 123.69, 128.36, 138.50, 173.12, 174.72. IR: 3302, 3137, 3061, 2953, 2940, 2869,

1736, 1662, 1600, 1542, 1499, 1442 cm^{-1}. LRMS (ESI, m/z): calculated for $[M+H]^+$ $C_{16}H_{23}NO_3H^+$, 278.18, found 278.17; calculated for $[M+Na]^+$ $C_{16}H_{23}O_3Na^+$, 300.16, found 300.10.

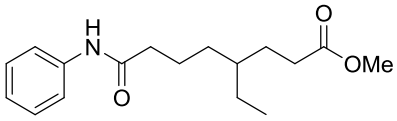

Synthesis of methyl 4-ethyl-8-oxo-8-(phenylamino)octanoate (18b): The procedure was similar to the last step of **18a** except the following reagents were used: DIPEA (319 mg, 2.47mmol), TBTU (594 mg, 1.85 mmol) and aniline (172 mg, 185 mmol). The extraction was done with dichloromethane (4 x 20 mL). The product was purified by silica gel flash chromatography (ethyl acetate:hexanes 1:4) to afford **18b** (250 mg, 75%). ^{1}HNMR (400 MHz, CD_3OD) δ (ppm): 0.87 (t, *J* = 7.2 Hz, 3H), 1.34 (m, 5H), 1.60 (m, 2H), 1.68 (m, 2H), 2.33 (m, 4H), 3.64 (s, 3H), 7.07 (t, 1H), 7.29 (t, *J* = 7.2 Hz, 2H), 7.53 (d, *J* = 7.2 Hz, 2H). ^{13}CNMR (100 MHz, CD_3OD) δ (ppm): 9.35, 22.23, 24.83, 27.55, 30.56, 31.63, 36.48, 37.83, 50.32, 119.55, 123.40, 128.06, 138.19, 172.82, 174.49. IR: 3302, 3198, 3137, 3062, 2955, 2930, 2862, 1737, 1663, 1600, 1542, 1499, 1442 cm^{-1}. LRMS (ESI, m/z): calculated for $[M+H]^+$ $C_{17}H_{25}O_3H^+$, 292.19, found 292.19; calculated for $[M+Na]^+$ $C_{17}H_{25}O_3Na^+$, 314.17, found 314.17.

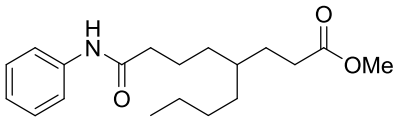

Synthesis of methyl 4-butyl-8-oxo-8-(phenylamino)octanoate (18c): The procedure was similar to that of **17b** except the following reagents were used: **16c** (1.2 g, 3.6 mmol) $Pd(OH)_2$ (504 mg of 20 wt. % $Pd(OH)_2$ on carbon, 0.72 mmol). The crude product was used in the following reaction.

The procedure was similar to that of **18a** except the following reagents were used: Crude **17c** from prior reaction, DIPEA (464 mg, 3.59 mmol), TBTU (865 mg, 2.69 mmol) and aniline (250 mg, 2.69 mmol). The product was purified by silica gel flash chromatography (ethyl acetate:hexanes 1:6) to afford **18c** (250 mg, 44% over two steps). ^{1}HNMR (400 MHz, CD_3OD) δ (ppm): 0.89 (t, *J* = 6.4 Hz, 3H), 1.31 (m, 9H), 1.60 (m, 2H), 1.68 (m, 2H), 2.32 (m, 4H), 2.82 (s, 3H), 7.06 (t, *J* = 7.2 Hz, 1H), 7.28 (t, *J* = 8 Hz, 2H), 7.53 (d, *J* = 8 Hz, 2H). ^{13}CNMR (100 MHz, CD_3OD) δ (ppm): 13.07, 22.48, 22.66, 28.29, 28.46, 30.84, 32.37, 32.55, 36.56, 36.77, 50.63, 119.84, 123.69, 128.36, 138.49, 173.10, 174.77. IR: 3302, 3198, 3137, 3041, 2953, 2928, 2859, 1737, 1661, 1600, 1541, 1499, 1441 cm^{-1}. LRMS (ESI, m/z): calculated for $[M+H]^+$ $C_{19}H_{29}NO_3H^+$, 320.22, found 320.21; calculated for $[M+Na]^+$ $C_{19}H_{29}NO_3Na^+$, 342.20, found 342.17.

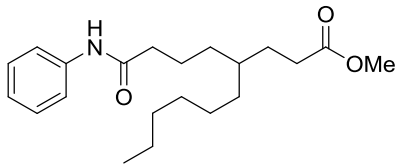

Synthesis of methyl 4-hexyl-8-oxo-8-(phenylamino)octanoate (18d): The procedure was similar to that of **16b** except the following reagents were used: **14** (460 mg, 3.24 mmol) dry THF (20 mL), copper(I)bromide dimethyl sulfide (2 g, 9.73 mmol), *n*-hexyllithium (8.46 ml of a 2.3 M solution in hexanes, 1.792 g, 19.46 mmol), chlorotrimethylsilane (3.17 g, 29.19 mmol), NaH (259 mg of 60% NaH in mineral oil, 6.48 mmol), benzyl diethyl phosphonoacetate **15b** (1.85 g, 6.48 mmol). The reaction was heated to reflux for 4.5 hours. The product was purified by silica gel flash chromatography (ethyl acetate:hexanes 1:10). The purified product was used in the following reaction.

The procedure was similar to that of **17b** except the following reagents were used: **16d** from prior reaction, $Pd(OH)_2$ (228 mg of 20 wt. % $Pd(OH)_2$ on carbon, 0.32 mmol). The crude product was used in the following reaction.

The procedure was similar to that of **18a** except the following: **17d** from prior reaction, acetonitrile (15 mL), DIPEA (838 mg, 6.48 mmol), TBTU (1.56 g, 4.86 mmol) and aniline (452 mg, 4.86 mmol). The reaction was quenched with 10% aqueous HCl (10 mL). The product was purified by silica gel flash chromatography (ethyl acetate:hexanes 1:6) to afford **18d** (214 mg, 19% over four steps). ^{1}HNMR (400 MHz, CD_3OD) δ (ppm): 0.88 (t, *J* = 6.8 Hz, 3H), 1.31 (m, 13H), 1.60 and 1.68 (overlapped quartet and quintet, *J* = 7.6 and 7.6 Hz, 4H), 2.32 (m, 4H), 3.64 (s, 3H), 7.07 (t, *J* = 7.2 Hz, 1H), 7.28 (t, *J* = 7.6 Hz, 2H), 7.53 (d, *J* = 7.6 Hz, 2H). ^{13}CNMR (100 MHz, CD_3OD) δ (ppm): 13.02, 22.30, 22.47, 26.14, 28.32, 29.34, 30.85, 31.61, 32.35, 32.86, 36.57, 36.75, 50.61, 119.86, 123.70, 128.34, 138.47, 173.13, 174.81. LRMS (ESI, m/z): calculated for $[M+H]^+$ $C_{21}H_{33}NO_3H^+$, 348.25, found 348.26; calculated for $[M+Na]^+$ $C_{21}H_{33}NO_3Na^+$, 370.24, found 370.22.

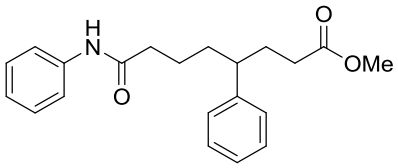

Synthesis of methyl 8-oxo-4-phenyl-8-(phenylamino)octanoate (18e): 8-Methoxy-8-oxo-5-phenyloctanoic acid **17e** (0.763 g, 2.89 mmol) was dissolved in dichloromethane (25 mL), then aniline (0.32 mL, 3.47 mmol) was added, followed by 4-(dimethylamino)pyridine (0.424 g, 3.47 mmol). The mixture was stirred until 4-(dimethylamino)pyridine was completely dissolved, then dicyclohexyl carbdiimide (0.716 g, 3.47 mmol) was added, and the reaction was stirred for 4 hours at room

temperature. The reaction was quenched with 10% aqueous HCl (40 mL), the organic layer was washed with a saturated $NaHCO_3$ solution, and then brine, dried over anhydrous Na_2SO_4, concentrated, and purified by column chromatography (acetone:petroleum ether 1:6) to give **18e** (704 mg, 72%). ^{1}HNMR (400 MHz, CD_3OD): 1.46 (m, 2H), 1.65 (m, 2H), 1.80 (m, 1H), 1.98 (m, 1H), 2.11 (m, 2H), 2.28 (m, 2H), 2.53 (m, 1H), 3.55 (s, 3H), 7.05 (t, *J* = 7.6 Hz, 1H), 7.16 (m, 3H), 7.26 (m, 4H), 7.52 (d, *J* = 8.4 Hz, 2H); ^{13}CNMR (100 MHz, CD_3OD): 23.59, 31.55, 31.58, 35.92, 36.50, 45.05, 50.59, 119.83, 123.71, 126.10, 127.41, 128.21, 128.39, 138.48, 144.07, 172.96, 174.34. IR: 3301, 3197, 3135, 3061, 3027, 2949, 2865, 1734, 1663, 1600, 1543, 1499, 1442 cm^{-1}. LRMS (ESI, m/z): calculated for $[M+H]^+$ $C_{21}H_{25}NO_3H^+$, 340.2; found 340.2; calculated for $[M+Na]^+$ $C_{21}H_{25}O_3Na^+$, 362.2; found 362.2.

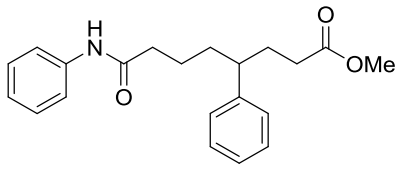

Synthesis of methyl 4-benzyl-8-oxo-8-(phenylamino)octanoate (18f):

The procedure was similar to that of **16b** except the following reagents were used: **14** (500 mg, 3.52 mmol), dry THF (20 mL), copper(I)bromide dimethyl sulfide (2.17 g, 10.56 mmol), benzylmagnesium chloride (21.11 ml of a 1.0 M solution in methyl THF, 3.189 g, 21.12 mmol), chlorotrimethylsilane (3.44 g, 31.68 mmol), NaH (282 mg of 60% NaH in mineral oil, 7.04 mmol) and benzyl diethyl phosphonoacetate **15b** (2.02 g, 7.04 mmol). The reaction was heated to reflux for 1 hour 45 minutes. The crude product was purified by silica gel flash chromatography (ethyl acetate:hexanes 1:9). The purified product was used in the following reaction.

The procedure was similar to that of **17b** except the following: **16f** from prior reaction, $Pd(OH)_2$ (247 mg of 20 wt. % $Pd(OH)_2$ on carbon, 0.35 mmol). The reaction was stirred for 4.5 hours under hydrogen, then it was filtered, and the solvent was evaporated. The crude product was used in the following reaction.

The procedure was similar to that of **18a** except the following: Crude **17f** from prior reaction, DIPEA (464 mg, 3.59 mmol), TBTU (865 mg, 3.59 mmol), and aniline (250 mg, 2.69 mmol). The reaction was stirred for 4 hours 45 minutes. The combined organic extracts were dried over anhydrous Na_2CO_3. The product was purified by silica gel flash chromatography (ethyl acetate:hexanes 1:3) to afford **18f** (340 mg, 27% over four steps). ^{1}HNMR (400 MHz, CD_3OD) δ (ppm): 1.35 (m, 2H), 1.60 and 1.72 (overlapped m and m, 5H), 2.34 (m, 4H), 2.55 (d, *J* = 6.8 Hz, 2H), 3.61 (s, 3H), 7.10 (m, 4H), 7.21 (t, *J* = 7.6 Hz, 2H), 7.28 (t, *J* = 7.2 Hz, 2H), 7.51 (d, *J* = 7.6 Hz, 2H). ^{13}CNMR (100 MHz, CD_3OD) δ (ppm): 22.35, 28.00, 30.84, 31.97, 36.66, 38.87, 39.61, 50.62, 119.90, 123.71, 125.47, 127.86, 128.34, 128.79, 138.44, 140.65, 173.04, 174.65. IR: 3302, 3026, 2929, 2863, 1734, 1661, 1599, 1542, 1498, 1441 cm^{-1}. LRMS (ESI, m/z): calculated for $[M+H]^+$ $C_{22}H_{27}NO_3H^+$, 354.21, found 354.22; calculated for $[M+Na]^+$ $C_{22}H_{27}NO_3Na^+$, 376.19, found 376.21.

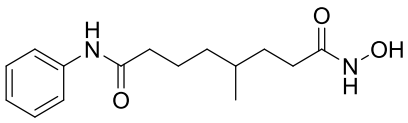

Synthesis of *N*^{1}-hydroxy-4-methyl-*N*^{8}-phenyloctanediamide (19a): In an acid washed flask, hydroxylamine HCl (1.09 g, 15.67 mmol) was dissolved in MeOH (10 mL). KOH (1.76 g, 31.33 mmol) was added at 0°C and allowed to stir for 20 minutes. An alcoholic solution of **18a** (434 mg, 1.57 mmol, in 10 mL MeOH) was

added, and the reaction was stirred for 4.5 hours at 0°C. The pH of the reaction mixture was adjusted to 6 with concentrated aqueous HCl, followed by dilution with distilled de-ionized water (30 mL). The reaction was extracted with ethyl acetate (3 x 30 mL). The organic extracts were collected together and dried over anhydrous Na_2SO_4. The product was purified by silica gel flash chromatography (acetone:dichloromethane 1:3) using iron-free silica gel to afford **19a** (312 mg, 72%). ^{1}HNMR (400 MHz, CD_3OD) δ (ppm): 0.92 (d, *J* = 6.0 Hz, 3H), 1.23 (m, 1H), 1.44 (m, 3H), 1.72 (m, 3H), 2.15 (m, 2H), 2.35 (t, *J* = 7.6 Hz, 2H), 7.07 (t, *J* = 7.2 Hz, 1H), 7.28 (t, *J* = 7.6 Hz, 2H), 7.53 (d, *J* = 7.6 Hz, 2H). ^{13}CNMR (100 MHz, CD_3OD) δ (ppm): 18.19, 22.89, 29.98, 32.01, 32.26, 35.76, 36.64, 119.87, 123.72, 128.35, 138.45, 171.79, 173.21. IR: 3308, 3138, 3063, 3030, 2954, 2930, 2861, 1737, 1695, 1663, 1601, 1543, 1500, 1443 cm^{-1}. HRMS (ESI-TOF, m/z): calculated for $[M+Na]^+$ $C_{15}H_{22}N_2O_3Na^+$, 301.1528, found 301.1520. HPLC analytical purity analysis 98.4%.

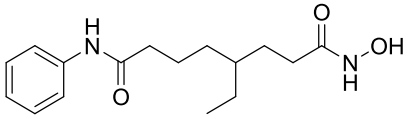

Synthesis of 4-ethyl-*N*^{1}-hydroxy-*N*^{8}-phenyloctanediamide (19b): The procedure was similar to that of **19a** except the following: hydroxylamine HCl (597 mg, 8.59 mmol), KOH (964 mg, 17.18 mmol), and **18b** (250 mg, 0.86 mmol). The reaction was left to stir for 4 hours at 0°C, then at room temperature overnight. The product was purified by silica gel flash chromatography (ethyl acetate:hexanes 1:4 to 1:3) using iron-free silica gel to afford **19b** (116 mg, 46%). ^{1}HNMR (400 MHz, CD_3OD) δ (ppm): 0.87 (t, *J* = 6.4 Hz, 3H), 1.32 (m, 5H), 1.59 and 1.67 (overlapped m and m, 4H), 2.08 (t, *J* = 7.2 Hz, 2H), 2.35 (t, *J* = 7.2 Hz, 2H), 7.06 (t, *J* = 7.2 Hz,

1H), 7.28 (t, *J* = 7.6 Hz, 2H), 7.54 (d, *J* = 8 Hz, 2H). ^{13}CNMR (100 MHz, CD_3OD) δ (ppm): 9.72, 22.52, 25.16, 28.67, 29.82, 31.90, 36.76, 38.14, 119.90, 123.76, 128.39, 138.45, 171.89, 173.25. IR: 3252, 3199, 3061, 2960, 2932, 2872, 1658, 1600, 1546, 1500, 1444 cm^{-1}. HRMS (ESI-TOF, m/z): calculated for $[M+Na]^+$ $C_{16}H_{24}N_2O_3Na^+$, 315.1685, found 315.1669. HPLC analytical purity analysis 97.5%.

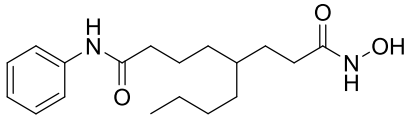

Synthesis of 4-butyl-*N*^{1}-hydroxy-*N*^{8}-phenyloctanediamide (19c): The procedure was similar to that of **19a** except the following: hydroxylamine HCl (538 mg, 7.74 mmol), KOH (869 mg, 15.49 mmol), and **18c** (247 mg, 0.77 mmol). The product was purified by silica gel flash chromatography (acetone:dichloromethane 1:4) using iron-free silica gel to afford **19c** (167 mg, 67%) ^{1}HNMR (400 MHz, CD_3OD) δ (ppm): 0.90 (t, *J* = 7.6 Hz, 3H), 1.33 (m, 9H), 1.60 and 1.69 (overlapped m and quintet, *J* = 7.2 Hz, 4H), 2.08 (t, *J* = 7.2 Hz, 2H), 2.35 (t, *J* = 7.2 Hz, 2H), 7.07 (t, *J* = 8.0 Hz, 1H), 7.29 (t, *J* = 7.6 Hz, 2H), 7.53 (d, *J* = 8.0 Hz, 2H). ^{13}CNMR (100 MHz, CD_3OD) δ (ppm): 13.06, 22.45, 22.68, 28.48, 29.11, 29.76, 32.30, 32.62, 36.62, 36.72, 119.86, 123.73, 128.36, 138.45, 171.87, 173.23. IR: 3288, 2972, 2927, 2872, 1647, 1600, 1545, 1499, 1443 cm^{-1}. HRMS (ESI-TOF, m/z): calculated for $[M+Na]^+$ $C_{18}H_{28}N_2O_3Na^+$, 343.1998, found 343.1985. HPLC analytical purity analysis 97.7%.

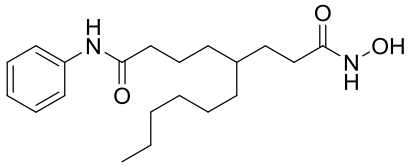

Synthesis of 4-hexyl-*N*^{1}-hydroxy-*N*^{8}-phenyloctanediamide (19d): The procedure was similar to that of **19a** except the following: hydroxylamine HCl (573

mg, 8.24 mmol), KOH (925 mg, 16.48 mmol), and **18d** (286 mg, 0.82 mmol). The reaction was stirred for 2 hours at 0°C, then pre-incubated solution of hydroxylamine HCl (573 mg, 8.24 mmol) and KOH (925 mg, 16.48 mmol) was added followed by stirring for 1.5 hour at 0°C. The product was purified by sequential silica gel flash chromatography (acetone:dichloromethane 1:3 and a second purification with acetone:dichloromethane 1:2) using iron-free silica gel. The compound was further purified by HPLC on a reverse phase HPLC semi-preparative column (YMC America, 250 x 10 mmI.D., 4µm, 8 nm) using a gradient of 60% to 10% of buffer A over 90 minutes (buffer A = 0.1% HPLC grade TFA in water; buffer B = HPLC grade acetonitrile) at a flow rate of 3.0 mL/min at room temperature to yield **19d** (49 mg, 17%). ^{1}HNMR (400 MHz, CD_3OD) δ (ppm): 0.88 (t, *J* = 6.8 Hz, 3H), 1.33 (m, 13H), 1.59 (m, 2H), 1.69 (quintet, *J* = 7.6 Hz, 2H), 2.08 (t, *J* = 8.0 Hz, 2H), 2.35 (t, *J* = 7.6 Hz, 2H), 7.07 (t, *J* = 7.6 Hz, 1H), 7.29 (t, *J* = 7.6 Hz, 2H), 7.52 (d, *J* = 7.6 Hz, 2H). ^{13}CNMR (100 MHz, CD_3OD) δ (ppm): 13.01, 22.30, 22.44, 26.20, 29.14, 29.38, 29.78, 31.63, 32.29, 32.96, 36.66, 36.71, 119.89, 123.71, 128.34, 138.45, 171.85, 173.21. IR: 3254, 3064, 2957, 2927, 2858, 1660, 1601. 1547, 1500, 1444 cm^{-1}. HRMS (ESI-TOF, m/z): calculated for $[M+Na]^+$ $C_{20}H_{32}N_2O_3Na^+$, 371.2311, found 371.2319. HPLC analytical purity analysis 98.2%.

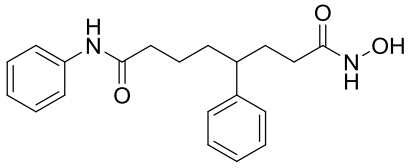

Synthesis of 4-hexyl-*N*^{1}-hydroxy-*N*^{8}-phenyloctanediamide (19e): The procedure was similar to that of **19a** except the following: hydroxylamine HCl (1.38 g, 19.91 mmol), MeOH (50 mL), KOH (2.23 g, 39.82 mmol), and **18e** (675 mg, 1.99

mmol). The reaction was stirred overnight. The product was purified by silica gel flash chromatography (5% MeOH in dichloromethane) using iron-free silica gel, followed by crystallization from MeOH to afford **19e** (350 mg, 52%). ^{1}HNMR (400 MHz, CD_3OD): 1.53 (m, 2H), 1.68 (m, 2H), 1.85 (m, 3H), 2.01 (m, 1H), 2.30 (m, 2H), 2.57 (m, 1H), 7.06 (t, *J* = 7.6 Hz, 1H), 7.18 (m, 3H), 7.28 (m, 4H), 7.50 (d, *J* = 7.2 Hz, 2H). ^{13}CNMR (100 MHz, CD_3OD): 23.58, 30.50, 32.22, 35.90, 36.43, 45.14, 119.84, 123.69, 126.04, 127.40, 128.21, 128.34, 138.42, 144.19, 171.5, 173.02. IR: 3253, 3199, 3061, 3027, 2929, 2866, 1657, 1600, 1545, 1499, 1444 cm^{-1}. HRMS (ESI-TOF, m/z): calculated for $[M+Na]^+$ $C_{20}H_{24}N_2O_3Na^+$, 363.1685, found 363.1686. HPLC analytical purity analysis 98.8%.

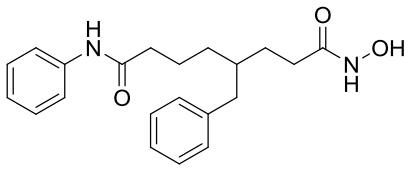

Synthesis of 4-benzyl-*N*^{1}-hydroxy-*N*^{8}-phenyloctanediamide (19f): The procedure was similar to that of **19a** except the following: hydroxylamine HCl (600 mg, 8.64 mmol), KOH (970 mg, 17.28 mmol), and **18f** (305 mg, 0.86 mmol). The reaction was stirred for 2 hours at 0°C, then another premixed solution of hydroxylamine HCl (600 mg, 8.64 mmol) and KOH (970 mg, 17.28 mmol) was added followed by stirring for 1.5 hour at 0°C. The product was purified by silica gel flash chromatography (acetone:dichloromethane 1:2) using iron-free silica gel to afford **19f** (158 mg, 51%). ^{1}HNMR (400 MHz, CD_3OD) δ (ppm): 1.33 (m, 2H), 1.67 (m 5H), 2.12 (m, 2H), 2.29 (m, 2H), 2.56 (m, 2H), 7.15 (m, 6H), 7.28 (t, *J* = 7.6 Hz, 2H), 7.51 (d, *J* = 7.6 Hz, 2H). ^{13}CNMR (100 MHz, CD_3OD) δ (ppm): 22.28, 28.83, 29.77, 31.72, 36.64, 38.93, 39.57, 119.91, 123.73, 125.46, 127.86, 128.352, 128.846,

138.43, 140.65, 171.70, 173.13. IR: 3253, 3063, 3027, 2972, 2927, 1660, 1600, 1547, 1499, 1444 cm^{-1}. HRMS (ESI-TOF, m/z): calculated for $[M+Na]^+$ $C_{21}H_{26}N_2O_3Na^+$, 377.1841, found 377.1824. HPLC analytical purity analysis 98.9%.

3.8.2.2. Enantioselective synthesis procedures for (*R*)-19f and (*S*)-19f

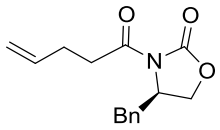

Synthesis of (*R*)-4-benzyl-3-(pent-4-enoyl)oxazolidin-2-one ((*R*)-20). The compound was synthesized in a similar way to the reported procedure.[134] Briefly, **(*R*)-8** (1.0 g, 5.64 mmol) was dissolved in dry THF (25 mL) followed by the addition of *n*-butyl lithium (2.5 mL of 2.5 M solution, 5.64 mmol) drop wise under argon at -78°C. The reaction was stirred at that temperature for 10 minutes, then 4-pentenoyl chloride (0.81 mL, 6.77 mmol) was added drop wise. Stirring was continued for 30 minutes at -78°C, then the reaction temperature was raised to gradually room temperature over 30 minutes. The reaction was diluted with saturated solution of ammonium chloride (30 mL) and saturated solution of sodium carbonate (30 mL) and stirred for 15 minutes at room temperature. The solution was extracted with ethyl acetate (3 x 40 mL). The organic extracts were combined, evaporated and the product was purified by Flash silica-gel chromatography (ethyl acetate:hexanes 1:9-1:3) which yielded the product **(*R*)-20** (954 mg, 65%). ^{1}HNMR (400 MHz, $CDCl_3$) δ (ppm): 2.45 (q, *J* = 6.8 Hz, 2H), 2.61 (dd, *J* = 3.6 Hz and 13.2, 1H), 3.04 (m, 2H), 3.31 (dd, *J* = 2.8 and 13.2 Hz, 1H), 4.17 (m, 2H), 4.68 (m, 1H), 5.07 (overlapped d and d, *J* = 10.4 and 17.2 Hz, 2H), 5.87 (m, 1H), 7.21 (d, *J* = 7.2 Hz, 2H), 7.31 (m, 3H); ^{13}CNMR (100 MHz, $CDCl_3$) δ (ppm): 28.16, 34.81, 37.92, 55.16, 66.21, 115.74,

127.36, 128.96, 129.42, 135.26, 136.69, 153.46, 172.55. LRMS (LC-SQMS, m/z); found: [M+H], 260.01, calculated for $C_{15}H_{18}NO_3$, 260.13, found: [M+Na], 281.97, calculated for $C_{15}H_{17}NO_3Na$, 282.11. Spectral data were consistent with the reported spectra.[134]

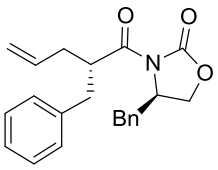

Synthesis of (*R*)-4-benzyl-3-((*S*)-2-benzylpent-4-enoyl)oxazolidin-2-one ((*RS*)-21). To compound **(*R*)-20** (951 mg, 3.67 mmol) was added dry THF (20 mL) followed by reduction of the temperature to -78°C. NaHMDS (2.0 mL of 2 M solution, 4.04 mmol) was added drop wise under Argon and the reaction was stirred at -78°C for 30 minutes. Benzyl bromide (0.86 mL, 7.34 mmol) was then added drop wise, and the reaction was stirred at -78°C for 5 hours, then the temperature was increased gradually to room temperature overnight. The reaction was then quenched with saturated ammonium chloride solution (15 mL) and was left to stir at room temperature for 15 minutes. The reaction was extracted with ethyl acetate (2 x 30 mL). The extracts were combined, evaporated, and the product was purified by Flash silica-gel chromatography (ethyl acetate:hexanes 1:15-1:10) which yielded **(*RS*)-21** as a white solid (730 mg, 57%). ^{1}HNMR (400 MHz, $CDCl_3$) δ (ppm): 2.29 (m, 1H), 2.47 (m, 2H), 2.83 (dd, *J* = 6.8 and 13.6 Hz, 1H), 3.03 (overlapped dd and dd, *J* = 3.2, 13.2, 8.4, and 13.6 Hz, 2H), 4.05 (dd, *J* = 3.2, and 9.2 Hz, 1H), 4.11 (t, *J* = 7.6 Hz, 1H), 4.35 (m, 1H), 4.62 (m, 1H), 5.05 (m, 2H), 5.81 (m, 1H), 7.01 (dd, *J* = 2.4, and 8.0 Hz, 2H), 7.20 (m, 1H), 7.25 (m, 3H), 7.28 (m, 4H); ^{13}CNMR (100 MHz, $CDCl_3$) δ (ppm): 36.34, 37.56, 38.13, 44.27, 55.05, 65.77, 117.28, 126.47, 127.24,

128.38, 128.88, 129.37, 129.38, 135.18, 138.90, 153.07, 175.26. LRMS (LC-SQMS, m/z); found: [M+H], 349.98, calculated for $C_{22}H_{24}NO_3$, 350.18, found: [M+Na], 371.95, calculated for $C_{22}H_{23}NO_3Na$, 372.16. $[\alpha]_D^{23}$ = -48.40 (*c* = 1.00, CH_2Cl_2). Spectral data were consistent with the reported spectra.[135] Diastereomeric ratio of 99:1 was calculated from the integration of peaks of both the major and the minor diastereomers in the ^{1}HNMR spectrum (See Figure B.78).

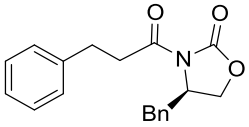

Synthesis of (*R*)-4-benzyl-3-(3-phenylpropanoyl)oxazolidin-2-one ((*R*)-23). The procedure was similar to that of **(*R*)-20** except the following reagents were used: **(*R*)-8** (1.5 g, 8.47 mmol), *n*-butyl lithium (4.1 mL of 2.5 M solution, 10.16 mmol), and 3-phenyl propanoyl chloride (1.64 mL, 11 mmol). The reaction gave **(*R*)-23** in 90% yield (2.36 g). ^{1}HNMR (400 MHz, $CDCl_3$) δ (ppm): 2.75 (dd, *J* = 9.6 Hz and 13.2, 1H), 3.03 (m, 2H), 3.29 (m, 3H), 4.16 (m, 2H), 4.67 (m, 1H), 7.22 (m, 3H), 7.32 (m, 7H); ^{13}CNMR (100 MHz, $CDCl_3$) δ (ppm): 30.26, 37.13, 37.82, 55.11, 66.18, 126.28, 127.36, 128.48, 128.58, 128.96, 129.42, 135.19, 140.44, 153.41, 172.41. LRMS (LC-SQMS, m/z); found: [M+H], 310.31, calculated for $C_{19}H_{20}NO_3$, 310.14, found: [M+Na], 332.31, calculated for $C_{19}H_{19}NO_3Na$, 332.13. Spectral data are consistent with the reported spectra.[136]

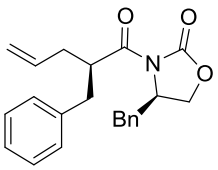

Synthesis of (*R*)-4-benzyl-3-((*R*)-2-benzylpent-4-enoyl)oxazolidin-2-one ((*RR*-21). The procedure was similar to that of **(*RS*)-21** except the following reagents

were used: **(*R*)-23** (2.35 g, 7.59 mmol), NaHMDS (4.18 mL of 2 M solution, 8.35 mmol), and allyl bromide (1.97 mL, 22.8 mmol). The product was purified by Flash silica-gel chromatography (ethyl acetate:hexanes 1:15) which yielded **(*RS*)-21** as an oily product (1.84 g, 69%). ^{1}HNMR (400 MHz, $CDCl_3$) δ (ppm): 2.37 (m, 1H), 2.52-2.67 (overlapped m and dd, *J* = 10.0 and 13.2 Hz, 2H), 2.84 (dd, *J* = 6.4 and 13.2 Hz, 1H), 2.96 (dd, *J* = 8.8 and 13.2 Hz, 1H), 3.23 (dd, *J* = 3.2, and 13.2 Hz, 1H), 3.82 (t, *J* = 8.4 Hz, 1H), 4.01 (d, *J* = 9.2 Hz, 1H), 4.33 (m, 1H), 4.45 (m, 1H), 5.10 (m, 2H), 5.86 (m, 1H), 7.17-7.33 (m, 10H); ^{13}CNMR (100 MHz, $CDCl_3$) δ (ppm): 36.32, 38.03, 38.29, 43.95, 55.49, 65.84, 117.41, 126.41, 127.29, 128.35, 128.90, 129.11, 129.42, 135.05, 135.36, 138.91, 153.01, 175.30. LRMS (LC-SQMS, m/z); found: [M+H], 350.45, calculated for $C_{22}H_{24}NO_3$, 350.18, found: [M+Na], 372.47, calculated for $C_{22}H_{23}NO_3Na$, 372.16. $[\alpha]_D^{23}$ = -121.5 (*c* = 1.00, CH_2Cl_2). Spectral data were consistent with the reported spectra.[135-136] Diastereomeric ratio of 97:3 was calculated from the integration of peaks of both the major and the minor diastereomers in the ^{1}HNMR spectrum (See Figure B.87).

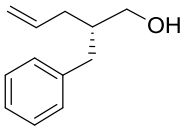

Synthesis of (*S*)-2-benzylpent-4-en-1-ol ((*S*)-22). A solution of **(*RS*)-21** (901 mg, 2.58 mmol) in dry THF (7 mL) was cooled and stirred at 0°C in ice bath for 15 minutes. Lithium aluminum hydride (295 mg, 7.77 mmol) was added portion wise and the reaction was stirred at 0°C for 2 hours. The reaction was quenched by careful drop wise addition of 1M solution of NaOH until no effervescence was observed, then diluted with water (3 mL). Extraction of the aqueous layer was done

with ethyl acetate (3 x 40 mL). The organic extracts were combined, evaporated, and the product was purified by Flash silica-gel chromatography (ethyl acetate:hexanes 1:15-1:10) which afforded **(*S*)-22** (402 mg, 88%). ^{1}HNMR (400 MHz, $CDCl_3$) δ (ppm): 1.38 (br s, 1H), 2.14 (t, *J* = 7.2 Hz, 2H), 2.64 (m, 2H), 3.55 (m, 2H), 5.06 (m, 2H), 5.83 (m, 1H), 7.19 (m, 3H), 7.28 (m, 2H); ^{13}CNMR (100 MHz, $CDCl_3$) δ (ppm): 35.50, 37.24, 42.37, 64.74, 116.61, 125.97, 128.35, 129.17, 136.83, 140.48. $[\alpha]_D^{23}$ = -13.96 (*c* = 0.824, CH_2Cl_2). Compound characterization and specific rotation were consistent with literature.[137]

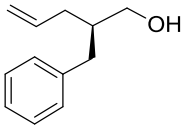

Synthesis of (*R*)-2-benzylpent-4-en-1-ol ((*R*)-22). The procedure was similar to that of **(*S*)-22** except the following reagents were used: **(*RR*)-21** (1.83 g, 5.23 mmol) in dry THF (25 mL), Lithium aluminum hydride (595 mg, 15.68 mmol). The reaction afforded **(*R*)-22** in 70% yield (645 mg). ^{1}HNMR (400 MHz, $CDCl_3$) δ (ppm): 42 (t, *J* = 5.6 Hz, 1H), 1.92 (m, 1H), 2.15 (m, 2H), 2.65 (m, 2H), 3.55 (m, 2H), 5.07 (m, 2H), 5.83 (m, 1H), 7.21 (m, 3H), 7.28 (m, 2H); ^{13}CNMR (100 MHz, $CDCl_3$) δ (ppm): 35.49, 37.24, 42.37, 64.71, 116.62, 125.97, 128.35, 129.18, 136.84, 140.50. $[\alpha]_D^{23}$ = +15.80 (*c* = 1, CH_2Cl_2). Compound characterization and specific rotation were consistent with its enantiomer (**(*S*)-22**) and with literature.[137-138]

3.8.2.3. Synthesis procedure for Mosher's esters of (*S*)-11-(*R*)-MTPA and (*R*)-11-(*R*)-MTPA

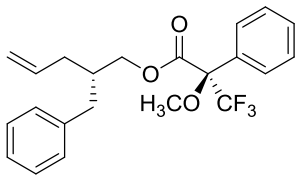

Synthesis of (*S*)-2-benzylpent-4-en-1-yl (*R*)-3,3,3-trifluoro-2-methoxy-2-phenylpropanoate ((*S*)-22-(*R*)-MTPA). Alcohol **(*S*)-22** (35 mg, 0.2 mmol) was dissolved in dry DCM (4 mL) followed by replacement of air with argon. and (*R*)-(+)-a-Methoxy-a-trifluoromethylphenylacetic acid (**(*R*)-MTPA**) (71 mg, 0.3 mmol), EDCI (116 mg, 0.6 mmol), and 4-(dimethylamino)pyridine (73 mg, 0.6 mmol). The reaction was stirred overnight at room temperature. Solvent was evaporated and the residue was suspended in 1N HCl (5 mL) and then extracted with ethyl acetate (2 x 15 mL). The combined extracts were combined, evaporated, and purified by silica gel flash chromatography (ethyl acetate:hexanes 1:15) to afford **(*S*)-22-(*R*)-MTPA** (49 mg, 63%). ^{1}HNMR (600 MHz, $CDCl_3$) δ (ppm): 2.03 (m, 3H), 2.51 (m, 2H), 3.49 (s, 3H), 4.06-4.13 (overlapped dd and dd, *J* = 2.8 and 7.2 Hz, 2H), 4.99 (m, 2H), 5.68 (m, 1H), 6.96 (d, *J* = 4.8 Hz, 2H), 7.12 (t, *J* = 5.2 Hz, 1H), 7.18 (d, *J* = 5.6 Hz, 2H), 7.35 (m, 3H), 7.46 (m, 2H). ^{13}CNMR (150 MHz, $CDCl_3$) δ (ppm): 35.15, 36.97, 39.26, 55.46, 67.18, 117.45, 121.99, 124.85, 126.23, 127.38, 128.45, 129.07, 129.67, 132.31, 135.48, 139.38, 166.57. ^{19}FNMR (400 MHz, $CDCl_3$) δ (ppm): -71.30. LRMS (LC-SQMS, m/z); found: [M+Na], 415.13, calculated for $C_{22}H_{23}F_3O_3Na$, 415.15.

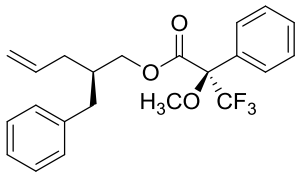

Synthesis of (*R*)-2-benzylpent-4-en-1-yl (*R*)-3,3,3-trifluoro-2-methoxy-2-phenylpropanoate ((*R*)-22-(*R*)-MTPA). The procedure was similar to that of **(S*R*)-18** except the following reagents were used **(*R*)-22** (15.8 mg, 0.09 mmol), (*R*)-(+)-a-Methoxy-a-trifluoromethylphenylacetic acid (**(*R*)-MTPA**) (46 mg, 0.2 mmol), EDCI (35 mg, 0.27 mmol), and 4-(dimethylamino)pyridine (33 mg, 0.27 mmol). The reaction was stirred at room temperature for 3 hours. The product was purified by silica gel flash chromatography (ethyl acetate:hexanes 1:50) and afforded **(*R*)-22-(*R*)-MTPA** in 89% yield (32 mg). ^{1}HNMR (600 MHz, $CDCl_3$) δ (ppm): 2.03 (m, 3H), 2.54 (m, 2H), 3.48 (s, 3H), 4.01 (dd, *J* = 2.8 and 7.2 Hz, 1H), 4.20 (dd, *J* = 2.8 and 7.2 Hz, 1H), 4.97 (m, 2H), 5.66 (m, 1H), 7.01 (d, *J* = 4.8 Hz, 2H), 7.13 (t, *J* = 5.2 Hz, 1H), 7.20 (d, *J* = 5.6 Hz, 2H), 7.35 (m, 3H), 7.46 (m, 2H). ^{13}CNMR (150 MHz, $CDCl_3$) δ (ppm): 34.99, 37.05, 39.15, 55.41, 67.19, 117.48, 121.98, 124.85, 126.26, 127.43, 128.45, 129.10, 129.67, 132.28, 135.42, 139.34, 166.55. ^{19}FNMR (400 MHz, $CDCl_3$) δ (ppm): -71.26. LRMS (LC-SQMS, m/z); found: [M+Na], 415.17, calculated for $C_{22}H_{23}F_3O_3Na$, 415.15.

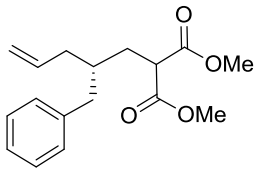

Synthesis of dimethyl (*R*)-2-(2-benzylpent-4-en-1-yl)malonate ((*R*)-24). A solution of **(*S*)-22** (400 mg, 2.27 mmol) in dry DCM (10 mL) was cooled to 0°C in ice bath followed by addition of triethyl amine (265 µL, 3.41 mmol), then

methanesulfonyl chloride (476 µL, 3.41 mmol) drop wise. The reaction was stirred for 10 minutes at 0°C, then for 1 hour at room temperature. The reaction was diluted with water (10 mL) followed by concentration at reduced pressure. The aqueous layer was extracted with ethyl acetate (3 x 20 mL). The organic extracts were combined, dried over anhydrous sodium sulfate, and evaporated. The crude product was used in the following reaction with no purification.

In a 2-neck flame dried flask, air was purged with argon, NaH (273 mg of 60% NaH in mineral oil, 6.82 mmol) was dissolved in dry THF (20 mL). The reaction was then cooled to 0°C and dimethyl malonate (0.78 mL, 6.82 mmol) was added drop wise with stirring. The reaction was allowed to stir for 15 minutes at 0°C, then the crude product from previous reaction was added (in 10 mL dry THF). The reaction was heated under reflux for 20 hours, then another solution of malonate anion (prepared in the same way as described above) was added to the reaction and reflux was continued for another 20 hours. The reaction was then quenched with saturated ammonium chloride solution (20 mL) and extracted with ethyl acetate (3 x 30 mL). The extracts were combined, evaporated, and the product was purified by Flash silica-gel chromatography (ethyl acetate:hexanes 1:9) which yielded **(*R*)-24** in 49% yield (269 mg) over two steps. ^{1}HNMR (400 MHz, $CDCl_3$) δ (ppm): 1.67 (m, 1H), 1.83-2.12 (m, 4H), 2.58 (m, 2H), 3.50 (t, *J* = 7.6 Hz, 1H) 3.69 (s, 3H), 3.73 (s, 3H), 5.05 (m, 2H), 5.76 (m, 1H), 7.13 (d, *J* = 7.2 Hz, 2H), 7.19 (m, 1H), 7.24 (m ,2H); ^{13}CNMR (100 MHz, $CDCl_3$) δ (ppm): 32.47, 37.16, 37.37, 39.85, 49.70, 52.48, 52.50, 117.22, 126.02, 128.30, 129.16, 135.70, 140.16, 169.82, 169.89. IR: 3065, 3027,

2953, 2924, 2853, 1733, 1651, 1623, 1592, 1575, 1496, 1436 cm^{-1}. LRMS (LC-SQMS, m/z); found: [M+H], 291.19, calculated for $C_{17}H_{23}O_4$, 291.16,

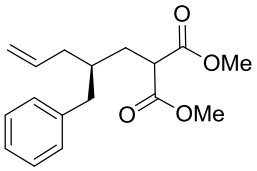

Synthesis of dimethyl (*S*)-2-(2-benzylpent-4-en-1-yl)malonate ((*S*)-24). The procedure was similar to that of **(*R*)-24** except the following reagents were used: **(*R*)-22** (597 mg, 3.34 mmol), triethyl amine (710 µL, 5.09 mmol), methanesulfonyl chloride (394 µL, 5.09 mmol), and the reaction was stirred at room temperature for 3 hours. For the next reaction, the following reagents were used once only, NaH (407 mg of 60% NaH in mineral oil, 10.17 mmol), dimethyl malonate (1.16 mL, 10.17 mmol) and the reaction was refluxed for 20 hours. The reaction afforded **(*S*)-13** in 66% yield (648 mg) over two steps. ^{1}HNMR (400 MHz, $CDCl_3$) δ (ppm): 1.74 (m, 1H), 1.88-2.08 (m, 4H), 2.56 (m, 2H), 3.50 (t, *J* = 7.6 Hz, 1H) 3.69 (s, 3H), 3.72 (s, 3H), 5.05 (m, 2H), 5.75 (m, 1H), 7.13 (d, *J* = 6.8 Hz, 2H), 7.19 (m, 1H), 7.29 (m ,2H); ^{13}CNMR (100 MHz, $CDCl_3$) δ (ppm): 32.47, 37.16, 37.37, 39.85, 49.70, 52.48, 52.50, 117.22, 126.02, 128.30, 129.16, 135.70, 140.16, 169.82, 169.89. IR: 3066, 3028, 2953, 2924, 1733, 1657, 1638, 1621, 1605, 1497, 1436 cm^{-1}. LRMS (LC-SQMS, m/z); found: [M+H], 291.37, calculated for $C_{17}H_{23}O_4$, 291.16, found: [M+Na], 313.38, calculated for $C_{17}H_{22}O_4Na$, 313.34.

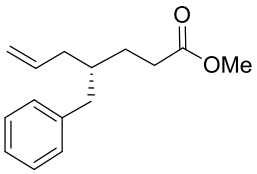

Synthesis of methyl (*S*)-4-benzylhept-6-enoate ((*S*)-25). (*R*)-24 (269 mg, 0.93 mmol) was dissolved in DMSO (15 mL) followed by addition of LiCl (394 mg, 9.3 mmol) and water (167 µL, 9.3 mmol). The reaction was heated under reflux (150-160 °C) overnight. Water (20 mL) was added to the reaction and the product was extracted with ethyl acetate (2 x 30 mL). The organic layer was evaporated and the product was purified by Flash silica-gel chromatography (ethyl acetate:hexanes 1:15) which yielded **(*S*)-25** in 75% yield (162 mg). ^{1}HNMR (400 MHz, $CDCl_3$) δ (ppm): 1.64 (m, 2H), 1.77 (m, 1H), 2.04 (m, 2H), 2.33 (m, 2H), 2.57 (m, 2H), 3.65 (s, 3H), 5.04 (m, 2H), 5.78 (m, 1H), 7.19 (m, 3H), 7.24 (t, *J* = 7.2 Hz, 2H); ^{13}CNMR (100 MHz, $CDCl_3$) δ (ppm): 28.14, 31.61, 37.20, 39.07, 39.91, 51.52, 116.76, 125.89, 128.27, 129.17, 136.29, 140.67, 174.17. IR: 3062, 3027, 2953, 2924, 2855, 1735, 1658, 1640, 1595, 1574, 1511, 1497, 1445 cm^{-1}. LRMS (LC-SQMS, m/z); found: [M+Na], 255.12, calculated for $C_{15}H_{20}O_2Na$, 255.14.

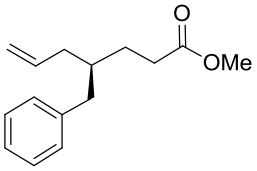

Synthesis of methyl (*R*)-4-benzylhept-6-enoate ((*R*)-25). The procedure was similar to that of **(*S*)-25** except the following reagents were used **(*S*)-24** (617 mg, 2.13 mmol), LiCl (270 mg, 6.38 mmol), water (115 µL, 6.38 mmol). The reaction afforded **(*R*)-25** in 65% yield (321 mg). ^{1}HNMR (400 MHz, $CDCl_3$) δ (ppm): 1.63 (m,

2H), 1.77 (m, 1H), 2.05 (m, 2H), 2.33 (m, 2H), 2.56 (m, 2H), 3.65 (s, 3H), 5.04 (m, 2H), 5.77 (m, 1H), 7.17 (m, 3H), 7.26 (m, 2H); ^{13}CNMR (100 MHz, $CDCl_3$) δ (ppm): 28.13, 31.61, 37.19, 39.07, 39.91, 51.53, 116.76, 125.89, 128.26, 129.16, 136.29, 140.67, 174.19. IR: 3063, 3027, 2924, 2856, 1736, 1657, 1640, 1596, 1511, 1497, 1436 cm^{-1}. LRMS (LC-SQMS, m/z); found: [M+Na], 255.26, calculated for $C_{15}H_{20}O_2Na$, 255.14.

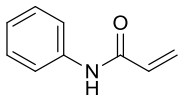

Synthesis of *N*-phenylacrylamide (26). The compound was synthesized similar to the reported procedure.[139] Briefly, aniline (3.03 mL, 33.15 mmol) and triethyl amine (6 mL, 66.29 mmol) were dissolved in dry DCM (30 mL) and the temperature of the solution was lowered to 0°C. A solution of acryloyl chloride (2.69 mL, 33.15 mmol) in dry DCM (10 mL) was added drop wise. The reaction temperature was increased gradually from 0°C to room temperature and stirring was continued overnight at room temperature. Solvent was evaporated and the residue was suspended in 10% HCl (20 mL) and then extracted with DCM (2 x 30 mL). The combined organic extracts were washed with saturated solution of sodium carbonate (20 mL), dried over anhydrous sodium sulfate and evaporated to give the product **26** as a yellow solid (4.44 g, 91%). ^{1}HNMR (400 MHz, $CDCl_3$) δ (ppm): 5.71 (dd, *J* = 1.6 and 10.0 Hz, 1H), 6.30 (dd, *J* = 10.0 and 16.8 Hz, 1H), 6.41 (dd, *J* = 1.6 and 16.8 Hz, 1H), 7.12 (t, *J* = 7.6, 1H), 7.28 (m, 2H), 7.60 (d, *J* = 8.0 Hz, 2H), 7.98 (s, 1H); ^{13}CNMR (100 MHz, $CDCl_3$) δ (ppm): 120.15, 124.51, 127.69, 128.99, 131.29,

137.85, 163.86. The spectral data for the synthesized compound was consistent with the reported data in literature.[139]

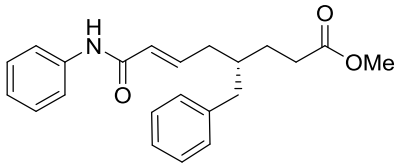

Synthesis of methyl (*S*,*E*)-4-benzyl-8-oxo-8-(phenylamino)oct-6-enoate ((*S*)-27). To a solution of **(*S*)-25** (162 mg, 0.7 mmol) in dry DCM (20 mL) was added **26** (103 mg, 0.7 mmol), then air was replaced with argon. Grubbs' second-generation catalyst (35 mg, 5 mol%) was added and the reaction was heated to 50-60°C for 20 hours. A second addition of Grubbs' second generation catalyst (35 mg, 5 mol%) was done and the reaction was heated to 50-60°C for 28 hours. The solvent was evaporated and the product was purified by Flash silica-gel chromatography (ethyl acetate:hexanes 1:15 followed by 1:7-1:3) which yielded **(*S*)-27** in 46% yield (112 mg). ^{1}HNMR (400 MHz, $CDCl_3$) δ (ppm): 1.67 (m, 2H), 1.88 (m, 1H), 2.18 (m, 2H), 2.33 (t, *J* = 8.0 Hz, 2H), 2.51 (dd, *J* = 7.6 and 13.6 Hz, 1H), 2.63 (dd, *J* = 6.4 and 13.6 Hz, 1H), 3.66 (s, 3H), 5.92 (d, *J* = 15.2 Hz, 1H), 6.91 (m, 1H), 7.12 (m, 3H), 7.21 (t, *J* = 7.2 Hz, 1H), 7.31 (m, 4H), 7.36 (s, 1H), 7.57 (dd, *J* = 7.6 Hz, 2H); ^{13}CNMR (100 MHz, $CDCl_3$) ð (ppm): 28.45, 31.67, 35.61, 38.93, 40.07, 51.65, 119.81, 124.27, 126.00, 126.16, 128.41, 129.01, 129.13, 138.02, 140.03, 143.84, 163.75, 173.97. IR: 3301, 3136, 3062, 3027, 2926, 1733, 1670, 1640, 1600, 1542, 1497, 1441 cm^{-1}. LRMS (LC-SQMS, m/z); found: [M+H], 352.07, calculated for $C_{22}H_{26}NO_3$, 352.19, found: [M+Na], 374.05, calculated for $C_{22}H_{25}NO_3Na$, 374.17.

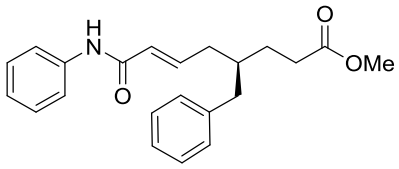

Synthesis of methyl (*R*,*E*)-4-benzyl-8-oxo-8-(phenylamino)oct-6-enoate ((*R*)-27). A similar to that of **(*S*)-27** was followed except the following reagents were used **(*R*)-25** (321 mg, 1.38 mmol), **26** (204 mg, 1.38 mmol), and Grubbs' second-generation catalyst (59 mg, 5 mol%). The reaction afforded **(*R*)-27** in 48% yield (233 mg). ^{1}HNMR (400 MHz, $CDCl_3$) δ (ppm): 1.66 (m, 2H), 1.87 (m, 1H), 2.17 (m, 2H), 2.34 (t, *J* = 8.0 Hz, 2H), 2.52 (dd, *J* = 7.6 and 13.6 Hz, 1H), 2.62 (dd, *J* = 6.4 and 13.6 Hz, 1H), 3.65 (s, 3H), 5.93 (d, *J* = 15.2 Hz, 1H), 6.91 (m, 1H), 7.11 (m, 3H), 7.20 (t, *J* = 7.6 Hz, 1H), 7.30 (m, 4H), 7.51 (s, 1H), 7.58 (d, *J* = 7.2 Hz, 2H); ^{13}CNMR (100 MHz, $CDCl_3$) δ (ppm): 28.43, 31.66, 35.60, 38.92, 40.04, 51.66, 119.85, 124.26, 126.01, 126.15, 128.41, 129.00, 129.13, 138.06, 140.03, 143.79, 163.83, 173.00. IR: 3401, 3062, 3026, 2924, 2856, 1736, 1658, 1640, 1597, 1574, 1512, 1437 cm^{-1}. LRMS (LC-SQMS, m/z); found: [M+H], 352.07, calculated for $C_{22}H_{26}NO_3$, 352.19, found: [M+Na], 374.02, calculated for $C_{22}H_{25}NO_3Na$, 374.17.

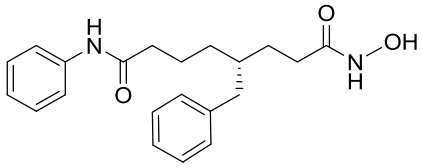

Synthesis of (*R*)-4-benzyl-*N*^{1}-hydroxy-*N*^{8}-phenyloctanediamide ((*R*)-19f). **(*S*)-27** (112 mg, 0.32 mmol) was dissolved in MeOH (15 mL), then Pd (30 mg of 20 wt.% Pd on carbon) was added to the solution. Air inside the flask was purged with argon (three times), then with hydrogen gas (three times). The reaction was stirred

under hydrogen overnight. The reaction was filtered, and the solvent was evaporated. The crude product was used in the next reaction with no purification.

In an acid washed flask, hydroxylamine HCl (222 mg, 3.19 mmol) was dissolved in MeOH (10 mL). KOH (358 mg, 6.38 mmol) was added at 0°C and allowed to stir for 10 minutes. An alcoholic solution of the crude product from the previous reaction (in 5 mL MeOH) was added, and the reaction was stirred for 3.5 hours at 0°C, then another premixed solution of hydroxylamine HCl (222 mg, 3.19 mmol) and KOH (358 mg, 6.38 mmol) was added followed by stirring for 4 hour at 0°C. The pH of the reaction mixture was adjusted to 6 with concentrated aqueous HCl, followed by dilution with distilled de-ionized water (10 mL). The reaction was extracted with ethyl acetate (2 x 20 mL). The product was purified by silica gel flash chromatography (acetone:dichloromethane 1:4-1:2) using iron-free silica gel to afford **(*R*)-19f** (84 mg, 74% over two steps). ^{1}HNMR (400 MHz, CD_3OD) δ (ppm): 1.32 (m, 2H), 1.69 (m 5H), 2.12 (m, 2H), 2.29 (m, 2H), 2.52 (dd, *J* = 7.2 and 13.2 Hz, 2H), 2.61 (dd, *J* = 6.4 and 13.6 Hz, 2H), 7.05-7.15 (m, 4H), 7.21 (t, *J* = 7.2 Hz, 2H), 7.28 (t, *J* = 7.6 Hz, 2H), 7.51 (d, *J* = 8.0 Hz, 2H). ^{13}CNMR (100 MHz, CD_3OD) δ (ppm): 22.28, 28.84, 29.77, 31.72, 36.63, 38.93, 39.57, 119.92, 123.73, 125.46, 127.86, 128.35, 128.85, 138.43, 140.65, 171.70, 173.13. IR: 3230, 3061, 3026, 2925, 2864, 1648, 1598, 1543, 1497, 1443 cm^{-1}. HRMS (ESI-TOF, m/z): calculated for $[M+Na]^+$ $C_{21}H_{26}N_2O_3Na^+$, 377.1841, found 377.1837. HPLC analytical purity analysis 95.6%.

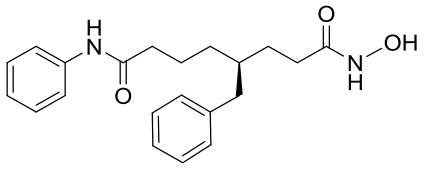

Synthesis of (*S*)-4-benzyl-*N*^{1}-hydroxy-*N*^{8}-phenyloctanediamide ((*S*)-19f). similar to that of **(*R*)-19f** was followed except the following reagents were used **(*R*)-27** (283 mg, 0.8 mmol), Pd (58 mg of 20 wt.% Pd on carbon). Hydroxylamine HCl (557 mg, 8.02 mmol) and KOH (900 mg, 16.03 mmol) were added once only and the reaction was stirred for 3 hours at 0°C. The product was purified by silica gel flash chromatography (acetone:dichloromethane 1:4-1:2) using iron-free silica gel to afford **(*S*)-19f** (133 mg, 47% over two steps). ^{1}HNMR (400 MHz, CD_3OD) δ (ppm): 1.33 (m, 2H), 1.59-1.82 (m 5H), 2.14 (m, 2H), 2.30 (m, 2H), 2.53 (dd, *J* = 7.2 and 13.6 Hz, 2H), 2.61 (dd, *J* = 6.8 and 13.6 Hz, 2H), 7.05-7.16 (m, 4H), 7.21 (t, *J* = 7.2 Hz, 2H), 7.28 (t, *J* = 7.6 Hz, 2H), 7.51 (d, *J* = 7.6 Hz, 2H). ^{13}CNMR (100 MHz, CD_3OD) δ (ppm): 22.28, 28.83, 29.76, 31.71, 36.62, 38.93, 39.57, 119.91, 123.73, 125.46, 127.86, 128.34, 128.84, 138.43, 140.65, 171.70, 173.13. IR: 3232, 3026, 2926, 2865, 1645, 1598, 1543, 1497, 1443 cm^{-1}. HRMS (ESI-TOF, m/z): calculated for $[M+Na]^+$ $C_{21}H_{26}N_2O_3Na^+$, 377.1841, found 377.1848. HPLC analytical purity analysis 95.6%.

3.8.3. Procedures for biological screenings

3.8.3.1. HeLa cell lysis

Details were provided in Section 2.7.3.1 of Chapter 2.

3.8.3.2. Global HDAC inhibition

To measure global HDAC inhibition, HeLa cell lysates (1 µg total protein) were mixed with HDAC-Glo™ buffer (Promega) in polystyrene 96-well half area white plate (Corning) to a final volume of 12 µL, followed by addition of inhibitors in

DMSO (0.5 µL) and incubation for 15 min at room temperature without rocking. An uninhibited control reaction was also included that contained DMSO (0.5 µL) in HDAC-Glo™ buffer (12 µL). Deacetylase activity was measured using the HDAC-Glo™ assay kit as per the manufacturer's protocol (Promega). Specifically, the HDAC-Glo™ substrate (1 mL) and developer (1 µL) were first premixed to form the HDAC-Glo™ reagents. Then, to monitor deacetylase activity, HDAC-Glo™ reagent (5µL) and HDAC-Glo™ buffer (7.5 µL) were added to each well (25 µL total volume) and incubated for 35 min at room temperature without rocking. The deacetylase activity was measured as luminescent signal using a GeniosPlus Fluorimeter (Tecan) at optimal gain. The concentrations of inhibitors reported in the dose-dependent studies are final concentrations after addition of HDAC-Glo™ reagent and HDAC-Glo™ buffer. The luminescent signal was first background corrected with the signal from a negative control reaction where no lysates was added to that reaction. Percent deacetylase activity was calculated by dividing the background corrected signal for each reaction by the background corrected signal of the uninhibited control, and then multiplying by 100. IC_{50} values were calculated by fitting the percent deacetylase activity remaining as a function of inhibitor concentration to a sigmoidal dose-response curve ($y = 100/(1+(x/IC_{50})^{Z})$, where y = percent deacetylase activity and x = inhibitor concentration) using non-linear regression with KaleidaGraph 4.1.3 software. Results are reported in Tables 3.1, and B.1, and Figure B.140.

3.8.3.3. Inhibitor testing with HDAC isoforms [93]

Details were provided in Section 2.7.3.2 of Chapter 2. Results are reported in Figures 3.2 and B.141-B.147, and Tables 4.2 and B.2-B.9.

3.8.3.4. *In cellulo* selectivity testing

Details were provided in Sections 2.7.3.3-2.7.3.5 of Chapter 2. Results are reported in Figures 3.3 and B.148.

3.8.3.5. *In vitro* cell growth inhibition

Details were provided in Section 2.7.3.6 of Chapter 2. Results are reported in Figures B.149-B.152 and Tables 3.3 B.11-B.12.

3.8.4. Docking procedure

The AutoDock 4.2 and Autodock tools programs [119, 127] were used to perform the docking studies. HDAC6 catalytic domain 2 (CD2) (PDB: 5G0H)[13] and HDAC3 (PDB: 4A69)[100] crystal structures were downloaded from the protein data bank. PyMOL program (Schrodinger, LLC) was used to delete the co-crystallized inhibitor (*S*-trichostatin A), ethylene glycol molecules, potassium ions and all water molecules in HDAC6 crystal structure. With HDAC3 crystal, chain A, deacetylase-activation-domain (DAD) (from the SMRT corepressor), glycerol, D-myo-inositol-1,4,5,6-tetrakisphosphate and glycerol molecules, acetate, potassium and sulfate ions, and all water molecules were deleted. Only the zinc atom remained in both crystal structures. AutoDockTools-1.5.4 program [119, 127] was used to add all polar hydrogen atoms, modify histidine protonation (H573 and H574 residues of HDAC6, and H134 and H135 of HDAC3) by adding only HD1, compute Gasteiger charges, and merge all non polar hydrogen, followed by generation of the pdbqt output file. The charge of the zinc atom was manually changed from zero to +2. For HDAC6, a grid box with a

spacing of 0.375 Å, size of 42 x 40 x 44, and coordinates for the center of the grid box (-13.000, -2.000, -5.000) were used. For HDAC3, a grid box of size 58 X 58 X 54 $Å^3$ with a spacing of 0.375 Å and centered at (8.166, 76.663, 21.318) were used. The rest of binding sites preparation procedure and all docking parameters were similar to was mentioned in Section 2.7.4 of Chapter 2.

CHAPTER 4 - SYNTHESIS AND BIOLOGICAL EVALUATION OF SAHA DERIVATIVES SUBSTITUTED AT C5 POSITION

Some of the text in this chapter was reprinted or modified from: Negmeldin, A. T. and Pflum, M. K. H., The structural requirements of histone deacetylase Inhibitors: SAHA analogs modified at the C5 Position Display dual HDAC6/8 Selectivity, *Bioorganic & medicinal chemistry letters* **2017** (*Accepted*).

4.1. Rationale for synthesis and screening of C5-modified SAHA analogs

Guided by the promising modifications of the C4 position in the linker of SAHA that led to substantial improvement in selectivity with a modest reduction in potency compared to SAHA, we explored the effect of modifications on the C5 position in the linker (Figure 4.1). Based on the experimental and computational studies done for the C4-modified SAHA analogs, we expected that the C5-modified SAHA analogs would show similar selectivity to HDAC6 and HDAC8. As discussed in the previous two chapters, some of the C2-SAHA analogs showed about 30-fold reduction in potency against HDAC6, while some of the C4-SAHA analogs showed only about 2.5-fold reduction in potency against HDAC6 compared to SAHA. The question that needed to be answered was to what extent modification of SAHA at the C5 position would affect both potency and selectivity. In this chapter, SAHA analogs substituted at the C5 of the linker region were synthesized (Figure 4.1 and scheme 4.1) and tested for potency and selectivity both *in vitro* and *in cellulo*. Several analogs showed dual HDAC6/8 selectivity over HDAC1, 2, and 3, with a modest reduction in HDAC6 inhibition but enhanced HDAC8 inhibition compared to SAHA. This chapter documents that modifying the linker region of SAHA can alter its selectivity with minimal effect on potency.

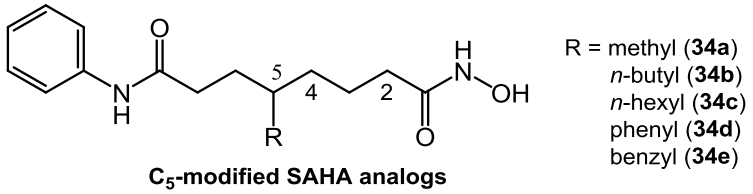

Figure 4.1. Chemical structures of C5-modified SAHA analogs (**34a**-**e**).

4.2. Synthesis of C5-substituted SAHA derivatives

C5-modified SAHA analogs **34a-e** were synthesized as shown in Scheme 4.1. The synthesis started from a coupling reaction of 4-pentenoic acid **28** with aniline using TBTU to obtain amide **29**. Intermediate amide **29** was then reacted with crotonaldehyde **13** via a cross metathesis reaction using Grubbs' second-generation catalyst to afford the α,β-unsaturated aldehyde **30**. Aldehyde **30** was substituted with different groups through a 1,4-conjugate addition using organolithium or organomagnesium cuprates, which yielded intermediates **31a-e**. Horner–Wadsworth–Emmons olefination of **31a-e** with trimethyl phosphonoacetate **32** followed by reduction gave amide esters **33a-e** with a saturated linker. Finally, amide esters **33a-e** were reacted with hydroxylamine to afford the C5-substituted SAHA derivatives **34a-e** as racemic mixtures.[140]

Scheme 4.1. Synthesis of C5-SAHA analogs (**34a-e**)

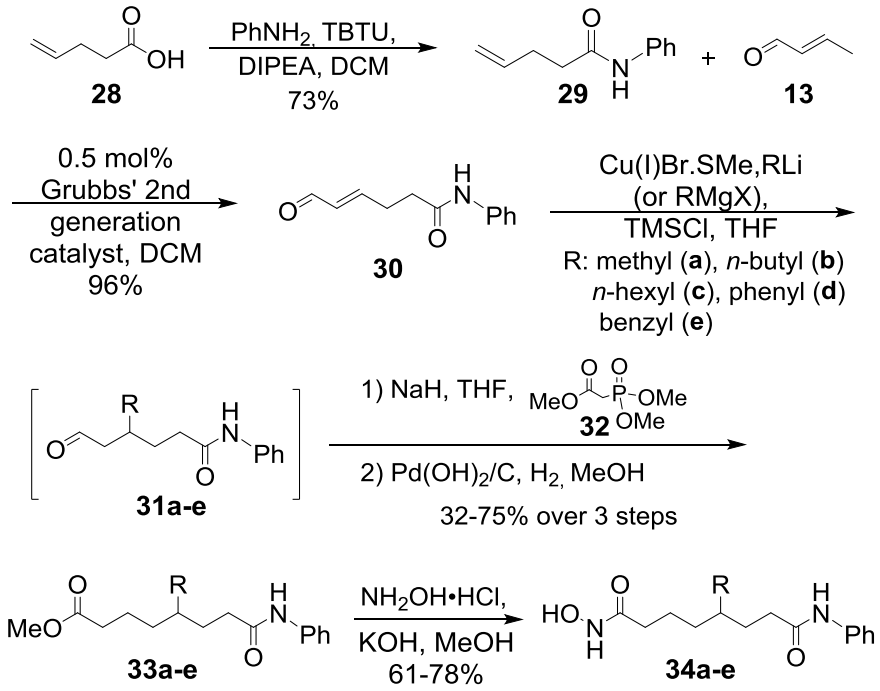

4.3. *In vitro* screening of C5-modified SAHA derivatives

As a preliminary screen, the new analogs were tested for their global HDAC inhibition with HeLa cell lysates as the source of all HDAC proteins (Table 4.1). SAHA was also tested as the parent unsubstituted control molecule. The inhibitory activities of the analogs were measured with the HDAC-Glo™ I/II substrate (see section 2.2). C5-methyl SAHA analog **34a** showed greater potency compared to SAHA (100 nM vs. 200 nM IC_{50} values, Table 4.1). However, all other analogs showed weaker potency than SAHA (11- to 33-fold reduction in potency), with IC_{50} values from 2.2 to 6.5 µM (Table 4.1). The observed lower potencies of compounds **34b**-**34e** may be due to selectivity for specific HDAC isoform(s), which lowered the potency against lysates that contain all HDAC isoforms. The lower potency observed

here was similar to what was observed with both the C2- and the C4-modified SAHA analogs (see sections in 2.2 and 3.3 Chapters 2 and 3).

Table 4.1. IC_{50} values for SAHA, and C5-modified SAHA analogs (**34a-e**) with HeLa cell lysates.[a]

Compound	R	IC_{50} (μM)
SAHA		0.20 ± 0.02
34a	methyl	0.10 ± 0.01
34b	*n*-butyl	5.0 ± 0.4
34c	*n*-hexyl	6.5 ± 0.1
34d	Phenyl	2.2 ± 0.1
34e	benzyl	6.2 ± 0.2

[a] Mean IC_{50} value and standard error of at least three independent trials are shown (Figure C.52 and Table C.1).

To test isoform selectivity, the parent molecule, SAHA, and all the C5-modified SAHA analogs were tested at a single concentration using the recently developed ELISA-based HDAC activity assay (see section 2.2).[93] SAHA, as expected, showed no selectivity among HDAC1, 2, 3, and 6 (Figure 4.2).[93] Interestingly, several C5-SAHA analogs displayed more potent inhibition against HDAC6 compared to HDAC1, HDAC2, and HDAC3 (Figure 4.2). The analogs that showed the greater difference in potency with HDAC6 versus the other isoforms were C5-*n*-butyl (**34b**), C5-*n*-hexyl (**34c**), and C5-benzyl (**34e**). The C5-methyl SAHA (**34a**) and C5-phenyl SAHA (**34d**) showed only a small difference in potency comparing HDAC6 to the others (Figure 4.2).

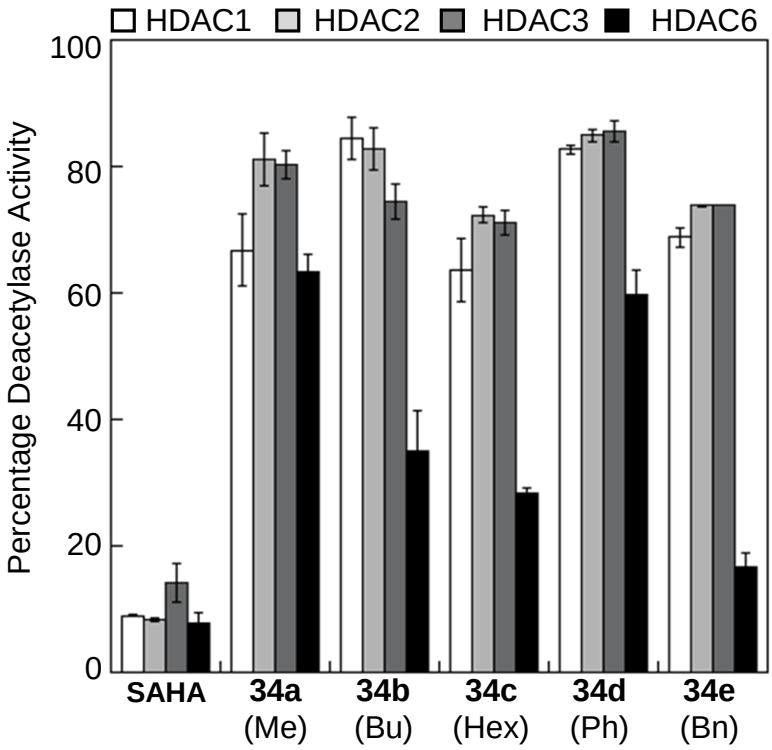

Figure 4.2. *In vitro* isoform selectivity screening of C5-modified SAHA analogs (**34a-e**) against HDAC1, HDAC2, HDAC3, and HDAC6 using the ELISA-based HDAC activity assay. Analogs **34a-e** were tested at 0.025, 0.25, 1.25, 0.125, and 1.25 μM final concentrations, respectively. SAHA was tested at 1 μM concentration in a previous report using the same assay procedure.[93] Mean percent deacetylase activities from a minimum of two independent trials with standard errors were plotted (Table C.2).

IC_{50} values for the most selective derivatives **34b**, **34c**, and **34e** were determined with HDAC1, HDAC2, HDAC3, HDAC6, and HDAC8 isoforms to quantitatively assess the selectivity (Table 4.2). The IC_{50} values of SAHA as the parent compound were included as well (Table 4.2).[93] SAHA displayed similar IC_{50} values against HDAC1, 2, 3, and 6, with 6- to 27-fold selectivity against HDAC8 (Tables 4.2 and C.6).[93, 112] Both C5-*n*-butyl (**34b**) and C5-*n*-hexyl (**34c**) SAHA analogs displayed the modest selectivity, with 3- to 5-fold and 5- to 7-fold selectivities for HDAC6 and HDAC8 over HDAC1, 2, and 3 (Tables 4.2, C.3, C.4 and C.6 and Figures C.53 and C.54). In addition, **34b** and **34c** showed modest reduction

in HDAC6 potency (IC_{50} values of 320 nM and 410 nM), but similar potency against HDAC8 (430 and 420 nM) compared to SAHA. The most potent and selective analog was C5-benzyl SAHA (**34e**), which displayed 8- to 21-fold selectivity for HDAC6 and HDAC8 over HDAC1, 2, and 3 and IC_{50} values of 270 and 380 nM with HDAC6 and HDAC8, respectively (Tables 4.2, C.5 and C.6, and Figure C.55). The selectivity was due to a dramatic reduction in potency with HDAC1, 2, and 3 (14- to 80-fold), but only a modest potency reduction in HDAC6 (8.5- to 12-fold) and similar potency with HDAC8 (380 – 540 nM), compared to SAHA. Modification of SAHA at the C5 position of the linker region led to selectivity for HDAC6 and 8 over HDAC1, 2, and 3.

Table 4.2. IC_{50} values for SAHA and C5-modified SAHA analogs **34c, 34d,** and **34e** against HDAC1, 2, 3, 6 and 8.[a]

Compound	IC_{50} values (μM)				
	HDAC1	HDAC2	HDAC3	HDAC6	HDAC8
SAHA[b]	33 ± 1	96 ± 10	20 ± 1	33 ± 3	540 ± 10
34b (*n*-butyl)	1,100 ± 100	1,300 ± 100	1,600 ± 100	320 ± 30	430 ± 10
34c (*n*-hexyl)	2,100 ± 100	2,500 ± 100	2,900 ± 300	410 ± 60	420 ± 20
34e (benzyl)	2,900 ± 300	3,500 ± 100	5,800 ± 800	270 ± 20	380 ± 20

[a] Mean IC_{50} value and standard error of at least three independent trials are shown (Figures C.53-C.55 and Tables C.3-C.5). [b] Previously reported IC_{50} values using the same assay procedure.[93]

4.4. *In cellulo* selectivity testing

To test the analogs in a more biological context, the C5-benzyl (**34e**) SAHA analog was tested for selectivity in cells. The inhibition of HDAC6 was monitored by detecting the levels of its known substrate acetyl-α-tubulin (AcTub), whereas Class I HDAC (HDAC1, 2, and 3) inhibition was monitored by observing the known substrate, acetyl-histone 3 (AcH3). SAHA or C5-benzyl SAHA **34e** were incubated

with U937 leukemia cells before lysis and western blot analysis of protein acetylation (Figure 4.3). As expected, SAHA increased the levels of both acetyl-α-tubulin and acetyl-histone H3 to a similar extent (Figure 4.3, lane 1), which is consistent with its non-selective inhibition of HDAC1, 2, 3, and 6 isoforms. On the other hand, C5-benzyl SAHA analog **34e** showed a dose-dependent selective increase in levels of acetyl-α-tubulin (Figure 4.3, lanes 3-5, AcTub), which was greater than the increased levels of acetyl histone H3 (Figure 4.3, lanes 3-5, AcH3) compared to the DMSO control (Figure 4.3, lane 2). The observed HDAC6 selectivity of the C5-benzyl SAHA **34e** in cells is consistent with the selectivity observed in the *in vitro* screening (Table 4.2 and Figure 4.3).

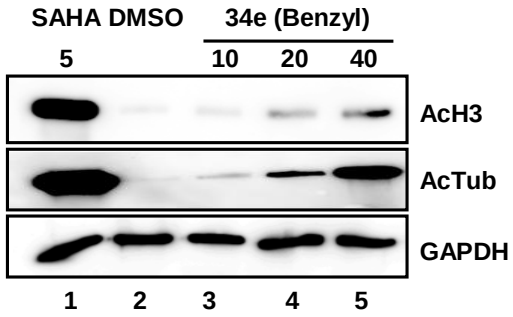

Figure 4.3. Cell based selectivity assessment of the C5-benzyl SAHA analog. Western blot analysis of acetyl-lysine 9 of histone H3 (AcH3), and acetyl-lysine 40 of α-tubulin (AcTub) after treatment with SAHA or C5-benzyl SAHA **34e**. U937 cells were treated with DMSO (1%), SAHA (5 μM), or increasing concentrations of C5-benzyl SAHA (**34e**) analog (10-40 μM), before lysis, SDS-PAGE separation, transfer to a PVDF membrane, and western analysis with AcH3 or AcTub antibodies. GAPDH levels in the samples were also probed as a gel load control. A DMSO control sample was included for comparison to inhibitor-treated samples. Repetitive trials are shown in Figure C.56.

4.5. *In vitro* cancer cell growth inhibition

To evaluate the ability of the C5-modified SAHA analogs to influence cell growth, the most selective analogs were tested. C5-*n*-butyl (**34b**), C5-*n*-hexyl (**34c**), and C5-benzyl (**34e**) SAHA analogs were tested at single concentrations using the

MTT assay with T-cell lymphoma derived cancer Jurkat cell line (Figure 4.4). The tested analogs displayed cytotoxicity against the cell line, with 39%, 24%, and 50% cell viability with C5-*n*-butyl SAHA (**34b**), C5-*n*-hexyl SAHA (**34c**), and C5-benzyl SAHA (**34e**) at 10 μM concentrations, respectively (Figure 4.4 and Table C.7). On the other hand, SAHA demonstrated higher cytotoxicity than the C5-modified SAHA analogs, with 49% cell viability at 1 μM. The reduced cytotoxicity of the analogs compared to SAHA can be due to their lower potency (8- to 12-fold reduction in IC_{50} values with HDAC6 compared to SAHA, Table 4.2). In addition, the nonselective inhibition of most HDAC isoforms by SAHA might contribute to its higher cytotoxicity (Table 4.2 and Figure 4.4).

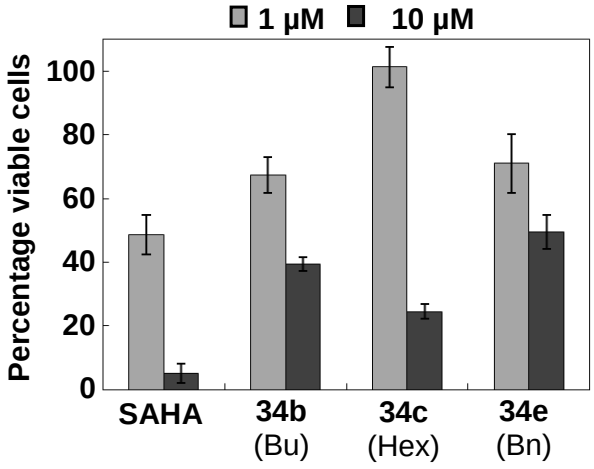

Figure 4.4. Cytotoxicity screening of SAHA and C5-modified SAHA analogs **34b**, **34c**, and **34e** with the Jurkat cells. Compounds were tested at 1 and 10 μM concentrations using MTT assay. Mean percent cell viability from a minimum of three independent trials with standard errors were plotted (Table C.7).

In conclusion, C5-modified SAHA analogs displayed dual HDAC6/8 selectivity. The best compound was C5-benzyl SAHA (**34e**), which showed up to 21-fold selectivity for HDAC6 and 8 compared to HDAC1, 2, and 3, and IC_{50} values of 270 and 380 nM with HDAC6 and 8, respectively. Compared to SAHA C5-modified

SAHA analogs **34b-e** exhibited 8- to 12-fold reduction in potency towards HDAC6, while similar IC_{50} values with HDAC8 were observed. C5-benzyl SAHA (**34e**) was tested for isoform selectivity in cells and showed selectivity consistent to what was observed *in vitro*. The fold selectivities observed with the C5-modified SAHA analogs were reduced compared to previously reported HDAC6/8-selective C2-modified SAHA analogs (49- to 300- fold selective for HDAC6 and 8 over HDAC1, 2, and 3 for the C2-hexyl SAHA).[112] On the other hand, the C5-modified SAHA analogs were more potent against HDAC6 and 8 (270 to 430 nM IC_{50} values) compared to C2-modifed SAHA analogs (600 to 2,000 nM IC_{50} values for C2-hexyl SAHA). Moreover, by comparing the effect of modifications on the C5 position of the linker region of SAHA to the C4 analogs mentioned in Chapter 3, we can conclude that modifying the C4 position led to more potent inhibition of both HDAC6 and HDAC8 compared to the C5 analogs (57 to 140 nM vs. 270 to 430 nM IC_{50} values for HDAC6 and 8) (Tables 3.2 and 4.2). In addition, the fold selectivities of the C4-SAHA analogs to HDAC6 and HDAC8 over HDAC1, 2, and 3 were higher compared to C5-SAHA analogs with the same modifications (171- to 740-fold vs. 3- to 21-fold for C4- and C5- butyl, hexyl, and benzyl)(Tables 3.2, 4.2, B.10 and C.6). The position of the modification in the linker region of SAHA is critical and can greatly affect both potency and selectivity of the analogs. In general, this study, along with chapters 2, 3, and previous reports[104-105, 112], indicate that modifying SAHA in the linker region can alter the selectivity of HDAC inhibitors. In particular, the reduced potency of SAHA against HDAC8 was switched in the C5-modified analogs to poor potency with HDAC1, 2, and 3, which resulted in dual HDAC6/8 preference. HDAC6/8 dual

selective inhibitors can be used as biological tools to study both HDAC6 and HDAC8-related cancer biology, and as leads for development of more effective anti-cancer agents targeting both HDAC6 and HDAC8.

4.6. Experimental Procedures

4.6.1. Materials and instrumentation

Details were provided in Section 2.7.1 of Chapter 2.

4.6.2. Synthesis procedure

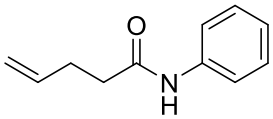

Synthesis of *N*-phenylpent-4-enamide (29): TBTU (614 mg, 1.91 mmol) was dissolved in dry dichloromethane (10 mL), followed by addition of pent-4-enoic acid **28** (127 mg, 1.27 mmol), DIPEA (329 mg, 2.55 mmol), and aniline (178 mg, 1.91 mmol). The reaction was stirred for 4.5 hours. The reaction was quenched with 1M HCl (20 mL) and extracted with dichloromethane (3X30 mL). The organic extract was dried over anhydrous Na_2SO_4 and concentrated. The product was purified by silica-gel flash chromatography (ethyl acetate/hexanes 1:4) to afford **29** (162 mg, 73%). ^{1}HNMR (400 MHz, $CDCl_3$) δ (ppm): 2.38 (m, 4H), 4.96 (d, *J* = 9.6 Hz, 1H), 5.02 (d, *J* = 16.4 Hz, 1H), 5.80 (m, 1H), 7.01 (t, *J* = 7.2 Hz, 1H), 7.22 (t, *J* = 8.0 Hz, 2H), 7.43 (d, *J* = 8.4 Hz, 2H), 7.57 (br s, 1H). ^{13}CNMR (100 MHz, $CDCl_3$) δ (ppm): 29.48, 36.74, 115.88, 119.99, 124.27, 128.95, 136.85, 137.90, 170.84. The spectral data for the synthesized compound was consistent with the reported data in literature.[141]

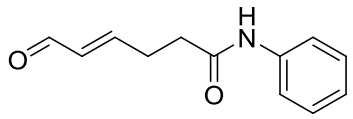

Synthesis of (E)-6-oxo-*N*-phenylhex-4-enamide (30): In a flame dried 2-neck 100 mL flask and condenser, air was replaced with argon and Grubbs' second-generation catalyst (58.2 mg, 0.068 mmol, 1.5 mol%) was dissolved in dry dichloromethane (20 mL), followed by the addition of crotonaldehyde **13** (3.20 g, 45.68 mmol) and **29** (800 mg, 4.57 mmol). The reaction was heated with reflux for 11 hours under argon. The reaction was cooled to room temperature, concentrated, and purified by silica-gel flash chromatography (ethyl acetate /Hexanes 1:1.5) to afford **30** (845 mg, 91%)**.** ^{1}HNMR (400 MHz, $CDCl_3$) δ (ppm): 2.56 (t, *J* = 7.2 Hz, 2H), 2.74 (q, *J* = 6.8 Hz, 2H), 6.14 (dd, *J* = 7.6 Hz, 1H), 6.91 (dt, *J* = 15.6 and 6.4 Hz, 1H), 7.11 (t, *J* = 7.2 Hz, 1H), 7.31 (t, *J* = 7.6 Hz, 2H), 7.50 (d, *J* = 7.6 Hz, 2H), 7.68 (br s, 1H), 9.49 (d, *J* = 7.6 Hz, 1H). ^{13}CNMR (100 MHz, $CDCl_3$) δ (ppm): 27.95, 34.94, 119.95, 124.53, 129.04, 133.22, 137.64, 156.71, 169.37, 194.03. IR: 3313, 3064, 2971, 2928, 1668, 1598, 1545, 1498, 757, 694 cm^{-1}. LRMS (ESI, *m/z*): calculated for $[M+H]^+$ $C_{12}H_{14}NO_2$, 204.10, found 204.14; calculated for $[M+Na]^+$ $C_{12}H_{13}NO_2Na^+$, 226.08, found 226.11.

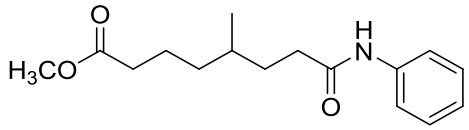

Synthesis of methyl 5-methyl-8-oxo-8-(phenylamino)octanoate (33a): In a 200 mL 2-neck dry flask, Copper(I)bromide dimethyl sulfide complex (1.52 g, 7.39 mmol) was dissolved in dry THF (20 mL). Air was replaced with argon, and then the temperature was reduced to -15°C. Methyllithium (9.12 mL of 1.6 M solution,

321 mg, 14.78 mmol) was added drop wise with stirring, and the mixture was allowed to stir for additional 20 minutes at -15°C. The temperature was then reduced to -78°C followed by the addition of chlorotrimethylsilane (2.40 g, 22.17 mmol) drop wise, and then **30** (500 mg, 2.46 mmol). The reaction was allowed to stir for 3.5 hours at -78°C. The reaction was quenched with a solution of saturated ammonium chloride in ammonia (1:1) portion wise until the reaction color turned blue. The organic layer was collected and the aqueous layer was extracted with ethyl acetate (3X30 mL). The combined organic layers were dried over anhydrous Na_2SO_4, filtered, and rotavaped to an oily crude product **31a**, which was used in the next reaction.

In a 200 mL 2-neck flame dried flask, air was replaced with argon, NaH (168 mg of 60% NaH, 4.19 mmol) dissolved in dry THF (25 mL) was added, and the reaction was cooled to 0°C. Trimethyl phosphonoacetate (763 mg, 4.19 mmol) was added dropwise with stirring. The reaction was allowed to stir for 15 minutes at 0°C, and then the crude product **31a** from the previous reaction dissolved in dry THF (8 mL) was added. The reaction was stirred for another 30 minutes at 0°C, followed by stirring for 90 minutes at room temperature. The reaction was quenched with a saturated aqueous ammonium chloride solution (15 mL) and the organic layer was collected. The aqueous layer was extracted with ethyl acetate (3 times with 30 mL) and the combined organic layers were dried over anhydrous $MgSO_4$, filtered, and concentrated. The crude product was used in the following reaction without further purification.

In a 50 mL flask the crude product from the previous reaction was dissolved in MeOH (20 mL), and then $Pd(OH)_2$ (173 mg of 20 wt.% $Pd(OH)_2$ on carbon, 0.25 mmol) was added. Air inside the flask was replaced with argon (3 times), and then with hydrogen gas (three times). The reaction was allowed to stir under hydrogen for 3.5 hours at room temperature. The reaction was filtered through a celite plug and the solvent was evaporated. The product was purified by silica-gel flash chromatography (ethyl acetate/hexanes 1:4) to afford **33a** (295 mg, 43% over three steps). ^{1}HNMR (400 MHz, CD_3OD) δ (ppm): 0.94 (d, *J* = 5.6 Hz, 3H), 1.19 (m, 1H), 1.35 (m, 1H), 1.50 (m, 2H), 1.70 (m, 3H), 2.36 (m, 4H), 3.64 (s, 3H), 7.07 (t, *J* = 7.6 Hz, 1H), 7.28 (t, *J* = 8.4 Hz, 2H), 7.53 (d, *J* = 8.0 Hz, 2H). ^{13}CNMR (100 MHz, CD_3OD) δ (ppm): 18.25, 22.04, 32.17, 32.38, 33.53, 34.27, 35.74, 50.58, 119.82, 123.69, 128.35, 138.51, 173.40, 174.52. IR: 3302, 2953, 2930, 2870, 1736, 1719, 1661, 1599, 1543, 1499, 1441, 754, 692 cm^{-1}. LRMS (ESI, *m/z*): calculated for $[M+H]^+$ $C_{16}H_{24}NO_3$, 278.18, found 278.18; calculated for $[M+Na]^+$ $C_{16}H_{23}NO_3Na^+$, 300.16, found 300.17.

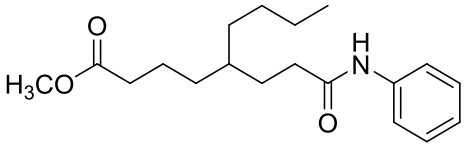

Synthesis of methyl 5-(3-oxo-3-(phenylamino)propyl)nonanoate (33b): The procedure was similar to **33a** except *n*-butyllithium (5.9 mL of 2.5 M solution, 0.95 g, 14.78 mmol) was used in place of methyllithium. The product was purified by silica-gel flash chromatography (ethyl acetate/hexanes 1:5) to afford **33b** (493 mg, 63% over three steps). ^{1}HNMR (400 MHz, CD_3OD) δ (ppm): 0.91 (t, *J* = 6.80 Hz, 3H), 1.35 (m, 9H), 1.64 (m, 4H), 2.33 (m, 4H), 3.64 (s, 3H), 7.07 (t, *J* = 7.2 Hz, 1H),

7.29 (t, *J* = 7.2 Hz, 2H), 7.53 (d, *J* = 7.2 Hz, 2H). ^{13}CNMR (100 MHz, CD_3OD) δ (ppm): 13.05, 21.63, 22.70, 28.47, 29.17, 32.37, 32.64, 33.59, 33.95, 36.79, 50.57, 119.82, 123.67, 128.34, 138.51, 173.40, 174.52. IR: 3302, 3138, 3062, 2955, 2928, 2860, 1737, 1721, 1663, 1600, 1543, 1499, 1442, 754, 692 cm^{-1}. LRMS (ESI, *m/z*): calculated for $[M+H]^+$ $C_{19}H_{30}NO_3$, 320.22, found 320.26; calculated for $[M+Na]^+$ $C_{19}H_{29}NO_3Na^+$, 342.20, found 342.26.

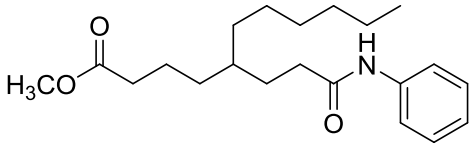

Synthesis of methyl 5-(3-oxo-3-(phenylamino)propyl)undecanoate (33c): The procedure was similar to **33a** except the following reagents were used: Copper(I)bromide dimethyl sulfide complex (1.37 g, 6.65 mmol), *n*-hexyllithium (5.78 mL of 2.3 M solution, 1.23 g, 13.30 mmol), chlorotrimethylsilane (2.16 g, 19.95 mmol), **30** (450 mg, 2.22 mmol), NaH (151 mg of 60% NaH, 3.77 mmol), trimethyl phosphonoacetate (686 mg, 3.77 mmol), and $Pd(OH)_2$ (156 mg of 20% $Pd(OH)_2$/C, 0.22 mmol). The product was purified by silica-gel flash chromatography (ethyl acetate/hexanes 1:6 to 1:5) to afford **33c** (577 mg, 75% over three steps). ^{1}HNMR (400 MHz, CD_3OD) δ (ppm): 0.89 (t, *J* = 7.2 Hz, 3H), 1.33 (m, 13H), 1.63 (m, 4H), 2.33 (m, 4H), 3.64 (s, 3H), 7.06 (t, *J* = 7.6 Hz, 1H), 7.28 (t, *J* = 7.6 Hz, 2H), 7.54 (d, *J* = 7.2 Hz, 2H). ^{13}CNMR (100 MHz, CD_3OD) δ (ppm): 13.10, 21.63, 22.36, 26.19, 29.18, 29.42, 31.65, 32.38, 32.95, 33.61, 33.99, 36.79, 50.60, 119.81, 123.66, 128.35, 138.54, 173.40, 174.49. IR: 3302, 3138, 3061, 2953, 2926, 2856, 1737, 1661, 1600, 1543, 1499, 1441, 754, 692 cm^{-1}. LRMS (ESI, *m/z*): calculated for $[M+H]^+$

$C_{21}H_{34}NO_3$, 348.25, found 348.28; calculated for $[M+Na]^+$ $C_{21}H_{33}NO_3Na^+$, 370.24, found 370.26.

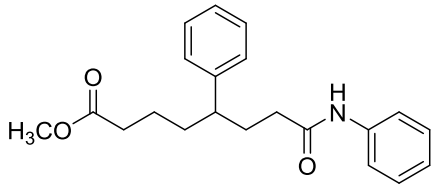

Synthesis of methyl 8-oxo-5-phenyl-8-(phenylamino)octanoate (33d): The procedure was similar to **33a** except the following reagents were used: phenyllithium (7.38 mL of 2 M solution, 1.24 g, 14.78 mmol) and $Pd(OH)_2$ (692 mg of 20% $Pd(OH)_2$/C, 0.99 mmol). The product was purified by silica-gel flash chromatography (ethyl acetate/hexanes 1:3) to afford **33d** (539 mg, 64% over three steps). ^{1}HNMR (500 MHz, CD_3OD) δ (ppm): 1.46 (m, 2H), 1.63 (m, 2H), 1.89 (m, 1H), 2.15 (m, 5H), 2.58 (m, 1H), 3.59 (s, 3H), 7.05 (t, 1H), 7.18 (d, *J* = 7.2 Hz, 3H), 7.27 (m, 4H), 7.48 (d, *J* = 8.0 Hz, 2H). ^{13}CNMR (125 MHz, CD_3OD) δ (ppm): 22.68, 32.22, 33.27, 34.61, 35.84, 45.24, 50.54, 119.81, 123.63, 126.06, 127.44, 128.21, 128.31, 138.46, 144.25, 172.85, 174.35. IR: 3303, 3137, 3028, 2928, 2859, 1737, 1663, 1600, 1545, 1500, 756, 693 cm^{-1}. LRMS (ESI, *m/z*): calculated for $[M+H]^+$ $C_{21}H_{26}NO_3$, 340.19, found 340.14; calculated for $[M+Na]^+$ $C_{21}H_{25}NO_3Na^+$, 362.17, found 362.12.

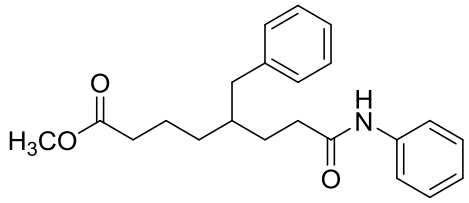

Synthesis of methyl 5-benzyl-8-oxo-8-(phenylamino)octanoate (33e): The procedure was similar to **33a** except benzylmagnesium chloride (14.78 mL of 1 M solution, 2.23 g, 14.78 mmol) was used in place of methyllithium. The product was

purified by silica-gel flash chromatography (ethyl acetate/hexanes 1:3) to afford **33e** (274 mg, 32% over three steps). ^{1}HNMR (400 MHz, CD_3OD) δ (ppm): 1.31 (q, *J* = 5.6 Hz, 2H), 1.67 (m, 5H), 2.26 (t, *J* = 7.2 Hz , 2H), 2.39 (m, 2H), 2.60 (m, 2H), 3.61 (s, 3H), 7.07 (t, *J* = 7.2 Hz, 1H), 7.15 (m, 3H), 7.26 (m, 4H), 7.51 (d, *J* = 8.4 Hz, 2H). ^{13}CNMR (100 MHz, CD_3OD) δ (ppm): 21.50, 28.93, 31.87, 33.50, 33.94, 39.08, 39.69, 50.54, 119.88, 123.70, 125.47, 127.86, 128.34, 128.81, 138.47, 140.74, 173.24, 174.47. IR: 3302, 3027, 2927, 2866, 1734, 1661, 1599, 1542, 1498, 1442, 755, 694 cm^{-1}. LRMS (ESI, *m/z*): calculated for $[M+H]^+$ $C_{22}H_{28}NO_3$, 354.21, found 354.20; calculated for $[M+Na]^+$ $C_{22}H_{27}NO_3Na^+$, 376.19, found 376.19.

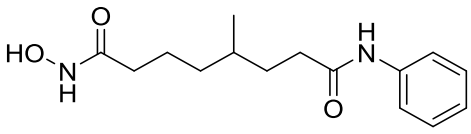

Synthesis of *N*^{8}-hydroxy-4-methyl-*N*^{1}-phenyloctanediamide (34a): In an acid-washed flask, hydroxylamine HCl (877 mg, 12.60 mmol) was dissolved in MeOH (10 mL). KOH (1.42 g, 25.24 mmol) was added at 0°C and left to stir for 20 minutes. An alcoholic solution of **33a** (350 mg, 1.26 mmol, in 10 mL methanol) was added and the reaction was left to stir for 2.5 hours at 0°C. The pH of the reaction mixture was adjusted to 6.0 with concentrated aqueous HCl, followed by dilution with distilled de-ionized water (30 mL). The reaction was extracted with ethyl acetate (3X30 mL). The organic extracts were collected together and dried over anhydrous Na_2SO_4. The product was purified with acid-washed silica-gel flash chromatography (acetone/DCM 1:3) to afford **34a** (214 mg, 61%). ^{1}HNMR (400 MHz, CD_3OD) δ (ppm): 0.94 (d, *J* = 6.4 Hz, 3H), 1.21 (m ,1H), 1.39 (m, 1H), 1.48-1.78 (m, 5H), 2.08 (t, *J* = 7.6 Hz, 2H), 2.38 (m, 2H), 7.07 (t, *J* = 7.2 Hz, 1H), 7.28 (t, *J* = 7.6

Hz, 2H), 7.52 (d, *J* = 7.6 Hz, 2H). ^{13}CNMR (100 MHz, CD_3OD) δ (ppm): 18.26, 22.75, 32.09, 32.37, 32.50, 34.24, 35.68, 119.87, 123.69, 128.33, 138.50, 171.54, 173.43. IR: 3291, 2955, 2928, 2871, 1736, 1660, 1600, 1546, 1500, 1444, 756, 693 cm^{-1}. HRMS (ESI-TOF, *m/z):* calculated for $[M+Na]^+$ $C_{15}H_{22}N_2O_3Na^+$, 301.1528, found 301.1540. HPLC analytical purity analysis 97.1%.

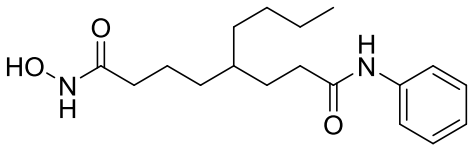

Synthesis of 4-butyl-*N*^{8}-hydroxy-*N*^{1}-phenyloctanediamide (34b): The procedure was similar to **34a** except for the following: MeOH (15 mL), hydroxylamine HCl (1.0 g, 14.46 mmol), KOH (1.62 g, 28.92 mmol), **33b** (462 mg, 1.45 mmol). The reaction was stirred for 2 hours at 0°C. The product was purified with acid-washed silica-gel flash chromatography (acetone/DCM 1:4) to afford **34b** (363 mg, 78%). ^{1}HNMR (400 MHz, CD_3OD) δ (ppm): 0.91 (t, *J* = 6.8 Hz, 3H), 1.34 (m, 9H), 1.65 (m, 4H), 2.08 (t *J* = 7.6 Hz, 2H), 2.35 (t, *J* = 7.2 Hz, 2H), 7.07 (t, *J* = 7.2 Hz, 1H), 7.29 (t, *J* = 7.2 Hz, 2H), 7.53 (d, *J* = 8.0 Hz, 2H). ^{13}CNMR (100 MHz, CD_3OD) δ (ppm): 13.06, 22.34, 22.70, 28.49, 29.18, 32.31, 32.57, 32.70, 33.92, 36.73, 119.85, 123.70, 128.35, 138.51, 171.56, 173.50. IR: 3242, 2955, 2926, 2858, 1645, 1599, 1543, 1499, 1443, 1047, 754, 691 cm^{-1}. HRMS (ESI-TOF, *m/z):* calculated for $[M+Na]^+$ $C_{18}H_{28}N_2O_3Na^+$, 343.1998, found 343.1988. HPLC analytical purity analysis 98.0%.

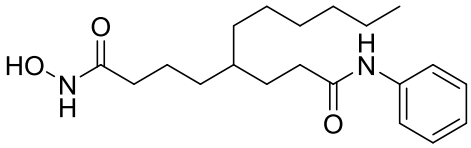

Synthesis of 4-hexyl-*N*^{8}-hydroxy-*N*^{1}-phenyloctanediamide (34c): The procedure was similar to **34a** except for the following: hydroxylamine HCl (1.06 g, 15.20 mmol), KOH (1.71 g, 30.40 mmol), **33c** (529 mg, 1.52 mmol). The reaction was stirred for 3 hours at 0°C. The product was purified with acid-washed silica-gel flash chromatography (acetone/DCM 1:4) to afford **34c** (326 mg, 61%). ^{1}HNMR (400 MHz, CD_3OD) δ (ppm): 0.88 (t, *J* = 6.8 Hz, 3H), 1.35 (m, 13 H), 1.64 (m, 4H), 2.08 (t, *J* = 7.2 Hz, 2H), 2.35 (t, *J* = 7.6 Hz, 2H), 7.07 (t, *J* = 7.2 Hz, 1H), 7.28 (t, *J* = 8.0 Hz, 2H), 7.53 (d, *J* = 8.0 Hz, 2H). ^{13}CNMR (100 MHz, CD_3OD) δ (ppm): 13.04, 22.33, 22.36, 26.22, 29.19, 29.40, 31.63, 32.36, 32.58, 33.04, 33.95, 36.75, 119.89, 123.70, 128.34, 138.50, 171.56, 173.49. IR: 3243, 3199, 3061, 2953, 2925, 2856, 1651, 1600, 1545, 1499, 1443, 755, 692 cm^{-1}. HRMS (ESI-TOF, *m/z):* calculated for $[M+Na]^+$ $C_{20}H_{32}N_2O_3Na^+$, 371.2311, found 371.2311. HPLC analytical purity analysis 96.7%.

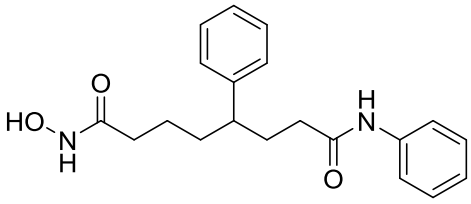

Synthesis of *N*^{8}-hydroxy-*N*^{1},4-diphenyloctanediamide (34d): The procedure was similar to **34a** except for the following: hydroxylamine HCl (1.08 g, 15.50 mmol), KOH (0.87 g, 15.50 mmol), **33d** (526 mg, 1.55 mmol). The reaction was stirred overnight at room temperature, then another 820 mg KOH was added and left to stir for 7 hours. The product was purified with acid-washed silica-gel flash chromatography (acetone/DCM 1:3) to afford **34d** (329 mg, 62%). ^{1}HNMR (500

MHz, CD_3OD) δ (ppm): 1.35 (m, 2H), 1.57 (m, 2H), 1.81 (m, 1H), 2.02 (m 5H), 2.49 (m, 1H), 6.95 (t, *J* = 7.5 Hz, 1H), 7.08 (m, 3H), 7.18 (m, 4H) 7.38 (d, *J* = 8.5 Hz, 2H). ^{13}CNMR (125 MHz, CD_3OD) δ (ppm): 23.47, 32.14, 32.28, 34.59, 35.92, 45.20, 119.84, 123.66, 126.06, 127.45, 128.22, 128.31, 138.44, 144.26, 171.40, 172.91. IR: 3255, 3065, 3022, 2906, 2847,1683, 1600, 1541, 1499, 1442, 552, 686 cm^{-1}. HRMS (ESI-TOF, *m/z):* calculated for $[M+Na]^+$ $C_{20}H_{24}N_2O_3Na^+$, 363.1685, found 363.1680. HPLC analytical purity analysis 96.0%.

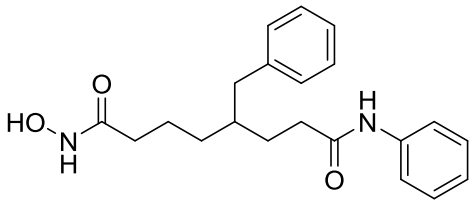

Synthesis of 4-benzyl-*N*^{8}-hydroxy-*N*^{1}-phenyloctanediamide (34e): The procedure was similar to **34a** except for the following: hydroxylamine HCl (522 mg, 7.50 mmol), KOH (842 mg, 15.00 mmol), **33e** (265 mg, 0.75 mmol). The reaction was stirred for 2 hours at 0°C, followed by the second addition of hydroxylamine HCl (522 mg, 7.50 mmol), KOH (842 mg, 15.00 mmol) and stirring for additional 3.5 hours at 0°C. The product was purified with acid-washed silica-gel flash chromatography (acetone/DCM 1:3) to afford **34e** (183 mg, 69%). ^{1}HNMR (400 MHz, CD_3OD) δ (ppm): 1.32 (q, *J* = 8.0 Hz, 2H), 1.69 (m, 5H), 2.02 (m, 2H), 2.39 (m, 2H), 2.59 (m, 2H), 7.07 (t, *J* = 7.6 Hz, 1H), 7.14 (m, 3H), 7.23 and 7.28 (overlapped t and t, *J* = 7.2 and 7.6 Hz, 4H), 7.51 (d, *J* = 7.6 Hz, 2H). ^{13}CNMR (100 MHz, CD_3OD) δ (ppm): 22.19, 28.91, 31.86, 32.50, 33.90, 39.00, 39.70, 119.89, 123.72, 125.48, 127.89, 128.35, 128.82, 138.46, 140.72, 171.46, 173.29. IR: 3244, 3061, 3026, 2923, 2867, 1638, 1599, 1542, 1498, 1443, 754, 700 cm^{-1}. HRMS (ESI-TOF, *m/z):* calculated

for $[M+Na]^+$ $C_{21}H_{26}N_2O_3Na^+$, 377.1841, found 377.1831. HPLC analytical purity analysis 98.7%.

4.6.3. Procedures for biological screenings

4.6.3.1. HeLa cell lysis

Details were provided in Section 2.7.3.1 of Chapter 2.

4.6.3.2. Global HDAC inhibition

Details were provided in Section 3.6.3.2 of Chapter 3. Results are reported in Figures 4.2 and C.52, and Tables 4.2 and C.1.

4.6.3.3. Inhibitor testing with HDAC isoforms [93]

Details were provided in Section 2.7.3.2 of Chapter 2. Results are reported in Figures 4.2 and C.53-C.55, and Tables 4.2 and C.2-C.5.

4.6.3.4. *In cellulo* selectivity testing

Details were provided in Section 2.7.3.3-2.7.3.5 of Chapter 2. Results are reported in Figures 4.3 and C.56.

4.6.3.5. *In vitro* cell growth inhibition

Details were provided in Section 2.7.3.6 of Chapter 2. Results are reported in Figure 4.4 and Table C.7.

CHAPTER 5 - DOCKING STUDY OF *N*-SUBSTITUTED SAHA ANALOGS [102]

Some of the text in this chapter was reprinted or modified from: Bieliauskas, A. V.; Weerasinghe, S. V. W.; Negmeldin, A. T.; Pflum, M. K. H., Structural Requirements of Histone Deacetylase Inhibitors: SAHA Analogs Modified on the Hydroxamic Acid, *Archiv der Pharmazie (Weinheim, Ger.)* **2016,** *349*, 373-382.

5.1. Rationale for synthesis, screening, and docking of *N*-substituted SAHA analogs (35 a-e)

Towards creating isoform selective inhibitors, the three structural regions of HDAC inhibitors (Figure 5.1) have been modified, focusing primarily on the capping region and metal binding moiety.[12] The high sequence similarity within the active sites of the isoforms makes inhibitor design problematic.[12] Recently, the structures of HDAC1, HDAC2, HDAC3, HDAC4, HDAC6, HDAC7 and HDAC8 were reported, [13-21] along with homology models of the other HDAC isoforms.[22-23] According to structural analysis, a 14Å internal cavity exists deep within the HDAC active site near the catalytic metal atom, which functions as an exit channel for release of the acetate byproduct after acetyl-lysine deacetylation (see section 1.4 in Chapter 1).[98, 142-143] Important for inhibitor development, several compounds have been designed to target the internal cavity by appending large aromatic groups to the metal binding moiety.[19, 144-145] For example, **Cpd-60** (Figure 5.1) displays selectivity for HDAC1 and HDAC2 compared to HDAC3-8 (Table 1.1) .[84, 92] Docking studies of **Cpd-60** into the HDAC1 and HDAC3 homology models suggested that selectivity was due to differential interactions of the aryl group on the metal binding group with residues in the 14Å internal cavity.[84] A significant conclusion of these studies is that the metal binding moiety can be modified to create selective HDAC inhibitors.

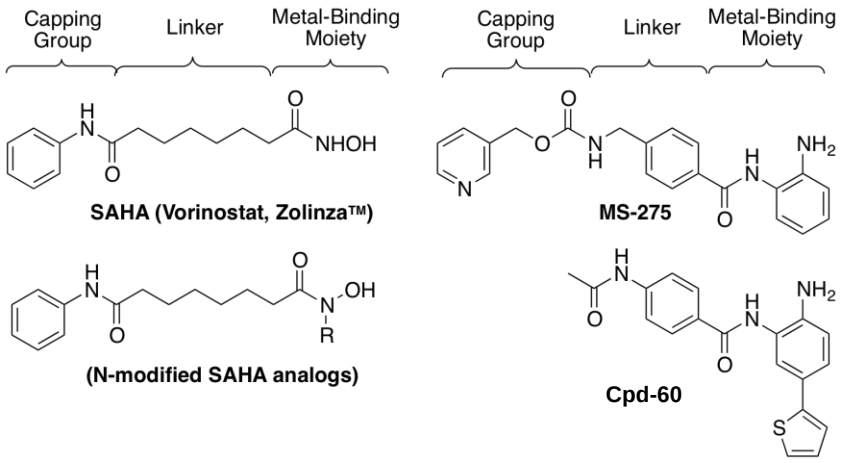

Figure 5.1. Structures of select HDAC inhibitors with the structural regions indicated at the top.

To further exploit the 14 Å internal cavity for selective inhibitor design, we created SAHA analogs functionalized on the amine of the hydroxamic acid metal binding moiety. Like the benzamide of **Cpd-60** [19], crystallographic and modeling analyses indicate that the hydroxamic acid is positioned at the base of the active site channel adjacent to the internal cavity.[15-16, 19-23, 25, 99-100] Given the HDAC1/2 selectivity of **Cpd-60** [84], we hypothesized that alkyl or aryl groups attached to the hydroxamic acid of SAHA would also impart selectivity.

In this work, *N*-substituted SAHA analogs (Figure 5.1) were synthesized by Dr. Anton Bieliauskas and screened by Dr. Sujith Weerasinghe to explore the effect of hydroxamic acid substitution on the activity and selectivity of SAHA.[102] The *N*-substituted SAHA analogs displayed reduced potency and solubility, but greater selectivity, compared to SAHA.

To assess selectivity, the analogs were screened by Dr. Sujith Weerasinghe against three individual HDAC isoforms, HDAC 1, HDAC3, and HDAC6.[102] HDAC1 and HDAC3 were included because **Cpd-60** was able to discriminate between them

in prior work.[84, 92] HDAC6 was also tested to assess class II selectivity. The analogs were initially screened against the isoforms at a single concentration of 125 μM (Figure 5.2). The compounds containing aliphatic substituents (**35a**, methyl, and **35b**, pentyl) displayed little to no isoform selectivity, similar to SAHA.[78] Likewise, the *N*-homobenzyl analog **35d** also showed roughly similar potency against the isoforms. In contrast, the *N*-benzyl **35c** and N-biphenyl **35e** variants displayed some degree of HDAC1 selective inhibition, similar to **Cpd-60**. Among these two analogs, N-biphenyl SAHA **35e** demonstrated the most selectivity, with 58 ± 2% activity remaining with HDAC1, but statistically insignificant inhibition observed with both HDAC3 and HDAC6. The single concentration selectivity screen points to *N*-biphenyl **35e** as an HDAC1 selective inhibitor, similar to compound **Cpd-60**.

Based on the observation that the benzyl **35c** and biphenyl **35e** variants displayed some level of HDAC1 selectivity at 125 μM concentration, IC_{50} values were determined by Dr. Sujith Weerasinghe (Table 5.1).[102] As expected,[78] the pan-inhibitor SAHA displayed less than a 1.5-fold preference for any HDAC isoform tested.[104] The benzyl variant **35c** displayed slightly greater selectivity for HDAC1 versus HDAC3 (2.5-fold). Interestingly, the *N*-biphenyl variant **35e** displayed preferential inhibition for HDAC1 with an IC_{50} for HDAC1 of 233 ± 40 μM. Unfortunately, due to solubility issues at high concentrations, IC_{50} values for HDAC3 and HDAC6 could not be determined. However, at the highest concentration possible (250 μM), no inhibitory activity was observed with either HDAC3 or HDAC6 (Table 5.1), suggesting a preference for HDAC1.

Docking studies discussed here were done to account for the lower potency and the enhanced selectivity observed with the *N*-substituted SAHA analogs. Docking studies showed that the *N*-substituent accesses the 14 Å internal cavity to impart preferential inhibition of HDAC1. These studies with *N*-substituted SAHA analogs are consistent with the strategy exploiting the 14Å internal cavity of HDAC proteins to create HDAC1/2 selective inhibitors.

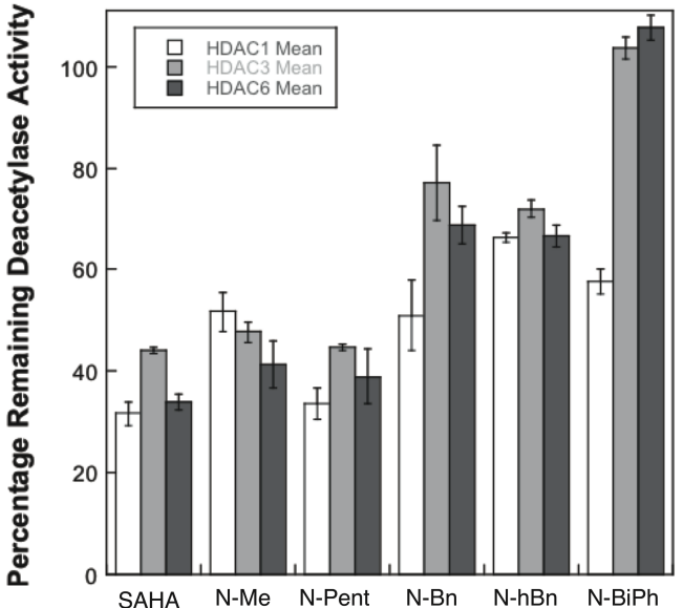

Figure 5.2. HDAC inhibitory activities of the *N*-modified SAHA analogs were measured at 125 μM against HDAC1, HDAC3 and HDAC6. Data provided by Dr. Sujith Weerasinghe).[102]

Table 5.1. IC_{50} values for SAHA, *N*-benzyl **35c**, and *N*-biphenyl **35e** against HDAC1, HDAC3, and HDAC6.[a]

	HDAC1	HDAC3	HDAC6
SAHA	96 ± 16 nM	146 ± 12 nM	74 ± 9 nM
35c	177 ± 21 μM	440 ± 23 μM	287 ± 9 μM
35e	233 ± 40 μM	105 ± 2 %[b]	108 ± 3 %[b]

[a]Values are the means of at least three independent trials with standard error. [b]Deacetylase activity remaining at 250 μM concentration of inhibitor is shown because solubility issues prevented IC_{50} value determination. Data provided by Dr. Sujith Weerasinghe.[102]

5.2. Docking studies with HDAC1 and HDAC3 crystal structures

Docking studies were performed to rationalize the lower potency and HDAC1 selectivity of the *N*-modified SAHA analogs. SAHA, along with the *N*-pentyl **35b** and N-biphenyl **35e** analogs, were docked into the HDAC1 crystal structure.[99] SAHA maintained five interactions (1.1 to 3.8 Å distances) with the bound Zn^{2+} metal and nearby amino acids (H140, H141, and Y303, Figure 5.3A, see residues in blue). In contrast, the *N*-pentyl **35b** variant maintained only three of these interactions (with Zn^{2+}, H141, and Y303, Figure 5.3B), while the *N*-biphenyl **2e** analog displayed only two (with Zn^{2+} and Y303, Figure 5.3C). The loss of hydrogen binding capability of the hydroxamic acid amine likely accounts for the fewer stabilizing interactions with the analogs. In addition, the orientation of the hydroxamic acid is also altered by the *N*-modification. Specifically, SAHA positions the carbonyl adjacent to Y303, the amine near H141, and the hydroxyl next to H140. Due to the *N*-modification, the hydroxyl amine orientation is flipped, with *N*-pentyl **35b** positioning the hydroxyl near H141. Likewise, the *N*-biphenyl analog adopts an alternative pose with the carbonyl interacting with Zn^{2+} and the hydroxyl interacting with Y303. The docking experiments point towards fewer interactions between the hydroxamic acid and the active site, likely due to flipping of the *N*-modification into the 14Å cavity and loss of hydrogen bonding capability of the modified amine, which account for the reduced potency.

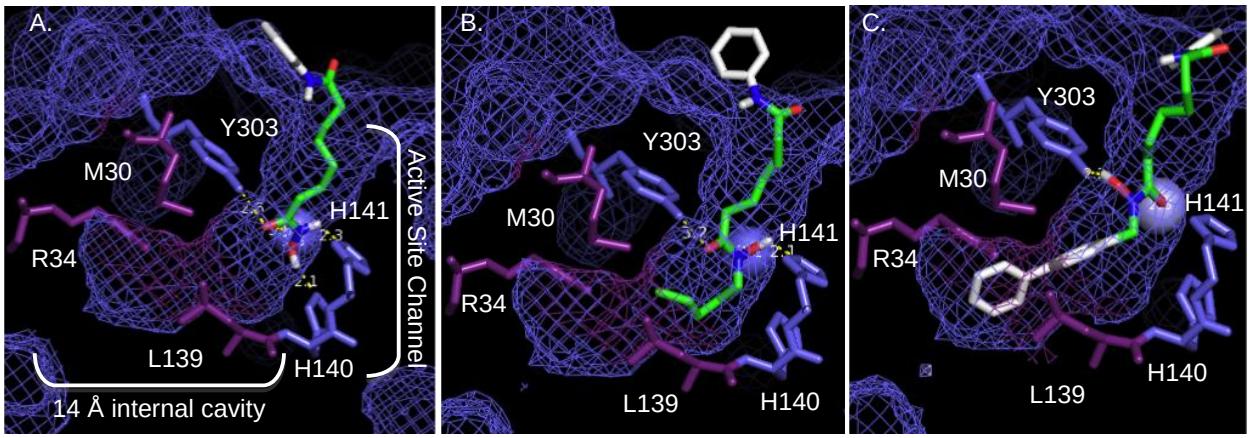

Figure 5.3. Docking of SAHA (A), *N*-pentyl SAHA **35b** (B), and N-biphenyl SAHA **35e** (C) into the HDAC1 crystal structure (PBD 4BKX). The HDAC structure is represented as blue mesh, the Zn^{2+} metal as a blue orb, and the inhibitor and amino acids as ball and sticks. The atoms of the inhibitor are color-coded (C= green/white; O = red; N = blue, H = white).

In addition to the loss of bonding interactions, another significant observation from the docking studies is the positioning of the *N*-modification within the 14Å internal cavity. The narrowest section of the cavity is created by M30, R34, and L139 (Figure 5.3A and Figure 5.4A, see resides in purple). While the pentyl group of **35b** is positioned up to this constricted point in the cavity (Figure 5.3B), the biphenyl group of **35e** extends beyond the narrow opening (Figure 5.3C). Therefore, the reduced potency of *N*-biphenyl SAHA **35e** may also be due to the narrowing of the cavity near M30, R34 and L139 to constrict binding (Figure 5.4A). Consistent with the extent and orientation of interactions, the energies of the inhibitor/HDAC1 complexes for SAHA, *N*-pentyl SAHA **35b,** and *N*-biphenyl SAHA **35e** were -5.46, -4.25, and -3.28 kcal/mole, respectively. The energies are consistent with the experimental data indicating that SAHA is the most potent compound, whereas the N-biphenyl **35e** analog is the least potent (Table 5.1).

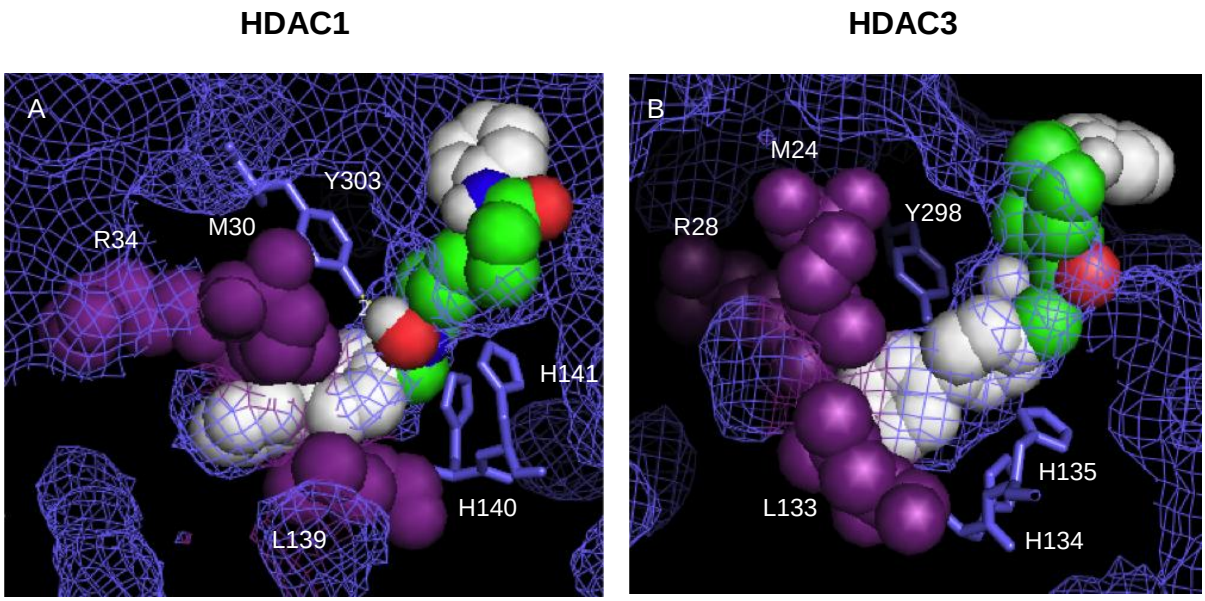

Figure 5.4. Docking of *N*-biphenyl SAHA **35e** into the crystal structures of HDAC1 and HDAC3. (A) This image is identical to that in Figure 5.3C, except that SAHA, M30, R34, and L139 are shown as space filling models. (B) This image is identical to that in Figure 5.5C, except that SAHA, M24, R28, and L133 are shown as space filling models. The HDAC structure is represented as blue mesh, while amino acids interacting with the hydroxamic acid in HDAC1 are shown as blue ball and sticks. The atoms on the inhibitor are color-coded (C= green/white; O = red; N = blue, H = white).

The docking studies were further analyzed to explain the enhanced preference of **35e** compared to SAHA and **35b** (Table 5.2). Prior docking analysis with **Cpd-60** suggested that selectivity for HDAC1 compared to HDAC3 was a result of congestion in the 14 Å cavity due to a tyrosine in HDAC3; HDAC1 contains serine at the same position, which allows the cavity to accommodate bulky aromatic groups.[84] Docking of SAHA into the HDAC3 structure revealed that Y107 is positioned relatively distant to the 14Å cavity (Figure 5.5A).[100] Likewise, S113 in the HDAC1 crystal structure is also located adjacent to the cavity (Figure 5.6). In addition, previous mutagenesis studies indicated that S113 is only partially responsible for the potency of **Cpd-60** with HDAC1.[98]

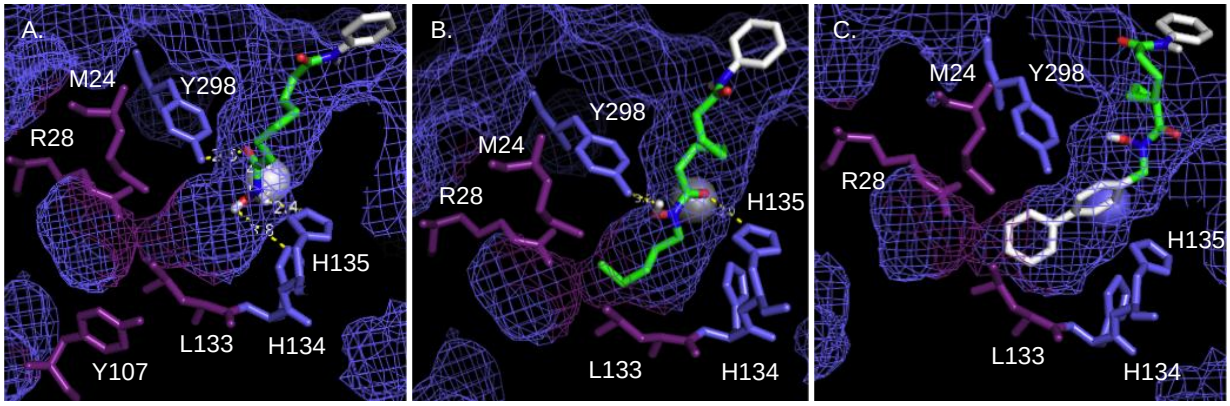

Figure 5.5. Docking of SAHA (A), *N*-pentyl SAHA **35b** (B), and *N*-biphenyl SAHA **35e** (C) into the HDAC3 crystal structure (PBD 4A69). The HDAC structure is represented as blue mesh, the Zn^{2+} metal as a grey orb, and the inhibitor and amino acids as ball and sticks. The atoms of the inhibitor are color-coded (C= green/white; O = red; N = blue, H = white).

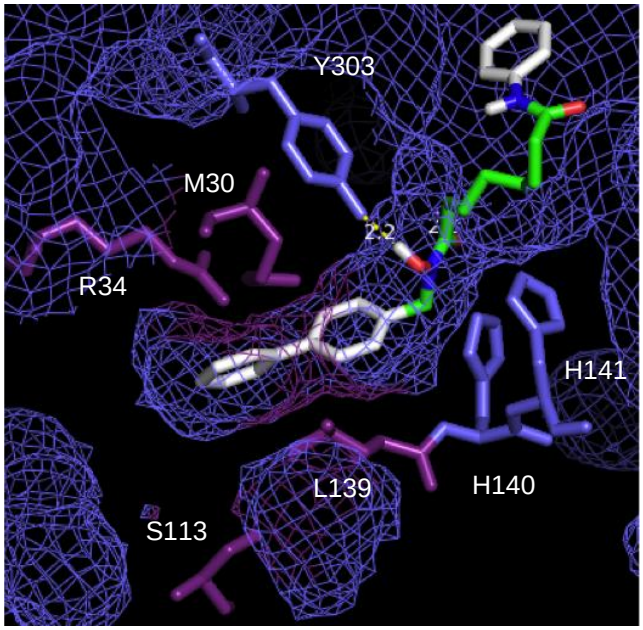

Figure 5.6. Docking of *N*-biphenyl **35e** into the HDAC1 crystal structure (PBD 4BKX). The HDAC structure is represented as blue mesh, the Zn^{2+} metal as a grey orb, and the inhibitor and amino acids as ball and sticks. The atoms on the inhibitor are color-coded (C= green/white; O = red; N = blue, H = white). This image is identical to that in Figure 5.3C, except that S113 is shown here.

An alternative hypothesis explaining the HDAC1 preference of **Cpd-60** and HDAC1 preference of *N*-biphenyl SAHA **35e** emerges when considering the narrowest point in the 14Å internal cavities of HDAC1 and HDAC3. HDAC3

maintains a considerably more constricted 14Å internal cavity than HDAC1 (compare Figures 5.3A to Figure 5.5A and 54.A to 5.4B). The residues M24, R28, and L133 of HDAC3 appear to block the cavity and may restrict access to bulky *N*-modified inhibitors. Docking of *N*-biphenyl **35e** into the HDAC3 crystal structure produced no poses that were consistent with the expected metal/hydroxamic binding interaction. Instead, the biphenyl group was positioned up to the narrowest section of the cavity, near M24, R28, and L133 of HDAC3 (Figure 5.4B and Figure 5.5C). In this case, the biphenyl group is unable to extend beyond the constricted region to access the 14 Å internal cavity of HDAC3, as was seen with HDAC1 (Figure 5.3C and Figure 5.4A). As a result of the blocked cavity, the hydroxamic acid is positioned at the outside edge of the active site channel, unable to interact with the metal ion. Therefore, docking suggests that the poor potency observed with **35e** and HDAC3 is due to restricted access of the *N*-biphenyl to the 14Å internal cavity, which prevents favorable metal/hydroxamic acid interactions. In contrast, the straight chain *N*-pentyl analog **35b** is positioned up to the constriction point (Figure 5.5B), similar to HDAC1 (Figure 5.3B), which allows effective binding and better potency. In total, the docking studies are consistent with accessibility of the 14Å cavity to large aromatic groups as a significant factor leading to the HDAC1 preference of inhibitors bearing substituents on the metal binding group, including **Cpd-60** and *N*-biphenyl SAHA **35e**.

In conclusion, *N*-modified SAHA analogs (**35a-e**) displayed significantly reduced potency compared to the parent SAHA. Interestingly, the benzyl and pentyl substituents are tolerated to a greater extent than any of the other *N*-substituted

analogs. Docking studies are consistent with the pentyl groups accessing the 14Å internal cavities of HDAC1 and HDAC3 (Figure 5.3B and 5.5B). However, the additional interactions in the cavity were unable to overcome the lost hydrogen bonding due to the presence of the *N*-modification. The results suggest that any group, regardless of size, incorporated directly on the hydroxamic acid will result in decreased inhibitory activity compared to the unsubstituted analog. These studies are consistent with prior work reporting reduced potencies of HDAC inhibitors as a result of *N*-methylation of the hydroxamic acid group.[146-147]

While the *N*-modified SAHA analogs showed reduced potency compared to SAHA, one compound displayed selectivity. The *N*-biphenyl variant **35e** showed preference for HDAC1 over HDAC3 and HDAC6. Docking analysis with the HDAC1 and HDAC3 crystal structures suggests that that accessibility to the 14Å internal cavity is differentially restricted, leading to preferential binding to HDAC1 over HDAC3. Therefore, the combined experimental and computation analysis of *N*-modified SAHA analogs further validates the concept of creating isoform-selective HDAC inhibitors by positioning aromatic substituents in the 14Å internal cavity. These studies guide future inhibitor design by suggesting that additional substituted metal binding groups can be created to take advantage of the altered cavity accessibility of the HDAC isoforms.

5.3. Experimental procedure

5.3.1. Docking procedure

Crystal structures for HDAC1 and HDAC3 were downloaded from the RCSB protein data bank (HDAC1: 4BKX and HDAC3: 4A69). PyMOL (Schrodinger, LLC) was used to delete the MTA1 corepressor chain, acetate, potassium and sulfate ions

in HDAC1 crystal structure. In the case of the HDAC3 crystal structure, the water molecules, chain A, deacetylase-activation-domain (DAD) (from the SMRT corepressor), glycerol, D-myo-inositol-1,4,5,6-tetrakisphosphate molecules, acetate, potassium and sulfate ions were deleted. AutoDockTools-1.5.4 program [119, 127] was used to add all hydrogen atoms, modify histidine protonation (H140 and H141 residues for HDAC1, His134 His135 for HDAC3) by adding only HD1, compute Gasteiger charges, and merge all non polar hydrogen, followed by generation of the pdbqt output file. The charge of the zinc atom was manually changed from zero to +2. A grid box with a spacing of 0.375 Å, size of 56 x 42 x 38, and coordinates for the center of the grid box (-48.000, 18.000, -3.750) were used for HDAC1, while the values for HDAC3 were 58 x 58 x 54 and (8.166, 76.663, 21.318). All docking procedure and parameters were similar to what mentioned in Chapter 2, Section 2.7.4.

CHAPTER 6 - SYNTHESIS AND SCREENING OF BIARYL INDOLYL BENZAMIDE HDAC INHIBITORS

6.1. Rationale for design, synthesis and screening of biaryl indolyl benzamide HDAC inhibitors

The objective of this project was to generate HDAC1-selective inhibitors to study HDAC1-related cancer biology. No selective inhibitor for HDAC1 has been identified to date. Rational design of HDAC1-selective inhibitors is a challenge due to the high sequence similarity and active site similarity between HDAC1 and HDAC2.[12] In addition to studying HDAC1-related cancer biology, creating HDAC1-selective inhibitors will be a step forward in the development of HDAC1-selective anticancer drugs, which can lead to more effective cancer treatment compared to non-selective inhibitors or inhibitors that are selective for more than one HDAC isoform.

Several HDAC1/HDAC2 selective inhibitors have been reported.[84, 92] Most of the HDAC1/2 selective inhibitor are benzamide derivatives, where the metal binding group is a 1,2-diamino benzamide chelating group (such as **Cpd-60,** an HDAC1/2 selective inhibitors (Figure 6.1)). According to literature, the selectivity of the HDAC1/2 benzamide inhibitors came from the use of bulky aromatic rings (Figure 6.1, red rings in **Cpd-60**), which will not fit in the 14 Å channel of HDAC3 protein.[84, 102] The presence of the biaryl group can impart selectivity to HDAC1 and 2 over HDAC3, and can be used to develop an HDAC1-selective inhibitor.

In 2012, several hydroxamic acid derivatives were reported to be HDAC1/HDAC3 dual selective inhibitors.[117] The study showed that the selectivity came from preferential interaction of the capping group (Figure 6.1, blue part in **36**)

with the solvent exposed region of the active sites of HDAC1 and HDAC3 over HDAC2. The capping group that imparted selectivity against HDAC2 can successfully be used to generate an HDAC1-selective inhibitor.

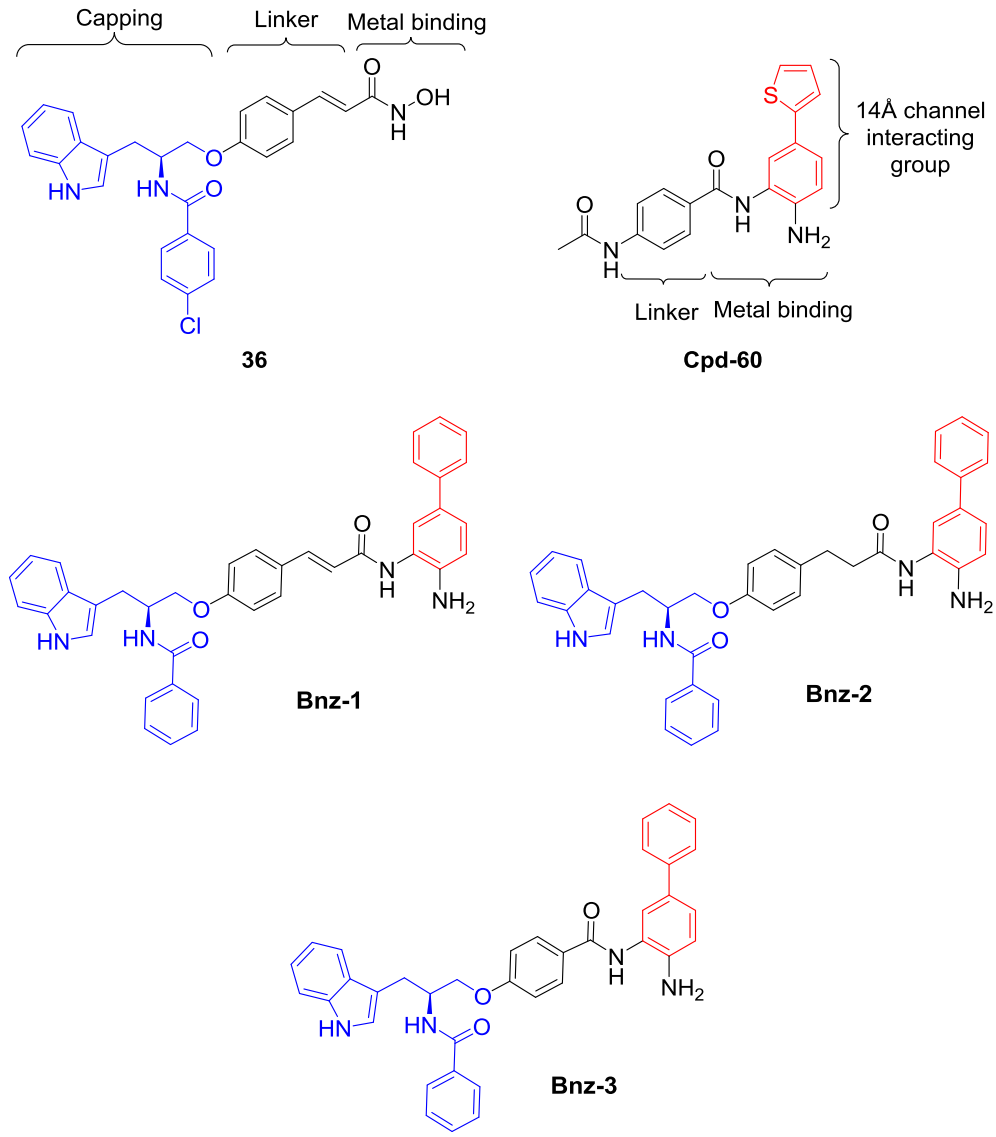

Figure 6.1. Structures of HDAC1/3 selective inhibitor **36**, HDAC1/2 selective inhibitor **Cpd-60**, and the biaryl indolyl benzamide HDAC inhibitors **Bnz-1**, **Bnz-2**, and **Bnz-3**.

In this work we combined both the functional groups from the HDAC1/2 selective inhibitors and HDAC1/3 selective inhibitor in order to generate HDAC1 selective analogs. The hypothesis was to combine the biaryl group (Figure 6.1, red

part of Cpd-60) which discriminated against HDAC3, with the capping group of the HDAC1/3 selective inhibitors (Figure 6.1, blue part of **36**) which discriminated against HDAC2. By combining these two fragments we designed three potential HDAC1-selective inhibitor (Figure 6.1, **Bnz-1**, **Bnz-2**, and **Bnz-3**).

6.2. Docking studies of Cpd-60 with HDAC1, 2, 3, and 7

To validate the design of the HDAC1-selective inhibitors, and to understand the binding of selective inhibitors to HDAC1, **Cpd-60** was docked in the crystal structures of class I HDAC1 (PDB: 4BKX), HDAC2 (PDB: 3MAX), and HDAC3 (PDB: 4A69), and class II HDAC7 (PDB: 3C0Z) using Autodock program[119]. The docking studies revealed the amino acids that are critical for the selectivity, and more importantly, showed the preference of **Cpd-60** binding to HDAC1 and HDAC2 (Figure 6.2). For both HDAC1 and HDAC2, Cpd-60 showed the expected binding, with the metal binding group of **Cpd-60** (Figure 6.1) well positioned in the metal binding region of the active site and the biaryl ring system positioned in the 14 Å channel (Figures 6.1, 6.2A and B). It's worth mentioning that the crystal structures of both HDAC1 and HDAC2 showed a difference in the width of the 14 Å channel (Figure 6.2A and B). HDAC2 displayed a wider channel than HDAC1, with a slight constriction in HDAC1 crystal structure 14 Å channel created by M30, R34, and L139 (gold mesh in Figure 6.2A). But the compound still bound well to both active sites. On the other hand, in HDAC3 **Cpd-60** didn't fit in the active site due to the presence of a constriction created by M30, R34, and L139 blocking the 14 Å channel (Figure 6.2, see arrow), similar to the *N*-library docking results (section 5.4 in Chapter 5).[102] The constriction in the 14 Å cavity of HDAC3 prevented the biaryl ring system from fitting, which led to a pose that placed the metal binding group of the

compound away from the metal binding region in HDAC3 active site (gold mesh in Figure 6.2C). In HDAC7, a similar disfavored binding or no binding was observed due to the absence or blocking of the 14 Å channel (gold mesh in Figure 6.2D).

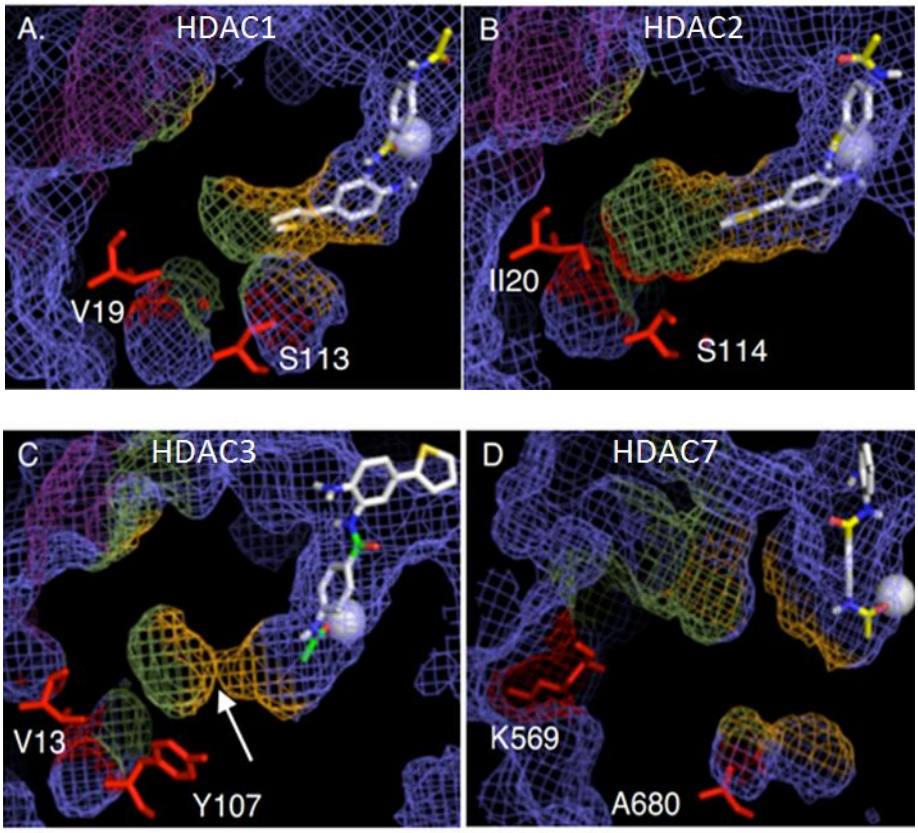

Figure 6.2. Docking of **Cpd-60** into the crystal structures of (A) HDAC1, (B) HDAC2, (C) HDAC3 and (D) HDAC7. The Zn^{2+} metal is represented as a grey orb, the inhibitor as ball and sticks, and the HDAC structure as color-coded mesh (gold = 14 Å cavity constriction point; green = base of the 14 Å cavity; blue = all other regions). Residues differing in their position at the cavity surface in HDAC2 versus 1, 3, or 7 are shown in red.

6.3. Synthesis of the biaryl indolyl benzamide HDAC inhibitors

The biaryl indolyl benzamide inhibitors were synthesized according to Schemes 6.1-6.4. First, synthesis of intermediates **44a** and **44b** commenced with reduction of (*tert*-butoxycarbonyl)-*L*-tryptophan **37** with $LiAlH_4$, which afforded the protected tryptophanol **40**. Another method for the synthesis of **40** was also followed

by BOC protection of methyl *L*-tryptophanate HCl salt **38**, then reduction with $LiAlH_4$ (Scheme 6.1). The coupling partner esters **42a** and **42b** were synthesized from their corresponding carboxylic acids, (*E*)-3-(4-hydroxyphenyl)acrylic acid **41a** or 4-hydroxy benzoic acid **41b**, by esterification with methanol. Mitsunobu coupling of **40** with **42a** or **42b** gave **43a** or **43b**, respectively. Deprotection of **43a** or **43b** with HCl/EtOAc, and coupling with benzoic acid using TBTU and DIPEA afforded **44a** or **44b** intermediates.

Scheme 6.1. Synthesis of intermediates **44a** and **44b**

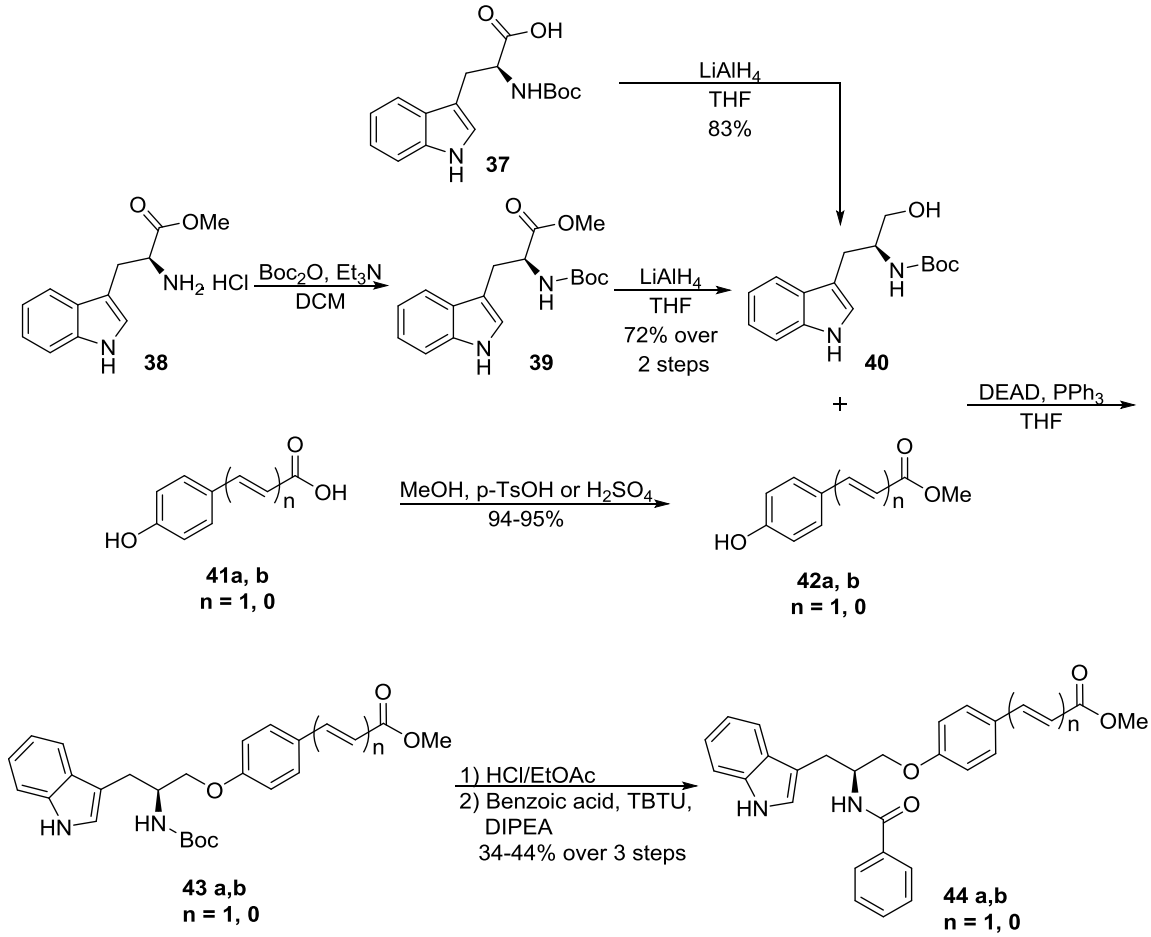

The biaryl fragment of the molecules (biaryl amine **49**) was synthesized by BOC protection of 4-bromo-2-nitro aniline **46** using di-tert-butyl dicarbonate and a catalytic amount of DMAP to form the mono BOC amine **47** (Scheme 6.2).

Compound **47** was then subjected to Suzuki coupling using phenyl boronic acid, potassium carbonate, and bis triphenylphosphine palladium dichloride to give **48**, which was then reduced by Pd/C and hydrogen gas to afford **49** (Scheme 6.2).

Scheme 6.2. Synthesis of the biaryl amine **49**

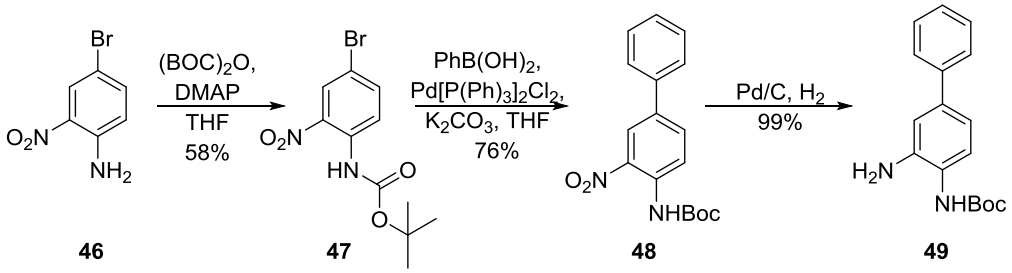

Synthesis of **Bnz-1** and **Bnz-3** was done according to Scheme 6.3. Hydrolysis of **44a** and **44b** with NaOH gave the free carboxylic acids **45a** and **45b**. Coupling of **45a** or **45b** with the BOC-protected biaryl amine **49** was achieved with PyBOP and afforded the BOC-protected **50a** and **50b**. The final products **Bnz-1** and **Bnz-3** were obtained by BOC deprotection of with 50% TFA/DCM. **Bnz-2** was synthesized by reduction of **45a**, followed by coupling with the biaryl amine **49** and finally BOC deprotection with 50%TFA/DCM (Scheme 6.4).

Scheme 6.3. Synthesis of **Bnz-1** and **Bnz-3**

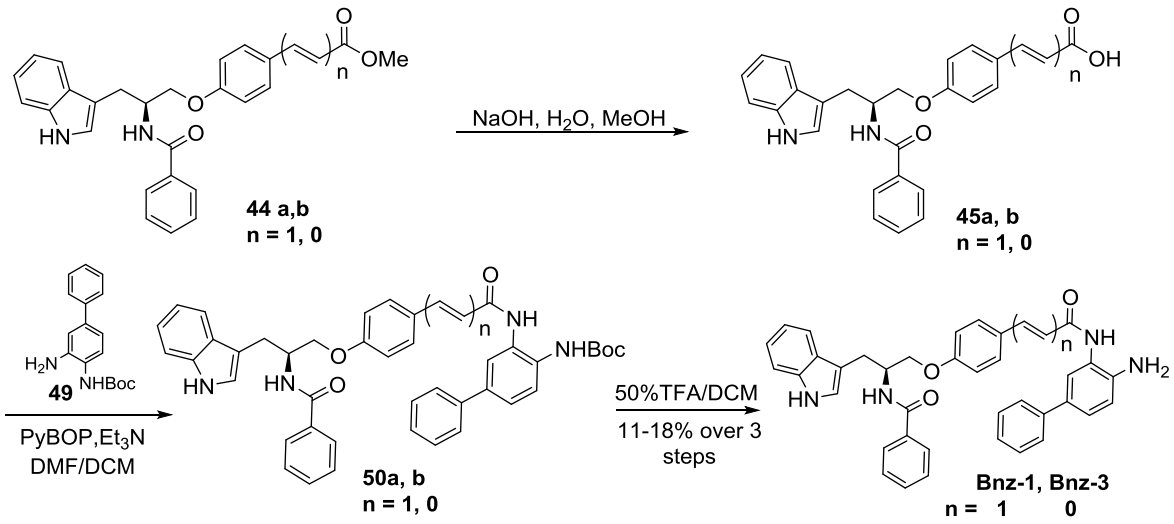

Scheme 6.4. Synthesis of **Bnz-2**

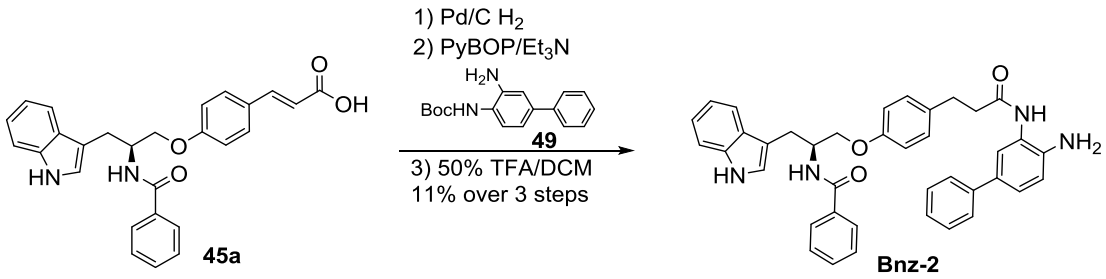

6.4. *In vitro* screening of biaryl indolyl benzamide HDAC inhibitors

To assess isoform selectivity, the three new compounds were screened against recombinant HDAC1 and HDAC2 using the HDAC-Glo assay (Figure 6.3). **Bnz-3** was further tested with HDAC3 and HDAC6. Cpd-60, as a HDAC1/2 selective inhibitor, and SAHA, as a non-selective compound, were tested as well with recombinant HDAC1, 2, 3, and 6. As expected, SAHA showed almost the same inhibitory activity with HDAC1, 2, 3, and 6 (Figure 6.3). The HDAC1/2 selective inhibitor **Cpd-60** demonstrated selectivity for HDAC1 and 2 over HDAC3 and 6. The new analogs showed several interesting results. First, **Bnz-3** displayed the highest inhibitory activity among the three analogs, with about ten- to 100-fold higher potency compared to **Bnz-2** and **Bnz-1**, respectively (compare HDAC1 or HDAC2

activity at 2 µM for **Bnz-3** to 20 and 200µM for **Bnz-2** and **Bnz-1**, or at 0.2 µM for **Bnz-3** to 2 and 20 µM for **Bnz-2** and **Bnz-1**) (Figure 6.3). Second, all the analogs showed selectivity for HDAC1 over HDAC2, with the best selectivity observed for HDAC1 with **Bnz-3** at 2 µM (Figure 6.3). The presence of the saturated linker in **Bnz-2** led to about 10-fold improvement in potency compared to the unsaturated linker in **Bnz-1** (Figures 6.1 and 6.3). Interestingly, removing the linker in **Bnz-3** led to another 10-fold enhancement in the activity compared to **Bnz-2**, and about 100-fold compared to **Bnz-1** (Figures 6.1 and 6.3).

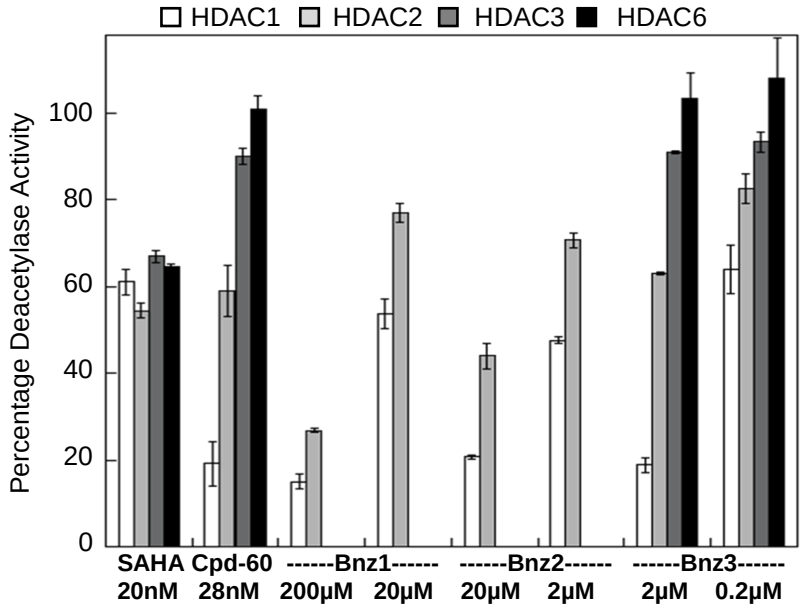

Figure 6.3. *In vitro* isoform selectivity screening of SAHA, Cpd-60, Bnz-1, Bnz-2, and Bnz-3 against HDAC1, HDAC2, HDAC3, and HDAC6. The concentrations shown for each compound are final concentrations. Mean percent deacetylase activities from a minimum of two independent trials with standard errors were plotted (Table D.1).

To further assess the selectivity of **Bnz-3** as the best analog, IC_{50} values were determined for both **Bnz-3** and **Cpd-60** using recombinant HDAC1 and HDAC2 (Table 6.1). **Cpd-60** showed about 7.3-fold selectivity for HDAC1 over HDAC2, with 10.4 nM IC_{50} value with HDAC1. On the other hand, **Bnz-3** displayed about 10.6-fold

selectivity for HDAC1 over HDAC2, with an IC_{50} value of 548 nM with HDAC1. The IC_{50} values show that the potency of **Bnz-3** was about 53-fold less potent than **Cpd-60** in inhibiting HDAC1, while the selectivity for HDAC1 was modestly enhanced to 10.6-fold compared to 7.3-fold with Cpd-60 (Table 6.1).

In conclusion, several biaryl indolyl benzamide inhibitors were designed, synthesized, and screened for isoform selectivity. The design was based on combining two different fragments to discriminate against HDAC2 and HDAC3, to get a potential HDAC1-selective inhibitor. **Bnz-3** was the best analog in terms of potency and selectivity. **Bnz-3** displayed about 10-fold higher potency than **Bnz-2**, and about 100-fold higher potency than **Bnz-1**. **Bnz-3** exhibited a modest inhibitory potency with HDAC1 (548 nM). In terms of selectivity, **Bnz-3** showed HDAC1 preference, but the observed fold selectivity to HDAC1 over HDAC2 (7.3-fold) was far less than what we expected (30- to 50-fold) when we designed these inhibitors.

Table 6.1. IC_{50} values and fold selectivity for **Cpd-60** and **Bnz-3** against HDAC1 and HDAC2 using recombinant proteins.[a]

Compound	IC_{50} values (nM)		
	HDAC1	HDAC2	HDAC1/HDAC2 fold selectivity
Cpd-60	10.4 ± 0.7	75.9 ± 7.9	7.3
Bnz-3	548 ± 50	5800 ± 380	10.6

[a] Mean IC_{50} value and standard error of at least three independent trials are shown (Figures D.24 and D.25 and Tables D.2 and D.3).

6.5. Experimental Procedures

6.5.1. Materials and instrumentation

Details were provided in Section 2.7.1 of Chapter 2.

6.5.2. Docking procedure

Crystal structures of HDAC1 and HDAC3 were prepared in a similar way as mentioned previously and all box sizes dimensions were the same (Chapter 5, section 5.5.1). For HDAC2, a similar preparation procedure, box dimensions and position to Chapter 2, section 2.7.4 were followed. for HDAC7, the crystal structure was downloaded from the protein data bank (pdb ID: 3C0Z)[21], a grid box of size 26 X 26 X 26 $Å^3$ with a spacing of 0.375 Å and centered at (-32.876, -29.000, -19.000) was used. The PyMOL program was used to delete all water molecules, metal ions (potassium), ethanol, and glycerol molecules and the cocrystallized ligand in the active site from the crystal structure; only the zinc atoms remained. All docking procedure and parameters were similar to what mentioned in Chapter 2, Section 2.7.4.

6.5.3. Synthesis procedure

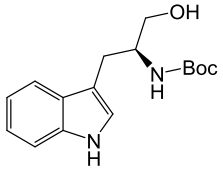

Synthesis of *tert*-butyl (S)-(1-hydroxy-3-(1H-indol-3-yl)propan-2-yl)carbamate (40): Method A: In a 50 mL flask, (*tert*-butoxycarbonyl)-*L*-tryptophan **37** (1 g, 3.29 mmol) was dissolved in dry THF (15 mL). $LiAlH_4$ (499 mg, 13.14 mmol) was added at 0ºC portion wise, and then the temperature was increased to room temperature and the reaction was left to stir for 5 hours under argon. The reaction was quenched with careful dropwise addition of a citric acid solution (10 mL of 1M solution in water). The organic layer was separated, and the aqueous layer was extracted with ethyl acetate (2X30 mL). The organic layers were collected, dried

over anhydrous Na_2SO_4, and evaporated. The product was purified by silica-gel flash chromatography (acetone/petroleum ether 1:3) to afford **40** (655 mg, 83%). Melting point: 117-120 ºC (reported 118-120 ºC)[148]. ^{1}HNMR (400 MHz, DMSO-d_6) δ (ppm): 1.34 (s, 9H), 2.70 (dd, *J* = 7.2 and 14.4 Hz, 1H), 2.87 (dd, *J* = 6.4 and 14.4 Hz, 1H), 3.33 (m, 2H), 3.66 (m, 1H), 4.60 (t, *J* = 5.6 Hz, 1H), 6.48 (d, *J* = 8.4 Hz, 1H), 6.95 (t, *J* = 8.0 Hz, 1H), 7.04 and 7.07 (overlapped t and s, *J* = 7.4 Hz, 2H), 7.30 (d, *J* = 8.0 Hz, 1H), 7.55 (d, *J* = 7.6 Hz, 1H), 10.75 (br s, 1H). Spectral data for the synthesized compound was consistent with the reported data in literature.[149]

Method B: The compound was synthesized similar to the reported procedure.[149] In a 50 mL flask, methyl *L*-tryptophanate HCl salt **38** (1g, 3.93 mmol) was dissolved in dry DCM (10 mL), followed by the addition of triethyl amine (874 mg, 8.64 mmol) and di-tert-butyl dicarbonate (943 mg, 4.32 mmol). The reaction was stirred overnight, washed with citric acid (2x5mL of 1M solution in water) AND then brine (10 mL), dried over anhydrous Na_2SO_4, and evaporated to give **39**. Without purification, **39** was dissolved in dry THF (20 mL), followed by the addition of $LiAlH_4$ (571 mg, 15.04 mmol) portion wise at 0ºC. The same procedure as method A was followed. The product was purified by silica-gel flash chromatography (ethyl acetate/hexanes 1/2) to afford **40** (850 mg, 72% over two steps). Melting point: 118-119 ºC (reported 118-120 ºC)[148].

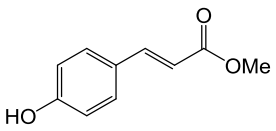

Synthesis of methyl (*E*)-3-(4-hydroxyphenyl)acrylate (42a): The compound was synthesized according to the reported procedure.[150] (*E*)-3-(4-

hydroxyphenyl)acrylic acid **41a** (4 g, 24.37 mmol) was dissolved in methanol (40 mL). *p*-Toluenesulfonic acid (927 mg, 4.87 mmol) was added and the reaction was heated at reflux for 19 hours. The solvent was evaporated, and the residue was dissolved in ethyl acetate (40 mL), washed with saturated $NaHCO_3$ solution (30 mL), dried over anhydrous Na_2SO_4, and evaporated to afford **42a** (4.14 g, 95%). Melting point: 134-137 ºC. ^{1}HNMR (400 MHz, $CDCl_3$) δ (ppm): 3.80 (s, 3H), 6.30 (d, *J* = 16 Hz, 1H), 6.85 (d, *J* = 8.4 Hz, 2H), 7.42 (d, *J* = 8.8 Hz, 2H), 7.63 (d, *J* = 16 Hz, 1H). Spectral data for the synthesized compound was consistent with the reported data in literature.[150]

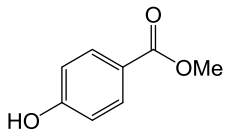

Synthesis of methyl 4-hydroxy benzoate (42b): The compound was synthesized similar to the reported procedure.[151] 4-hydroxybenzoic acid **41b** (4 g, 24.37 mmol) was dissolved in methanol (100 mL), sulfuric acid (0.5 mL) was added, and the reaction was heated to reflux for 6 hours. The solvent was evaporated, and the residue was dissolved in ethyl acetate (40 mL), washed with saturated $NaHCO_3$ solution (30 mL), dried over anhydrous Na_2SO_4, and evaporated to afford **42b** (4.14 g, 94%). ^{1}HNMR (400 MHz, $CDCl_3$) δ (ppm): 3.90 (s, 3H), 6.28 (br s, 1H) 6.88 (dd, *J* = 2, 4.8 Hz, 2H), 7.95 (dd, *J* = 2, 4.8 Hz, 2H). Spectral data for the synthesized compound was consistent with the reported data in literature.[151]

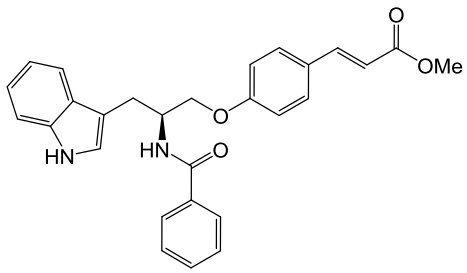

Synthesis of methyl (*S*,*E*)-3-(4-(2-benzamido-3-(1H-indol-3-yl)propoxy)phenyl)acrylate (44a): The compound was synthesized according to the reported procedure.[117] In dry THF (10 mL), **40** (850 mg , 2.89 mmol), **42a** (567 mg, 3.18 mmol) and triphenyl phosphine (834 mg, 3.18 mmol) were dissolved, followed by the addition of diethyl azodicarboxylate (554 mg, 3.18 mmol) drop wise at 0 ºC. The reaction was stirred at room temperature for 4 hours. The solvent was evaporated, and the product was purified by silica-gel flash chromatography (EtOAc/Hexanes 1:3) to afford **43a**.

Compound **43a** was dissolved in EtOAc (10 mL), then EtOAc saturated with HCl (10 mL) was added. The reaction was left to stir at RT for 8.5 hours. The solvent was evaporated and the crude product was used in the following reaction directly with no further purification.

Benzoic acid (493 mg, 4.04 mmol) was dissolved in dry DCM (15 mL), then DIPEA (1.05 mL, 6.05 mmol) was added, followed by TBTU (1.94 gm, 6.05 mmol). The reaction was left to stir at room temperature for 30 min, followed by the addition of the intermediate from previous step and another portion of DIPEA (1.05 mL, 6.03 mmol). The reaction was left to stir for 3.5 hours. The solvent was evaporated and the product was purified by flash silica-gel chromatography (EtOAc/Hexanes 1:2-1:1.5) to afford **44a** (34% over three steps). ^{1}HNMR (400 MHz, DMSO-d6) δ (ppm):

3.08 (d, *J* = 7.2 Hz, 2H), 3.68 (s, 3H), 4.09 (m, 1H), 4.18 (m, 1H), 4.57 (m, 1H), 6.44 (d, *J* = 16 , 1H), 6.94 (m ,3H), 7.04 (t, *J* = 7.2 , 1H), 7.16 (s, 1H), 7.30 (d, *J* = 8, 1H), 7.43 (t, *J* = 7.2, 2H), 7.50 (t, *J* = 6.8, 1H), 7.62 (m, 3H), 7.81 (d, *J* = 7.6, 2H), 8.47 (d, *J* = 7.6 , 1H), 8.96 (br s, 1H), 10.78 (br s, 1H). Spectral data for the synthesized compound was consistent with the reported data in literature.[117]

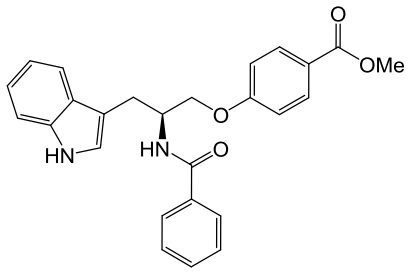

Synthesis of methyl (*S*)-4-(2-benzamido-3-(1H-indol-3-yl)propoxy)benzoate (44b): The compound was synthesized similar to **44a** except the following, **40** (1.88 g , 6.47 mmol), **42b** (1.08 g, 7.12 mmol), triphenyl phosphine (1.87 g, 7.12 mmol), diethyl azodicarboxylate (1.13 mL, 6.47 mmol), benzoic acid (210 mg, 1.72 mmol), DIPEA (449 uL, 2.58 mmol), TBTU (828 mg, 2.58 mmol), **43b** (620 mg, 1.72 mmol) and DIPEA (449 uL, 2.58 mmol). The product was purified by flash silica-gel chromatography (EtOAc/Hexanes 1:2-1:1.5) to afford **44b** (44% over three steps). ^{1}HNMR (400 MHz, DMSO-d6) δ (ppm): 3.10 (d, *J* = 6.8 Hz, 2H), 3.78 (s, 3H), 4.12 (m, 1H), 4.21 (m, 1H), 4.59 (m, 1H), 6.95 (t, *J* = 7.2 Hz, 1H), 7.04 (t, *J* = 8.8 , 3H), 7.18 (s, 1H), 7.31 (d, *J* = 8, 1H), 7.43-7.50 (t and t, *J* = 6.8, and 7.2 3H), 7.62 (d, *J* = 8, 1H), 7.83 (m, 4H), 8.52 (d, *J* = 8, 1H), 10.82 (br s, 1H).

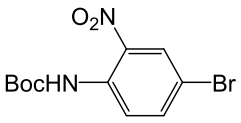

Synthesis of *tert*-butyl (4-bromo-2-nitrophenyl)carbamate (47): The compound was synthesized according to the reported procedure.[152] 4-bromo-2-

nitroaniline **46** (2g, 9.2 mmol) was dissolved in dry DCM (20 mL), followed by addition of DMAP (113 mg, 0.09 mmol). A solution of di-tert-butyl dicarbonate (2.2 g, 10.13 mmol) in dry DCM (20 mL) was added drop wise over 1 hour. The reaction was left to stir at room temperature for 3 hours. The solvent was evaporated and the reaction was purified by flash silica-gel chromatography (EtOAc/Hexanes 1:20) to afford **47** (1.7 g, 58%). ^{1}HNMR (400 MHz, $CDCl_3$) δ (ppm): 1.54 (s, 9H), 7.67 (dd, *J* = 2.3, 9.2 Hz, 1H), 8.32 (d, *J* = 2.4 Hz, 1H), 8.50 (d, *J* = 9.2 Hz, 1H), 9.60 (br s, 1H). Spectral data for the synthesized compound was consistent with the reported data in literature.[152]

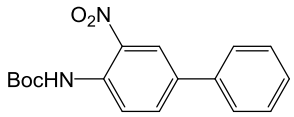

Synthesis of *tert*-butyl (3-nitro-[1,1'-biphenyl]-4-yl)carbamate (48): The compound was synthesized similar to the reported procedure.[152] Compound **47** (1.7 g, 5.36 mmol) was dissolved in dry THF (20 mL), followed by degassing with argon gas for 30 minutes. Phenyl boronic acid (1.05 g, 8.58 mmol), potassium carbonate (2.37 g, 17.16 mmol), and $Pd[PPh_3]_2Cl_2$ (85 mg, 5% w/w) were added. The reaction was heated under reflux for 23 hours, then the solvent was evaporated. The residue was suspended in diethyl ether (30 mL), filtered, and the solvent was evaporated. The residue was purified by flash silica-gel chromatography (EtOAc:Hexanes 1:20) and recrystallization of the impure column fractions from EtOH afforded **48** (1.23 g, 76%). ^{1}HNMR (400 MHz, $CDCl_3$) δ (ppm): 1.56 (s, 9H), 7.37 (m, 1H), 7.48 (m, *2*H), 7.58 (m, 2H), 7.85 (dd, *J* = 2.4, 8.8 Hz, 1H), 8.42 (d, *J* = 2.0 Hz, 1H), 8.63 (d, *J* = 8.8

Hz, 1H), 9.67 (br s, 1H). Spectral data for the synthesized compound was consistent with the reported data in literature.[152]

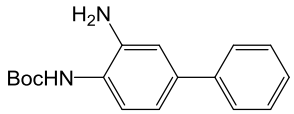

Synthesis of *tert*-butyl (3-amino-[1,1'-biphenyl]-4-yl)carbamate (49): The compound was synthesized similar to the reported procedure.[152] Compound **48** (1.21 g, 4.26 mmol) was suspended in EtOH (80 mL), and Pd/C (121 mg, 10% w/w) was added. The air inside the flask was replaced with argon (X3) then with hydrogen gas (X3). The reaction was allowed to stir under hydrogen overnight at room temperature. The reaction was filtered and concentrated to afford **49** (1.08 g, 99%). ^{1}HNMR (400 MHz, $CDCl_3$) δ (ppm): 1.51 (s, 9H), 5.28 (br s, 2H), 6.60 (br s, 1H), 7.11 (m, 1H), 7.18 (s, 1H), 7.36 (m, 4H), 7.51 (d, *J* = 8.4 Hz, 2H). Spectral data for the synthesized compound was consistent with the reported data in literature.[152]

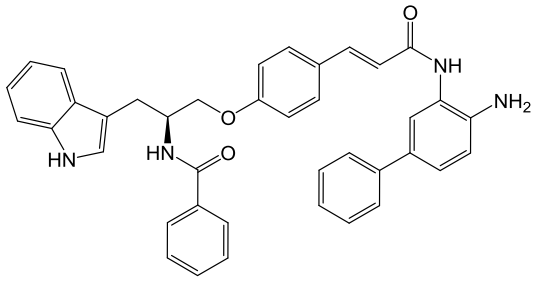

Synthesis of (*S*,*E*)-N-(1-(4-(3-((4-amino-[1,1'-biphenyl]-3-yl)amino)-3-oxoprop-1-en-1-yl)phenoxy)-3-(1H-indol-3-yl)propan-2-yl)benzamide (Bnz-1): **44a** (1.82 g, 4 mmol) was dissolved in MeOH (50 mL), followed by the addition of NaOH (1.6 g, 40 mmol) in water (10 mL). The reaction was left to stir at room temperature for 18 hours. Then the reaction was concentrated under vacuum. HCl (10 N solution in water) was added drop wise until the pH was 6. The reaction was

diluted with water and extracted with ethyl acetate (3X50 mL), dried over MgSO4, evaporated to give **45a**.

Crude product **45a** was dissolved in dry DMF (8 mL) followed by the addition on triethyl amine (0.195 mL, 1.5 mmol). PyBOP (729 mg, 1.5 mmol) was dissolved in dry DCM (5 mL) and added to the reaction, followed by the biaryl amine **49** (362 mg, 1.36 mmol) in dry DCM (5 mL). The reaction was left to stir for 19 hours at room temperature, and then was concentrated under reduced pressure, diluted with water (15 mL), and extracted with ethyl acetate (3x30 mL). The reaction was purified by flash silica-gel chromatography (EtOAc/Hexanes 1:2-1:1) to afford **50a**.

Compound **50a** (175 mg, 0.25 mmol) was dissolved in dry DCM (4mL), then TFA (4 mL) was added. The reaction was left to stir at room temperature for 4 hours. The reaction was then concentrated under vacuum and a saturated solution of $NaHCO_3$ was added dropwise until no effervescence was observed. The product was extracted with EtOAc (3x15mL) and purified by flash silica-gel chromatography (EtOAc/Hexanes 1:1.5-1:1) to afford **Bnz-1** (150 mg, 11% over three steps). ^{1}HNMR (400 MHz, DMSO-d6) δ (ppm): 3.10 (d, *J* = 7.2 Hz, 2H), 4.09 (m, 1H), 4.20 (m, 1H), 4.59 (m, 1H), 5.12 (br s, 2H), 6.76 (d, *J* = 15.6, 1H), 6.82 (d, *J* = 8.4, 1H), 6.96 (m, 4H), 7.22 (m, 3H), 7.31 (d, *J* = 8, 1H), 7.37 (t, *J* = 7.6, 2H), 7.49 (overlapped m, 8H), 7.62 (d, *J* = 7.6, 1H), 7.71 (br s, 1H), 7.83 (d, *J* = 8.4 , 2H), 8.50 (d, *J* = 7.6, 1H), 9.36 (br s, 1H), 10.80 (br s, 1H); ^{13}CNMR (100 MHz, CD_3OD) δ (ppm): 27.16, 50.29, 69.45, 111.20, 111.86, 115.53, 116.78, 118.78, 120.28, 121.39, 123.21, 123.88, 124.37, 125.99, 126.46, 127.78, 128.01, 128.64, 129.24, 129.73, 131.62, 134.98, 136.64, 139.90, 140.80, 141.62, 160.25, 164.40, 166.79; HRMS (ESI-TOF, *m/z):*

calculated for $[M+H]^+$ $C_{39}H_{34}N_4O_3H^+$, 607.2709, found 607.2736. HPLC analytical purity analysis 94.9%.

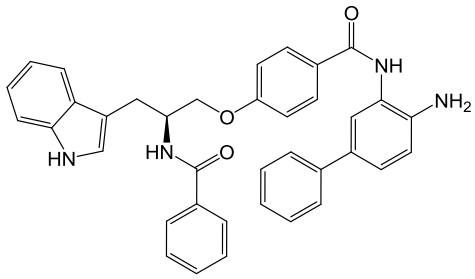

Synthesis of (*S*)-*N*-(4-amino-[1,1'-biphenyl]-3-yl)-4-(2-benzamido-3-(1H-indol-3-yl) propoxybenzamide (Bnz-3): Compound **44b** (630 mg, 1.47 mmol) was dissolved in MeOH (25 mL), followed by the addition of NaOH (588 mg, 14.7 mmol) in H_2O (5 mL). The reaction was left to stir at room temperature for 18 hours. Then the reaction was concentrated under vacuum. HCl (10 N) was added drop wise until the pH was 6. The reaction was diluted with water (10 mL) and extracted with EtOAc (3X30 mL), dried over $MgSO_4$, and evaporated to give **45b**.

Crude product **45b** was dissolved in dry DMF (5 mL), followed by the addition on triethyl amine (0.22 mL, 1.57 mmol). PyBOP (446 mg, 1.57 mmol) was dissolved in dry DCM (5 mL) and added to the reaction, followed by the biaryl amine **49** (817 mg, 1.57 mmol) in dry DCM (5 mL). The reaction was left to stir for 21 hours. The reaction was then concentrated under reduced pressure, diluted with water (10 mL), and extracted with ethyl acetate (3x30mL). The reaction was purified by flash silica-gel chromatography (EtOAc:Hexanes 1:2-1:1) to afford **50b**, which was used in the next reaction with no characterization.

Compound **50b** was dissolved in dry DCM (4mL), then TFA (4 mL) was added. The reaction was left to stir at room temperature for 4 hours. The reaction

was then concentrated under vacuum and a saturated solution of $NaHCO_3$ was added till no effervescence was observed. The product was extracted with EtOAc (3x20mL), purified by flash silica-gel chromatography (EtOAc:Hexanes 1:1.5-1:1) and afforded **Bnz-3** (18% over three steps). ^{1}HNMR (400 MHz, DMSO-d6) δ (ppm): 3.11 (d, *J* = 6.0 Hz, 2H), 4.12 (m, 1H), 4.23 (m, 1H), 4.61 (m, 1H), 5.06 (br s, 2H), 6.84 (d, *J* = 8.8, 1H), 6.97 (t, *J* = 7.2, 1H), 7.05 (m, 3H), 7.20 (m, 2H), 7.29-7.39 (overlapped t and t, *J* = 8, 4H), 7.44-7.53 (m, 6H), 7.63 (d, *J* = 8, 1H), 7.84 (d, *J* = 7.2, 2H), 7.95 (d, *J* = 8.4 , 2H), 8.53 (d, *J* = 8.4, 1H), 9.61 (br s, 1H), 10.82 (br s, 1H); ^{13}CNMR (100 MHz, CD_3OD) δ (ppm): 27.17, 50.24, 69.52, 111.18, 111.87, 114.54, 116.98, 118.79, 121.40, 123.90, 125.24, 125.95, 126.45, 127.24, 127.79, 127.86, 128.58, 128.66, 129.25, 130.17, 131.65, 134.96, 136.62, 140.66, 143.25, 161.54, 166.79; HRMS (ESI-TOF, *m/z):* calculated for $[M+H]^+$ $C_{37}H_{32}N_4O_3H^+$, 581.2553, found 581.2573. HPLC analytical purity analysis 94.9%.

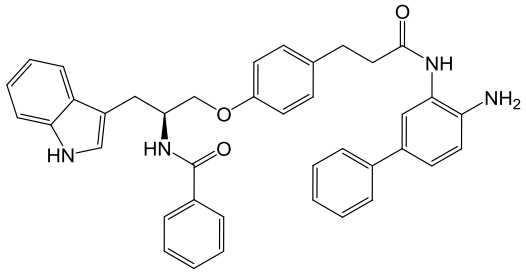

Synthesis of (*S*)-*N*-(1-(4-(3-((4-amino-[1,1'-biphenyl]-3-yl)amino)-3-oxopropyl)phenoxy) -3-(1H-indol-3-yl)propan-2-yl)benzamide (Bnz-2): Compound **45a** (600 mg, 1.36 mmol) was dissolved in MeOH (15 mL), followed by the addition of Pd/C (60 mg, 10% w/w). Air was replaced with argon (3X), then hydrogen gas (3X). The reaction was left to stir overnight under hydrogen at room

temperature. The reaction was then filtered, evaporated and the crude product was used in the next reaction.

The crude product **30** was dissolved in dry DMF (10 mL), followed by the addition of triethyl amine (0.244 mL, 1.75 mmol). PyBOP (911 mg, 1.75 mmol) was dissolved in dry DCM (5 mL) and added to the reaction, followed by amine **49** (451 mg, 1.59 mmol) in dry DCM (5 mL). The reaction was left to stir overnight at room temperature. The reaction was then concentrated under reduced pressure, diluted with water (15 mL), and extracted with ethyl acetate (3x20mL). The reaction was purified by flash silica-gel chromatography (EtOAc:Hexanes 1:2-1:1) and the product was used in the next reaction with no characterization.

The crude product from previous reaction was dissolved in dry DCM (4 mL), then TFA (4 mL, 52 mmol) was added. The reaction was left to stir at room temperature for 2 hours. The reaction was then concentrated under vacuum and a saturated solution of $NaHCO_3$ was added until no effervescence was observed. The product was extracted with ethyl acetate (3x15mL), purified by flash silica-gel chromatography (EtOAc:Hexanes 2:1-3:1), and afforded **Bnz-2** (11% over three steps). ^{1}HNMR (400 MHz, DMSO-d6) δ (ppm): 2.59 (t, *J* = 8.0 Hz, 2H), 2.84 (t, *J* = 7.2 Hz, 2H), 3.08 (d, *J* = 4.8 Hz, 2H), 3.95 (m, 1H), 4.10 (m, 1H), 4.56 (m, 1H), 4.95 (br s, 2H), 6.76 (d, *J* = 8.0, 1H), 6.86 (d, *J* = 8.4, 1H), 6.94 (t, *J* = 7.2, 1H), 7.03 (t, *J* = 7.2, 1H), 7.14-7.23 (m, 5H), 7.29-7.48 (m, 9H), 7.61 (d, *J* = 7.6, 1H), 7.82 (d, *J* = 7.2, 2H), 8.47 (d, *J* = 7.6, 1H), 9.18 (br s, 1H), 10.79 (br s, 1H); ^{13}CNMR (100 MHz, CD_3OD) δ (ppm): 27.20, 30.73. 38.21, 50.34, 69.36, 111.30, 111.83, 114.91, 116.54, 118.80, 121.37, 123.82, 123.92, 124.07, 124.46, 125.92, 126.41, 127.78, 127.87,

128.42, 128.63, 129.23, 129.73, 131.59, 133.76, 135.00, 136.62, 142.03, 157.29, 166.74, 171.06; HRMS (ESI-TOF, *m/z):* calculated for $[M+H]^+$ $C_{39}H_{36}N_4O_3H^+$, 609.2866, found 607.2854. HPLC analytical purity analysis 94.3%.

6.5.4. Procedures for biological screenings

6.4.3.1. Inhibitor testing with HDAC isoforms

To measure HDAC isoforms inhibition, individual baclovirus-expressed HDAC isoform (50 ng for HDAC1 (Enzo Life), 3 ng HDAC1 (BPS Bioscience), 0.5 ng for HDAC2 (BPS Bioscience), 6 ng for HDAC3 (Enzo Life), and 65 ng for HDAC6 (Enzo Life)) was mixed with HDAC-Glo™ buffer (Promega) in polystyrene 96-well half area white plate (Corning). Inhibitor in DMSO (1 µL) was then added to a final volume of 25 µL, and pre-incubation for 2 hours at room temperature without rocking. An uninhibited control reaction was also included that contained DMSO (1 µL) with each HDAC enzyme in HDAC-Glo™ buffer (24 µL). Deacetylase activity was measured using the HDAC-Glo™ assay kit as per the manufacturer's protocol (Promega). Specifically, the HDAC-Glo™ substrate (1 mL) and developer (1 µL) were first premixed to form the HDAC-Glo™ reagent. Then, to monitor deacetylase activity, HDAC-Glo™ reagent (5 µL) diluted in HDAC-Glo™ buffer (20 µL) was added to each well (50 µL total volume) and incubated for 30-45 minutes at room temperature without rocking. The deacetylase activity was measured as luminescent signal using a GeniosPlus Fluorimeter (Tecan) at optimal gain. The concentrations of inhibitors reported in the dose-dependent studies are final concentrations after addition of HDAC-Glo™ reagent and HDAC-Glo™ buffer. Percent deacetylase activity was calculated by dividing the signal for each reaction by the signal of the uninhibited control, and

then multiplying by 100. IC_{50} values were calculated by fitting the percent deacetylase activity remaining as a function of inhibitor concentration to a sigmoidal dose-response curve ($y = 100/(1+(x/IC_{50})^{Z}$), where y = percent deacetylase activity and x = inhibitor concentration) using non-linear regression with KaleidaGraph 4.1.3 software. Results are reported in Figures 6.3, D.24 and D.25, and Tables 6.1, D.2 and D.3.

CHAPTER 7 - CONCLUSION

In this thesis, several HDAC inhibitors have been designed, synthesized, and screened for biological activity. Several SAHA (Vorinostat) analogs were modified at different positions in the linker region of SAHA. C2-modififed SAHA analogs were generated by Dr. Anton Bieliauskas. Herein, isoforms selectivity assessment, and *in cellulo* testing of the C2-SAHA analogs were performed. Several of the C2-modified SAHA analogs displayed selectivity for HDAC6 and HDAC8 over HDAC1, 2, and 3. C2-*n*-hexyl SAHA analog **1i**, showed the highest selectivity with 49- to 300-fold selectivity for HDAC6 and 8 over HDAC1, 2, and 3. Enantioselective syntheses of both the (*R*) and (*S*) enantiomers of C2-*n*-hexyl SAHA were performed, and both enantiomers exhibited similar potency and selectivity to the racemic C2-*n*-hexyl SAHA **1i**.

In addition, several other SAHA derivatives substituted at the C4 and C5 positions of the linker region were synthesized and screened. The C4-SAHA analogs showed up to 1300-fold dual selectivity for HDAC6 and HDAC8 over HDAC1, HDAC2, and HDAC3. C4-benzyl SAHA **19f**, was the best analogs, which showed the highest fold selectivity with 210- to 740-fold selectivity for HDAC6 and 8 compared to HDAC1, 2, and 3, and 140 and 57 nM IC_{50} with HDAC6 and HDAC8. *In cellulo* testing of the C4-benzyl SAHA analog showed consistent isoform selectivity with the *in vitro* screening. Both enantiomers of the C4-benzyl SAHA were synthesized via enantioselective syntheses. *In vitro* screening of the pure enantiomers revealed that (*R*)-C4-benzyl SAHA is more potent and selective than the (*S*) enantiomer, with 48 and 27 nM IC_{50} with HDAC6 and HDAC8, and 520- to

1300-fold selectivity for HDAC6 and 8 over HDAC1, 2, and 3. In addition, C5-modified SAHA analogs also displayed dual HDAC6/8 selectivity. The best analog, C5-benzyl SAHA, showed much lower selectivity (8- to 21-fold selectivity) compared to the C4-benzyl SAHA. The potency (IC_{50} values of 270 and 380 nM with HDAC6 and 8, respectively) was also lower compared to the C4-benzyl SAHA.

In terms of structure activity relationship (SAR), the position of the modification is critical and can greatly affect both potency and selectivity of the inhibitors. In the C2-modified SAHA analogs, high fold selectivities were observed (up to 300-fold) to HDAC6 and 8, but with micromolar to submicromolar IC_{50} values (0.6 to 2 μM). Modifications at the C4 position of the linker gave analogs with higher fold selectivity (up to 1300-fold) to HDAC6 and 8, and the potency was enhanced as well (48 and 27 nM IC_{50} values with HDAC6 and 8, respectively) compared to the C2-modified SAHA analogs. On the other hand, moving the same modification farther to the C5- position of the linker (C5-benzyl SAHA) resulted in reduction in both selectivity (8- to 12-fold only), and potency (270 and 380 nM IC_{50} values with HDAC6 and 8) compared to the C4-benzyl SAHA.

Docking studies were done for the (*R*)- and (*S*)-C2-*n*-hexyl SAHA, and (*R*)- and (*S*)-C4-benzyl SAHA, and showed that the presence of the hexyl or benzyl groups at the C2 or C4 positions in the linker region led to the dual HDAC6/HDAC8 selectivity over HDAC1, 2, and 3 due to steric clash between the substituents and the active site entrances of HDAC1, 2, and 3.

In another project, several biaryl indolyl benzamide derivatives were designed, synthesized, and screened as possible HDAC1-selective inhibitors. **Bnz-3**

showed the highest potency compared to **Bnz-1** and **Bnz-2**. **Bnz-3** displayed about 10-fold higher potency than **Bnz-2**, and about 100-fold higher potency than **Bnz-1**. **Bnz-3** exhibited a modest inhibitory potency with HDAC1 (548 nM), but only 7.3-fold selectivity for HDAC1 over HDAC2.

This thesis, along with previous reports[103-105], indicate that modifying SAHA in the linker region can alter the selectivity of HDAC inhibitors, and suggest that modifying current drugs can significantly improve their properties. The dual HDAC6/8 selective inhibitors reported in this work can be used as biological tools to study both HDAC6 and HDAC8-related cancer biology, and as leads for development of more effective anti-cancer agents targeting both HDAC6 and HDAC8.

The first future direction in this work is to test the (*R*)-C4-benzyl SAHA analog **(*R*)-19f** in mouse studies in a collaboration work with Dr. Ge at Karmanos Cancer institute. A second future direction is based on the unique dual HDAC6/8 selectivity that was observed upon substituting the C4 in the linker of SAHA, in which HDAC substrate bearing the benzyl group in its linker region will be synthesized and tested for isoform selectivity. Isoform selective HDAC substrate can be used for PET imaging, to monitor levels of HDAC isoforms in different types of tumors (like brain tumors) in order to monitor treatment effectiveness and disease progression in a collaboration with Dr. Gelovani at college of engineering, Wayne State University. Finally, to develop highly selective HDAC1 selective inhibitors, several analogs of Cpd-60 and other HDAC1/2 selective inhibitors will be designed and synthesized based on computer aided design. The design will be done by modifying chemical

structures of the HDAC1/2 selective inhibitors and then docking of the modified structures in the crystal structures of HDAC1 and HDAC2 using LeadIt program. The best hits that show selectivity to HDAC1 over HDAC2 will be synthesized and screened *in vitro* for isoform selectivity.

APPENDIX A

A.1. Compound characterization data of (*R*) and (*S*)-C2-*n*-hexyl SAHA (1i)

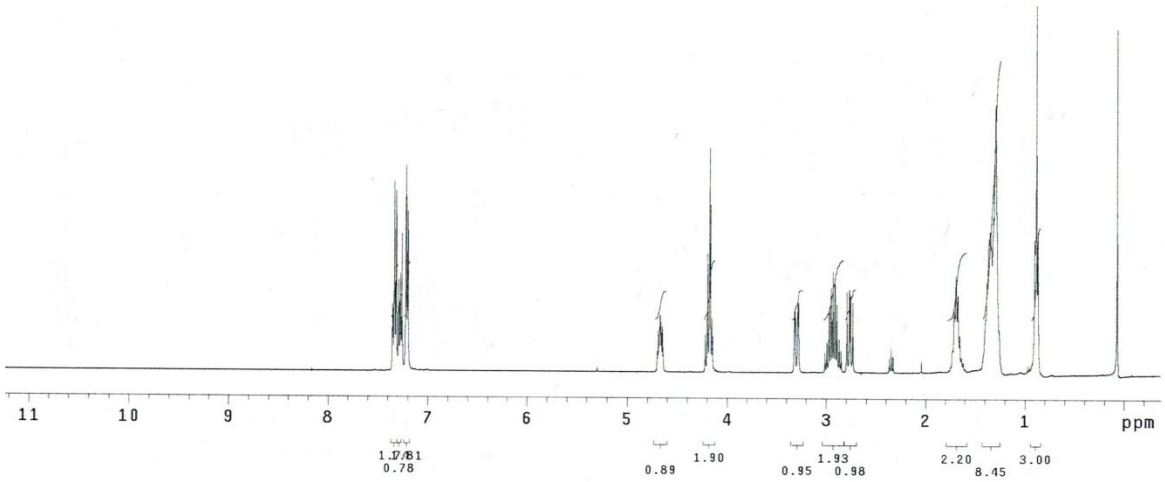

Figure A.1. ^{1}H NMR spectrum of **(*S*)-9**.

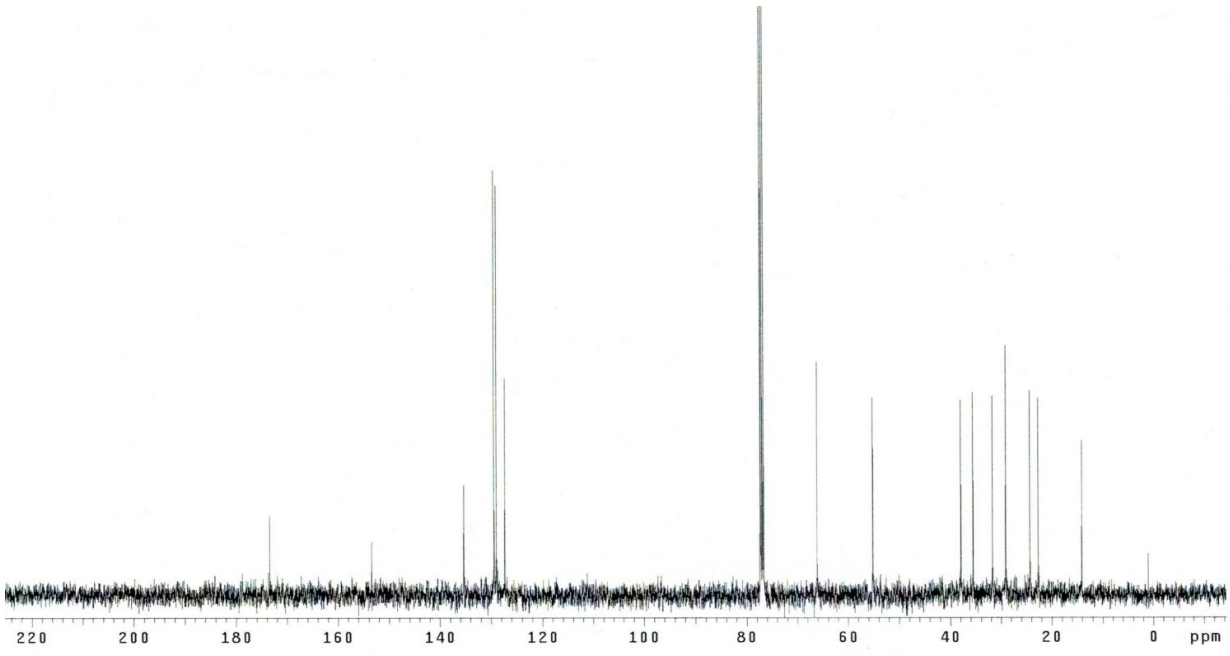

Figure A.2. ^{13}C NMR spectrum of **(*S*)-9**.

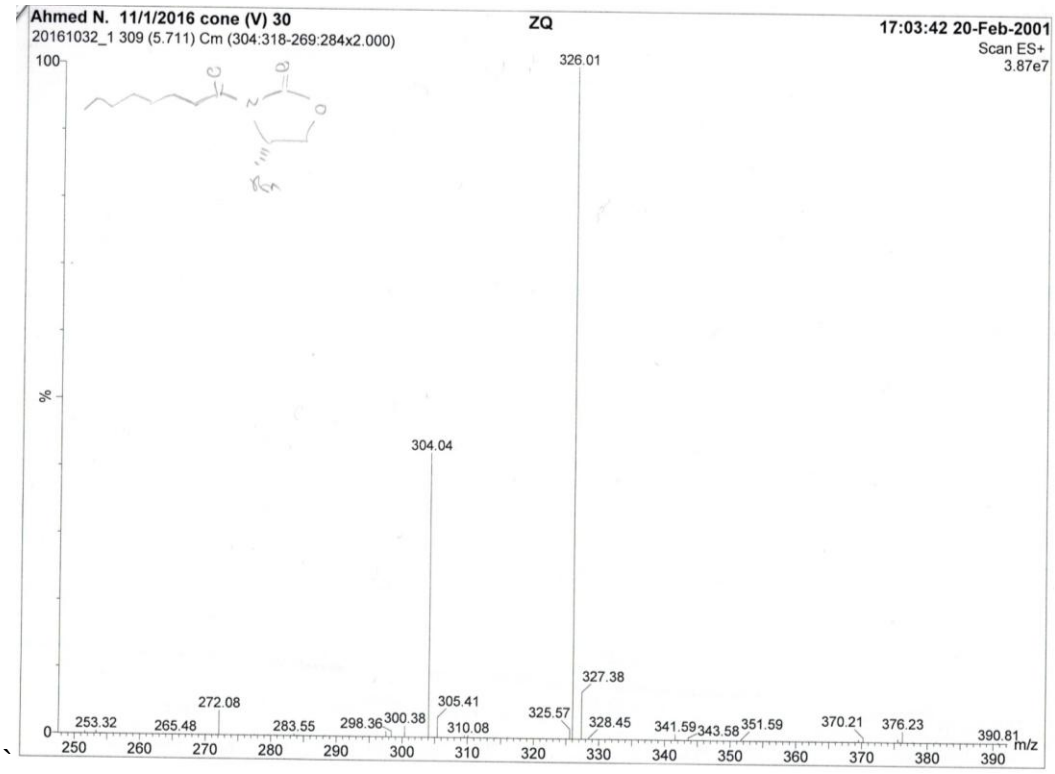

Figure A.3. Low resolution mass spectrum of **(*S*)-9.**

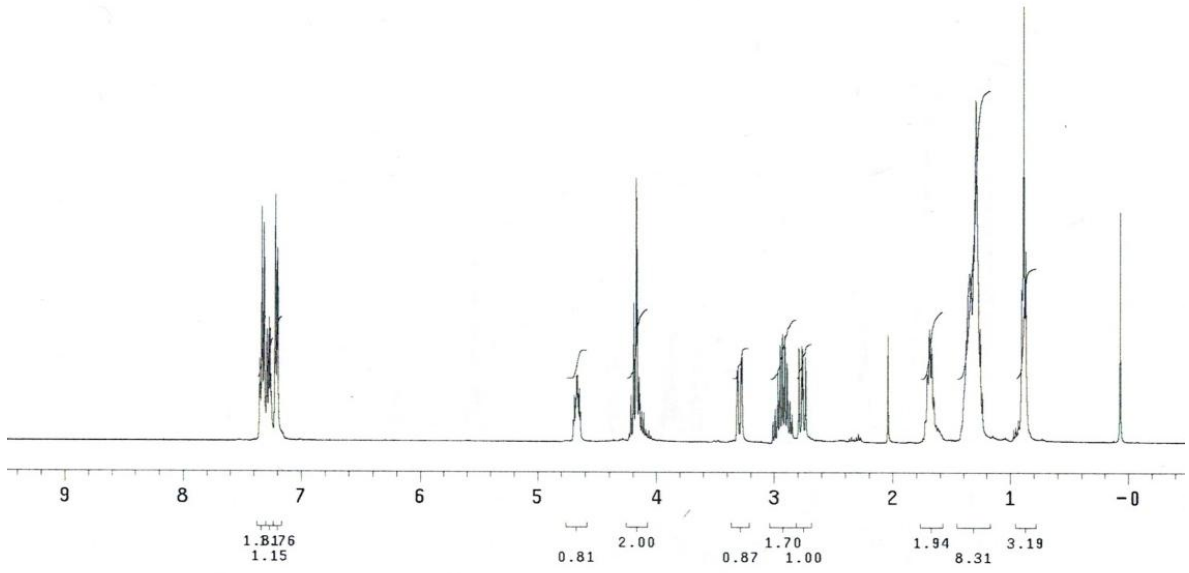

Figure A.4. ^{1}H NMR spectrum of **(*R*)-9.**

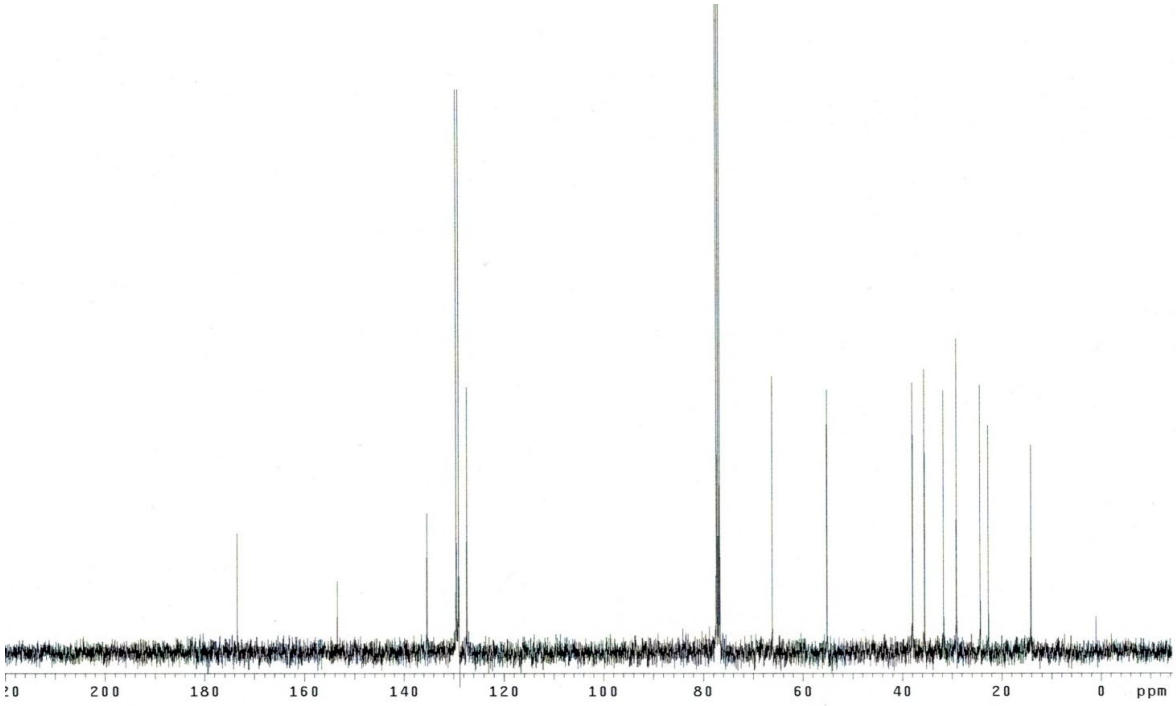

Figure A.5. ^{13}C NMR spectrum of **(*R*)-9.**

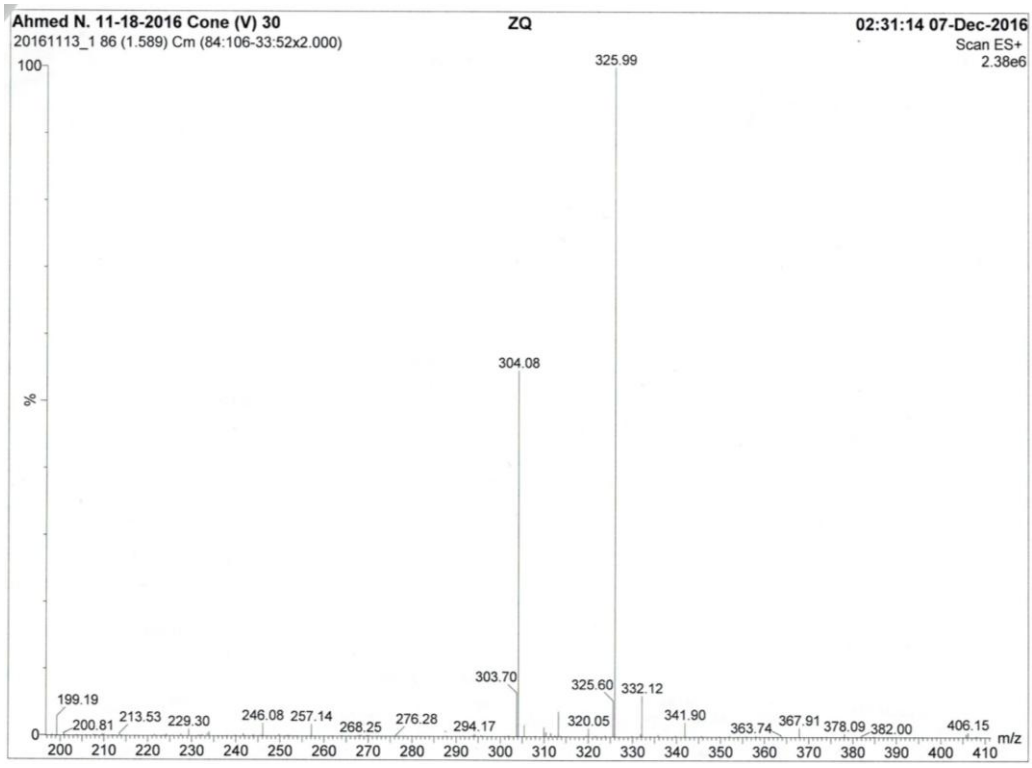

Figure A.6. Low resolution mass spectrum of **(*R*)-9.**

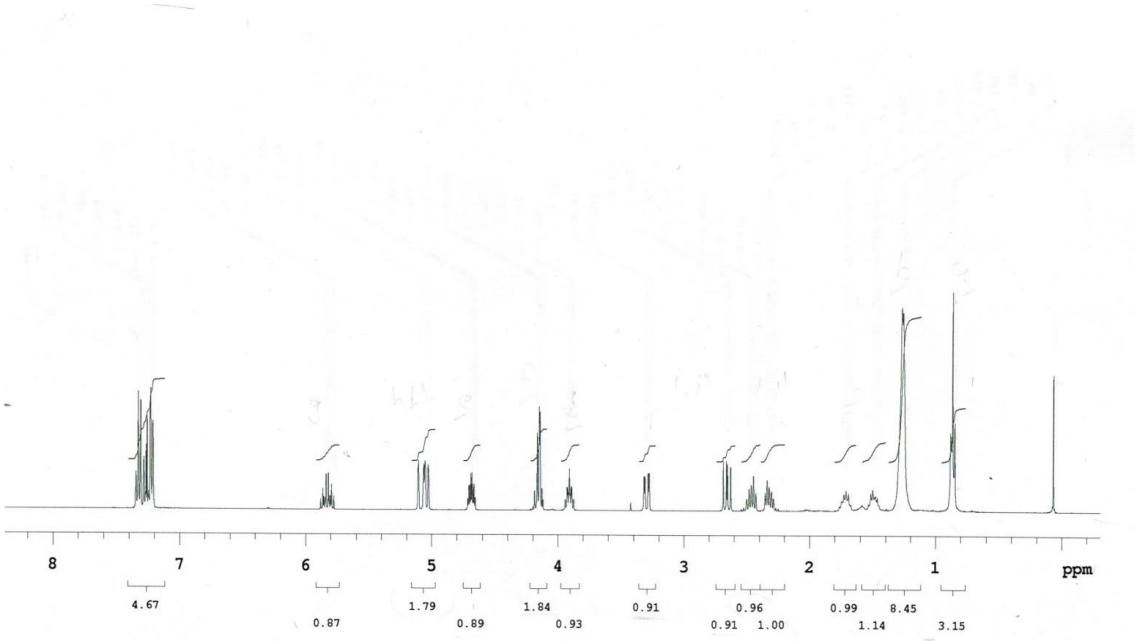

Figure A.7. ^{1}H NMR spectrum of **(*S*)-10.**

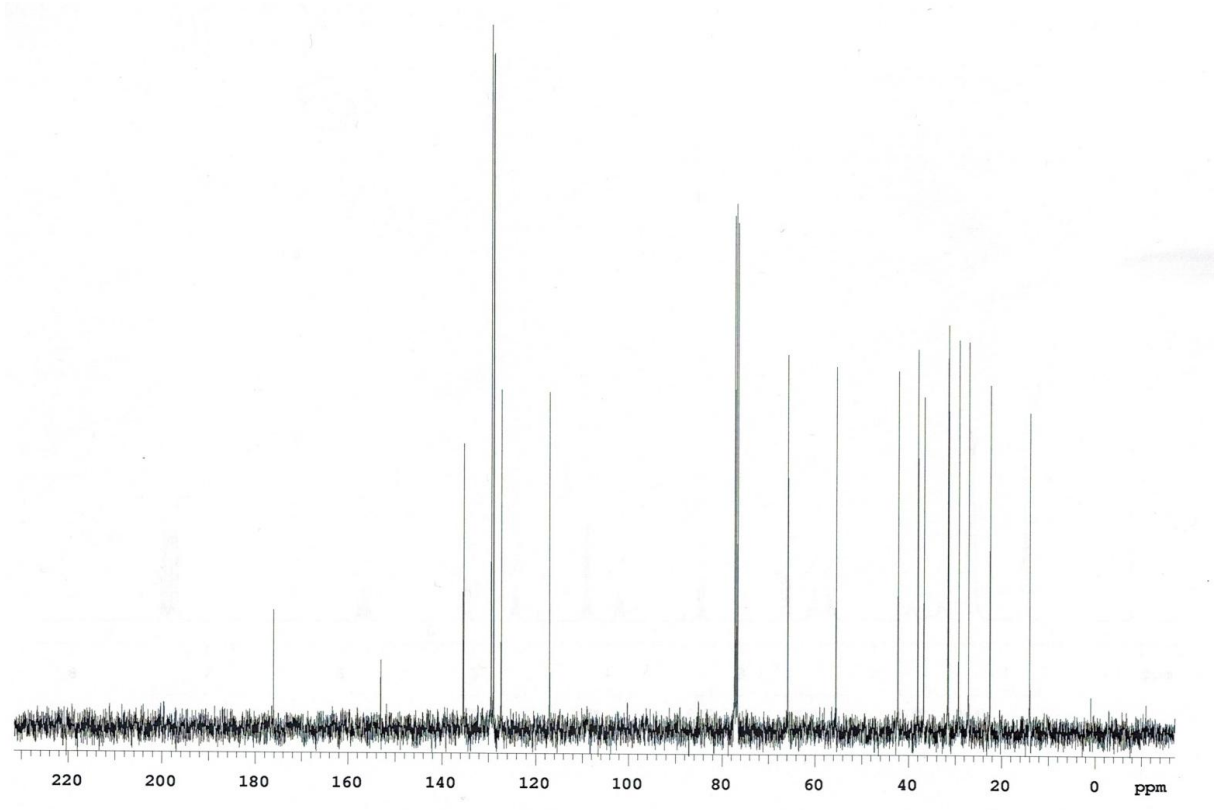

Figure A.8. ^{13}C NMR spectrum of **(*S*)-10.**

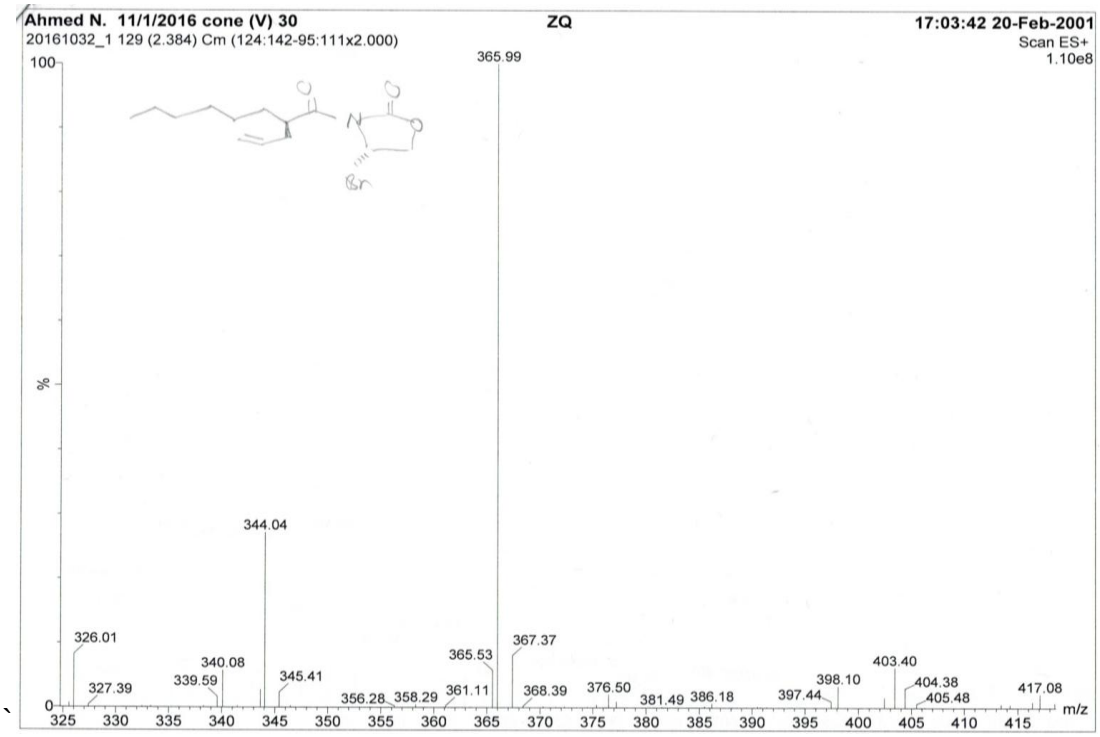

Figure A.9. Low resolution mass spectrum of **(*S*)-10.**

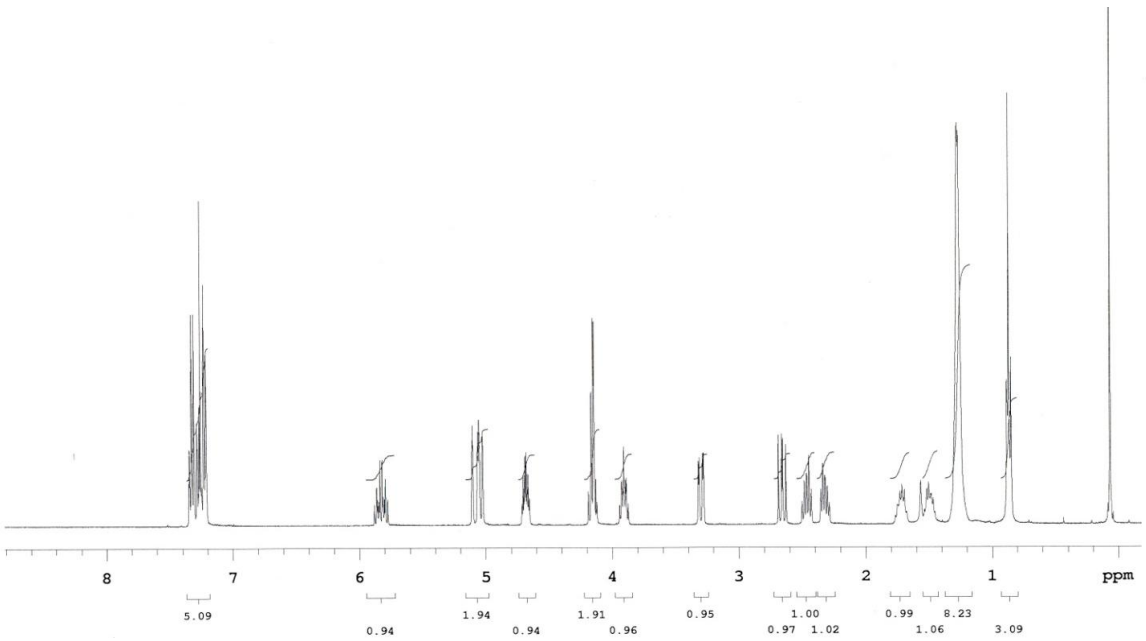

Figure A.10. ^{1}H NMR spectrum of **(*R*)-10.**

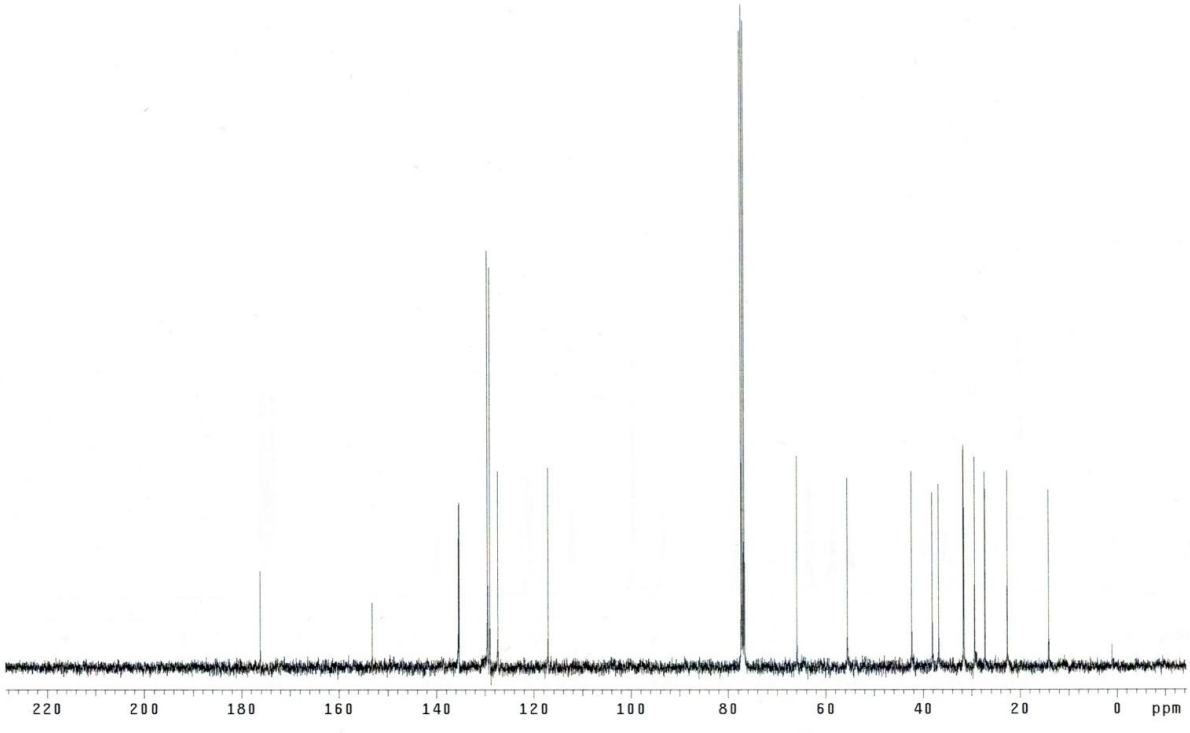

Figure A.11. ^{13}C NMR spectrum of **(*R*)-10.**

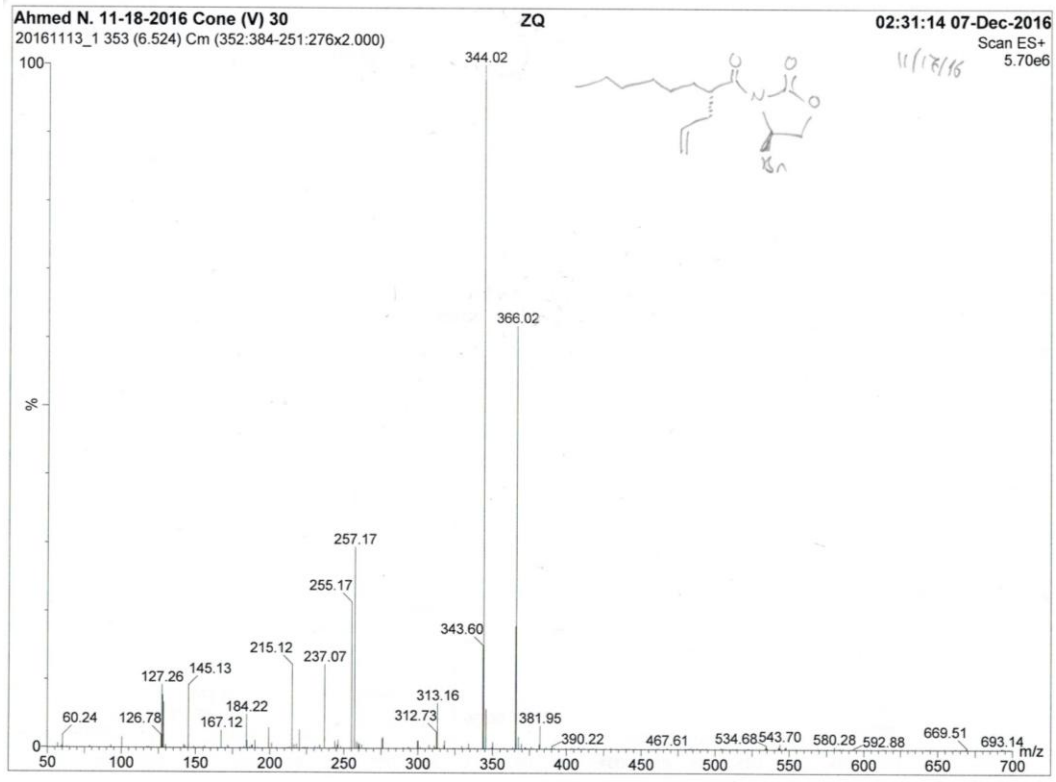

Figure A.12. Low resolution mass spectrum of **(*R*)-10.**

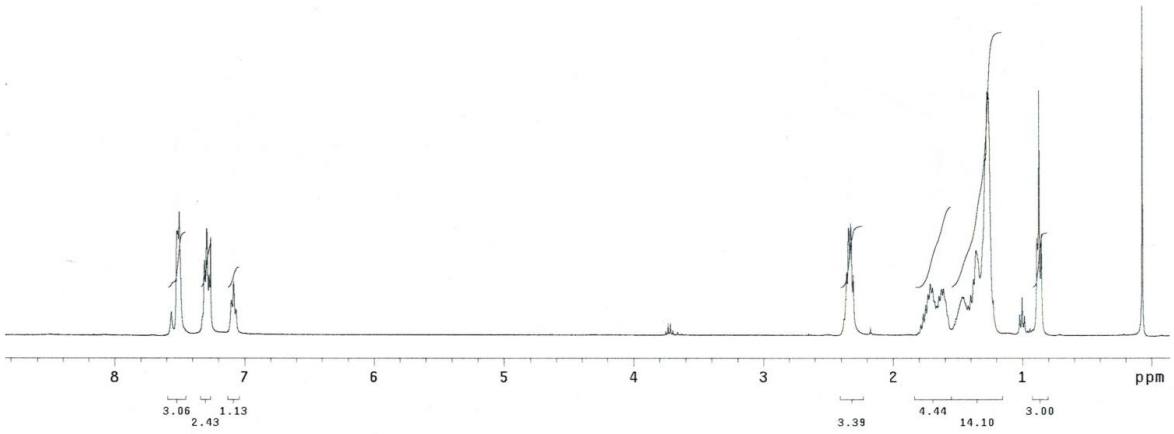

Figure A.13. ^{1}H NMR spectrum of **(*R*)-11.**

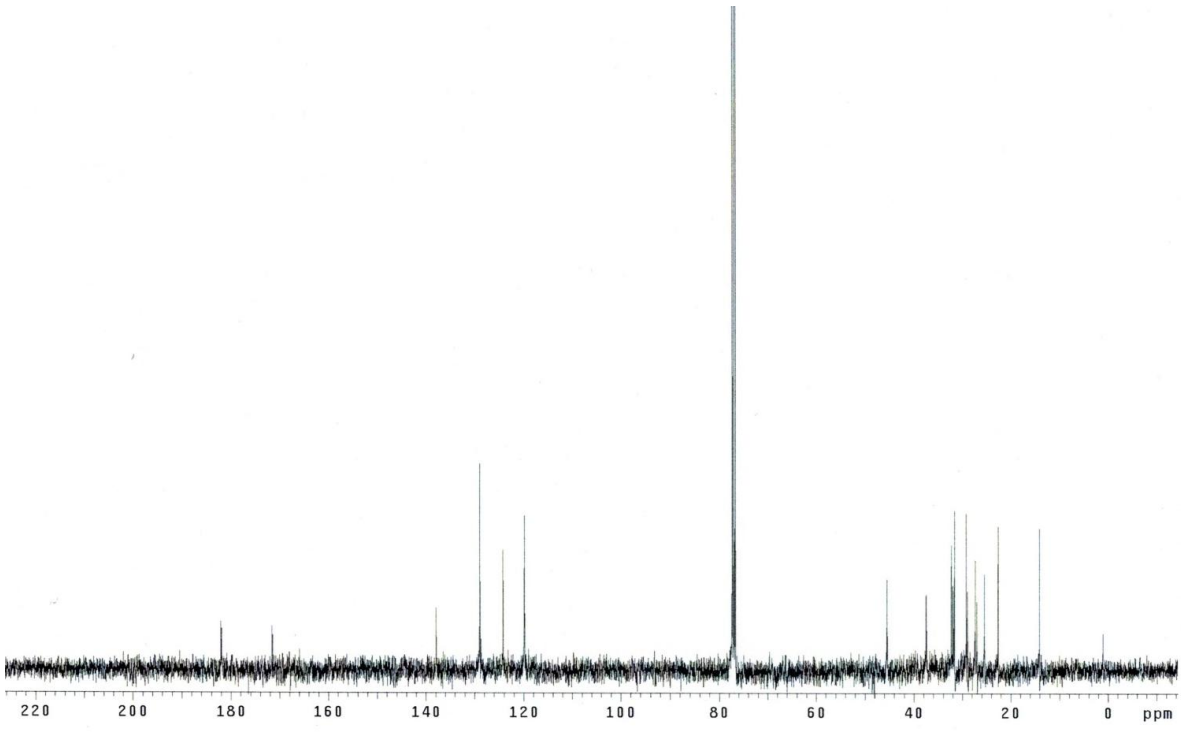

Figure A.14. ^{13}C NMR spectrum of **(*R*)-11.**

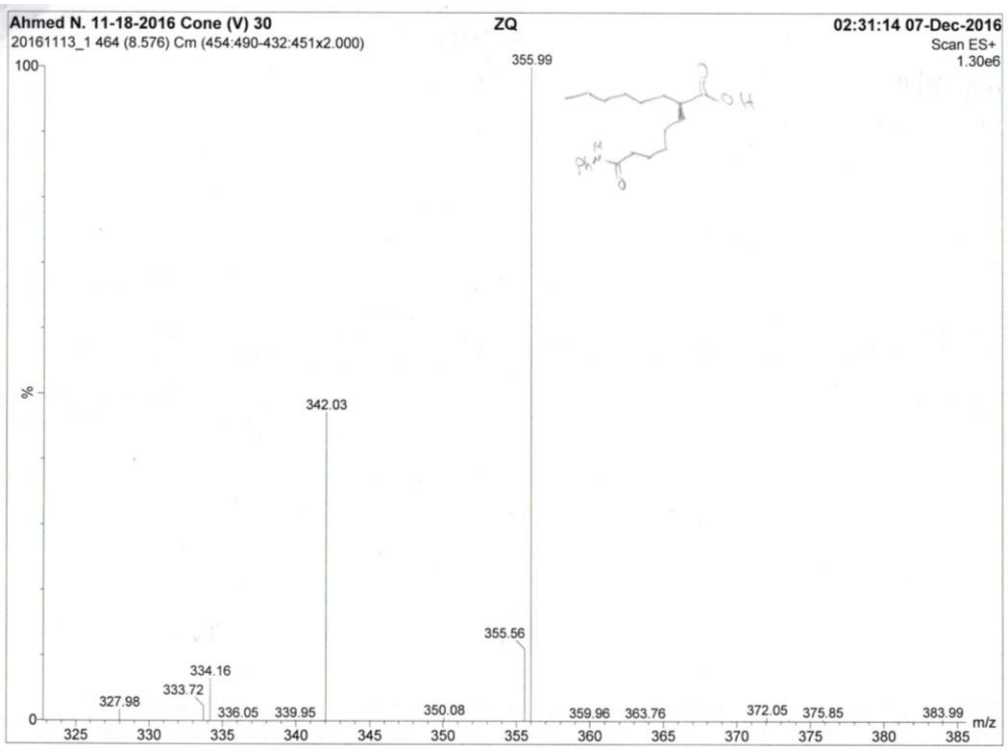

Figure A.15. Low resolution mass spectrum of **(*R*)-11.**

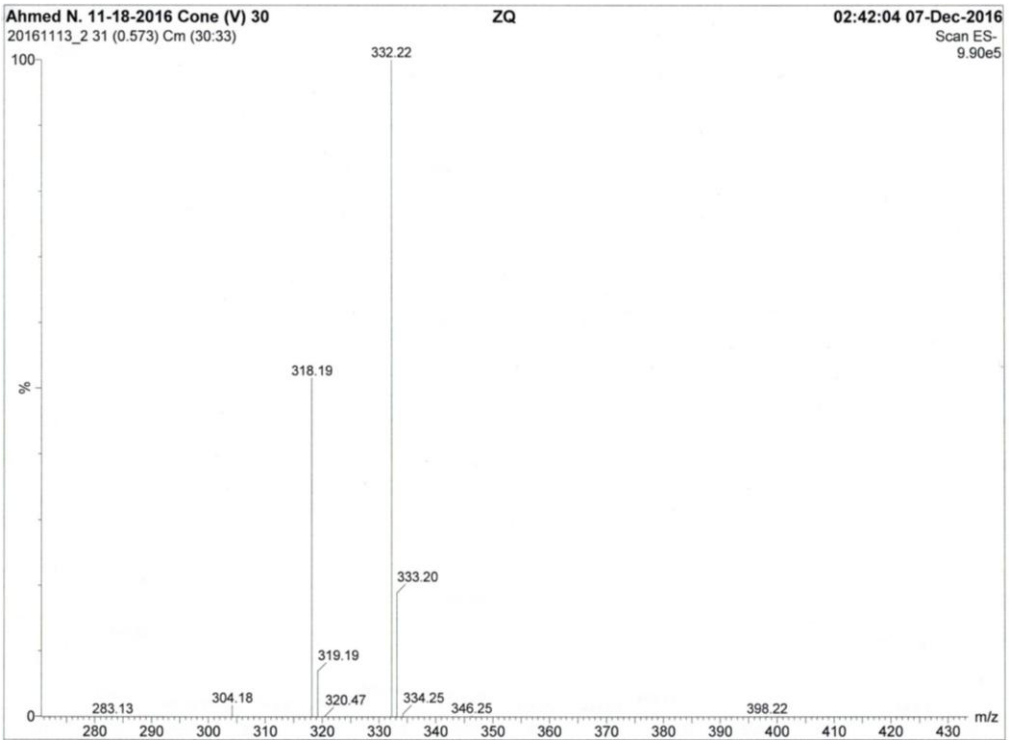

Figure A.16. Low resolution mass spectrum of **(*R*)-11.**

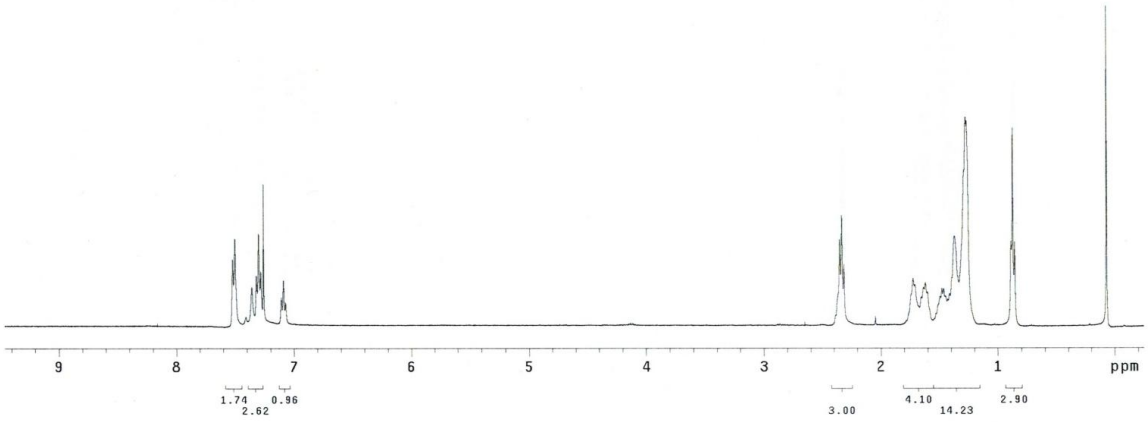

Figure A.17. ^{1}H NMR spectrum of **(*S*)-11.**

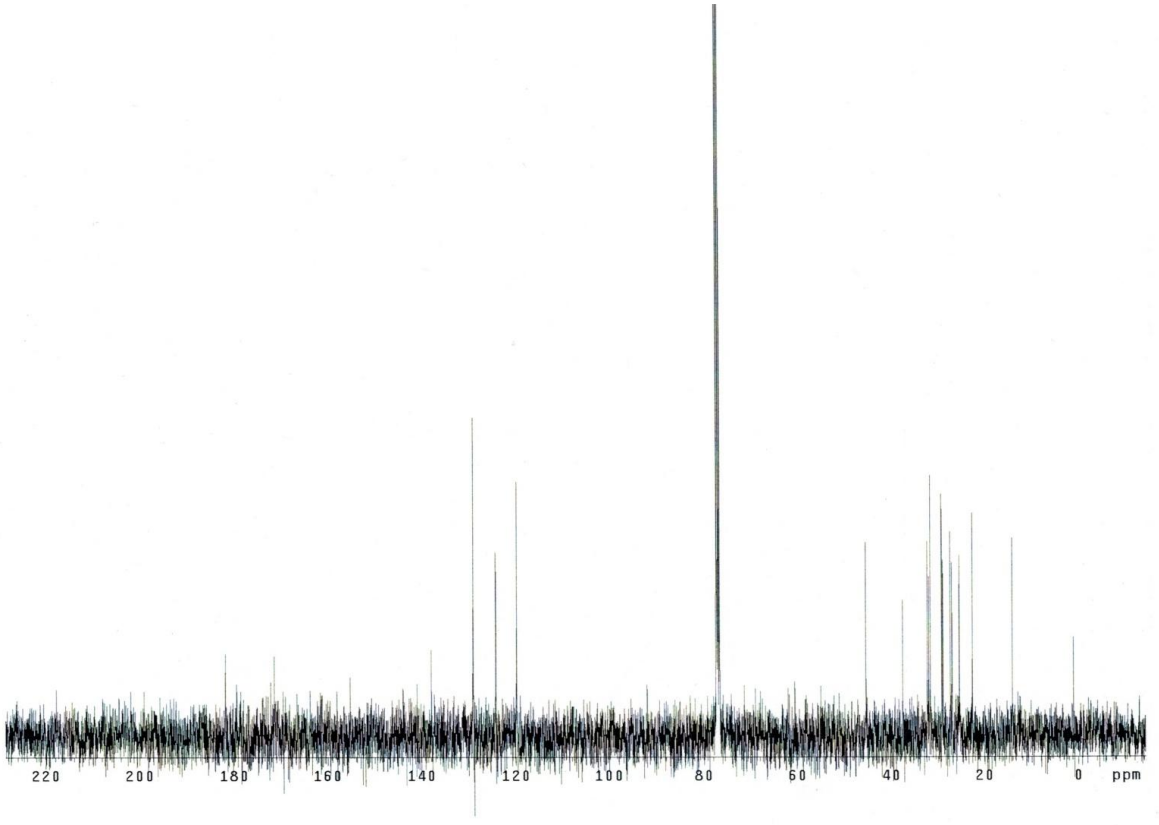

Figure A.18. ^{13}C NMR spectrum of **(*S*)-11.**

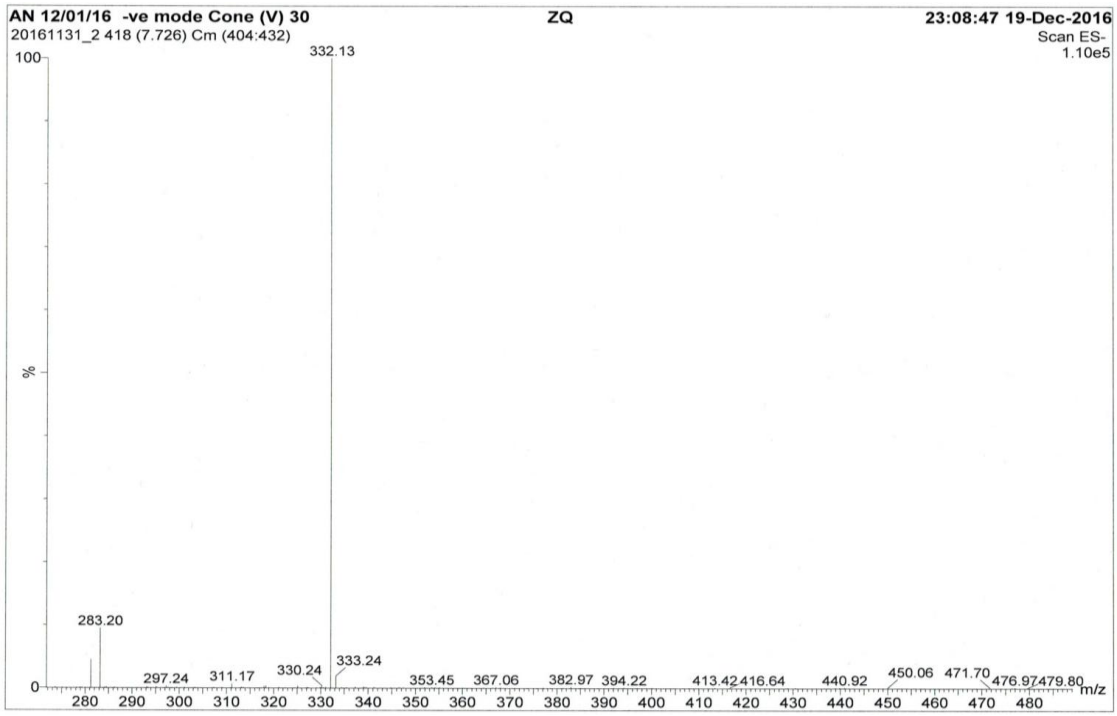

Figure A.19. Low resolution mass spectrum of **(*S*)-11.**

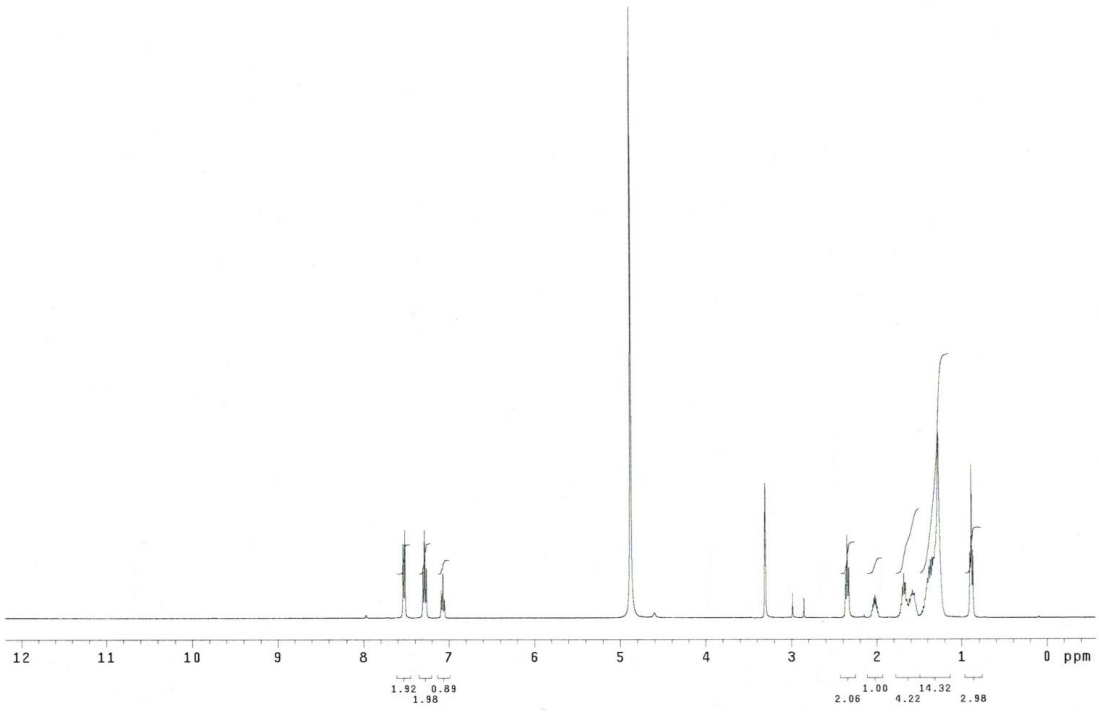

Figure A.20. ^{1}H NMR spectrum of *R*-C2-*n*-hexyl SAHA **(R)-1i.**

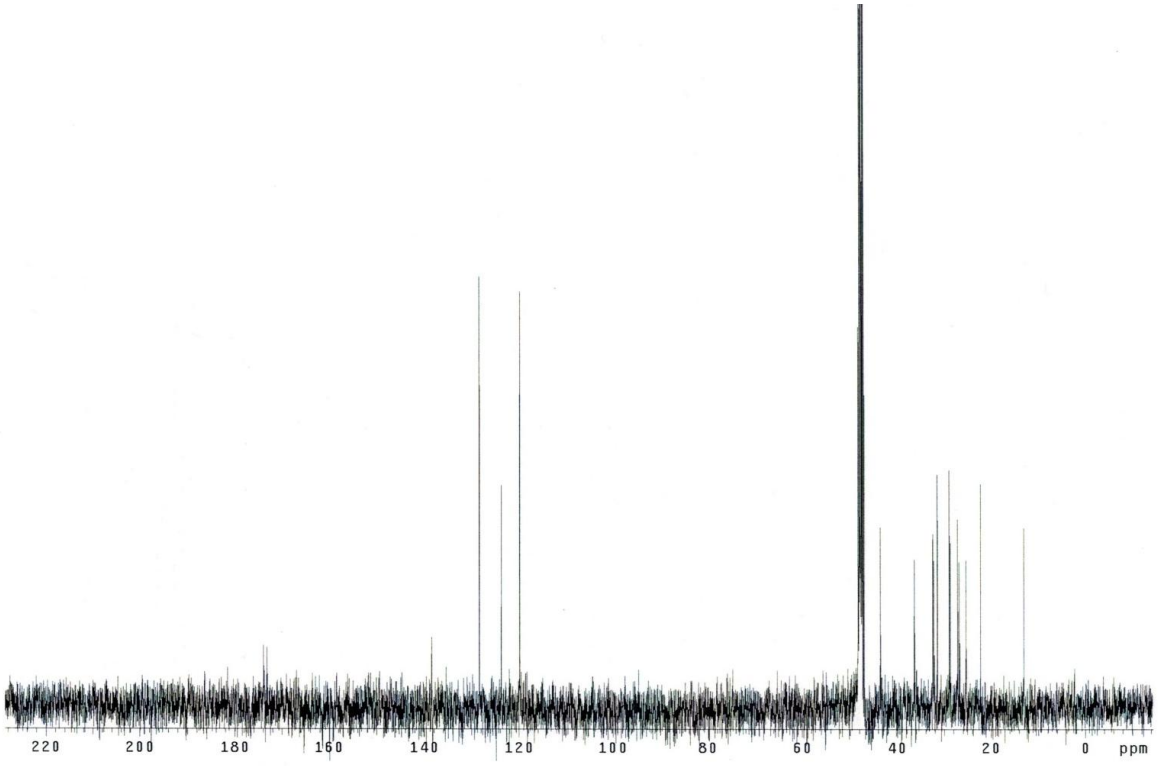

Figure A.21. ^{13}C NMR spectrum of *R*-C2-*n*-hexyl SAHA **(*R*)-1i.**

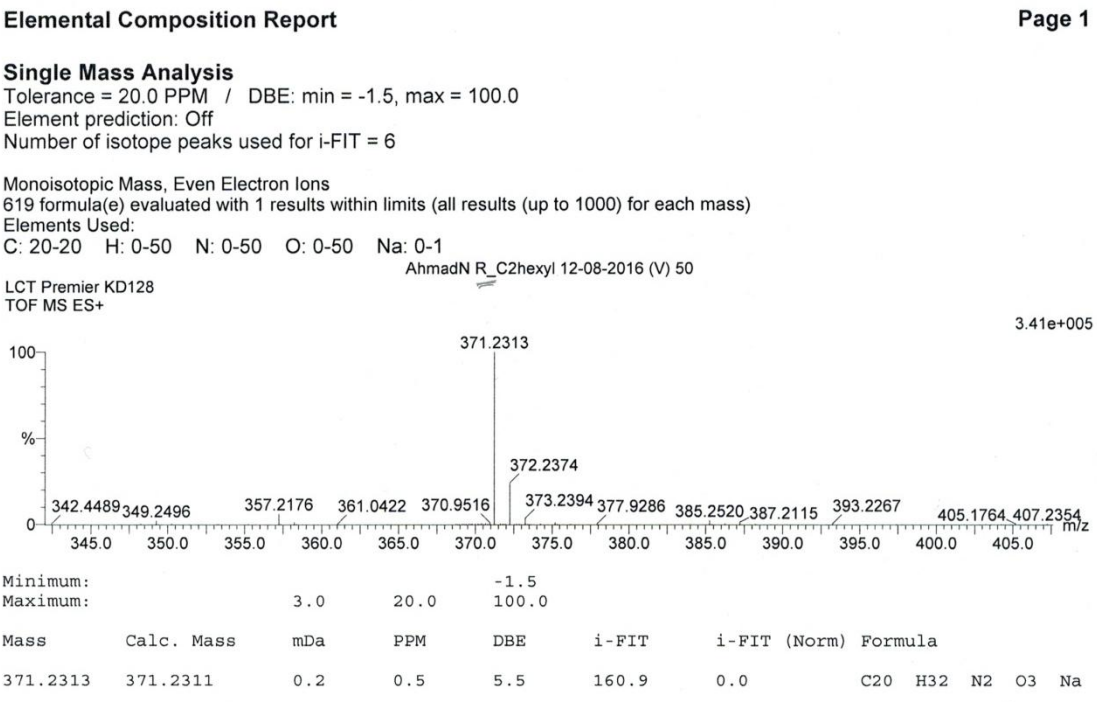

Figure A.22. High resolution mass spectrum of (*R*)-C2-*n*-hexyl SAHA **(R)-1i.**

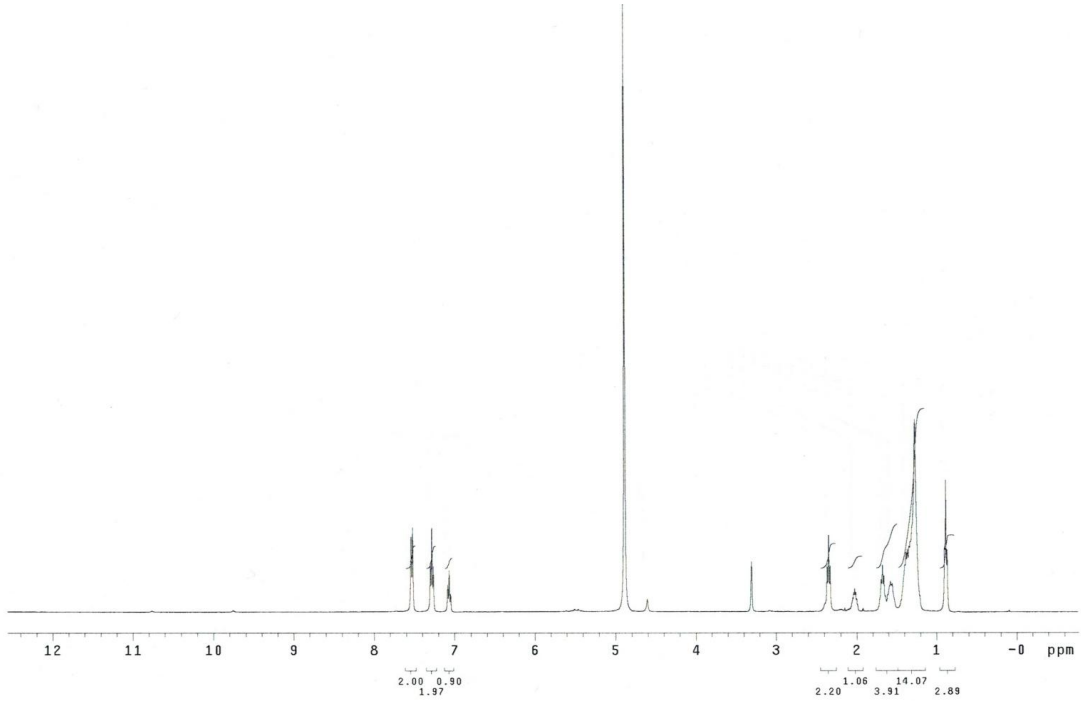

Figure A.23. ^{1}H NMR spectrum of (*S*)-C2-*n*-hexyl SAHA **(S)-1i.**

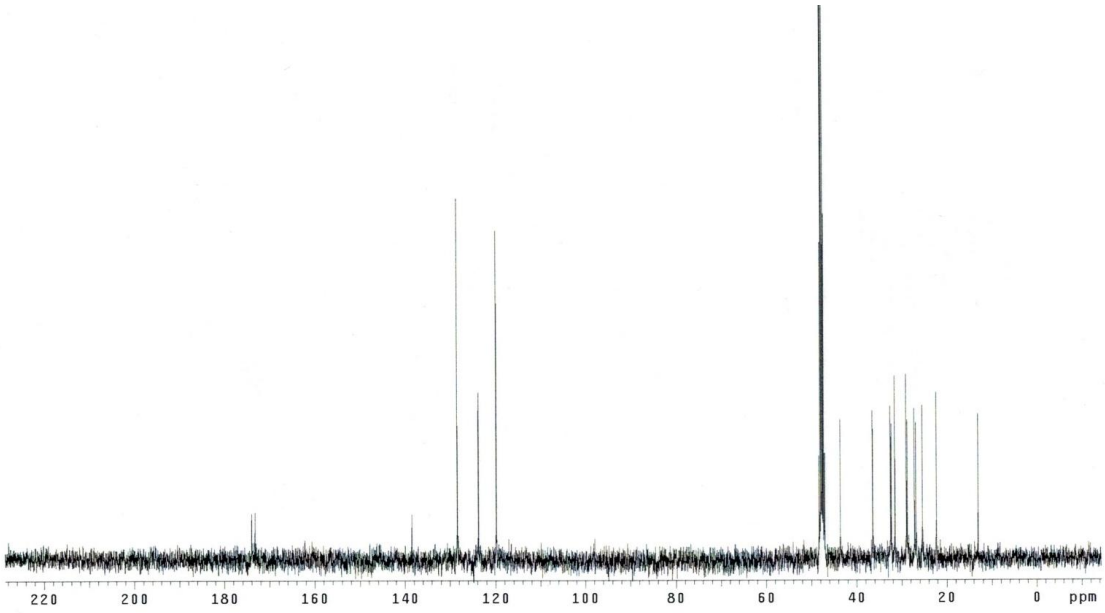

Figure A.24. ^{13}C NMR spectrum of (*S*)-C2-*n*-hexyl SAHA **(*S*)-1i**.

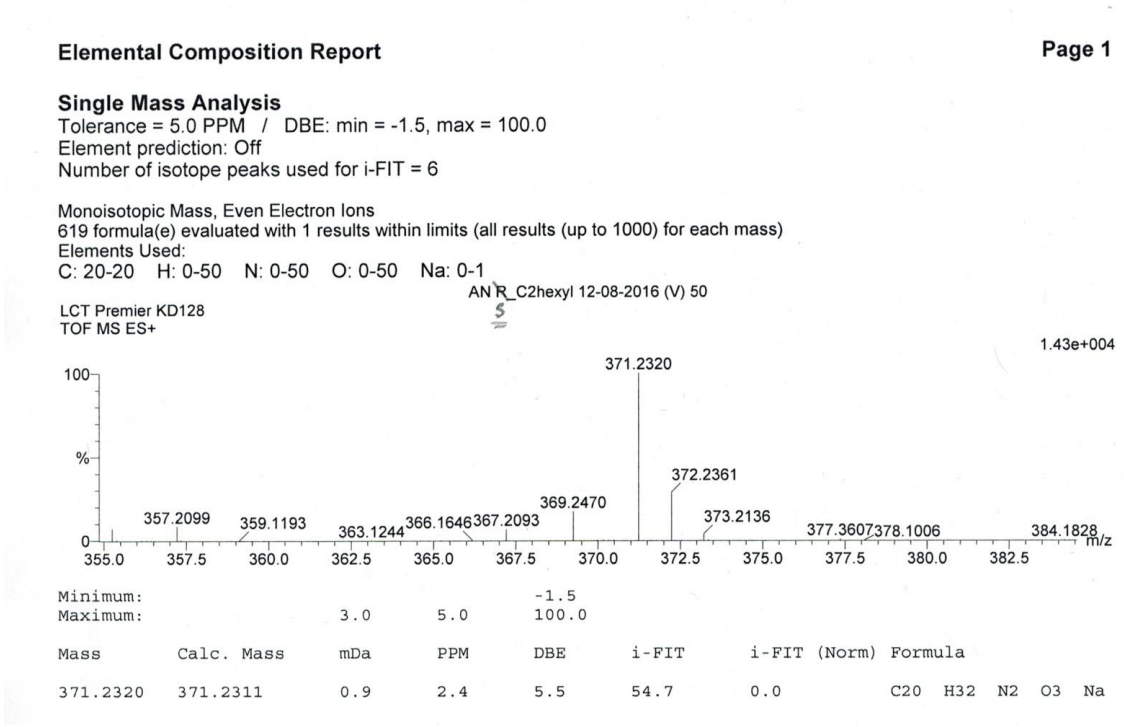

Elemental Composition Report Page 1

Single Mass Analysis
Tolerance = 5.0 PPM / DBE: min = -1.5, max = 100.0
Element prediction: Off
Number of isotope peaks used for i-FIT = 6

Monoisotopic Mass, Even Electron Ions
619 formula(e) evaluated with 1 results within limits (all results (up to 1000) for each mass)
Elements Used:
C: 20-20 H: 0-50 N: 0-50 O: 0-50 Na: 0-1

LCT Premier KD128
TOF MS ES+
AN R_C2hexyl 12-08-2016 (V) 50
1.43e+004

Minimum:				-1.5			
Maximum:		3.0	5.0	100.0			
Mass	Calc. Mass	mDa	PPM	DBE	i-FIT	i-FIT (Norm)	Formula
371.2320	371.2311	0.9	2.4	5.5	54.7	0.0	C20 H32 N2 O3 Na

Figure A.25. High resolution mass spectrum of (*S)*-C2-*n*-hexyl SAHA **(*S*)-1i.**

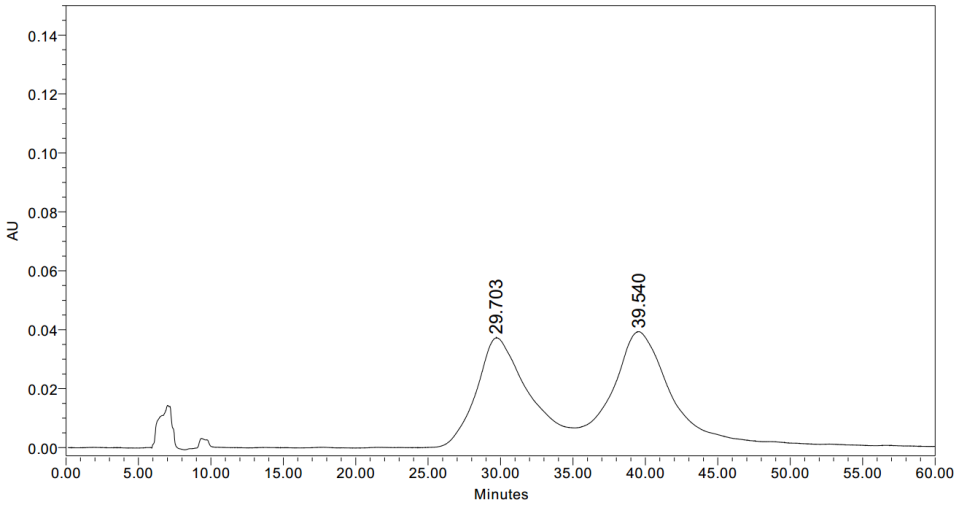

	RT	Area	% Area	Height
1	29.703	8936939	48.38	36430
2	39.540	9535849	51.62	37171

Figure A.26. Chiral HPLC spectrum taken at 254 nm of the C2-*n*-hexyl SAHA (**1i**) as a racemic mixture. The spectrum shows peaks for both the *R* and the *S* enantiomers. The calculated area and height under each peak, along with % area, is shown in the table below the spectrum.

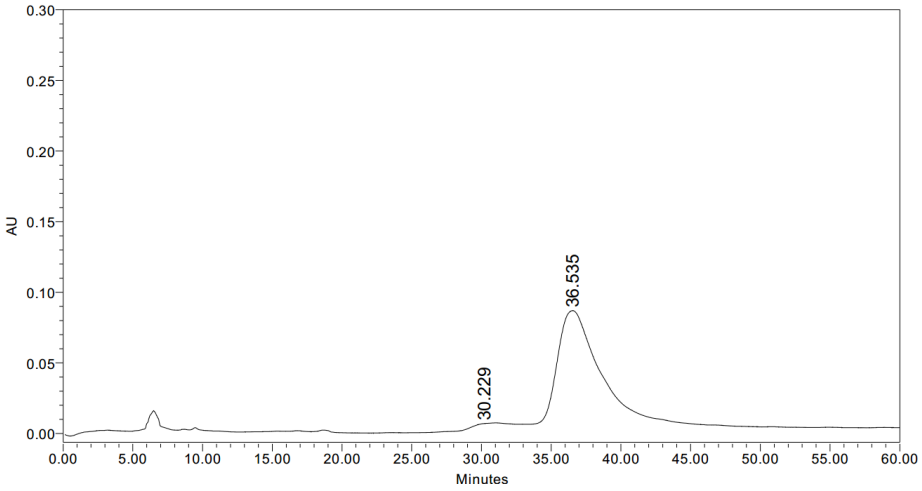

	RT	Area	% Area	Height
1	30.229	627338	3.97	3519
2	36.535	15190243	96.03	78984

Figure A.27. Chiral HPLC spectrum taken at 254 nm of the (*R*)-C2-*n*-hexyl SAHA **(*R*)-1i**. The major peak (at 36.5 min) represents the *R* enantiomer, while the minor peak (at 30.2 min) represents the *S* enantiomer. The calculated area and height under each peak, along with % area, is shown in the table below the spectrum.

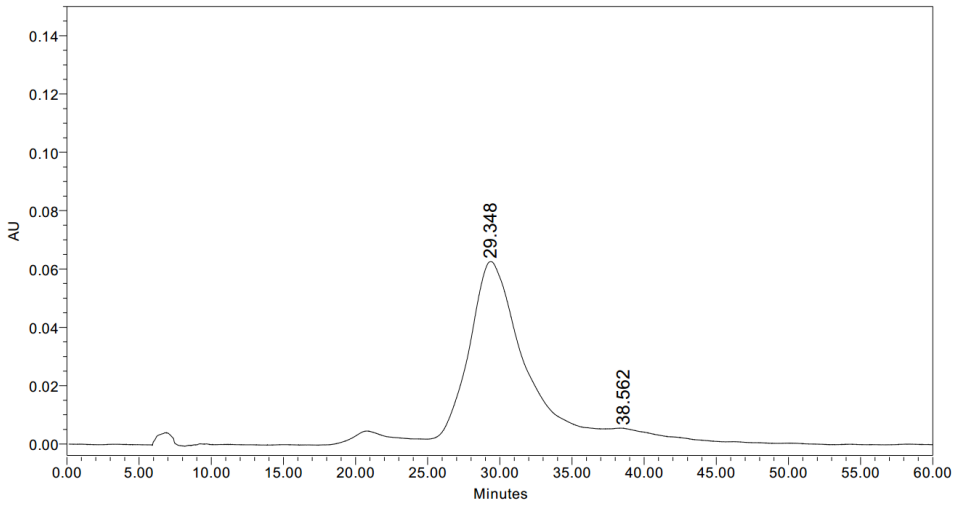

	RT	Area	% Area	Height
1	29.348	13214165	98.77	58447
2	38.562	163917	1.23	1143

Figure A.28. Chiral HPLC spectrum taken at 254 nm of the (*S*)-C2-*n*-hexyl SAHA (*S*-1i). The major peak (at 29.3 min) represents the *S* enantiomer, while the minor peak (at 38.6 min) represents the *R* enantiomer. The calculated area and height under each peak, along with % area, is shown in the table below the spectrum.

A.2. *In vitro* HDAC activity screening data

Table A.1. Percent remaining deacetylase activity after incubation of a single concentration of SAHA and each C2-modified SAHA analog with HDAC1, HDAC2, HDAC3, and HDAC6 using the ELISA-based activity assay.[a]

	Deacetylase activity (%)			
compound	HDAC1	HDAC2	HDAC3	HDAC6
SAHA[93]	8.9±0.1	8.3±0.2	14±3	7.9±1.6
1a (methyl)	62±8	78±3	96±4	55±6
1b (ethyl)	76±5	65±6	88±5	52±6
1c (propyl)	75±4	69±1	86±7	49±5
1d (butyl)	69±8	82±4	78±6	39±4
1e (allyl)	83±6	78±3	90±3	52±7
1f (propargyl)	90±7	91±2	99±3	62±7
1g (benzyl)	92±4	99±1	92±8	30±6
1h (pentyl)	89±1	99±2	95±4	21±5
1i (hexyl)	91±4	98±1	100±3	26±2

[a] The means and standard errors for a minimum of three independent trials are shown. All analogs were used at 5μM final concentration, except SAHA and C2-butyl (**1d**) which were tested at 1μM and 10μM respectively. This data is associated with Figure 2.3.

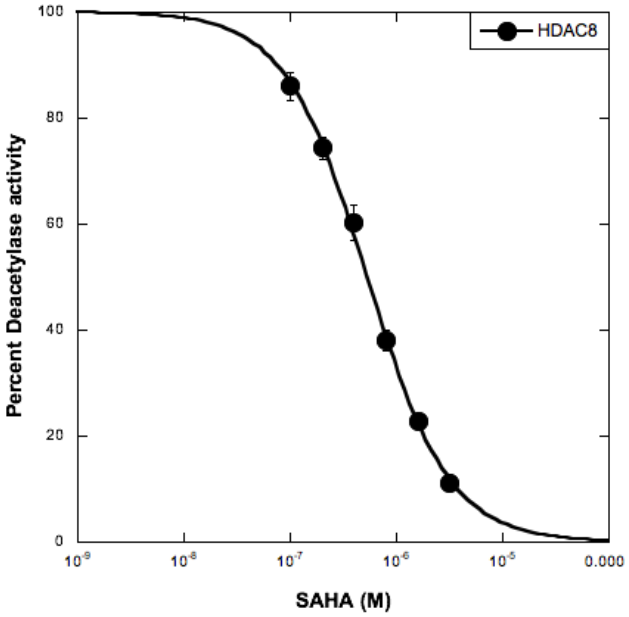

Figure A.29. Dose dependent curve of SAHA with HDAC8 isoform with error bars depicting the standard error of at three independent trials. In some cases, the error bars are smaller than the size of the filled circle. IC_{50} values associated with Table 2.2 were determined by fitting data to a sigmoidal curve using KaleidaGraph 4.1.3 (Synergy Software) (Table A.2).

Table A.2. Percentage remaining deacetylase activity after incubation of SAHA with HDAC8.[a]

Concentration (M)	Deacetylase activity (%)
3.2×10^{-6}	11±1
1.6×10^{-6}	23±1
8.0×10^{-7}	38±2
4.0×10^{-7}	60±3
2.0×10^{-7}	74±2
1.0×10^{-7}	86±3

[a] Means and standard errors of at three independent trials with the SAHA concentrations shown. Data is associated with Figure A.29 and Table 2.2.

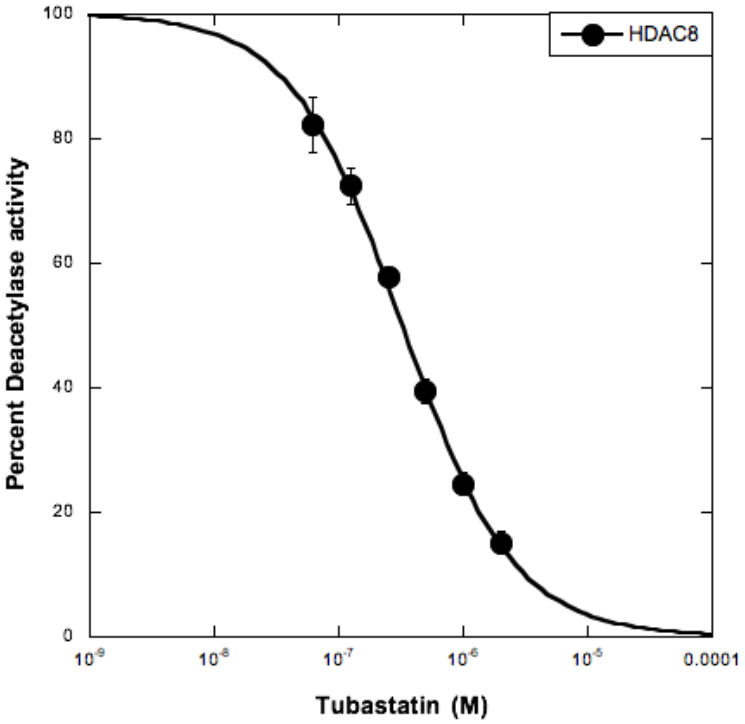

Figure A.30. Dose dependent curve of tubastatin with HDAC8 isoform with error bars depicting the standard error of at three independent trials. In some cases, the error bars are smaller than the size of the filled circle. IC_{50} values associated with Table 2.2 were determined by fitting data to a sigmoidal curve using KaleidaGraph 4.1.3 (Synergy Software) (Table A.3).

Table A.3. Percentage remaining deacetylase activity after incubation of tubastatin with HDAC8.[a]

Concentration (M)	Deacetylase activity (%)
2.0×10^{-6}	15±2
1.0×10^{-6}	25±2
5.0×10^{-7}	40±2
2.5×10^{-7}	58±1
1.25×10^{-7}	73±3
6.25×10^{-8}	82±4

[a] Means and standard errors of at three independent trials with the tubastatin concentrations shown. Data is associated with Figure A.30 and Table 2.2.

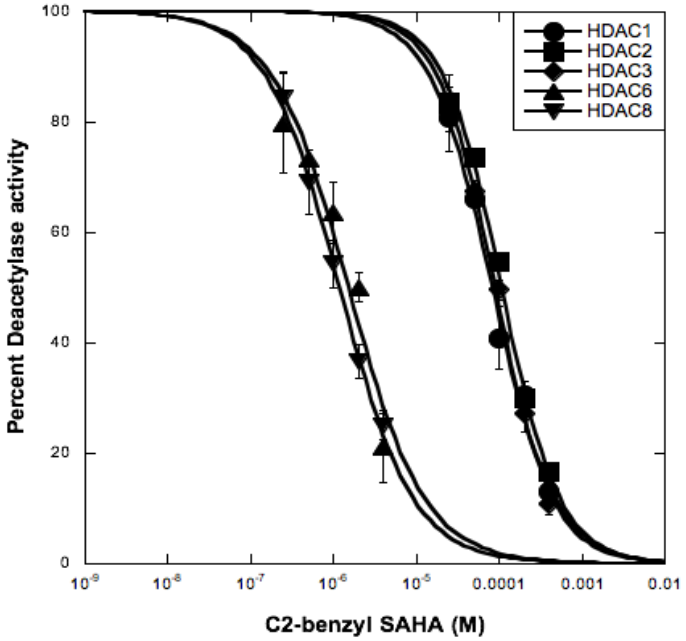

Figure A.31. Dose dependent curves of C2-benzyl SAHA analog (**1g**) with HDAC1, HDAC2, HDAC3, HDAC6, and HDAC8 isoforms with error bars depicting the standard error of at least two independent trials. IC_{50} values associated with Table 2.2 were determined by fitting data to a sigmoidal curve using KaleidaGraph 4.1.3 (Synergy Software) (Table A.4).

Table A.4. Percentage remaining deacetylase activity after incubation of C2-benzyl SAHA (**1g**) with HDAC1, HDAC2, HDAC3, HDAC6, and HDAC8.[a]

Concentration (M)	Deacetylase activity (%)				
	HDAC1	HDAC2	HDAC3	HDAC6	HDAC8
4.0×10^{-4}	13±1	17±1	11±2		
2.0×10^{-4}	31±2	30±2	27±3		
1.0×10^{-4}	41±6	55±1	50±2		
5.0×10^{-5}	66±1	74±1	68±2		
2.5×10^{-5}	81±3	84±3	82±7		
4.0×10^{-6}				21±7	25±2
2.0×10^{-6}				50±3	37±3
1.0×10^{-6}				64±6	54±4
5.0×10^{-7}				73±1	69±6
2.5×10^{-7}				80±9	84±5

[a] Means and standard errors of at least two independent trials with the C2-benzyl SAHA (**1g**) concentrations shown. Data is associated with Figure A.31 and Table 2.2.

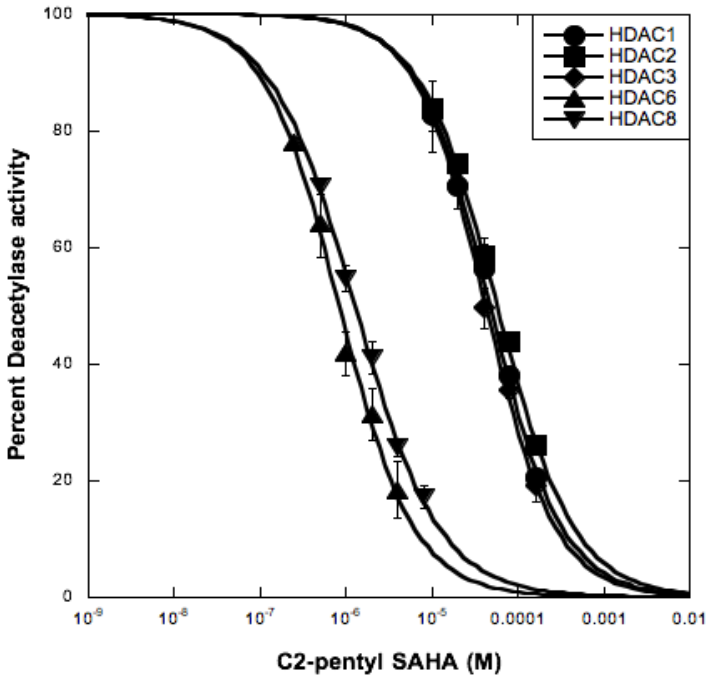

Figure A.32. Dose dependent curves of C2-*n*-pentyl SAHA analog (**1h**) with HDAC1, HDAC2, HDAC3, HDAC6, and HDAC8 isoforms with error bars depicting the standard error of at least two independent trials. IC_{50} values associated with Table 2.2 were determined by fitting data to a sigmoidal curve using KaleidaGraph 4.1.3 (Synergy Software) (Table A.5).

Table A.5. Percentage remaining deacetylase activity after incubation of C2-*n*-pentyl SAHA (**1h**) with HDAC1, HDAC2, HDAC3, HDAC6, and HDAC8.[a]

Concentration (M)	Deacetylase Activity (%)				
	HDAC1	HDAC2	HDAC3	HDAC6	HDAC8
1.6×10^{-4}	21±1	26±1	19±3		
8.0×10^{-5}	38±1	44±1	36±2		
4.0×10^{-5}	56±4	59±3	50±3		
2.0×10^{-5}	71±1	74±1	71±4		
1.0×10^{-5}	83±3	84±1	83±6		
8.0×10^{-6}					17±2
4.0×10^{-6}				18±5	26±1
2.0×10^{-6}				31±4	41±3
1.0×10^{-6}				42±4	55±2
5.0×10^{-7}				64±6	71±1
2.5×10^{-7}				78±1	

[a] Means and standard errors of at least two independent trials with the C2-*n*-pentyl SAHA (**1h**) concentrations shown. Data is associated with Figure A.32 and Table 2.2.

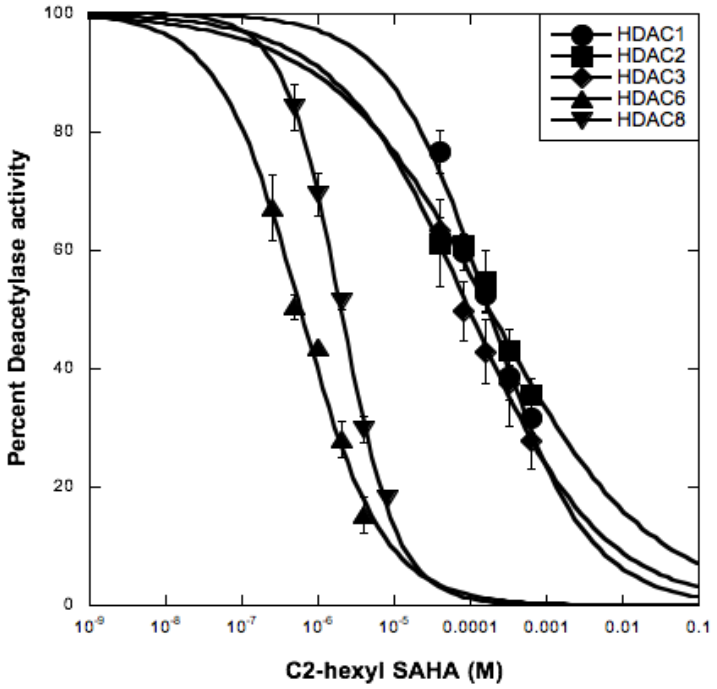

Figure A.33. Dose dependent curves of C2-*n*-hexyl SAHA derivative (**1i**) with HDAC1, HDAC2, HDAC3, HDAC6, and HDAC8 isoforms with error bars depicting the standard error of at least two independent trials. IC_{50} values associated with Table 2.2 were determined by fitting data to a sigmoidal curve using KaleidaGraph 4.1.3 (Synergy Software) (Table A.6).

Table A.6. Percentage of remaining HDAC deacetylase activity after incubation of C2-*n*-hexyl SAHA derivative (**1i**) HDAC1, HDAC2, HDAC3, HDAC6, and HDAC8.[a]

Concentration (M)	Deacetylase Activity (%)				
	HDAC1	HDAC2	HDAC3	HDAC6	HDAC8
6.4×10^{-4}	32±2	35±3	28±5		
3.2×10^{-4}	39±8	43±1	38±3		
1.6×10^{-4}	52±3	55±5	43±5		
8.0×10^{-5}	60±3	61±2	50±5		
4.0×10^{-5}	77±4	61±7	63±2		
8.0×10^{-6}					18±1
4.0×10^{-6}				15±3	30±2
2.0×10^{-6}				28±3	51±1
1.0×10^{-6}				44±1	70±4
5.0×10^{-7}				50±2	84±4
2.5×10^{-7}				67±6	

[a] Means and standard errors of at least two independent trials are shown. Data is associated with Figure A.33 and Table 2.2.

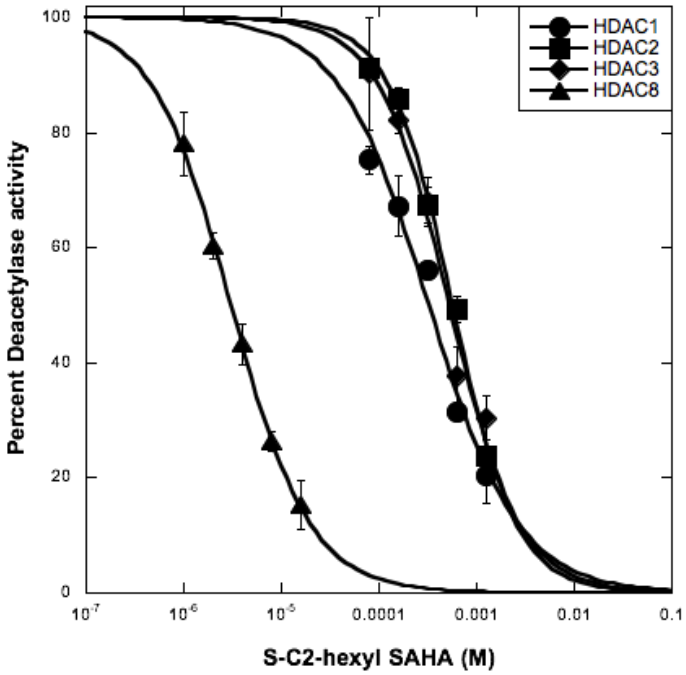

Figure A.34. Dose dependent curves of (*S*)-C2-*n*-hexyl SAHA ((***S***)-**1i**) with HDAC1, HDAC2, HDAC3, and HDAC8 isoforms with error bars depicting the standard error of at least two independent trials. IC_{50} values associated with Table 2.2 were determined by fitting data to a sigmoidal curve using KaleidaGraph 4.1.3 (Synergy Software) (Table A.7).

Table A.7. Percentage of remaining HDAC deacetylase activity after incubation of (*S*)-C2-*n*-hexyl SAHA ((***S***)-**1i**) HDAC1, HDAC2, HDAC3, and HDAC8.[a]

Concentration (M)	Deacetylase Activity (%)			
	HDAC1	HDAC2	HDAC3	HDAC8
1.28×10^{-3}	20±5	24±1	30±4	
6.4×10^{-4}	32±1	49±2	38±5	
3.2×10^{-4}	56±1	68±3	68±4	
1.6×10^{-4}	67±5	86±2	82±2	
8.0×10^{-5}	75±2	91±1	90±10	
1.6×10^{-5}				15±4
8.0×10^{-6}				26±2
4.0×10^{-6}				43±4
2.0×10^{-6}				60±2
1.0×10^{-6}				78±6

[a] Means and standard errors of at least two independent trials are shown. Data is associated with Figure A.34 and Table 2.2.

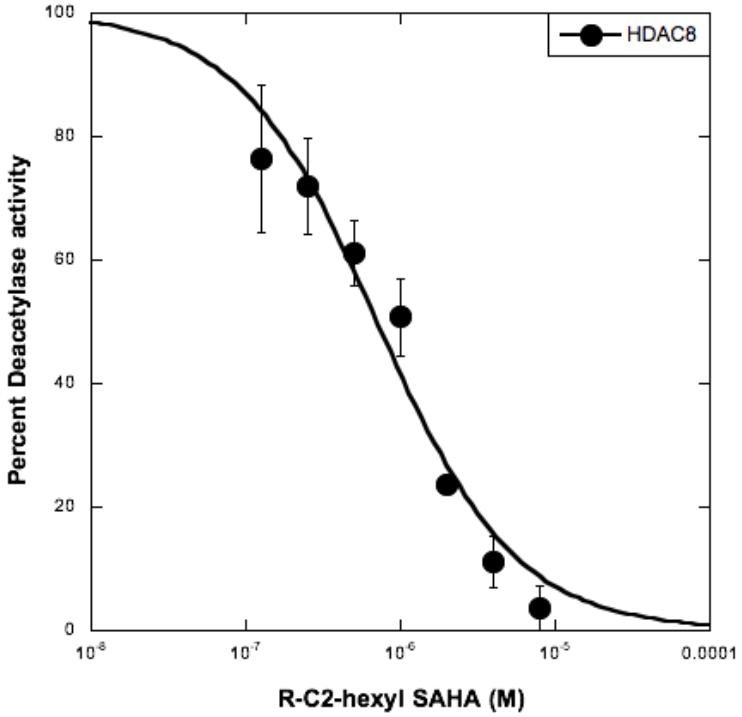

Figure A.35. Dose dependent curves of (*R*)-C2-*n*-hexyl SAHA derivative ((***S***)-**1i**) with HDAC8 isoform with error bars depicting the standard error of at least two independent trials. IC_{50} values associated with Table 2.2 were determined by fitting data to a sigmoidal curve using KaleidaGraph 4.1.3 (Synergy Software) (Table A.8).

Table A.8. Percentage of remaining HDAC deacetylase activity after incubation of (*R*)-C2-*n*-hexyl SAHA and HDAC8.[a]

Concentration (M)	Deacetylase Activity (%)
	HDAC8
8.0×10^{-6}	3.7±3.5
4.0×10^{-6}	11±4
2.0×10^{-6}	24±1
1.0×10^{-6}	50±6
5.0×10^{-7}	63±5
2.5×10^{-7}	72±8
1.25×10^{-7}	76±12

[a] Means and standard errors of at least two independent trials are shown. Data is associated with Figure A.35 and Table 2.2.

A.3. *In cellulo* selectivity data

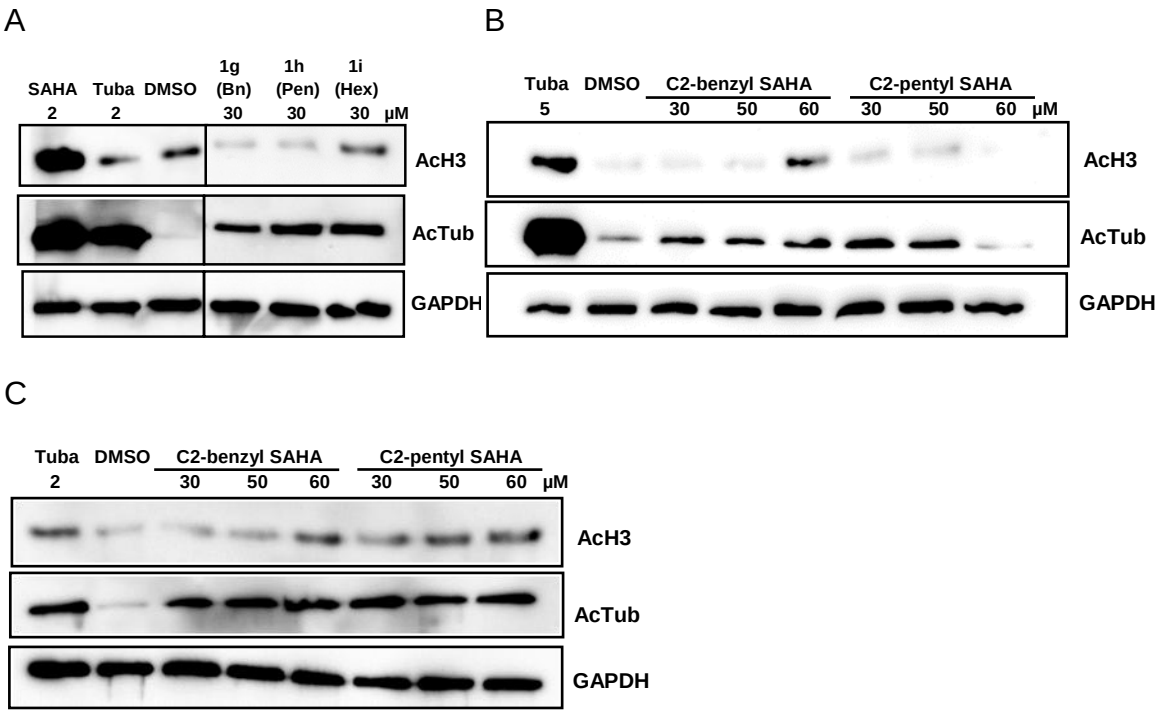

Figure A.36. Representative cell-based selectivity trials with SAHA, tubastatin and SAHA analogs. U937 cells were treated with DMSO (1%), SAHA, C2-benzyl SAHA (**1g**), C2-n-pentyl SAHA (**1h**), C2-n-hexyl SAHA (**1i**). After lysis and SDS-PAGE separation of the proteins in the lysates, western blots analysis of acetyl-histone H3 (AcH3) and acetyl-α-tubulin (AcTub) was performed. GAPDH was used as a loading control. DMSO was used as the no inhibitor control. These three trials (parts A-C) are associated with the fourth trial shown in Figure 2.4a.

Table A.9. Fold increase in acetyl-histone H3 and acetyl-tubulin at 30 μM of SAHA analogs **1g**, **1i**, and **1h**, compared to DMSO treated cells for the western blots images in figures 2.4a and A.36.[a]

Compound	Acetyl-histone H3		Acetyl-tubulin	
	Mean fold increase	Standard error	Mean fold increase	Standard error
1g (benzyl)	0.99	0.32	5.0	0.80
1i (pentyl)	1.6	0.84	7.5	3.2
1h (hexyl)	1.3	0.44	3.9	0.53

[a] Means and standard errors of four independent trials are shown. Data is associated with Figures 2.4a, A.36 and A.37.

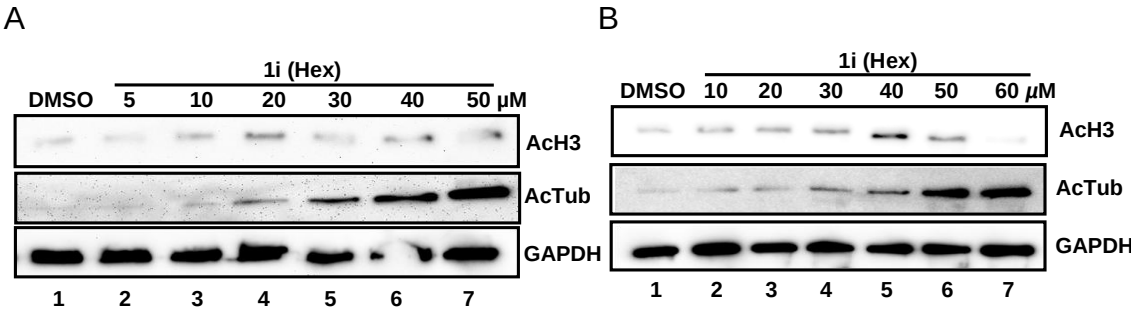

Figure A.37. Repetitive cell-based selectivity trials with C2-n-hexyl SAHA analog (**1i**). U937 cells were treated with increasing concentrations of C2-n-hexyl SAHA analog (**1i**, 10-60 μM or 5-50 μM). After lysis and SDS-PAGE separation of the proteins in the lysates, western blot analysis of acetyl-histone H3 (AcH3) and acetyl-α-tubulin (AcTub) was performed. GAPDH was used as a loading control. DMSO was used as the no inhibitor control. These two trials (parts a and b) are associated with the third trial shown in Figure 2.4b.

A.4. Cell growth inhibition data

Table A.10. Percentage of viable cells after treatment of Jurkat cell line with of C2-benzyl SAHA **1g**, C2-pentyl SAHA **1h**, C2-hexyl SAHA **1i**, and SAHA.[a]

	Viable cells (%)	
Compound	1 μM	10 μM
1g (benzyl)	100 ± 8	83 ± 2
1h (pentyl)	80 ± 13	92 ± 8
1i (hexyl)	88 ± 11	47 ± 9
SAHA	49 ± 6	5 ± 3

[a] Means and standard errors for a minimum of three independent trials are shown. All analogs were tested at 1 and 10μM final concentrations. Data is associated with Figure 2.5.

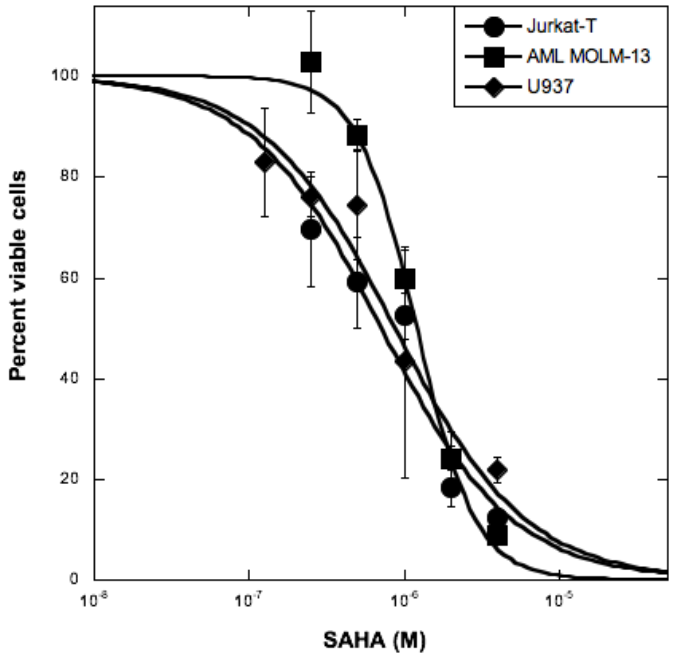

Figure A.38. Dose dependent cell viability of SAHA with Jurkat, AML MOLM-13, and U937 cell lines, with error bars depicting the standard error of at least three independent trials. EC_{50} values associated with Table 2.3 were determined by fitting data to a sigmoidal curve using KaleidaGraph 4.1.3 (Synergy Software) (Table A.11).

Table A.11. Percentage of viable cells after treatment of different cell lines with SAHA at the specified concentrations.[a]

Concentration (M)	Viable cells (%)		
	Jurkat	AML-MOL13	U937
4.0×10^{-6}	12 ± 1	9 ± 1	22 ± 3
2.0×10^{-6}	18 ± 4	24 ± 2	24 ± 6
1.0×10^{-6}	53 ± 5	60 ± 6	43 ± 23
5.0×10^{-7}	59 ± 9	88 ± 3	75 ± 11
2.5×10^{-7}	70 ± 11	103 ± 10	76 ± 4
1.25×10^{-7}			83 ± 11

[a] Standard errors of at least three independent trials are shown. Data is associated with Figure A.38 and Table 2.3.

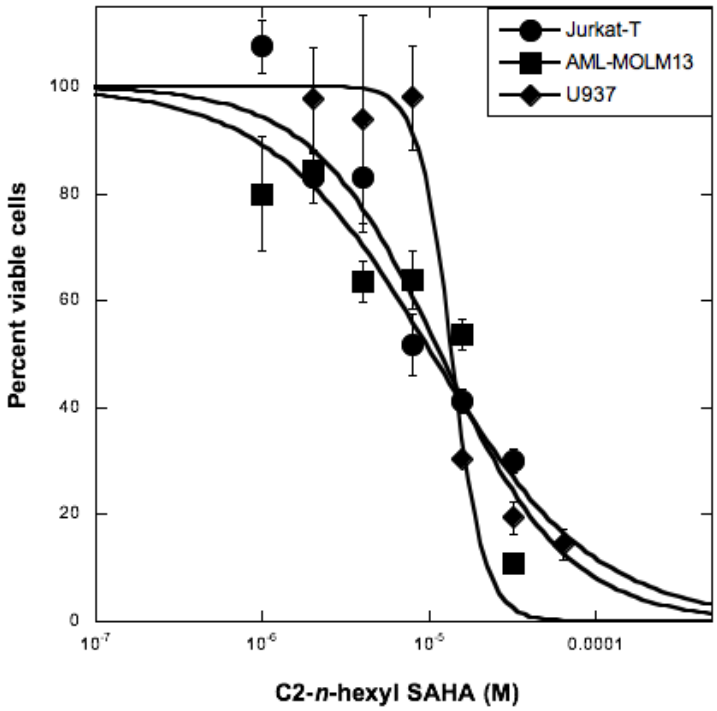

Figure A.39. Dose dependent cell viability of C2-*n*-hexyl SAHA (**1i**) with Jurkat, AML MOLM-13, and U937 cell lines, with error bars depicting the standard error of more than three independent trials. EC_{50} values associated with Table 2.3 were determined by fitting data to a sigmoidal curve using KaleidaGraph 4.1.3 (Synergy Software) (Table A.12).

Table A.12. Percentage of viable cells after treatment of different cell lines with of C2-*n*-hexyl SAHA (**1i**) at the specified concentrations.[a]

Concentration (M)	Viable cells (%)		
	Jurkat	AML-MOL13	U937
6.4×10^{-5}			14 ± 3
3.2×10^{-5}	30 ± 2	11 ± 1	19 ± 3
1.6×10^{-5}	41 ± 2	54 ± 3	30 ± 1
8.0×10^{-6}	52 ± 6	64 ± 5	98 ± 10
4.0×10^{-6}	83 ± 10	64 ± 4	94 ± 20
2.0×10^{-6}	83 ± 5	84 ± 3	98 ± 10
1.0×10^{-6}	108 ± 5	80 ± 11	

[a] Means and standard errors of at least three independent trials are shown. Data is associated with Figure A.39 and Table 2.3.

APPENDIX B

B.1. Compound characterization of the C4-modified SAHA analogs

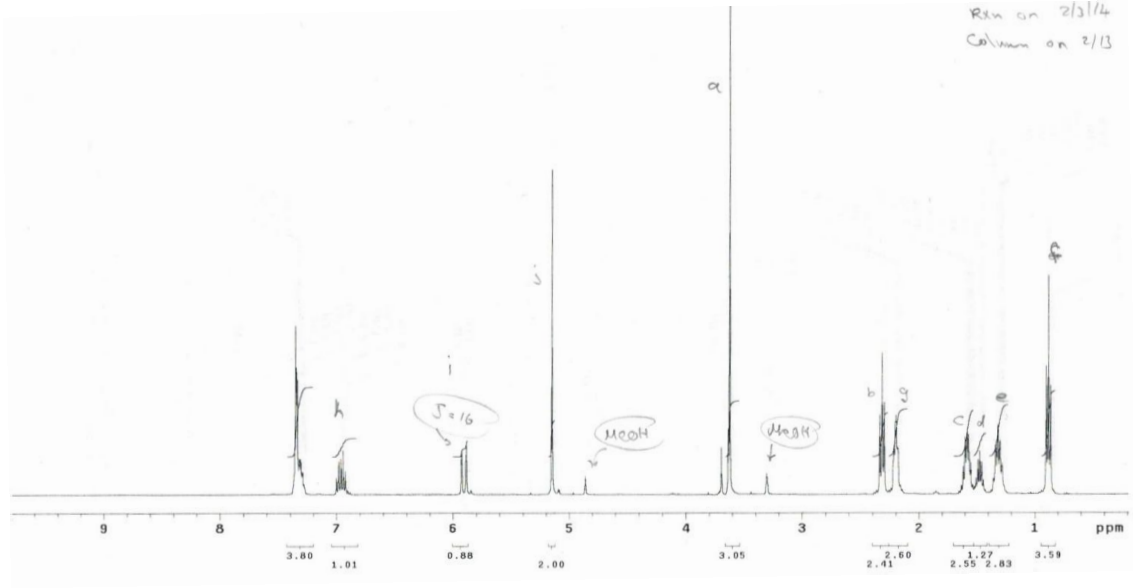

Figure B.1. ^{1}HNMR spectrum of **16b** in CD_3OD.

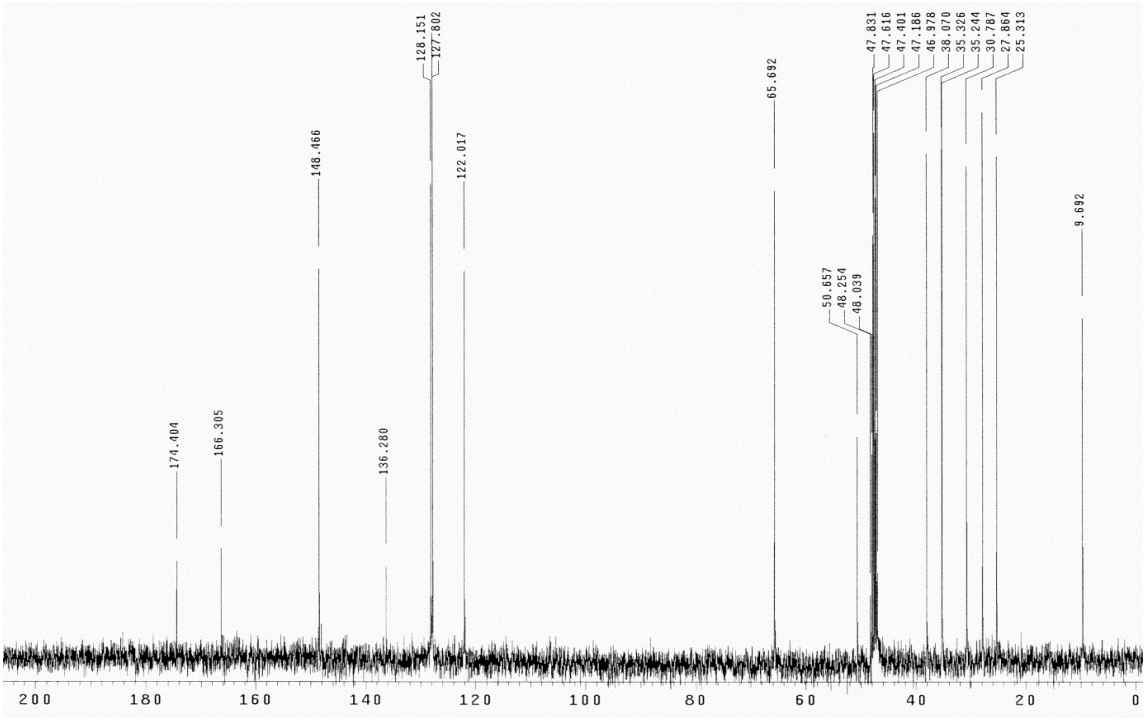

Figure B.2. ^{13}CNMR spectrum of **16b** in CD_3OD.

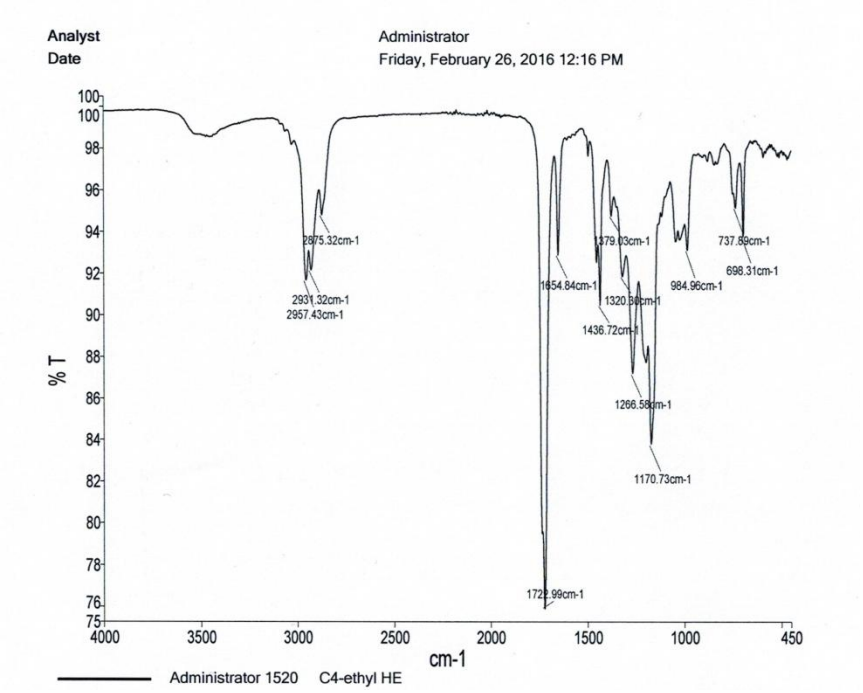

Figure B.3. IR spectrum of **16b** using a Perkin Elmer Spectrum Two ATR-FTIR.

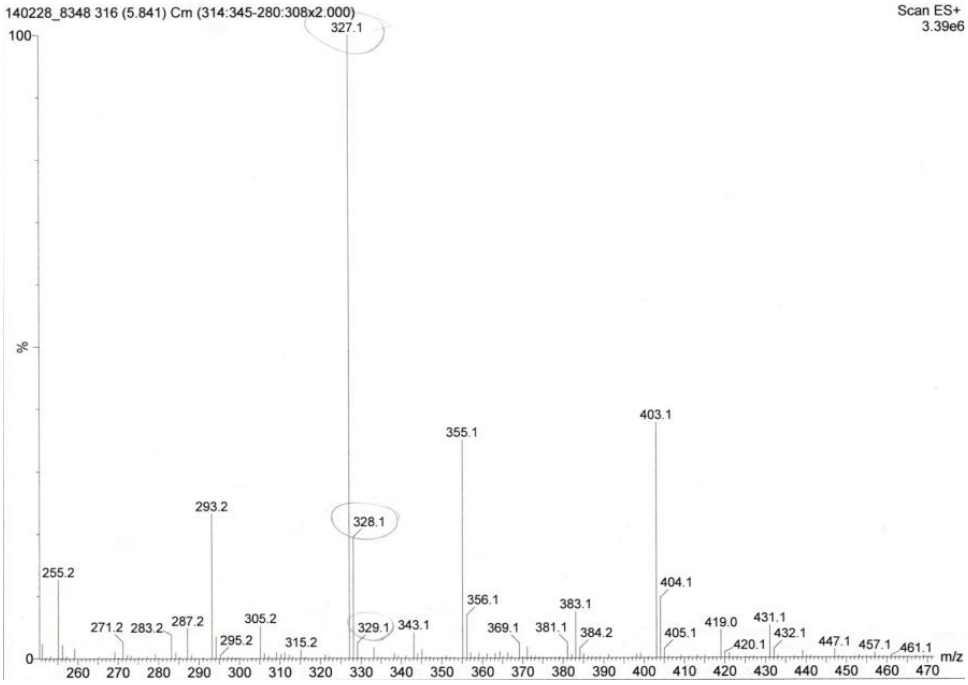

Figure B.4. Low resolution mass spectrum of **16b**.

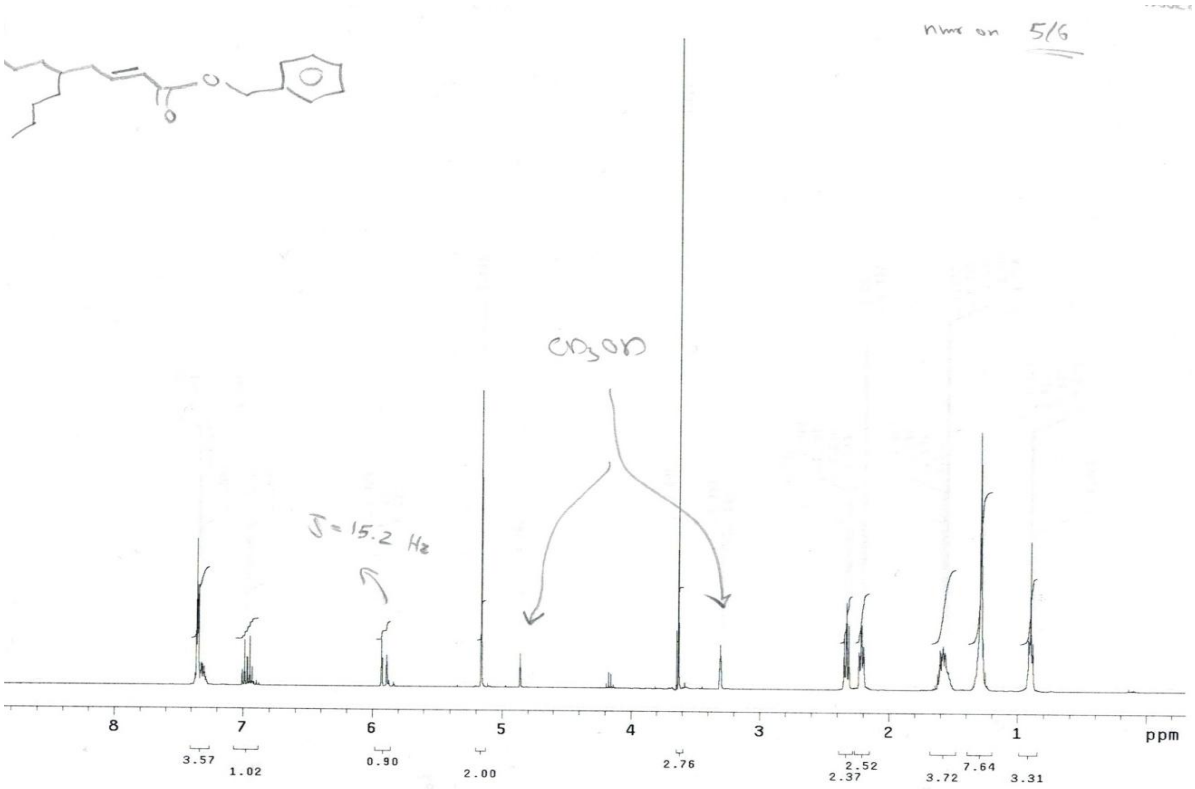

Figure B.5. ^{1}HNMR spectrum of **16c** in CD_3OD.

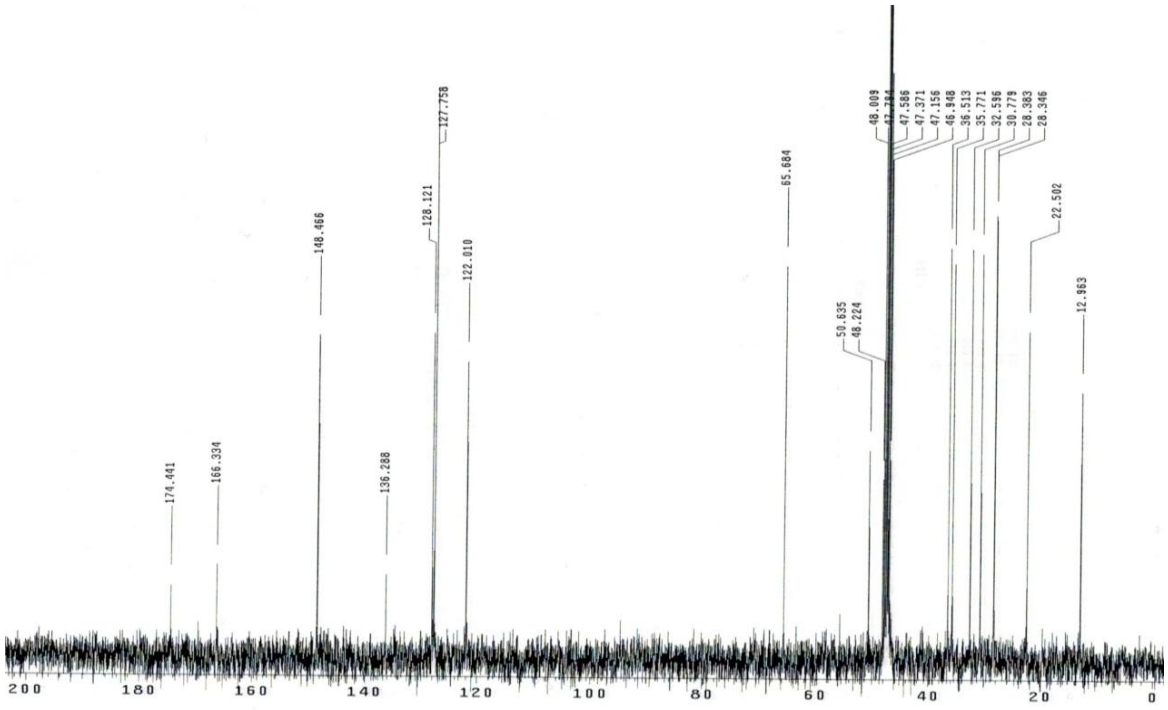

Figure B.6. ^{13}CNMR spectrum of **16c** in CD_3OD.

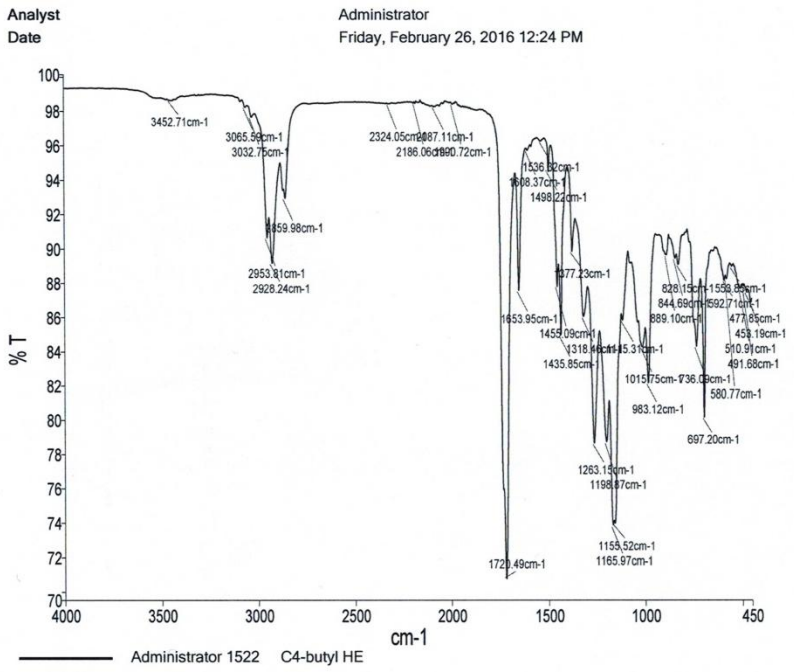

Figure B.7. IR spectrum of **16c** using a Perkin Elmer Spectrum Two ATR-FTIR.

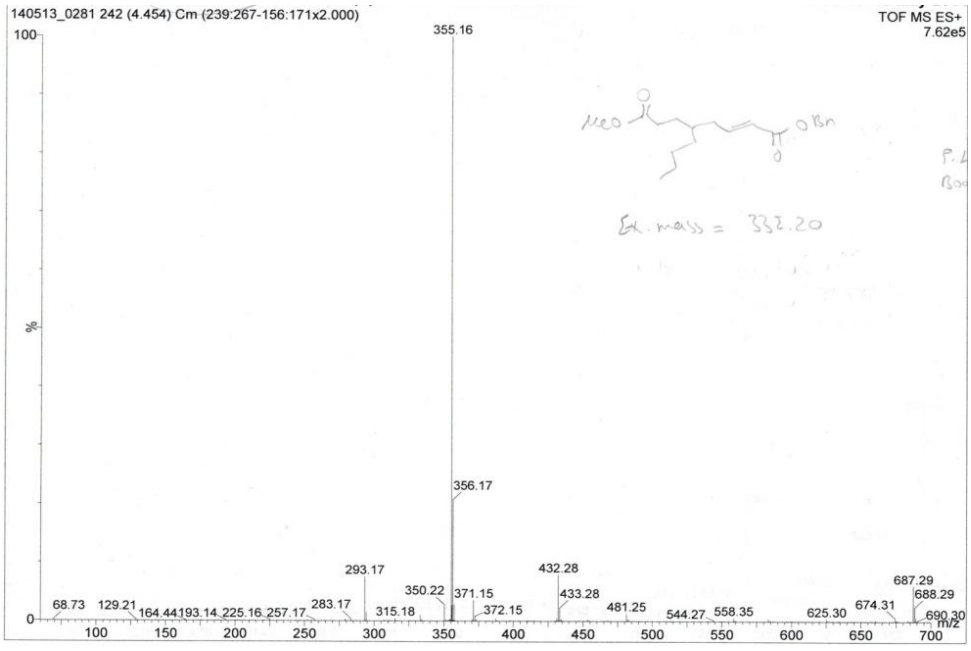

Figure B.8. Low resolution mass spectrum of **16c**.

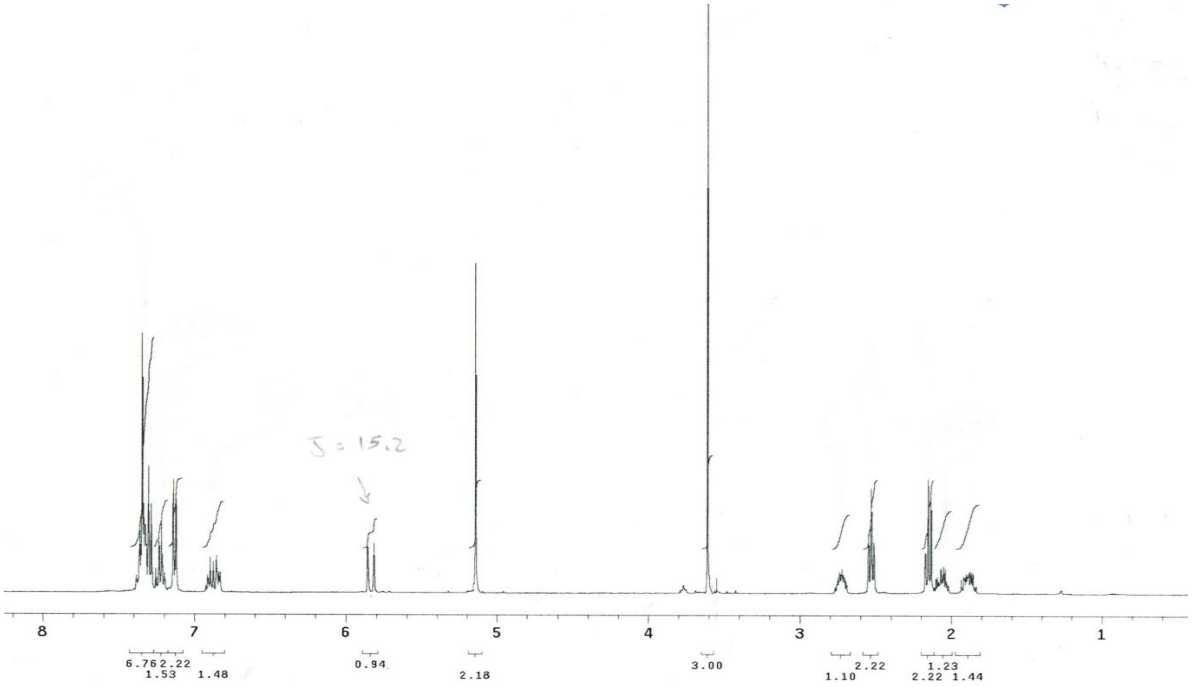

Figure B.9. ^{1}HNMR spectrum of **16e** in $CDCl_3$.

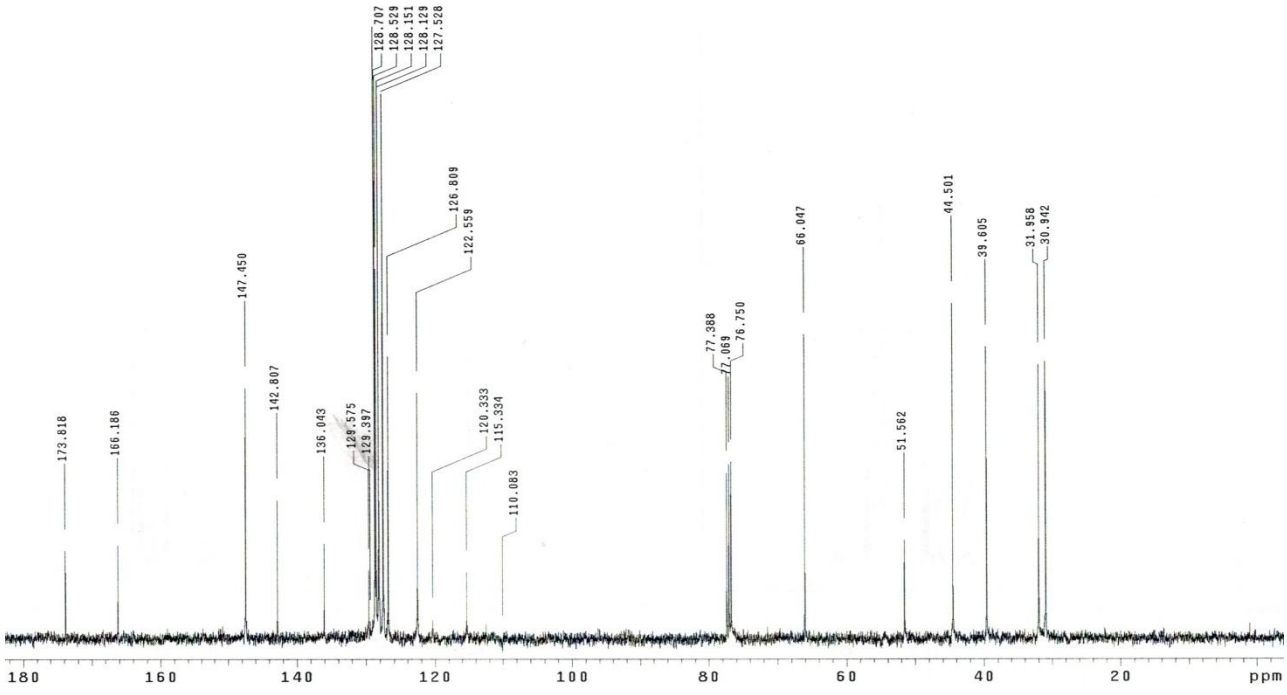

Figure B.10. ^{13}CNMR spectrum of **16e** in $CDCl_3$.

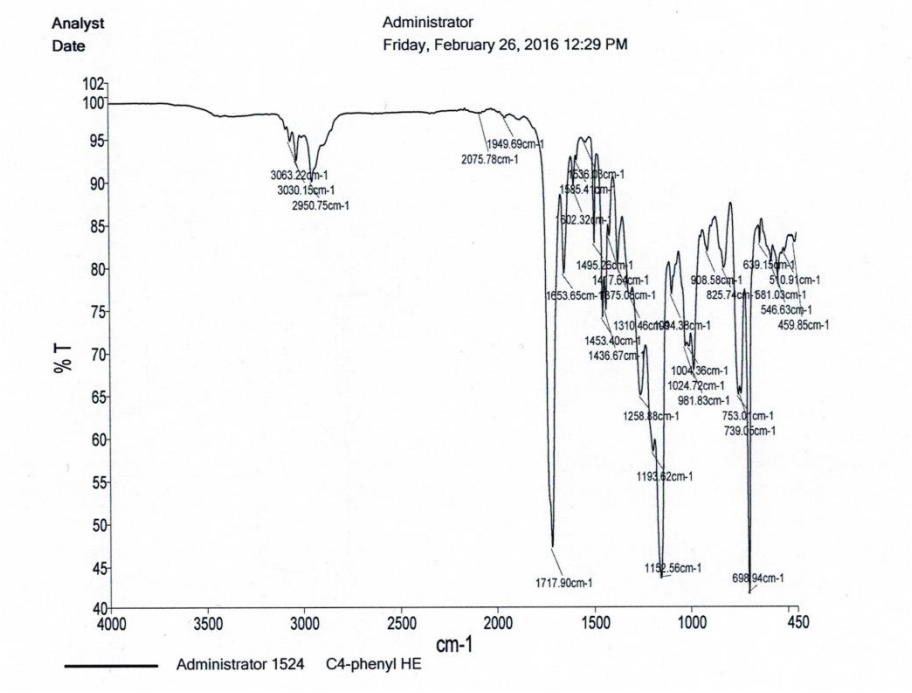

Figure B.11. IR spectrum of **16e** using a Perkin Elmer Spectrum Two ATR-FTIR.

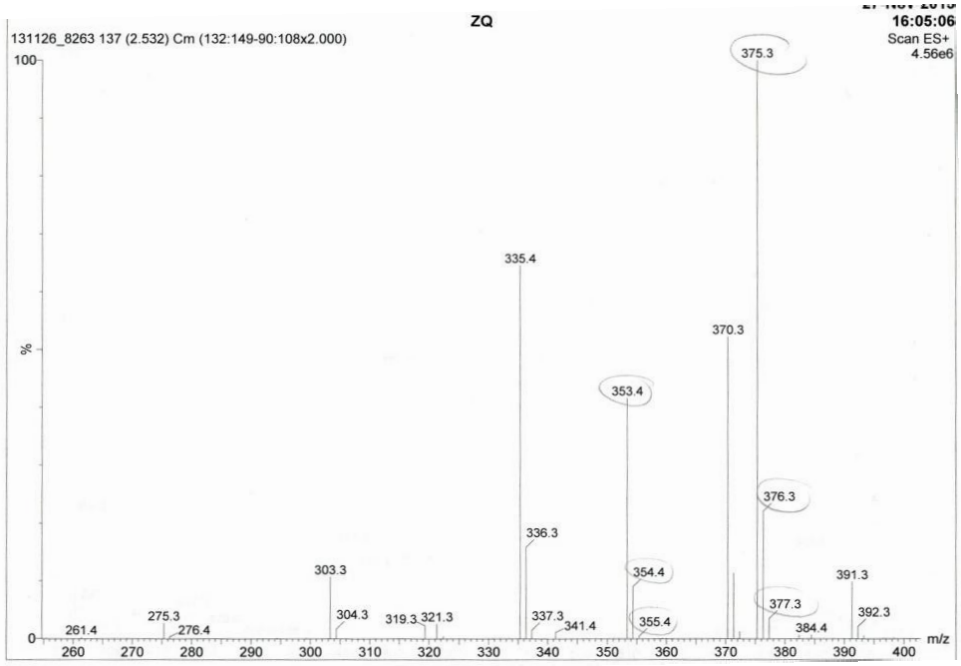

Figure B.12. Low resolution mass spectrum of **16e**.

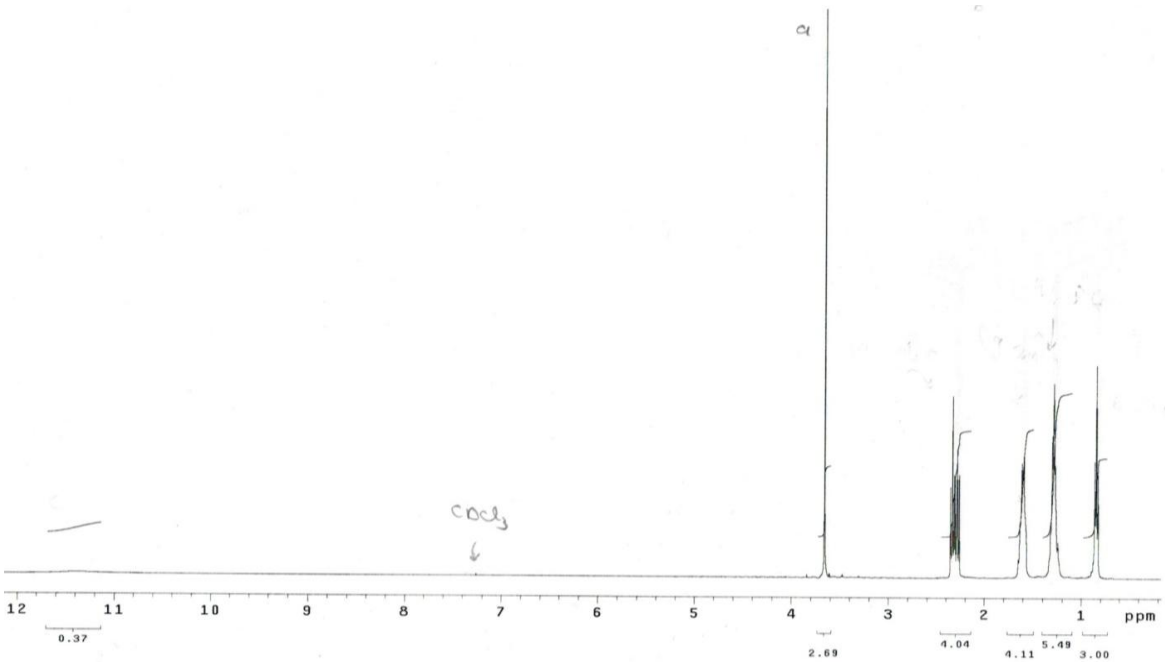

Figure B.13. ^{1}HNMR spectrum of **17b** in $CDCl_3$.

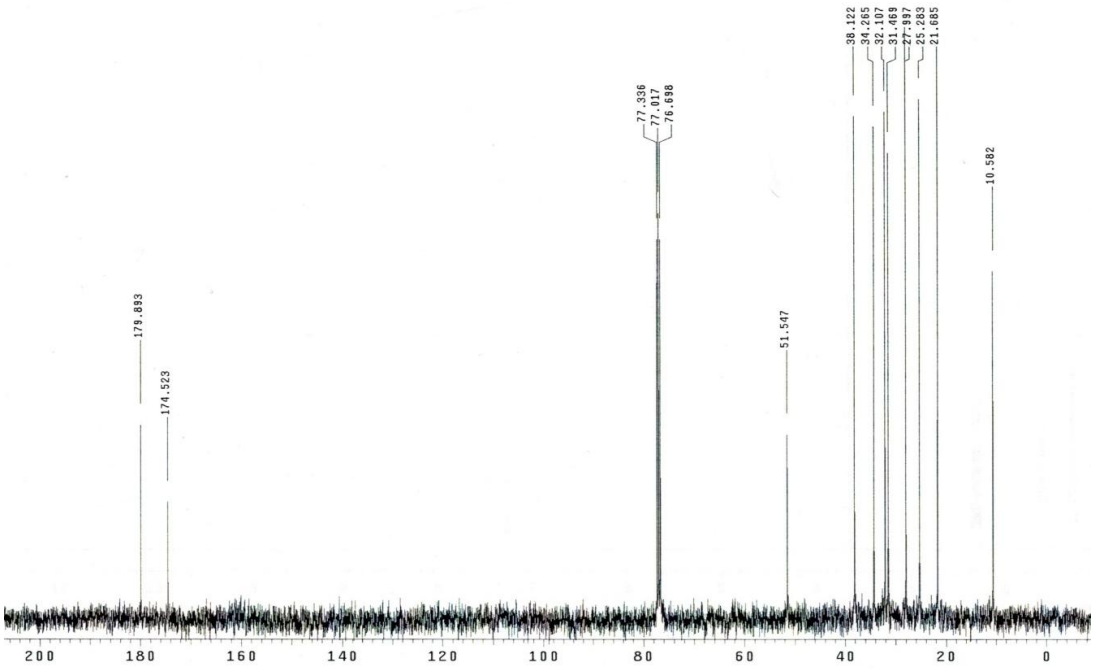

Figure B.14. ^{13}CNMR spectrum of **17b** in $CDCl_3$.

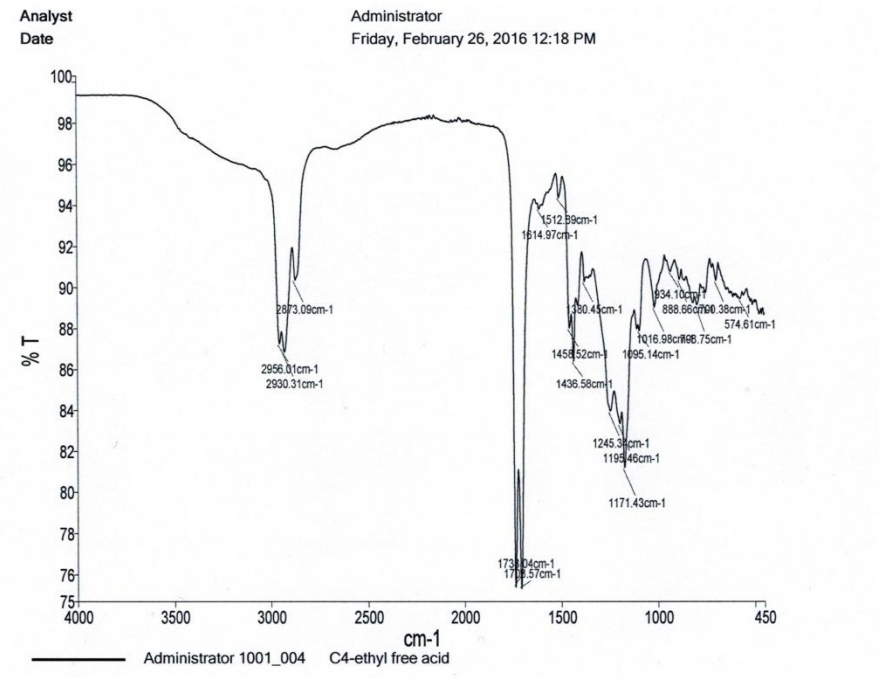

Figure B.15. IR spectrum of **17b** using a Perkin Elmer Spectrum Two ATR-FTIR.

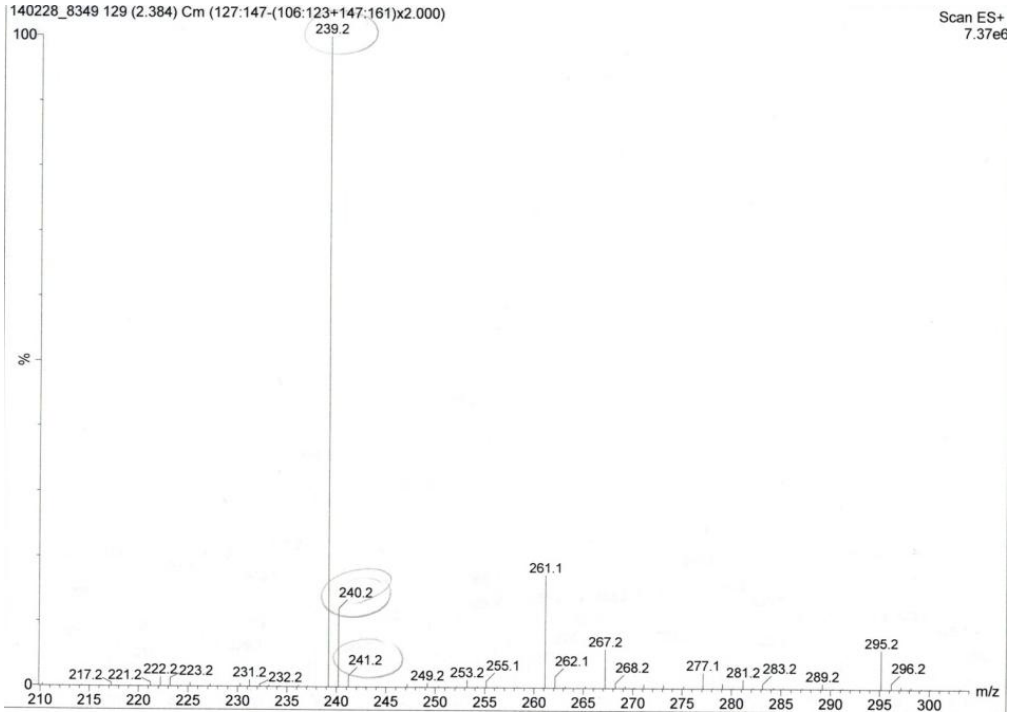

Figure B.16. Low resolution mass spectrum of **17b**.

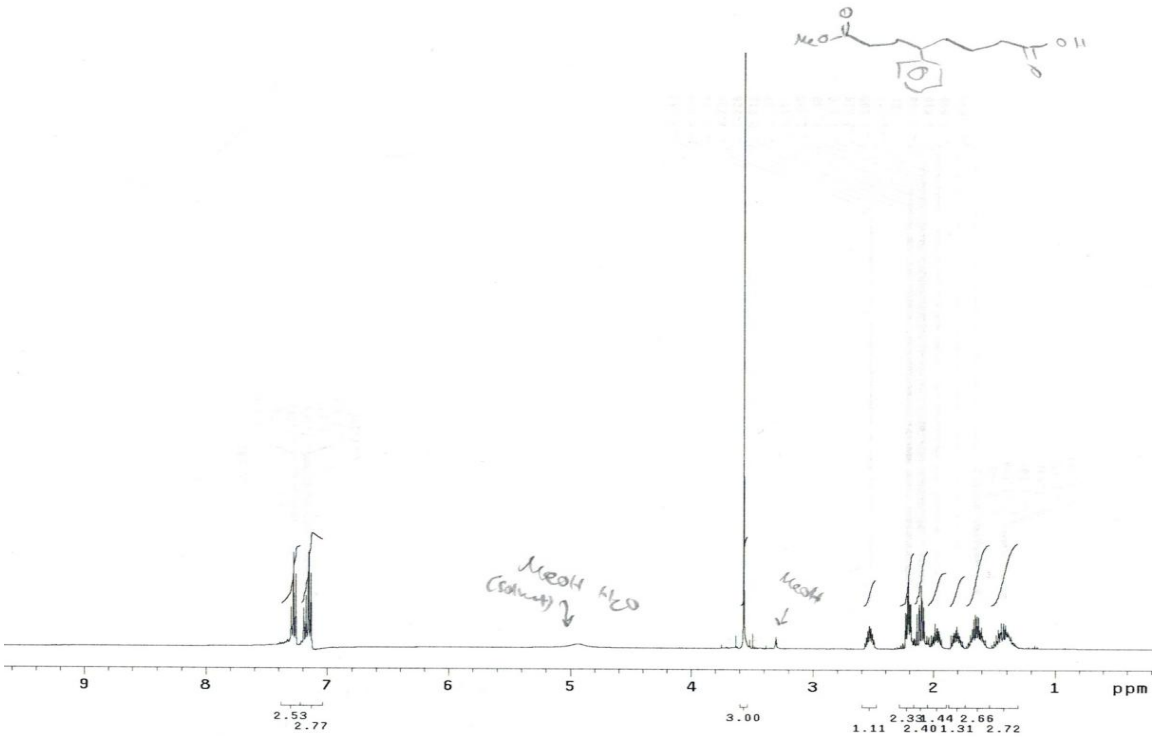

Figure B.17. ^{1}HNMR spectrum of **17e** in CD_3OD.

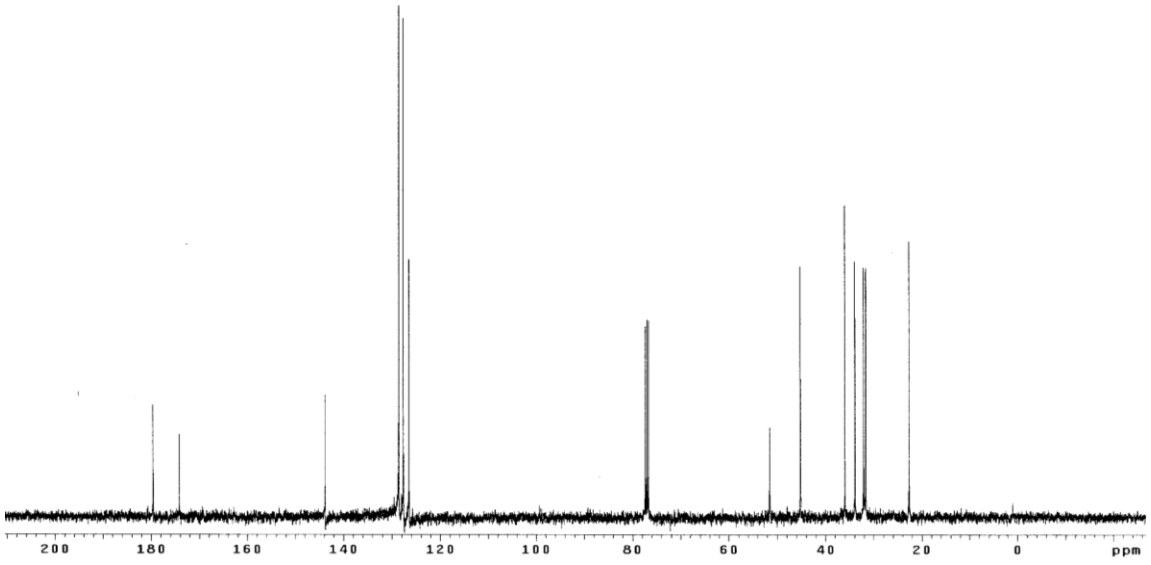

Figure B.18. ^{13}CNMR spectrum of **17e** in $CDCl_3$.

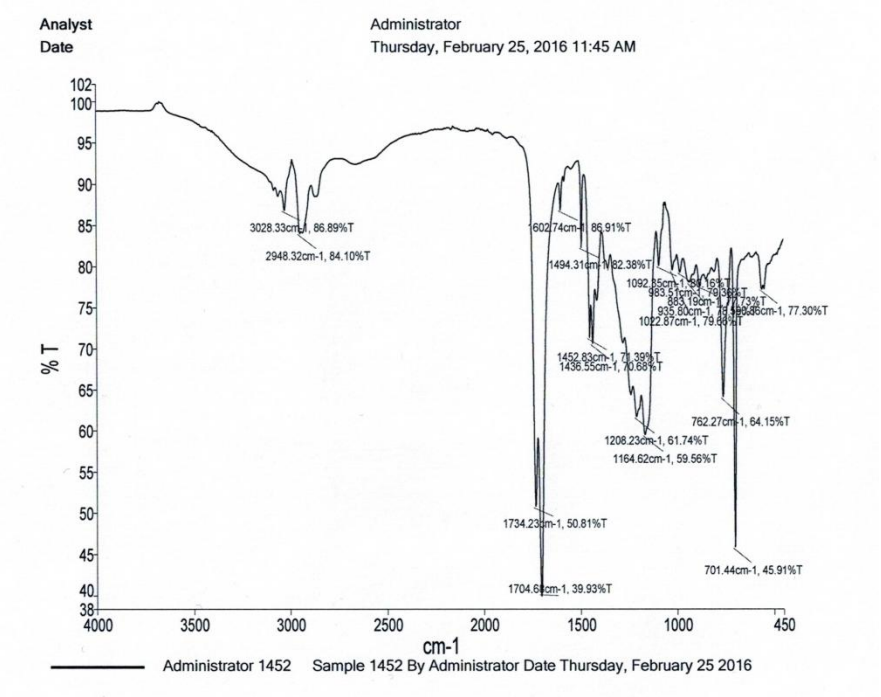

Figure B.19. IR spectrum of **17e** using a Perkin Elmer Spectrum Two ATR-FTIR.

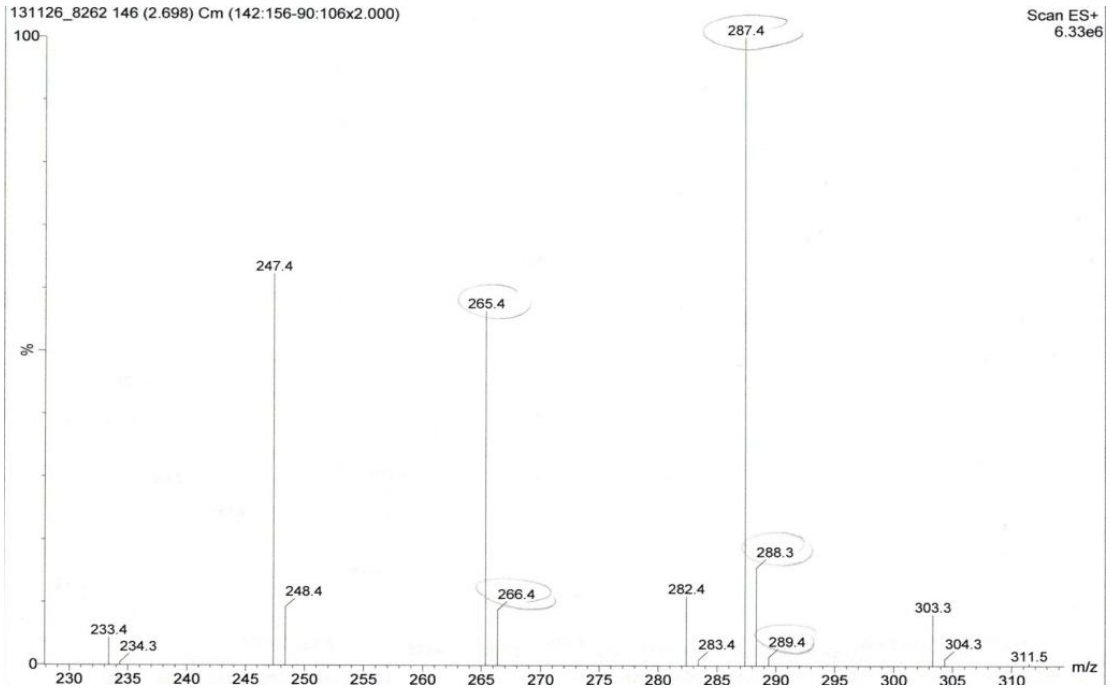

Figure B.20. Low resolution mass spectrum of **17e**.

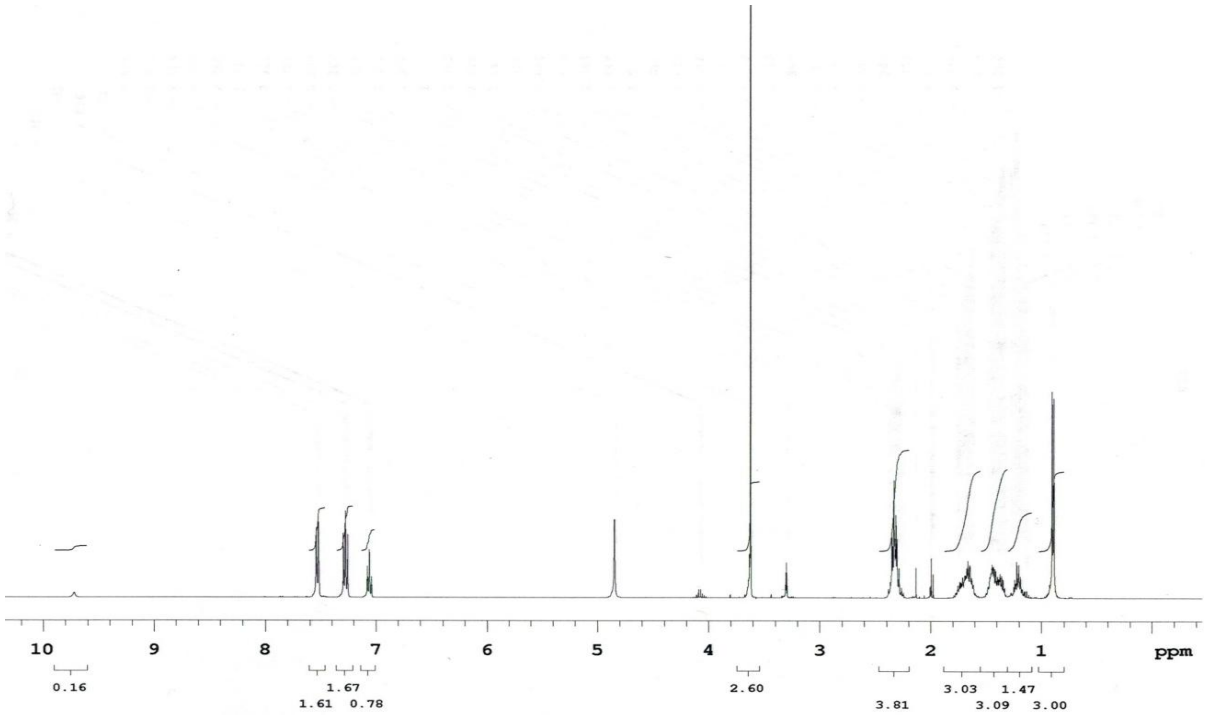

Figure B.21. ^{1}HNMR spectrum of **18a** in CD_3OD.

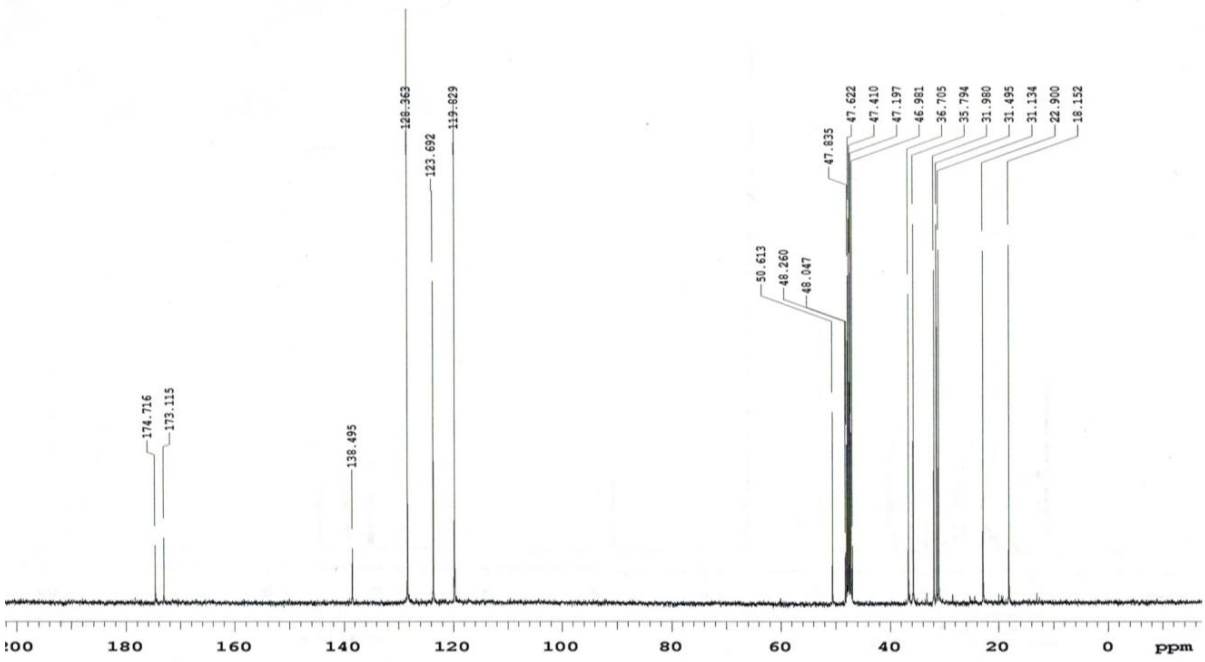

Figure B.22. ^{13}CNMR spectrum of **18a**.

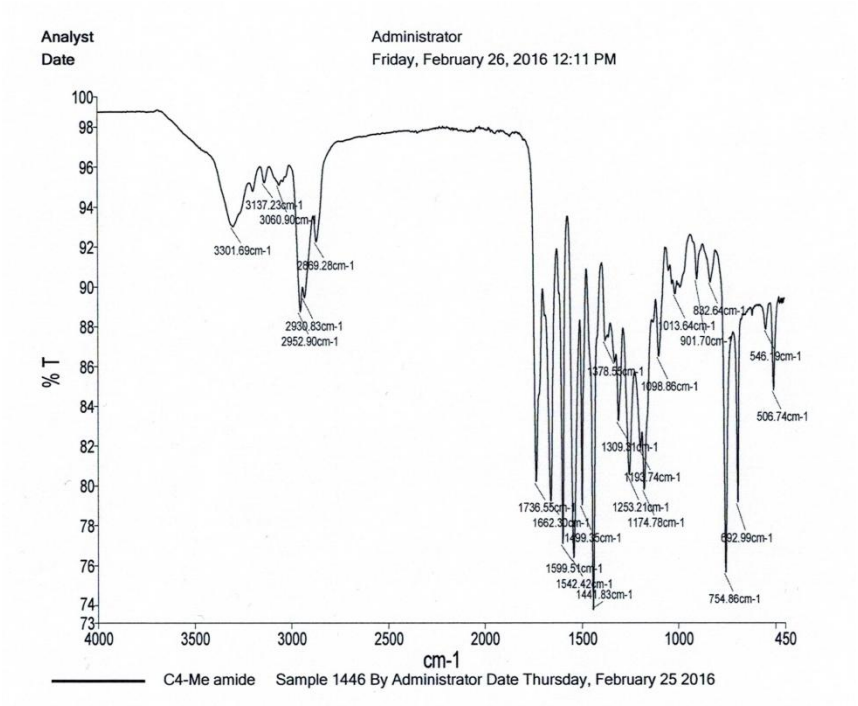

Figure B.23. IR spectrum of **18a** using a Perkin Elmer Spectrum Two ATR-FTIR.

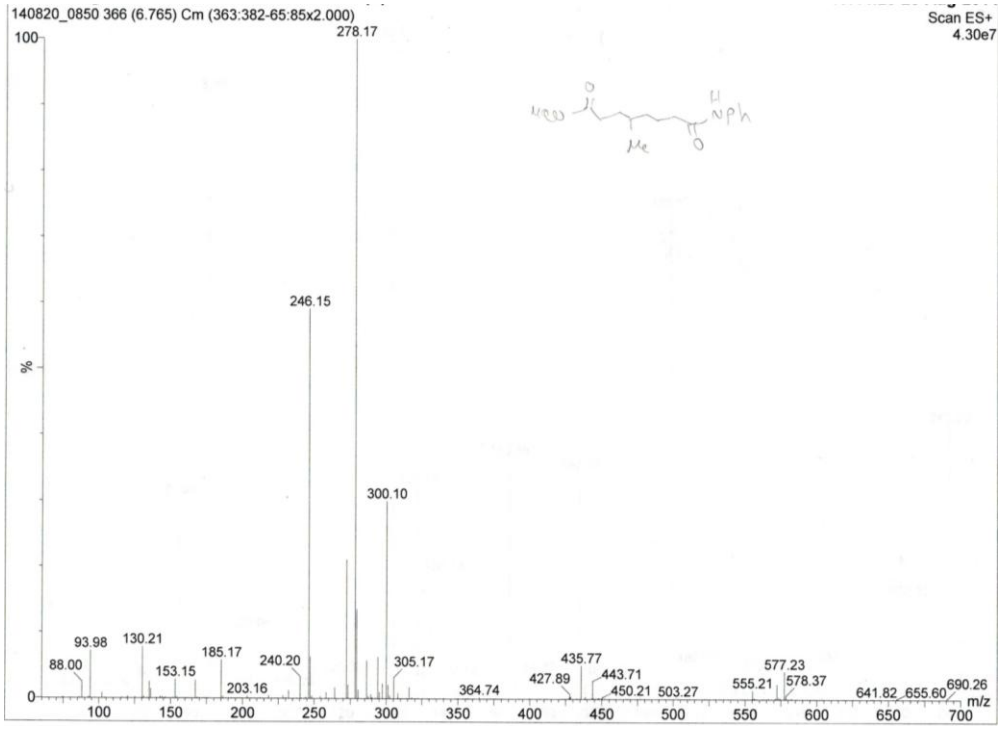

Figure B.24. Low resolution mass spectrum of **18a**.

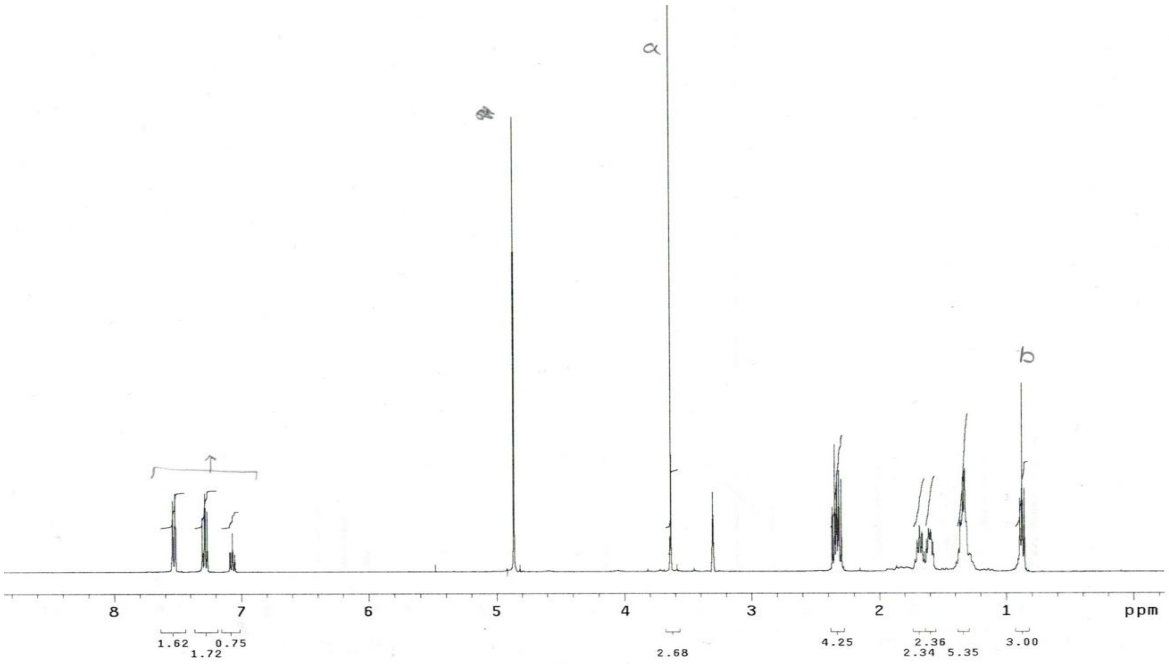

Figure B.25. ^{1}HNMR spectrum of **18b** in CD_3OD.

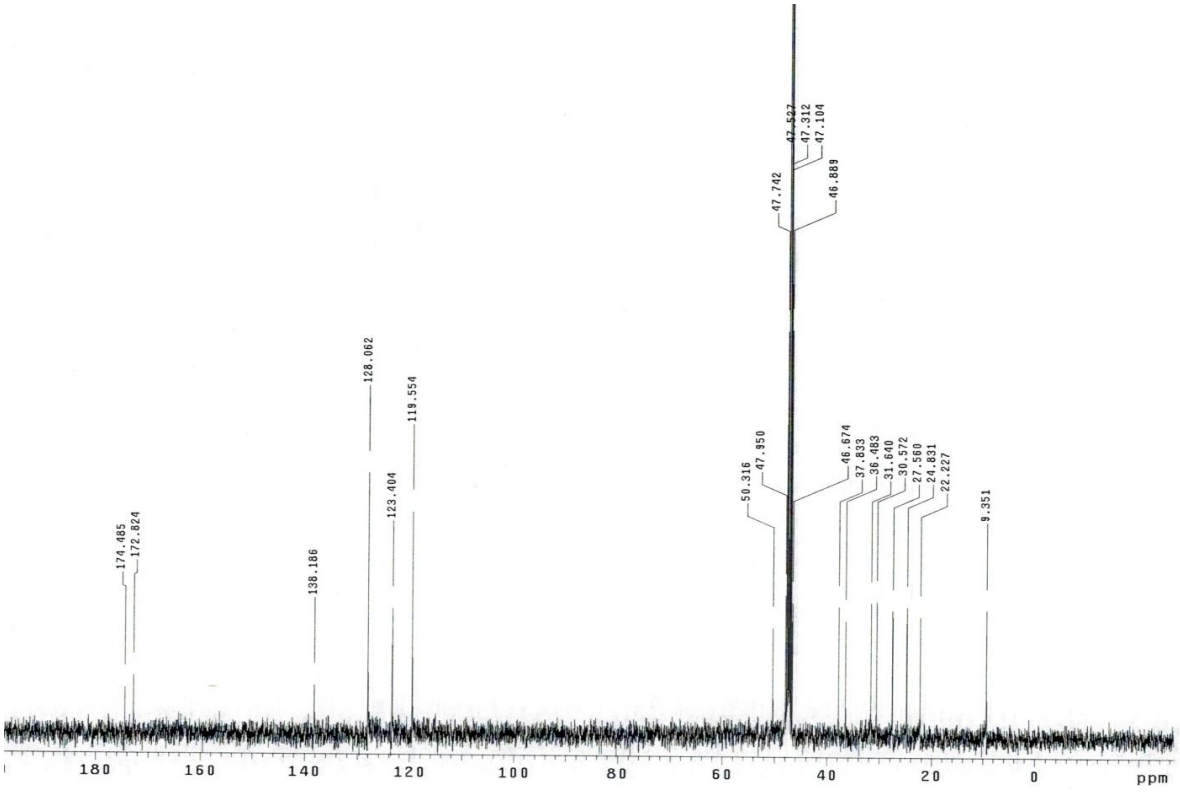

Figure B.26 ^{13}CNMR spectrum of **18b** in CD_3OD.

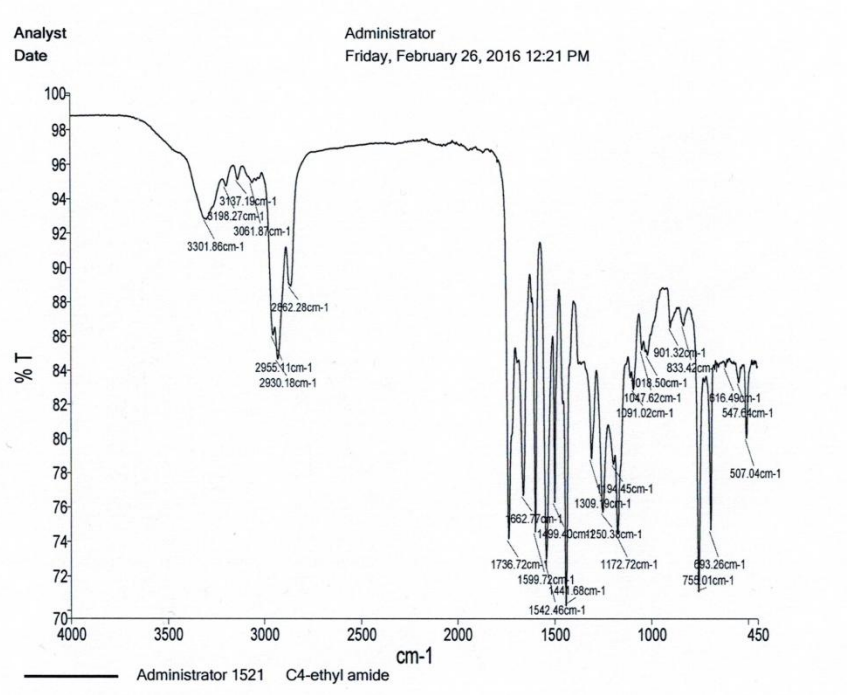

Figure B.27. IR spectrum of **18b** using a Perkin Elmer Spectrum Two ATR-FTIR.

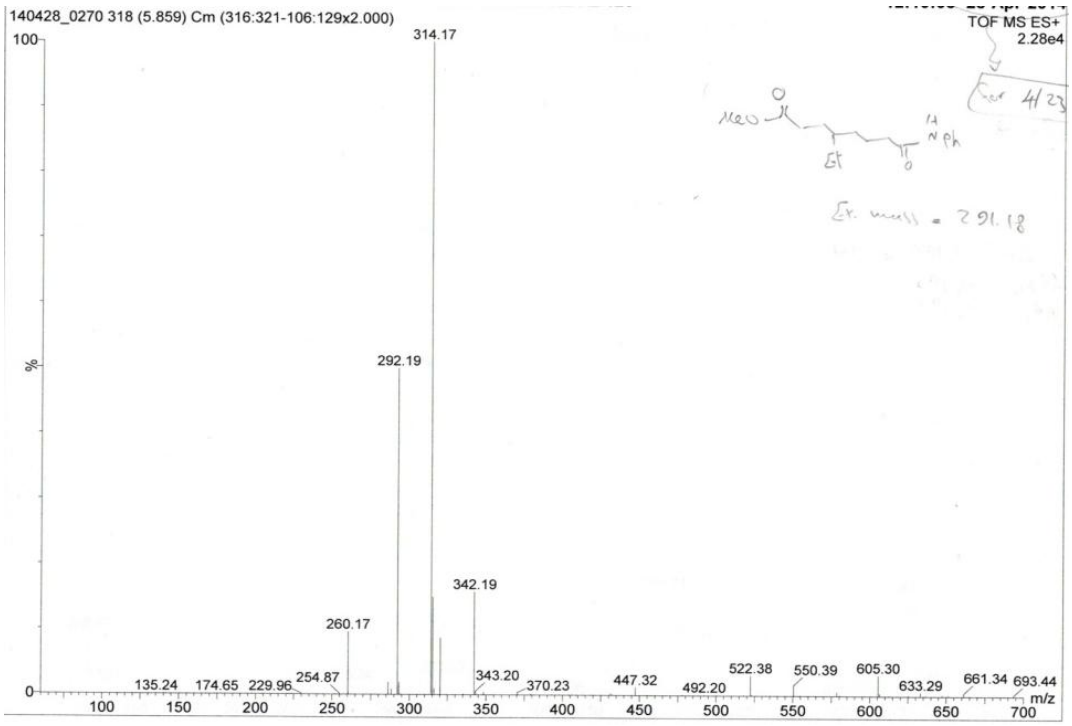

Figure B.28. Low resolution mass spectrum of **18b**.

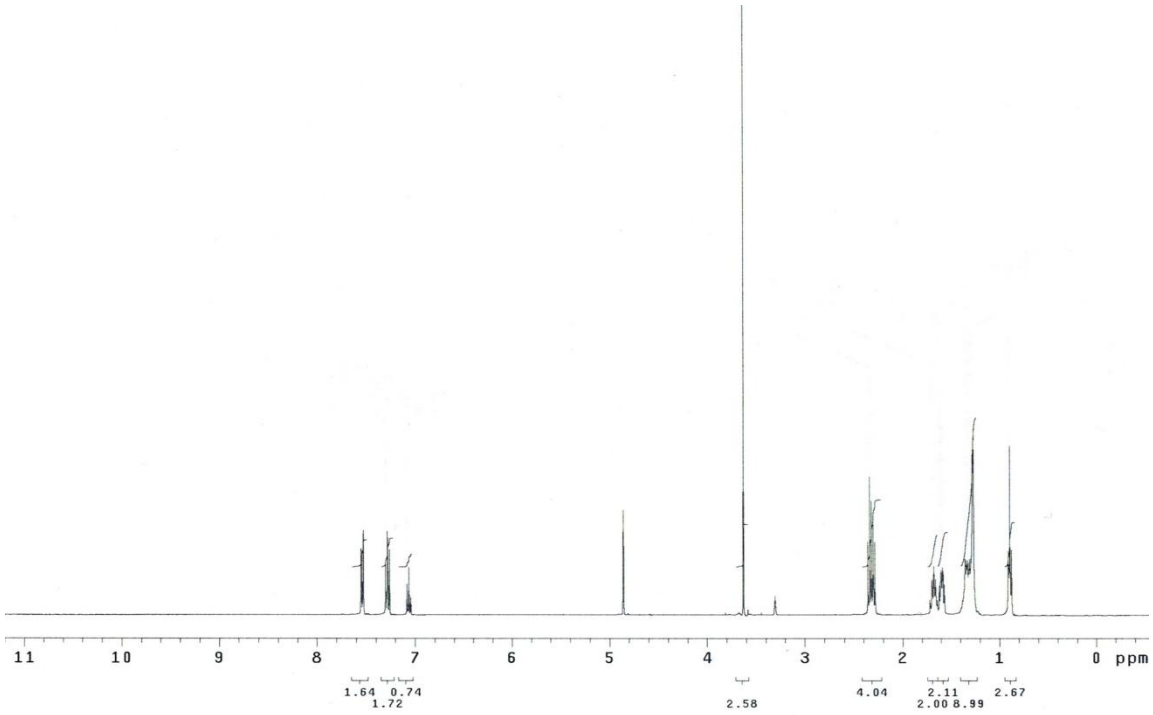

Figure B.29. ^{1}HNMR spectrum of **18c** in CD_3OD.

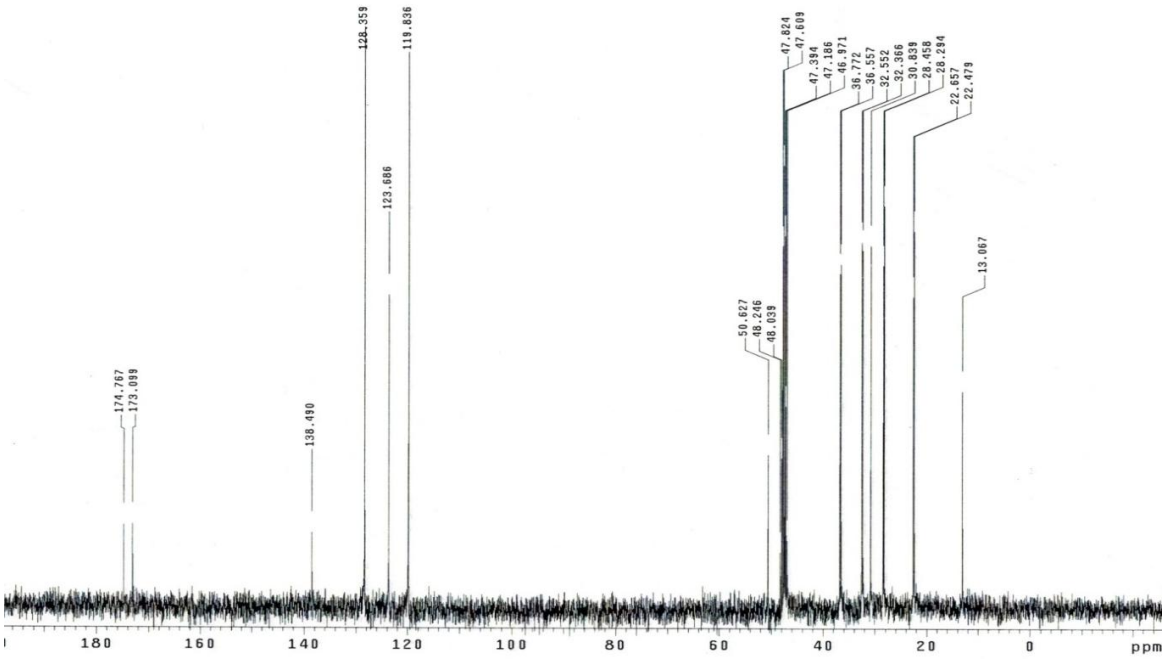

Figure B.30. ^{13}CNMR spectrum of **18c** in CD_3OD.

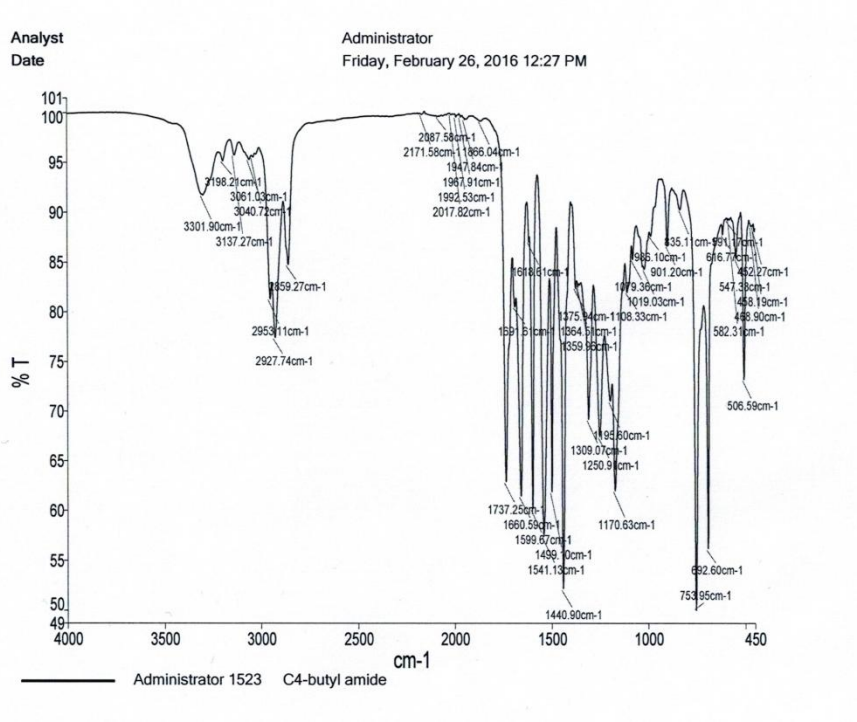

Figure B.31. IR spectrum of **18c** using a Perkin Elmer Spectrum Two ATR-FTIR.

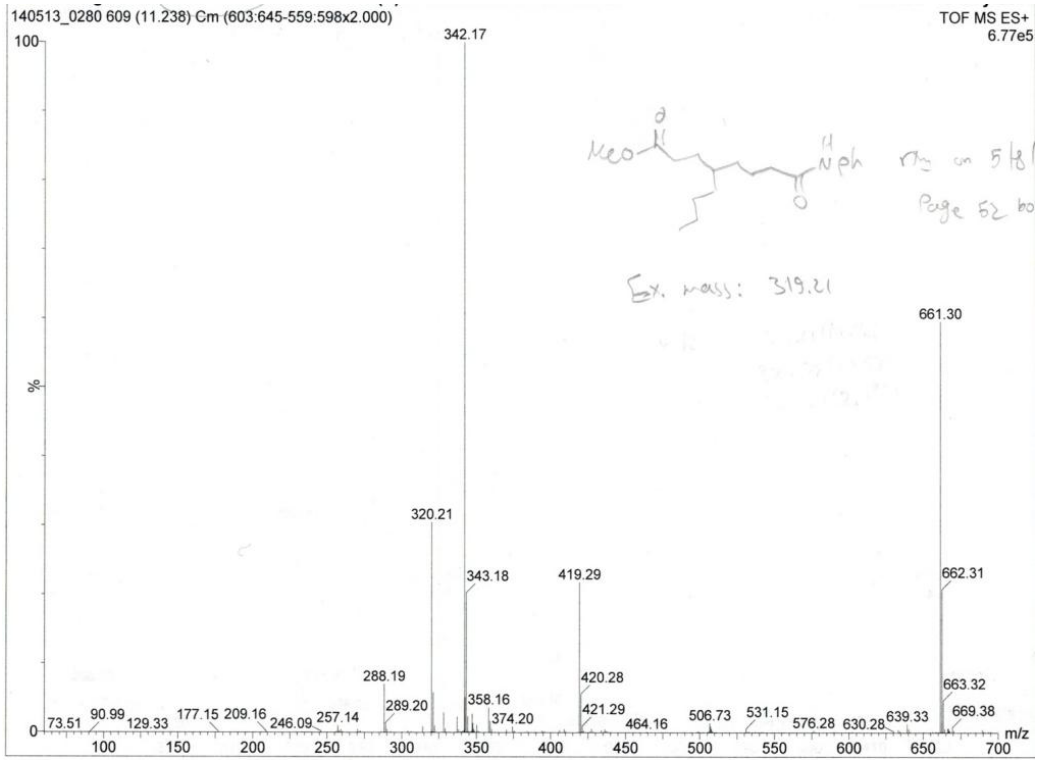

Figure B.32. Low resolution mass spectrum of **18c**.

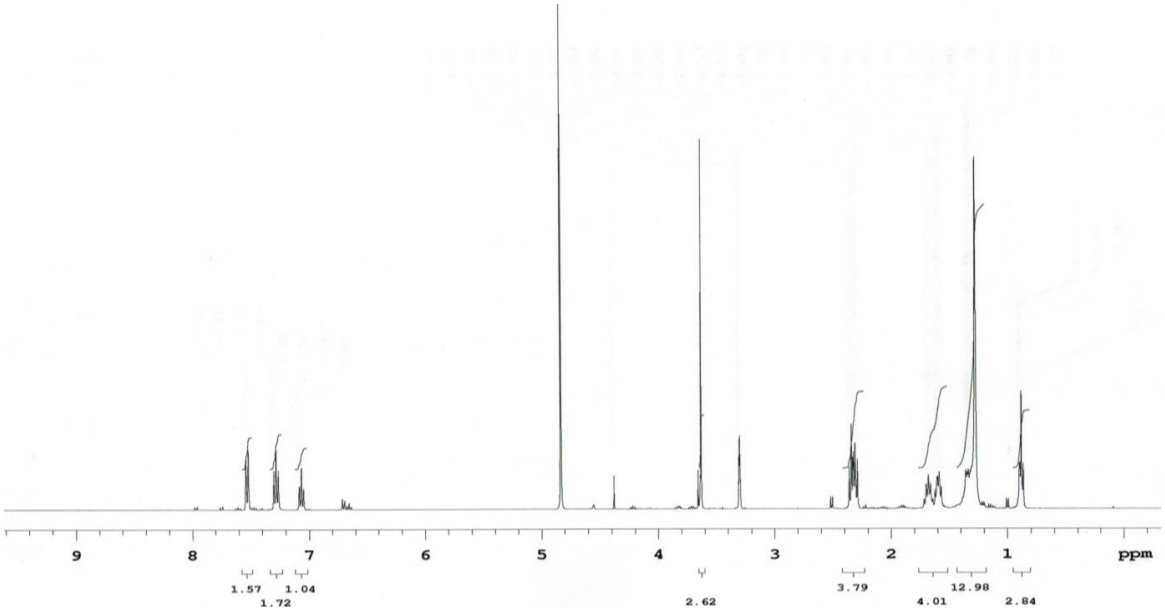

Figure B.33. ^{1}HNMR spectrum of **18d** in CD_3OD.

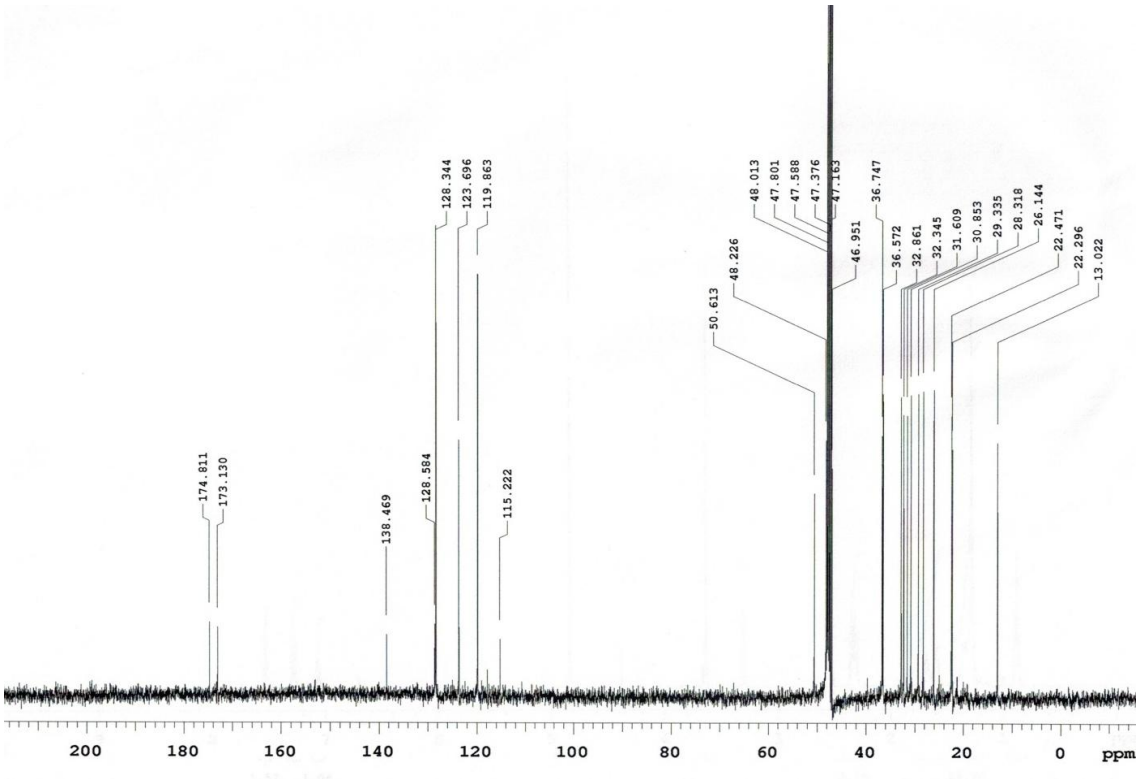

Figure B.34. ^{13}CNMR spectrum of **18d** in CD_3OD.

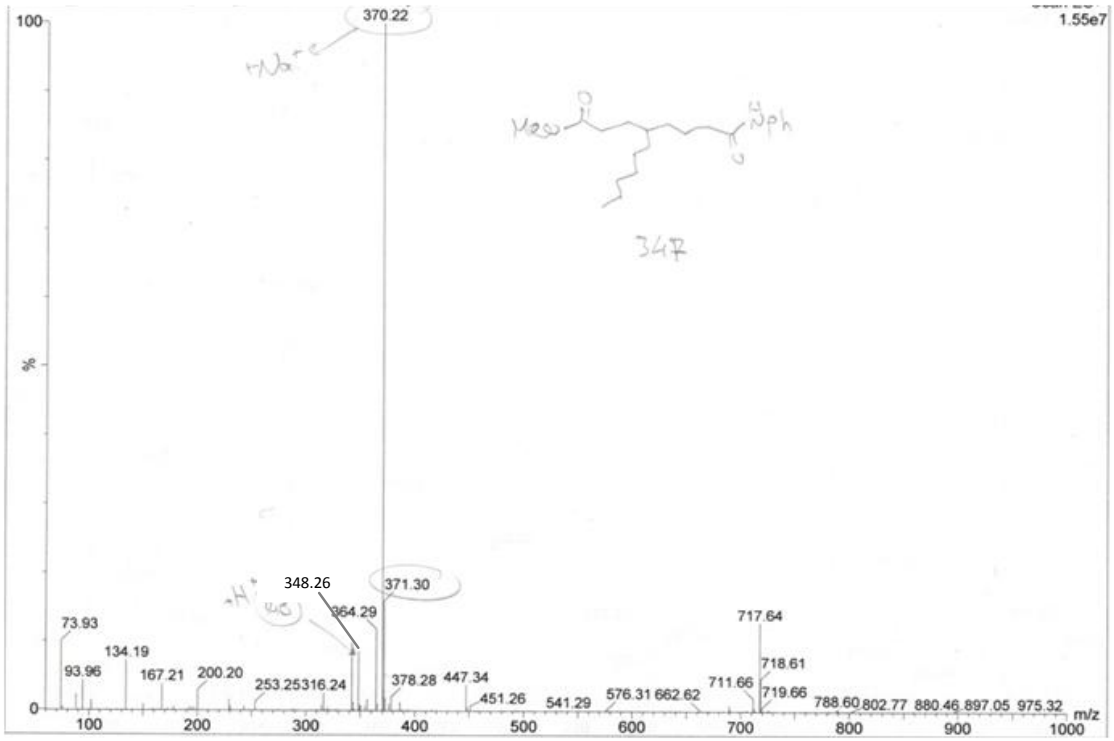

Figure B.35. Low resolution mass spectrum of **18d**.

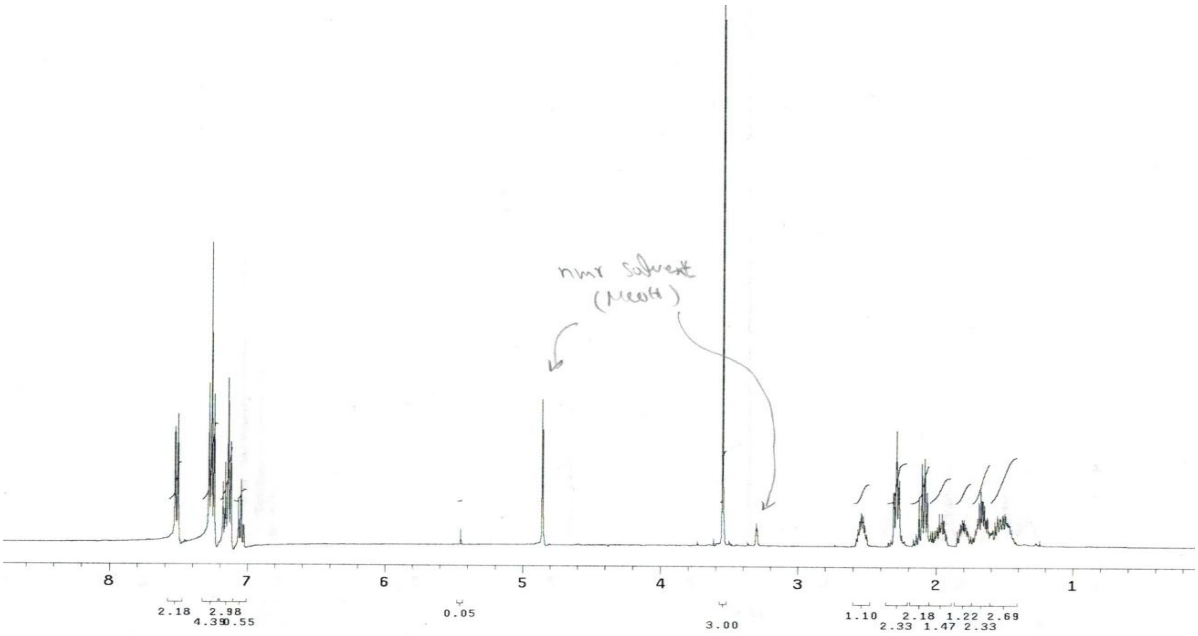

Figure B.36. ^{1}HNMR spectrum of **18e** in CD_3OD.

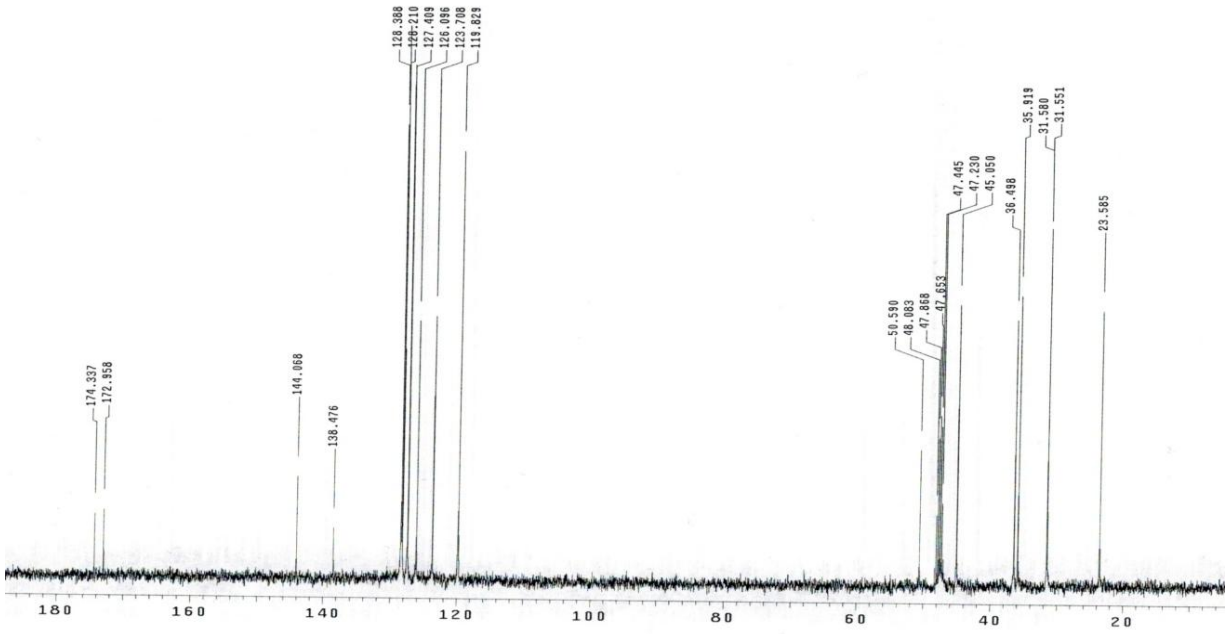

Figure B.37. ^{13}CNMR spectrum of **18e** in CD_3OD.

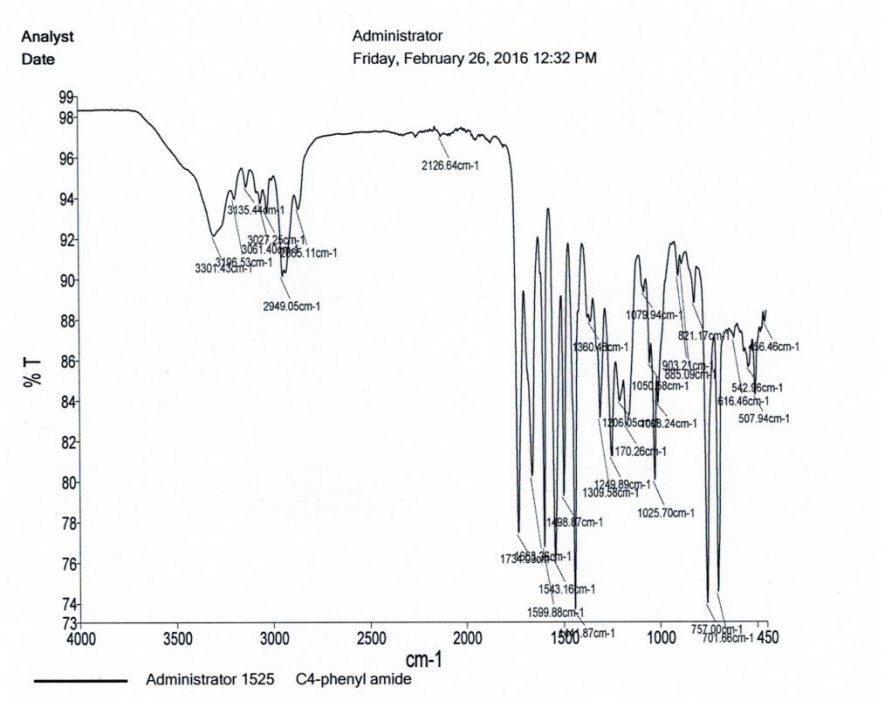

Figure B.38. IR spectrum of **18e** using a Perkin Elmer Spectrum Two ATR-FTIR.

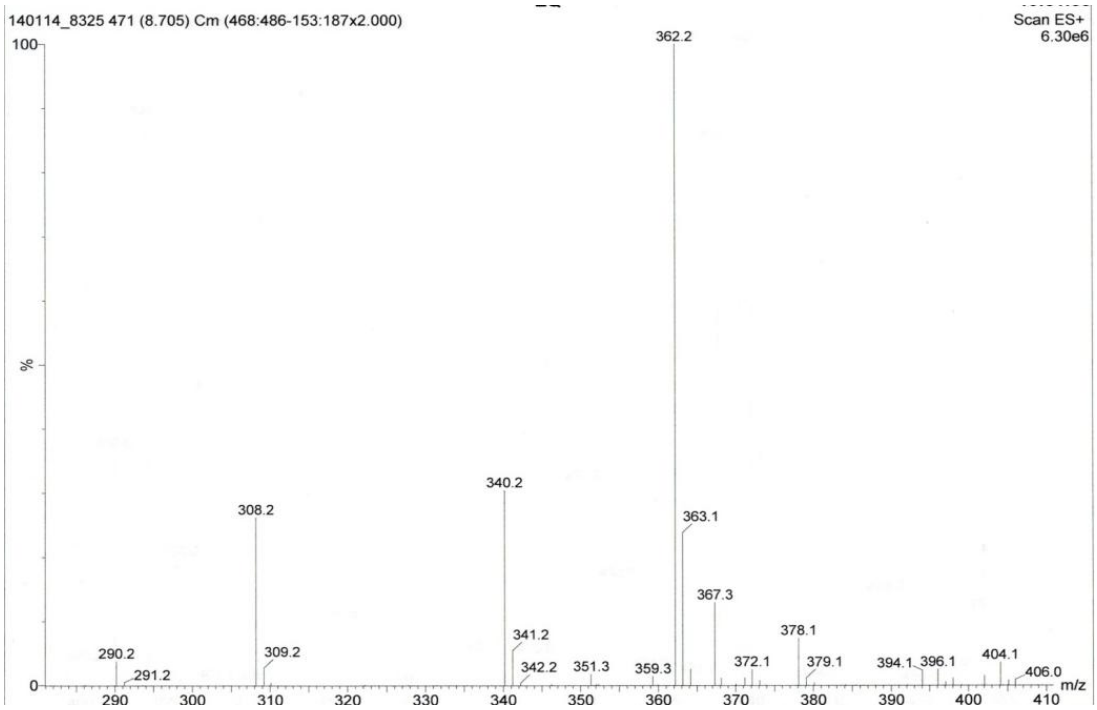

Figure B.39. Low resolution mass spectrum of **18e**.

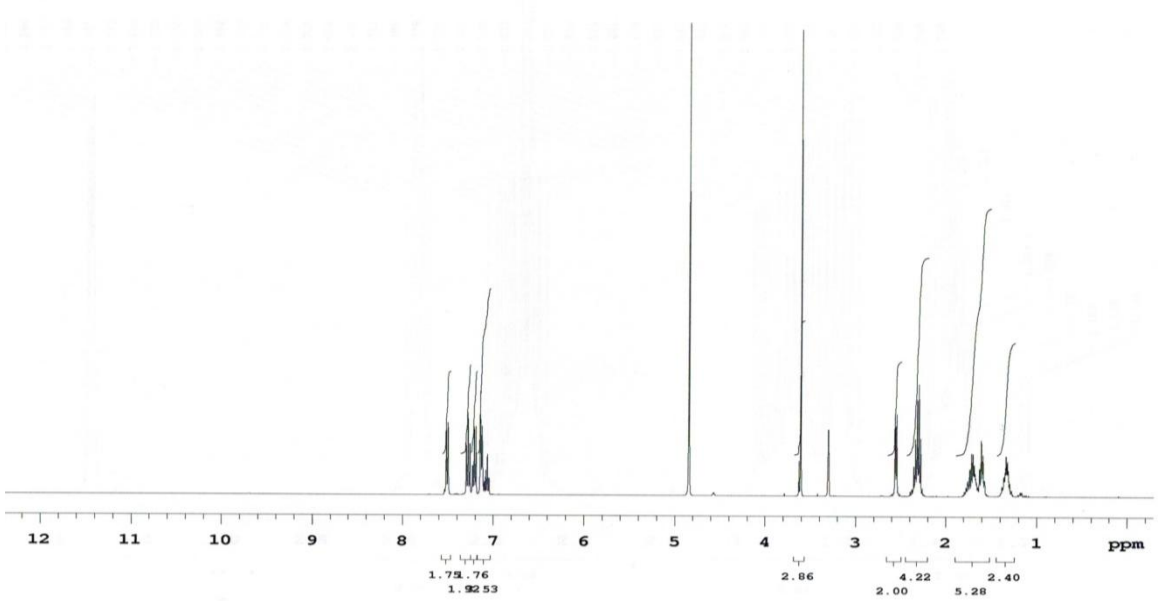

Figure B.40. ^{1}HNMR spectrum of **18f** in CD_3OD.

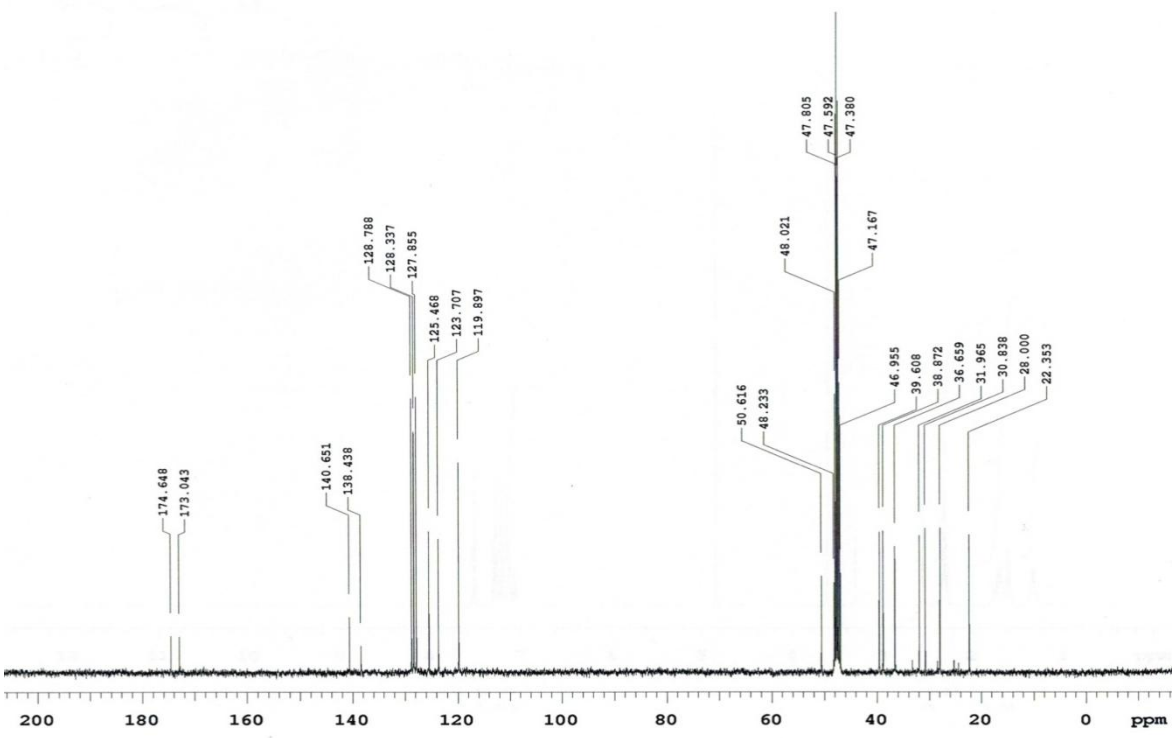

Figure B.41. ^{13}CNMR spectrum of **18f** in CD_3OD.

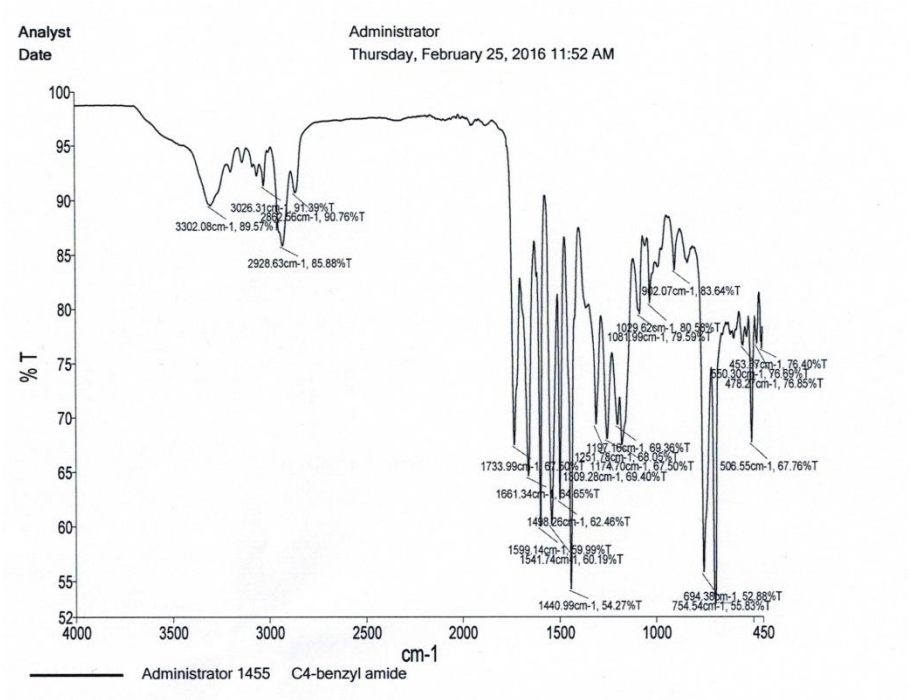

Figure B.42. IR spectrum of **18f** using a Perkin Elmer Spectrum Two ATR-FTIR.

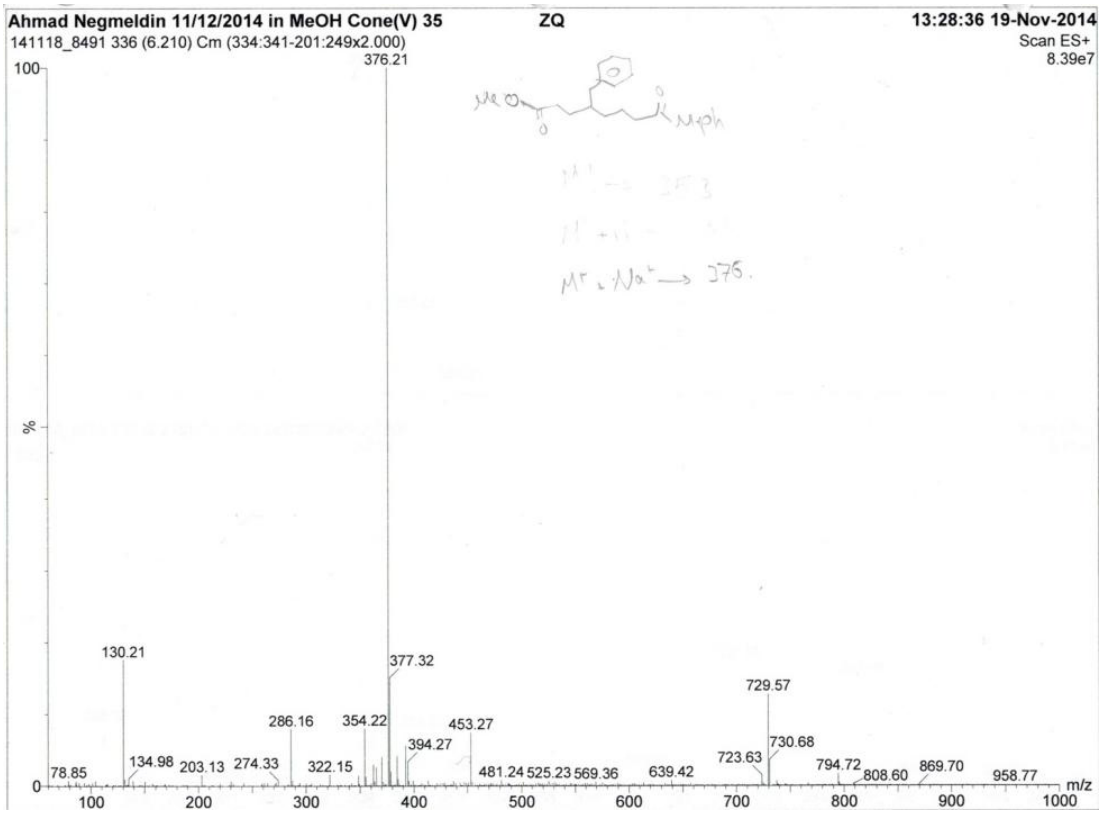

Figure B.43. Low resolution mass spectrum of **18f**.

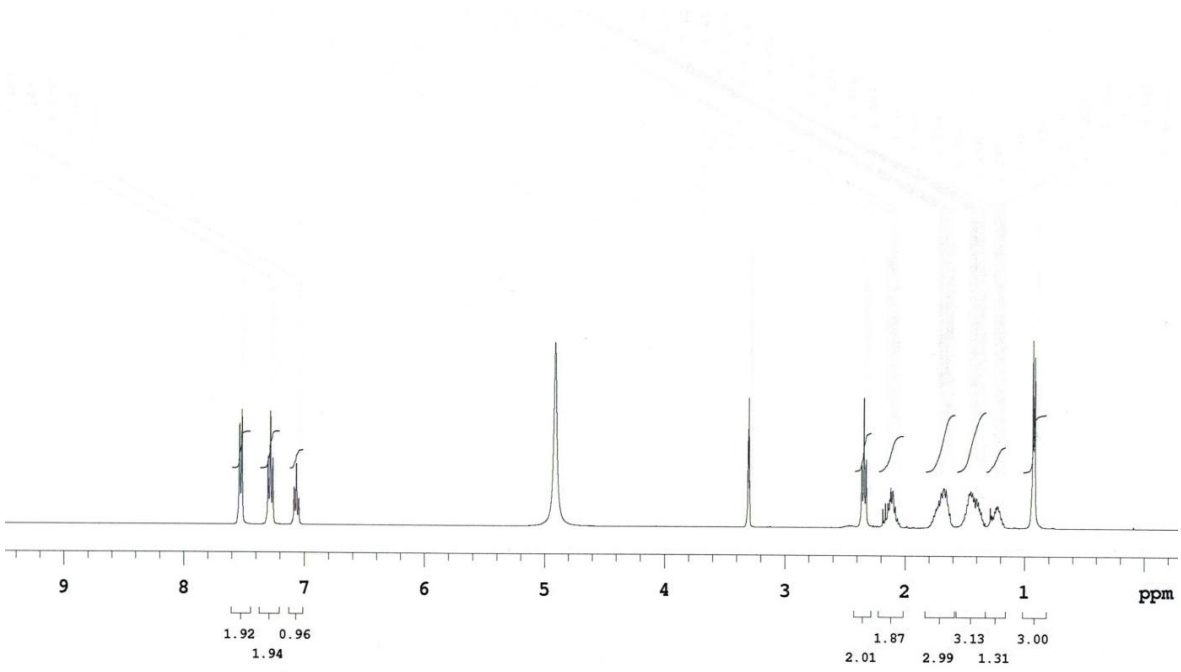

Figure B.44. ^{1}HNMR spectrum of **19a** in CD_3OD.

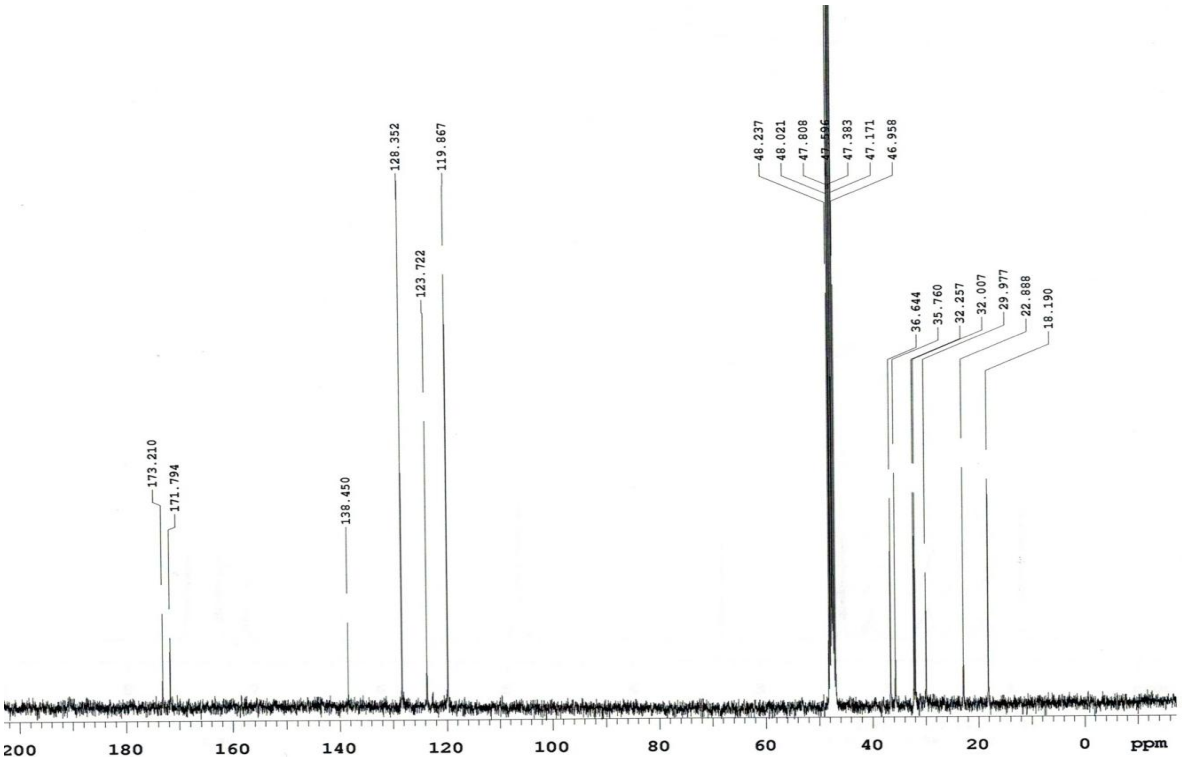

Figure B.45. ^{13}CNMR spectrum of **19a** in CD_3OD.

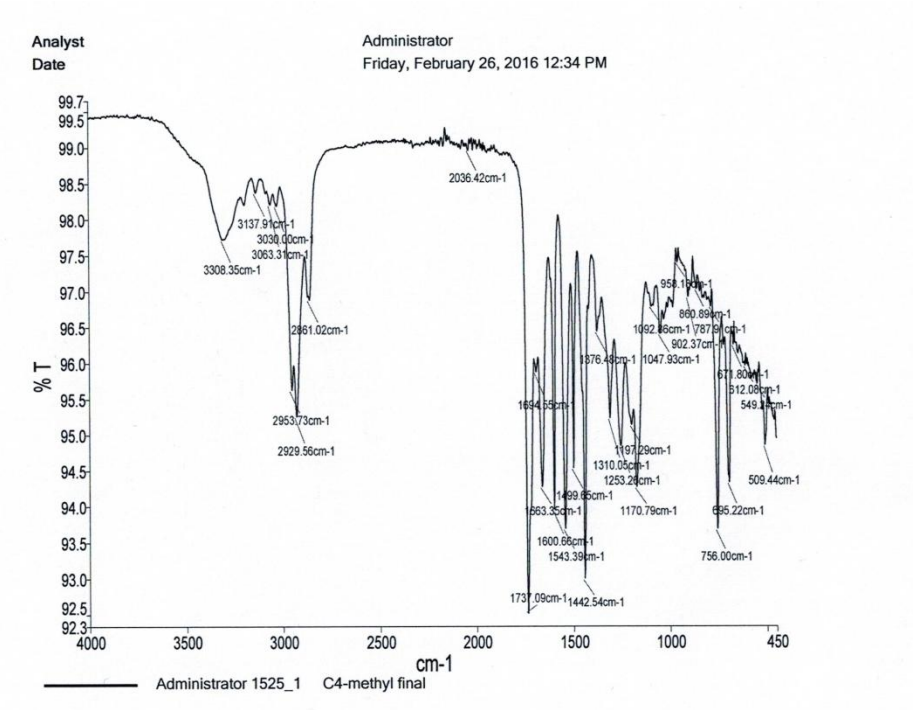

Figure B.46. IR spectrum of **19a** using a Perkin Elmer Spectrum Two ATR-FTIR.

Elemental Composition Report **Page 1**

Single Mass Analysis
Tolerance = 5.0 PPM / DBE: min = -1.5, max = 100.0
Element prediction: Off
Number of isotope peaks used for i-FIT = 6

Monoisotopic Mass, Even Electron Ions
60 formula(e) evaluated with 1 results within limits (all results (up to 1000) for each mass)
Elements Used:
C: 15-15 H: 0-30 N: 0-5 O: 0-5 23Na: 0-1

A.Negmeldin 4-Me in MeOH+DMSO Cone(V)50

LCT Premier KD128
TOF MS ES+

6.21e+005

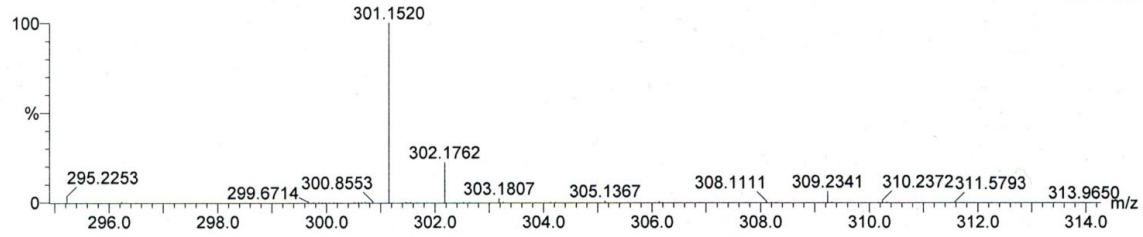

Minimum:				-1.5			
Maximum:		3.0	5.0	100.0			
Mass	Calc. Mass	mDa	PPM	DBE	i-FIT	i-FIT (Norm)	Formula
301.1520	301.1528	-0.8	-2.7	5.5	142.9	0.0	C15 H22 N2 O3 23Na

Figure B.47. High resolution mass spectrum of **19a**.

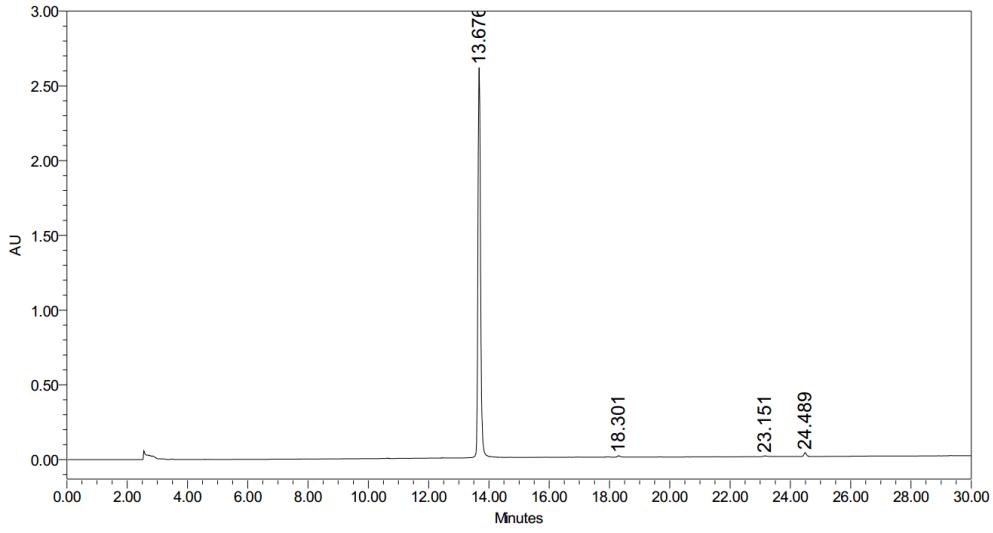

	RT	Area	% Area	Height
1	13.676	15693948	98.38	2608390
2	18.301	55905	0.35	8685
3	23.151	52098	0.33	4423
4	24.489	151167	0.95	24616

Figure B.48. HPLC spectrum taken at 254 nm of C4-methyl SAHA (**19a**). The peak at 13.676 is C4-methyl SAHA. The calculated area and height under each peak, along with % area, is shown in the table below the spectrum.

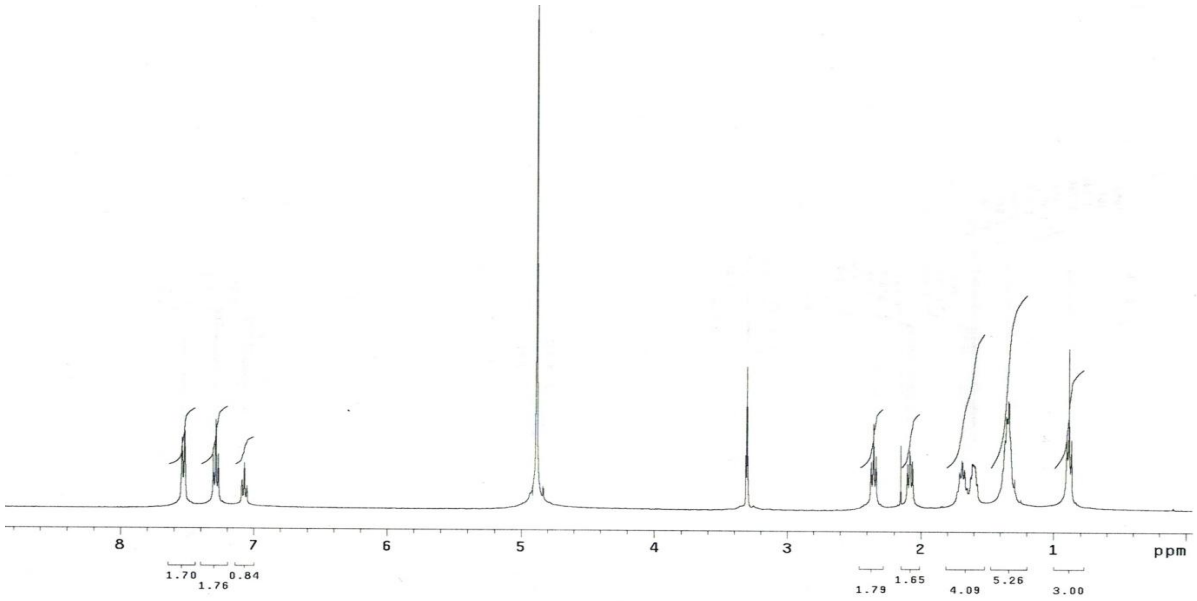

Figure B.49. ^{1}HNMR spectrum of **19b** in CD_3OD.

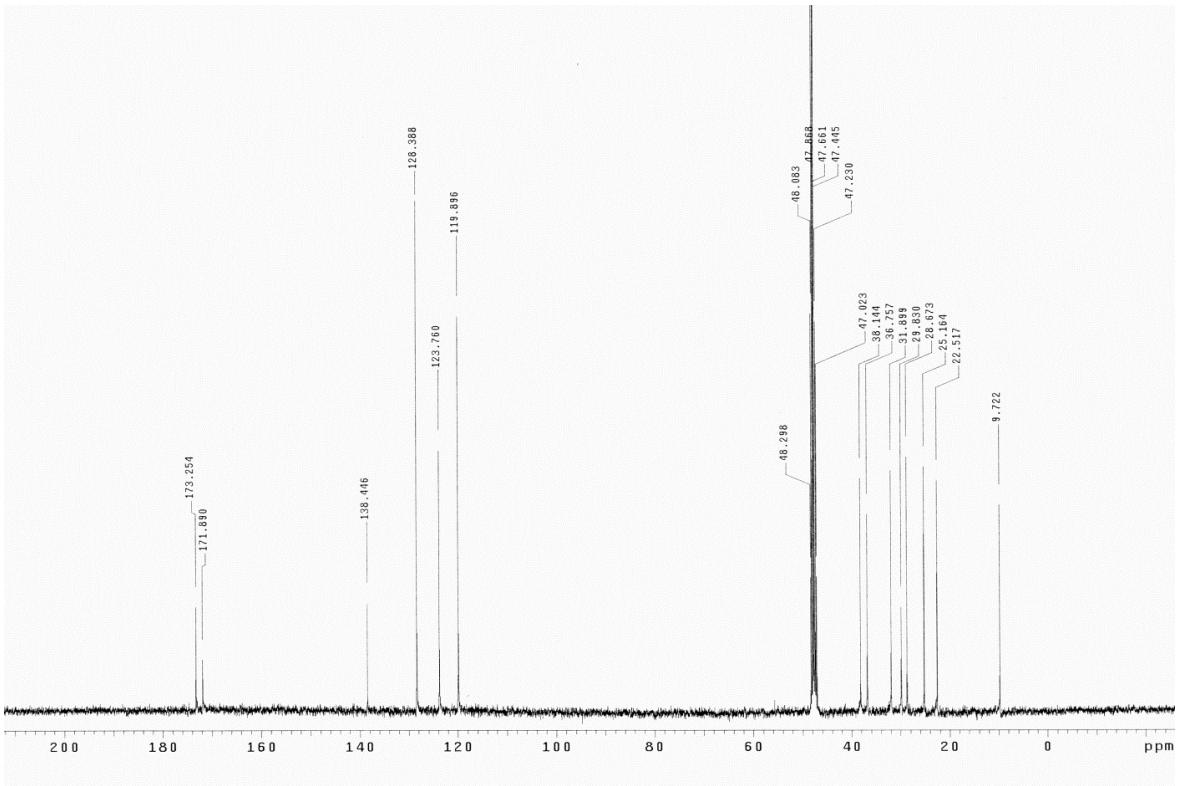

Figure B.50. ^{13}CNMR spectrum of **19b** in CD_3OD.

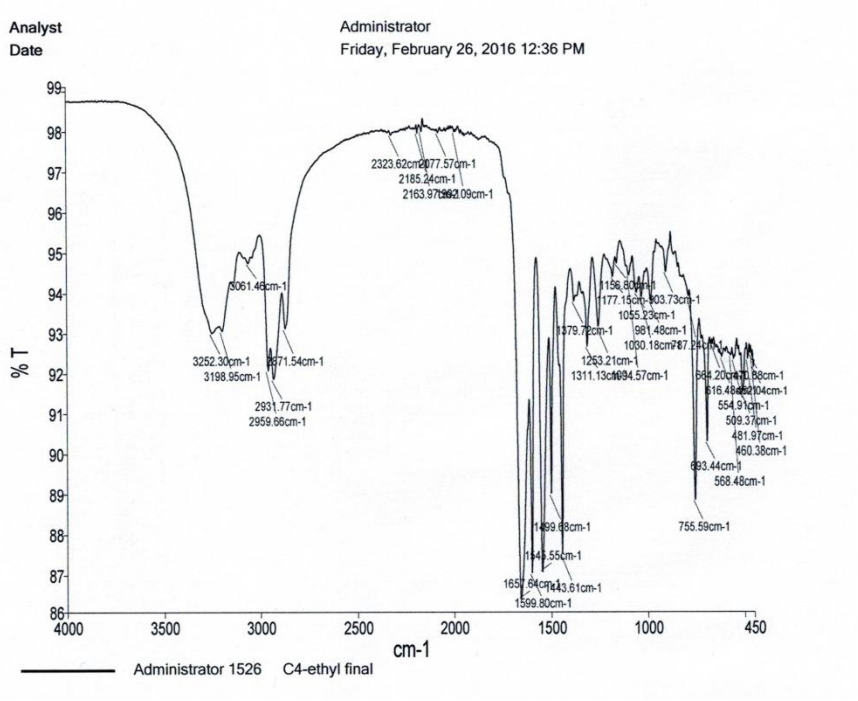

Figure B.51. IR spectrum of **19b** using a Perkin Elmer Spectrum Two ATR-FTIR.

Elemental Composition Report **Page 1**

Single Mass Analysis
Tolerance = 5.0 PPM / DBE: min = -1.5, max = 100.0
Element prediction: Off
Number of isotope peaks used for i-FIT = 6

Monoisotopic Mass, Even Electron Ions
208 formula(e) evaluated with 1 results within limits (all results (up to 1000) for each mass)
Elements Used:
C: 16-16 H: 0-100 N: 0-5 O: 0-5 Na: 0-5
1602126_038 2812 (51.988) Ahmed Negmeldin C4-ethyl SAHA in Water Cone(V)50
LCT Premier KD128
TOF MS ES+
2.91e+004

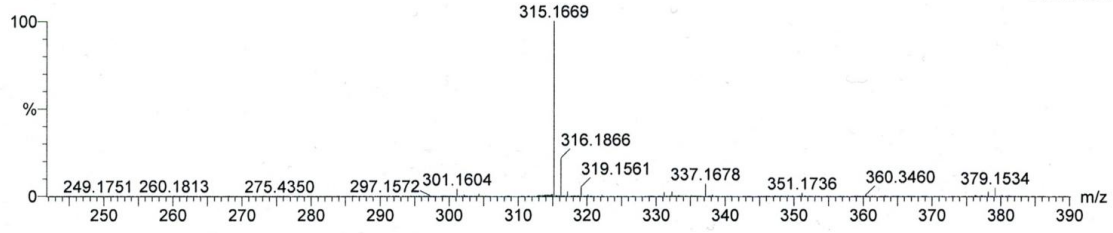

Minimum:				-1.5			
Maximum:		3.0	5.0	100.0			
Mass	Calc. Mass	mDa	PPM	DBE	i-FIT	i-FIT (Norm)	Formula
315.1671	315.1685	-1.4	-4.4	5.5	233.8	0.0	C16 H24 N2 O3 Na

Figure B.52. High resolution mass spectrum of **19b**.

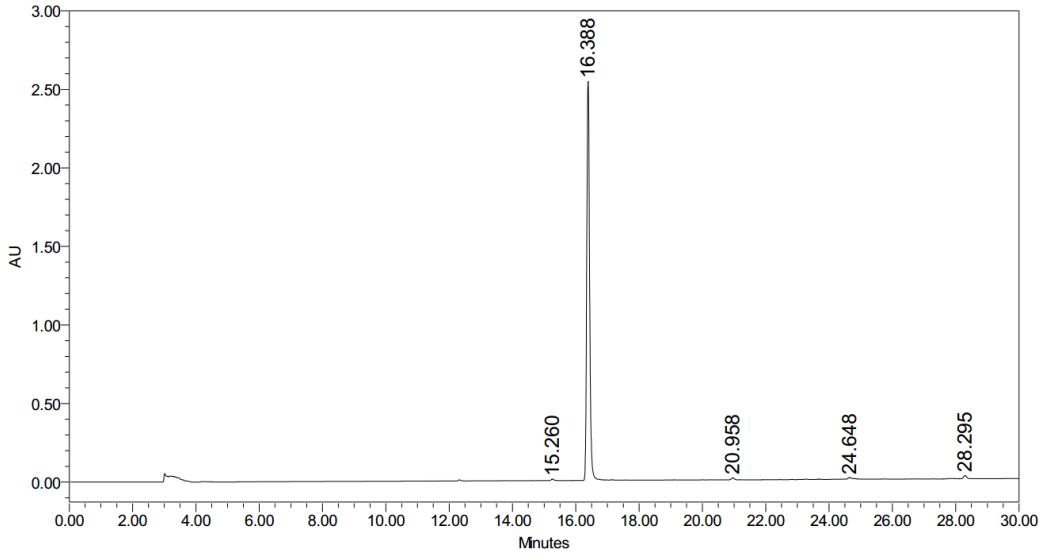

	RT	Area	% Area	Height
1	15.260	59780	0.36	9252
2	16.388	15985361	97.52	2539625
3	20.958	80291	0.49	12713
4	24.648	119953	0.73	10766
5	28.295	146013	0.89	20832

Figure B.53. HPLC spectrum taken at 254 nm of C4-ethyl SAHA (**19b**). The peak at 16.388 is C4-ethyl SAHA. The calculated area and height under each peak, along with % area, is shown in the table below the spectrum.

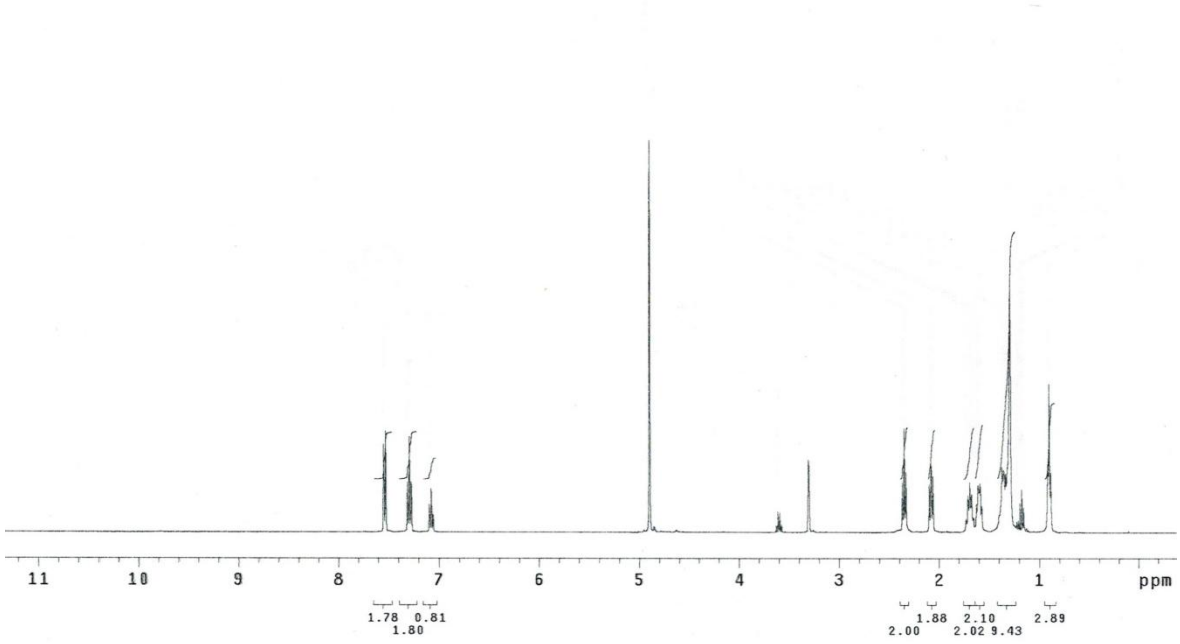

Figure B.54. ^{1}HNMR spectrum of **19c** in CD_3OD.

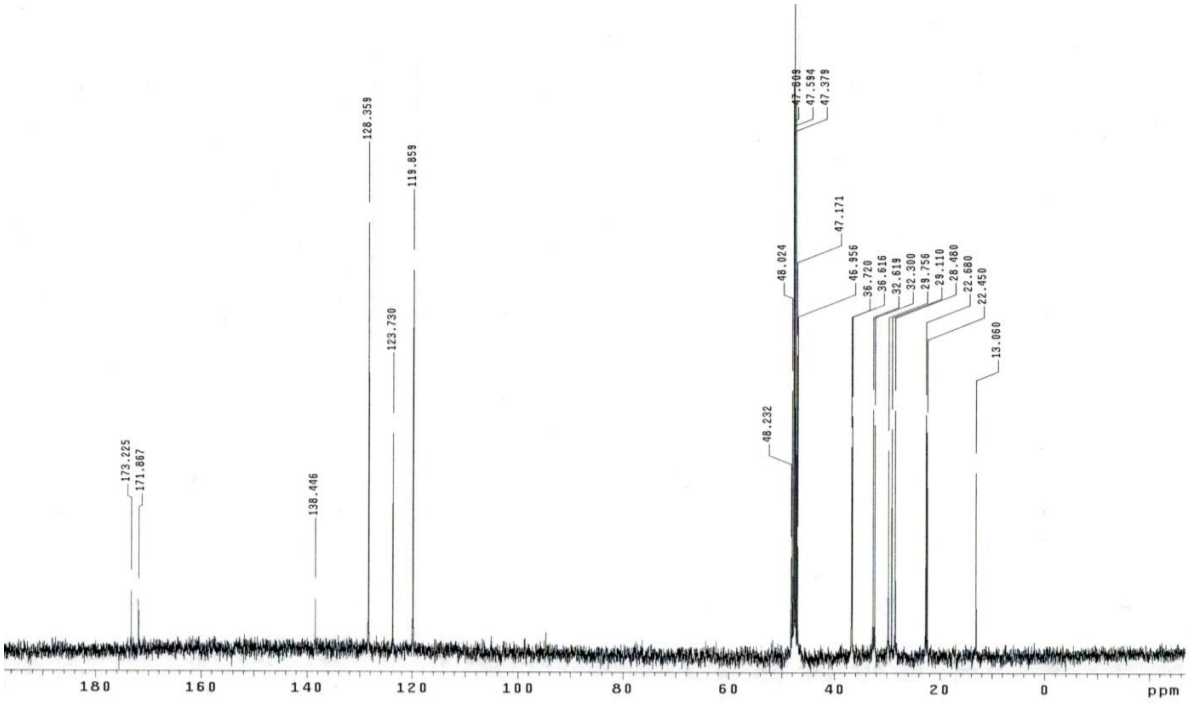

Figure B.55. ^{13}CNMR spectrum of **19c** in CD_3OD.

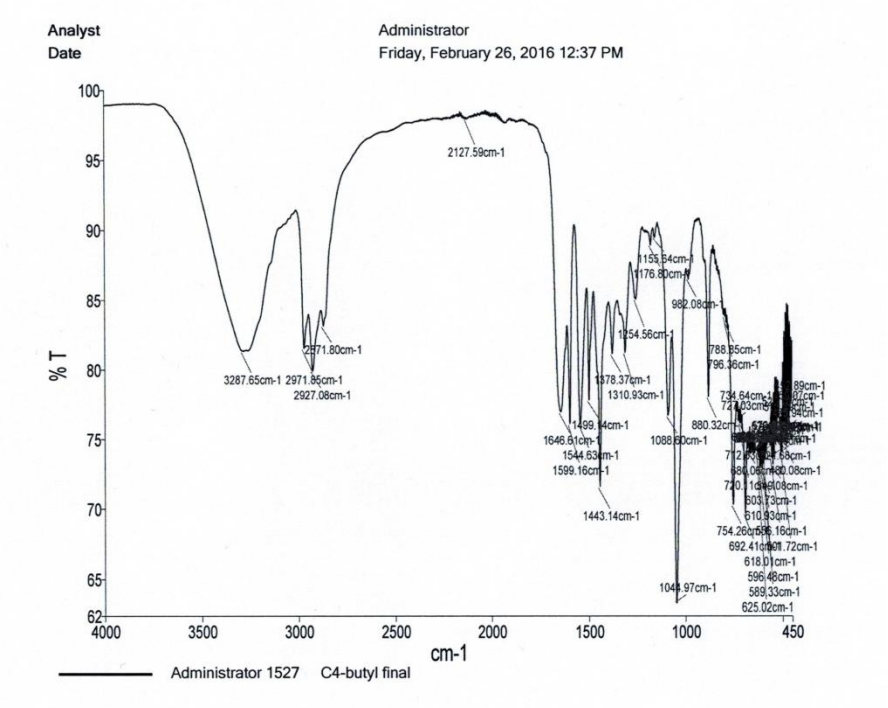

Figure B.56. IR spectrum of **19c** using a Perkin Elmer Spectrum Two ATR-FTIR.

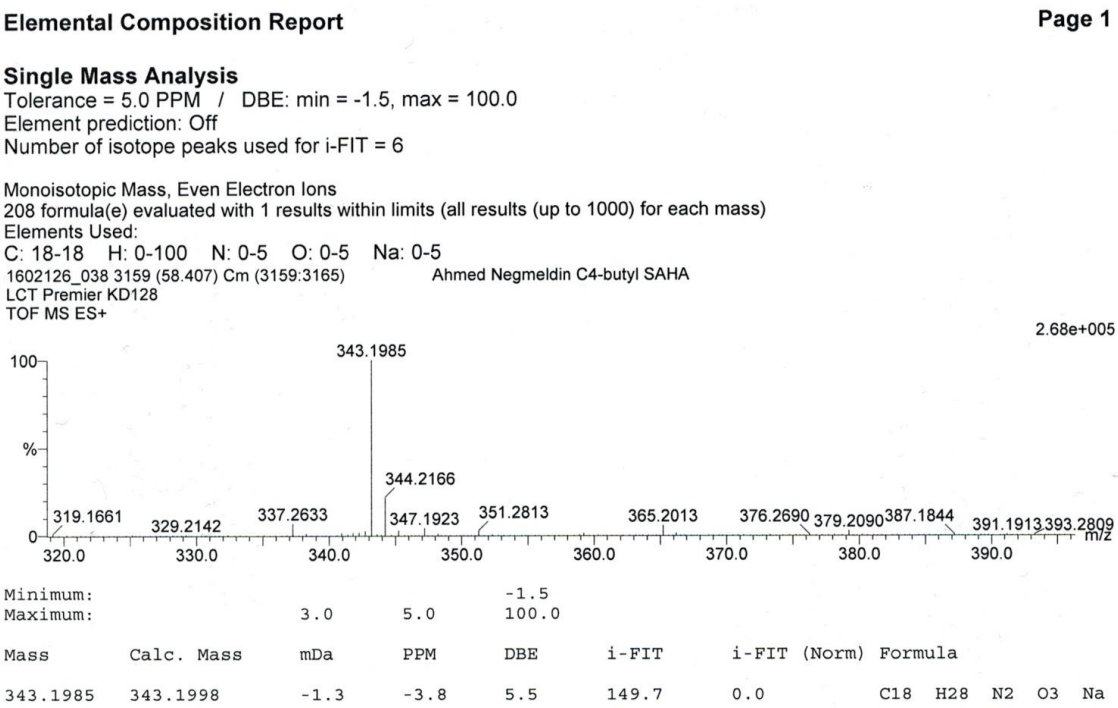

Figure B.57. High resolution mass spectrum of **19c**.

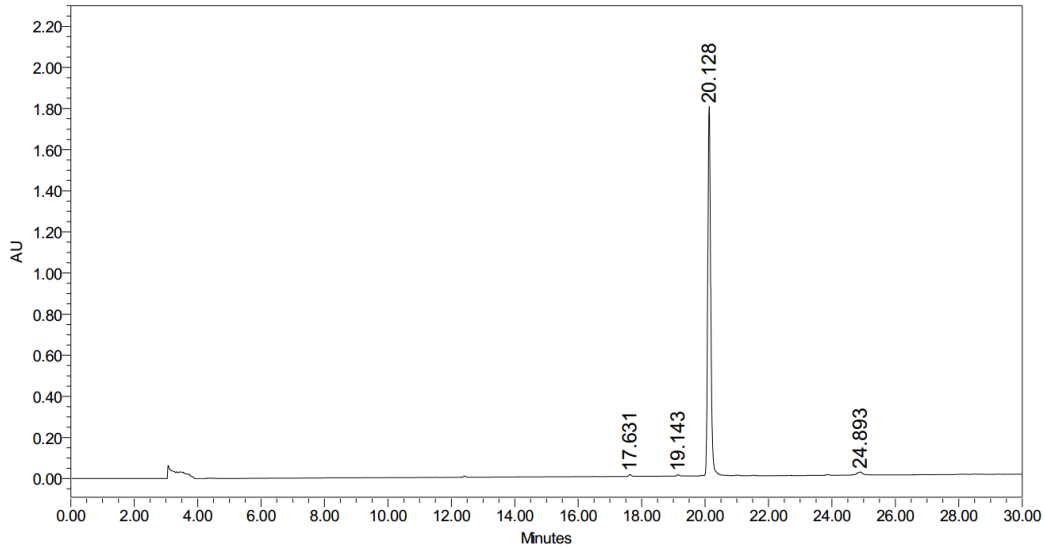

	RT	Area	% Area	Height
1	17.631	50506	0.42	8334
2	19.143	52712	0.44	6273
3	20.128	11819905	97.65	1796418
4	24.893	181171	1.50	14339

Figure B.58. HPLC spectrum taken at 254 nm of C4-*n*-butyl SAHA (**19c**). The peak at 20.128 is C4-*n*-butyl SAHA. The calculated area and height under each peak, along with % area, is shown in the table below the spectrum.

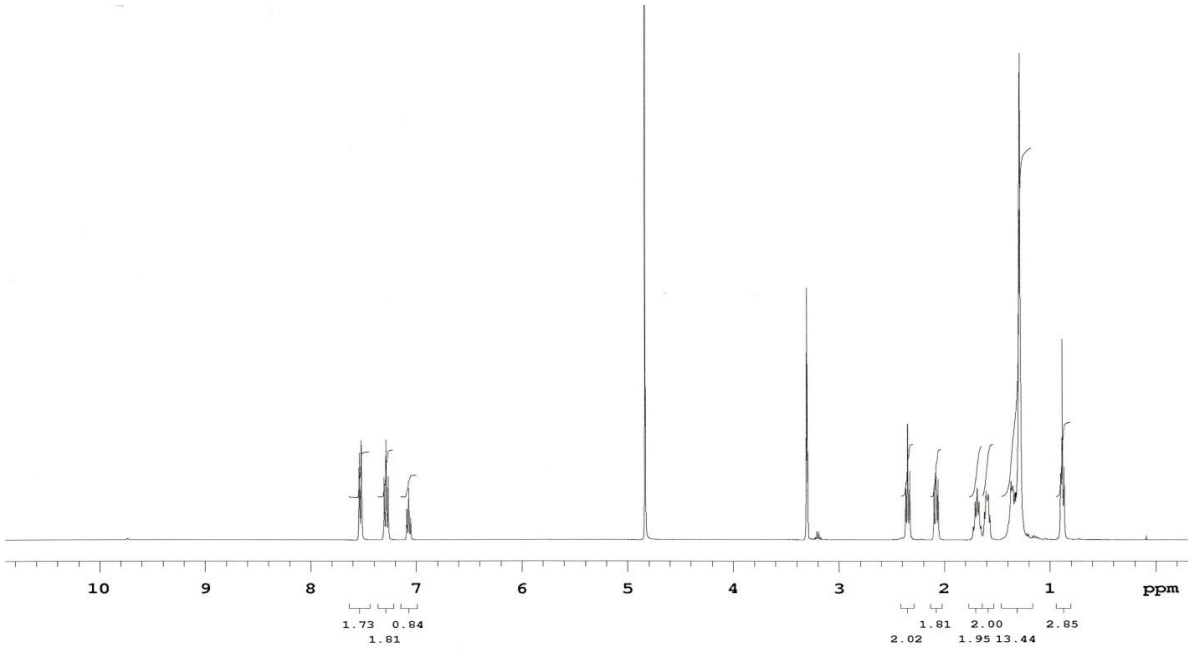

Figure B.59. ^{1}HNMR spectrum of **19d** in CD_3OD.

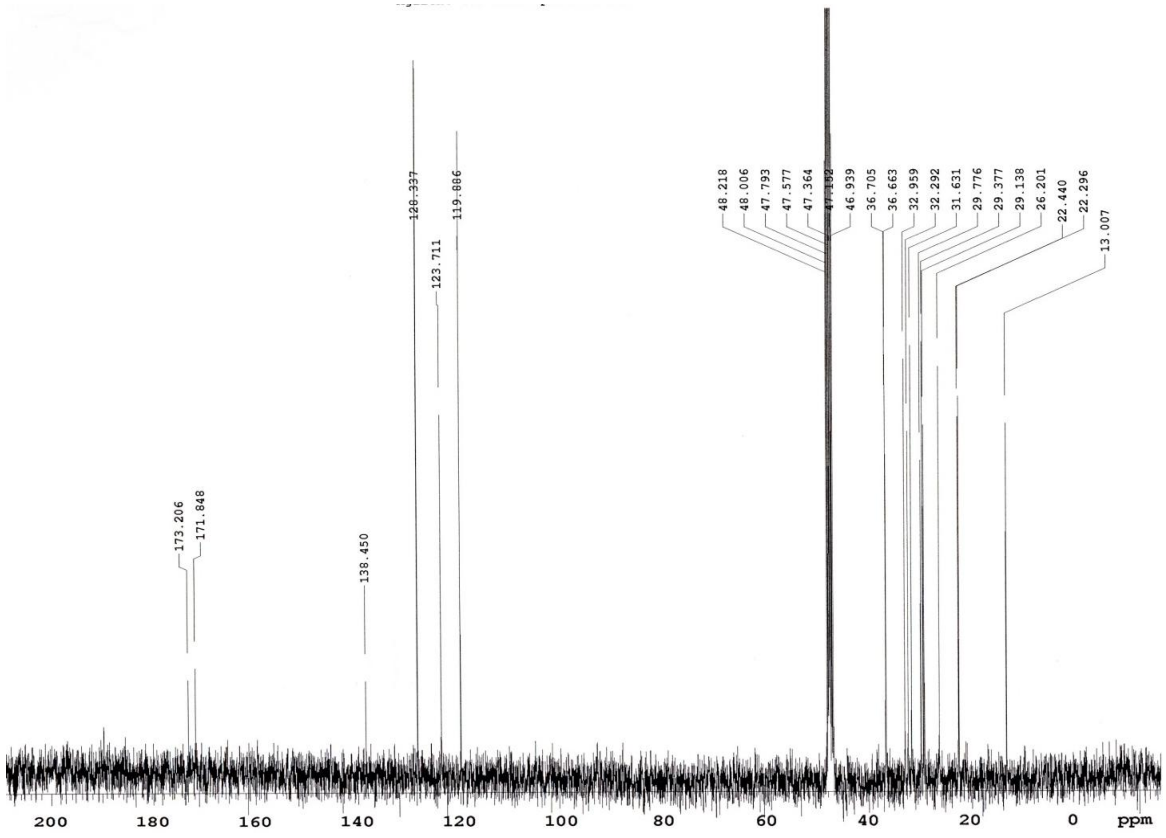

Figure B.60. ^{13}CNMR spectrum of **19d** in CD_3OD.

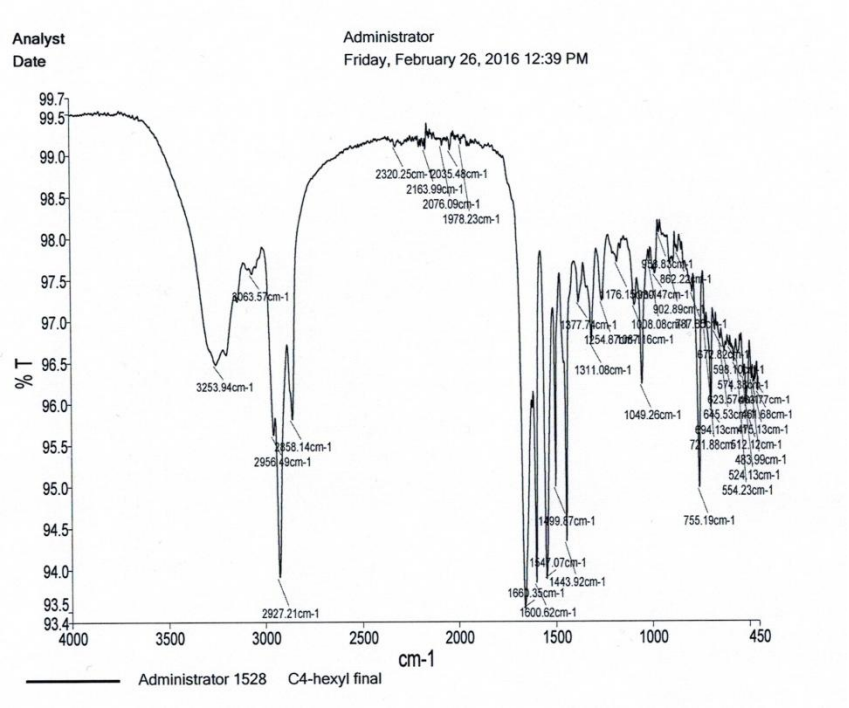

Figure B.61. IR spectrum of **19d** using a Perkin Elmer Spectrum Two ATR-FTIR.

Elemental Composition Report **Page 1**

Single Mass Analysis
Tolerance = 5.0 PPM / DBE: min = -1.5, max = 100.0
Element prediction: Off
Number of isotope peaks used for i-FIT = 6

Monoisotopic Mass, Even Electron Ions
209 formula(e) evaluated with 1 results within limits (all results (up to 1000) for each mass)
Elements Used:
C: 20-20 H: 0-100 N: 0-5 O: 0-5 Na: 0-5

Ahmed Negmeldin C4-hexyl SAHA in Water Cone(V)50

LCT Premier KD128
TOF MS ES+

7.12e+004

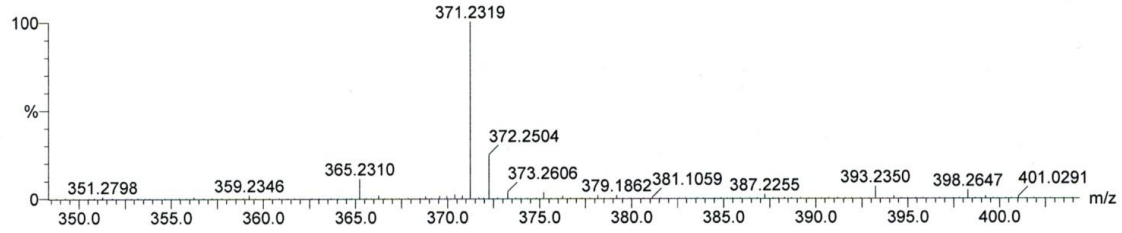

Minimum:				-1.5			
Maximum:		3.0	5.0	100.0			
Mass	Calc. Mass	mDa	PPM	DBE	i-FIT	i-FIT (Norm)	Formula
371.2319	371.2311	0.8	2.2	5.5	140.6	0.0	C20 H32 N2 O3 Na

Figure B.62. High resolution mass spectrum of **19d**.

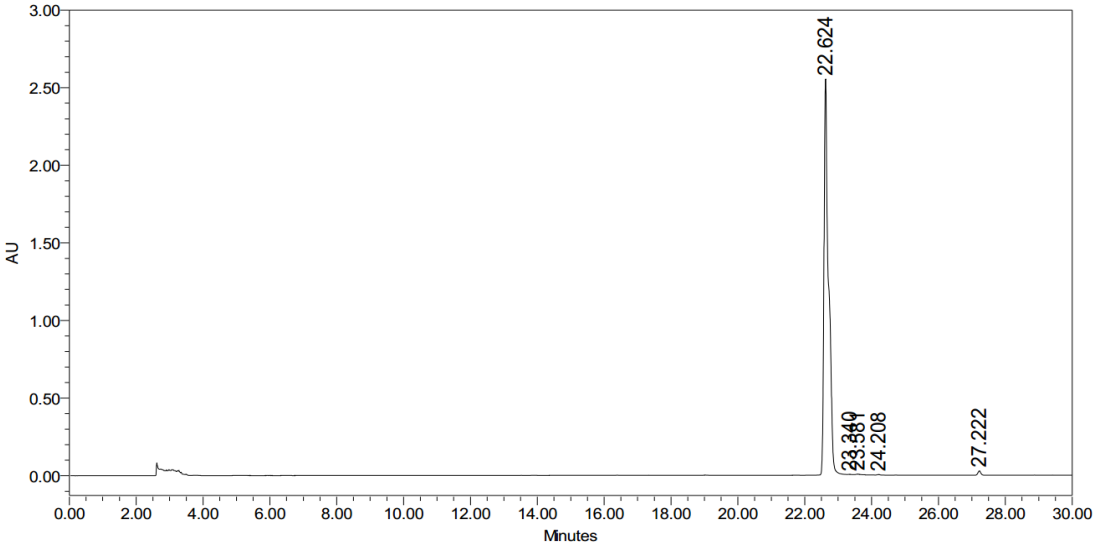

	RT	Area	% Area	Height
1	22.624	24434604	98.21	2552987
2	23.340	49285	0.20	5492
3	23.581	116591	0.47	7456
4	24.208	25421	0.10	3675
5	27.222	173207	0.70	27930
6	32.366	80119	0.32	13238

Figure B.63. HPLC spectrum taken at 254 nm of C4-*n*-hexyl SAHA (**19d**). The peak at 22.624 is C4-*n*-hexyl SAHA. The calculated area and height under each peak, along with % area, is shown in the table below the spectrum.

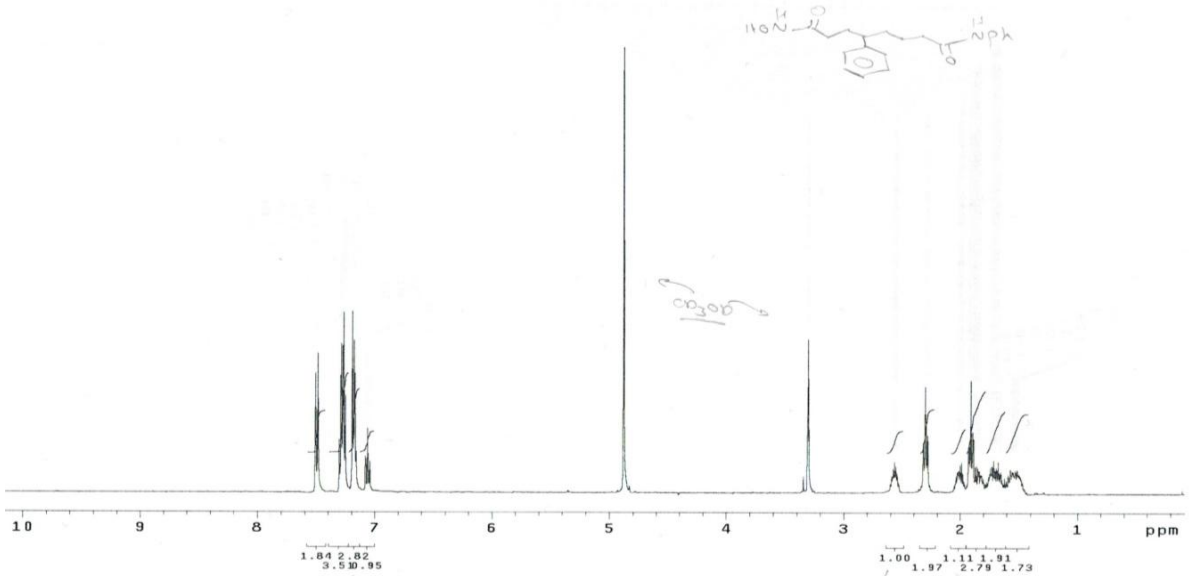

Figure B.64. ^{1}HNMR spectrum of **19e** in CD_3OD.

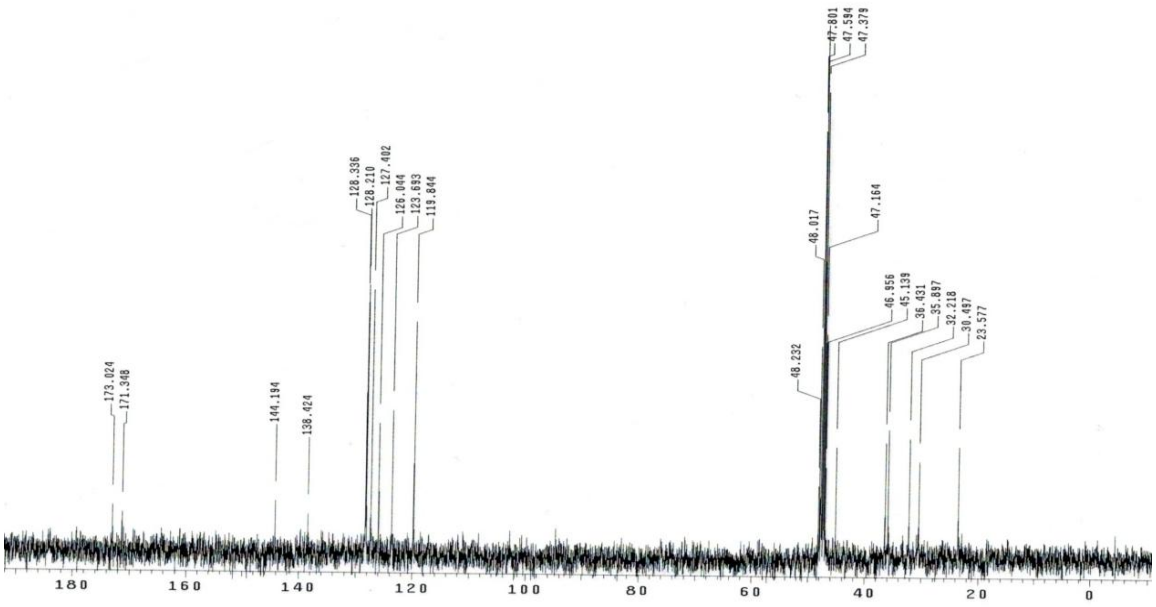

Figure B.65. ^{13}CNMR spectrum of **19e** in CD_3OD.

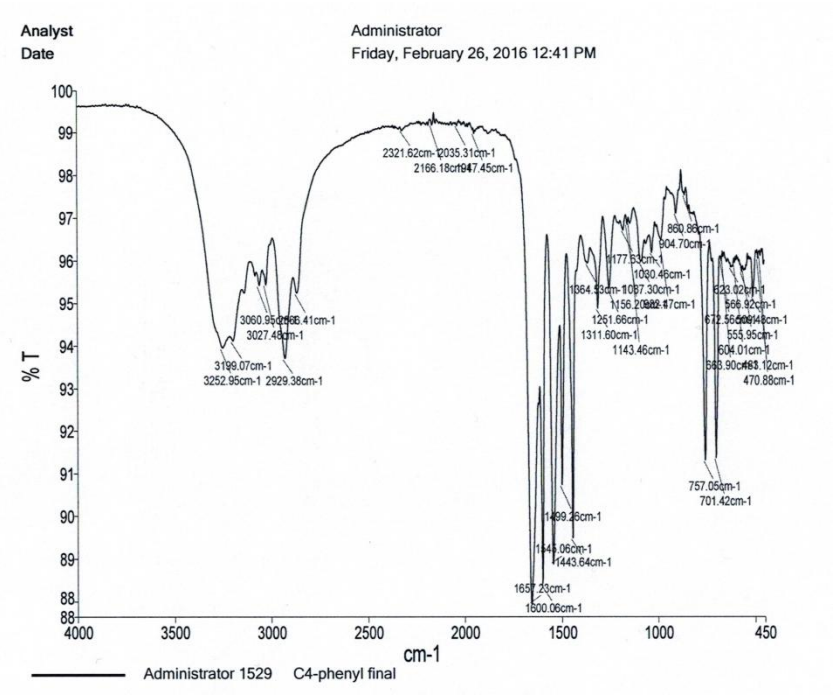

Figure B.66. IR spectrum of **19e** using a Perkin Elmer Spectrum Two ATR-FTIR.

Elemental Composition Report **Page 1**

Single Mass Analysis
Tolerance = 5.0 PPM / DBE: min = -1.5, max = 100.0
Element prediction: Off
Number of isotope peaks used for i-FIT = 6

Monoisotopic Mass, Even Electron Ions
208 formula(e) evaluated with 1 results within limits (all results (up to 1000) for each mass)
Elements Used:
C: 20-20 H: 0-100 N: 0-5 O: 0-5 Na: 0-5
1602126_039 541 (10.008) Cm (537:547) Ahmed Negmeldin C4-phenyl SAHA
LCT Premier KD128
TOF MS ES+

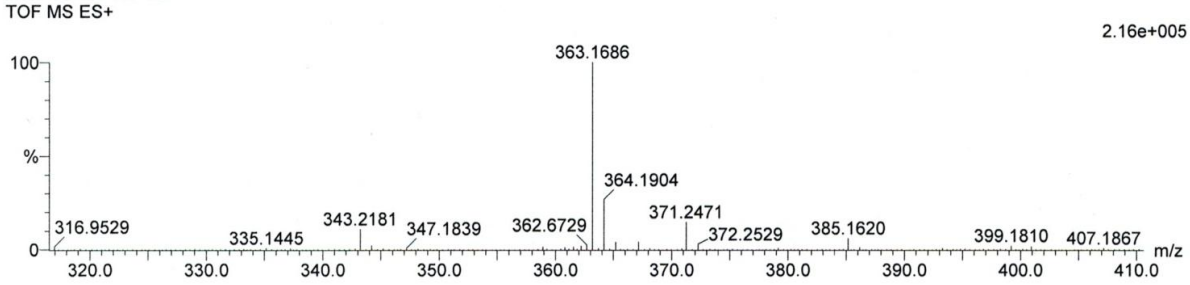

Minimum:				-1.5			
Maximum:		3.0	5.0	100.0			
Mass	Calc. Mass	mDa	PPM	DBE	i-FIT	i-FIT (Norm)	Formula
363.1686	363.1685	0.1	0.3	9.5	140.0	0.0	C20 H24 N2 O3 Na

Figure B.67. High resolution mass spectrum of **19e**.

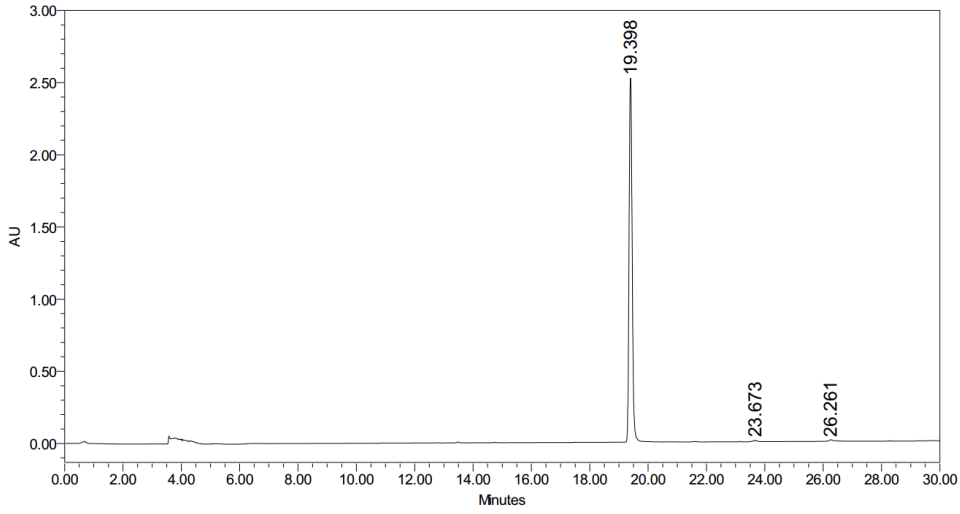

	RT	Area	% Area	Height
1	19.398	18503505	98.75	2521047
2	23.673	87733	0.47	9056
3	26.261	146288	0.78	10390

Figure B.68. HPLC spectrum taken at 254 nm of C4-phenyl SAHA (**19e**). The peak at 19.398 is C4-phenyl SAHA. The calculated area and height under each peak, along with % area, is shown in the table below the spectrum.

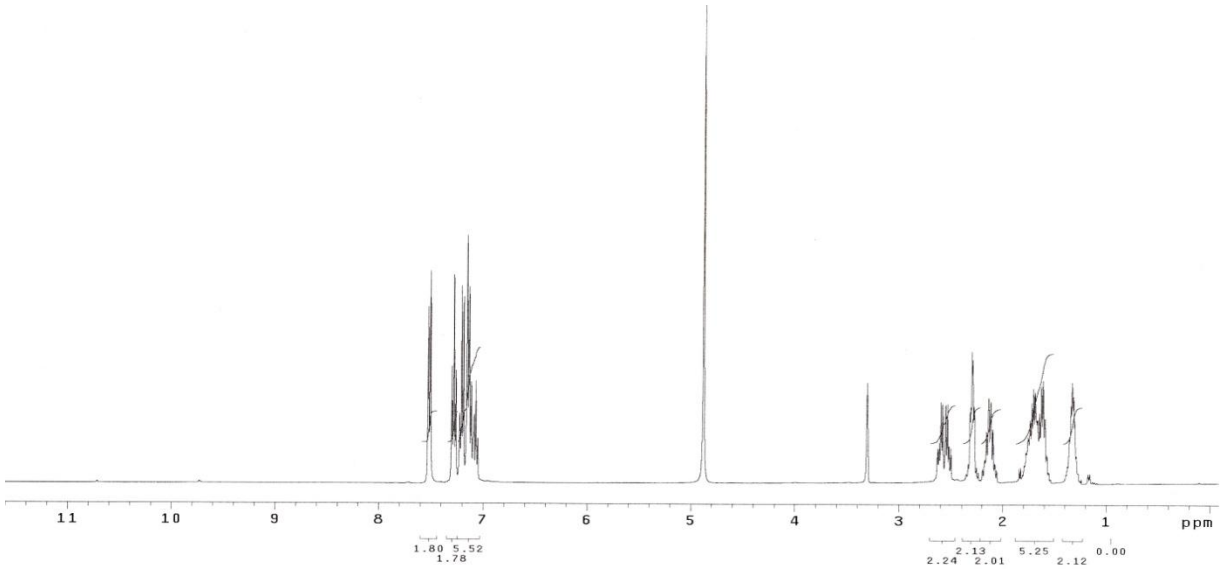

Figure B.69. ^{1}HNMR spectrum of **19f** in CD_3OD.

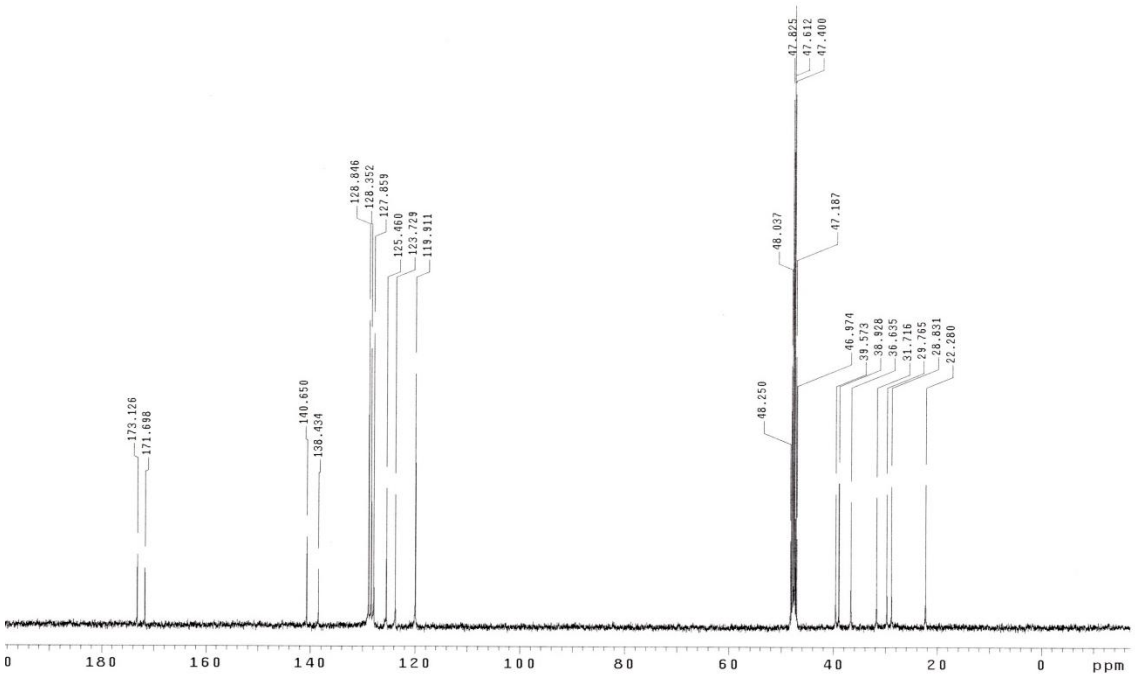

Figure B.70. ^{13}CNMR spectrum of **19f** in CD_3OD.

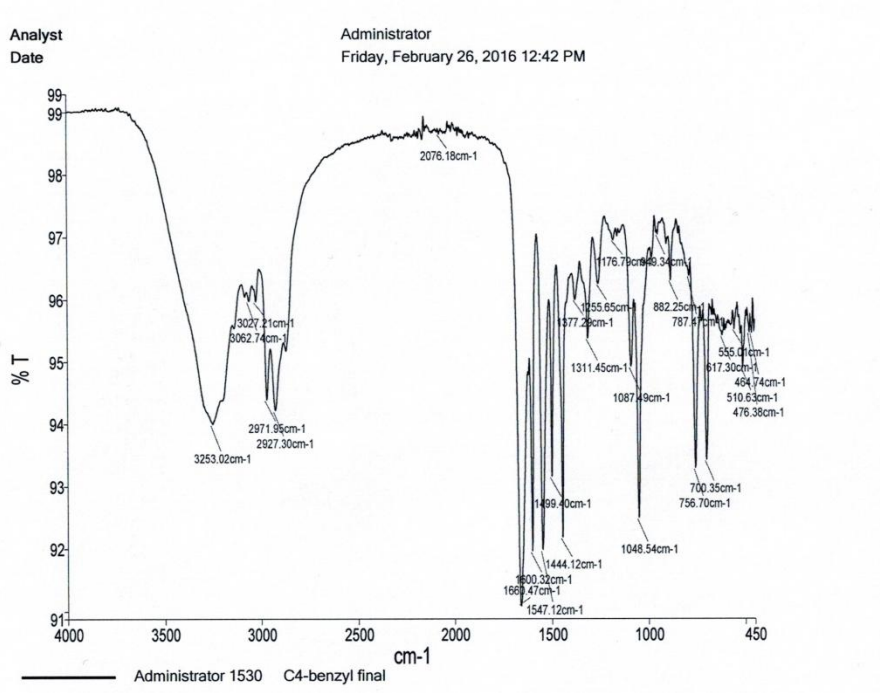

Figure B.71. IR spectrum of **19f** using a Perkin Elmer Spectrum Two ATR-FTIR.

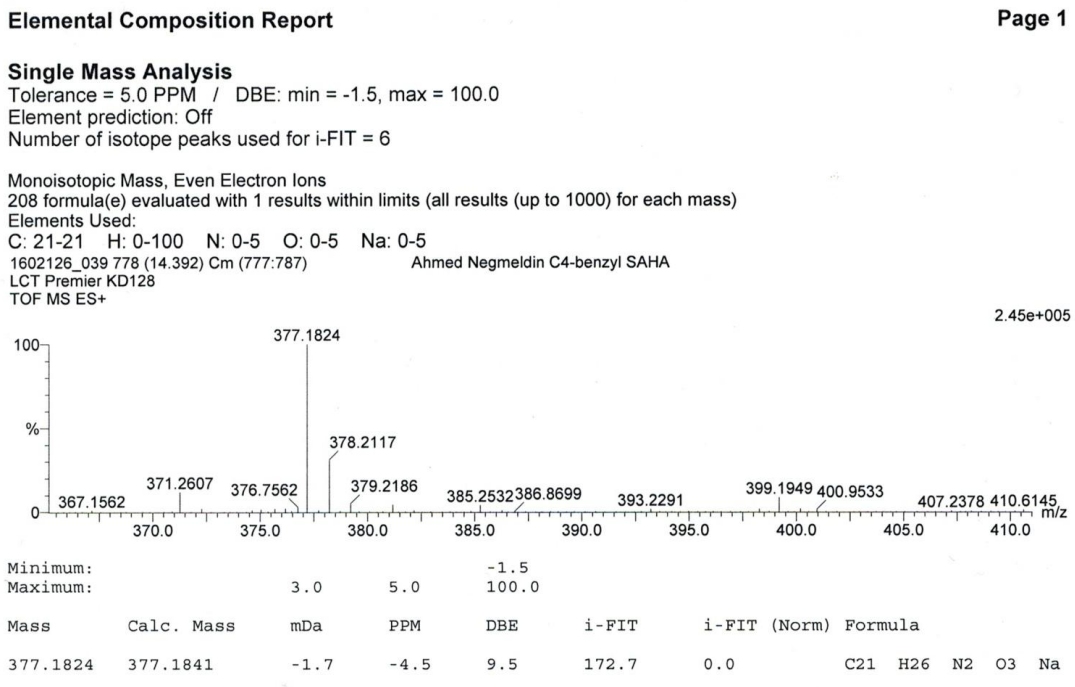

Figure B.72. High resolution mass spectrum of **19f**.

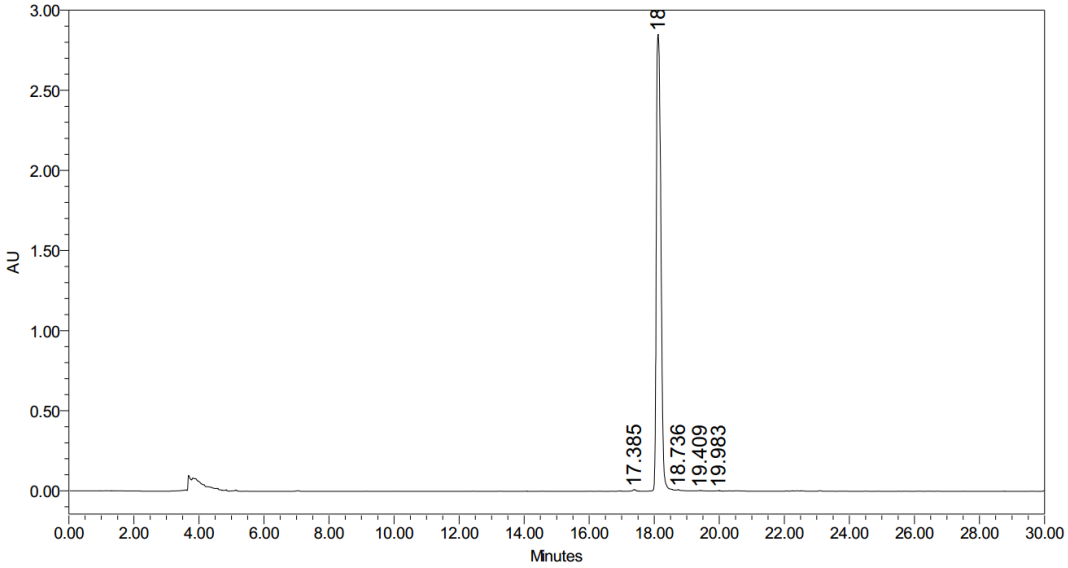

	RT	Area	% Area	Height
1	17.385	81871	0.29	10172
2	18.119	27839558	98.91	2850045
3	18.736	130855	0.46	9239
4	19.409	65425	0.23	4304
5	19.983	27953	0.10	3066

Figure B.73. HPLC spectrum taken at 254 nm of C4-benzyl SAHA (**19f**). The peak at 18.119 is C4-benzyl SAHA. The calculated area and height under each peak, along with % area, is shown in the table below the spectrum.

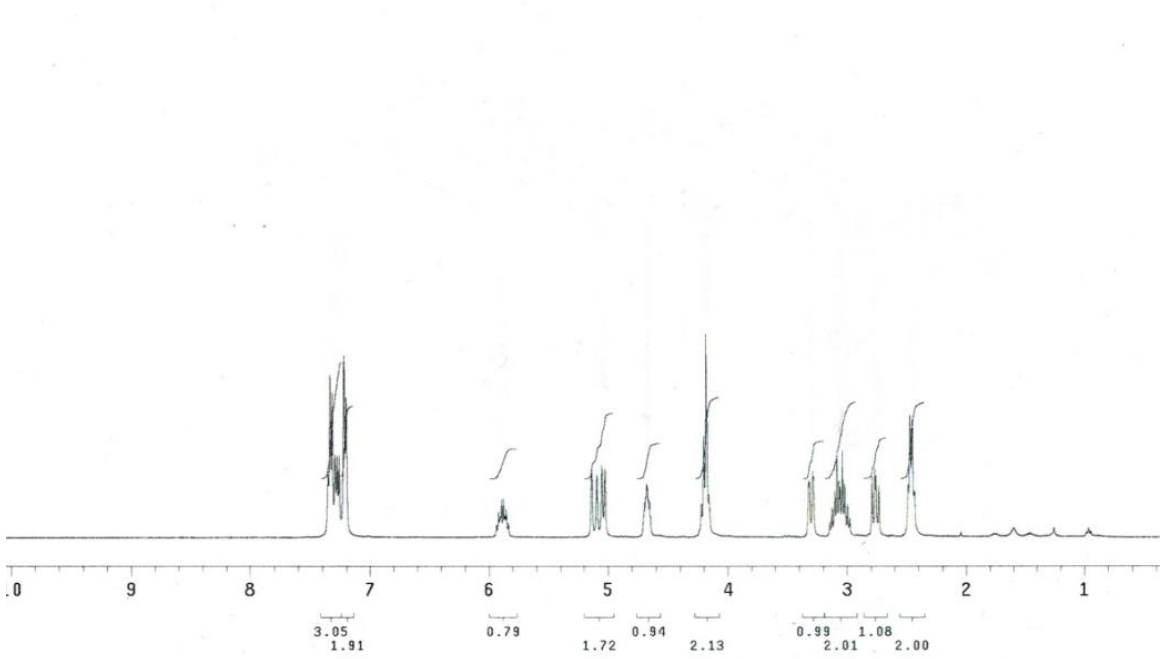

Figure B.74. ^{1}HNMR spectrum of **(*R*)-20** in $CDCl_3$.

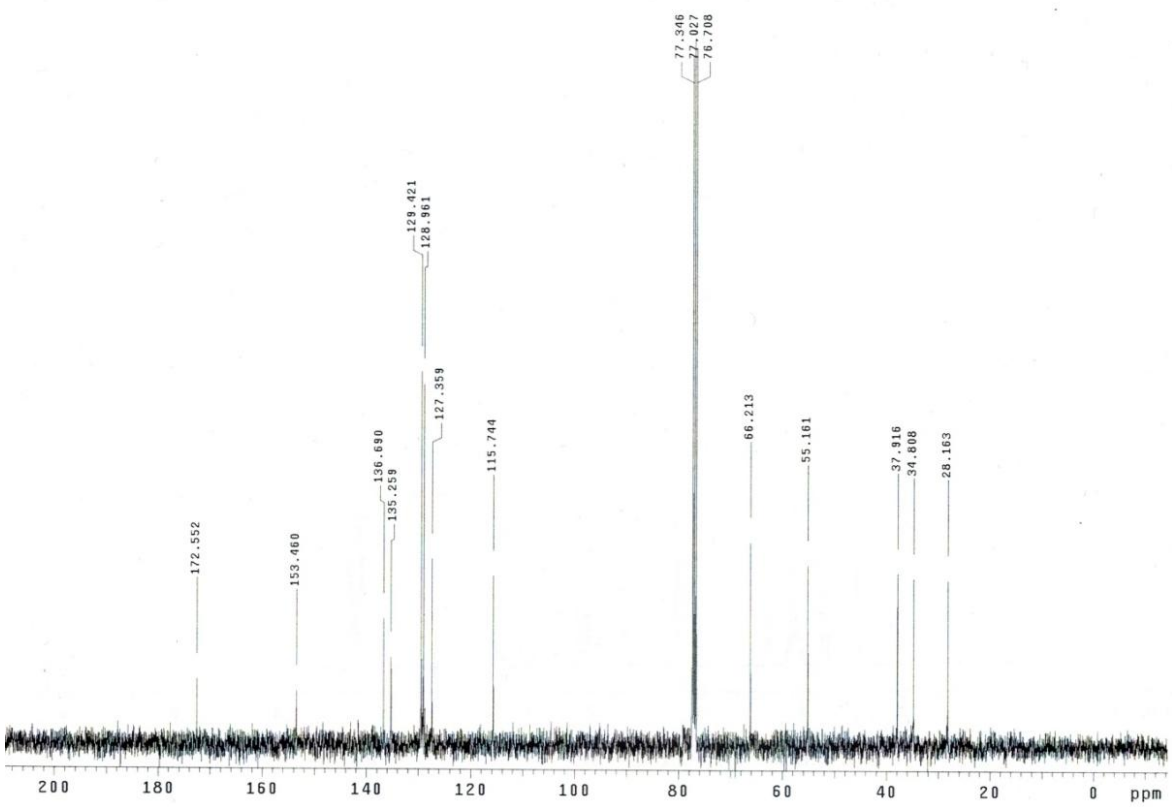

Figure B.75. ^{13}CNMR spectrum of **(*R*)-20** in $CDCl_3$.

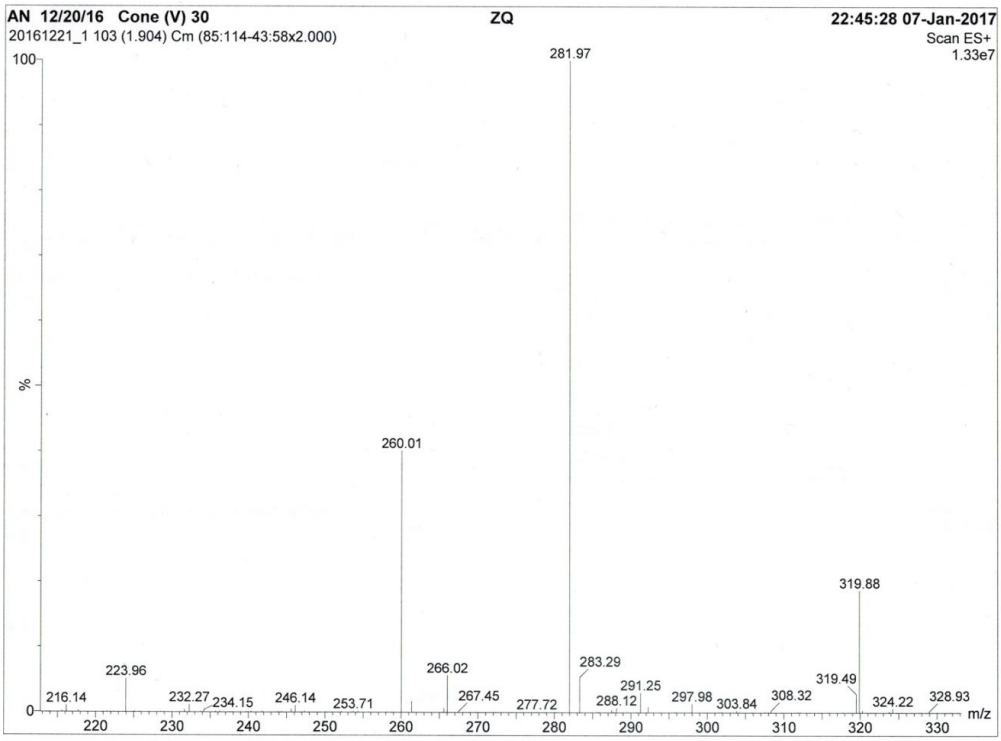

Figure B.76. Low resolution mass spectrum of **(*R*)-20**.

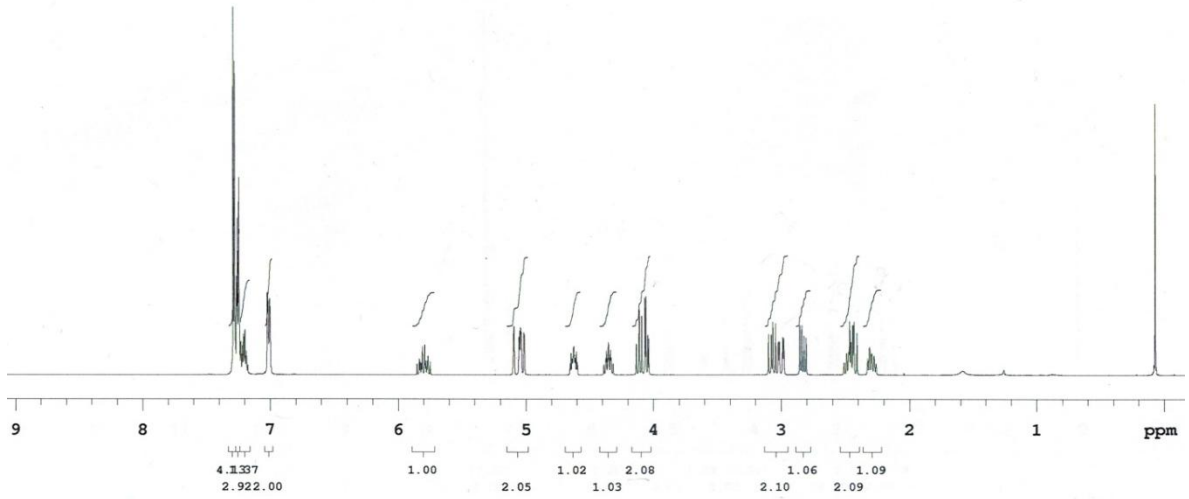

Figure B.77. ^{1}HNMR spectrum of **(*RS*)-21** in $CDCl_3$.

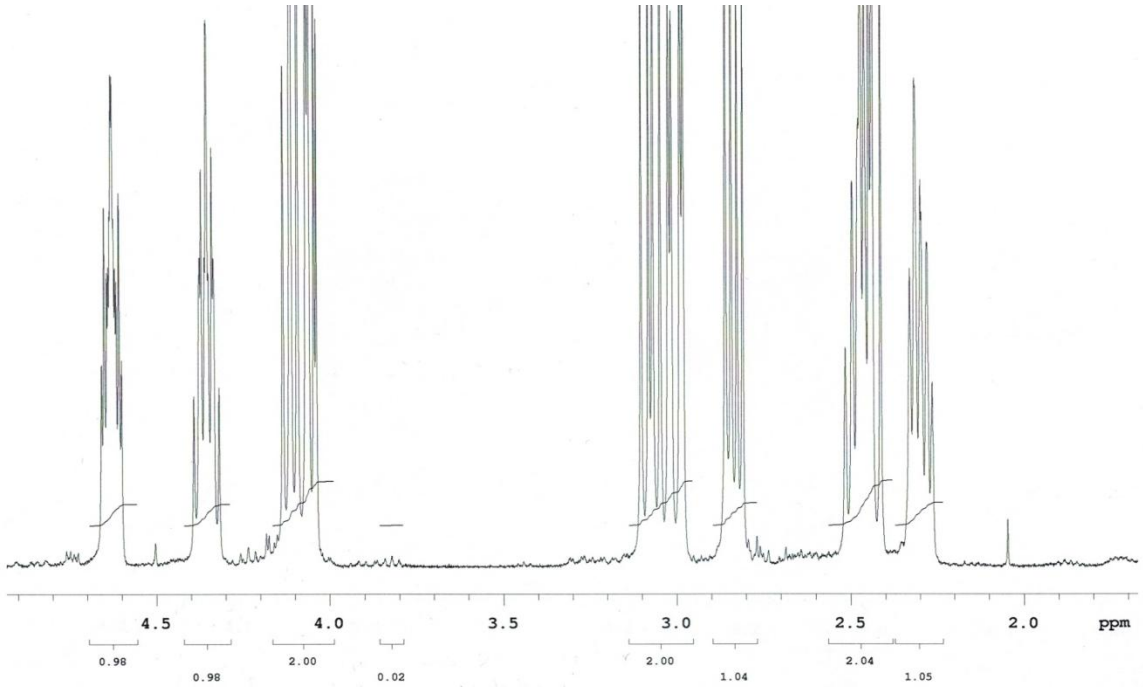

Figure B.78. Enlarged 1HNMR spectrum of **(*RS*)-21** showing a peak of the major diastereomer at 4.05 (overlapping with another peak) and a peak of the minor diastereomer **(*RR*)-21** at 3.82. Integration of these two peaks (2.00 and 0.02) was used to calculate the diastereomeric ratio (dr) discussed in the text (99:1 dr).

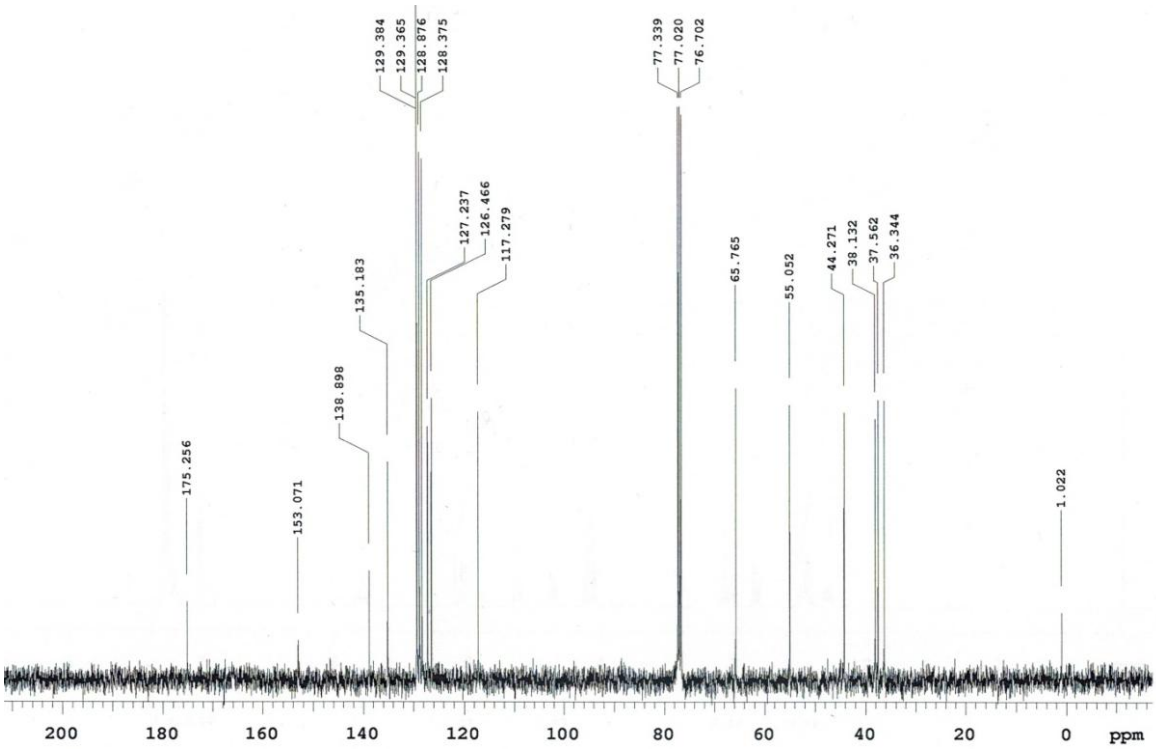

Figure B.79. ^{13}CNMR spectrum of **(*RS*)-21** in $CDCl_3$.

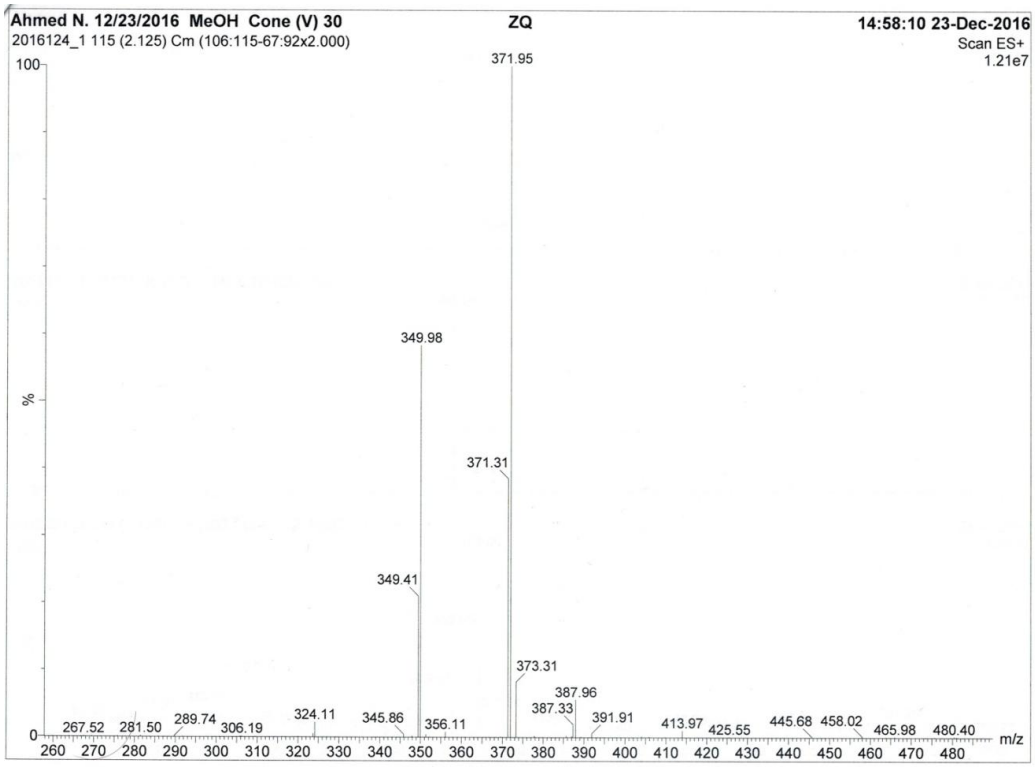

Figure B.80. Low resolution mass spectrum of **(*RS*)-21**.

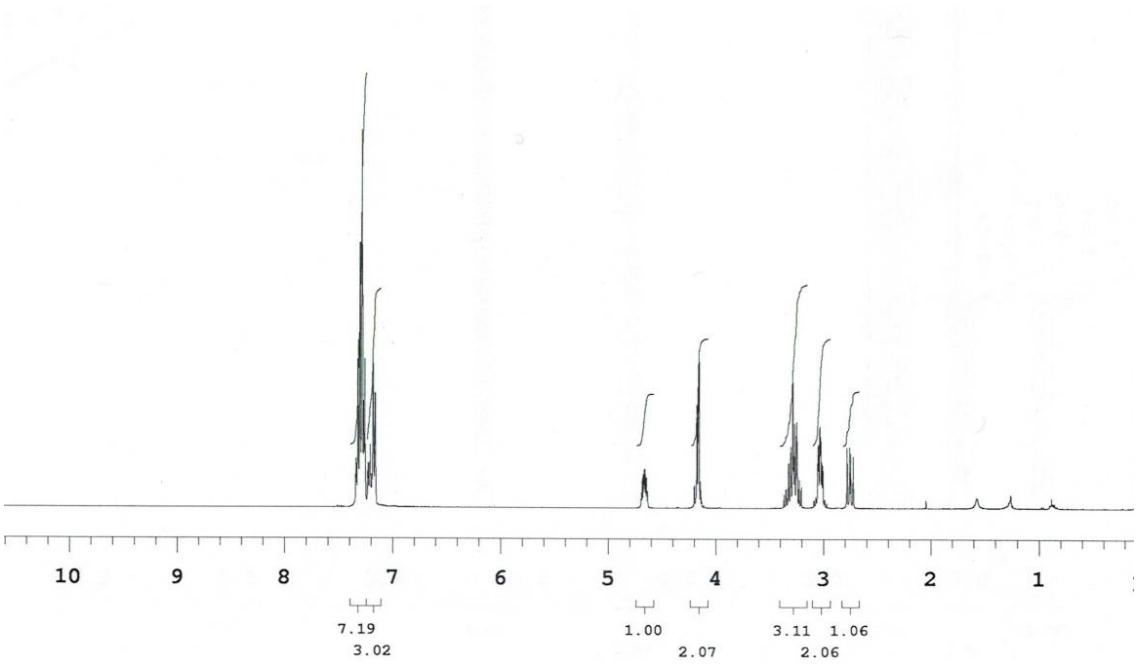

Figure B.81. ^{1}HNMR spectrum of **(*R*)-23** in $CDCl_3$.

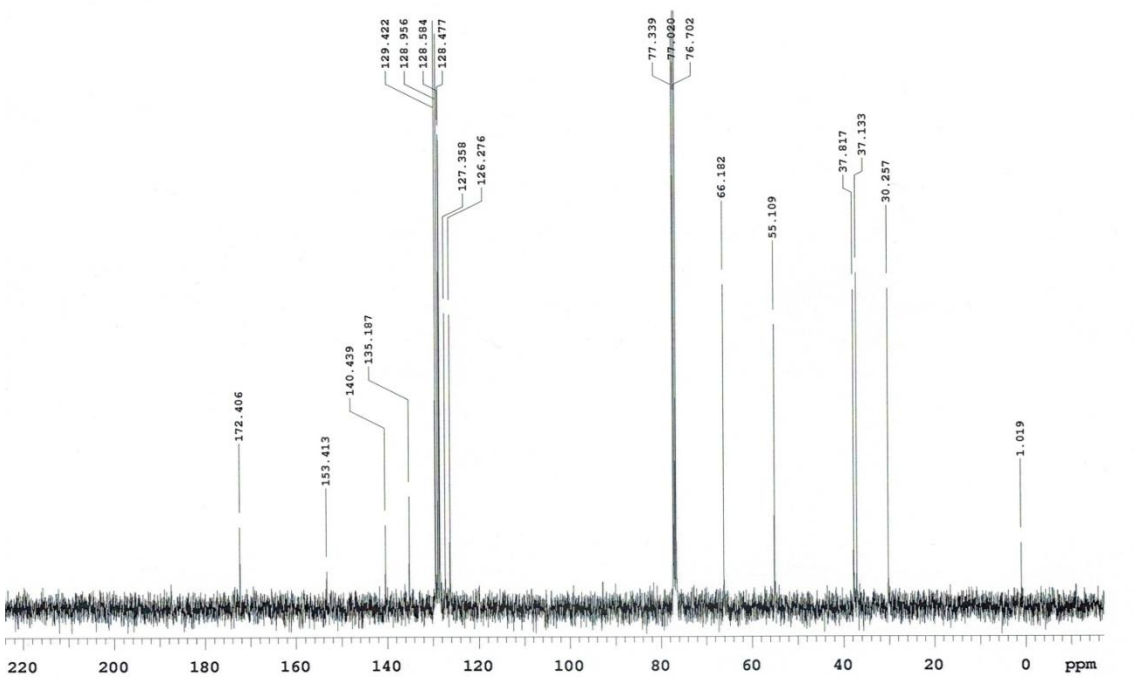

Figure B.82. ^{13}CNMR spectrum of **(*R*)-23** in $CDCl_3$.

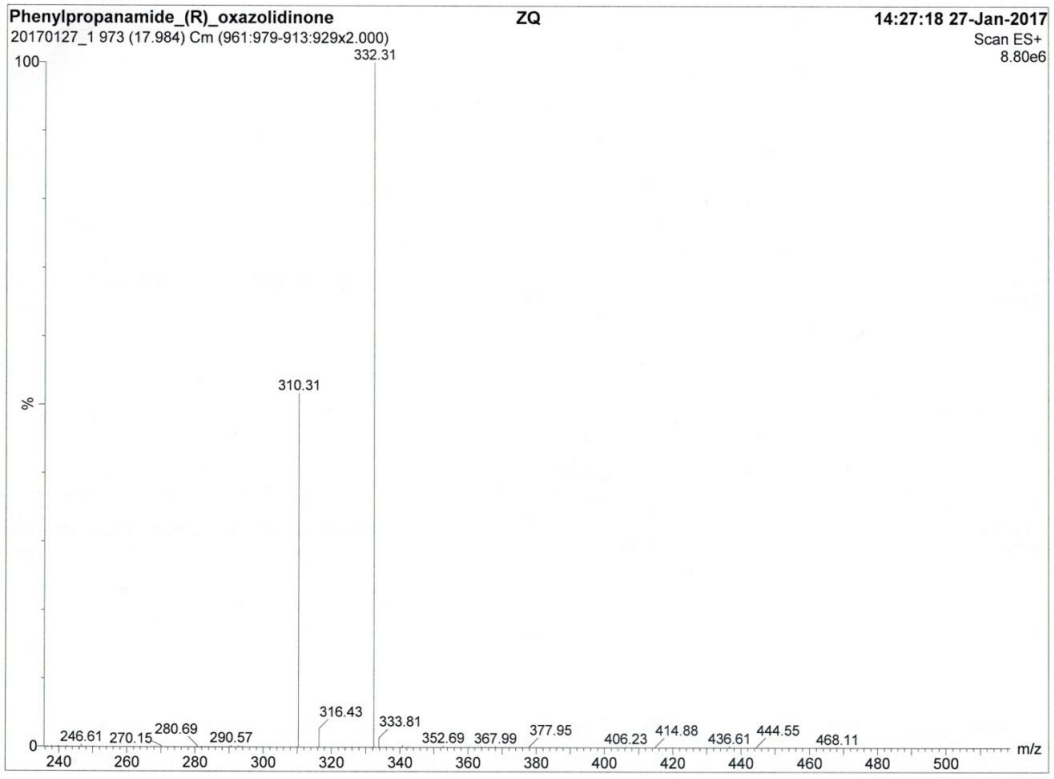

Figure B.83. Low resolution mass spectrum of **(*R*)-23**.

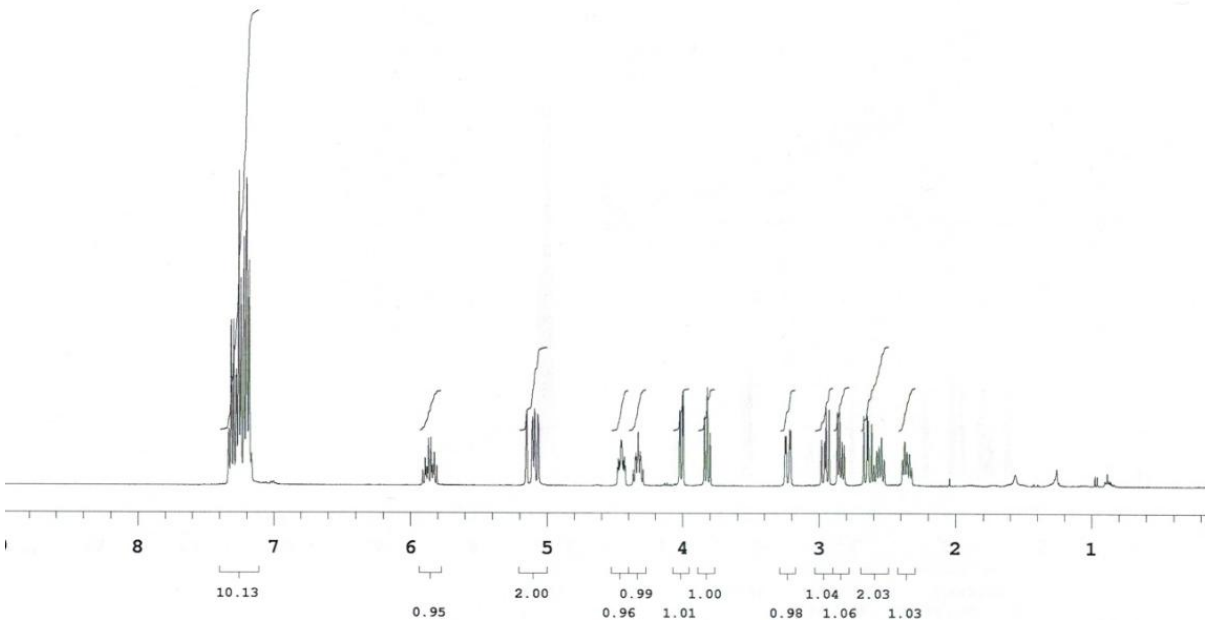

Figure B.84. ^{1}HNMR spectrum of **(*RR*)-21** in $CDCl_3$.

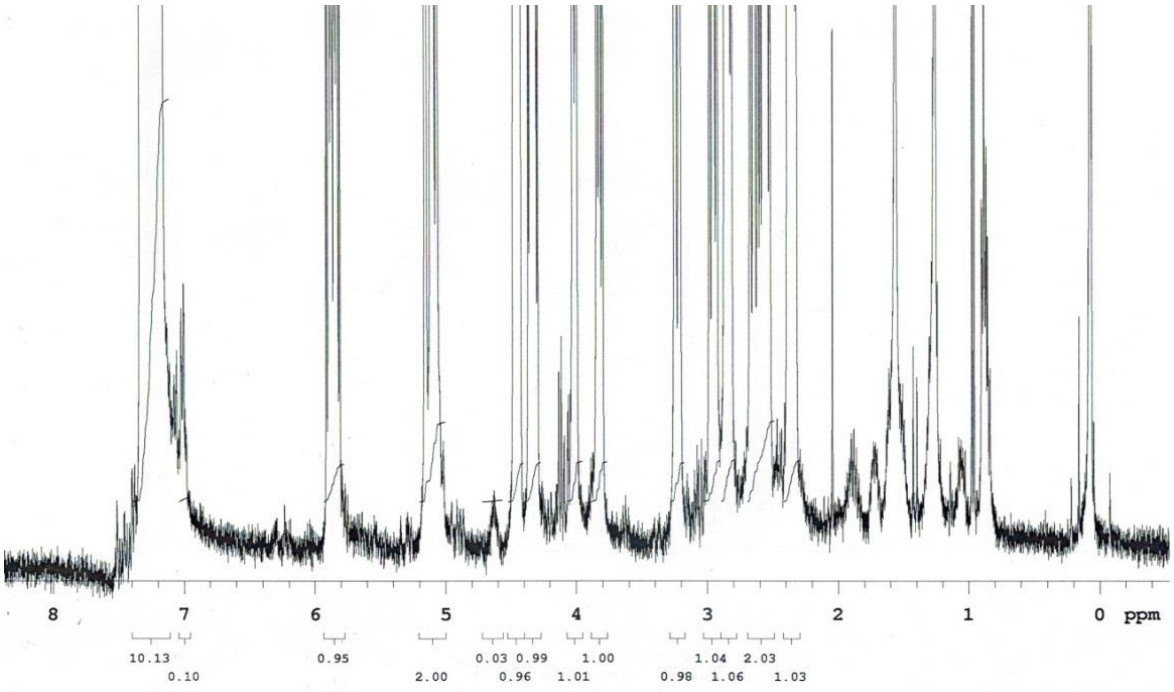

Figure B.85. Enlarged ^{1}HNMR spectrum of **(*RR*)-21** showing a peak of the major diastereomer at 4.45 and a peak of the minor diastereomer **(*RS*)-21** at 4.63. Integration of these two peaks (0.99 and 0.03) was used to calculate the diastereomeric ratio (dr) discussed in the text (97:3 dr).

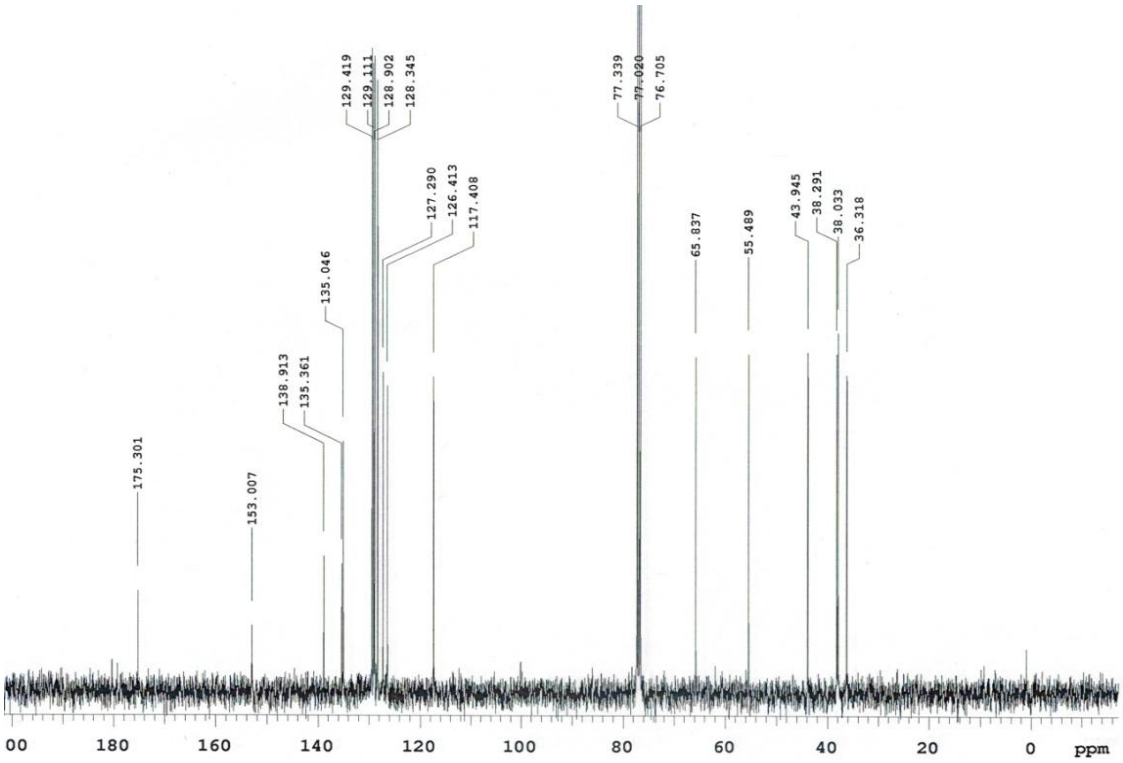

Figure B.86. ^{13}CNMR spectrum of **(*RR*)-21** in $CDCl_3$.

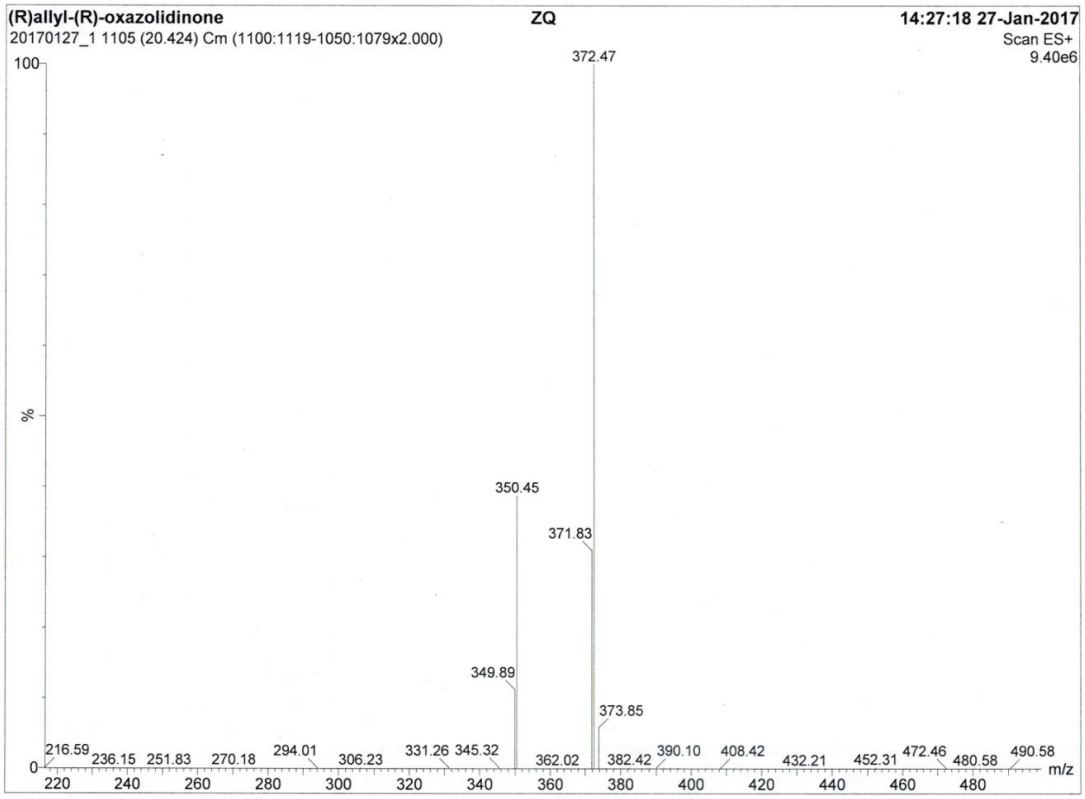

Figure B.87. Low resolution mass spectrum of **(*RR*)-21**.

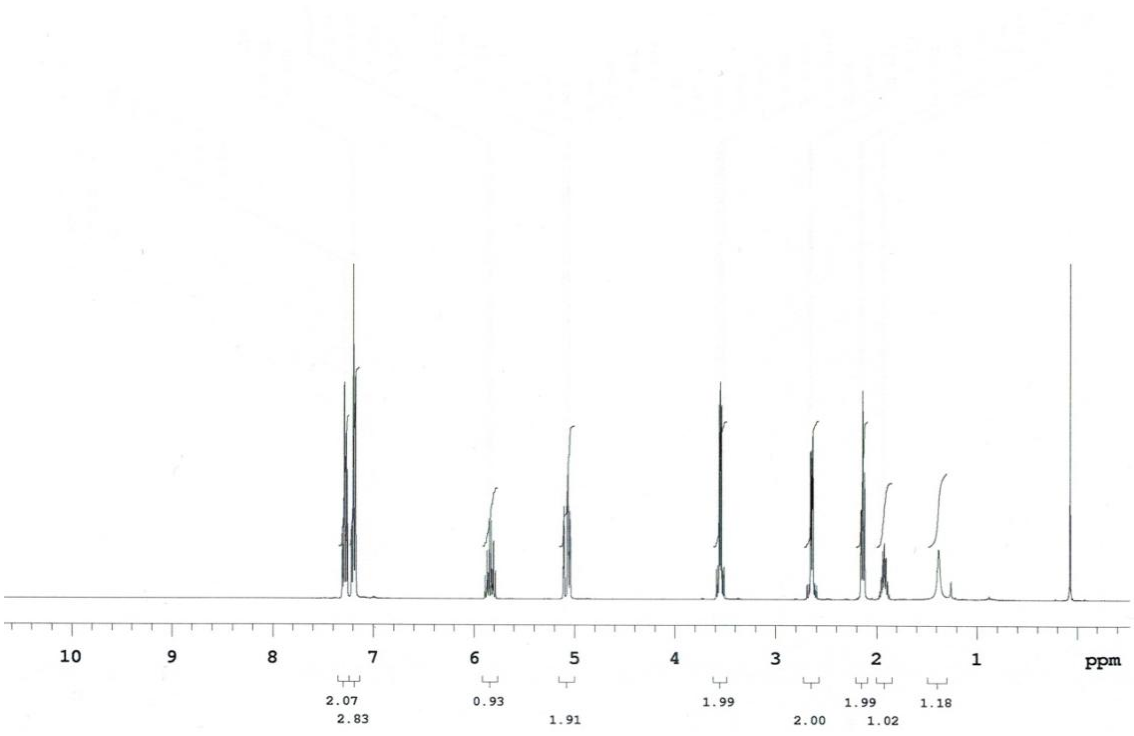

Figure B.88. ^{1}HNMR spectrum of **(*S*)-22** in $CDCl_3$.

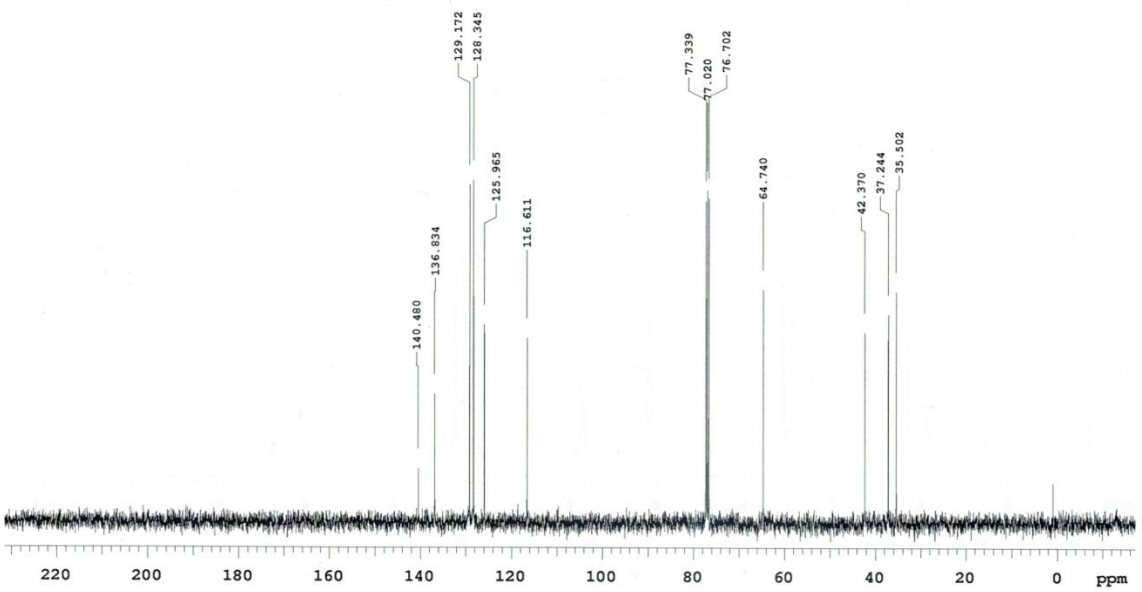

Figure B.89. ^{13}CNMR spectrum of **(*S*)-22** in $CDCl_3$.

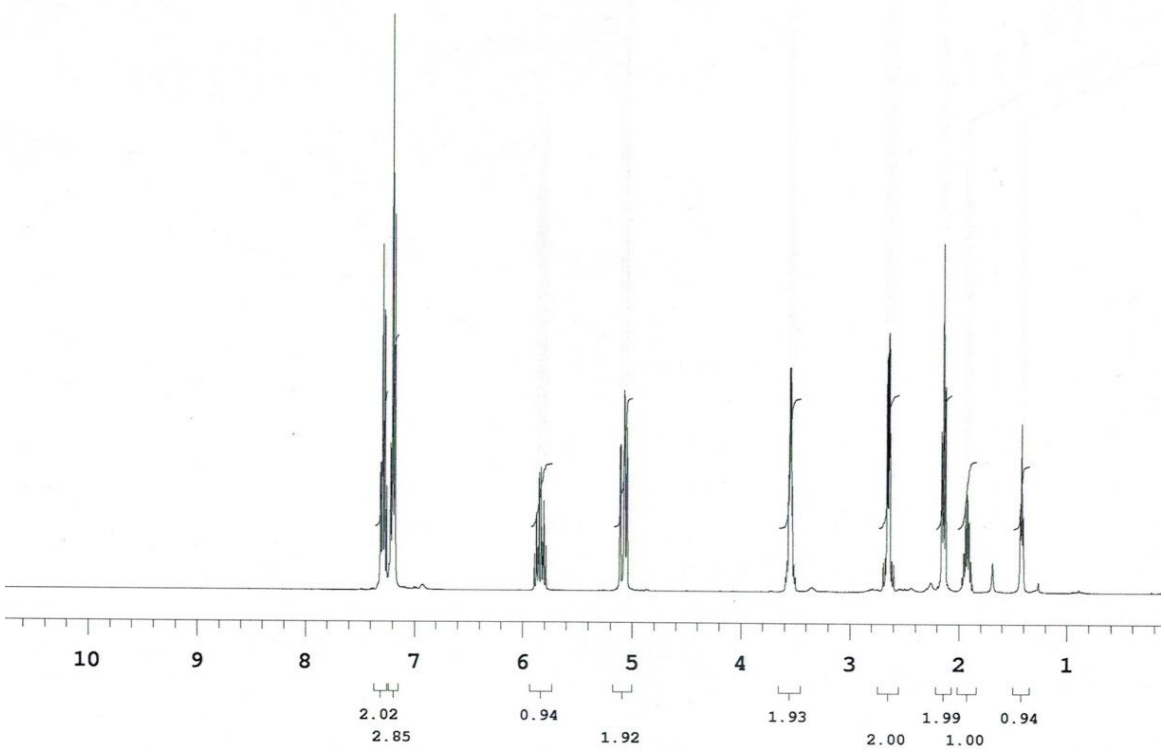

Figure B.90. ^{1}HNMR spectrum of **(*R*)-22** in $CDCl_3$.

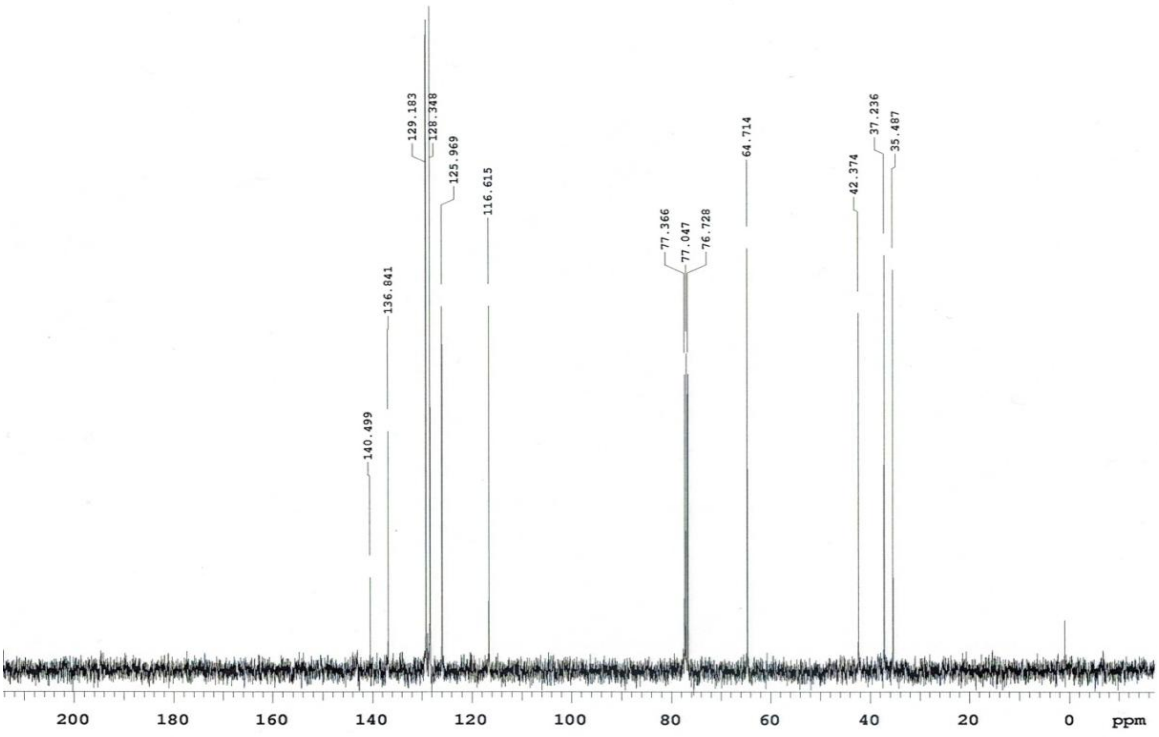

Figure B.91. ^{13}CNMR spectrum of **(*R*)-22** in $CDCl_3$.

B.2. Synthesis scheme for Mosher's esters

Scheme B.1: Synthesis of Mosher's esters **(*S*)-22-(*R*)-MTPA** and **(*R*)-22-(*R*)-MTPA** discussed in Chapter 3

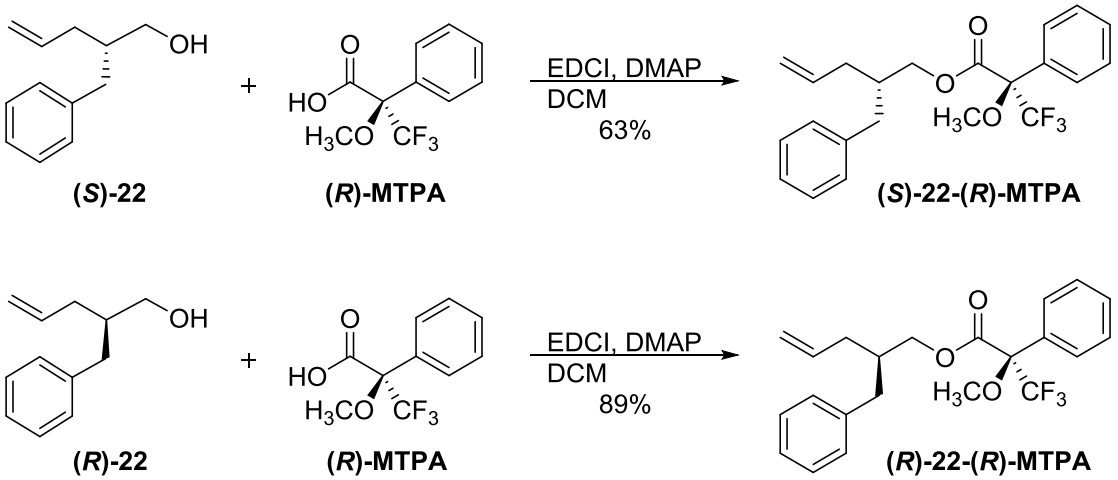

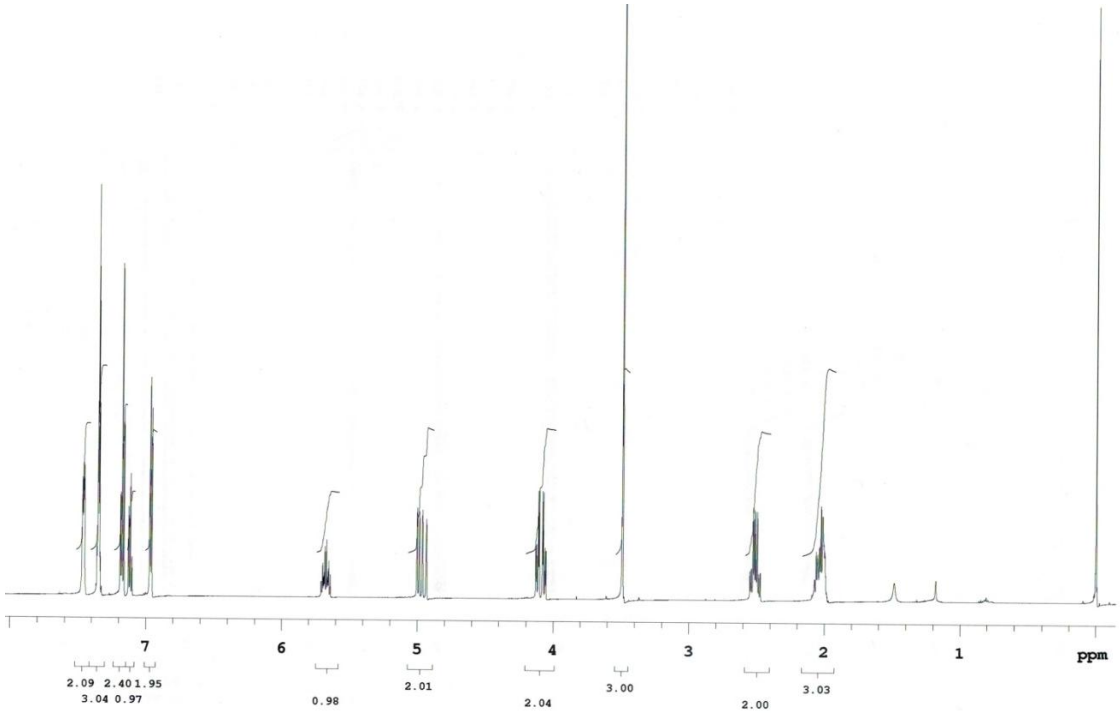

Figure B.92. ^{1}HNMR spectrum of **(*S*)-22-(*R*)-MTPA** in $CDCl_3$.

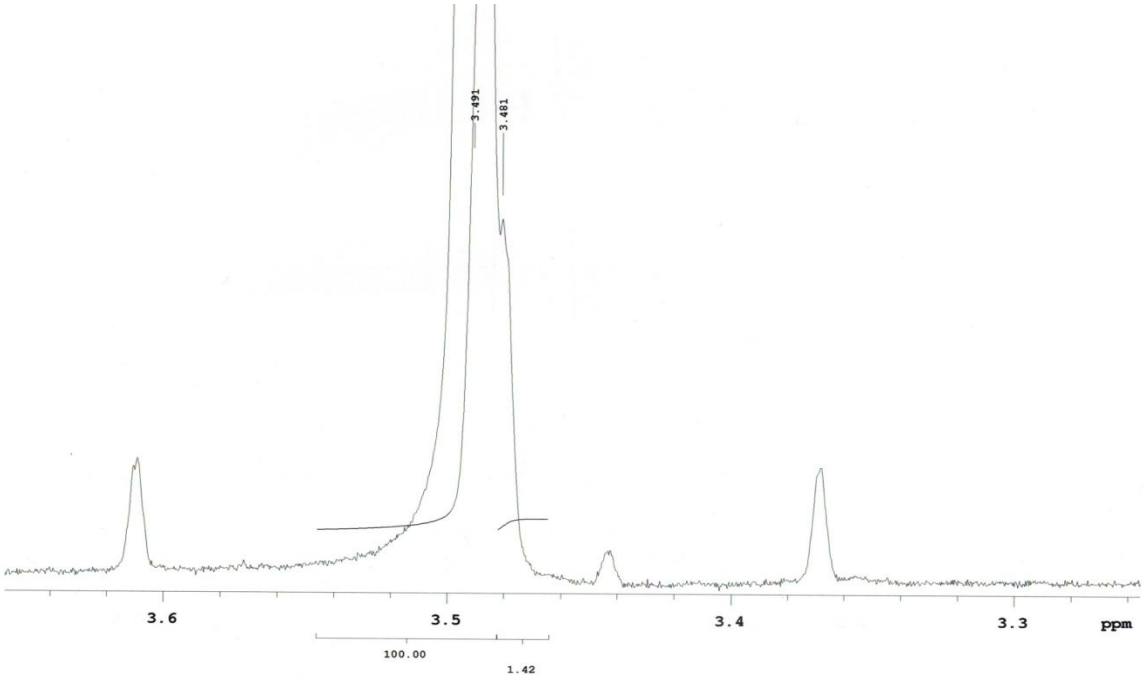

Figure B.93. Enlarged ^{1}HNMR spectrum of **(*S*)-22-(*R*)-MTPA** showing a singlet peak of the major diastereomer at 3.491, and another singlet peak of the minor diastereomer **(*R*)-22-(*R*)-MTPA** at 3.481. Integration of these two peaks (100.00 and 1.42) was used to calculate the diastereomeric ratio (dr) discussed in the text (99:1 dr).

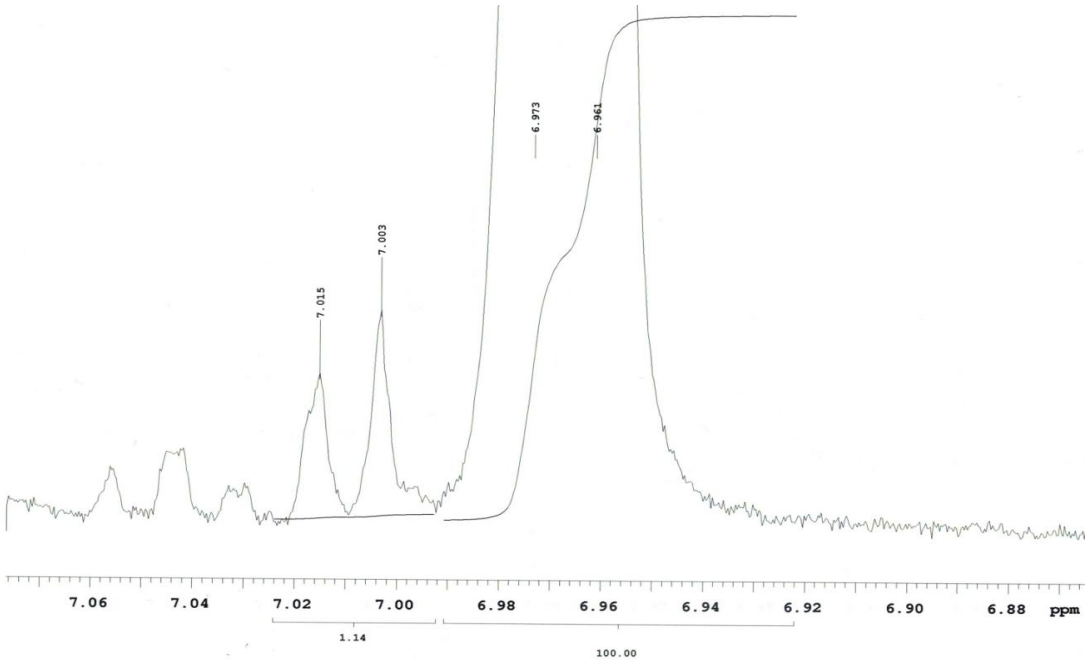

Figure B.94. Enlarged ^{1}HNMR spectrum of **(*S*)-22-(*R*)-MTPA** showing a doublet peak of the major diastereomer at 6.961 and 6.973, and another doublet peak of the minor diastereomer **(*R*)-22-(*R*)-MTPA** at 7.003 and 7.015. Integration of these two peaks (100.00 and 1.14) was used to calculate the diastereomeric ratio (dr) discussed in the text (99:1 dr).

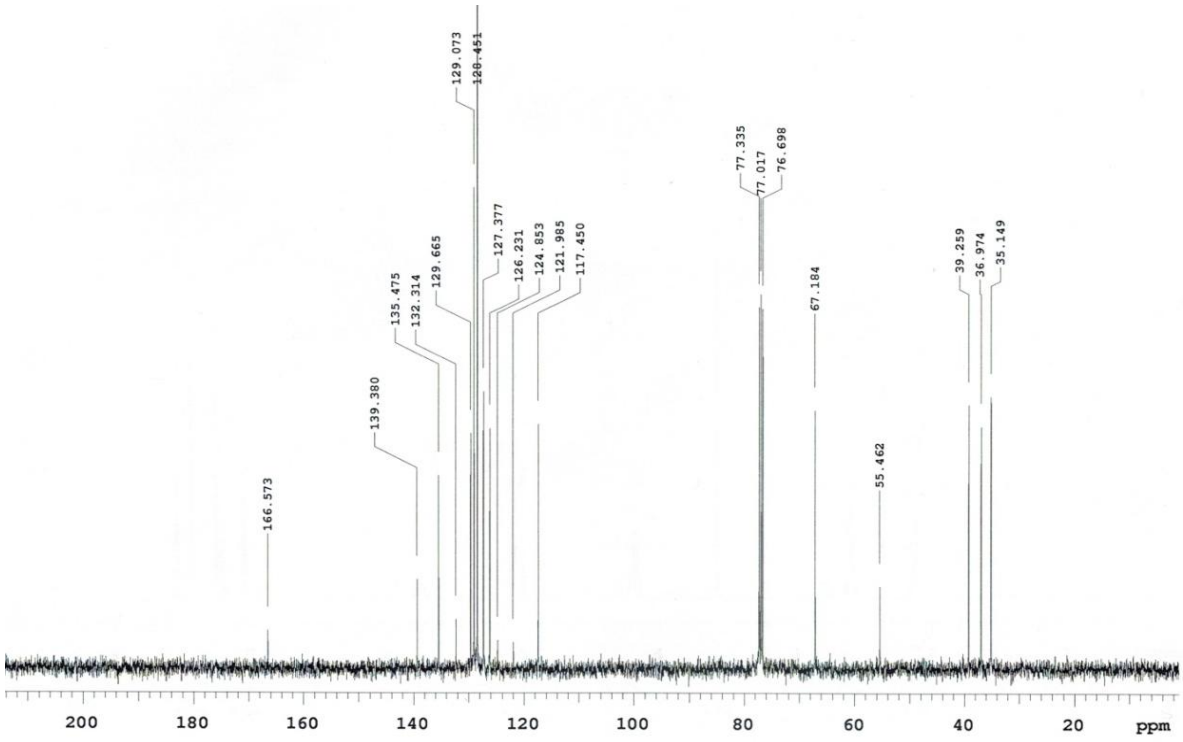

Figure B.95. ^{13}CNMR spectrum of **(*S*)-22-(*R*)-MTPA** in $CDCl_3$.

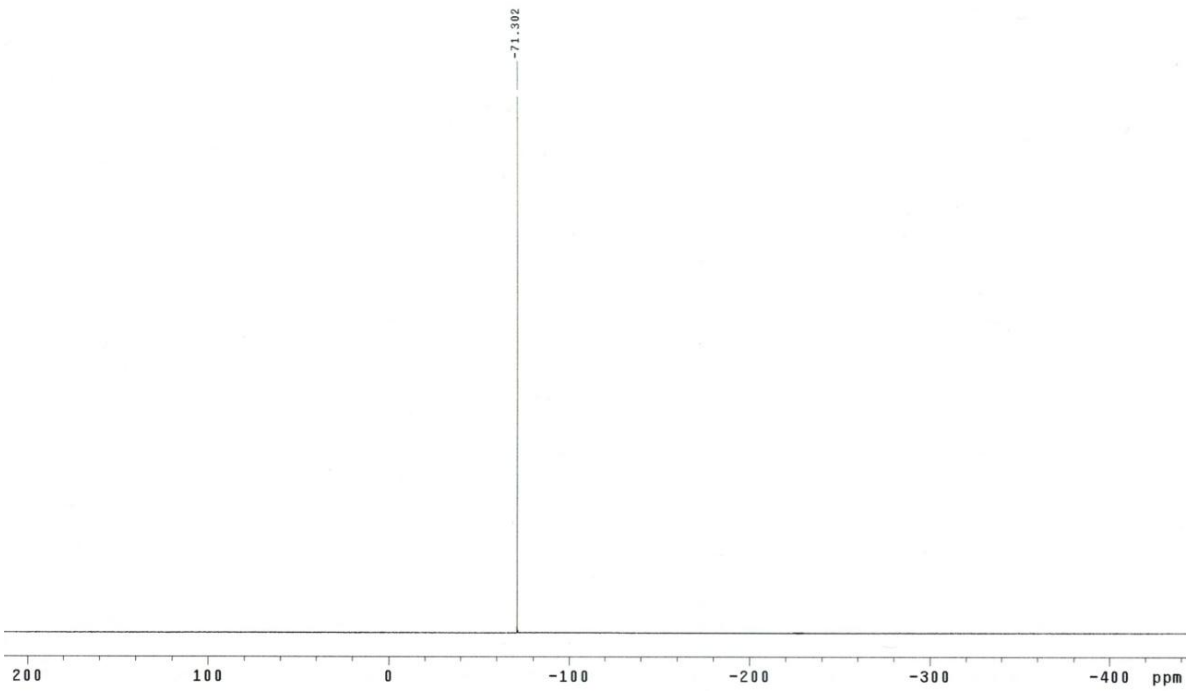

Figure B.96. ^{19}FNMR spectrum of **(*S*)-22-(*R*)-MTPA** in $CDCl_3$.

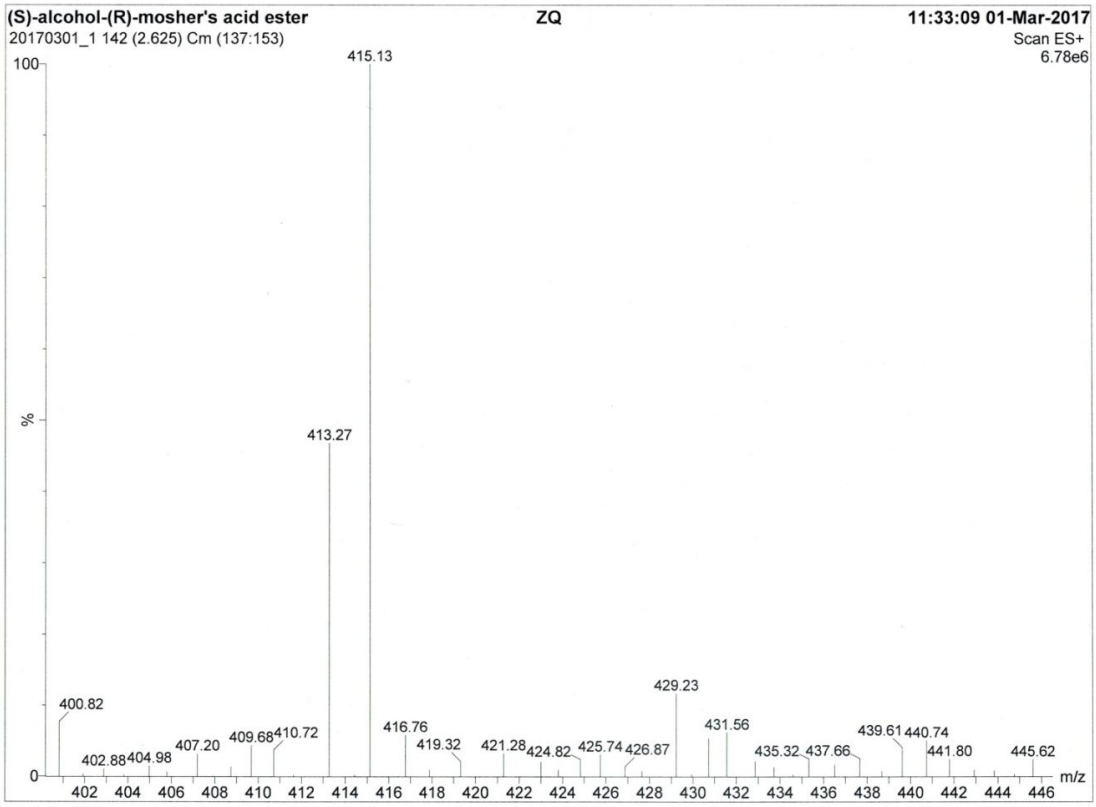

Figure B.97. Low resolution mass spectrum of **(*S*)-22-(R)-MTPA**.

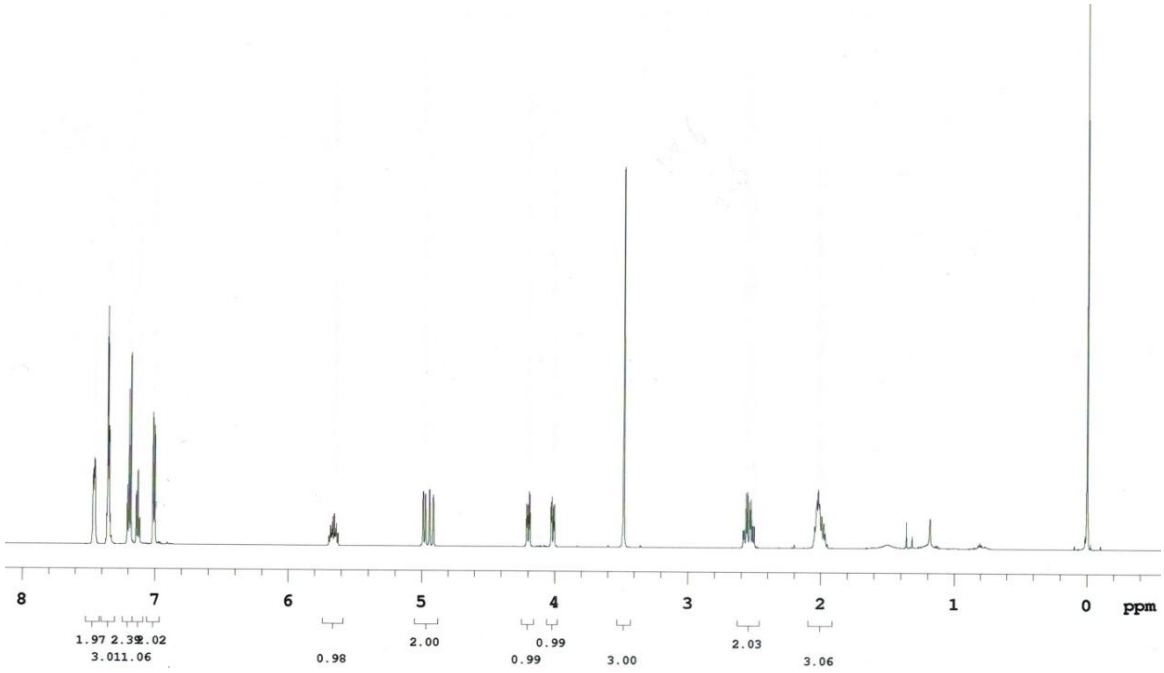

Figure B.98. ^{1}HNMR spectrum of **(*R*)-22-(R)-MTPA** in $CDCl_3$.

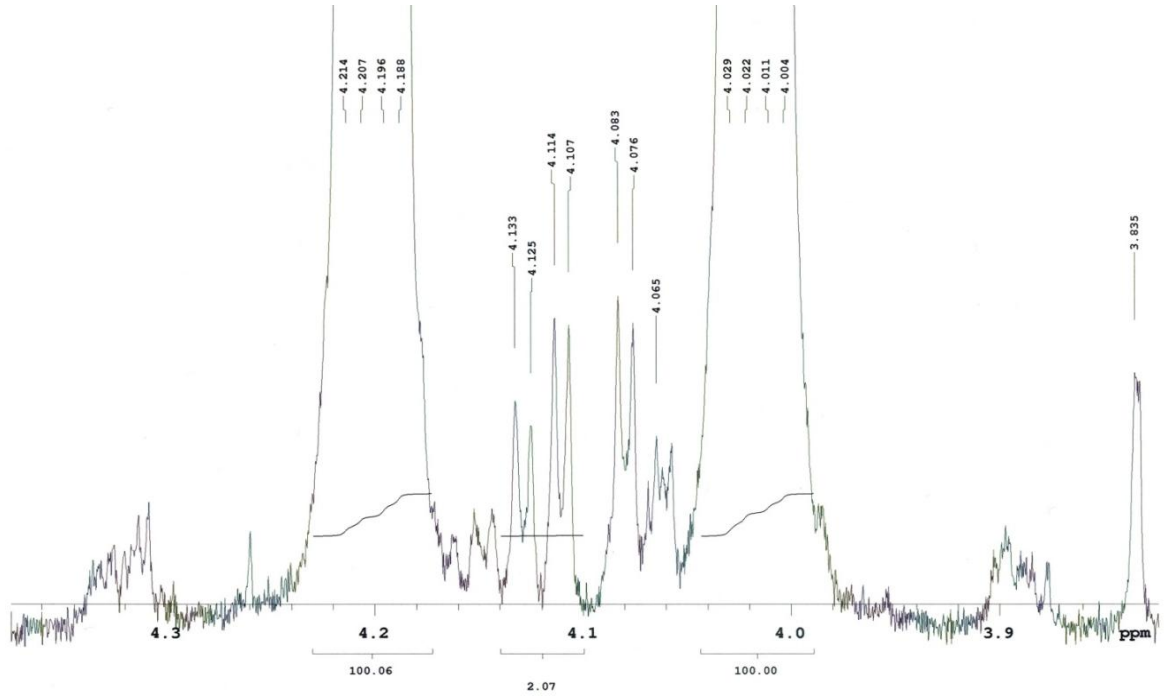

Figure B.99. Enlarged ^{1}HNMR spectrum of **(*R*)-22-(*R*)-MTPA** showing a doublet doublet peaks of the major diastereomer at 4.004-4.029 and another doublet doublet peak of the minor diastereomer **(*S*)-22-(*R*)-MTPA** at 4.107-4.133. Integration of these two peaks (100.06 and 2.07) was used to calculate the diastereomeric ratio (dr) discussed in the text (98:2 dr).

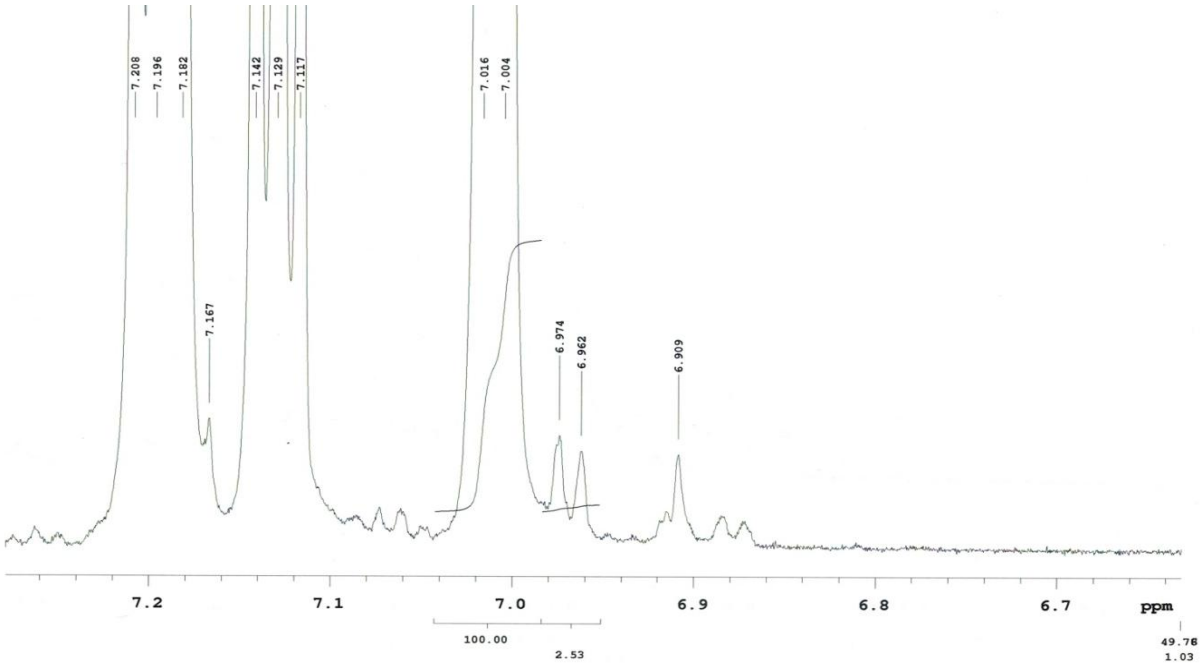

Figure B.100. Enlarged ^{1}HNMR spectrum of **(*R*)-22-(*R*)-MTPA** showing a doublet peak of the major diastereomer at 7.004 and 7.016, and another doublet peak of the minor diastereomer **(*S*)-22-(*R*)-MTPA** at 6.962 and 6.974. Integration of these two peaks (100.00 and 2.53) was used to calculate the diastereomeric ratio (dr) discussed in the text (98:2 dr).

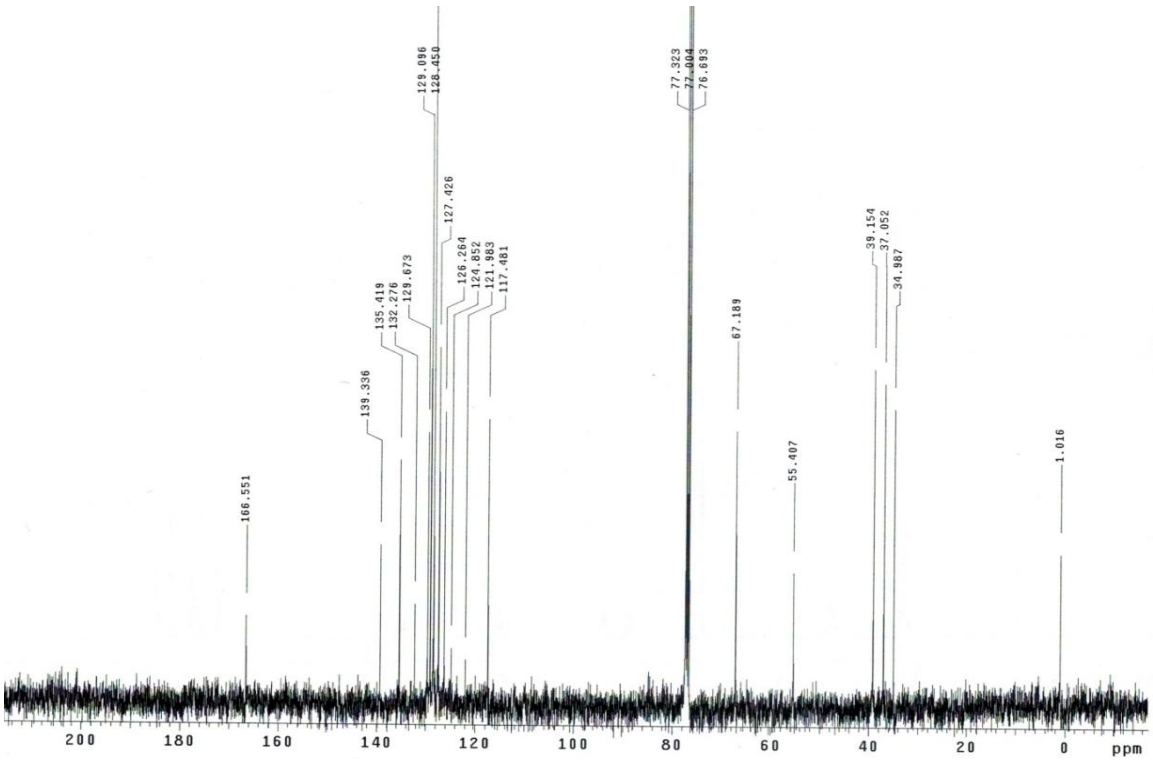

Figure B.101. ^{13}CNMR spectrum of **(*R*)-22-(R)-MTPA** in $CDCl_3$.

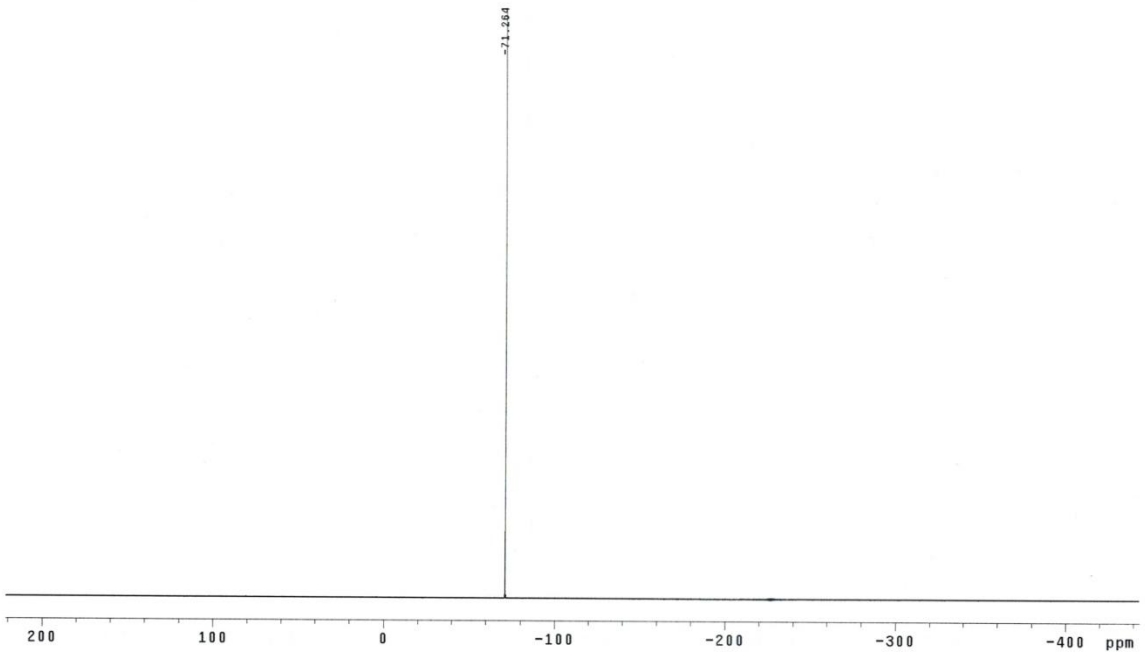

Figure B.102. ^{19}FNMR spectrum of **(*R*)-22-(*R*)-MTPA** in $CDCl_3$.

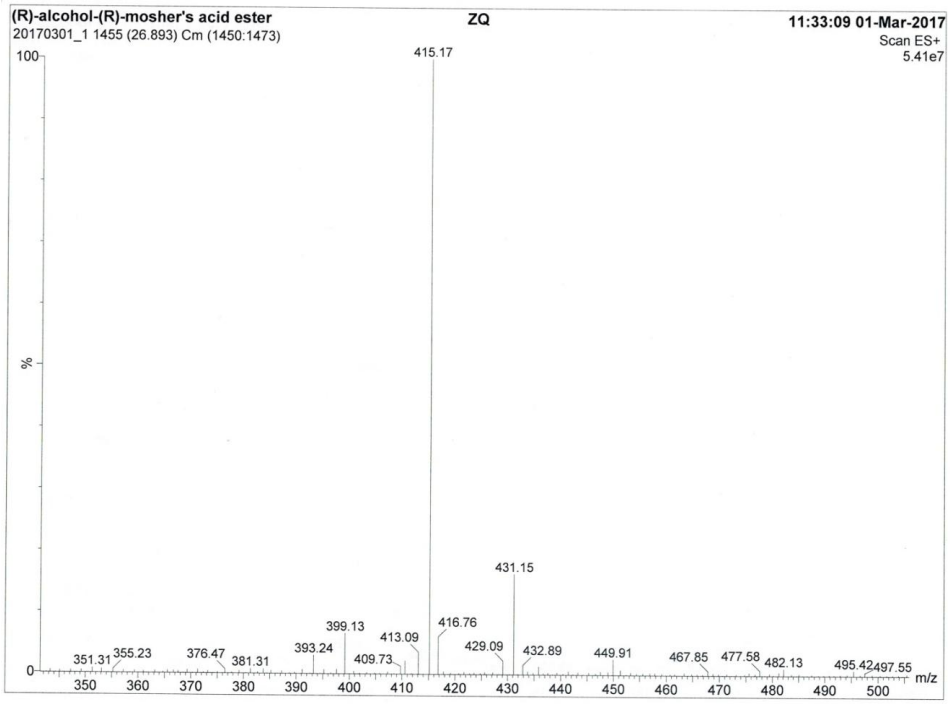

Figure B.103. Low resolution mass spectrum of **(*R*)-22-(*R*)-MTPA**.

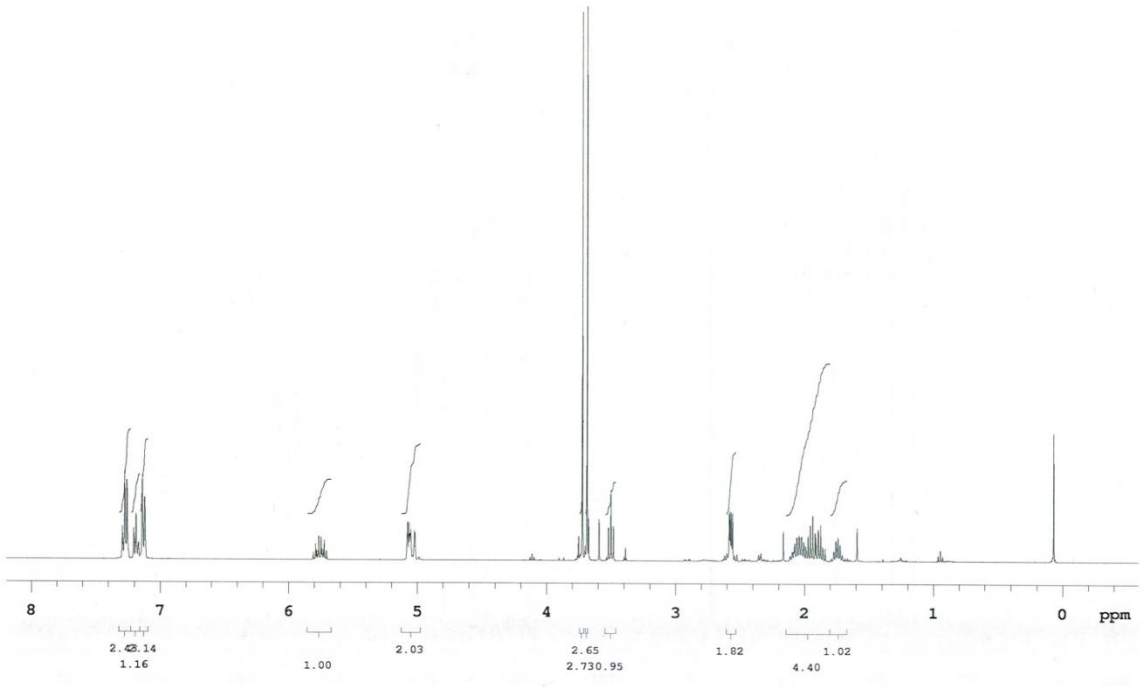

Figure B.104. ^{1}HNMR spectrum of **(*R*)-24** in $CDCl_3$.

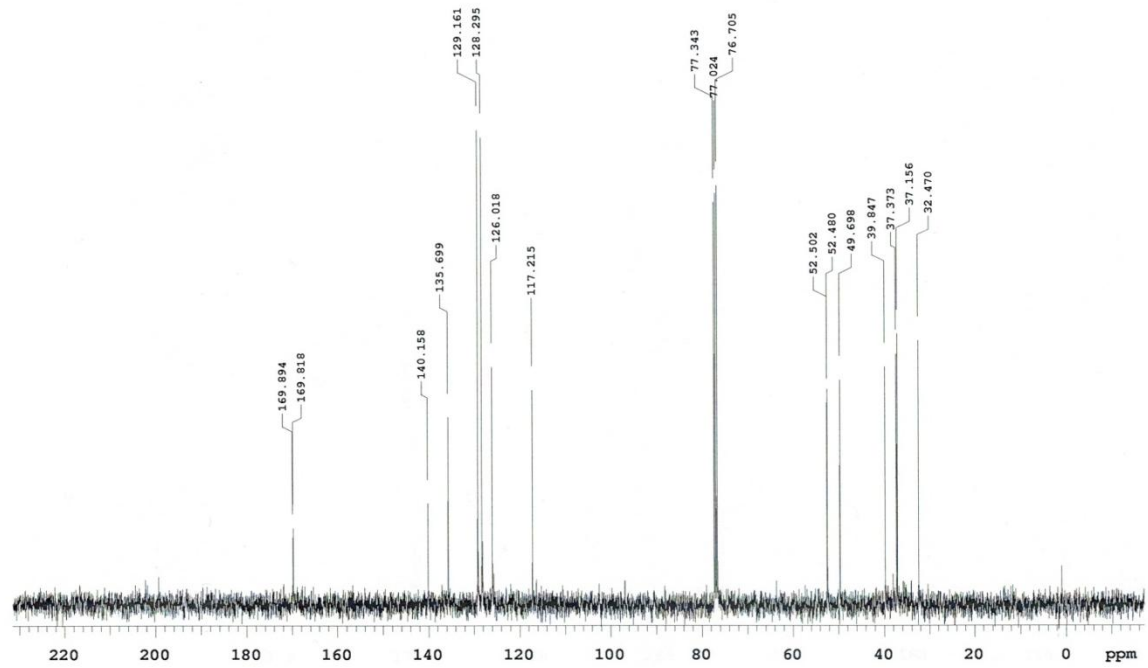

Figure B.105. ^{13}CNMR spectrum of **(*R*)-24** in $CDCl_3$.

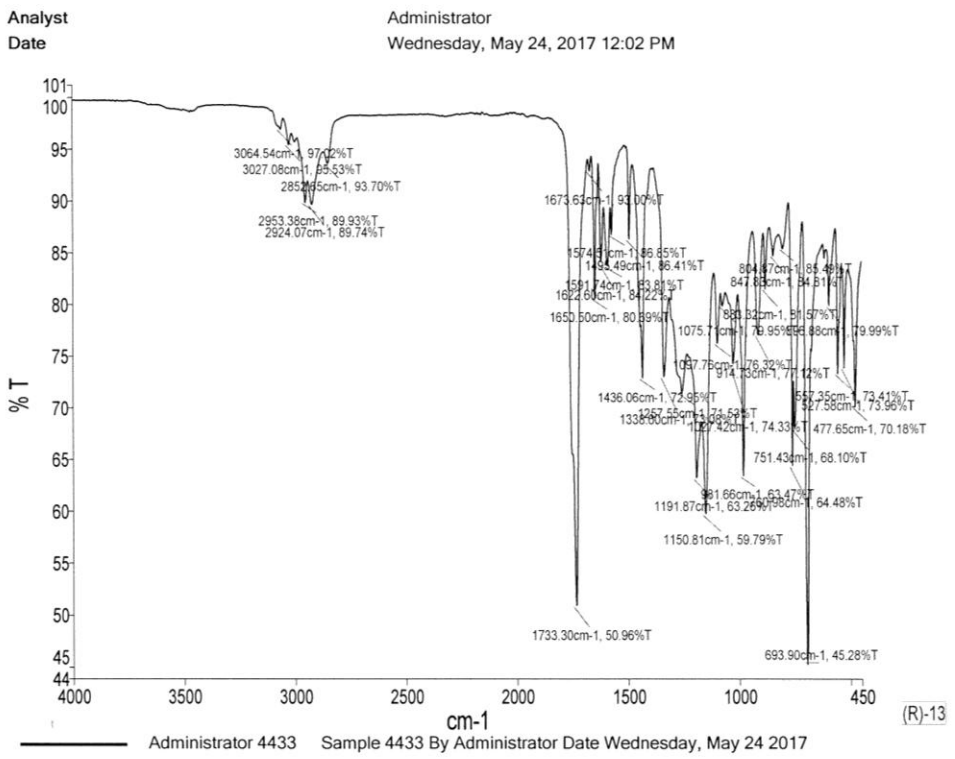

Figure B.106. IR spectrum of **(*R*)-24**.

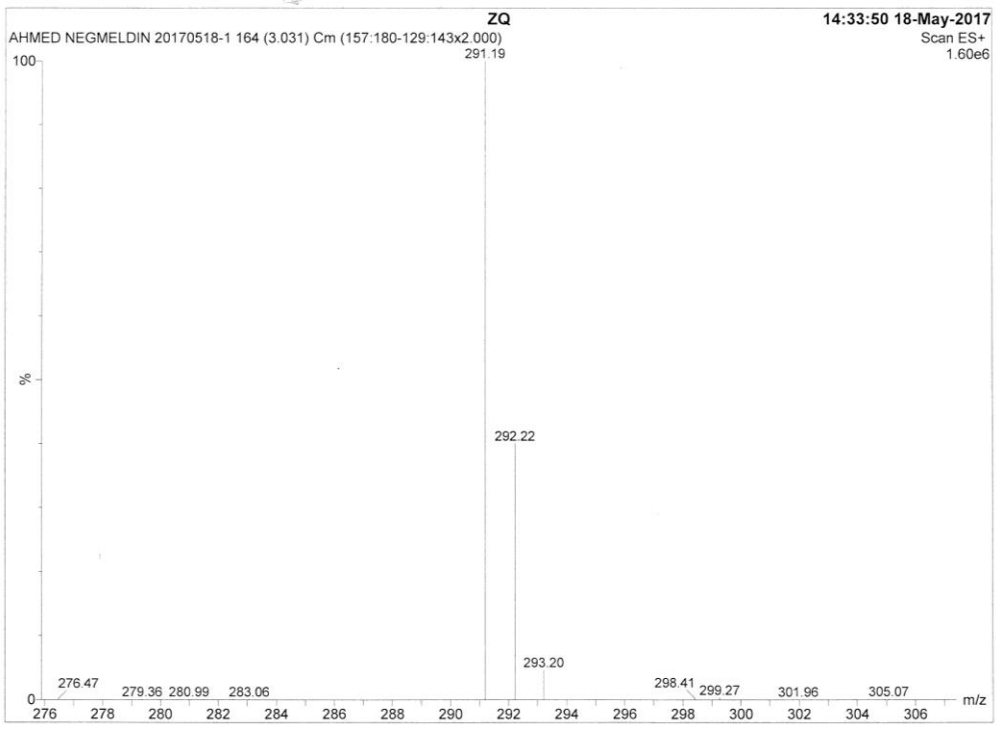

Figure B.107. Low resolution mass spectrum of **(*R*)-24**.

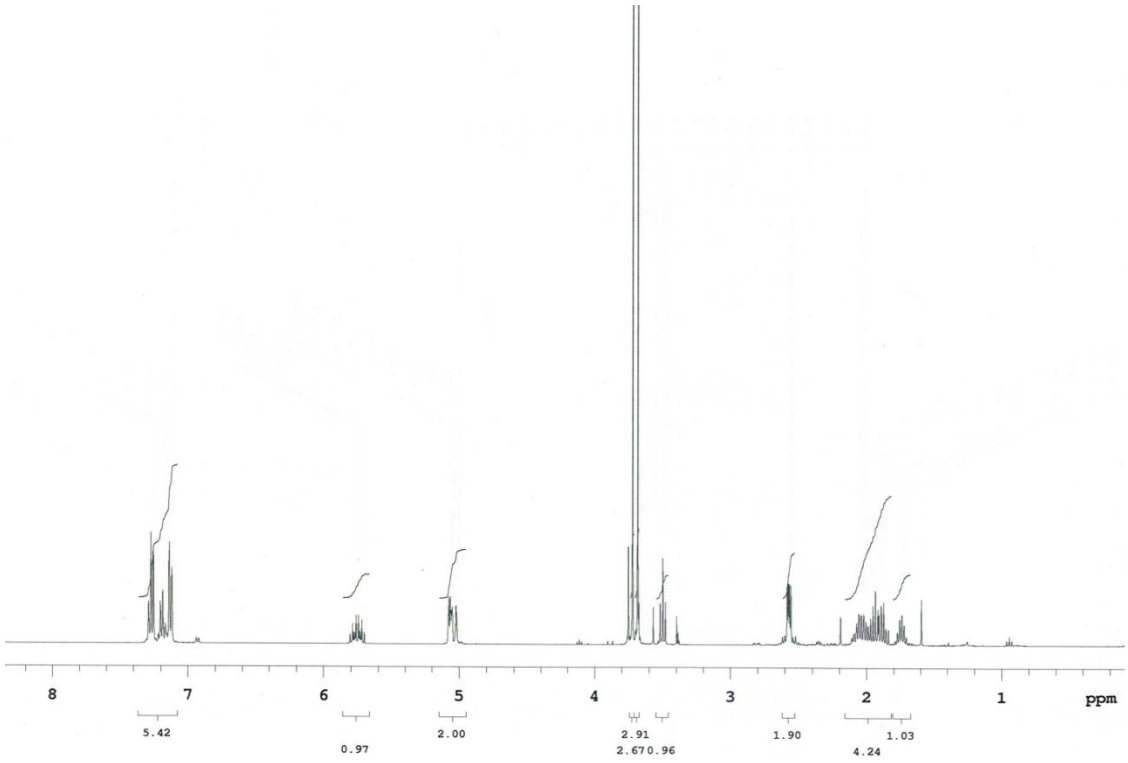

Figure B.108. ^{1}HNMR spectrum of **(*S*)-24** in $CDCl_3$.

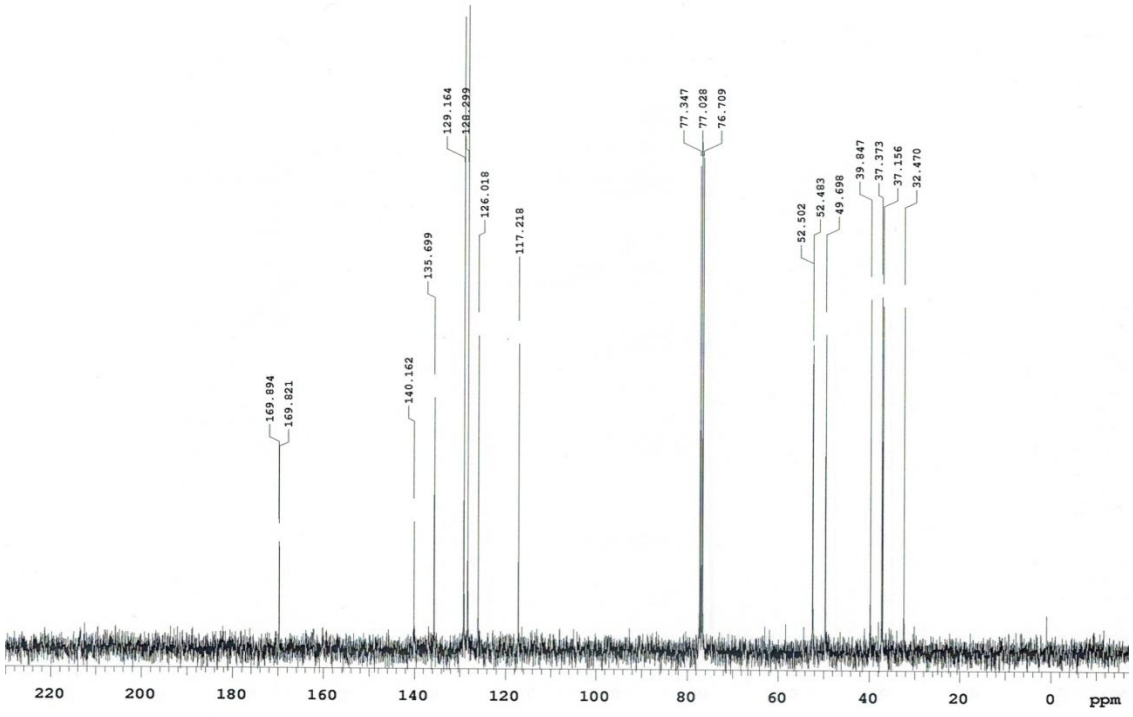

Figure B.109. ^{13}CNMR spectrum of **(*S*)-24** in $CDCl_3$.

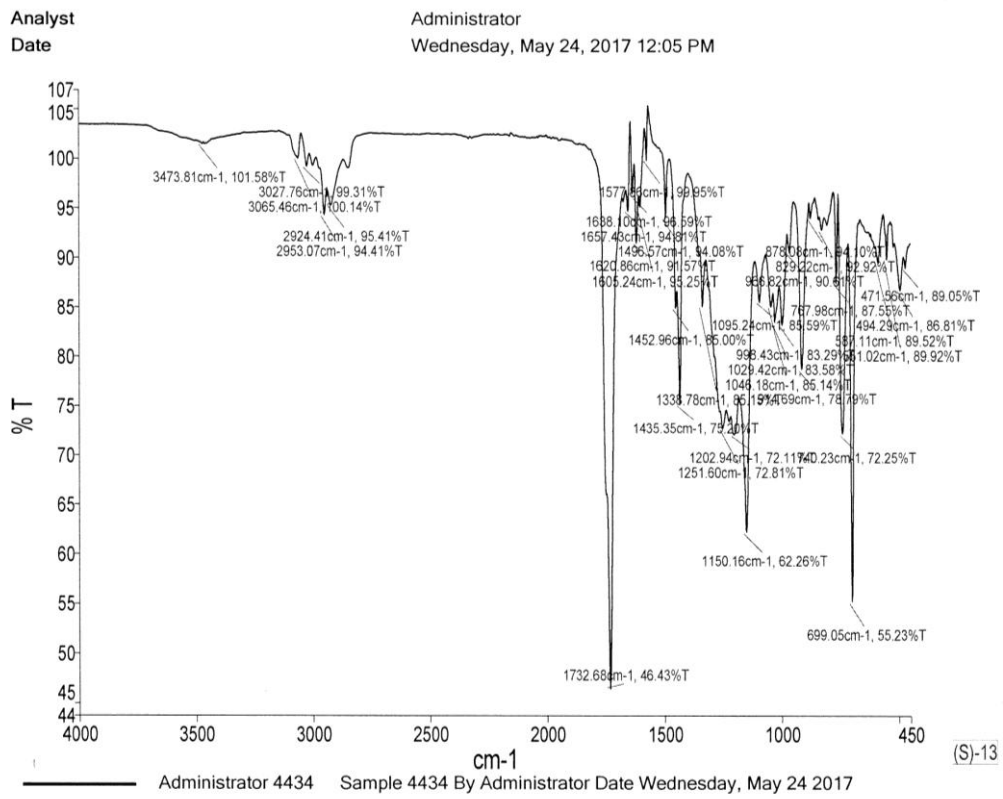

Figure B.110. IR spectrum of **(*S*)-24**.

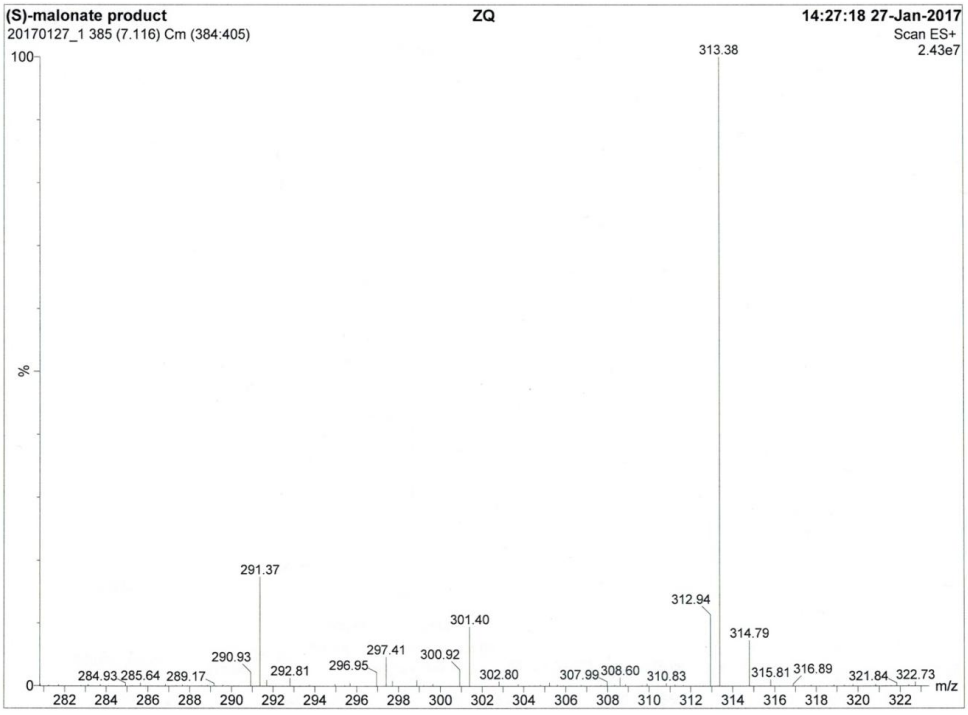

Figure B.111. Low resolution mass spectrum of **(*S*)-24**.

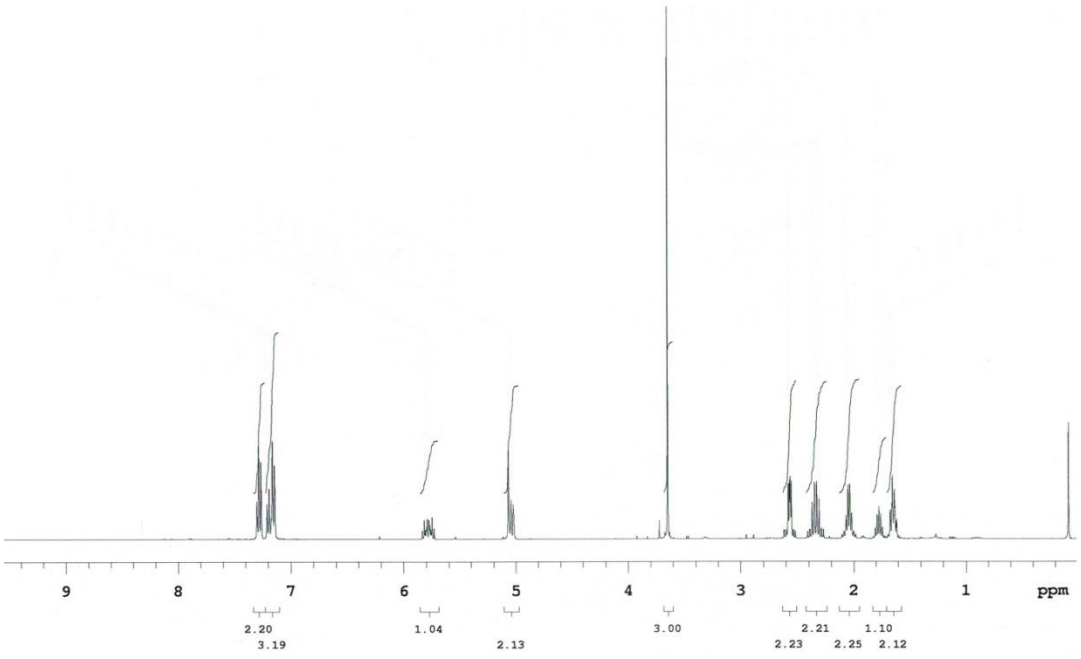

Figure B.112. ^{1}HNMR spectrum of **(*S*)-25** in $CDCl_3$.

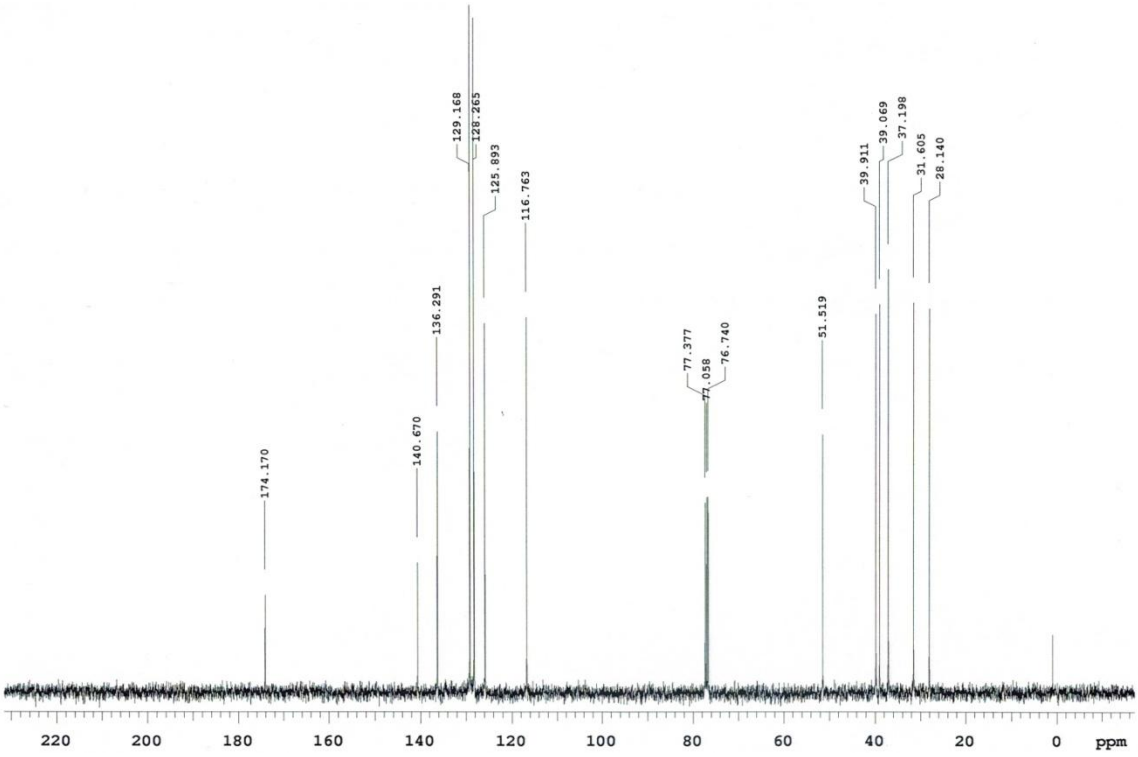

Figure B.113. ^{13}CNMR spectrum of **(*S*)-25** in $CDCl_3$.

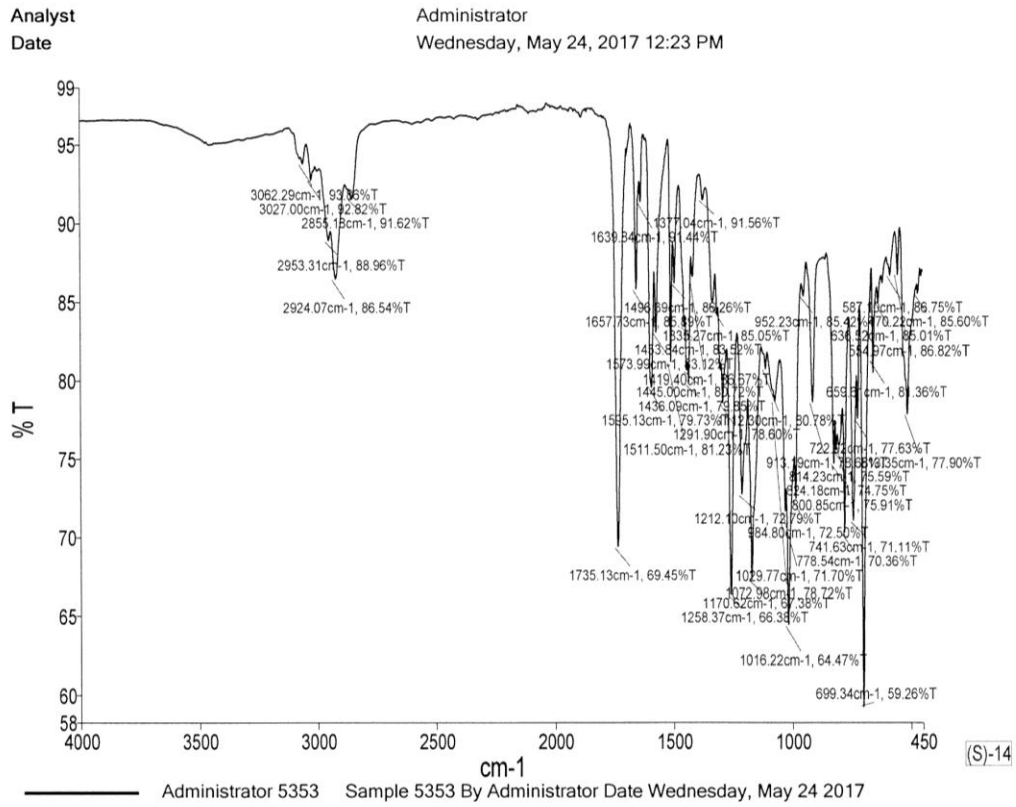

Figure B.114. IR spectrum of **(*S*)-25**.

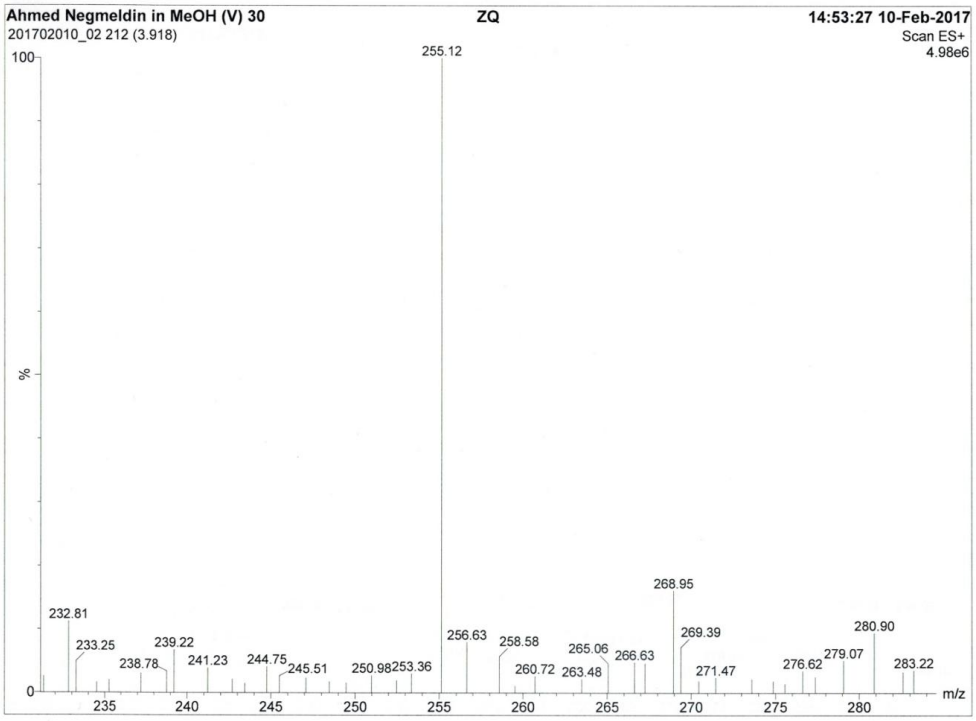

Figure B.115. Low resolution mass spectrum of **(*S*)-25**.

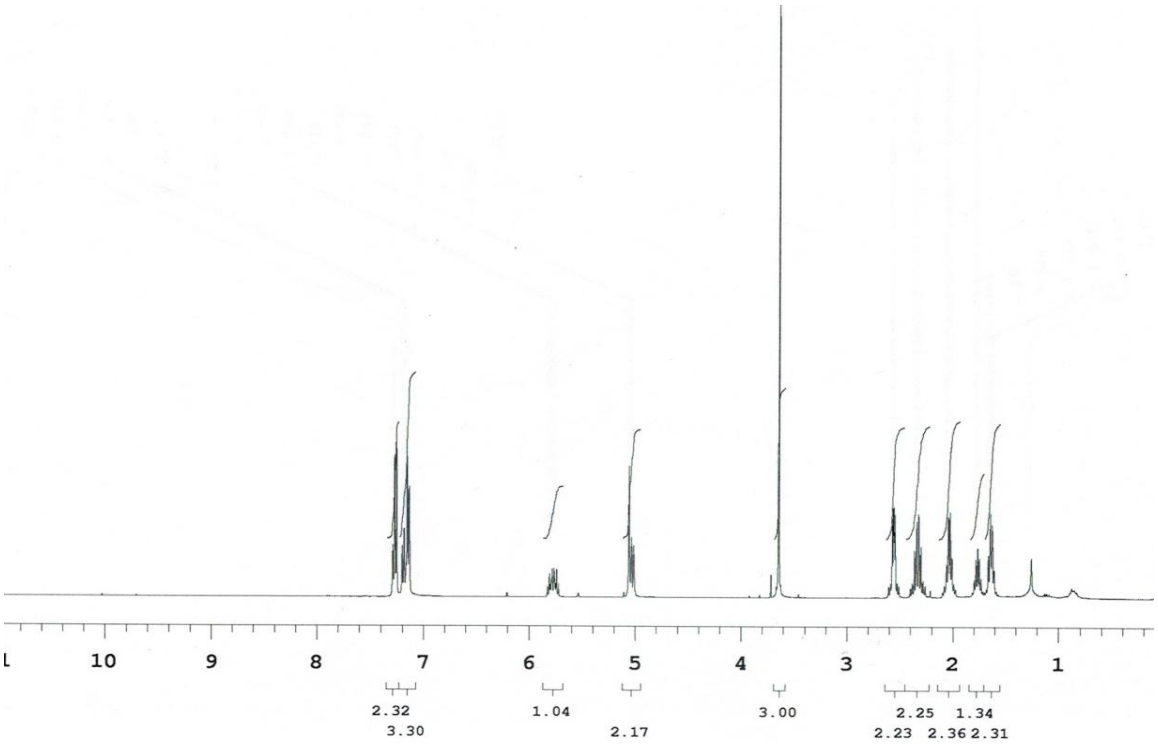

Figure B.116. ^{1}HNMR spectrum of **(*R*)-25** in $CDCl_3$.

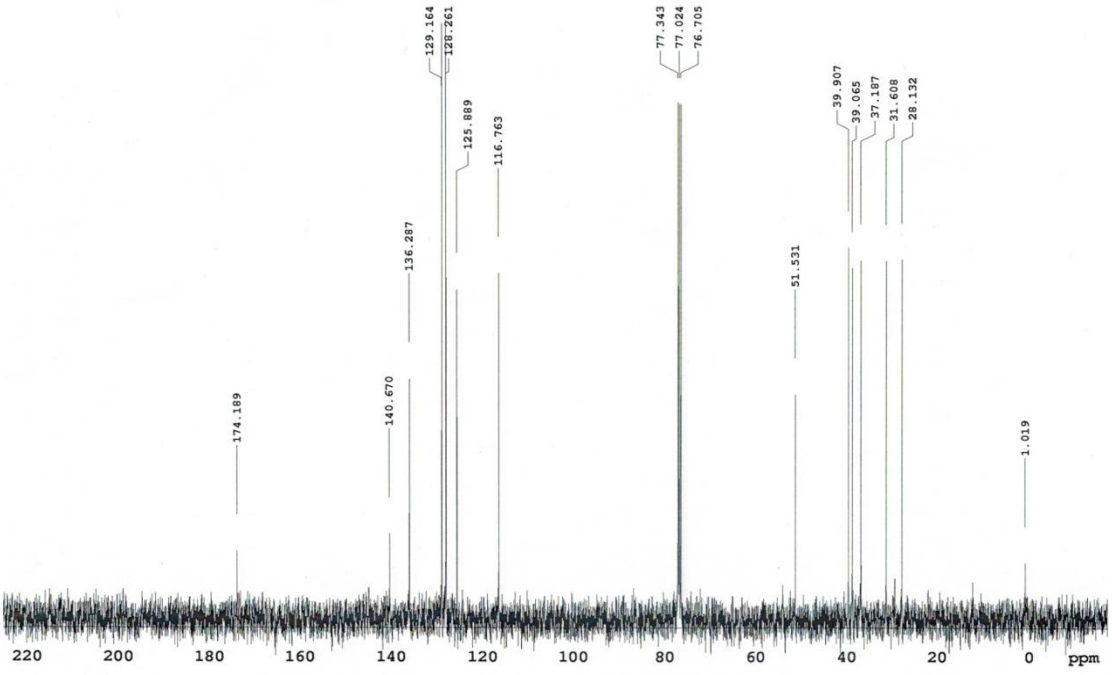

Figure B.117. ^{13}CNMR spectrum of **(*R*)-25** in $CDCl_3$.

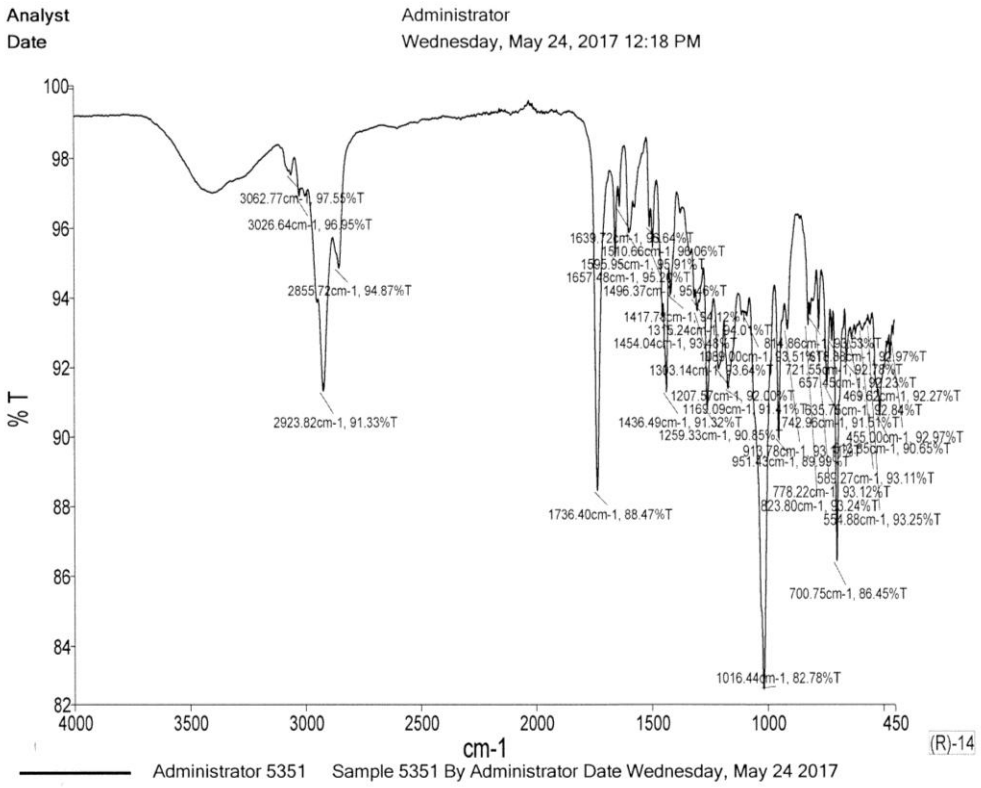

Figure B.118. IR spectrum of **(*R*)-25**.

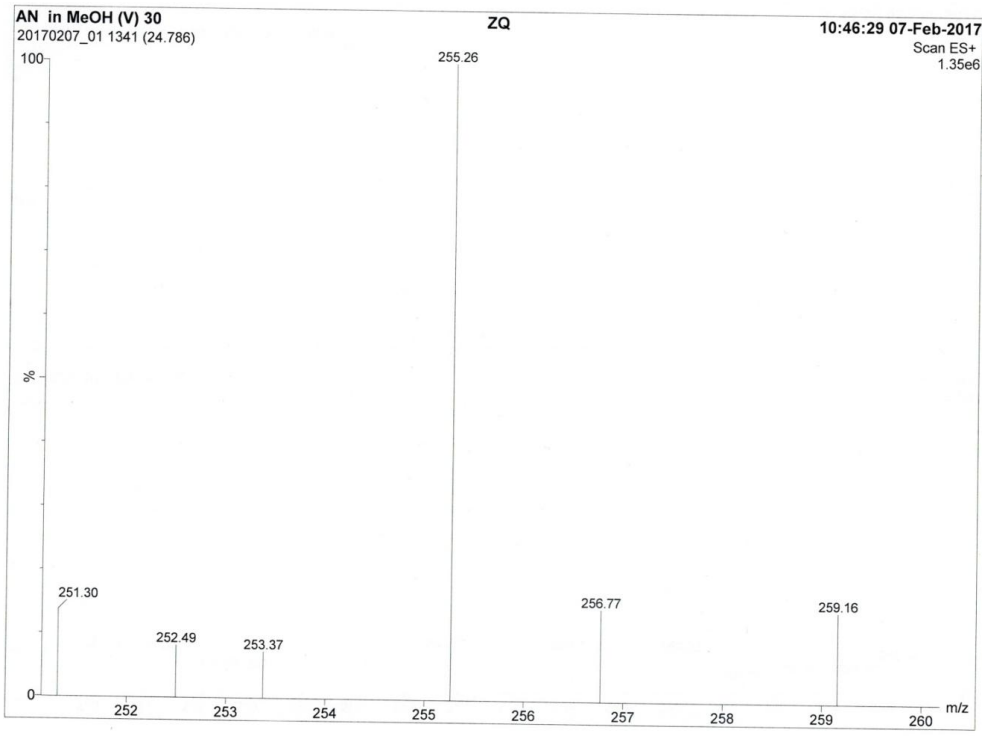

Figure B.119. Low resolution mass spectrum of **(*R*)-25**.

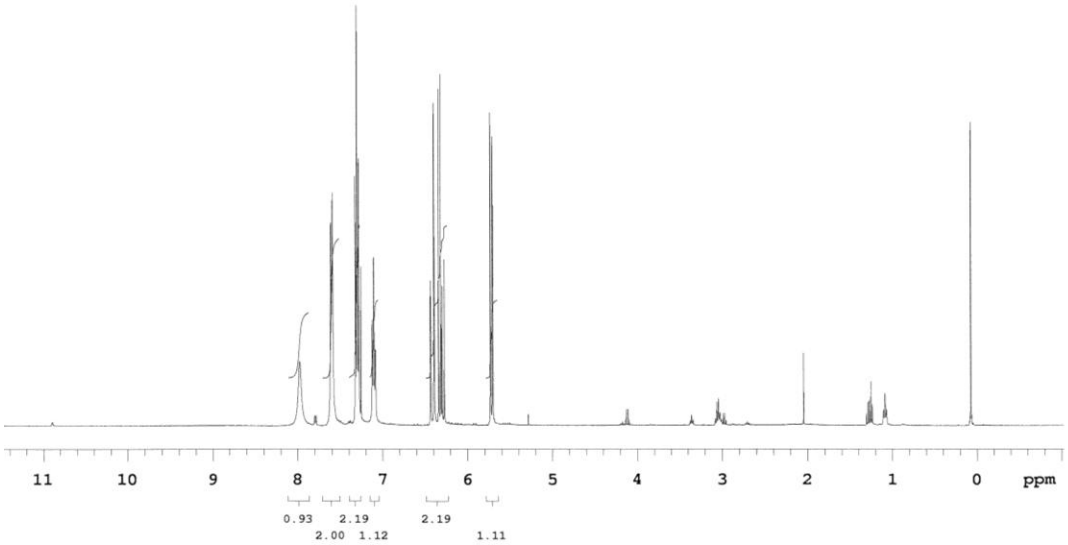

Figure B.120. ^{1}HNMR spectrum of **26** in $CDCl_3$.

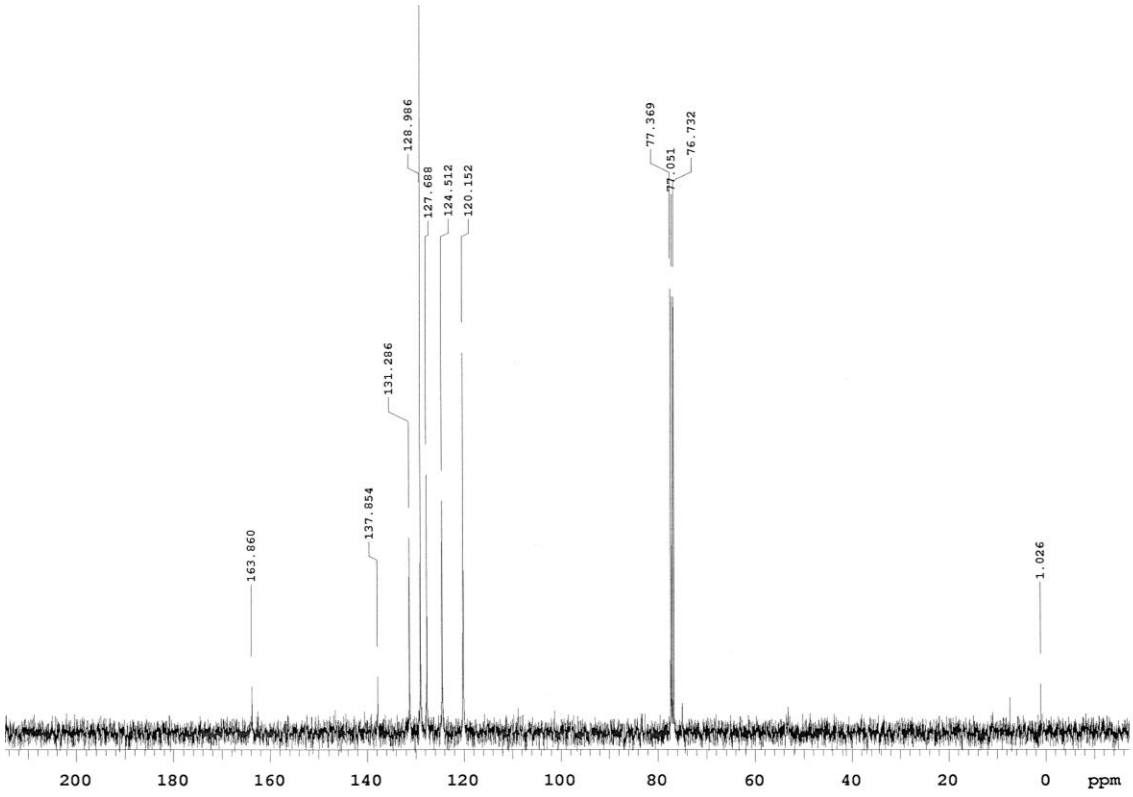

Figure B.121. ^{13}CNMR spectrum of **26** in $CDCl_3$.

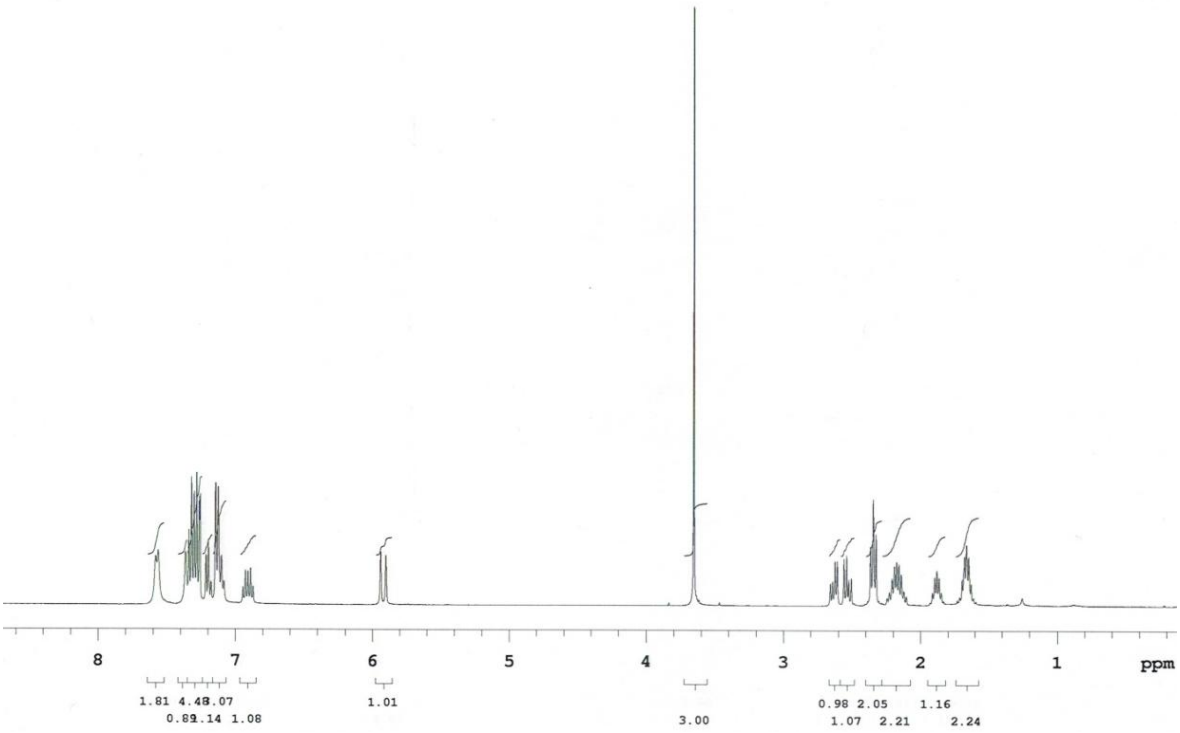

Figure B.122. ^{1}HNMR spectrum of **(*S*)-27** in $CDCl_3$.

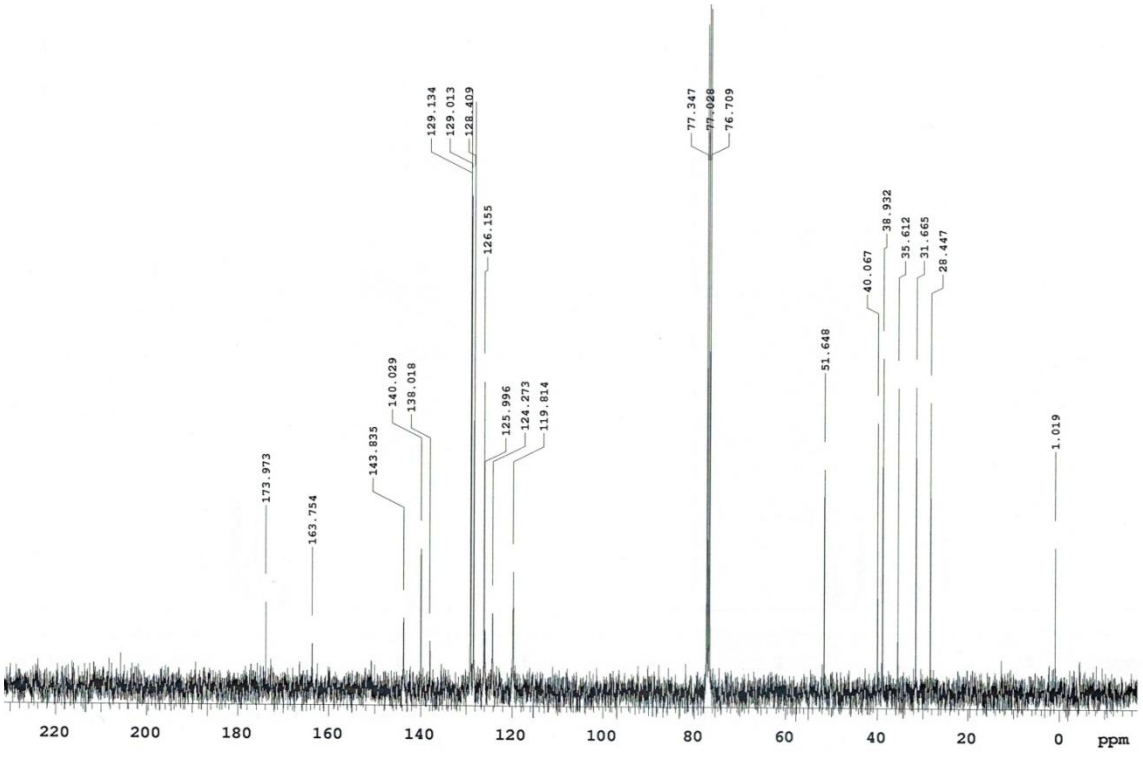

Figure B.123. ^{13}CNMR spectrum of **(*S*)-27** in $CDCl_3$.

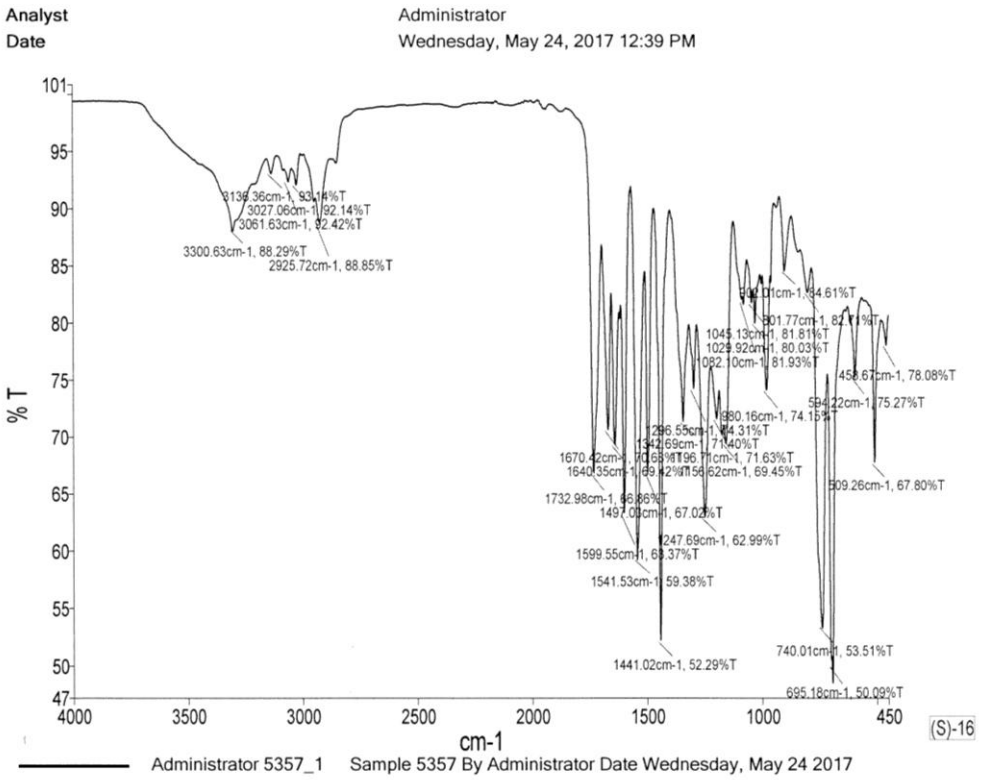

Figure B.124. IR spectrum of **(*S*)-27**.

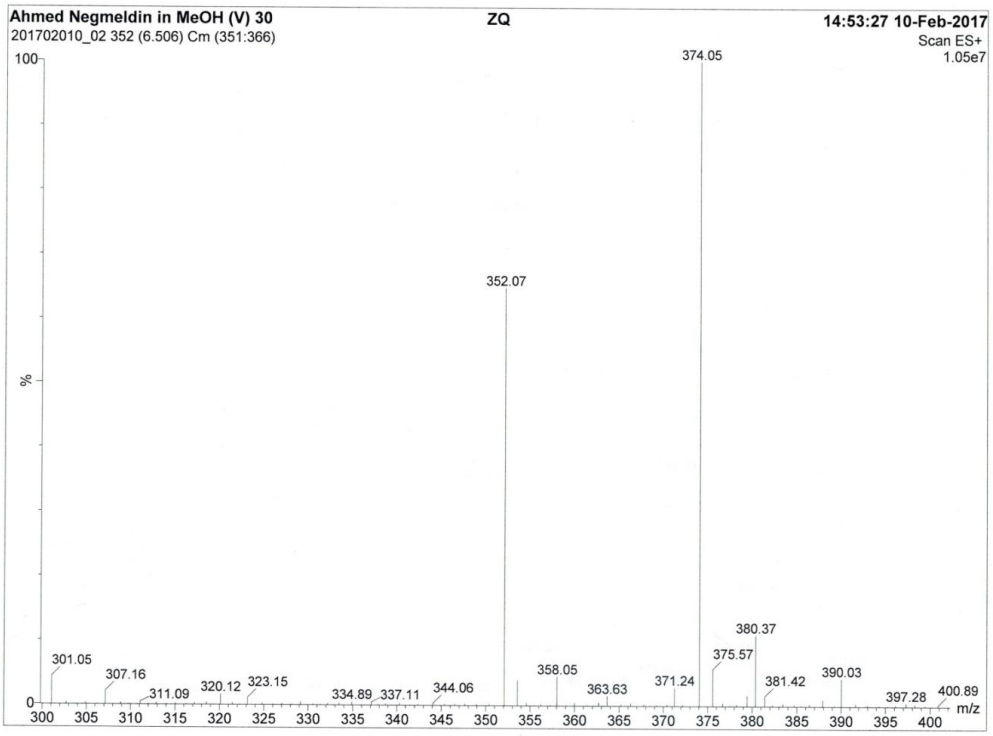

Figure B.125. Low resolution mass spectrum of **(*S*)-27**.

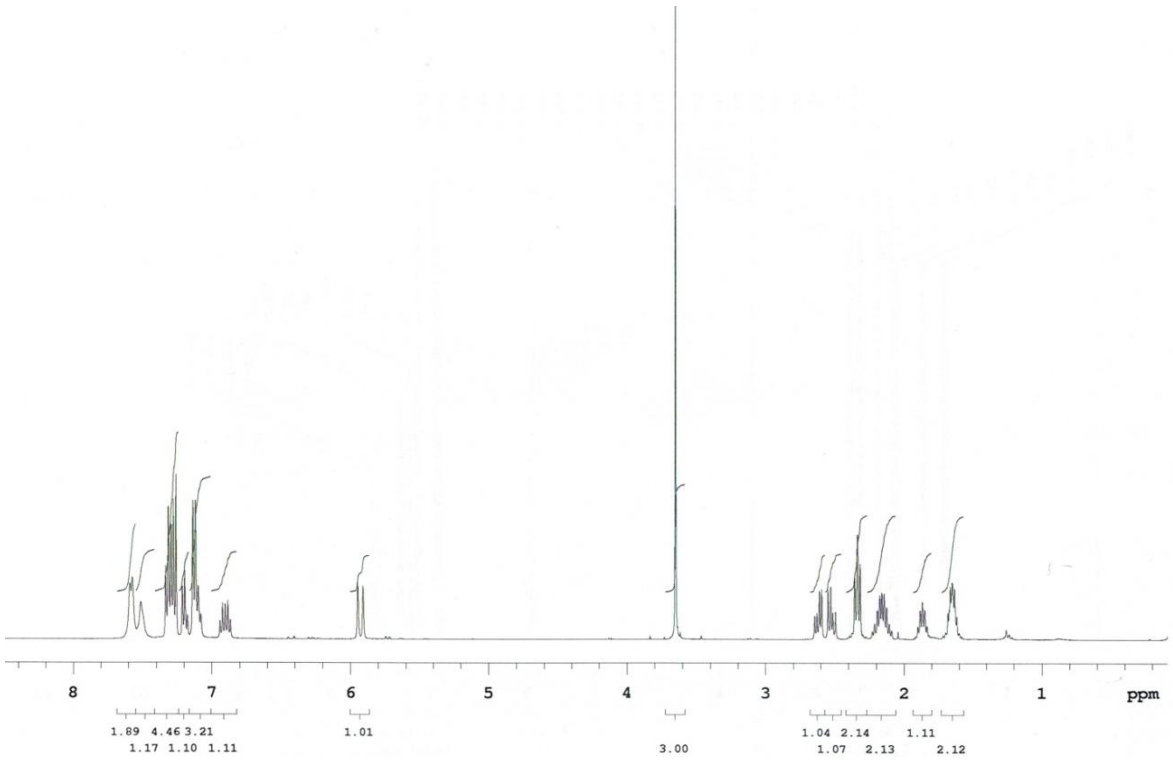

Figure B.126. ^{1}HNMR spectrum of **(*R*)-27** in $CDCl_3$.

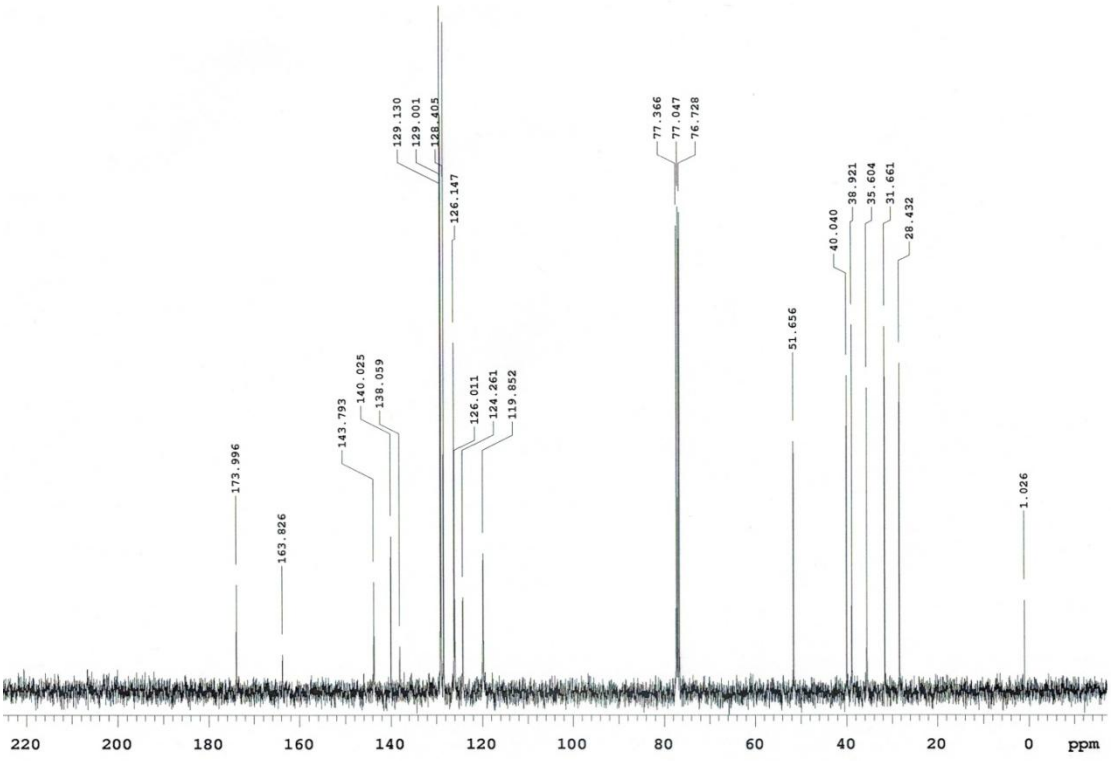

Figure B.127. ^{13}CNMR spectrum of **(*R*)-27** in $CDCl_3$.

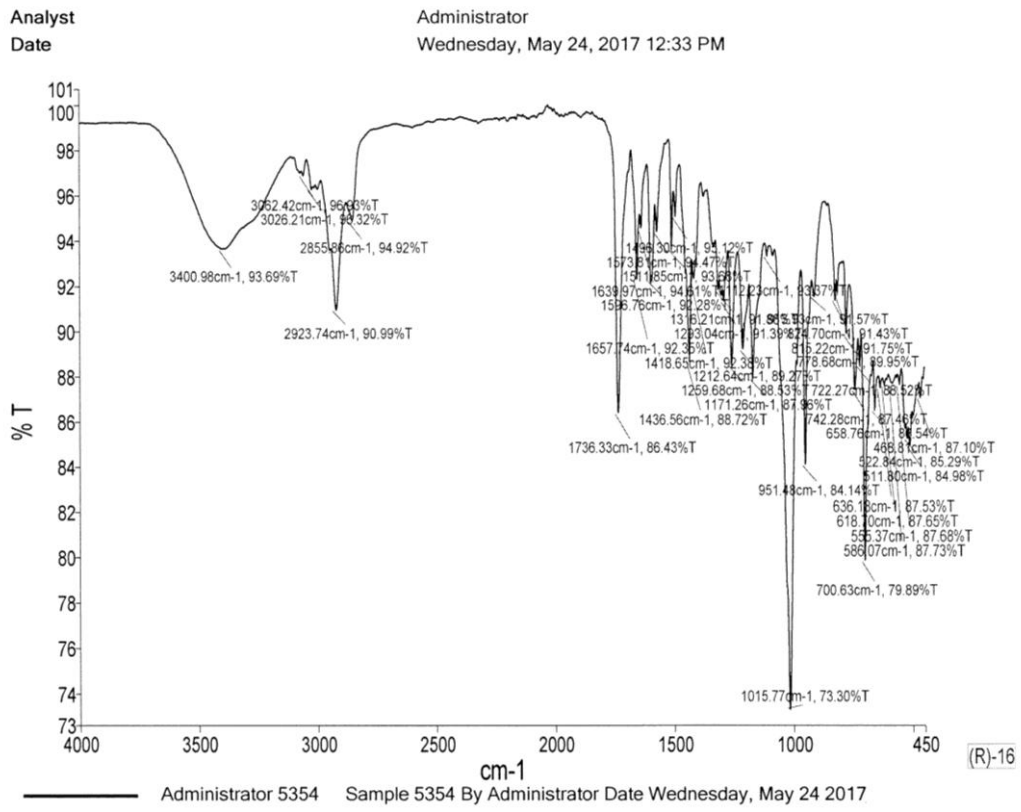

Figure B.128. IR spectrum of **(*R*)-27**.

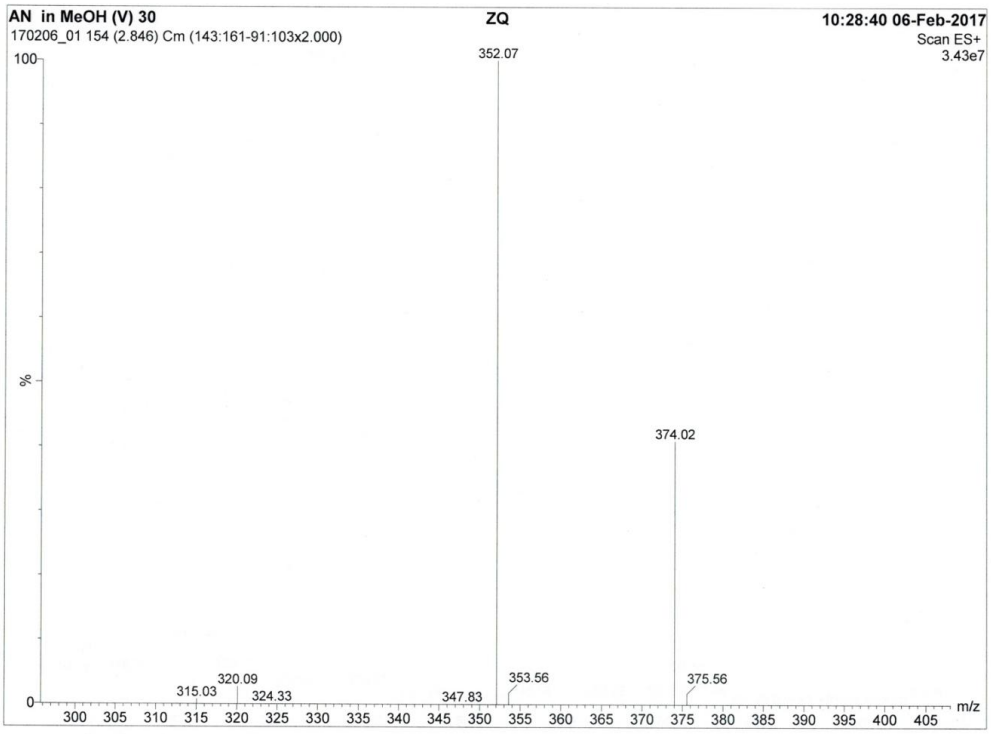

Figure B.129. Low resolution mass spectrum of **(*R*)-27**.

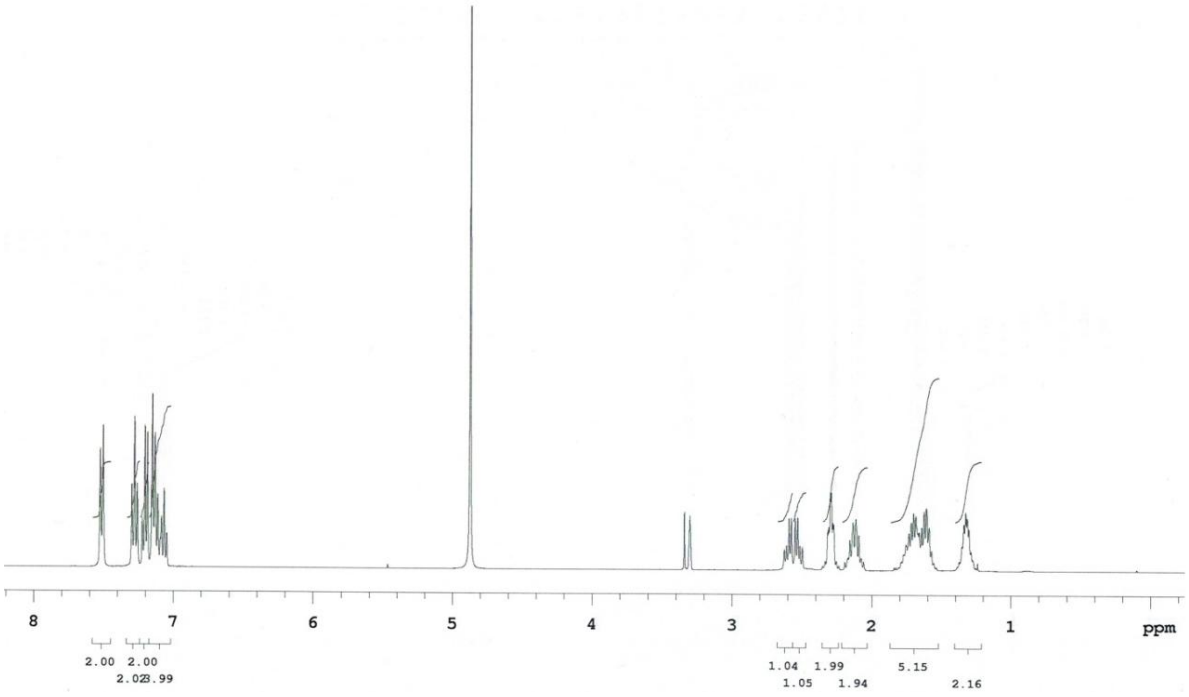

Figure B.130. ^{1}HNMR spectrum of **(*R*)-19f** in CD_3OD.

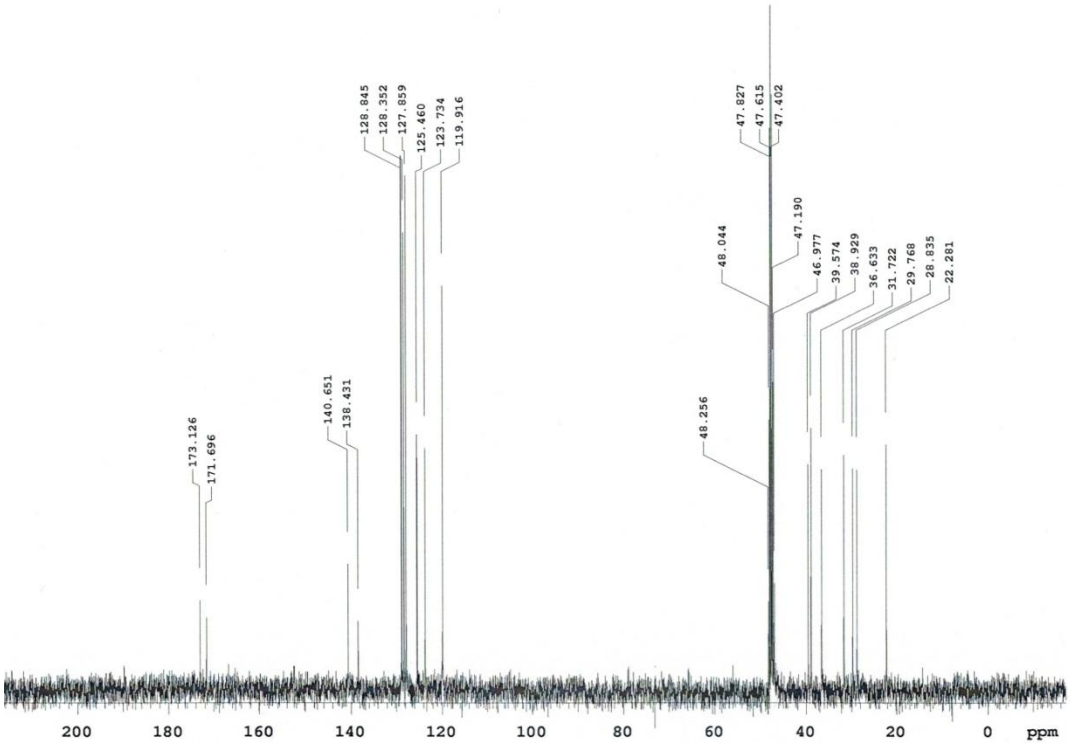

Figure B.131. ^{13}CNMR spectrum of **(*R*)-19f** in CD_3OD.

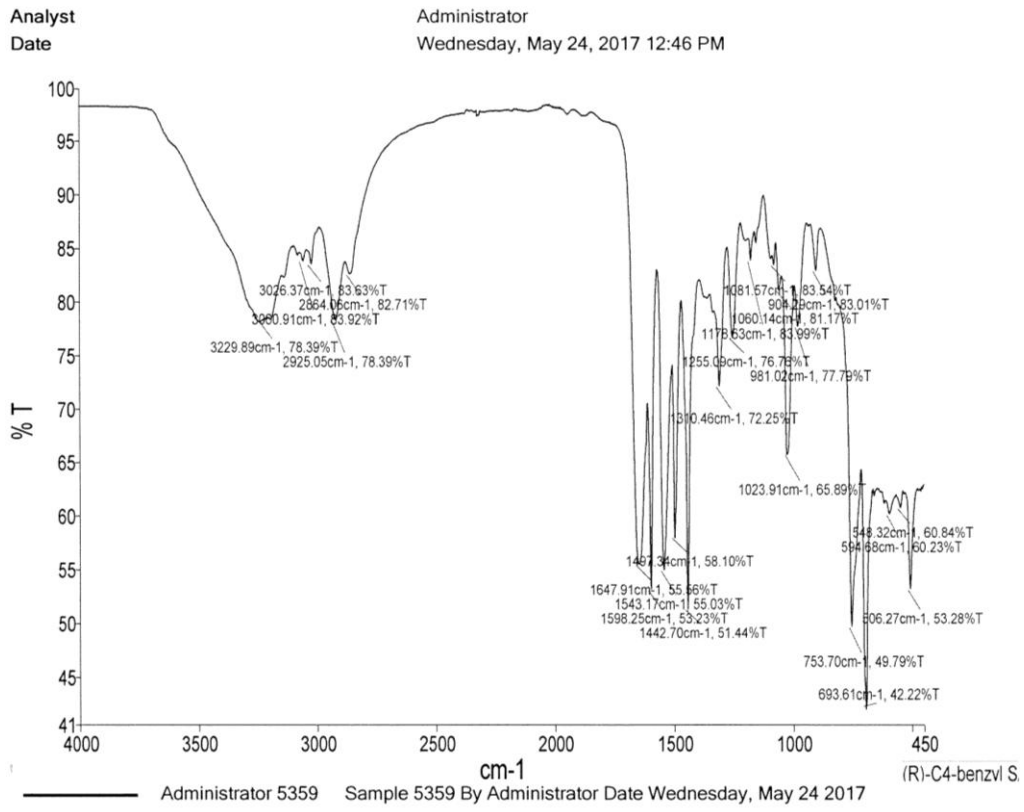

Figure B.132. IR spectrum of **(*R*)-1f**.

Elemental Composition Report **Page 1**

Single Mass Analysis
Tolerance = 5.0 PPM / DBE: min = -1.5, max = 100.0
Element prediction: Off
Number of isotope peaks used for i-FIT = 6

Monoisotopic Mass, Even Electron Ions
21 formula(e) evaluated with 1 results within limits (all results (up to 1000) for each mass)
Elements Used:
C: 21-21 H: 0-26 N: 0-2 O: 0-3 Na: 0-1
170317_046 735 (13.568) Cm (731:735) (R)-C4-benzyl SAHA
LCT Premier KD128
TOF MS ES+

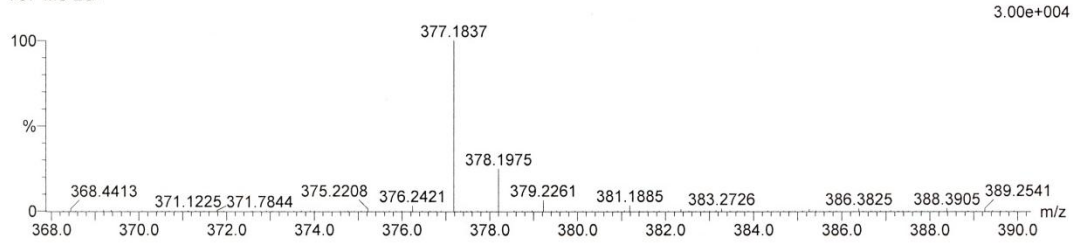

Minimum:				-1.5			
Maximum:		3.0	5.0	100.0			
Mass	Calc. Mass	mDa	PPM	DBE	i-FIT	i-FIT (Norm)	Formula
377.1837	377.1841	-0.4	-1.1	9.5	227.5	0.0	C21 H26 N2 O3 Na

Figure B.133. High resolution mass spectrum of **(*R*)-19f**.

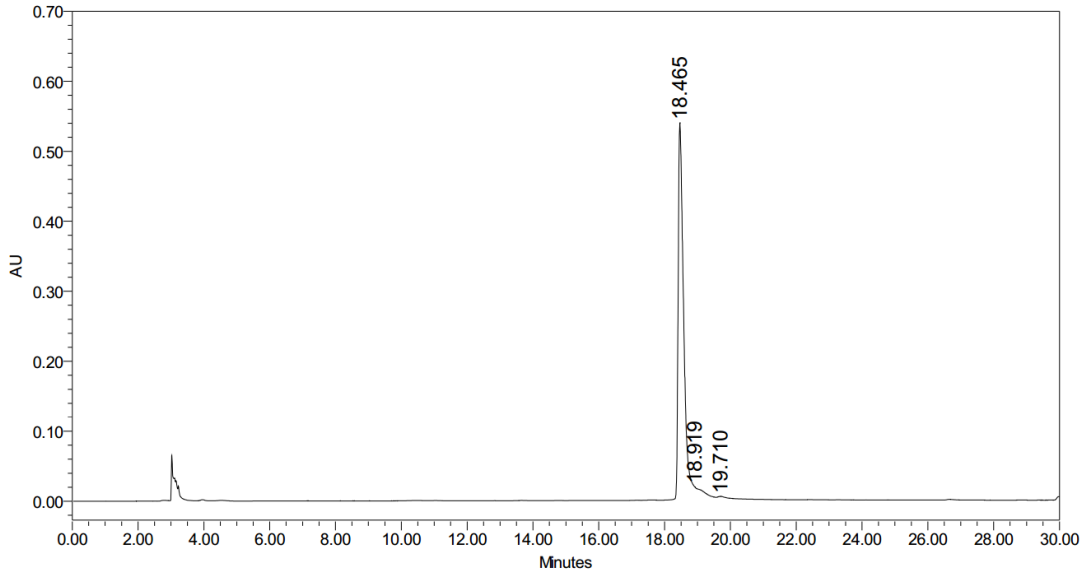

	RT	Area	% Area	Height
1	18.465	6135383	95.61	537896
2	18.919	259306	4.04	16077
3	19.710	22392	0.35	1787

Figure B.134. HPLC spectrum taken at 254 nm of *R*-C4-benzyl SAHA (**(*R*)-19f**). The peak at 18.465 is *R*-C4-benzyl SAHA. The calculated area and height under each peak, along with % area, is shown in the table below the spectrum.

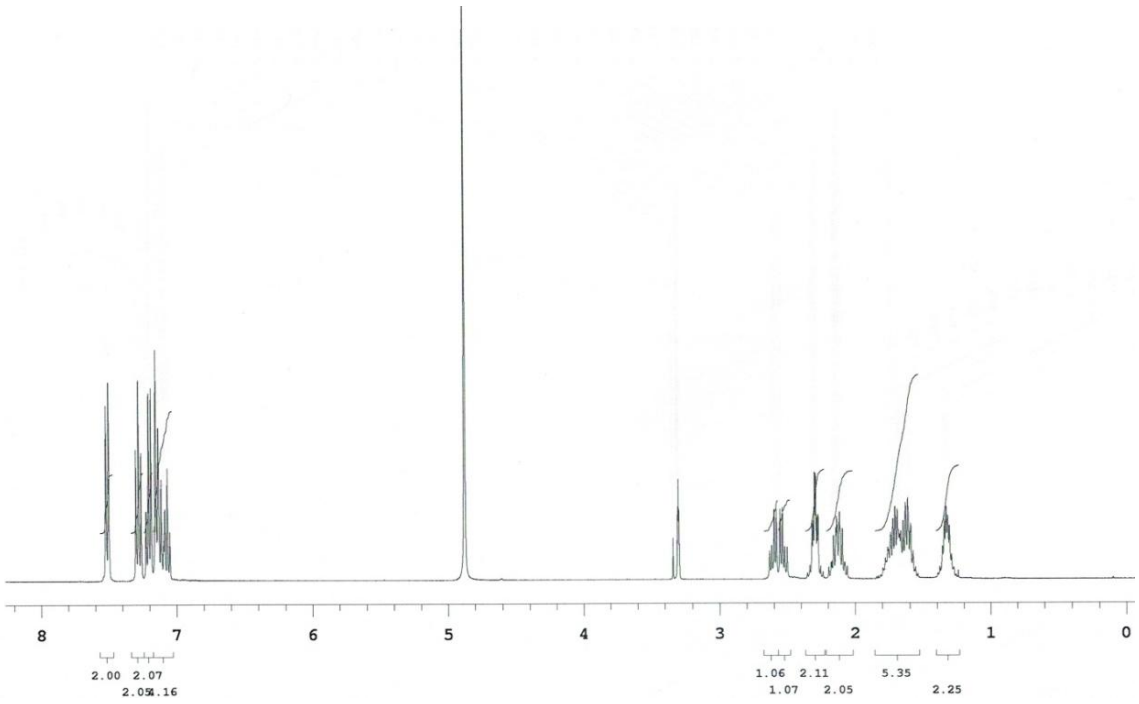

Figure B.135. ^{1}HNMR spectrum of **(*S*)-19f** in CD_3OD.

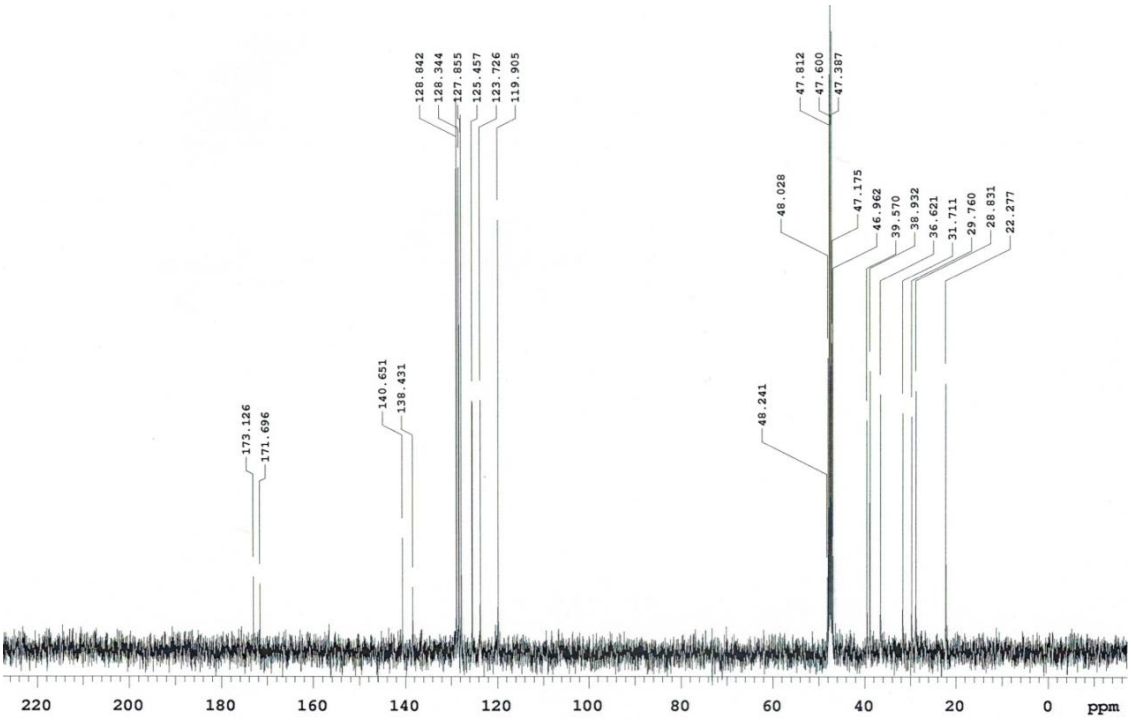

Figure B.136. ^{13}CNMR spectrum of **(*S*)-19f** in CD_3OD.

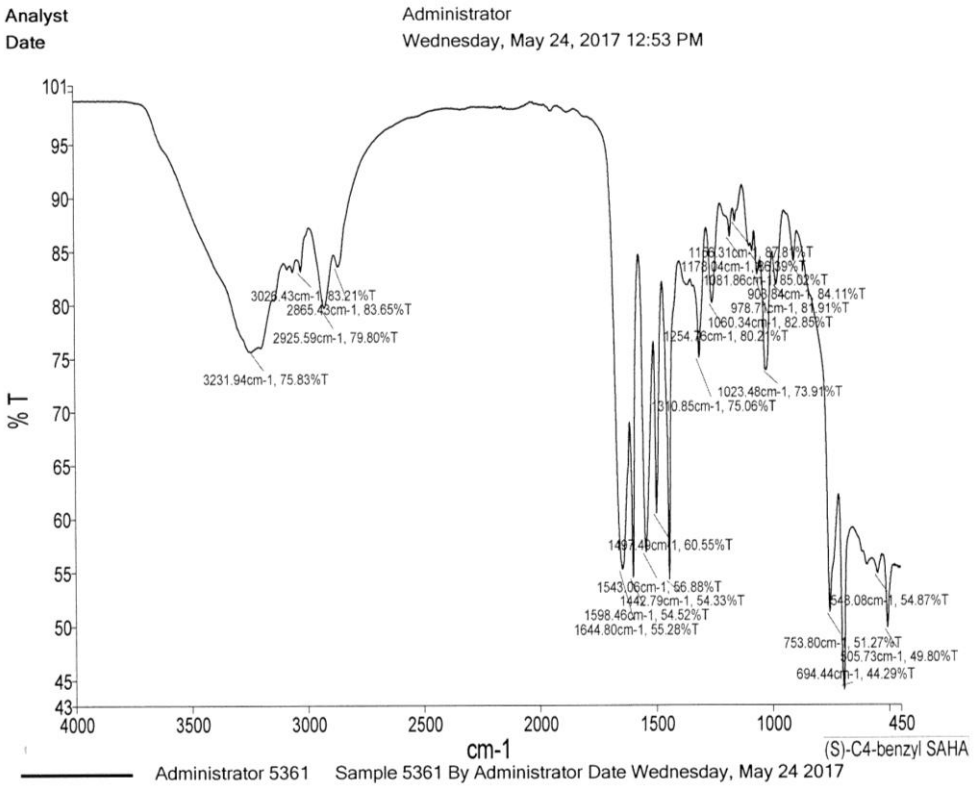

Figure B.137. IR spectrum of **(*S*)-1f**.

Elemental Composition Report **Page 1**

Single Mass Analysis
Tolerance = 5.0 PPM / DBE: min = -1.5, max = 100.0
Element prediction: Off
Number of isotope peaks used for i-FIT = 6

Monoisotopic Mass, Even Electron Ions
21 formula(e) evaluated with 1 results within limits (all results (up to 1000) for each mass)
Elements Used:
C: 21-21 H: 0-26 N: 0-2 O: 0-3 Na: 0-1
170317_046 135 (2.477) Cm (131:141) (S)-C4-benzyl SAHA
LCT Premier KD128
TOF MS ES+

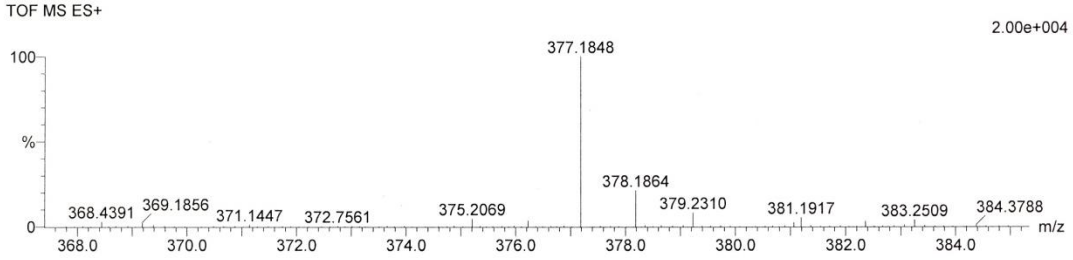

Minimum:				-1.5			
Maximum:		3.0	5.0	100.0			
Mass	Calc. Mass	mDa	PPM	DBE	i-FIT	i-FIT (Norm)	Formula
377.1848	377.1841	0.7	1.9	9.5	280.3	0.0	C21 H26 N2 O3 Na

Figure B.138. High resolution mass spectrum of **(*S*)-19f**.

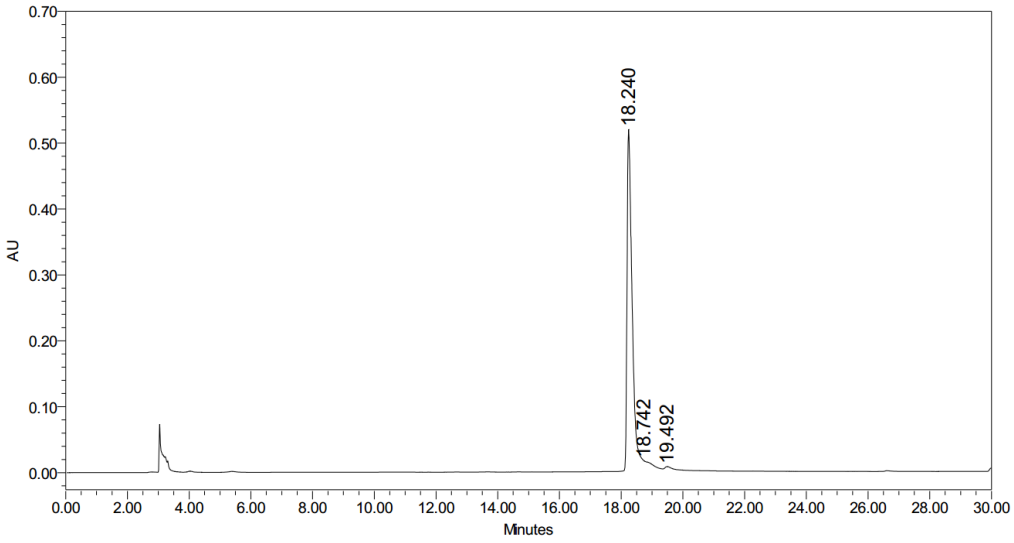

	RT	Area	% Area	Height
1	18.240	5967379	95.64	517781
2	18.742	221196	3.55	13508
3	19.492	51000	0.82	3857

Figure B.139. HPLC spectrum taken at 254 nm of *R*-C4-benzyl SAHA (**(*S*)-19f**). The peak at 18.240 is *R*-C4-benzyl SAHA. The calculated area and height under each peak, along with % area, is shown in the table below the spectrum.

B.3. *In vitro* screening with HDAC isoforms tables and figures

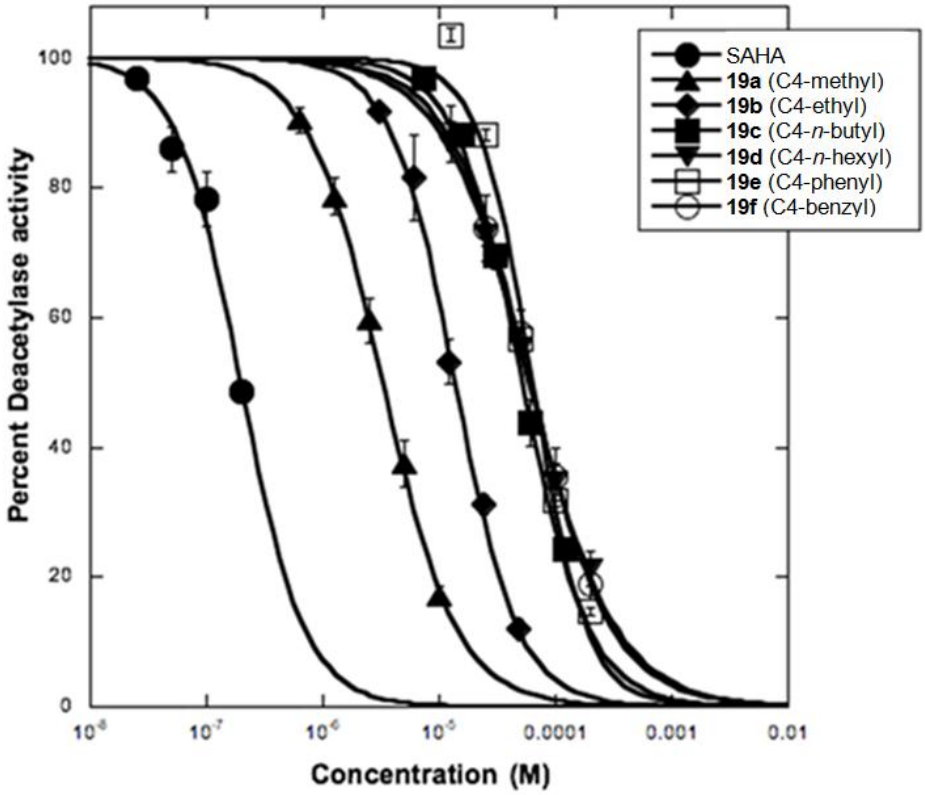

Figure B.140. Dose response curve of SAHA and C4-SAHA analogs **19a-f** tested using the HDAC activity in HeLa cells lysates from three independent trials with error bars indicating standard error (see Table S1). In some cases, the error bar is smaller than the marker size. Data were fit to the sigmoidal curve using KaleidaGraph 4.1.3 (Synergy Software) to determine the IC_{50}. The data are reported in Table 3.1.

Table B.1. Percent remaining HDAC activity after incubation of SAHA or C4-SAHA analogs **19a-f** with HeLa Lysates

	Deacetylase activity (%)						
Concentration (M)	SAHA	**19a**	**19b**	**19c**	**19d**	**19e**	**19f**
2.0×10^{-4}					21±3	15±1	19±2
1.0×10^{-4}					35±3	32±1	35±5
1.2×10^{-4}				24±1			
6.0×10^{-5}				44±4			
5.0×10^{-5}					56±2	57±2	58±4
4.8×10^{-5}			12±1				
3.0×10^{-5}				69±2			
2.5×10^{-5}					73±2	88±1	74±5
2.4×10^{-5}			31±2				
1.5×10^{-5}				88±1			
1.25×10^{-5}					87±1	104±1	88±4
1.2×10^{-5}			53±3				
1.0×10^{-5}		17±2					
7.5×10^{-6}				97±2			
6.0×10^{-6}			82±7				
5.0×10^{-6}		38±4					
3.0×10^{-6}			92±1				
2.5×10^{-6}		60±3					
1.25×10^{-6}		79±3					
6.25×10^{-6}		91±2					
2.0×10^{-7}	49±1						
1.0×10^{-7}	78±4						
5.0×10^{-8}	86±4						
2.5×10^{-8}	97±1						

[a] Mean percentage deacetylase activity and standard error of three trials are shown. This data is associated with Figure B.131 and Table 3.1.

Table B.2. Percent remaining deacetylase activity after incubation of a single concentration of each C4-modified SAHA analog with HDAC1, HDAC2, HDAC3, and HDAC6 using the ELISA-based activity assay.[a]

	Deacetylase activity (%)			
Compound	HDAC1	HDAC2	HDAC3	HDAC6
SAHA[93] 1 μM	8.9±0.1	8.3±0.2	14±3	7.9±1.6
19a (methyl) 0.75 μM	75±2	90±7	78±4	26±5
19b (ethyl) 0.75 μM	91±2	87±1	71±10	18±6
19c (butyl) 2.5 μM	88±2	87±1	85±2	5±3
19d (hexyl) 1.25 μM	97±3	101±2	100±6	21±2
19e (phenyl) 2.5 μM	86±1	85±3	85±5	17±7
19f (benzyl) 5 μM	87±4	92±4	90±3	2.9±0.5

[a] The means and standard errors for a minimum of two independent trials are shown. This data is associated with Figure 3.2.

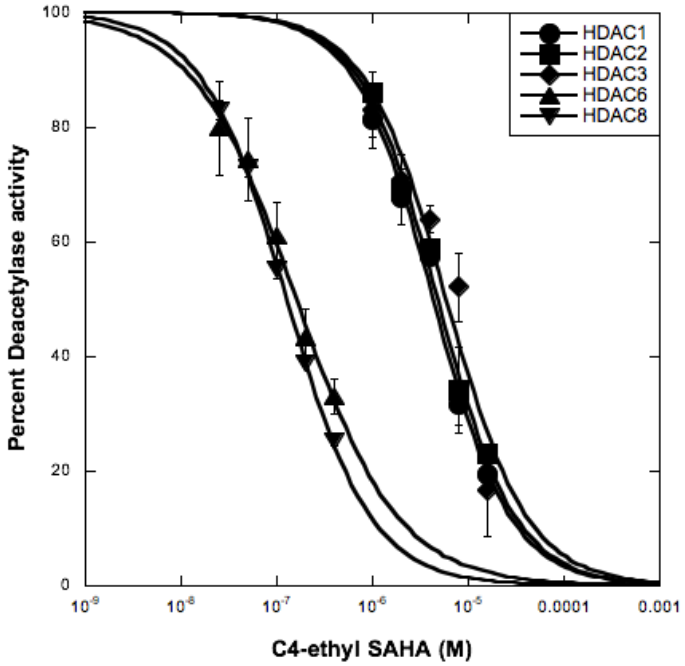

Figure B.141. Dose dependent curves of C4-ethyl SAHA analog (**19b**) with HDAC1, HDAC2, HDAC3, HDAC6, and HDAC8 isoforms with error bars depicting the standard error of at least three independent trials. IC_{50} values associated with Table 3.2 were determined by fitting data to a sigmoidal curve using KaleidaGraph 4.1.3 (Synergy Software) (Table B.3).

Table B.3. Percentage remaining deacetylase activity after incubation of C4-ethyl SAHA analog (**19b**) with HDAC1, HDAC2, HDAC3, HDAC6, and HDAC8.[a]

Concentration (M)	Deacetylase activity (%)				
	HDAC1	HDAC2	HDAC3	HDAC6	HDAC8
1.6×10^{-5}	19±1	23±2	17±8		
8.0×10^{-6}	32±4	34±7	52±6		
4.0×10^{-6}	58±1	59±2	64±2		
2.0×10^{-6}	68±5	69±1	71±4		
1.0×10^{-6}	81±3	86±2	83±7		
4.0×10^{-7}				33±3	25±1
2.0×10^{-7}				43±5	39±1
1.0×10^{-7}				61±6	55±2
5.0×10^{-8}				74±7	73±2
2.5×10^{-8}				80±8	83±2

[a] Means and standard errors of at least three independent trials with the C4-ethyl SAHA (**19b**) concentrations shown. Data is associated with Figure B.132 and Table 3.2.

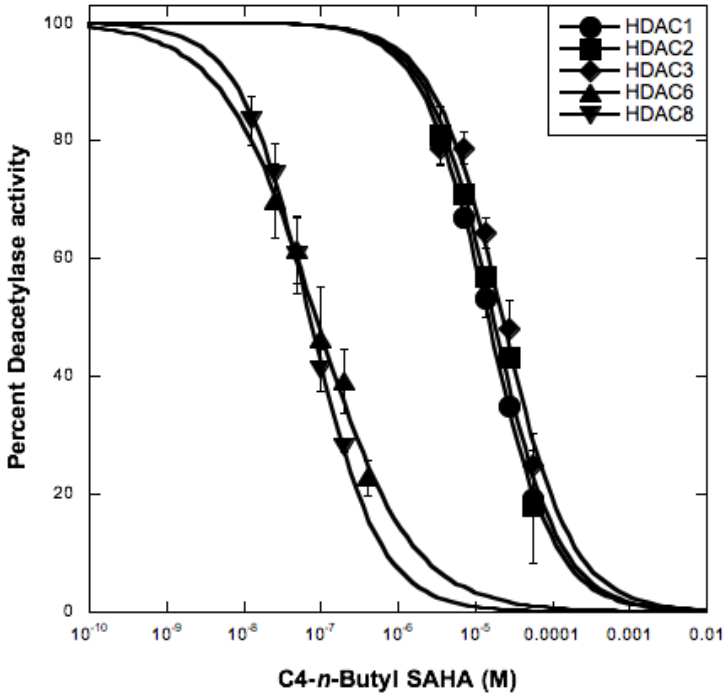

Figure B.142. Dose dependent curves of C4-butyl SAHA analog (**19c**) with HDAC1, HDAC2, HDAC3, HDAC6, and HDAC8 isoforms with error bars depicting the standard error of at least three independent trials. IC_{50} values associated with Table 3.2 were determined by fitting data to a sigmoidal curve using KaleidaGraph 4.1.3 (Synergy Software) (Table B.4).

Table B.4. Percentage remaining deacetylase activity after incubation of C4-butyl SAHA analog (**19c**) with HDAC1, HDAC2, HDAC3, HDAC6, and HDAC8.[a]

Concentration (M)	Deacetylase activity (%)				
	HDAC1	HDAC2	HDAC3	HDAC6	HDAC8
5.6×10^{-5}	19±1	18±10	25±5		
2.8×10^{-5}	35±1	43±2	48±5		
1.4×10^{-5}	53±3	57±1	64±2		
7.0×10^{-6}	67±2	71±2	79±3		
3.5×10^{-6}	81±1	81±5	79±3		
4.0×10^{-7}				23±3	
2.0×10^{-7}				39±5	28±4
1.0×10^{-7}				46±9	41±5
5.0×10^{-8}				61±6	61±7
2.5×10^{-8}				70±6	74±3
1.25×10^{-8}					84±1

[a] Means and standard errors of at least three independent trials with the C4-butyl SAHA (**19c**) concentrations shown. Data is associated with Figure B.133 and Table 3.2.

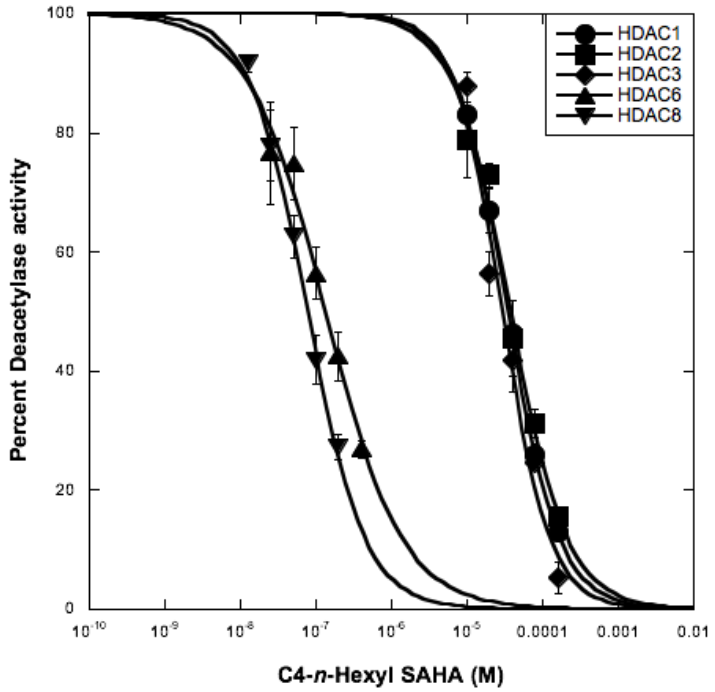

Figure B.143. Dose dependent curves of C4-*n*-hexyl SAHA analog (**19d**) HDAC1, HDAC2, HDAC3, HDAC6, and HDAC8 isoforms with error bars depicting the standard error of at least three independent trials. IC_{50} values associated with Table 3.2 were determined by fitting data to a sigmoidal curve using KaleidaGraph 4.1.3 (Synergy Software) (Table B.5).

Table B.5. Percentage remaining deacetylase activity after incubation of C4-*n*-hexyl SAHA analog (**19d**) with HDAC1, HDAC2, HDAC3, HDAC6, and HDAC8.[a]

Concentration (M)	Deacetylase activity (%)				
	HDAC1	HDAC2	HDAC3	HDAC6	HDAC8
1.6×10^{-4}	13±1	16±1	5±3		
8.0×10^{-5}	26±2	31±2	25±1		
4.0×10^{-5}	46±1	46±6	42±5		
2.0×10^{-5}	67±4	73±2	56±4		
1.0×10^{-5}	83±4	79±6	88±2		
4.0×10^{-7}				27±2	
2.0×10^{-7}				42±4	27±2
1.0×10^{-7}				56±4	42±4
5.0×10^{-8}				75±6	63±4
2.5×10^{-8}				77±9	78±6
1.25×10^{-8}					92±1

[a] Means and standard errors of at least three independent trials with the C4-*n*-hexyl SAHA (**19d**) concentrations shown. Data is associated with Figure B.134 and Table 3.2.

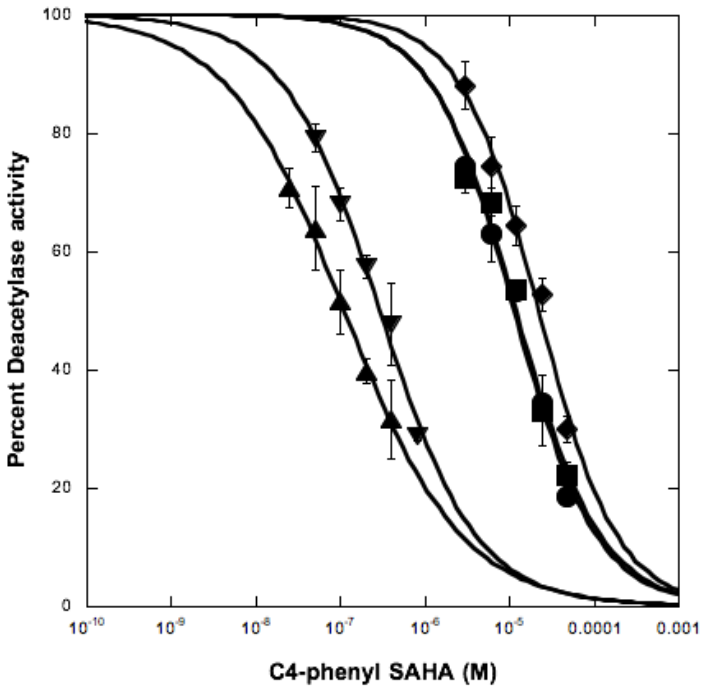

Figure B.144. Dose dependent curves of C4-phenyl SAHA analog (**19e**) with HDAC1, HDAC2, HDAC3, HDAC6, and HDAC8 isoforms with error bars depicting the standard error of at least three independent trials. IC_{50} values associated with Table 3.2 were determined by fitting data to a sigmoidal curve using KaleidaGraph 4.1.3 (Synergy Software) (Table B.6).

Table B.6. Percentage remaining deacetylase activity after incubation of C4-phenyl SAHA analog (**19e**) with HDAC1, HDAC2, HDAC3, HDAC6, and HDAC8.[a]

Concentration (M)	Deacetylase activity (%)				
	HDAC1	HDAC2	HDAC3	HDAC6	HDAC8
4.8×10^{-5}	19±1	22±2	30±2		
2.4×10^{-5}	34±1	33±6	53±3		
1.2×10^{-5}	53±2	53±1	64±3		
6.0×10^{-6}	63±5	68±2	74±5		
3.0×10^{-6}	74±2	72±3	88±4		
8.0×10^{-7}					29±1
4.0×10^{-7}				32±7	48±7
2.0×10^{-7}				40±2	57±2
1.0×10^{-7}				52±5	69±3
5.0×10^{-8}				64±7	80±2
2.5×10^{-8}				71±3	

[a] Means and standard errors of at least three independent trials with the C4-phenyl SAHA (**19e**) concentrations shown. Data is associated with Figure B.135 and Table 3.2.

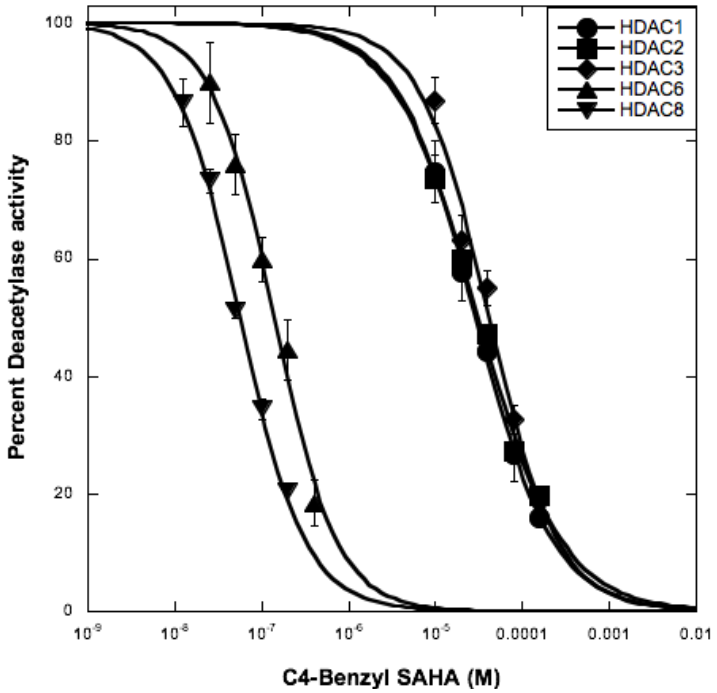

Figure B.145. Dose dependent curves of C4-benzyl SAHA analog (**19f**) with HDAC1, HDAC2, HDAC3, HDAC6, and HDAC8 isoforms with error bars depicting the standard error of at least three independent trials. IC_{50} values associated with Table 3.2 were determined by fitting data to a sigmoidal curve using KaleidaGraph 4.1.3 (Synergy Software) (Table B.7).

Table B.7. Percentage remaining deacetylase activity after incubation of C4-benzyl SAHA analog (**19f**) with HDAC1, HDAC2, HDAC3, HDAC6, and HDAC8.[a]

Concentration (M)	Deacetylase activity (%)				
	HDAC1	HDAC2	HDAC3	HDAC6	HDAC8
1.6×10^{-4}	16±1	20±1	19±2		
8.0×10^{-5}	27±2	27±5	33±2		
4.0×10^{-5}	44±2	47±1	55±3		
2.0×10^{-5}	58±5	60±1	63±5		
1.0×10^{-5}	75±5	74±4	87±4		
4.0×10^{-7}				18±4	
2.0×10^{-7}				45±5	21±1
1.0×10^{-7}				60±4	34±2
5.0×10^{-8}				76±5	51±1
2.5×10^{-8}				90±7	73±2
1.25×10^{-8}					87±4

[a] Means and standard errors of at least three independent trials with the C4-beznyl SAHA (**19f**) concentrations shown. Data is associated with Figure B.136 and Table 3.2.

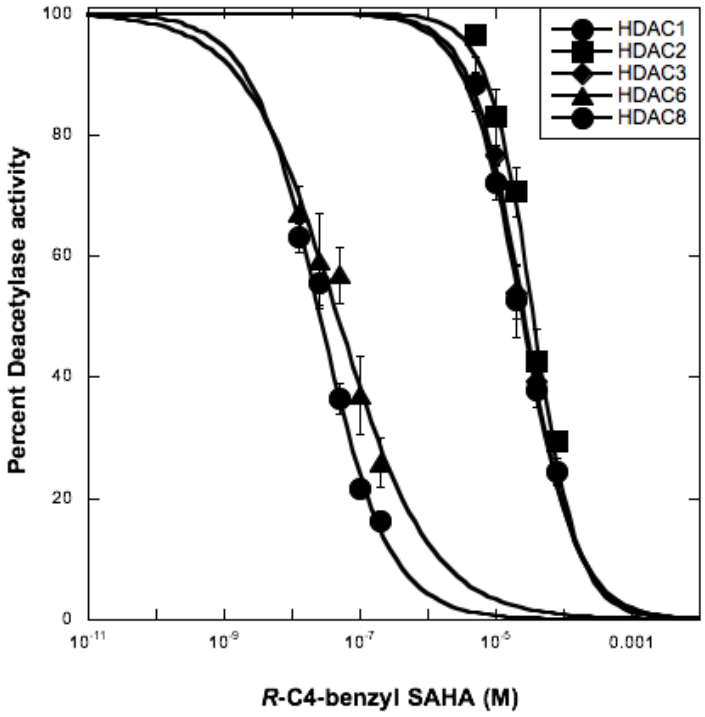

Figure B.146. Dose dependent curves of (*R*)-C4-benzyl SAHA analog (**(*R*)-19f**) with HDAC1, HDAC2, HDAC3, HDAC6, and HDAC8 isoforms with error bars depicting the standard error of at least three independent trials. IC_{50} values associated with Table 3.2 were determined by fitting data to a sigmoidal curve using KaleidaGraph 4.1.3 (Synergy Software) (Table B.8).

Table B.8. Percentage remaining deacetylase activity after incubation of C4-benzyl SAHA analog (**(*R*)-19f**) with HDAC1, HDAC2, HDAC3, HDAC6, and HDAC8.[a]

Concentration (M)	Deacetylase activity (%)				
	HDAC1	HDAC2	HDAC3	HDAC6	HDAC8
8.0×10^{-5}	24±2	29±1	25±2		
4.0×10^{-5}	38±3	43±5	39±2		
2.0×10^{-5}	53±6	71±4	54±4		
1.0×10^{-5}	72±3	83±5	77±2		
5.0×10^{-6}	88±4	96±1	89±2		
2.0×10^{-7}				26±4	16±1
1.0×10^{-7}				37±6	22±1
5.0×10^{-8}				57±5	37±3
2.5×10^{-8}				59±8	56±4
1.25×10^{-8}				67±4	64±2

[a] Means and standard errors of at least three independent trials with the (*S*)-C4-beznyl SAHA (**(*R*)-19f**) concentrations shown. Data is associated with Figure B.137 and Table 3.2.

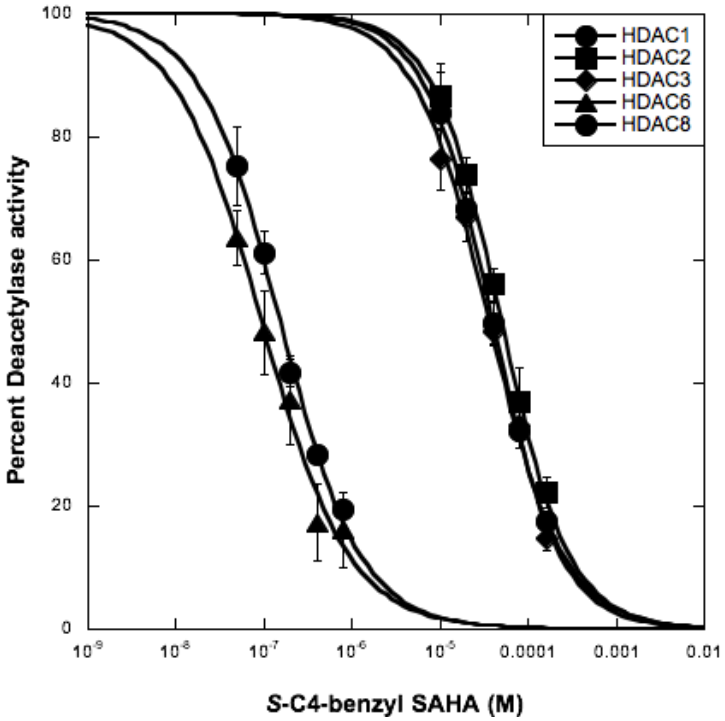

Figure B.147. Dose dependent curves of (*S*)-C4-benzyl SAHA analog (**(*S*)-19f**) with HDAC1, HDAC2, HDAC3, HDAC6, and HDAC8 isoforms with error bars depicting the standard error of at least three independent trials. IC_{50} values associated with Table 3.2 were determined by fitting data to a sigmoidal curve using KaleidaGraph 4.1.3 (Synergy Software) (Table B.9).

Table B.9. Percentage remaining deacetylase activity after incubation of C4-benzyl SAHA analog (**(*S*)-19f**) with HDAC1, HDAC2, HDAC3, HDAC6, and HDAC8.[a]

Concentration (M)	Deacetylase activity (%)				
	HDAC1	HDAC2	HDAC3	HDAC6	HDAC8
1.6×10^{-4}	17±1	22±2	15±2		
8.0×10^{-5}	32±2	37±6	33±4		
4.0×10^{-5}	50±3	56±3	48±2		
2.0×10^{-5}	68±3	74±3	67±4		
1.0×10^{-5}	84±7	87±5	76±5		
8.0×10^{-7}				16±6	19±1
4.0×10^{-7}				17±6	28±1
2.0×10^{-7}				37±7	42±2
1.0×10^{-7}				48±7	61±3
5.0×10^{-8}				64±4	75±6

[a] Means and standard errors of at least three independent trials with the (*S*)-C4-beznyl SAHA (**(*S*)-19f**) concentrations shown. Data is associated with Figure B.138 and Table 3.2.

Table B.10. Fold selectivity of SAHA, tubastatin, and C4-SAHA analogs **19b-19f** for HDAC6 and HDAC8 over HDAC1, 2, and 3.[a]

Compound	HDAC6 fold selectivity			HDAC8 fold selectivity		
	HDAC1	HDAC2	HDAC3	HDAC1	HDAC2	HDAC3
SAHA	1	3	0.6 [b]	0.06 [c]	0.2 [c]	0.04 [c]
Tubastatin	87	130	94	8.2	12	8.8
C4-ethyl SAHA **19b**	28	31	38	34	38	46
C4-butyl SAHA **19c**	170	200	260	200	240	310
C4-hexyl SAHA **19d**	250	270	210	440	480	380
C4-phenyl SAHA **19e**	100	350	210	38	130	79
C4-benzyl SAHA **19f**	210	270	300	510	670	740
(*S*)-C4-benzyl SAHA **(*S*)-19f**	520	750	560	930	1300	1000
(*R*)-C4-benzyl SAHA **(*R*)-19f**	420	540	390	260	330	240

[a] Fold selectivities were calculated from the IC_{50} values in tables 2 and 3. [b] SAHA displayed 1.65-fold preference for HDAC3 versus HDAC6. [c] SAHA displayed 16-fold, 6-fold, and 27-fold preference for HDAC1, 2, and 3, respectively, over HDAC8

B.4. *In cellulo* selectivity testing figure

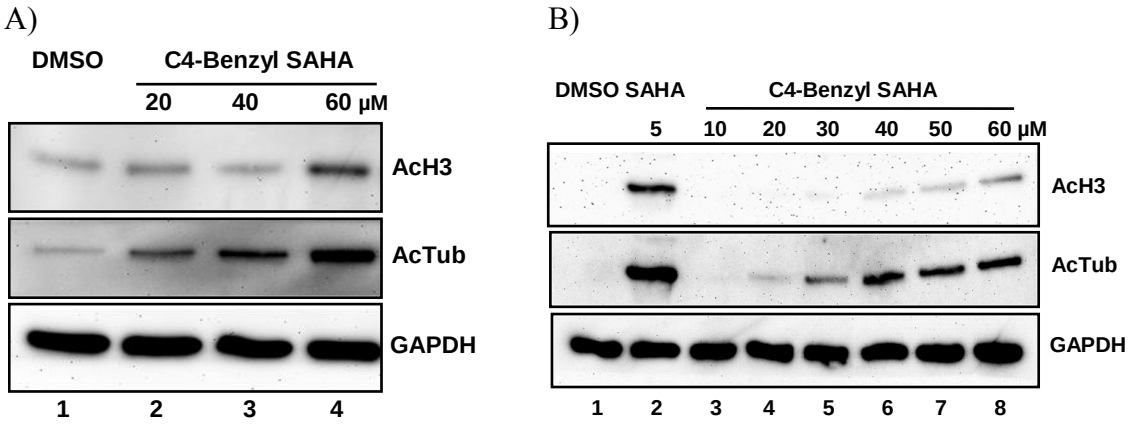

Figure B.148. Repetitive cell-based selectivity trials of the western blots analysis of acetyl-α-tubulin (AcTub) after treatment with SAHA or the SAHA analogs. U937 cells were treated with SAHA (5 μM), DMSO (1%), C4-benzyl SAHA (**19f**) analog before lysis, SDS-PAGE separation, transfer to a PVDF membrane, and western blotted with AcTub antibody. GAPDH levels in the samples were also probed as a gel load control. A DMSO control sample was included for comparison to inhibitor treated samples. These three trials are associated with the fourth trial shown in Figure 3.3.

B.5. *In vitro* cancer cell growth inhibition tables and figures

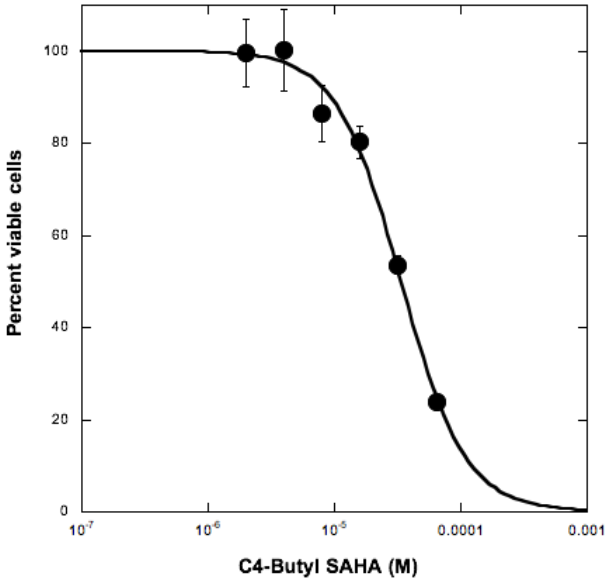

Figure B.149. Dose dependent cell viability of C4-*n*-butyl SAHA (**19c**) with U937 cell line, with error bars depicting the standard error of more than three independent trials. EC_{50} values associated with Table 3.2 were determined by fitting data to a sigmoidal curve using KaleidaGraph 4.1.3 (Synergy Software) (Table B.11).

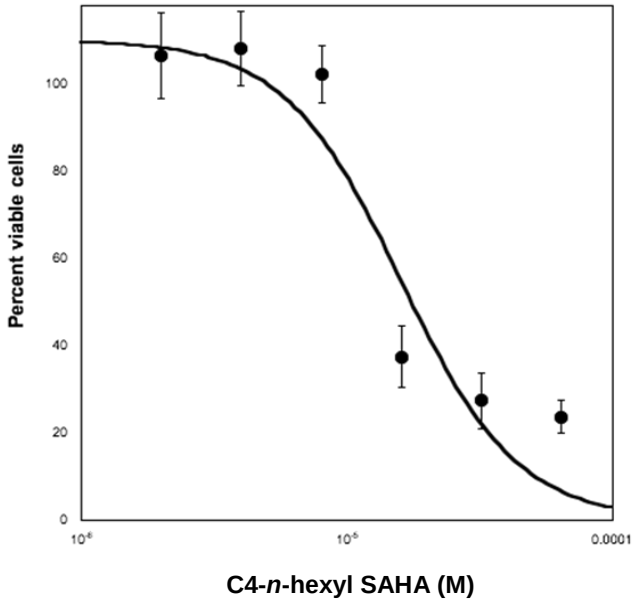

Figure B.150. Dose dependent cell viability of C4-*n*-hexyl SAHA (**19d**) with U937 cell line, with error bars depicting the standard error of six independent trials. EC_{50} values associated with Table 3.2 were determined by fitting data to a sigmoidal curve using KaleidaGraph 4.1.3 (Synergy Software) (Table B.11).

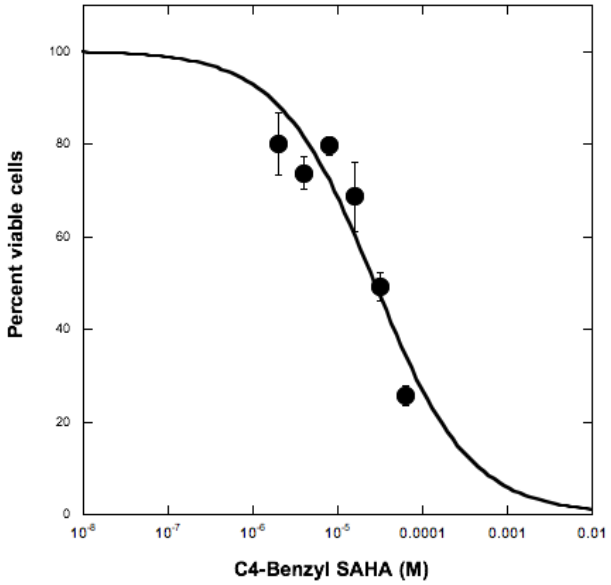

Figure B.151. Dose dependent cell viability of C4-benzyl SAHA (**19f**) with U937 cell line, with error bars depicting the standard error of more than three independent trials. EC_{50} values associated with Table 3.2 were determined by fitting data to a sigmoidal curve using KaleidaGraph 4.1.3 (Synergy Software) (Table B.11).

Table B.11. Percentage of viable cells after treatment of U937 cell line with C4-butyl SAHA (**19c**), C4-hexyl SAHA (**19d**) and C4-benzyl SAHA (**19f**) at the specified concentrations.[a]

Concentration (M)	Viable cells (%)		
	19c (butyl)	**19d** (hexyl)	**19f** (benzyl)
6.4×10^{-5}	24 ± 1	24 ± 4	26 ± 2
3.2×10^{-5}	54 ± 2	28 ± 6	49 ± 3
1.6×10^{-5}	80 ± 4	37 ± 7	69 ± 8
8.0×10^{-6}	87 ± 6	102 ± 7	80 ± 2
4.0×10^{-6}	100 ± 9	108 ± 9	74 ± 4
2.0×10^{-6}	100 ± 7	106 ± 10	80 ± 7

[a] Means and standard errors of at least three independent trials are shown. Data is associated with Figures B.140-B.142 and Table 3.3.

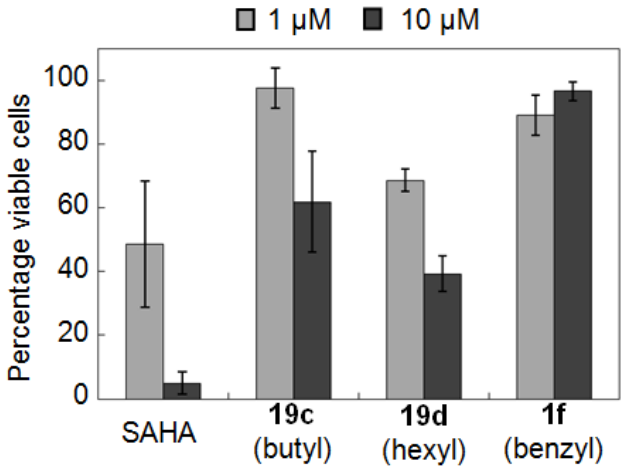

Figure B.152. Cytotoxicity screening of SAHA, and C4-SAHA analogs **19c**, **19d**, and **19f**, at 1 and 10 μM concentrations using an MTT assay with Jurkat cell line. Mean percent cell viability from a minimum of three independent trials with standard errors were plotted (Table B.12).

Table B.12. Percentage of viable cells after treatment of Jurkat cell line with of C4-butyl SAHA **19c**, C4-hexyl SAHA **19d**, C4-benzyl SAHA **19f**, and SAHA.[a]

	Viable cells (%)	
Compound	1 μM	10 μM
19c (butyl)	98 ± 6	62 ± 16
19d (hexyl)	69 ± 4	39 ± 6
19f (benzyl)	89 ± 20	97 ± 4
SAHA	49 ± 6	5 ± 3

[a] Means and standard errors for a minimum of four independent trials are shown. All analogs were tested at 1 and 10μM final concentrations. Data is associated with Figure B.143.

APPENDIX C

C.1. Compound characterization of the C5-modified SAHA analogs

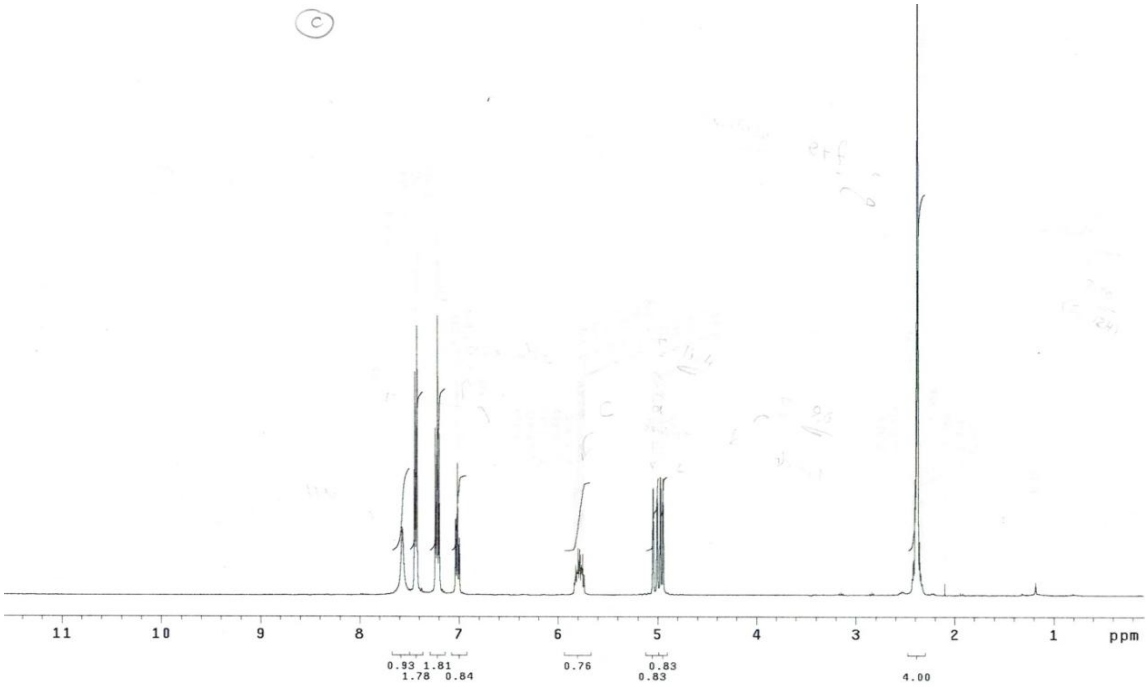

Figure C.1. ^{1}HNMR spectrum of **29**.

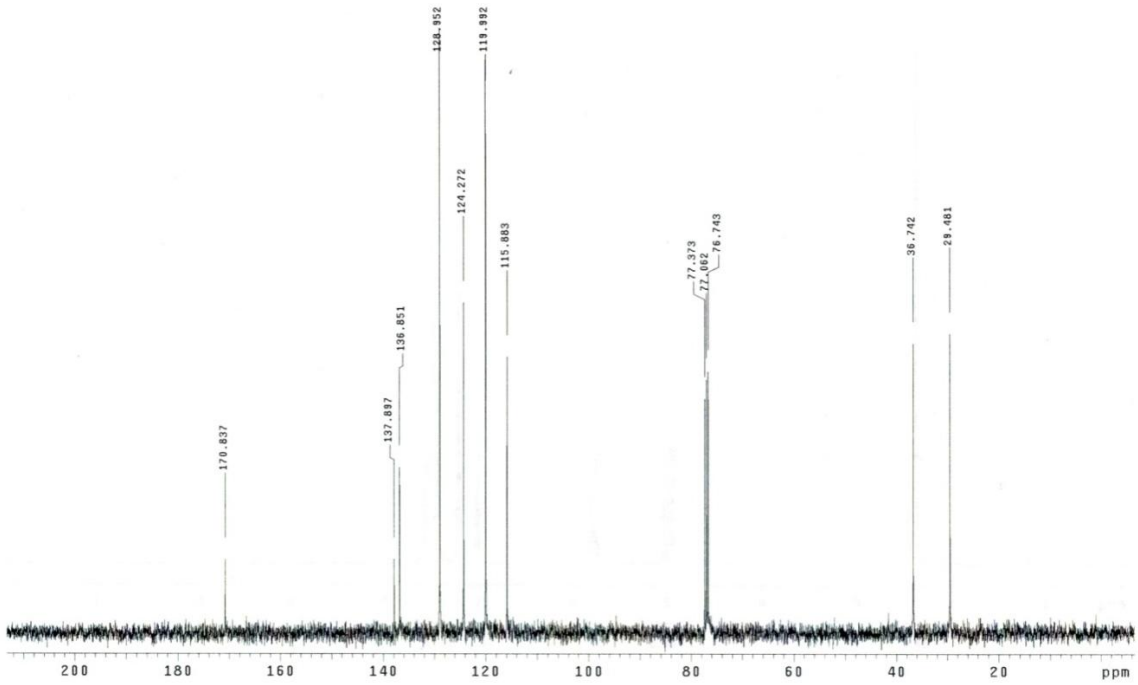

Figure C.2 ^{13}CNMR spectrum of **29**.

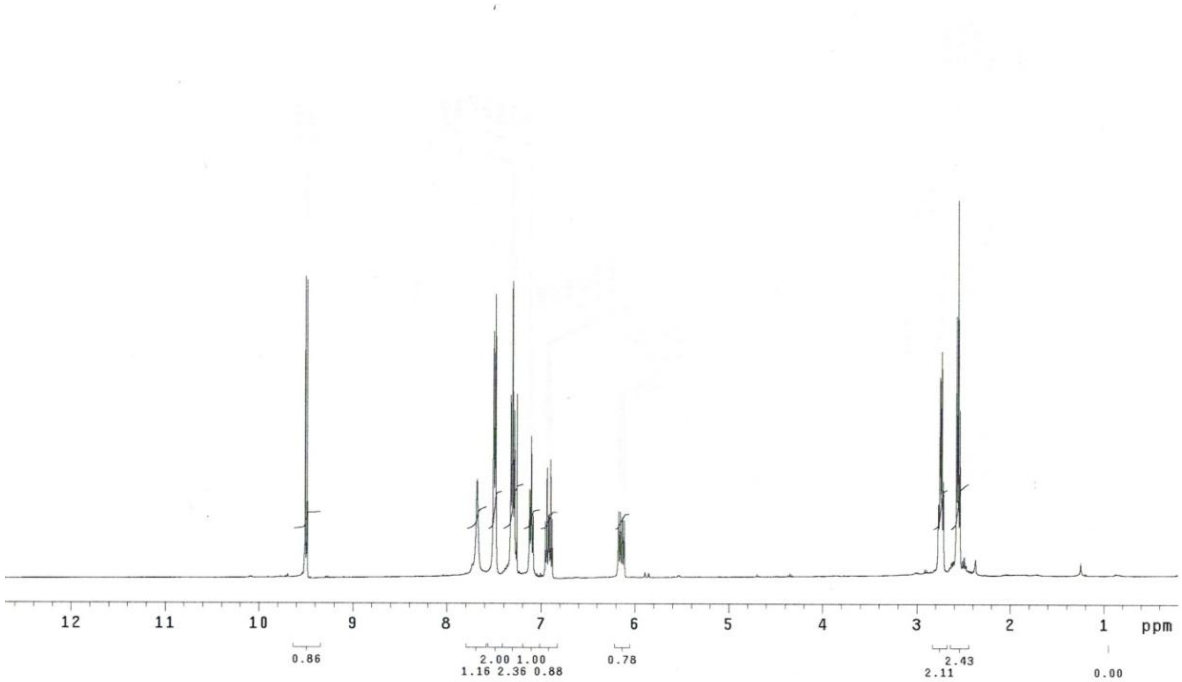

Figure C.3. ^{1}HNMR spectrum of **30**.

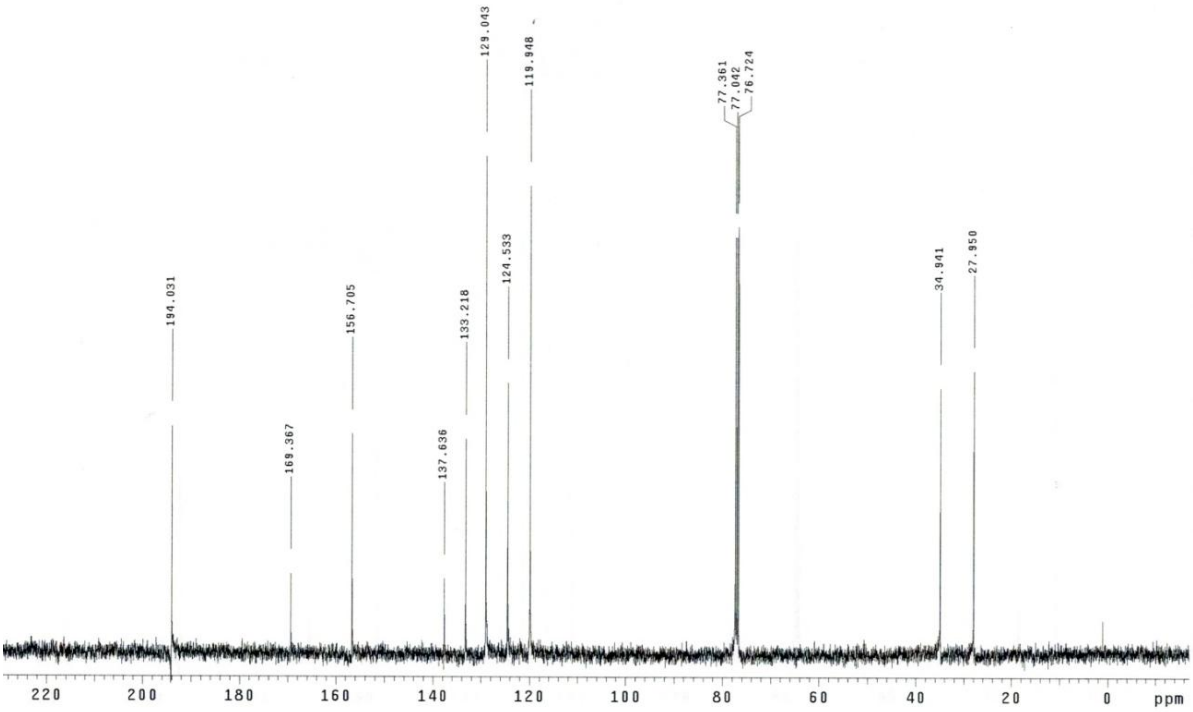

Figure C.4. ^{13}CNMR spectrum of **30**.

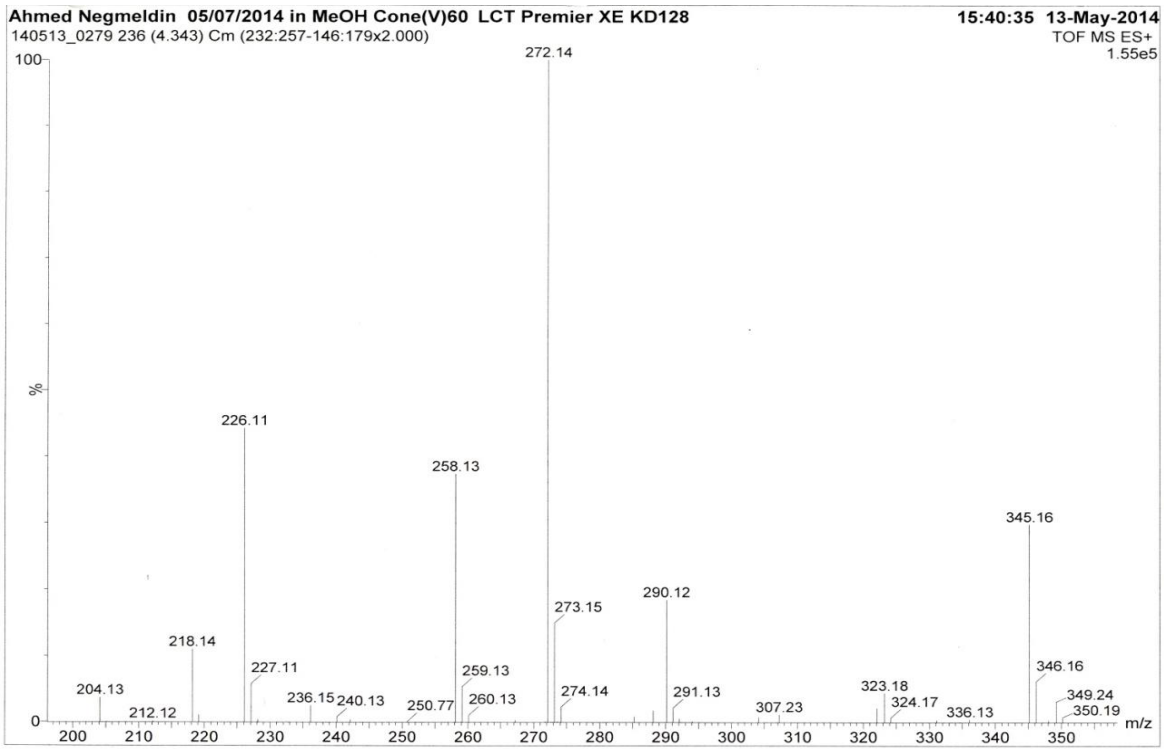

Figure C.5. Low resolution mass spectrum of **30** using a Waters ZQ LC-SQMS instrument.

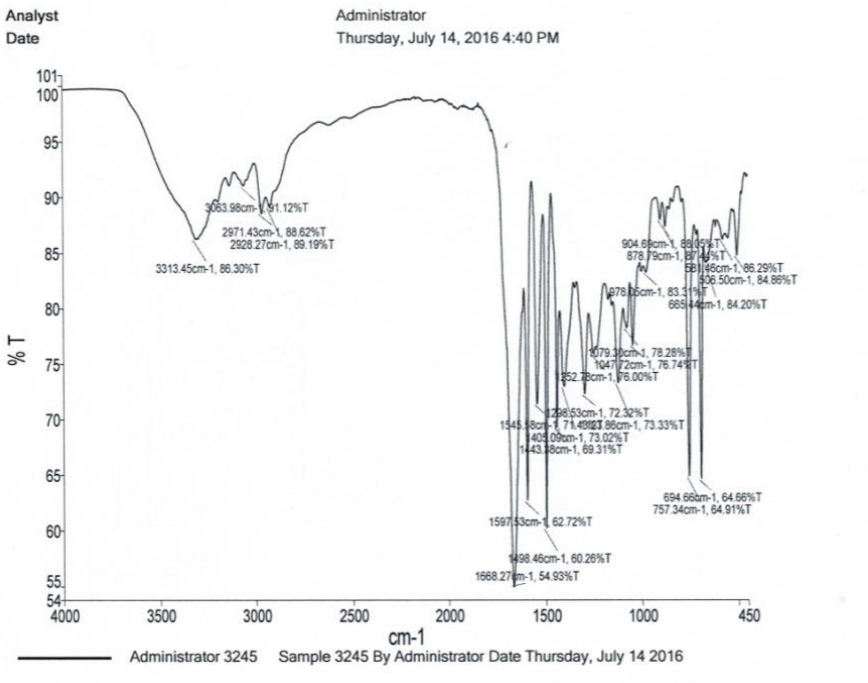

Figure C.6. IR spectrum of **30** using a Perkin Elmer Spectrum Two ATR-FTIR.

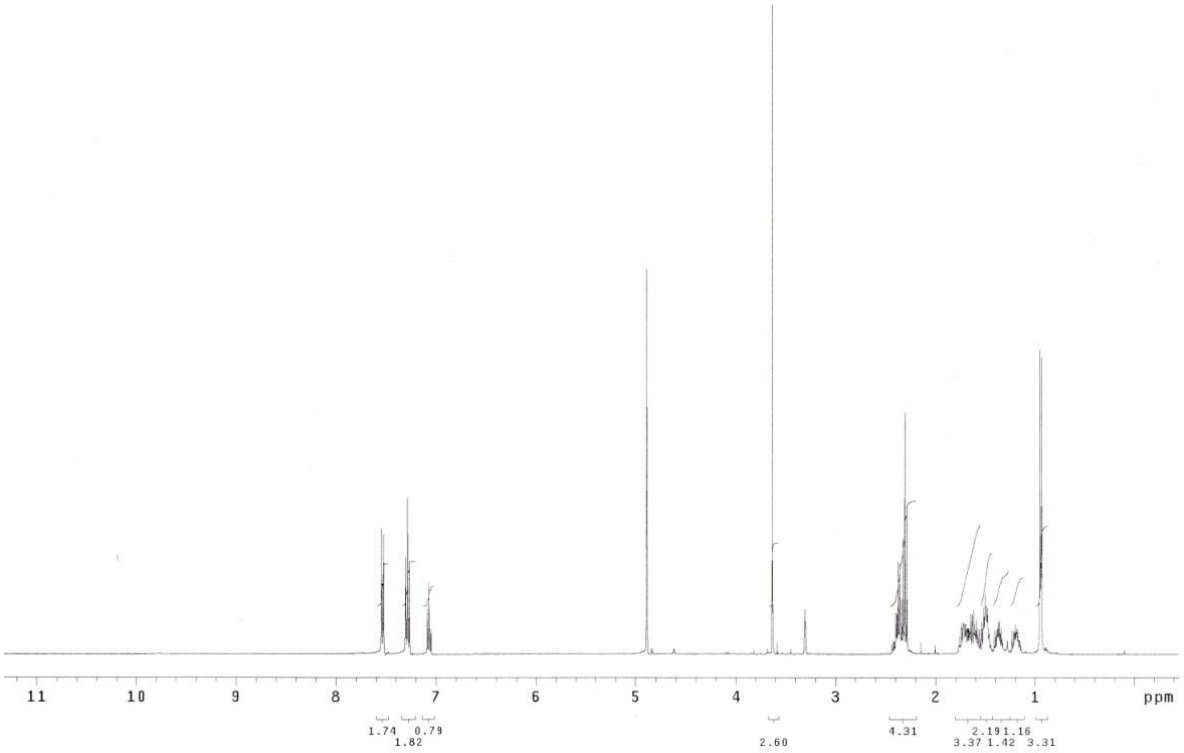

Figure C.7. ^{1}HNMR spectrum of **33a.**

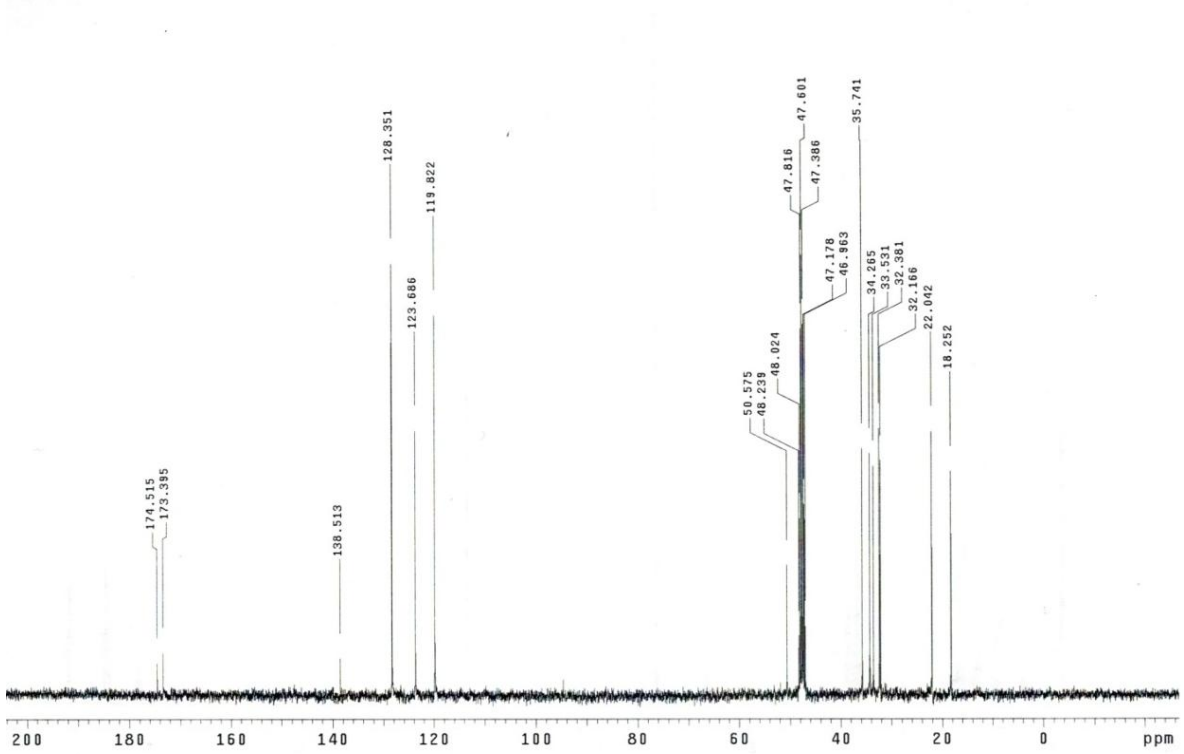

Figure C.8. ^{13}CNMR spectrum of **33a.**

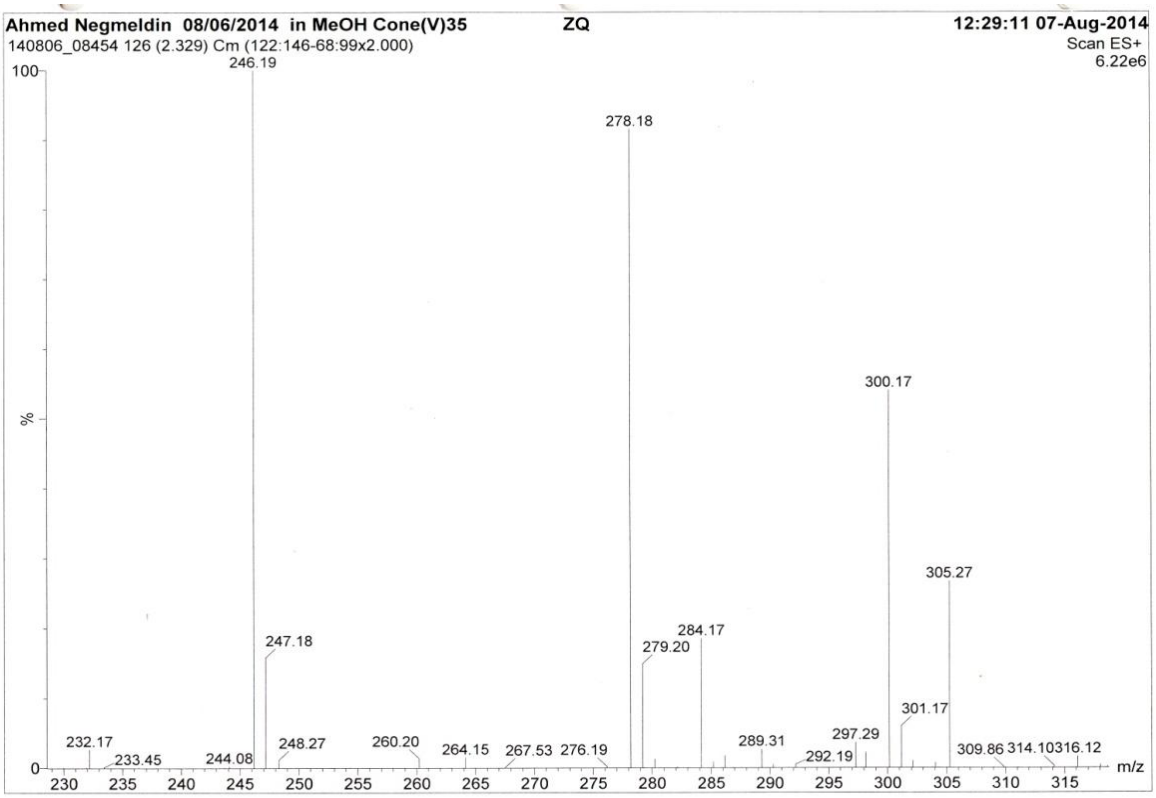

Figure C.9. Low resolution mass spectrum of **33a** using a Waters ZQ LC-SQMS instrument.

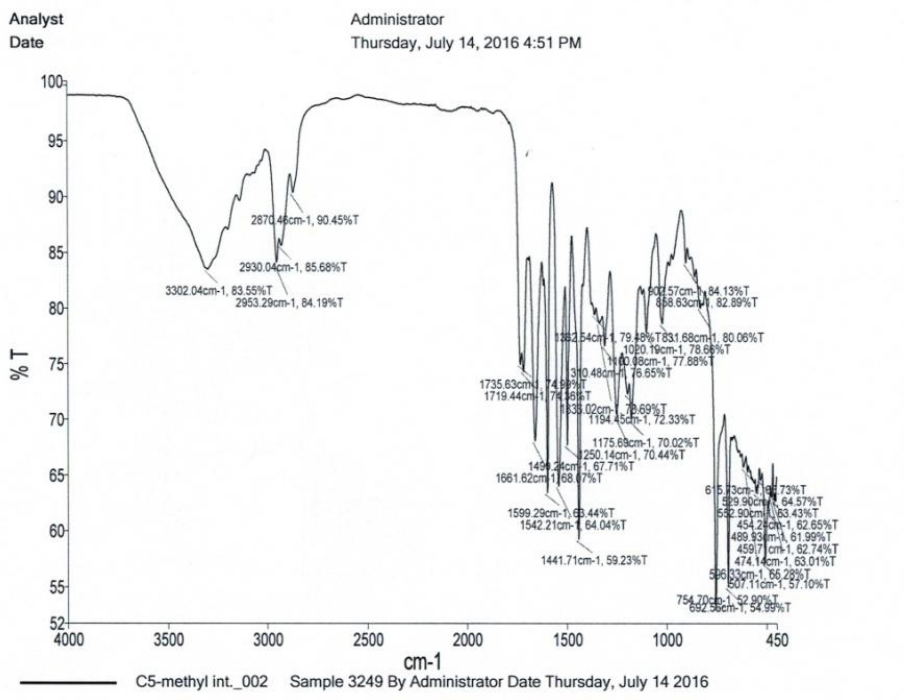

Figure C.10. IR spectrum of **33a** using a Perkin Elmer Spectrum Two ATR-FTIR.

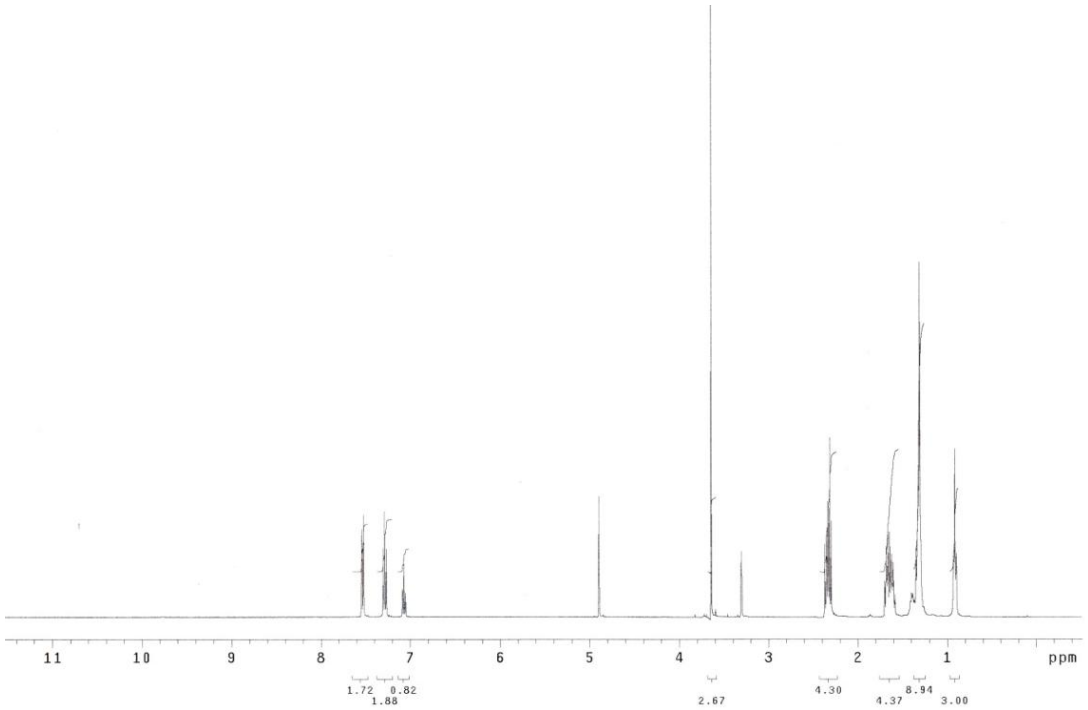

Figure C.11. ^{1}HNMR spectrum of **33b**.

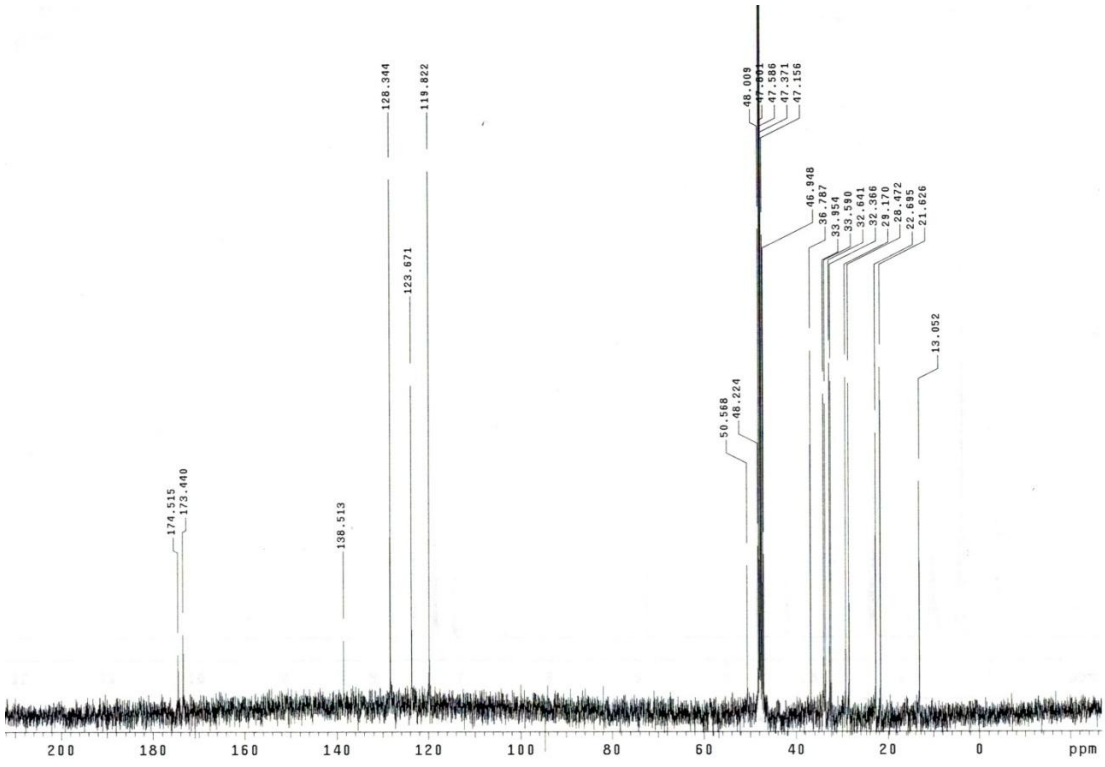

Figure C.12. ^{13}CNMR spectrum of **33b.**

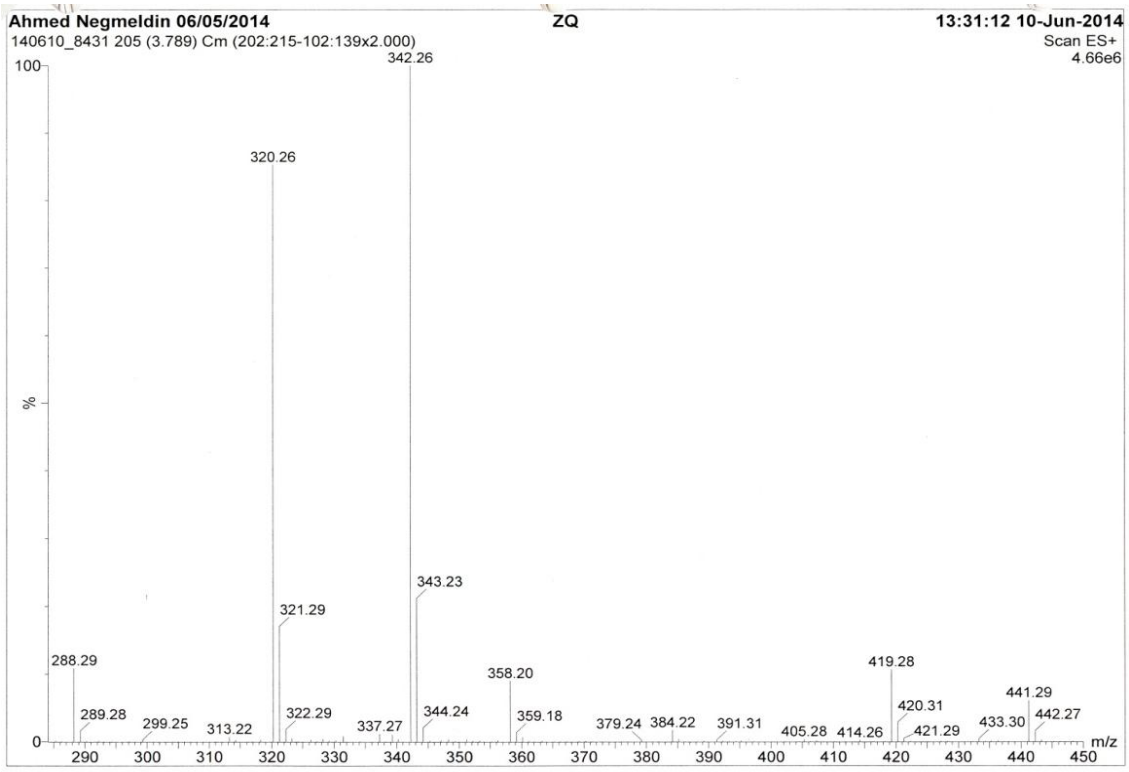

Figure C.13. Low resolution mass spectrum of **33b** using a Waters ZQ LC-SQMS instrument.

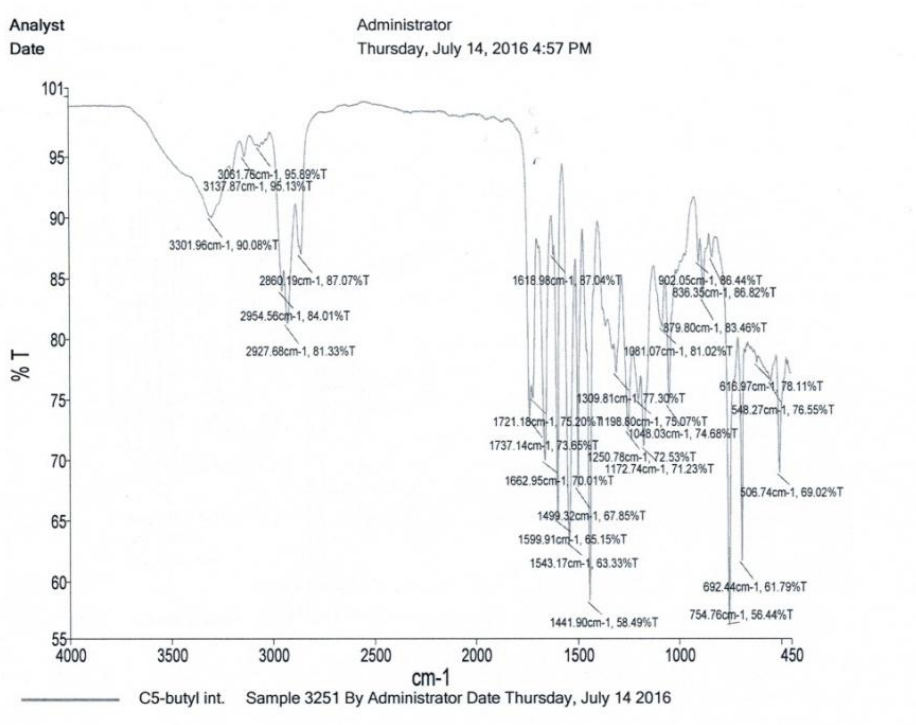

Figure C.14. IR spectrum of **33b** using a Perkin Elmer Spectrum Two ATR-FTIR.

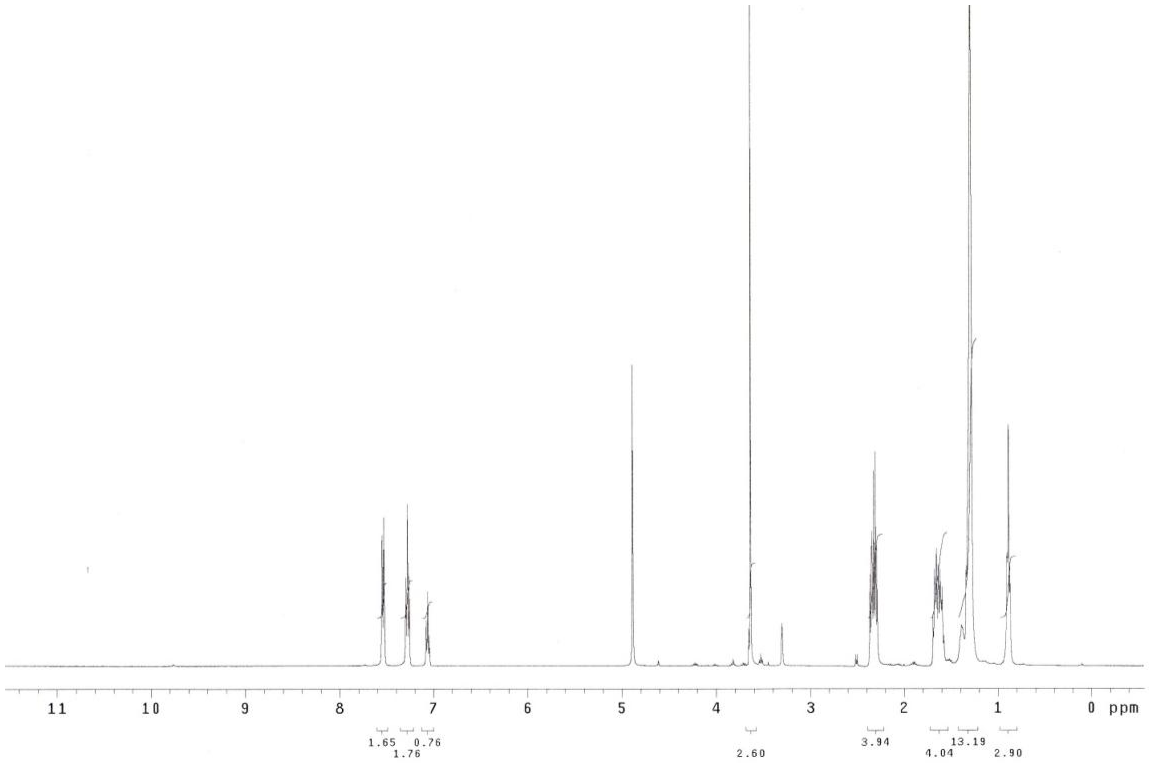

Figure C.15. ^{1}HNMR spectrum of **33c**.

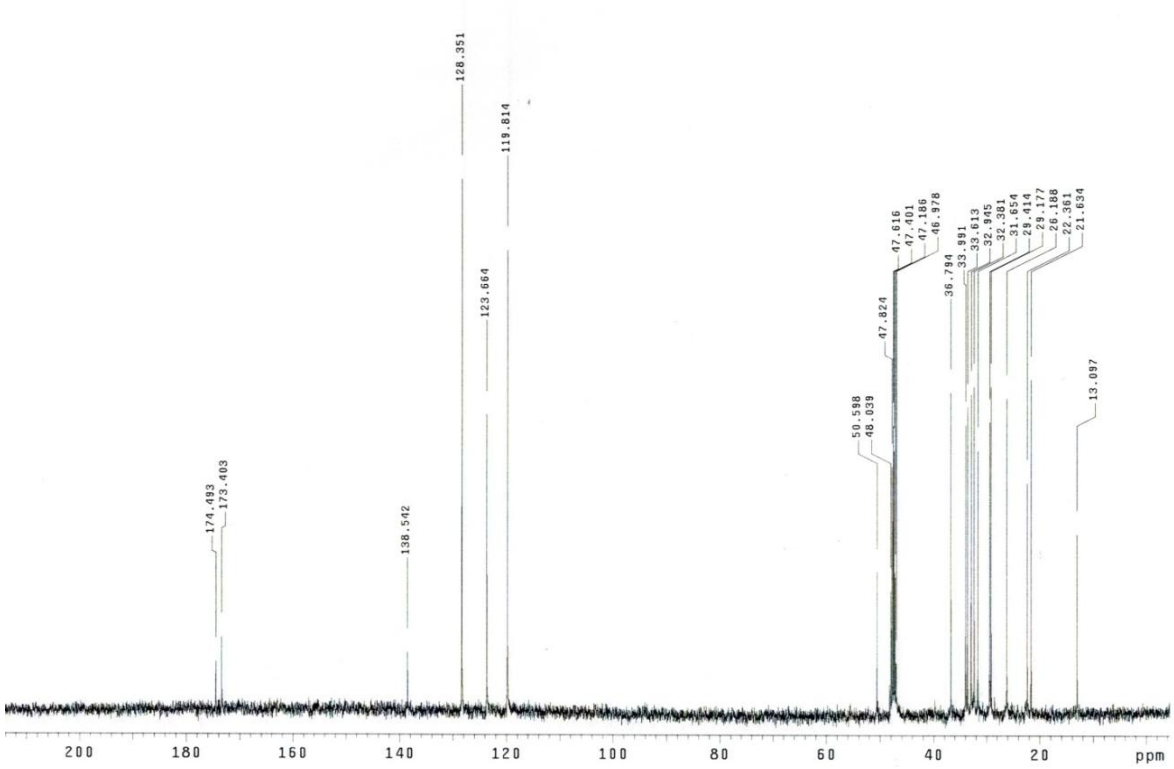

Figure C.16. ^{13}CNMR spectrum of **33c**.

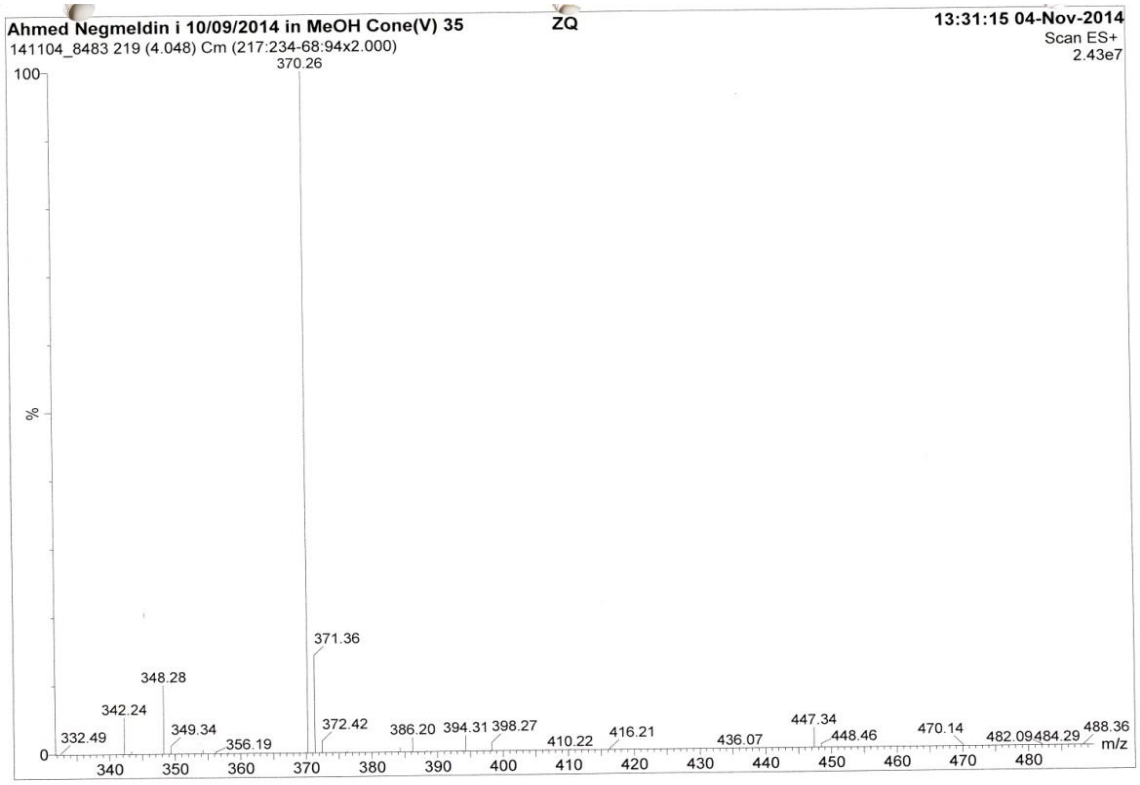

Figure C.17. Low resolution mass spectrum of **33c** using a Waters ZQ LC-SQMS instrument.

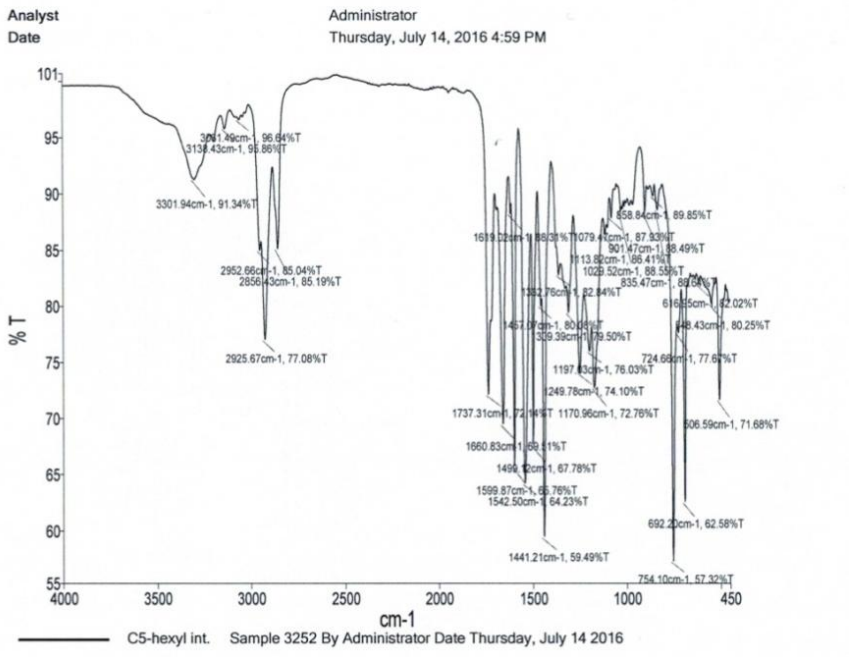

Figure C.18. IR spectrum of **33c** using a Perkin Elmer Spectrum Two ATR-FTIR.

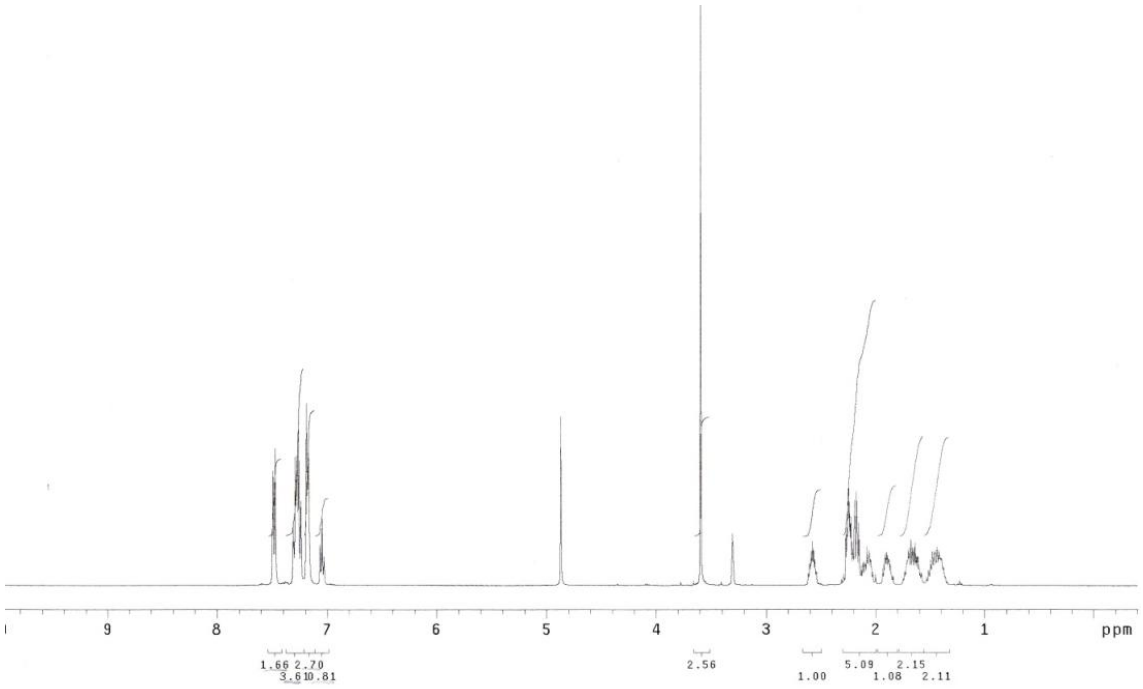

Figure C.19. [1]HNMR spectrum of **33d**.

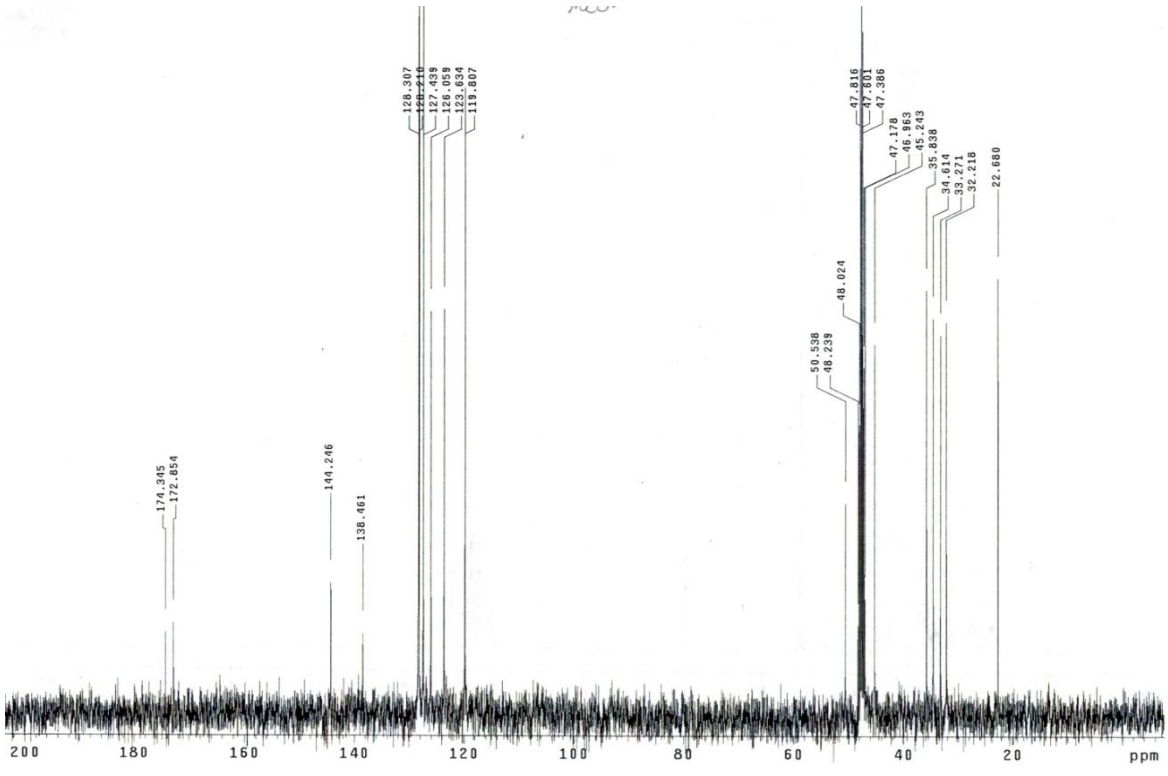

Figure C.20. [13]CNMR spectrum of **33d**.

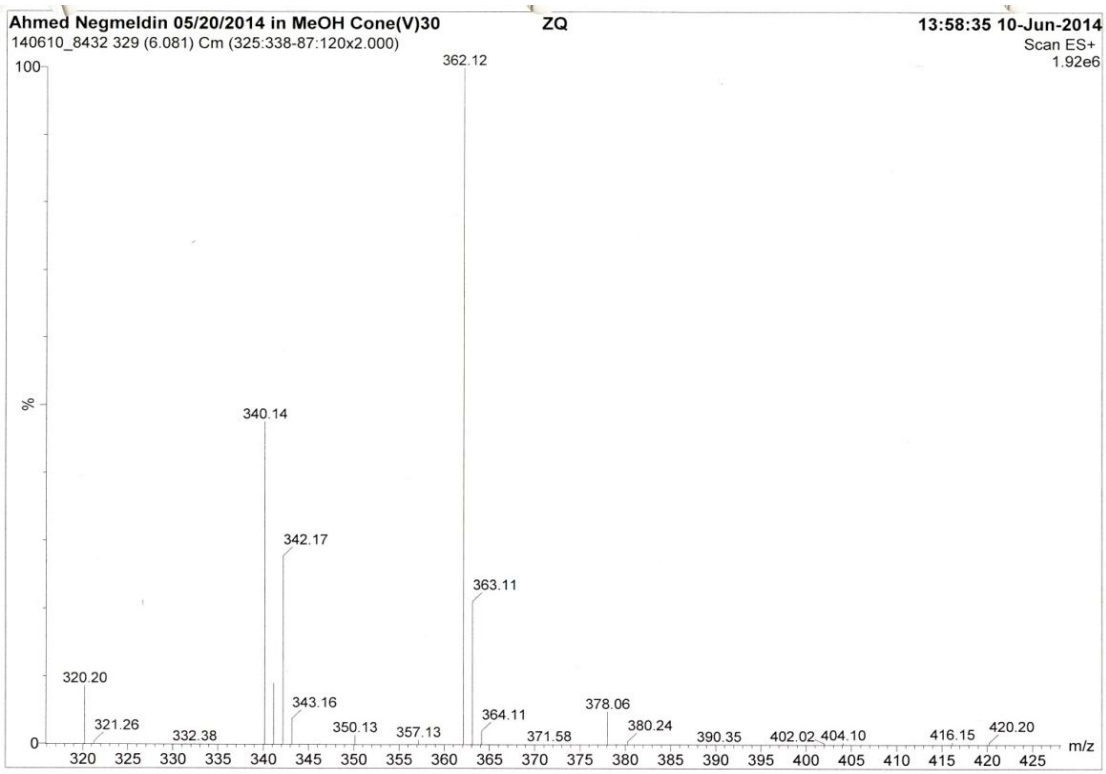

Figure C.21. Low resolution mass spectrum of **33d** using a Waters ZQ LC-SQMS instrument.

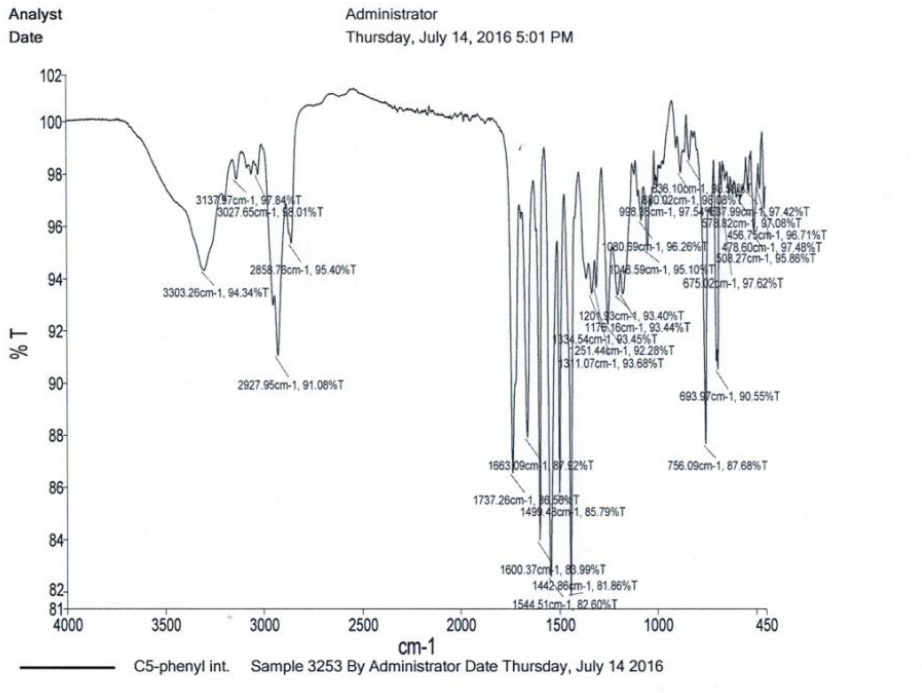

Figure C.22. IR spectrum of **33d** using a Perkin Elmer Spectrum Two ATR-FTIR.

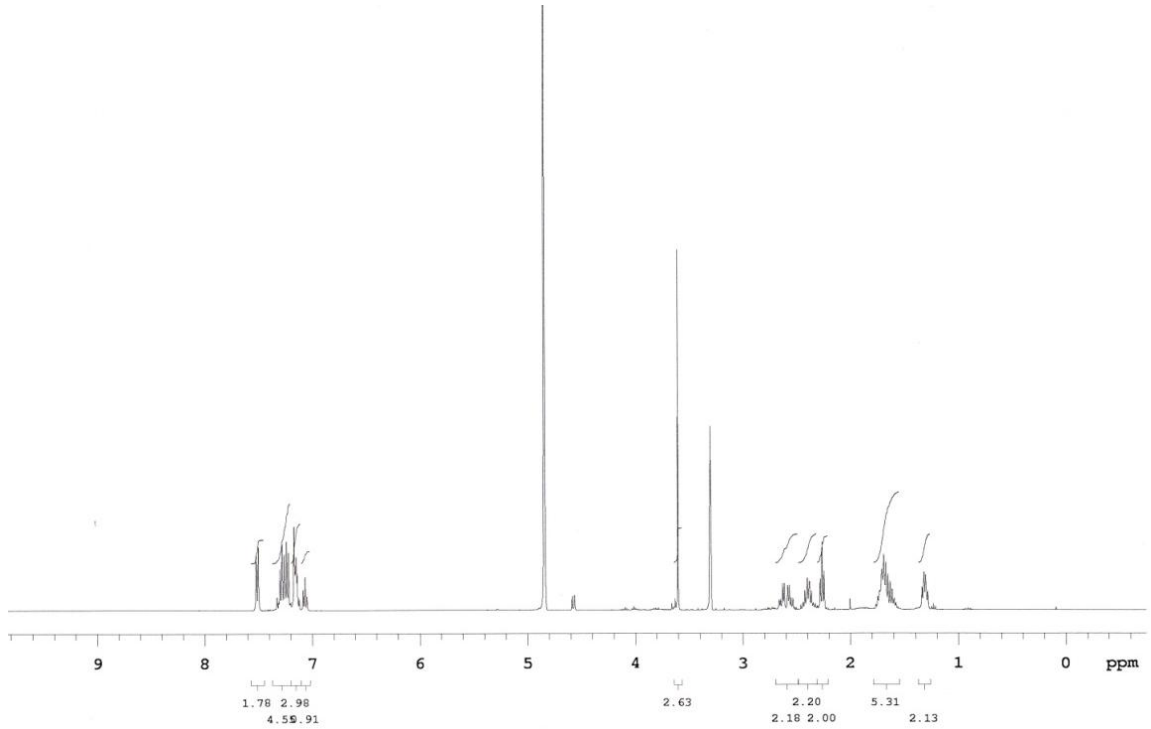

Figure C.23. ^{1}HNMR spectrum of **33e**.

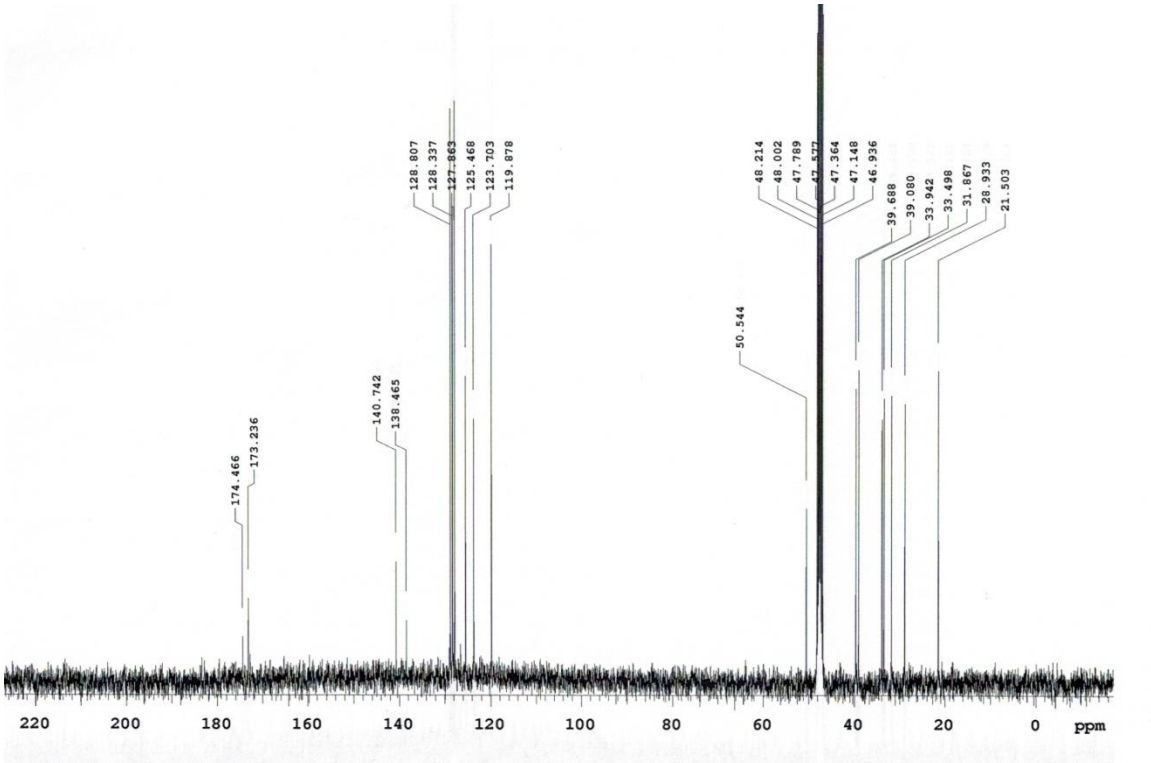

Figure C.24. ^{13}CNMR spectrum of **33e**.

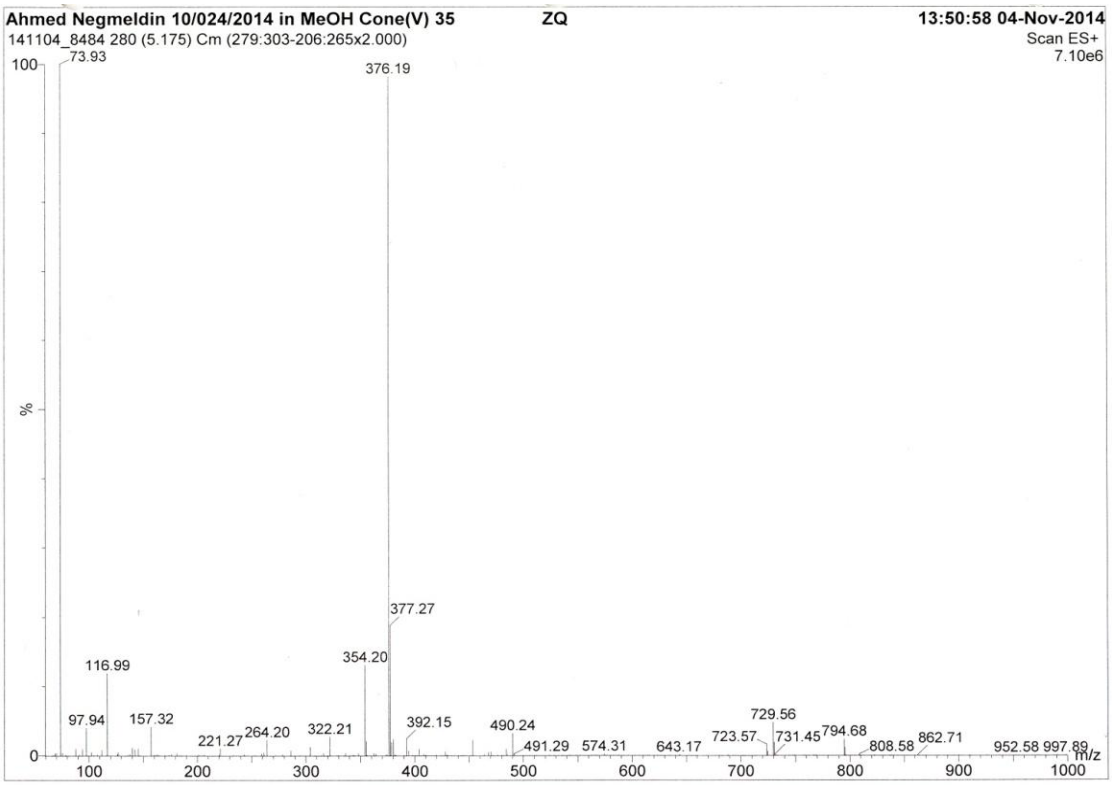

Figure C.25. Low resolution mass spectrum of **33e** using a Waters ZQ LC-SQMS instrument.

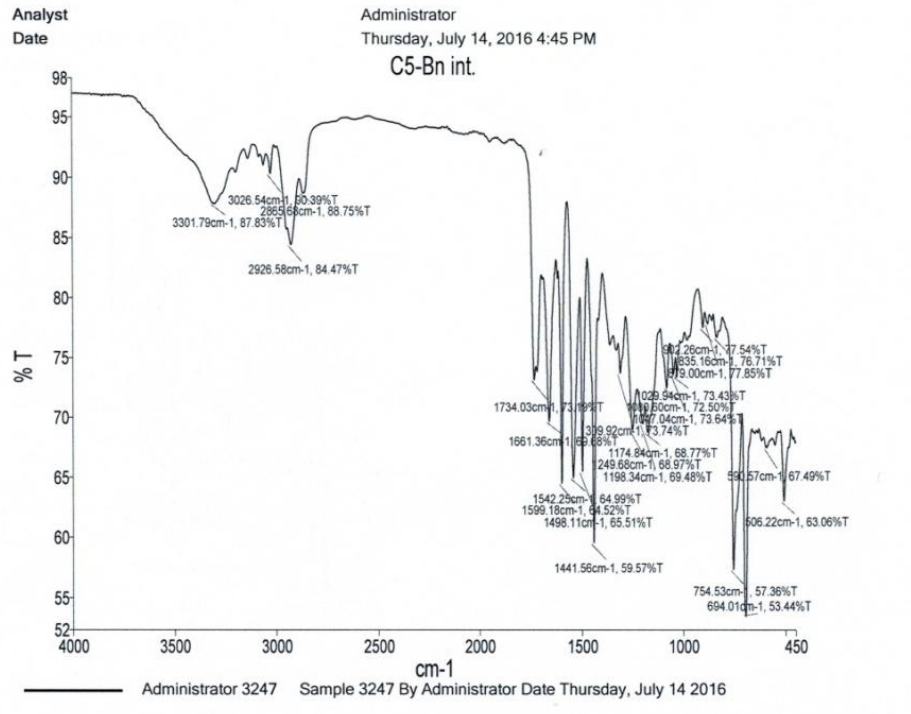

Figure C.26. IR spectrum of **33e** using a Perkin Elmer Spectrum Two ATR-FTIR.

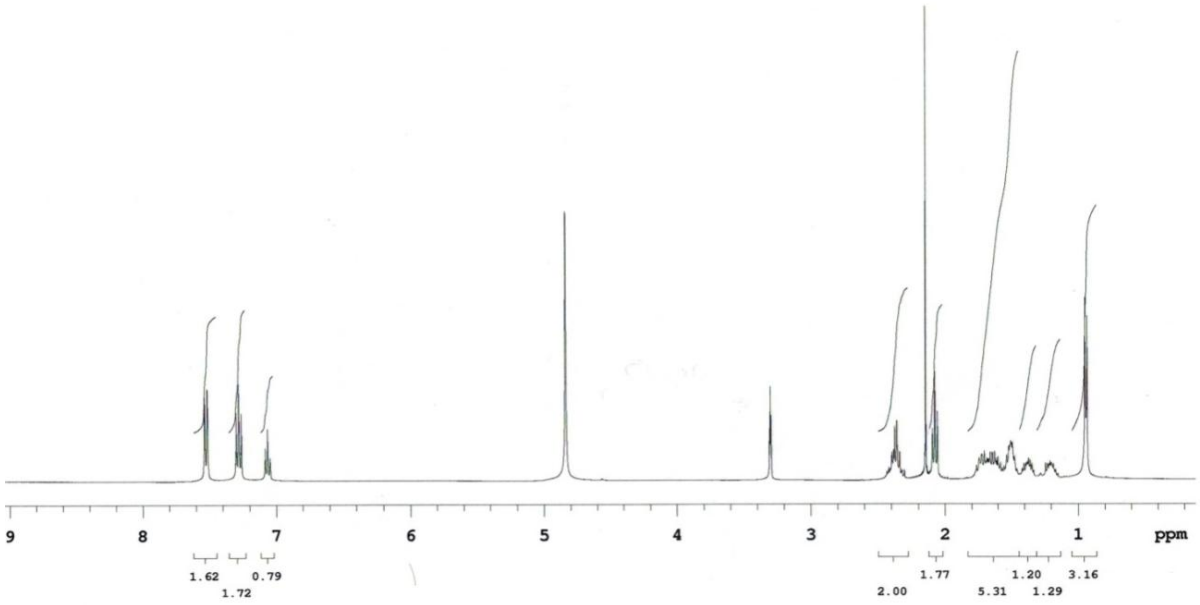

Figure C.27. ^{1}HNMR spectrum of **34a** in CD_3OD in the presence of trace amounts of acetone (2.15 ppm).[124]

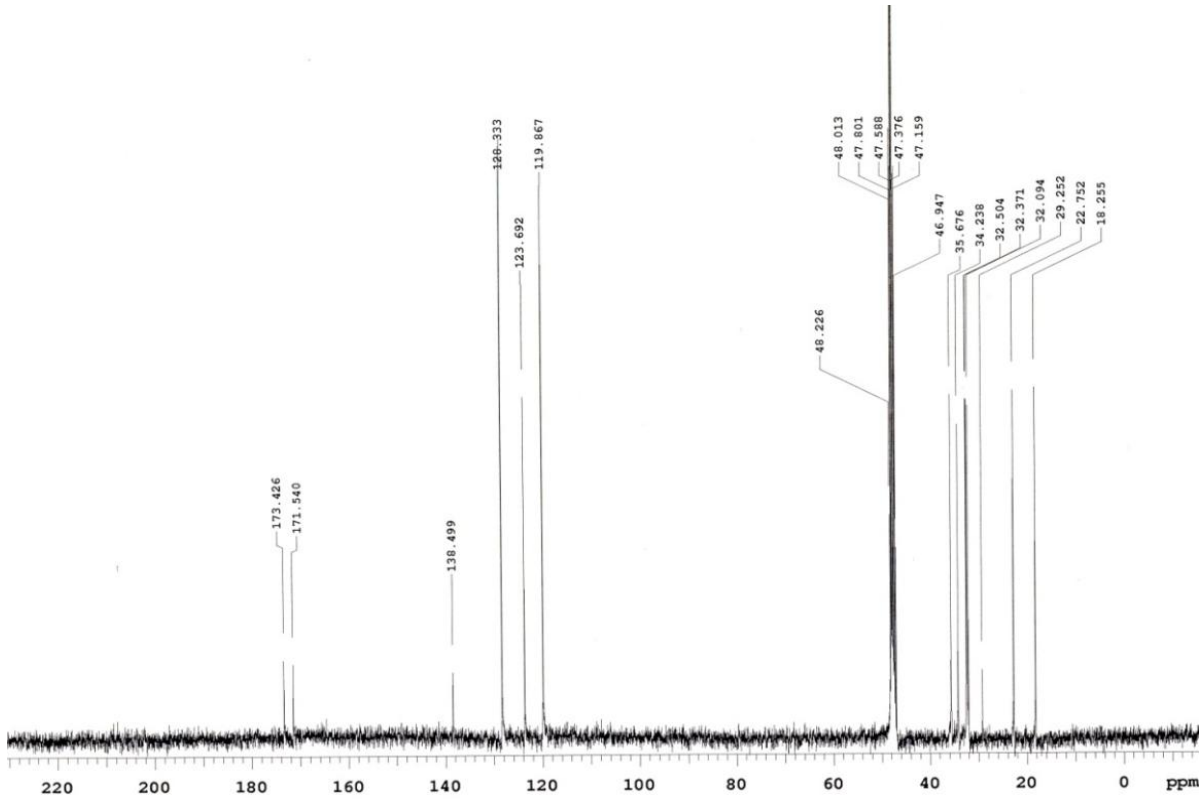

Figure C.28. ^{13}CNMR spectrum of **34a** in presence of trace amount of acetone (29.25 ppm).[124]

Elemental Composition Report **Page 1**

Single Mass Analysis
Tolerance = 5.0 PPM / DBE: min = -1.5, max = 100.0
Element prediction: Off
Number of isotope peaks used for i-FIT = 6

Monoisotopic Mass, Even Electron Ions
409 formula(e) evaluated with 1 results within limits (all results (up to 1000) for each mass)
Elements Used:
C: 15-15 H: 0-50 N: 0-50 O: 0-50 Na: 0-1
161209_1 192 (3.550) Cm ((184:222+130:151)) C5-methyl SAHA (V) 50
LCT Premier KD128
TOF MS ES+

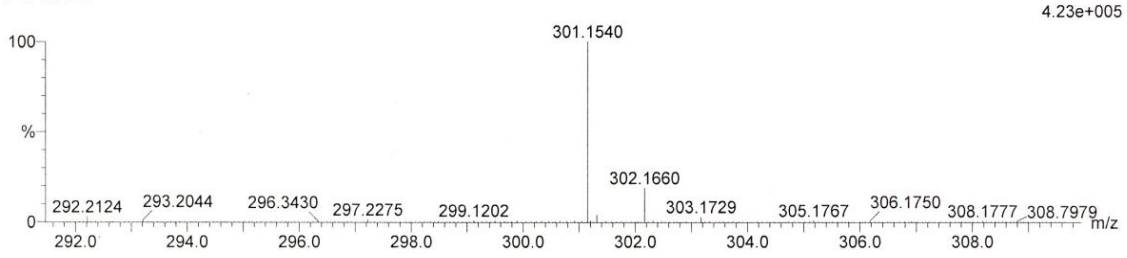

Minimum:				-1.5			
Maximum:		3.0	5.0	100.0			
Mass	Calc. Mass	mDa	PPM	DBE	i-FIT	i-FIT (Norm)	Formula
301.1540	301.1528	1.2	4.0	5.5	769.3	0.0	C15 H22 N2 O3 Na

Figure C.29. High resolution mass spectrum of **34a** using a Waters LCT-MS premier TOF instrument.

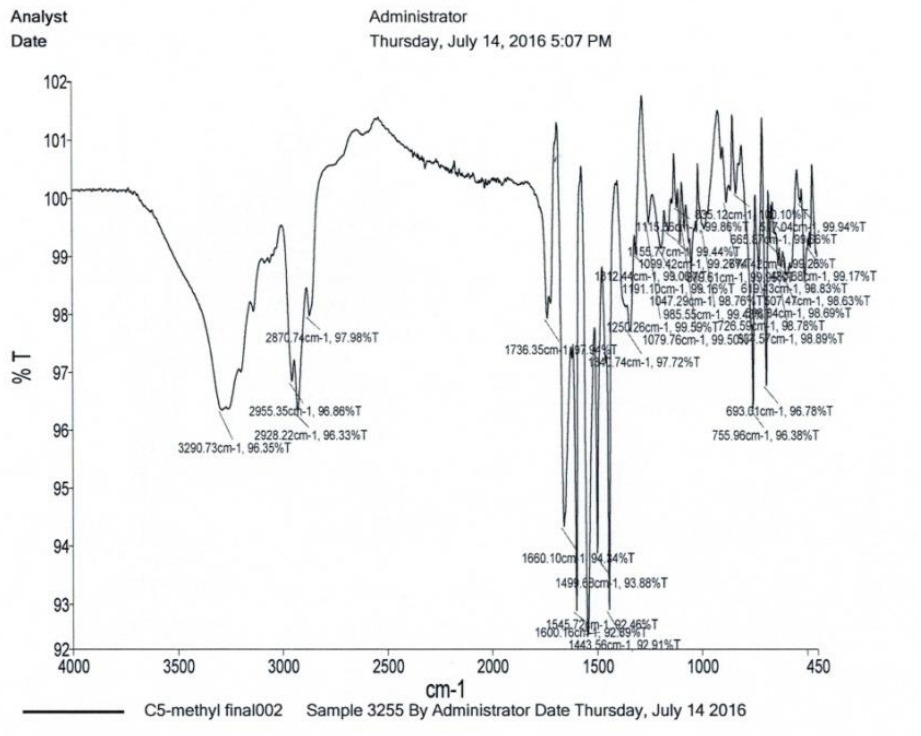

Figure C.30. IR spectrum of **34a** using a Perkin Elmer Spectrum Two ATR-FTIR.

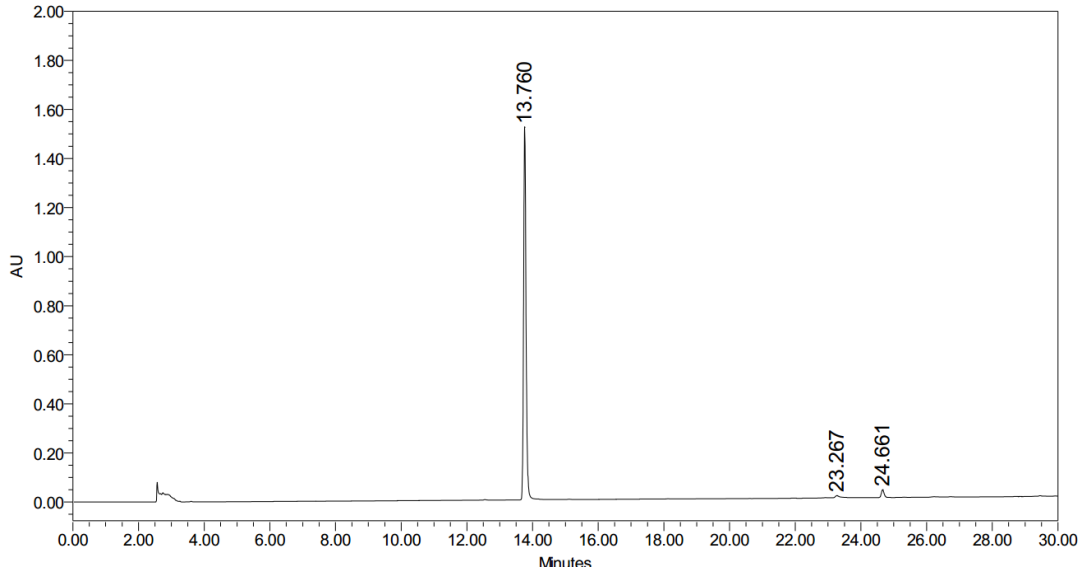

	RT	Area	% Area	Height
1	13.760	7830972	97.08	1520118
2	23.267	60686	0.75	7985
3	24.661	175204	2.17	31071

Figure C.31. HPLC spectrum taken at 254 nm of C5-methyl SAHA (**34a**). The peak at 13.760 is C5-methyl SAHA. The calculated area and height under each peak, along with % area, is shown in the table below the spectrum.

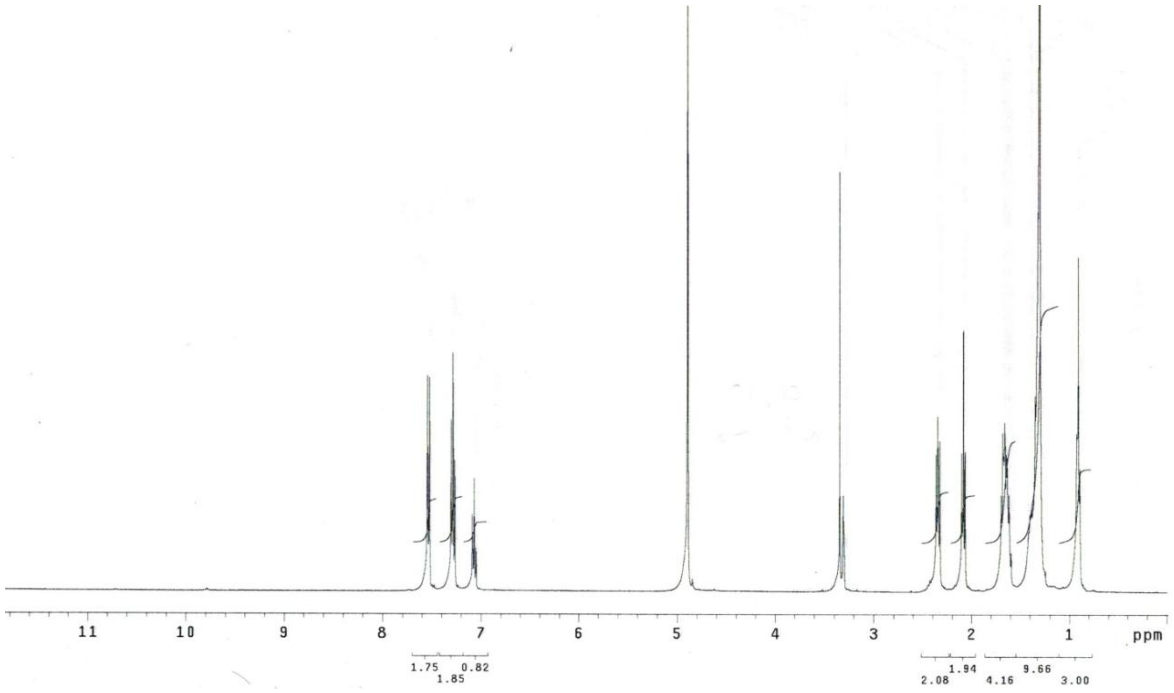

Figure C.32. ^{1}HNMR spectrum of **34b**.

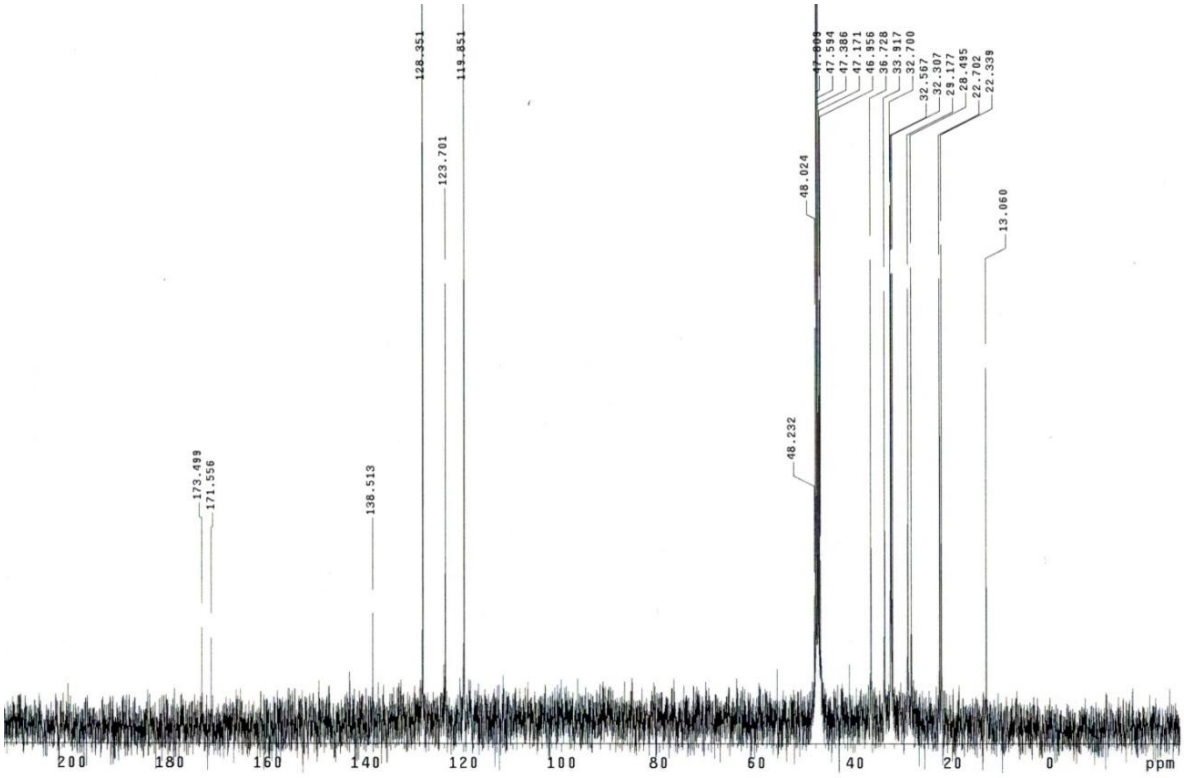

Figure C.33. ^{13}CNMR spectrum of **34b**.

Elemental Composition Report **Page 1**

Single Mass Analysis
Tolerance = 50.0 PPM / DBE: min = -1.5, max = 100.0
Element prediction: Off
Number of isotope peaks used for i-FIT = 6

Monoisotopic Mass, Even Electron Ions
7 formula(e) evaluated with 1 results within limits (all results (up to 1000) for each mass)
Elements Used:
C: 18-18 H: 0-28 N: 2-2 O: 0-3 Na: 0-1
161209_1 1446 (26.731) Cm (1445:1454) C5-butyl SAHA
LCT Premier KD128
TOF MS ES+

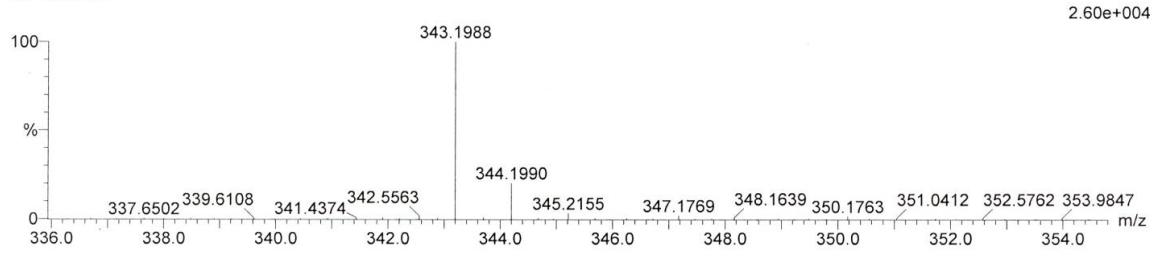

Minimum:				-1.5			
Maximum:		3.0	50.0	100.0			
Mass	Calc. Mass	mDa	PPM	DBE	i-FIT	i-FIT (Norm)	Formula
343.1988	343.1998	-1.0	-2.9	5.5	116.7	0.0	C18 H28 N2 O3 Na

Figure C.34. High resolution mass spectrum of **34b** using a Waters LCT-MS premier TOF instrument.

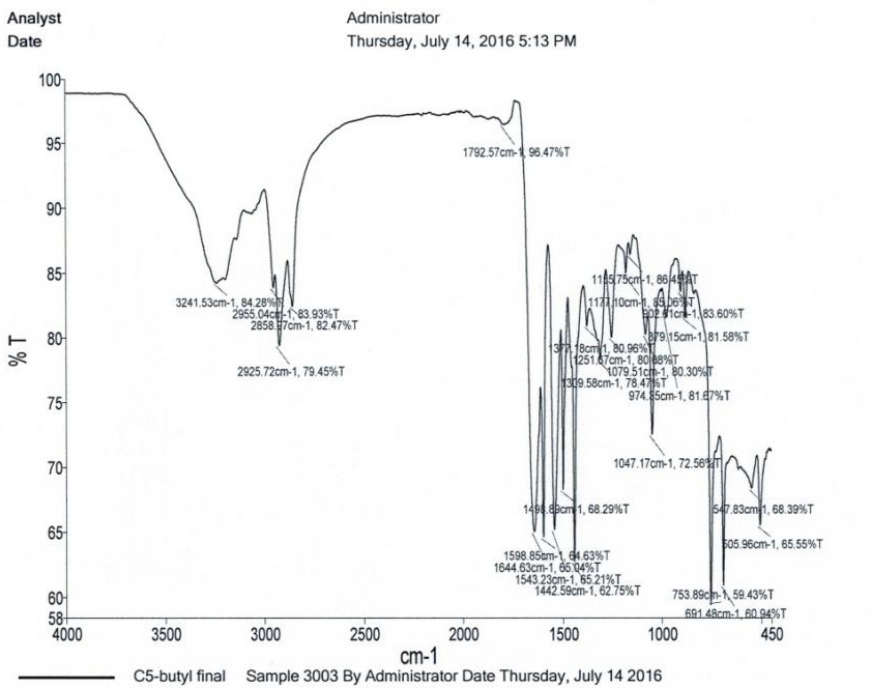

Figure C.35. IR spectrum of **34b** using a Perkin Elmer Spectrum Two ATR-FTIR.

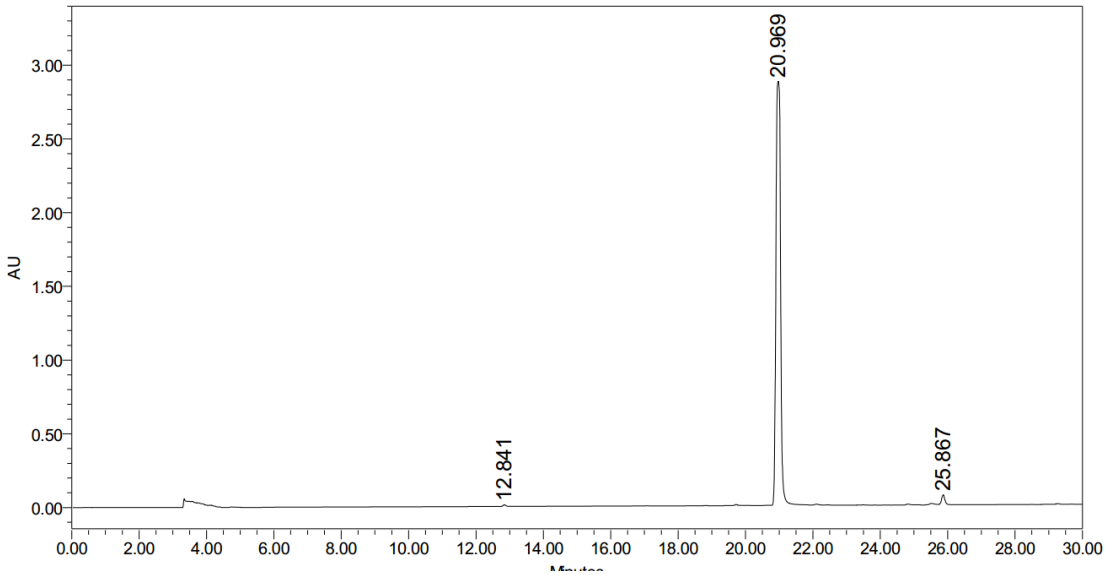

	RT	Area	% Area	Height
1	12.841	64214	0.23	11343
2	20.969	27475990	98.03	2876434
3	25.867	486640	1.74	68194

Figure C.36. HPLC spectrum taken at 254 nm of C5-butyl SAHA (**34b**). The peak at 20.969 is C5-butyl SAHA. The calculated area and height under each peak, along with % area, is shown in the table below the spectrum.

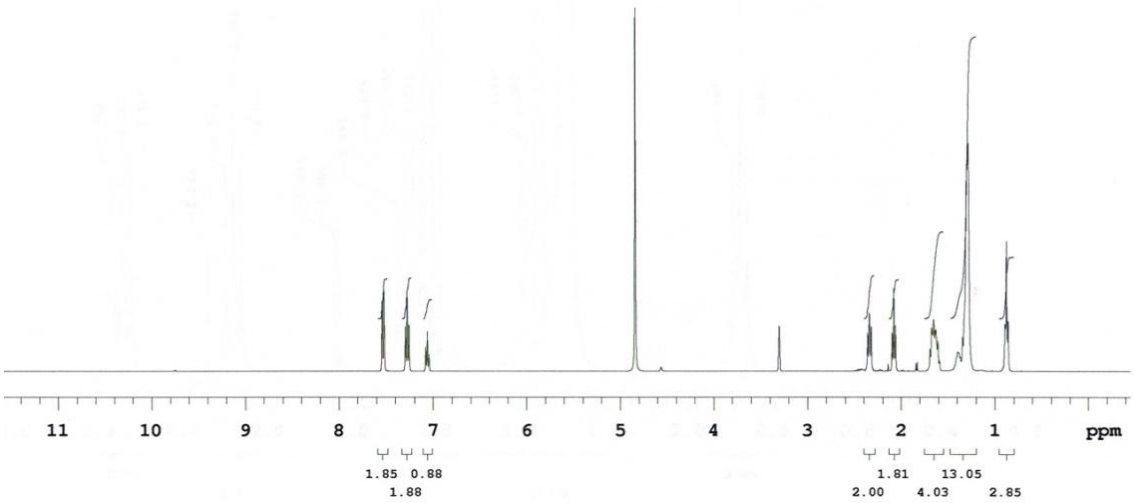

Figure C.37. [1]HNMR spectrum of **34c**.

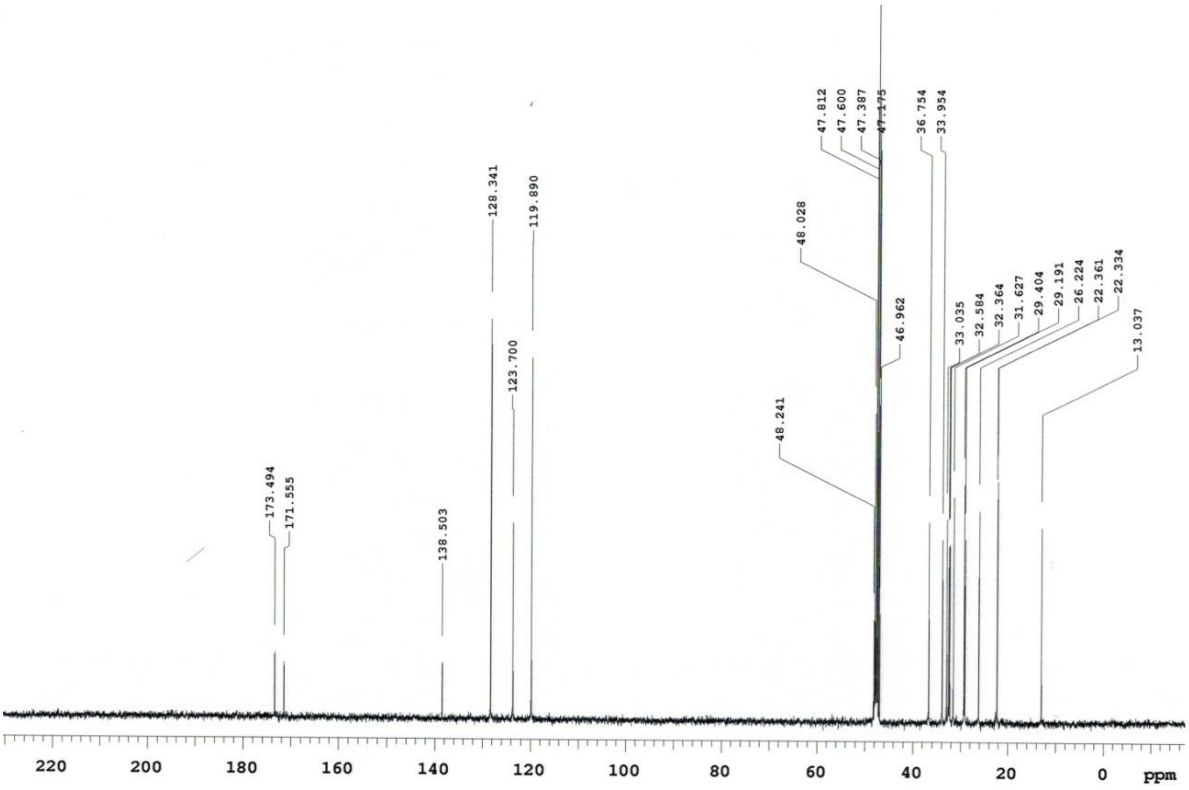

Figure C.38. [13]CNMR spectrum of **34c**.

Elemental Composition Report **Page 1**

Single Mass Analysis
Tolerance = 50.0 PPM / DBE: min = -1.5, max = 100.0
Element prediction: Off
Number of isotope peaks used for i-FIT = 6

Monoisotopic Mass, Even Electron Ions
7 formula(e) evaluated with 1 results within limits (all results (up to 1000) for each mass)
Elements Used:
C: 20-20 H: 0-32 N: 2-2 O: 0-3 Na: 0-1

161209_1 2261 (41.796) C5-hexyl SAHA
LCT Premier KD128
TOF MS ES+

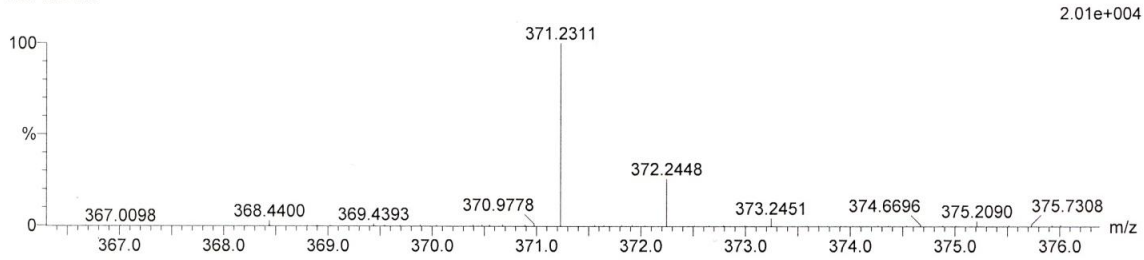

Minimum:				-1.5			
Maximum:		3.0	50.0	100.0			
Mass	Calc. Mass	mDa	PPM	DBE	i-FIT	i-FIT (Norm)	Formula
371.2311	371.2311	0.0	0.0	5.5	181.8	0.0	C20 H32 N2 O3 Na

Figure C.39. High resolution mass spectrum of **34c** using a Waters LCT-MS premier TOF instrument.

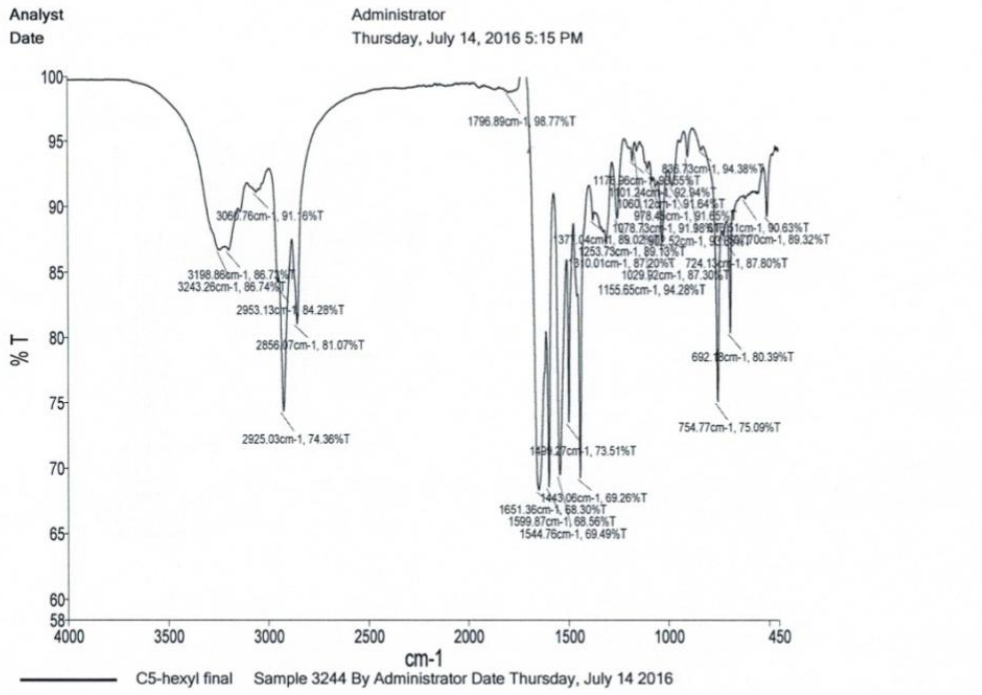

Figure C.40. IR spectrum of **34c** using a Perkin Elmer Spectrum Two ATR-FTIR.

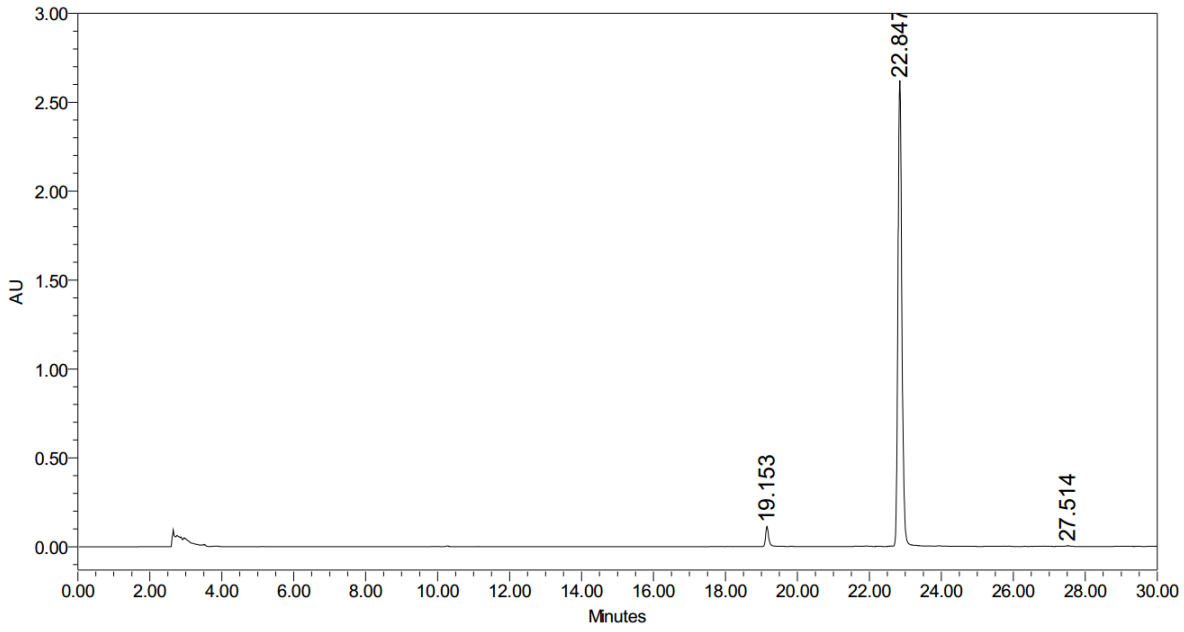

	RT	Area	% Area	Height
1	19.153	645449	3.16	110630
2	22.847	19764566	96.72	2617298
3	27.514	23863	0.12	3837

Figure C.41. HPLC spectrum taken at 254 nm of C5-hexyl SAHA (**34c**). The peak at 22.847 is C5-hexyl SAHA. The calculated area and height under each peak, along with % area, is shown in the table below the spectrum.

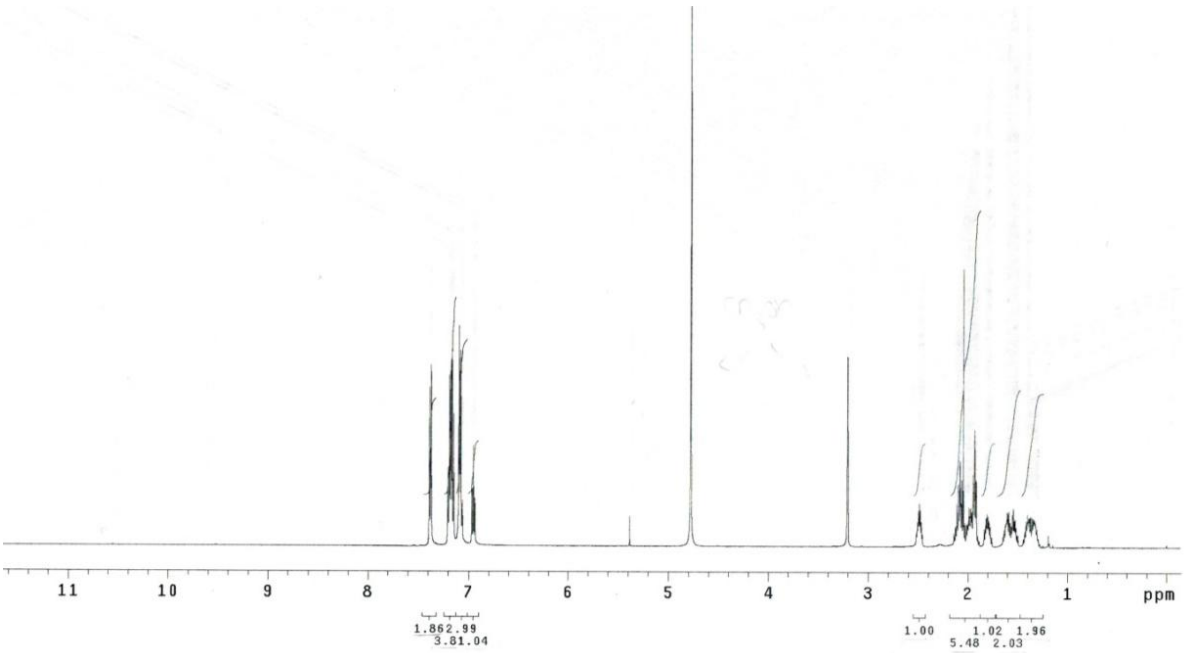

Figure C.42. ^{1}HNMR spectrum of **34d**.

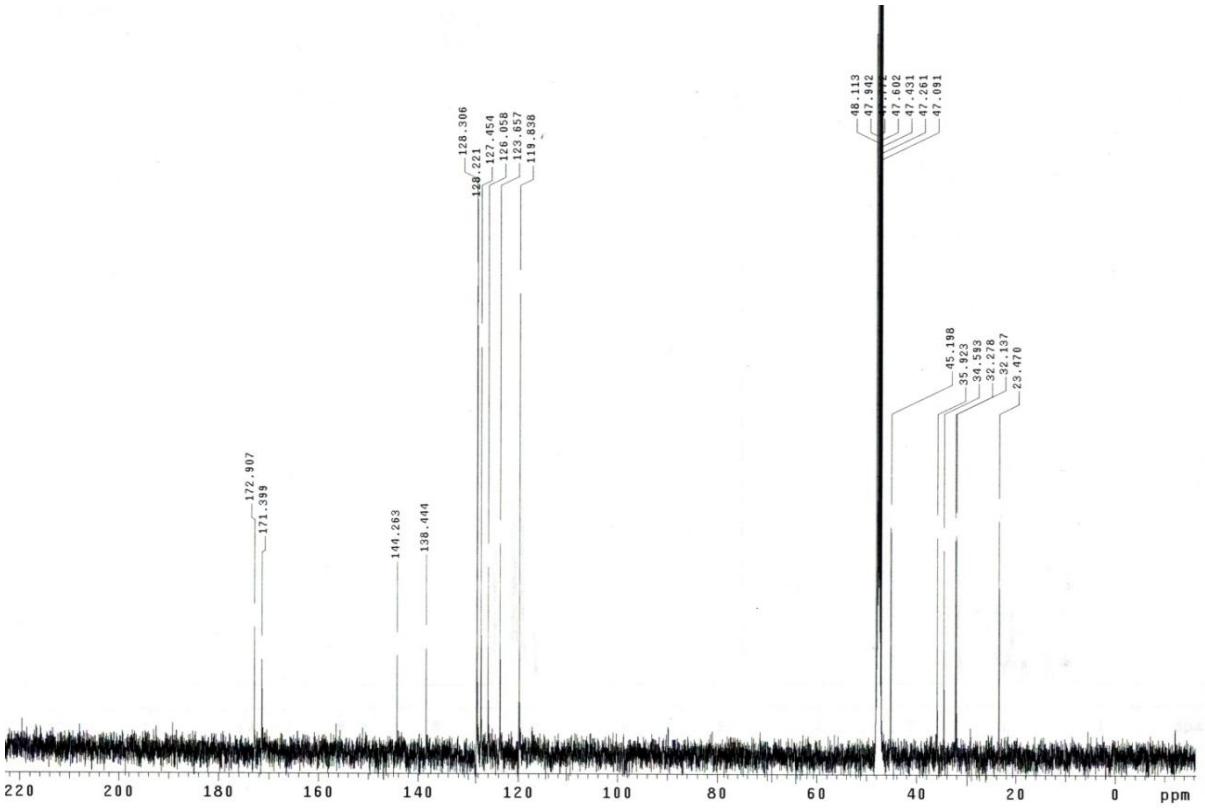

Figure C.43. ^{13}CNMR spectrum of **34d**.

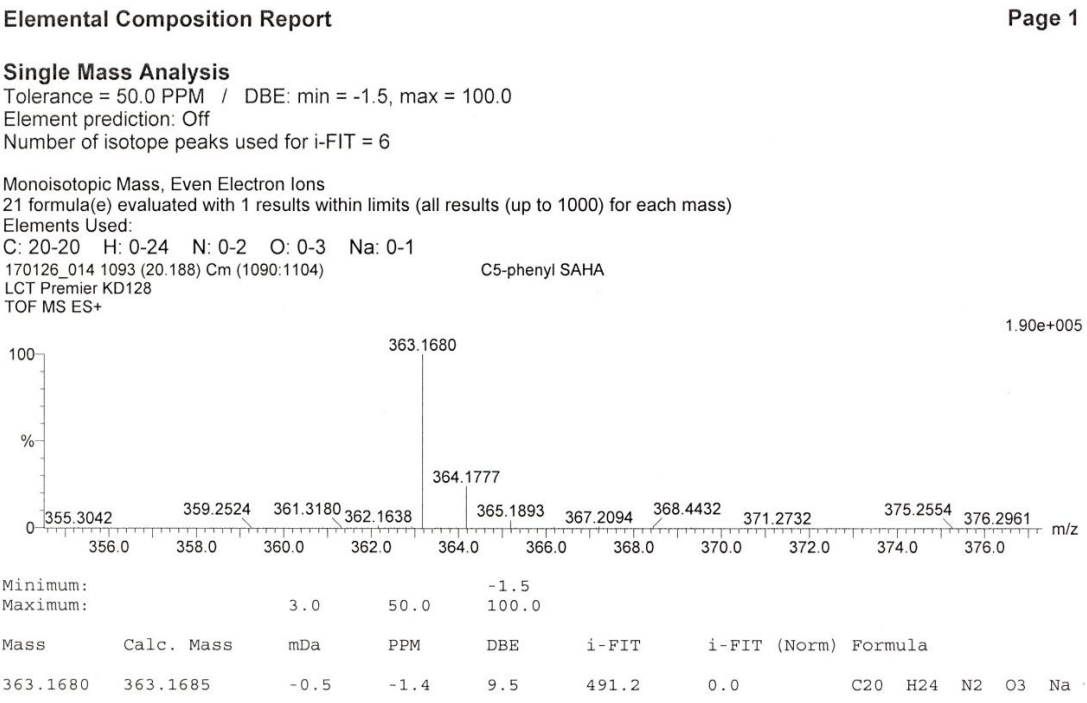

Figure C.44. High resolution mass spectrum of **34d** using a Waters LCT-MS premier TOF instrument.

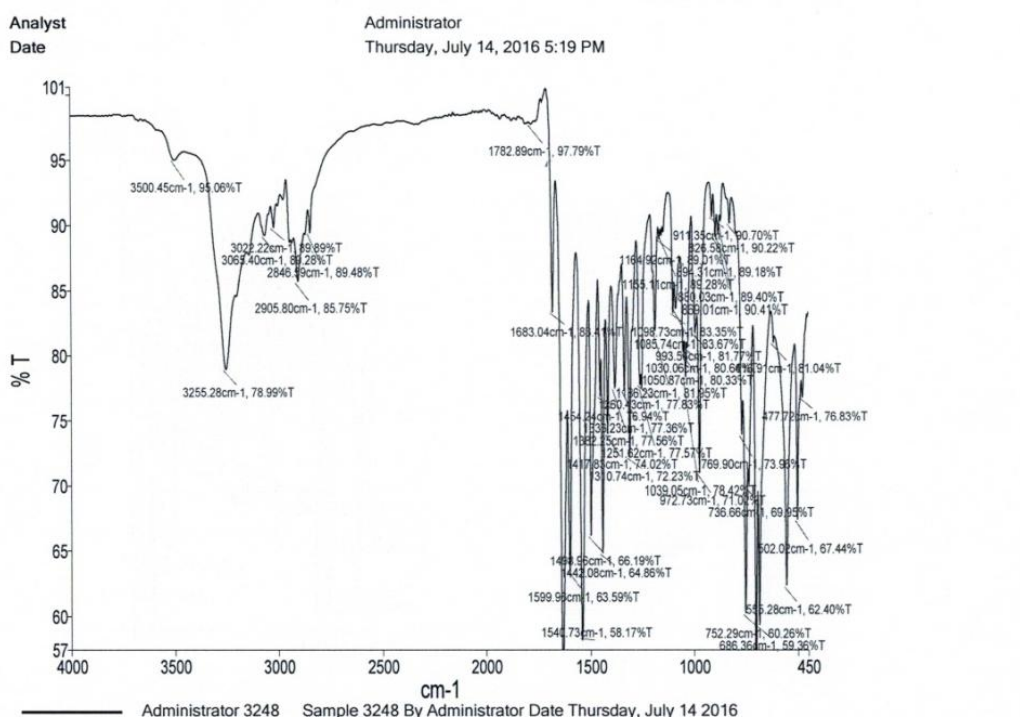

Figure C.45. IR spectrum of **34d** using a Perkin Elmer Spectrum Two ATR-FTIR.

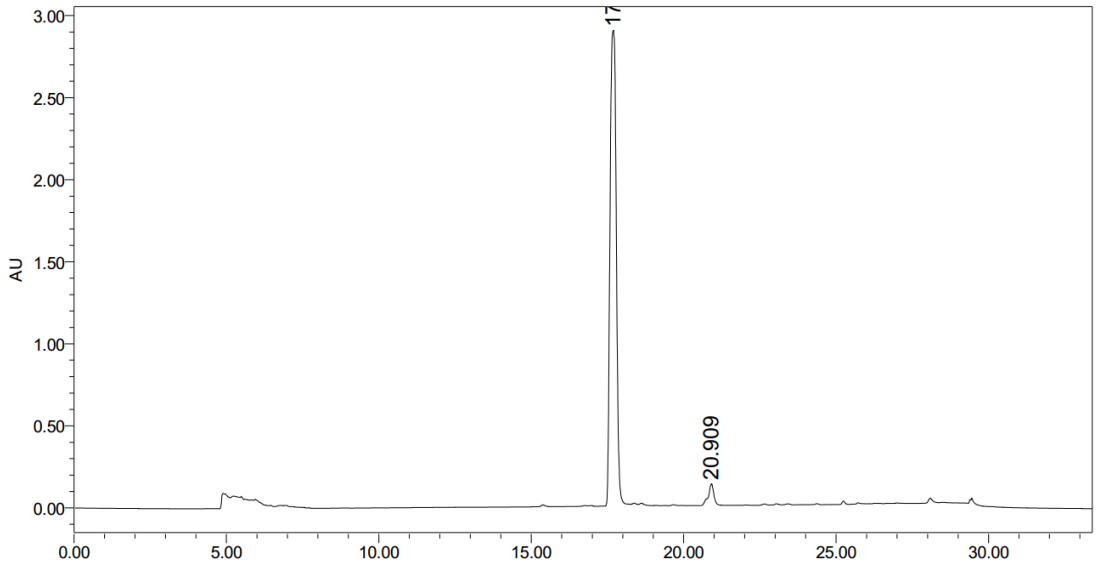

	RT	Area	% Area	Height
1	17.693	41437360	95.97	2898800
2	20.909	1741746	4.03	132705

Figure C.46. HPLC spectrum taken at 254 nm of C5-phenyl SAHA (**34d**). The peak at 17.693 is C5-phenyl SAHA. The calculated area and height under each peak, along with % area, is shown in the table below the spectrum.

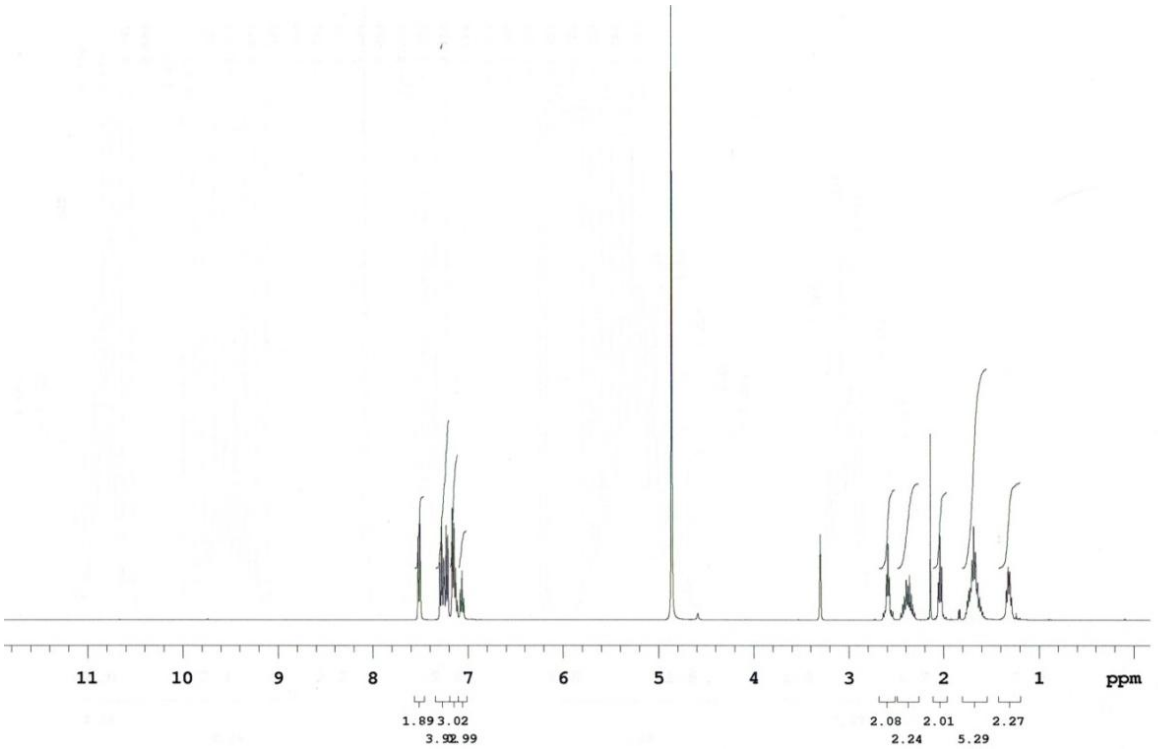

Figure C.47. ^{1}HNMR spectrum of **34e**.

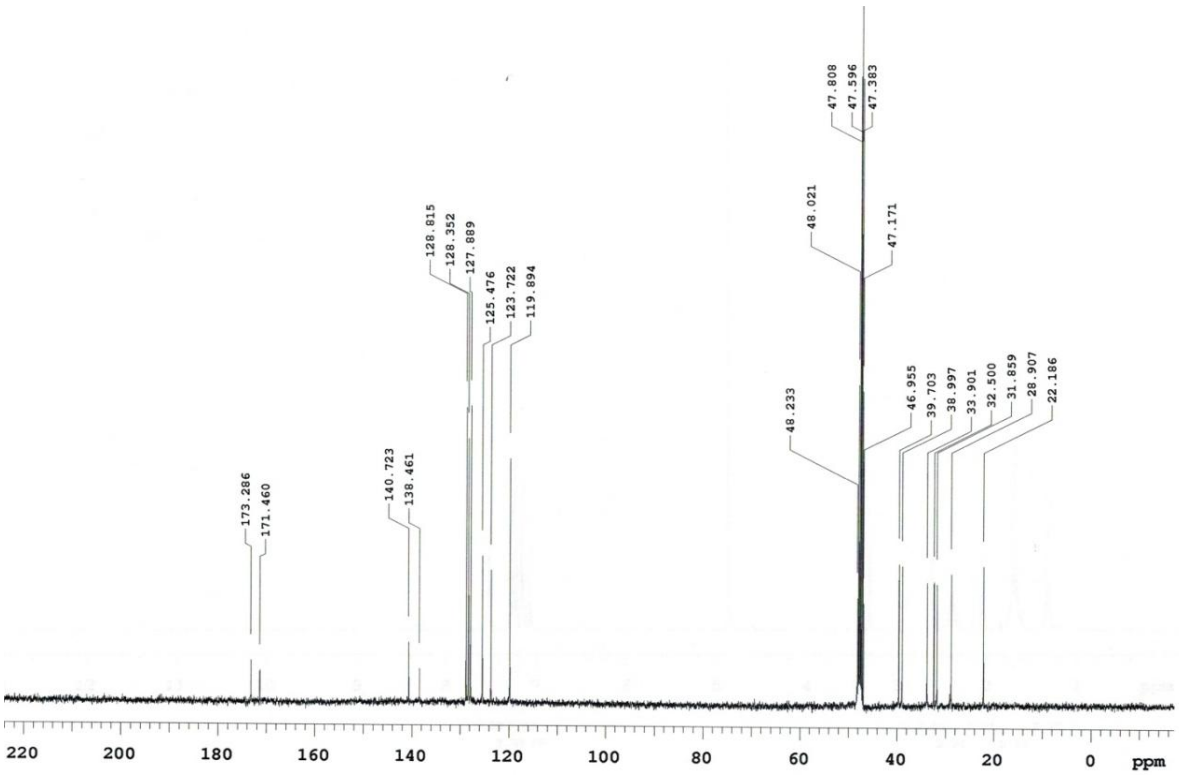

Figure C.48. ^{13}CNMR spectrum of **34e**.

Elemental Composition Report **Page 1**

Single Mass Analysis
Tolerance = 50.0 PPM / DBE: min = -1.5, max = 100.0
Element prediction: Off
Number of isotope peaks used for i-FIT = 6

Monoisotopic Mass, Even Electron Ions
6 formula(e) evaluated with 1 results within limits (all results (up to 1000) for each mass)
Elements Used:
C: 21-21 H: 0-26 N: 2-2 O: 0-3 Na: 0-1
170126_014 1654 (30.559) Cm (1654:1655) C5-benzyl SAHA
LCT Premier KD128
TOF MS ES+

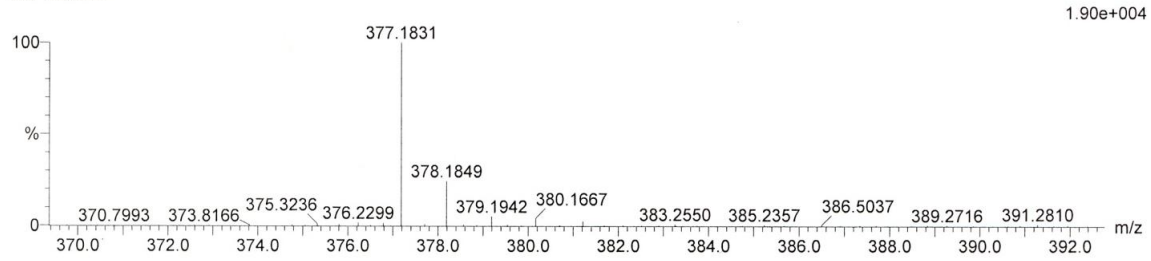

Minimum:				-1.5			
Maximum:		3.0	50.0	100.0			
Mass	Calc. Mass	mDa	PPM	DBE	i-FIT	i-FIT (Norm)	Formula
377.1831	377.1841	-1.0	-2.7	9.5	106.1	0.0	C21 H26 N2 O3 Na

Figure C.49. High resolution mass spectrum of **34e** using a Waters LCT-MS premier TOF instrument.

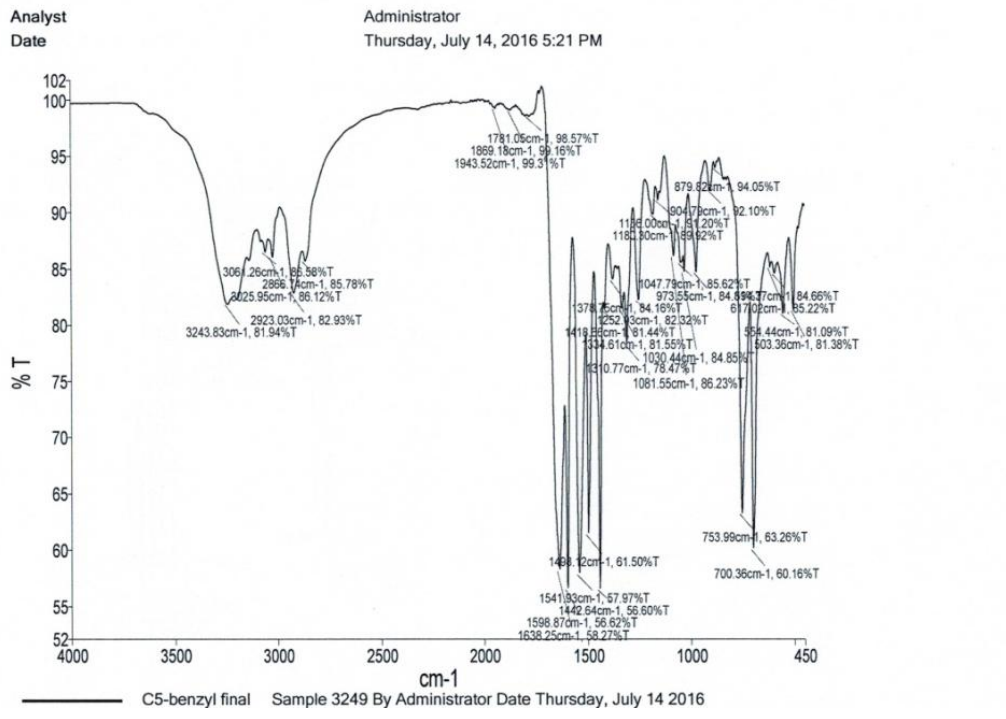

Figure C.50. IR spectrum of **34e** using a Perkin Elmer Spectrum Two ATR-FTIR.

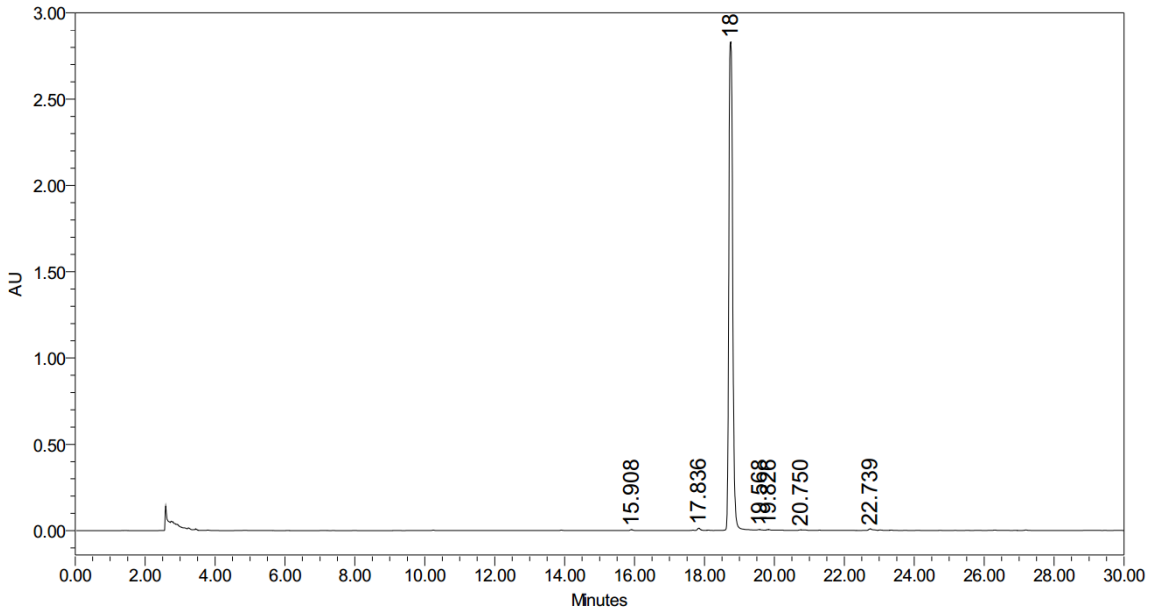

	RT	Area	% Area	Height
1	15.908	27014	0.12	4813
2	17.836	76472	0.34	12679
3	18.748	21901734	98.72	2831067
4	19.568	42470	0.19	4882
5	19.826	33684	0.15	4946
6	20.750	29145	0.13	2676
7	22.739	74733	0.34	8986

Figure C.51. HPLC spectrum taken at 254 nm of C5-benzyl SAHA (**34e**). The peak at 18.748 is C5-benzyl SAHA. The calculated area and height under each peak, along with % area, is shown in the table below the spectrum.

C.2. *In vitro* screening with HeLa cell lysates and HDAC isoforms

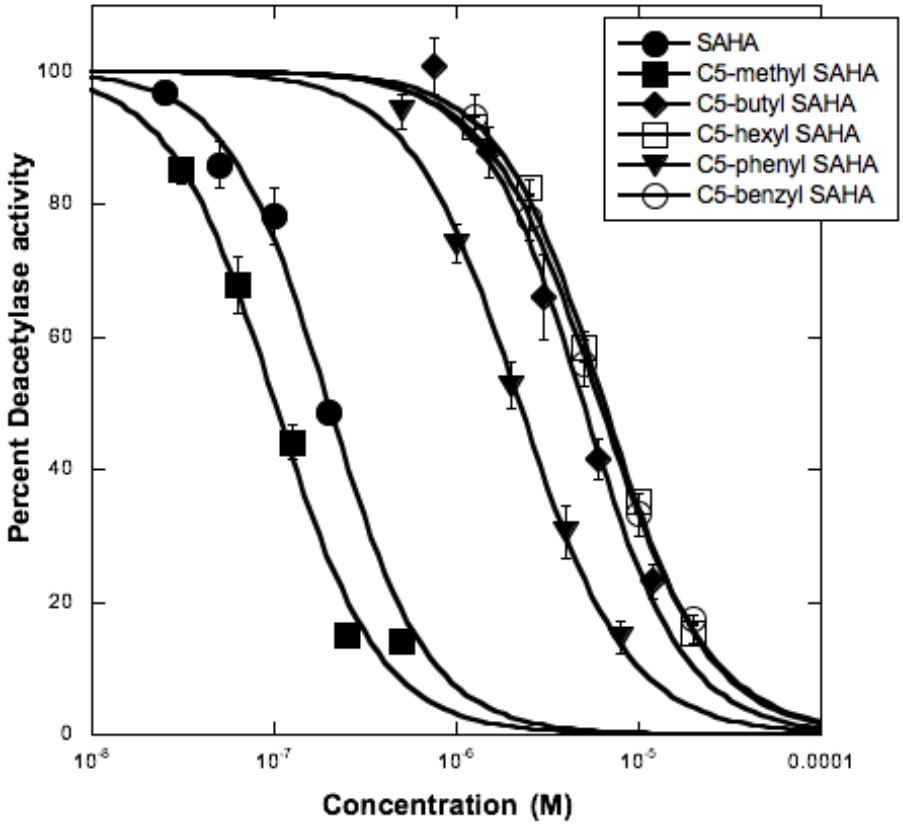

Figure C.52. Dose response curve of C5-modified SAHA analogs **34a-e** tested using the HDAC activity in HeLa cells lysates from three independent trials with error bars indicating standard error (see Table C.1). In some cases, the error bar is smaller than the marker size. Data were fit to the sigmoidal curve using KaleidaGraph 4.1.3 (Synergy Software) to determine the IC_{50}. The data are reported in Table 4.1.

Table C.1. Percent remaining HDAC activity after incubation of SAHA or C5-modified SAHA analogs **34a-e** with HeLa Lysates.[a]

	Deacetylase activity (%)					
Concentration (M)	SAHA	**34a** (methyl)	**34b** (butyl)	**34c**[93] (hexyl)	**34d** (phenyl)	**34e** (benzyl)
2.0×10^{-5}				15±2		17±1
1.2×10^{-5}			23±3			
1.0×10^{-5}				35±2		33±3
8.0×10^{-6}					15±2	
6.0×10^{-6}			42±3			
5.0×10^{-6}				58±2		56±4
4.0×10^{-6}					31±4	
3.0×10^{-6}			66±6			
2.5×10^{-6}				83±1		78±3
2.0×10^{-6}					53±3	
1.5×10^{-6}			88±4			
1.0×10^{-6}					74±3	
1.25×10^{-6}				92±2		93±4
7.5×10^{-7}			101±4			
5.0×10^{-7}		14±1			94±3	
2.5×10^{-7}		15±2				
2.0×10^{-7}	49±1					
1.25×10^{-7}		44±2				
1.0×10^{-7}	78±4					
6.25×10^{-8}		68±4				
5.0×10^{-8}	86±4					
3.13×10^{-8}		85±2				
2.5×10^{-8}	97±1					

[a] Mean percentage deacetylase activity and standard error of three trials are shown. This data is associated with Figure C.52 and Table 4.1.

Table C.2. Percent remaining deacetylase activity after incubation of a single concentration of each C5-modified SAHA analog with HDAC1, HDAC2, HDAC3, and HDAC6 using the ELISA-based activity assay.[a]

Compound	Deacetylase activity (%)			
	HDAC1	HDAC2	HDAC3	HDAC6
SAHA[b] 1 µM	8.9±0.1	8.3±0.2	14±3	7.9±1.6
34a (C5-methyl) 0.025 µM	67±6	81±3	80±2	63±3
34b (butyl) 0.25 µM	84±3	83±3	74±3	35±6
34c (hexyl) 1.25 µM	64±5	72±1	71±2	28±1
34d (phenyl) 0.125 µM	83±1	85±1	86±2	63±4
34e (benzyl) 1.25 µM	69±1	74±1	74±1	17±2

[a] The means and standard errors for a minimum of two independent trials are shown. This data is associated with Figure 4.2. [b] Previously reported values using the same assay procedure.[93]

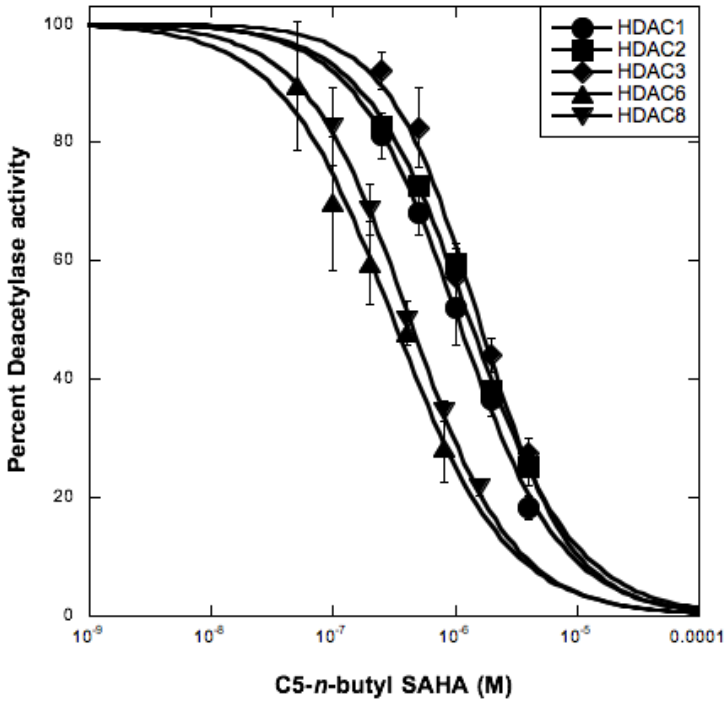

Figure C.53. Dose dependent curves of the C5-butyl SAHA analog (**34b**) with HDAC1, HDAC2, HDAC3, HDAC6 and HDAC8 isoforms, with error bars depicting the standard error of at least three independent trials. IC_{50} values associated with Table 4.2 were determined by fitting data to a sigmoidal curve using KaleidaGraph 4.1.3 (Synergy Software) (Table C.3).

Table C.3. Percentage remaining deacetylase activity after incubation of C5-butyl SAHA analog (**34b**) with HDAC1, HDAC2, HDAC3, HDAC6 and HDAC8.[a]

Concentration (M)	Deacetylase activity (%)				
	HDAC1	HDAC2	HDAC3	HDAC6	HDAC8
4.0×10^{-6}	18±2	25±3	27±3		
2.0×10^{-6}	37±3	38±1	44±3		
1.6×10^{-6}					22±2
1.0×10^{-6}	52±6	60±4	57±5		
8.0×10^{-7}				28±6	35±2
5.0×10^{-7}	68±4	73±1	83±7		
4.0×10^{-7}				48±2	50±3
2.5×10^{-7}	81±4	83±1	92±3		
2.0×10^{-7}				60±7	69±4
1.0×10^{-7}				70±11	83±6
5.0×10^{-8}				90±11	

[a] Means and standard errors of at least three independent trials with the C5-butyl SAHA (**34b**) concentrations shown. Data is associated with Figure C.53 and Table 4.2.

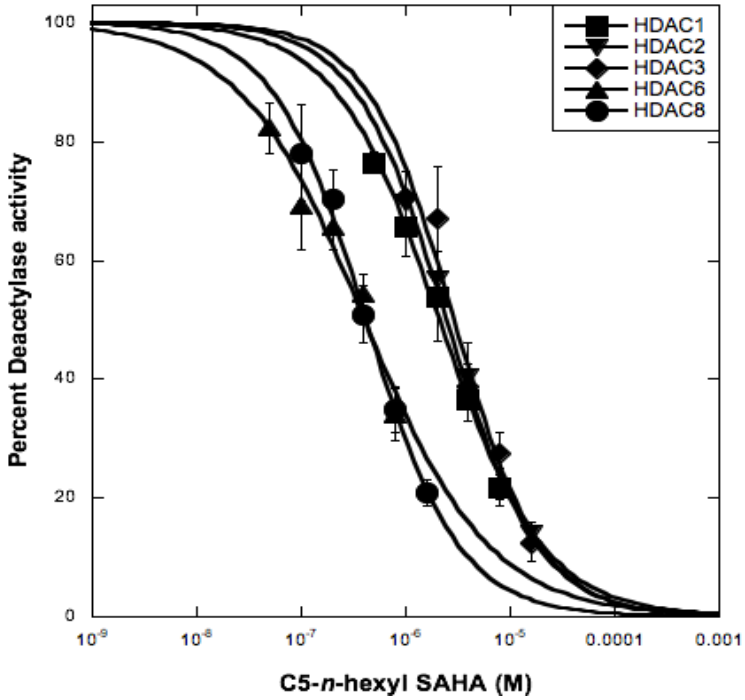

Figure C.54. Dose dependent curves of the C5-*n*-hexyl SAHA analog (**34c**) with HDAC1, HDAC2, HDAC3, HDAC6 and HDAC8 isoforms, with error bars depicting the standard error of at least three independent trials. IC_{50} values associated with Table 4.2 were determined by fitting data to a sigmoidal curve using KaleidaGraph 4.1.3 (Synergy Software) (Table C.4).

Table C.4. Percentage remaining deacetylase activity after incubation of C5-*n*-hexyl SAHA analog (**34c**) with HDAC1, HDAC2, HDAC3, HDAC6 and HDAC8.[a]

Concentration (M)	Deacetylase activity (%)				
	HDAC1	HDAC2	HDAC3	HDAC6	HDAC8
1.6×10^{-5}		14±2	12±3		
8.0×10^{-6}	22±3	21±1	27±4		
4.0×10^{-6}	37±±4	41±6	39±4		
2.0×10^{-6}	54±8	57±5	67±9		
1.6×10^{-6}					21±2
1.0×10^{-6}	66±5	70±5	71±1		
8.0×10^{-7}				34±4	35±4
5.0×10^{-7}	77±2				
4.0×10^{-7}				54±3	51±5
2.0×10^{-7}				66±4	70±5
1.0×10^{-7}				69±7	78±8
5.0×10^{-8}				82±4	

[a] Means and standard errors of at least three independent trials with the C5-*n*-hexyl SAHA (**34c**) concentrations shown. Data is associated with Figure C.54 and Table 4.2.

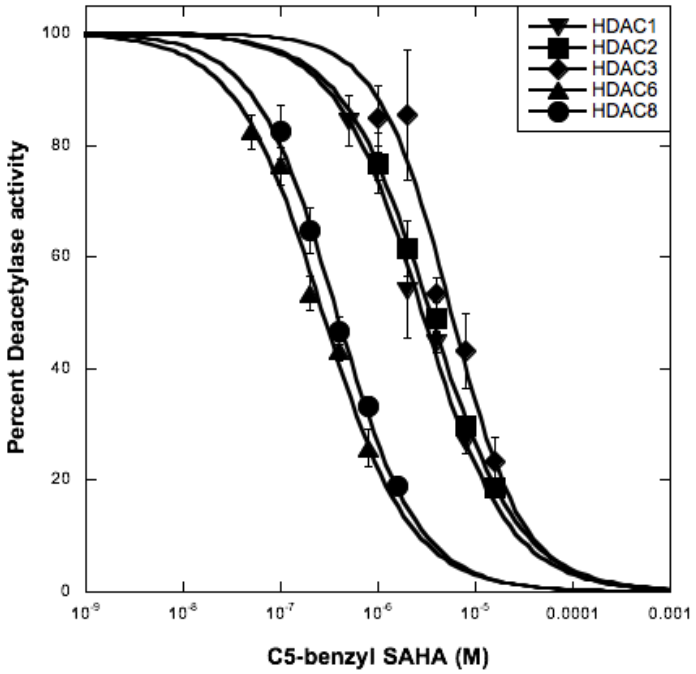

Figure C.55. Dose dependent curves of the C5-benzyl SAHA analog (**34e**) with HDAC1, HDAC2, HDAC3, HDAC6 and HDAC8 isoforms, with error bars depicting the standard error of at least three independent trials. IC_{50} values associated with Table 4.2 were determined by fitting data to a sigmoidal curve using KaleidaGraph 4.1.3 (Synergy Software) (Table C.5).

Table C.5. Percentage remaining deacetylase activity after incubation of C5-benzyl SAHA analog (**34e**) with HDAC1, HDAC2, HDAC3, HDAC6 and HDAC8.[a]

Concentration (M)	Deacetylase activity (%)				
	HDAC1	HDAC2	HDAC3	HDAC6	HDAC8
1.6×10^{-5}		19±1	23±4		
8.0×10^{-6}	27±2	30±1	43±7		
4.0×10^{-6}	45±2	49±3	53±3		
2.0×10^{-6}	54±8	62±5	85±12		
1.6×10^{-6}					19±1
1.0×10^{-6}	77±5	77±3	85±6		
8.0×10^{-7}				26±3	33±2
5.0×10^{-7}	84±4				
4.0×10^{-7}				43±2	47±2
2.0×10^{-7}				54±3	65±4
1.0×10^{-7}				76±3	82±5
5.0×10^{-8}				83±3	

[a] Means and standard errors of at least three independent trials with the C5-beznyl SAHA (**34e**) concentrations shown. Data is associated with Figure C.55 and Table 4.2.

Table C.6. Fold selectivity of SAHA and C5-SAHA analogs **34b**, **34c**, and **34e** for HDAC6 or HDAC8 over HDAC1, 2, and 3.[a]

Compound	HDAC6 fold selectivity			HDAC8 fold selectivity		
	HDAC1	HDAC2	HDAC3	HDAC1	HDAC2	HDAC3
SAHA	1	3	0.6 [b]	0.06 [c]	0.2 [c]	0.04 [c]
C5-butyl SAHA **34b**	3	4	5	3	3	4
C5-hexyl SAHA **34c**	5	6	7	5	6	7
C5-benzyl SAHA **34e**	11	13	21	8	9	15

[a] Fold selectivities were calculated from the IC_{50} values in Table 4.2. [b] SAHA displayed 1.65-fold preference for HDAC3 versus HDAC6. [c] SAHA displayed 16-fold, 6-fold, and 27-fold preference for HDAC1, 2, and 3, respectively, over HDAC8.

C.3. *In cellulo* selectivity testing

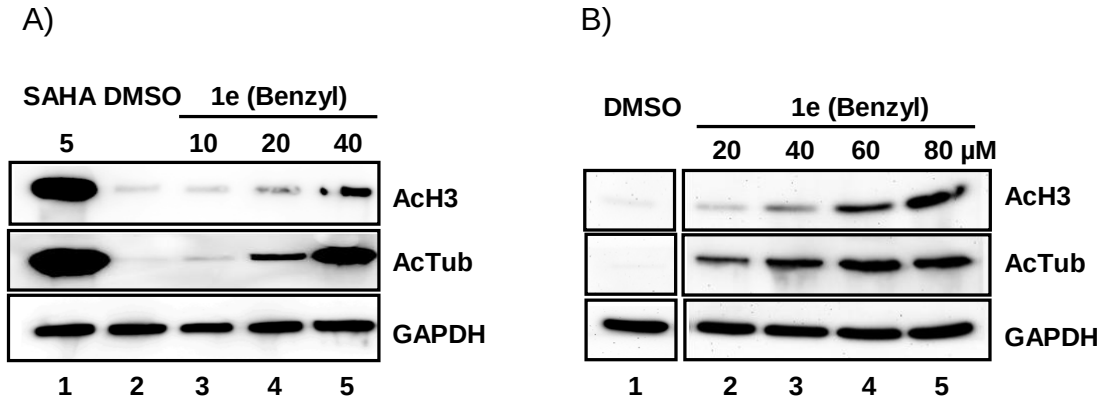

Figure C.56. Western blots analysis of acetyl-histone H3 (Lys9) (AcH3) and acetyl-α-tubulin (Lys40) (AcTub) after treatment with SAHA or the C5-benzyl SAHA analog **34e**. U937 cells were treated with SAHA (5 μM), DMSO (1%) or C5-benzyl SAHA analog **34e** at the specified concentrations, before lysis, SDS-PAGE separation, transfer to a PVDF membrane, and western blotted with AcH3 or AcTub antibodies. GAPDH levels in the samples were also probed as a gel load control. A DMSO control sample was included for comparison to inhibitor treated samples. These three trials (parts A-B) are associated with the third trial shown in Figure 4.3.

C.4. *In vitro* cancer cell growth inhibition

Table C.7. Percentage of viable cells after treatment of Jurkat cell line with of C5-butyl SAHA **34b**, C5-hexyl SAHA **34c**, C5-benzyl SAHA **34e**, and SAHA.[a]

	Viable cells (%)	
Compound	1 μM	10 μM
34b (butyl)	67 ± 6	39 ± 2
34c (hexyl)	101 ± 6	24 ± 2
34e (benzyl)	71 ± 9	50 ± 5
SAHA	49 ± 6	5 ± 3

[a] Means and standard errors for a minimum of four independent trials are shown. All analogs were tested at 1 and 10μM final concentrations. Data is associated with Figure 4.4.

APPENDIX D

D.1. Compound characterization of the biaryl indolyl benzamide inhibitors

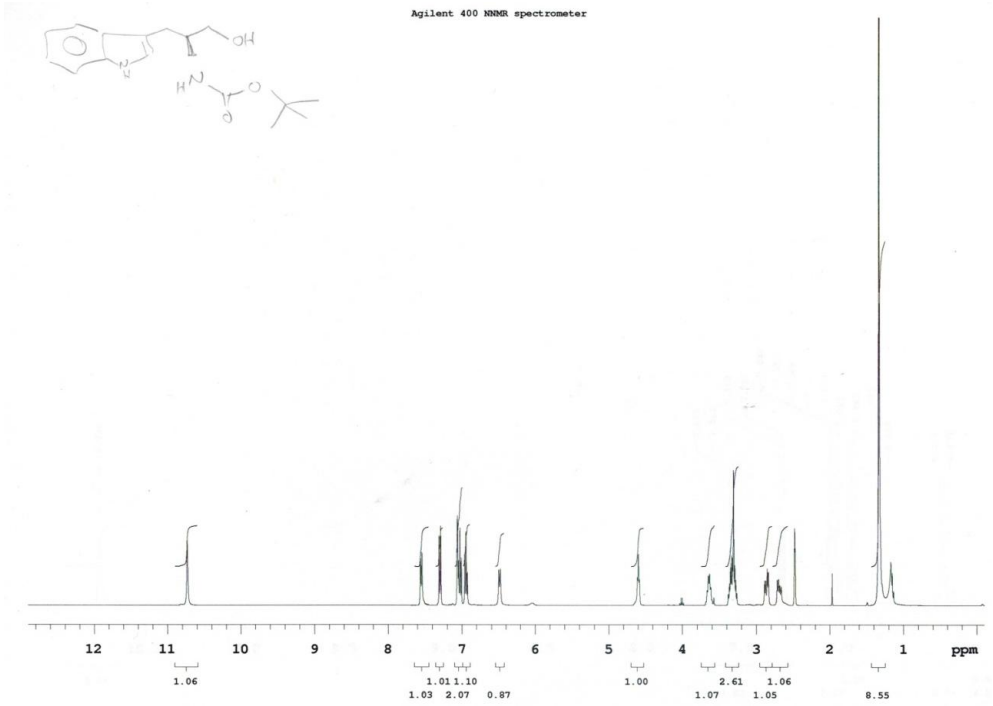

Figure D.1. ^{1}HNMR spectrum of **40**.

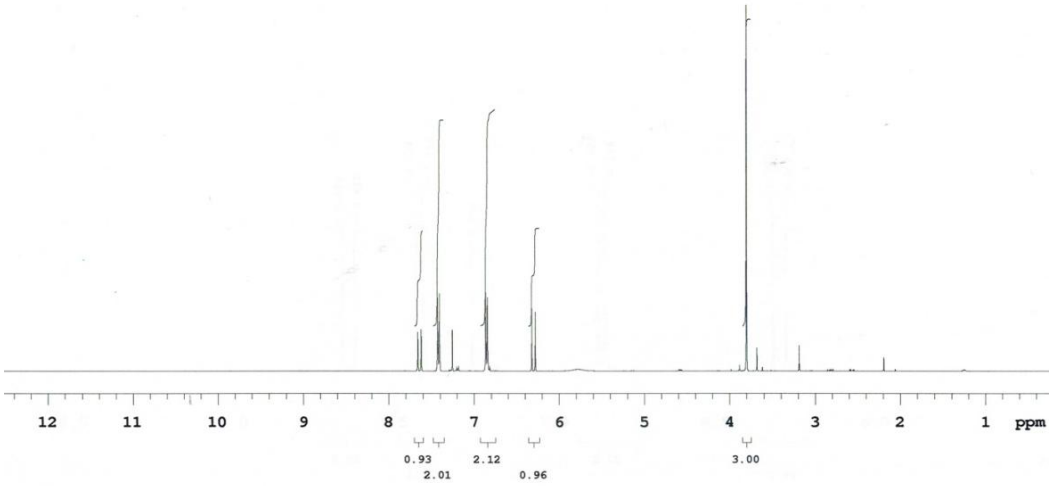

Figure D.2. ^{1}HNMR spectrum of **42a**.

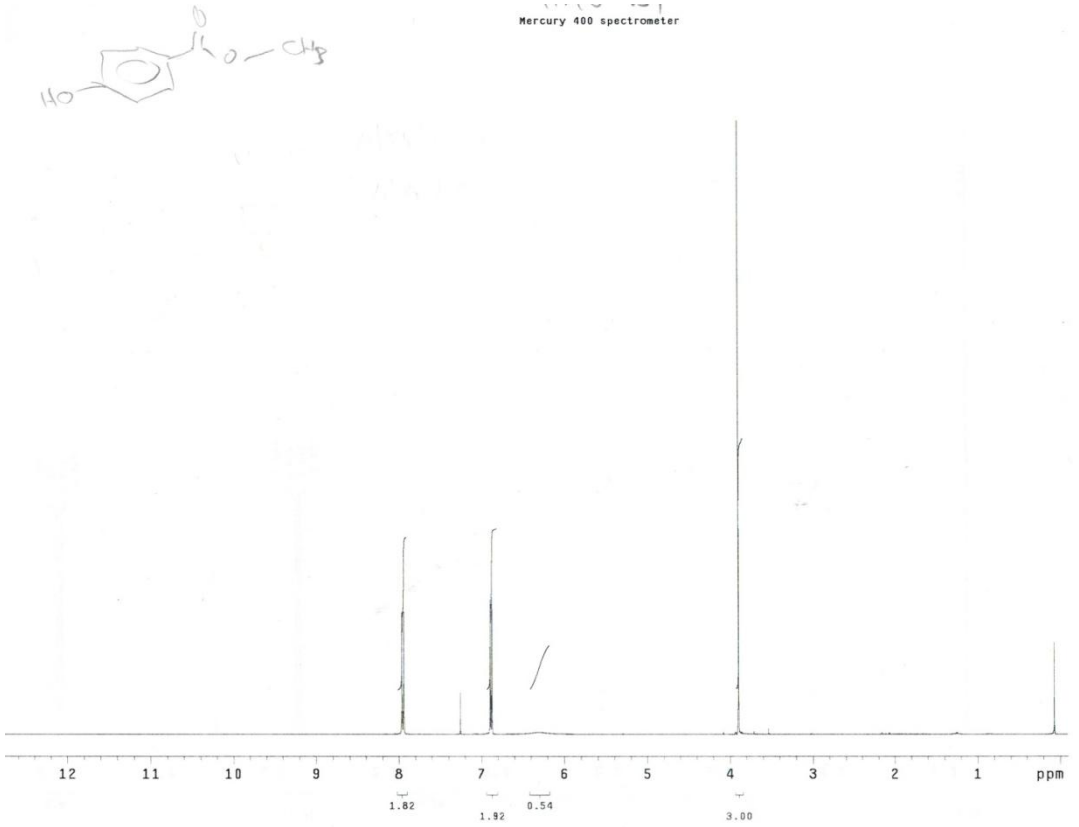

Figure D.3. [1]HNMR spectrum of **42b**.

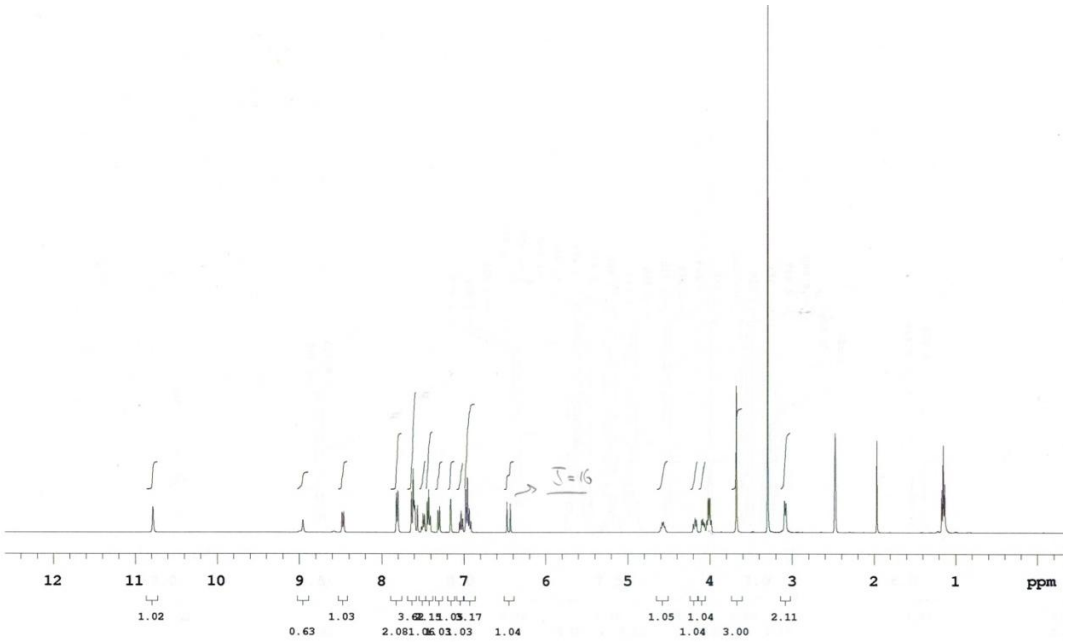

Figure D.4. [1]HNMR spectrum of **44a**.

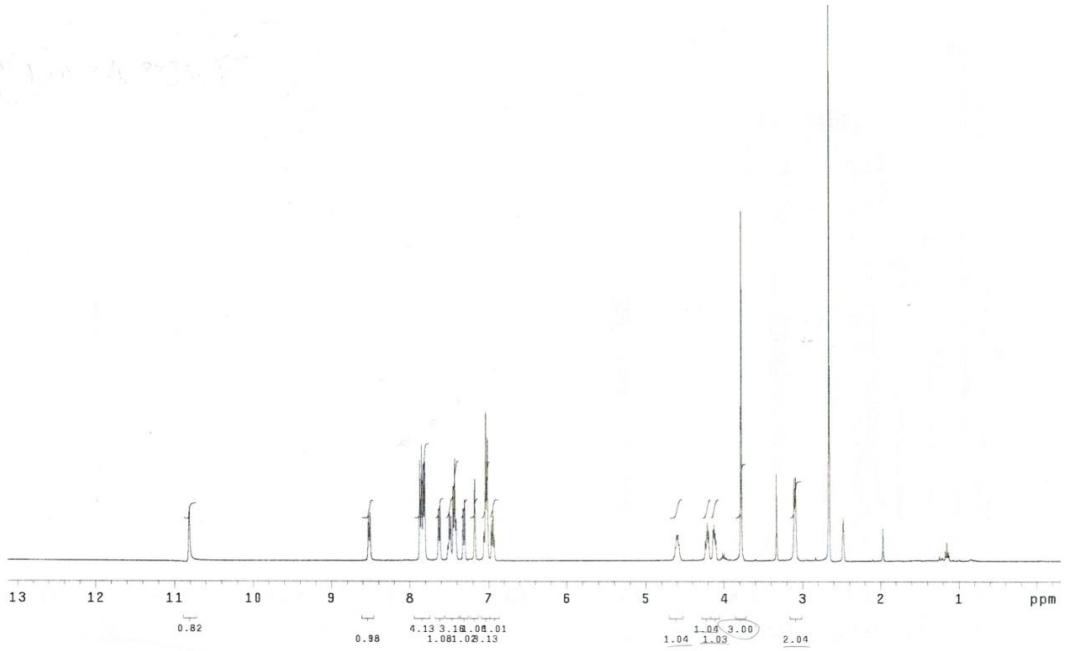

Figure D.5. [1]HNMR spectrum of **44b**.

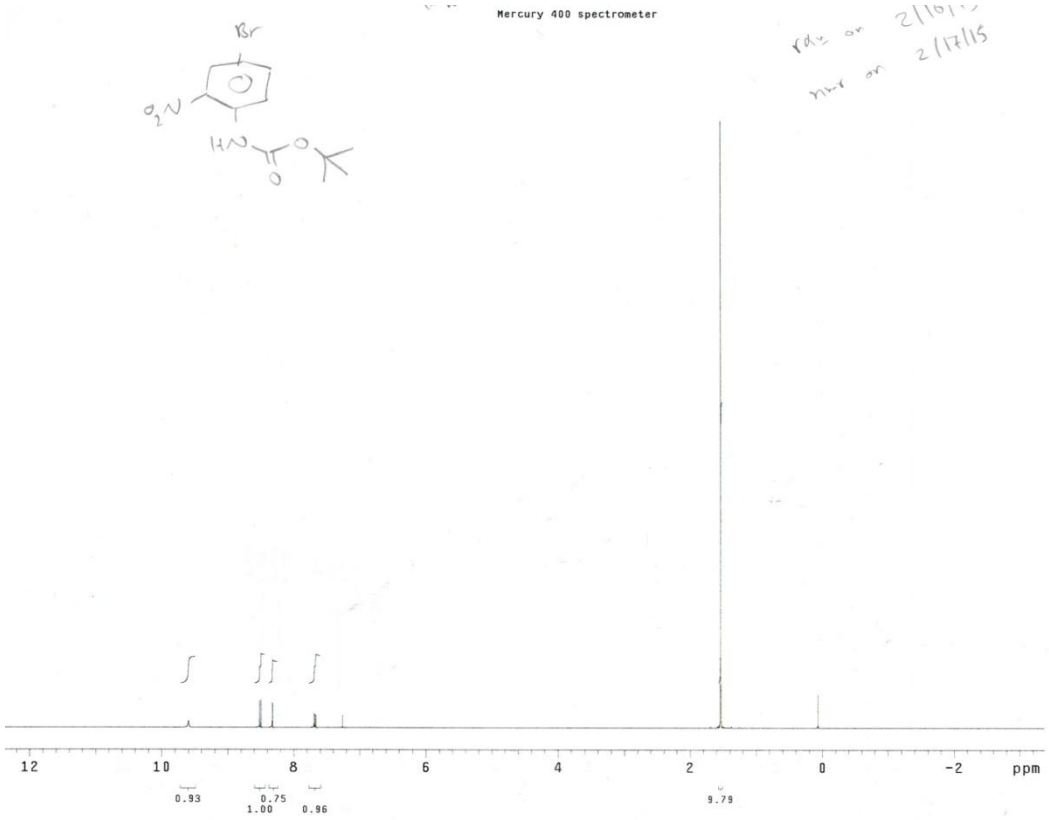

Figure D.6. [1]HNMR spectrum of **47**.

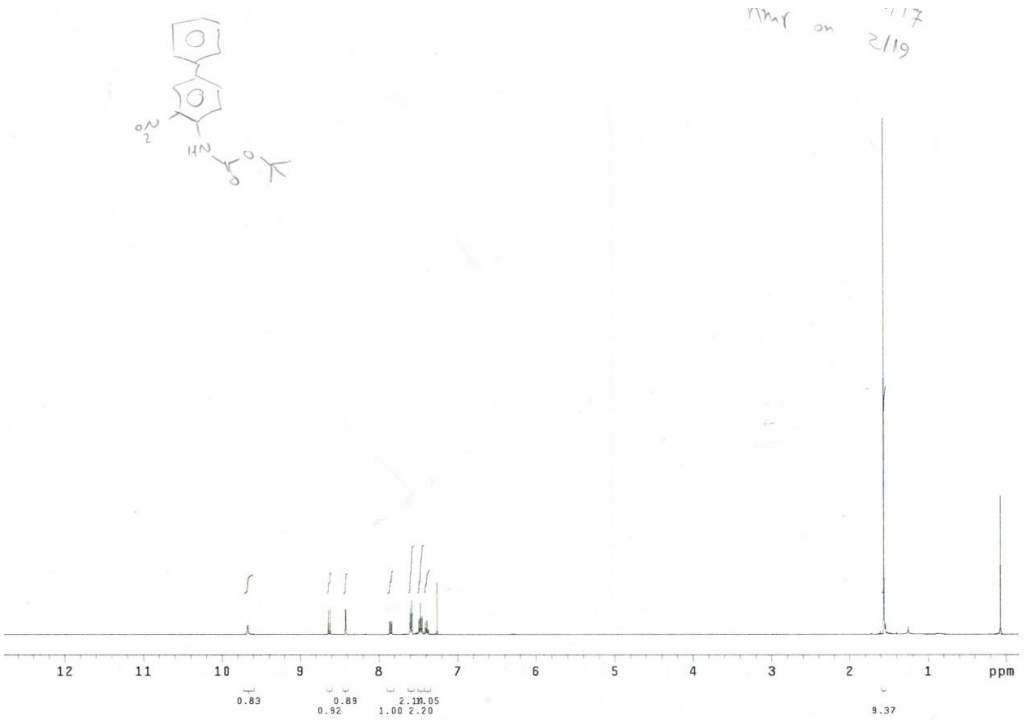

Figure D.7. ^{1}HNMR spectrum of **48**.

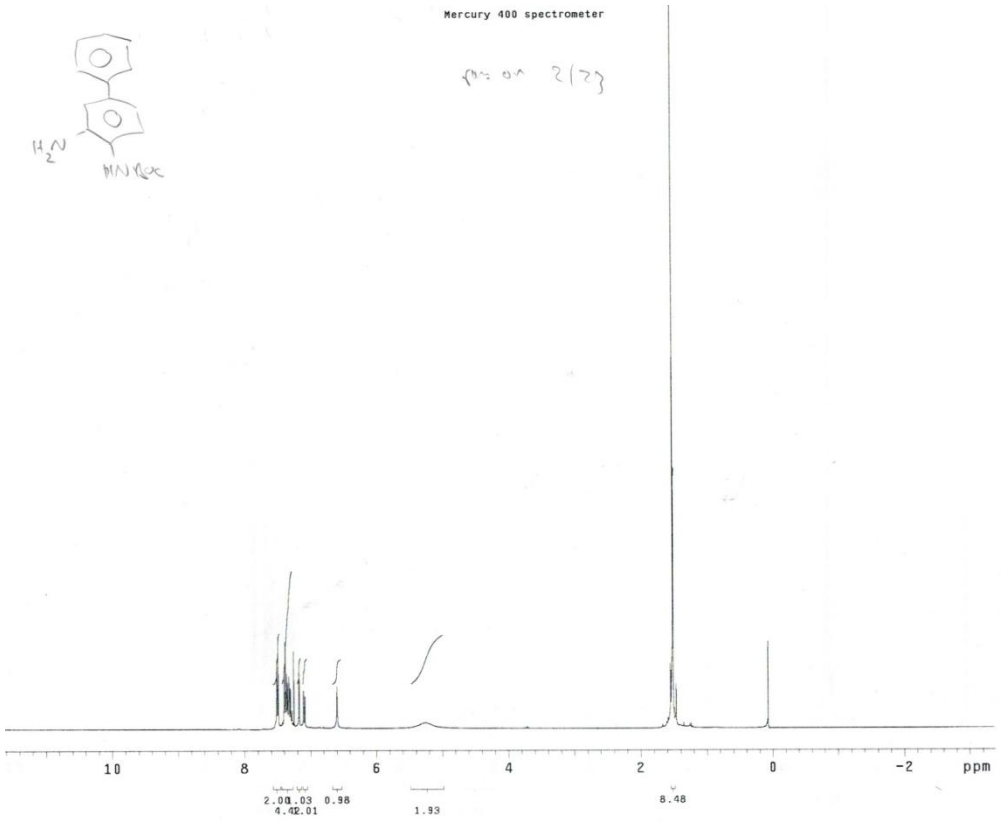

Figure D.8. ^{1}HNMR spectrum of **49**.

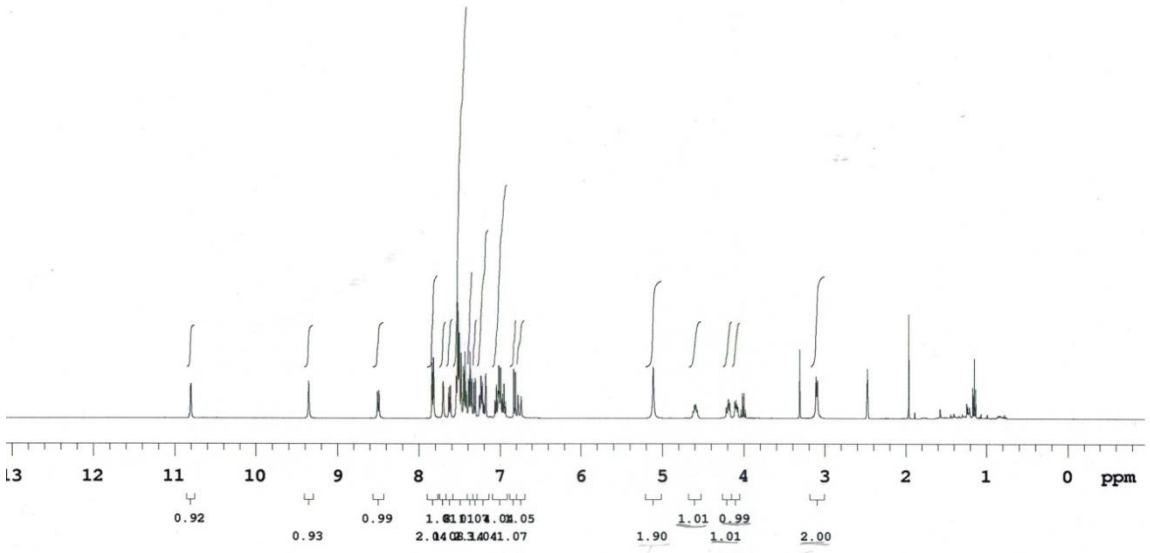

Figure D.9. [1]HNMR spectrum of **Bnz-1**.

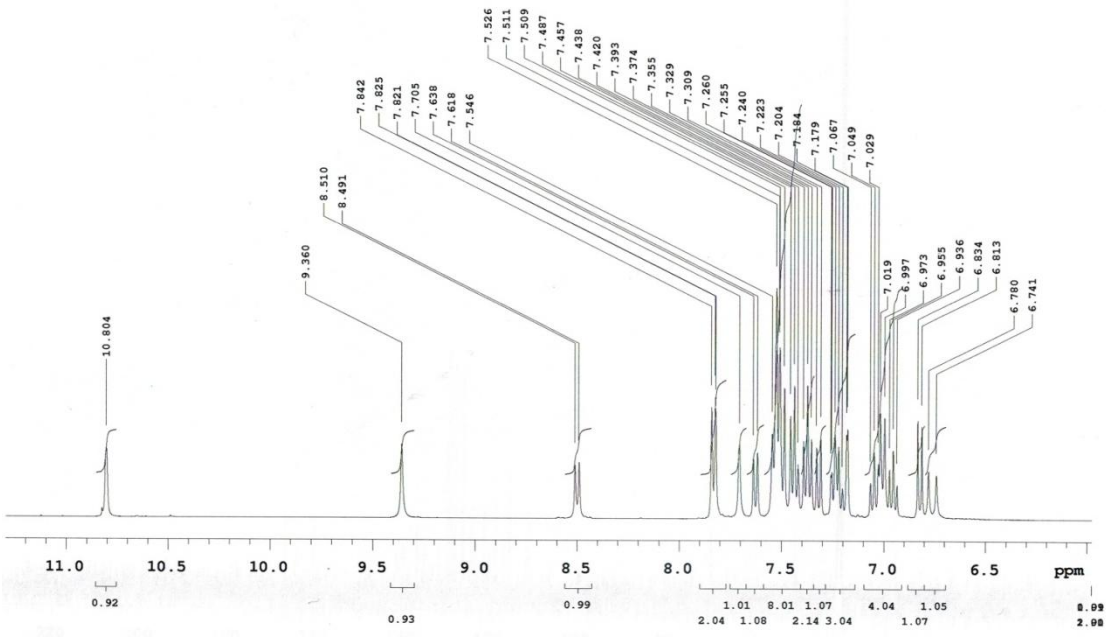

Figure D.10. [1]HNMR spectrum of **Bnz-1** enlarged in the aromatic protons region.

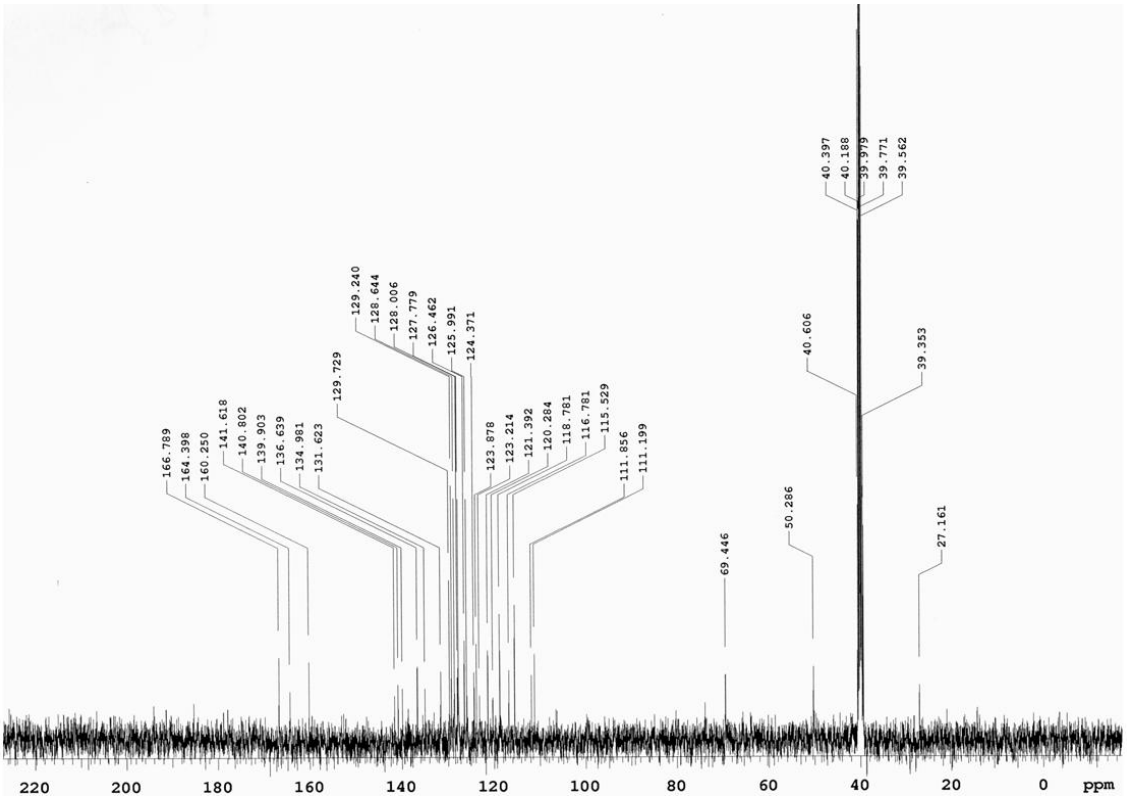

Figure D.11. ^{13}CNMR spectrum of **Bnz-1**.

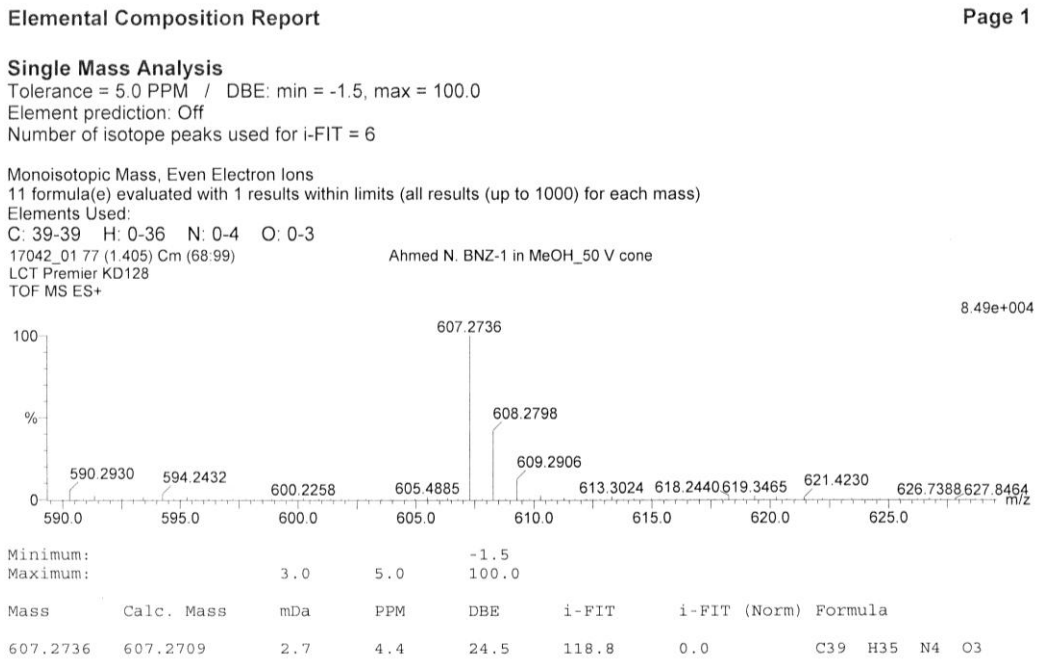

Figure D.12. High resolution mass spectrum of **Bnz-1** using a Waters LCT-MS premier TOF instrument.

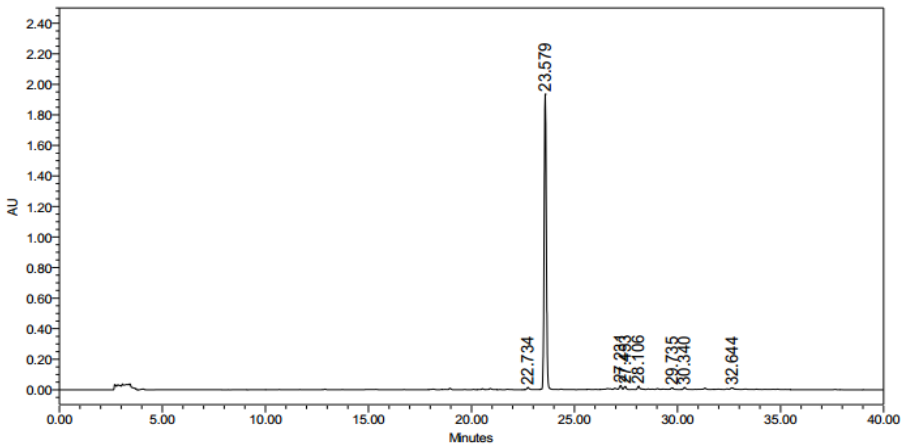

	RT	Area	% Area	Height
1	22.734	90287	0.60	11941
2	23.579	14265528	94.85	1935437
3	27.231	171313	1.14	24524
4	27.453	127129	0.85	18431
5	28.106	148072	0.98	18866
6	29.735	80387	0.53	9362
7	30.340	79764	0.53	10843
8	32.644	77860	0.52	8758

Figure D.13. HPLC spectrum taken at 254 nm of **Bnz-1**. The peak at 23.579 is **Bnz-1**. The calculated area and height under each peak, along with % area, is shown in the table below the spectrum.

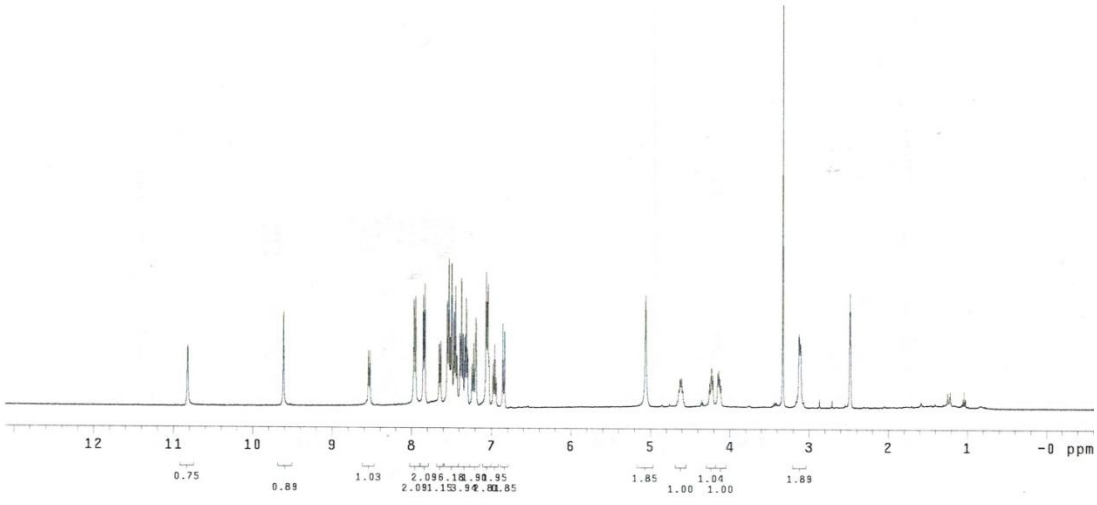

Figure D.14. ^{1}HNMR spectrum of **Bnz-3**.

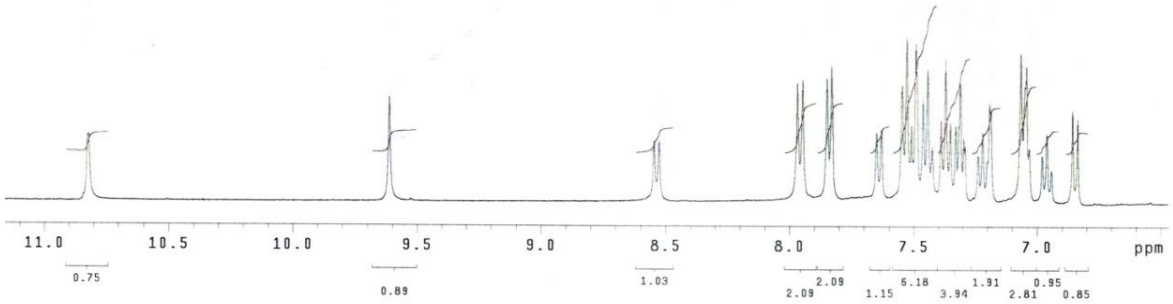

Figure D.15. ^{1}HNMR spectrum of **Bnz-3** enlarged in the aromatic protons region.

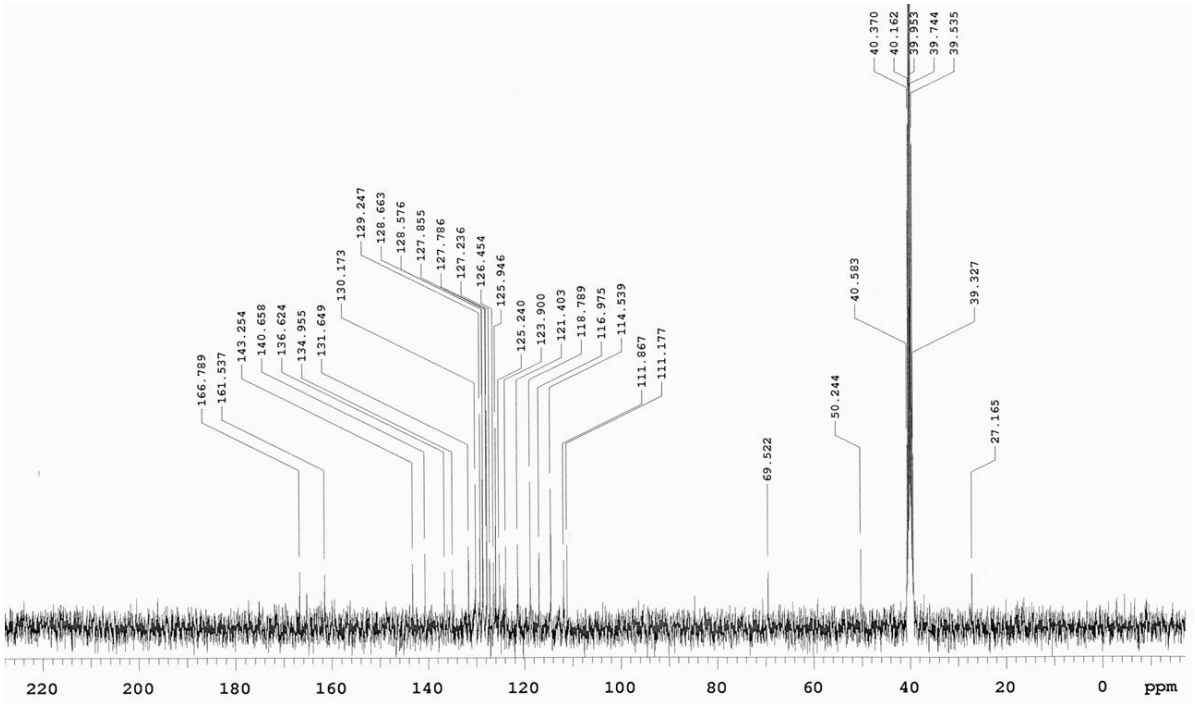

Figure D.16. ^{13}CNMR spectrum of **Bnz-3**.

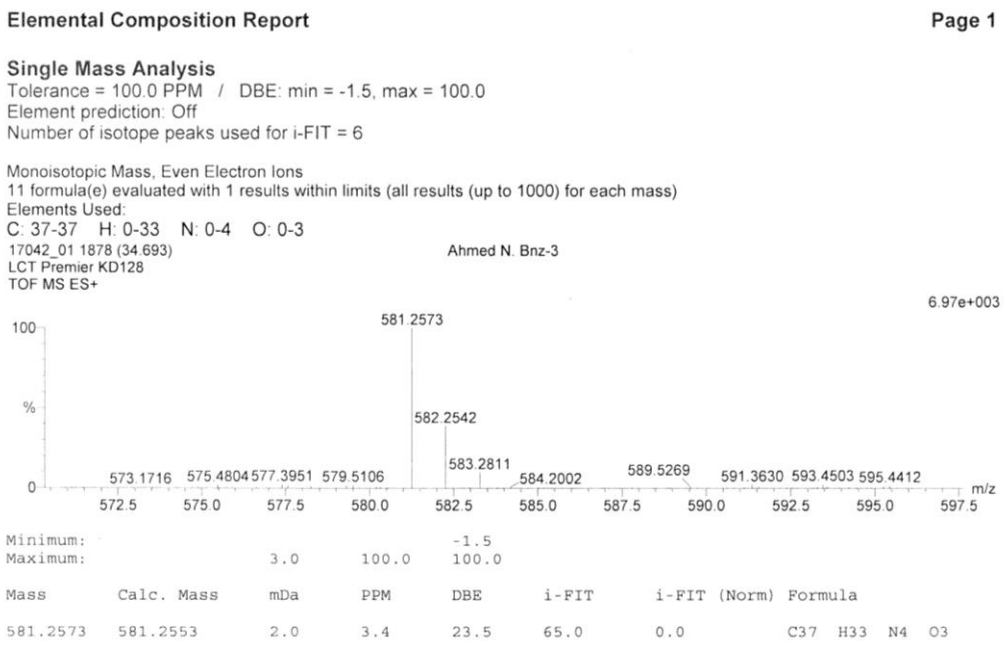

Elemental Composition Report Page 1

Single Mass Analysis
Tolerance = 100.0 PPM / DBE: min = -1.5, max = 100.0
Element prediction: Off
Number of isotope peaks used for i-FIT = 6

Monoisotopic Mass, Even Electron Ions
11 formula(e) evaluated with 1 results within limits (all results (up to 1000) for each mass)
Elements Used:
C: 37-37 H: 0-33 N: 0-4 O: 0-3

17042_01 1878 (34.693) Ahmed N. Bnz-3
LCT Premier KD128
TOF MS ES+
6.97e+003

Minimum:				-1.5			
Maximum:		3.0	100.0	100.0			
Mass	Calc. Mass	mDa	PPM	DBE	i-FIT	i-FIT (Norm)	Formula
581.2573	581.2553	2.0	3.4	23.5	65.0	0.0	C37 H33 N4 O3

Figure D.17. High resolution mass spectrum of **Bnz-3** using a Waters LCT-MS premier TOF instrument.

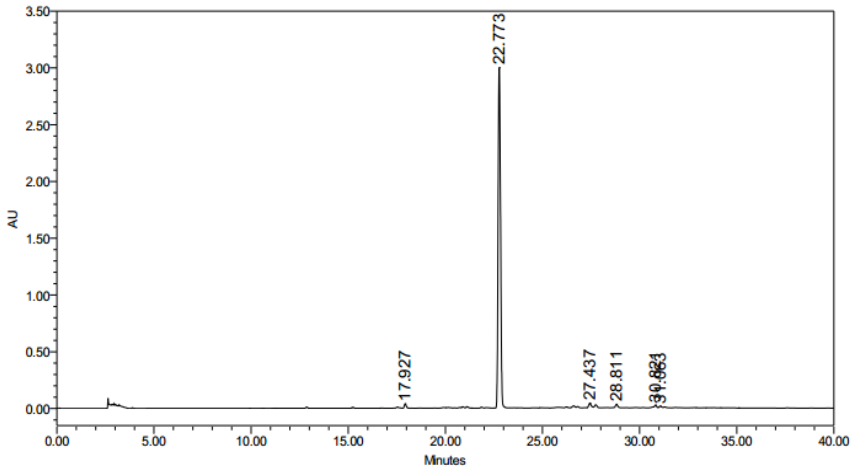

	RT	Area	% Area	Height
1	17.927	274725	1.00	37706
2	22.773	26093689	94.93	2998660
3	27.437	397087	1.44	41398
4	28.811	313349	1.14	32131
5	30.821	263727	0.96	24789
6	31.063	144676	0.53	15657

Figure D.18. HPLC spectrum taken at 254 nm of **Bnz-3**. The peak at 22.773 is **Bnz-3**. The calculated area and height under each peak, along with % area, is shown in the table below the spectrum.

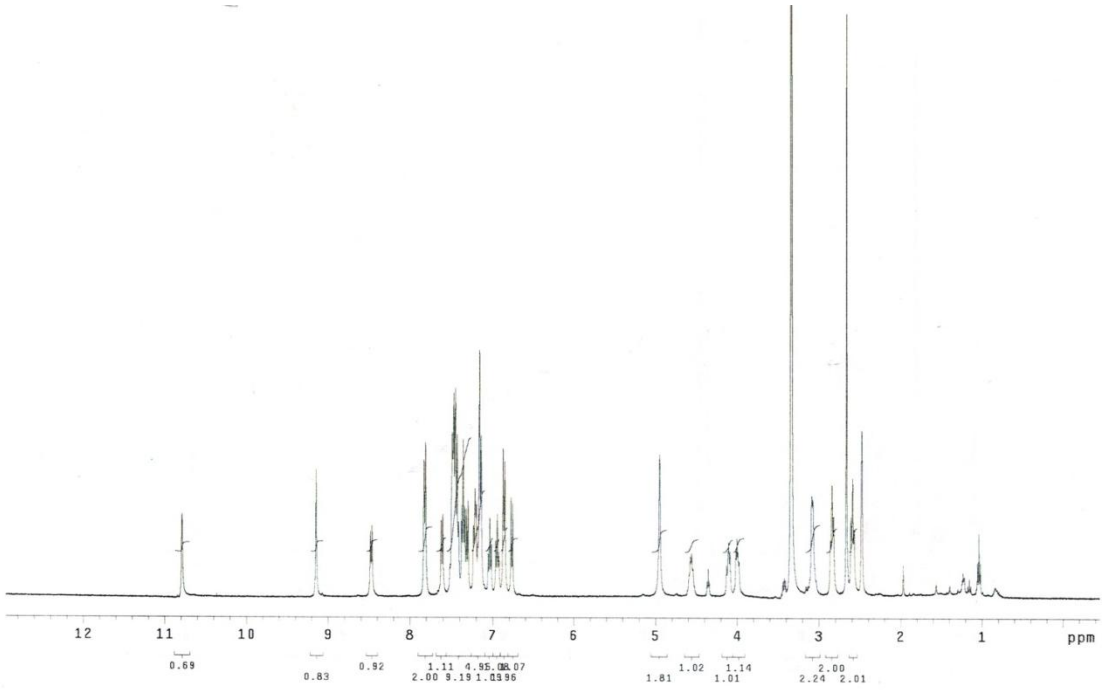

Figure D.19. [1]HNMR spectrum of **Bnz-2**.

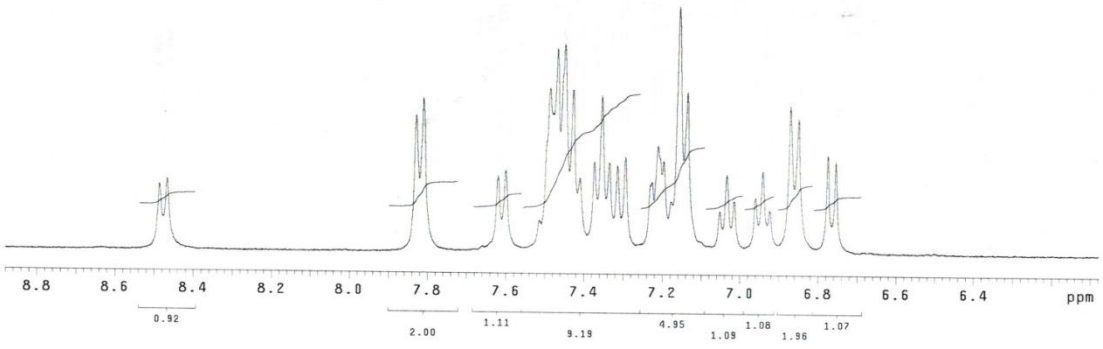

Figure D.20. [1]HNMR spectrum of **Bnz-2** enlarged in the aromatic protons region.

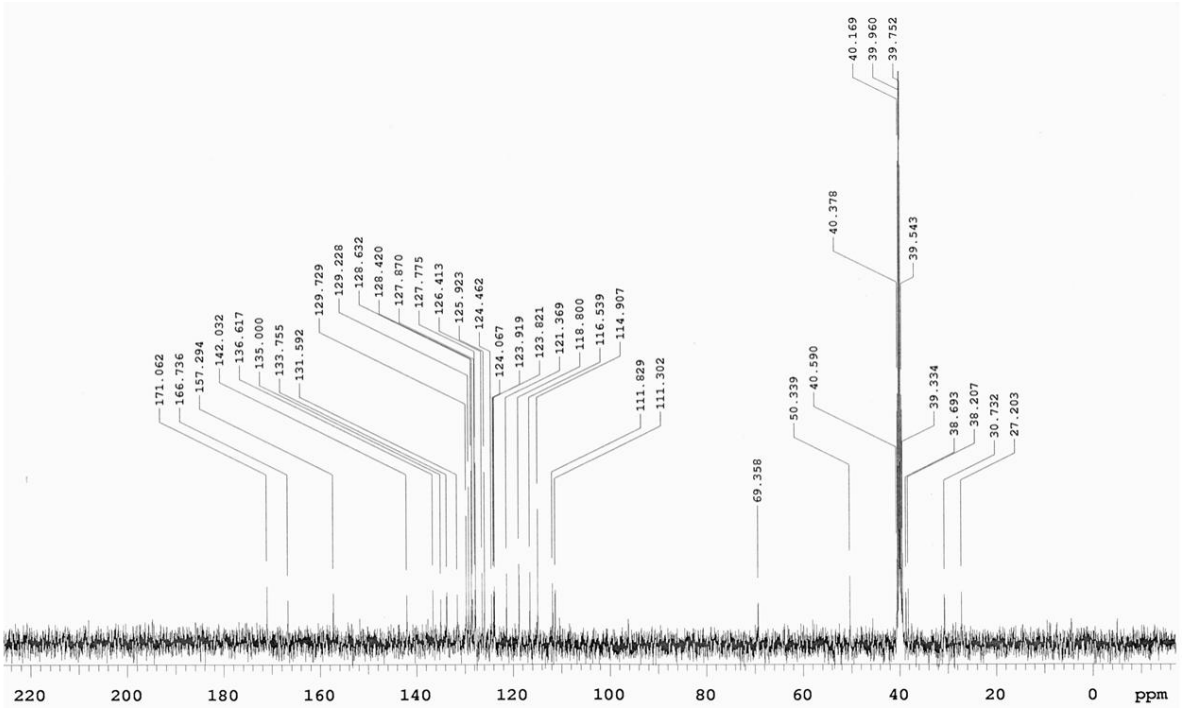

Figure D.21. ^{13}CNMR spectrum of **Bnz-2**.

Elemental Composition Report **Page 1**

Single Mass Analysis
Tolerance = 5.0 PPM / DBE: min = -1.5, max = 100.0
Element prediction: Off
Number of isotope peaks used for i-FIT = 6

Monoisotopic Mass, Even Electron Ions
11 formula(e) evaluated with 1 results within limits (all results (up to 1000) for each mass)
Elements Used:
C: 39-39 H: 0-37 N: 0-4 O: 0-3
17042_01 747 (13.789) Cm (747:768) Ahmed N. Bnz-2 in MeOH 70 V cone
LCT Premier KD128
TOF MS ES+

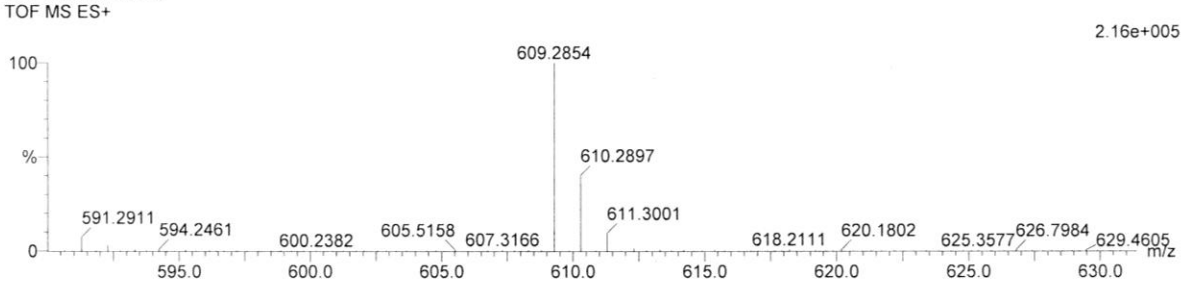

Minimum:				-1.5			
Maximum:		3.0	5.0	100.0			
Mass	Calc. Mass	mDa	PPM	DBE	i-FIT	i-FIT (Norm)	Formula
609.2854	609.2866	-1.2	-2.0	23.5	116.3	0.0	C39 H37 N4 O3

Figure D.22. High resolution mass spectrum of **Bnz-2** using a Waters LCT-MS premier TOF instrument.

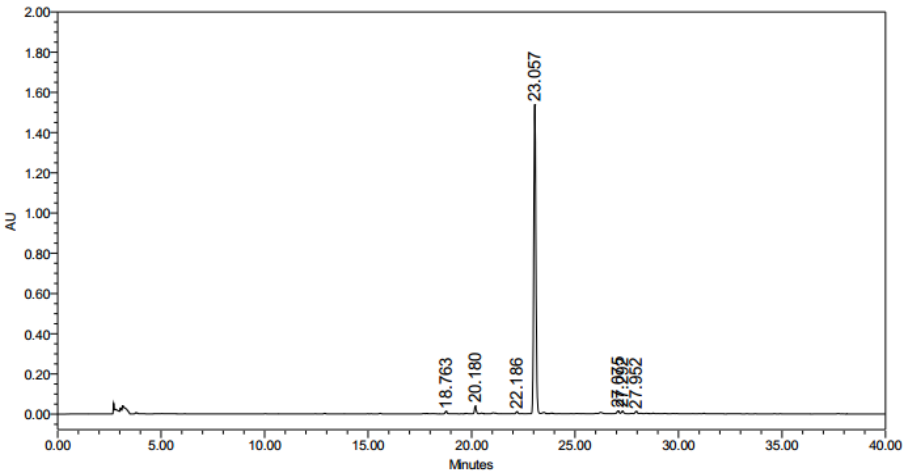

	RT	Area	% Area	Height
1	18.763	80458	0.70	12673
2	20.180	214703	1.86	37955
3	22.186	63697	0.55	9705
4	23.057	10907395	94.28	1539613
5	27.075	115303	1.00	13829
6	27.292	102610	0.89	12902
7	27.952	85155	0.74	11570

Figure D.23. HPLC spectrum taken at 254 nm of **Bnz-2**. The peak at 23.057 is **Bnz-2**. The calculated area and height under each peak, along with % area, is shown in the table below the spectrum.

D.2. *In vitro* screening with HDAC isoforms

Table D.1. Percent remaining deacetylase activity after incubation of a single concentration of each compound with HDAC1, HDAC2, HDAC3, and HDAC6.[a]

	Deacetylase activity (%)			
Compound	HDAC1	HDAC2	HDAC3	HDAC6
SAHA (20 nM)	61±3	55±2	67±1	65±1
Cpd-60 (28 nM)	19±5	59±6	90±2	101±3
Bnz-1 (200 µM)	15±2	27±1	-	-
Bnz-1 (20 µM)	54±3	77±2	-	-
Bnz-2 (20 µM)	21±1	44±3	-	-
Bnz-2 (2 µM)	48±1	71±2	-	-
Bnz-3 (2 µM)	19±2	63±1	91±1	103±6
Bnz-3 (200 nM)	64±6	83±3	93±2	108±9

[a] The means and standard errors for a minimum of two independent trials are shown. "-" not determined. This data is associated with Figure 6.3.

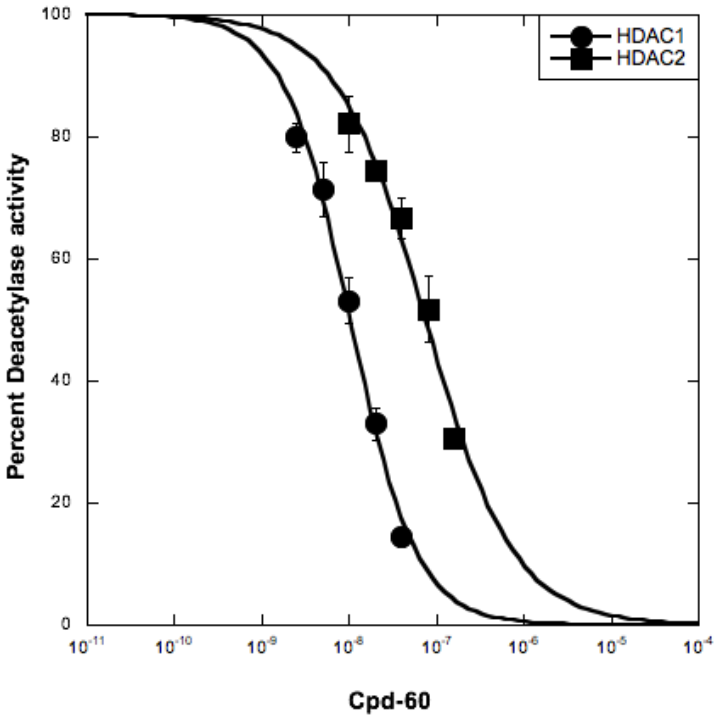

Figure D.24. Dose dependent curves of **Cpd-60** with HDAC1 and HDAC2 isoforms, with error bars depicting the standard error of at least three independent trials. IC_{50} values associated with Table 6.1 were determined by fitting data to a sigmoidal curve using KaleidaGraph 4.1.3 (Synergy Software) (Table D.2)

Table D.2. Percentage remaining deacetylase activity after incubation of **Cpd-60** with HDAC1 and HDAC2.[a]

Concentration (M)	Deacetylase activity (%)	
	HDAC1	HDAC2
1.6×10^{-7}		31 ± 1
8.0×10^{-8}		52 ± 5
4.0×10^{-8}	14 ± 1	67 ± 3
2.0×10^{-8}	33 ± 3	74 ± 1
1.0×10^{-8}	53 ± 4	82 ± 5
5.0×10^{-9}	71 ± 4	
2.5×10^{-9}	80 ± 2	

[a] Means and standard errors of at least three independent trials with the **Cpd-60** concentrations shown. Data is associated with Figure D.24 and Table 6.1.

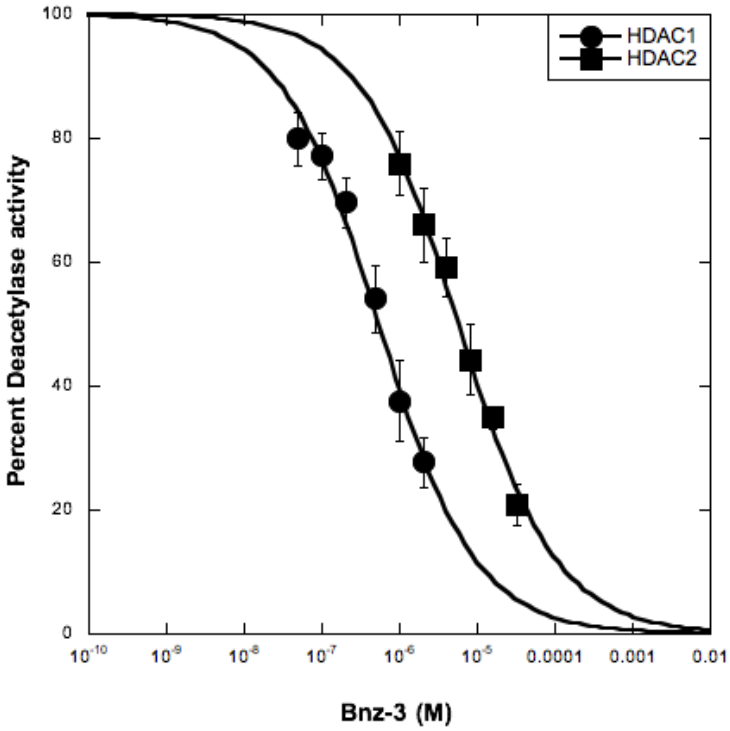

Figure D.25. Dose dependent curves of **Bnz-3** with HDAC1 and HDAC2 isoforms, with error bars depicting the standard error of at least three independent trials. IC_{50} values associated with Table 6.1 were determined by fitting data to a sigmoidal curve using KaleidaGraph 4.1.3 (Synergy Software) (Table D.3)

Table D.3. Percentage remaining deacetylase activity after incubation of **Bnz-3** with HDAC1 and HDAC2.[a]

Concentration (M)	Deacetylase activity (%)	
	HDAC1	HDAC2
2.0×10^{-6}	28 ± 4	
1.0×10^{-6}	38 ± 7	
5.0×10^{-7}	54 ± 5	
2.0×10^{-7}	70 ± 4	
1.0×10^{-7}	77 ± 4	
5.0×10^{-8}	80 ± 4	
3.2×10^{-5}		21 ± 3
1.6×10^{-5}		35 ± 2
8×10^{-6}		44 ± 6
4×10^{-6}		59 ± 5
2×10^{-6}		66 ± 6
1×10^{-6}		76 ± 2

[a] Means and standard errors of at least three independent trials with the **Bnz-3** concentrations shown. Data is associated with Figure D.25 and Table 6.1.

APPENDIX E

Copyrights permissions and reprint authorizations

Reprint authorization for Figure 1.1.

Order Completed

Thank you for your order.

This Agreement between Ahmed Negmeldin ("You") and Nature Publishing Group ("Nature Publishing Group") consists of your license details and the terms and conditions provided by Nature Publishing Group and Copyright Clearance Center.

Your confirmation email will contain your order number for future reference.

Printable details.

License Number	4111981079282
License date	May 18, 2017
Licensed Content Publisher	Nature Publishing Group
Licensed Content Publication	Nature Reviews Drug Discovery
Licensed Content Title	Epigenetic protein families: a new frontier for drug discovery
Licensed Content Author	Cheryl H. Arrowsmith, Chas Bountra, Paul V. Fish, Kevin Lee and Matthieu Schapira
Licensed Content Date	May 1, 2012
Licensed Content Volume	11
Licensed Content Issue	5
Type of Use	reuse in a dissertation / thesis
Requestor type	academic/educational
Format	print and electronic
Portion	figures/tables/illustrations
Number of figures/tables/illustrations	1
High-res required	no
Figures	Figure 1
Author of this NPG article	no
Your reference number	
Title of your thesis / dissertation	DESIGN, SYNTHESIS AND BIOLOGICAL EVALUATION OF HISTONE DEACETYLASE (HDAC) INHIBITORS: SAHA (VORINOSTAT) ANALOGS AND BIARYL INDOLYL BENZAMIDE INHIBITORS DISPLAY ISOFORM SELECTIVITY
Expected completion date	Jun 2017
Estimated size (number of pages)	360
Requestor Location	Ahmed Negmeldin 5101 Cass Ave Department of Chemistry DETROIT, MI 48202 United States Attn: Ahmed Negmeldin
Billing Type	Invoice
Billing address	Ahmed Negmeldin 5101 Cass Ave. Department of Chemistry DETROIT, MI 48202 United States Attn: Ahmed Negmeldin
Total	0.00 USD

ORDER MORE CLOSE WINDOW

Copyrights permission (Open access article "which permits unrestricted use, distribution, and reproduction in any medium, provided the original work is properly cited" as shown on the publisher's website) for Figure 1.2.

Nutrients **2014**, *6*(10), 4273-4301; doi:10.3390/nu6104273

Open Access Review

The Role of Dietary Histone Deacetylases (HDACs) Inhibitors in Health and Disease

Shalome A. Bassett [1,2,*] and **Matthew P. G. Barnett** [1,2]

[1] Food Nutrition & Health Team, Food & Bio-based Products Group, AgResearch Limited, Grasslands Research Centre, Tennent Drive, Palmerston North 4442, New Zealand
[2] Nutrigenomics New Zealand, Private Bag 92019, Auckland 1142, New Zealand

* Author to whom correspondence should be addressed.

Received: 31 July 2014 / Revised: 6 October 2014 / Accepted: 6 October 2014 / Published: 15 October 2014

(This article belongs to the Special Issue Nutritional Epigenetics)

Abstract

Modification of the histone proteins associated with DNA is an important process in the epigenetic regulation of DNA structure and function. There are several known modifications to histones, including methylation, acetylation, and phosphorylation, and a range of factors influence each of these. Histone deacetylases (HDACs) remove the acetyl group from lysine residues within a range of proteins, including transcription factors and histones. Whilst this means that their influence on cellular processes is more complex and far-reaching than histone modifications alone, their predominant function appears to relate to histones; through deacetylation of lysine residues they can influence expression of genes encoded by DNA linked to the histone molecule. HDAC inhibitors in turn regulate the activity of HDACs, and have been widely used as therapeutics in psychiatry and neurology, in which a number of adverse outcomes are associated with aberrant HDAC function. More recently, dietary HDAC inhibitors have been shown to have a regulatory effect similar to that of pharmacological HDAC inhibitors without the possible side-effects. Here, we discuss a number of dietary HDAC inhibitors, and how they may have therapeutic potential in the context of a whole food. View Full-Text

Keywords: nutritional epigenetics; histone deacetylase; lysine deacetylase; histone deacetylase inhibitors.

► Figures

Reprint authorization for Figure 1.3.

Copyright Clearance Center RightsLink®

Home | Account Info | Help

Title: Epigenomic regulation of host–microbiota interactions
Author: Theresa Alenghat,David Artis
Publication: Trends in Immunology
Publisher: Elsevier
Date: November 2014

Logged in as:
Ahmed Negmeldin
Account #: 3001041350
LOGOUT

Order Completed

Thank you for your order.

This Agreement between Ahmed Negmeldin ("You") and Elsevier ("Elsevier") consists of your license details and the terms and conditions provided by Elsevier and Copyright Clearance Center.

Your confirmation email will contain your order number for future reference.

Printable details.

License Number	4111981302918
License date	May 18, 2017
Licensed Content Publisher	Elsevier
Licensed Content Publication	Trends in Immunology
Licensed Content Title	Epigenomic regulation of host–microbiota interactions
Licensed Content Author	Theresa Alenghat,David Artis
Licensed Content Date	November 2014
Licensed Content Volume	35
Licensed Content Issue	11
Licensed Content Pages	8
Type of Use	reuse in a thesis/dissertation
Portion	figures/tables/illustrations
Number of figures/tables/illustrations	1
Format	both print and electronic
Are you the author of this Elsevier article?	No
Will you be translating?	No
Order reference number	
Original figure numbers	Figure 1
Title of your thesis/dissertation	DESIGN, SYNTHESIS AND BIOLOGICAL EVALUATION OF HISTONE DEACETYLASE (HDAC) INHIBITORS: SAHA (VORINOSTAT) ANALOGS AND BIARYL INDOLYL BENZAMIDE INHIBITORS DISPLAY ISOFORM SELECTIVITY
Expected completion date	Jun 2017
Estimated size (number of pages)	360
Elsevier VAT number	GB 494 6272 12
Requestor Location	Ahmed Negmeldin 5101 Cass Ave Department of Chemistry DETROIT, MI 48202 United States Attn: Ahmed Negmeldin
Publisher Tax ID	98-0397604
Total	0.00 USD

ORDER MORE | CLOSE WINDOW

Reprint authorization for Figure 1.4.

Copyright Clearance Center RightsLink®

Home | Account Info | Help

nature publishing group

Title: Histone deacetylase 6 structure and molecular basis of catalysis and inhibition
Author: Yang Hai, David W Christianson
Publication: Nature Chemical Biology
Publisher: Nature Publishing Group
Date: Jul 25, 2016

Logged in as:
Ahmed Negmeldin
Account #:
3001041350
LOGOUT

Order Completed

Thank you for your order.

This Agreement between Ahmed Negmeldin ("You") and Nature Publishing Group ("Nature Publishing Group") consists of your license details and the terms and conditions provided by Nature Publishing Group and Copyright Clearance Center.

Your confirmation email will contain your order number for future reference.

Printable details.

License Number	4111981452912
License date	May 18, 2017
Licensed Content Publisher	Nature Publishing Group
Licensed Content Publication	Nature Chemical Biology
Licensed Content Title	Histone deacetylase 6 structure and molecular basis of catalysis and inhibition
Licensed Content Author	Yang Hai, David W Christianson
Licensed Content Date	Jul 25, 2016
Licensed Content Volume	12
Licensed Content Issue	9
Type of Use	reuse in a dissertation / thesis
Requestor type	academic/educational
Format	print and electronic
Portion	figures/tables/illustrations
Number of figures/tables/illustrations	1
High-res required	no
Figures	Figure 2
Author of this NPG article	no
Your reference number	
Title of your thesis / dissertation	DESIGN, SYNTHESIS AND BIOLOGICAL EVALUATION OF HISTONE DEACETYLASE (HDAC) INHIBITORS: SAHA (VORINOSTAT) ANALOGS AND BIARYL INDOLYL BENZAMIDE INHIBITORS DISPLAY ISOFORM SELECTIVITY
Expected completion date	Jun 2017
Estimated size (number of pages)	360
Requestor Location	Ahmed Negmeldin 5101 Cass Ave Department of Chemistry DETROIT, MI 48202 United States Attn: Ahmed Negmeldin
Billing Type	Invoice
Billing address	Ahmed Negmeldin 5101 Cass Ave. Department of Chemistry DETROIT, MI 48202 United States Attn: Ahmed Negmeldin
Total	0.00 USD

ORDER MORE | CLOSE WINDOW

Reprint authorization for Figure 1.5.

Copyright Clearance Center RightsLink®

Home | Account Info | Help

nature publishing group

Title: Histone-deacetylase inhibitors: novel drugs for the treatment of cancer
Author: Ricky W. Johnstone
Publication: Nature Reviews Drug Discovery
Publisher: Nature Publishing Group
Date: Apr 1, 2002

Copyright © 2002, Rights Managed by Nature Publishing Group

Logged in as:
Ahmed Negmeldin
Account #:
3001041350
LOGOUT

Order Completed

Thank you for your order.

This Agreement between Ahmed Negmeldin ("You") and Nature Publishing Group ("Nature Publishing Group") consists of your license details and the terms and conditions provided by Nature Publishing Group and Copyright Clearance Center.

Your confirmation email will contain your order number for future reference.

Printable details.

License Number	4111990127781
License date	May 18, 2017
Licensed Content Publisher	Nature Publishing Group
Licensed Content Publication	Nature Reviews Drug Discovery
Licensed Content Title	Histone-deacetylase inhibitors: novel drugs for the treatment of cancer
Licensed Content Author	Ricky W. Johnstone
Licensed Content Date	Apr 1, 2002
Licensed Content Volume	1
Licensed Content Issue	4
Type of Use	reuse in a dissertation / thesis
Requestor type	academic/educational
Format	print and electronic
Portion	figures/tables/illustrations
Number of figures/tables/illustrations	1
High-res required	no
Figures	Figure 2
Author of this NPG article	no
Your reference number	
Title of your thesis / dissertation	DESIGN, SYNTHESIS AND BIOLOGICAL EVALUATION OF HISTONE DEACETYLASE (HDAC) INHIBITORS: SAHA (VORINOSTAT) ANALOGS AND BIARYL INDOLYL BENZAMIDE INHIBITORS DISPLAY ISOFORM SELECTIVITY
Expected completion date	Jun 2017
Estimated size (number of pages)	360
Requestor Location	Ahmed Negmeldin 5101 Cass Ave Department of Chemistry DETROIT, MI 48202 United States Attn: Ahmed Negmeldin
Billing Type	Invoice
Billing address	Ahmed Negmeldin 5101 Cass Ave. Department of Chemistry DETROIT, MI 48202 United States Attn: Ahmed Negmeldin
Total	0.00 USD

ORDER MORE | CLOSE WINDOW

Copyright © 2017 Copyright Clearance Center, Inc. All Rights Reserved. Privacy statement. Terms and Conditions.
Comments? We would like to hear from you. E-mail us at customercare@copyright.com

Reprint authorization for the C2-SAHA analogs publication: "Reprinted (adapted) with permission from (Structural Requirements of HDAC Inhibitors: SAHA Analogues Modified at the C2 Position Display HDAC6/8 Selectivity. *ACS Medicinal Chemistry Letters* **2017,** *8* (3), 281-286). Copyright (2017) American Chemical Society."

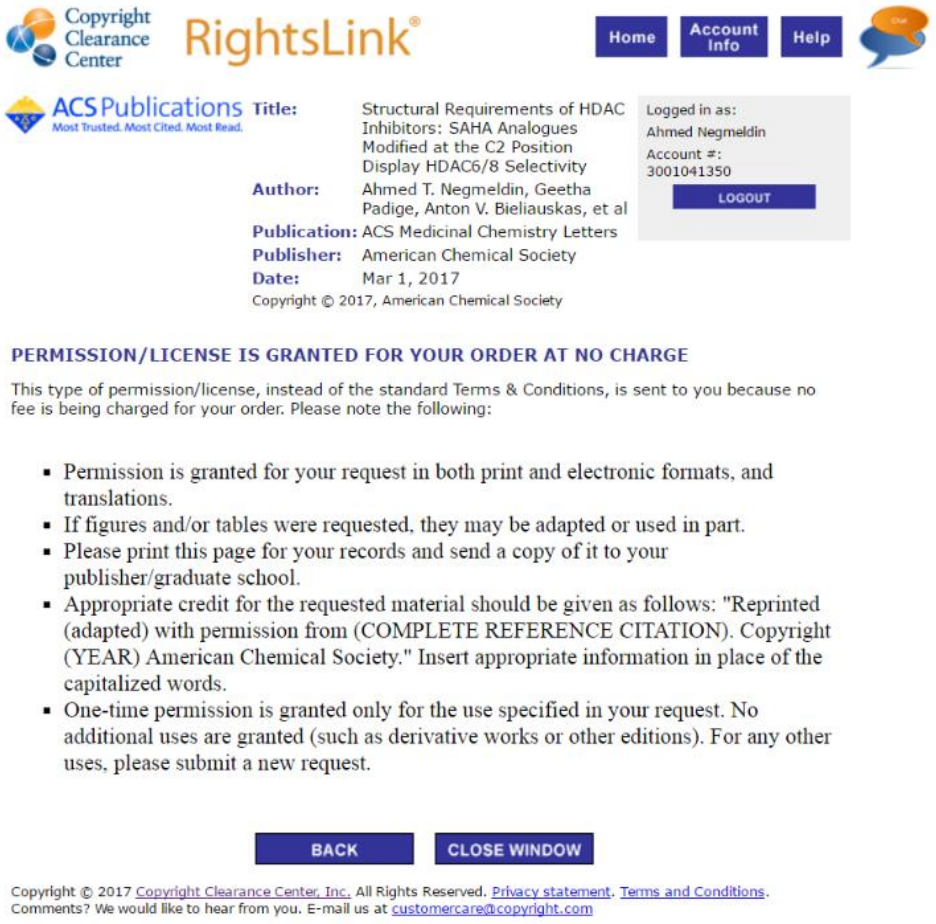

Copyright Clearance Center RightsLink®

Home | Account Info | Help

ACS Publications
Most Trusted. Most Cited. Most Read.

Title:	Structural Requirements of HDAC Inhibitors: SAHA Analogues Modified at the C2 Position Display HDAC6/8 Selectivity
Author:	Ahmed T. Negmeldin, Geetha Padige, Anton V. Bieliauskas, et al
Publication:	ACS Medicinal Chemistry Letters
Publisher:	American Chemical Society
Date:	Mar 1, 2017

Copyright © 2017, American Chemical Society

Logged in as:
Ahmed Negmeldin
Account #:
3001041350
LOGOUT

PERMISSION/LICENSE IS GRANTED FOR YOUR ORDER AT NO CHARGE

This type of permission/license, instead of the standard Terms & Conditions, is sent to you because no fee is being charged for your order. Please note the following:

- Permission is granted for your request in both print and electronic formats, and translations.
- If figures and/or tables were requested, they may be adapted or used in part.
- Please print this page for your records and send a copy of it to your publisher/graduate school.
- Appropriate credit for the requested material should be given as follows: "Reprinted (adapted) with permission from (COMPLETE REFERENCE CITATION). Copyright (YEAR) American Chemical Society." Insert appropriate information in place of the capitalized words.
- One-time permission is granted only for the use specified in your request. No additional uses are granted (such as derivative works or other editions). For any other uses, please submit a new request.

BACK | CLOSE WINDOW

Copyright © 2017 Copyright Clearance Center, Inc. All Rights Reserved. Privacy statement. Terms and Conditions.
Comments? We would like to hear from you. E-mail us at customercare@copyright.com

Reprint authorization for: "Structural Requirements of Histone Deacetylase Inhibitors: SAHA Analogs Modified on the Hydroxamic Acid". *Archiv der Pharmazie (Weinheim, Ger.)* **2016,** *349*, 373-382.

Copyright Clearance Center RightsLink®

Home | Account Info | Help

Title: Structural Requirements of Histone Deacetylase Inhibitors: SAHA Analogs Modified on the Hydroxamic Acid

Author: Anton V. Bieliauskas,Sujith V. W. Weerasinghe,Ahmed T. Negmeldin,Mary Kay H. Pflum

Publication: Archiv der Pharmazie

Publisher: John Wiley and Sons

Date: Apr 9, 2016

Logged in as:
Ahmed Negmeldin
Account #:
3001041350
LOGOUT

Order Completed

Thank you for your order.

This Agreement between Ahmed Negmeldin ("You") and John Wiley and Sons ("John Wiley and Sons") consists of your license details and the terms and conditions provided by John Wiley and Sons and Copyright Clearance Center.

Your confirmation email will contain your order number for future reference.

Printable details.

License Number	4111990593264
License date	May 18, 2017
Licensed Content Publisher	John Wiley and Sons
Licensed Content Publication	Archiv der Pharmazie
Licensed Content Title	Structural Requirements of Histone Deacetylase Inhibitors: SAHA Analogs Modified on the Hydroxamic Acid
Licensed Content Author	Anton V. Bieliauskas,Sujith V. W. Weerasinghe,Ahmed T. Negmeldin,Mary Kay H. Pflum
Licensed Content Date	Apr 9, 2016
Licensed Content Pages	10
Type of use	Dissertation/Thesis
Requestor type	Author of this Wiley article
Format	Print and electronic
Portion	Full article
Will you be translating?	No
Title of your thesis / dissertation	DESIGN, SYNTHESIS AND BIOLOGICAL EVALUATION OF HISTONE DEACETYLASE (HDAC) INHIBITORS: SAHA (VORINOSTAT) ANALOGS AND BIARYL INDOLYL BENZAMIDE INHIBITORS DISPLAY ISOFORM SELECTIVITY
Expected completion date	Jun 2017
Expected size (number of pages)	360
Requestor Location	Ahmed Negmeldin 5101 Cass Ave Department of Chemistry DETROIT, MI 48202 United States Attn: Ahmed Negmeldin
Publisher Tax ID	EU826007151
Billing Type	Invoice
Billing address	Ahmed Negmeldin 5101 Cass Ave. Department of Chemistry DETROIT, MI 48202 United States Attn: Ahmed Negmeldin
Total	0.00 USD

Would you like to purchase the full text of this article? If so, please continue on to the content ordering system located here: Purchase PDF

If you click on the buttons below or close this window, you will not be able to return to the content ordering system.

ORDER MORE | CLOSE WINDOW

REFERENCES

(1) Moving AHEAD with an international human epigenome project. *Nature* **2008,** *454* (7205), 711-715.

(2) Arrowsmith, C. H.; Bountra, C.; Fish, P. V.; Lee, K.; Schapira, M., Epigenetic protein families: a new frontier for drug discovery. *Nat Rev Drug Discov* **2012,** *11* (5), 384-400.

(3) Coppedè, F., The role of epigenetics in colorectal cancer. *Expert Review of Gastroenterology & Hepatology* **2014,** *8* (8), 935-948.

(4) Dawson, Mark A.; Kouzarides, T., Cancer Epigenetics: From Mechanism to Therapy. *Cell* **2012,** *150* (1), 12-27.

(5) Bassett, S. A.; Barnett, M. P. G., The Role of Dietary Histone Deacetylases (HDACs) Inhibitors in Health and Disease. *Nutrients* **2014,** *6* (10), 4273-4301.

(6) Rodd, A. L.; Ververis, K.; Karagiannis, T. C., Current and emerging therapeutics for cutaneous T-Cell lymphoma: histone deacetylase inhibitors. *Lymphoma* **2012,** *2012*, 10.

(7) Gregoretti, I.; Lee, Y.-M.; Goodson, H. V., Molecular evolution of the histone deacetylase family: functional implications of phylogenetic analysis. *J. Mol. Biol.* **2004,** *338* (1), 17-31.

(8) Alenghat, T.; Artis, D., Epigenomic regulation of host–microbiota interactions. *Trends in Immunology* **2014,** *35* (11), 518-525.

(9) Marks, P. A., Histone deacetylase inhibitors: A chemical genetics approach to understanding cellular functions. *Biochimica et Biophysica Acta (BBA) - Gene Regulatory Mechanisms* **2010,** *1799* (10–12), 717-725.

(10) Yang, X.-J.; Seto, E., The Rpd3/Hda1 family of lysine deacetylases: from bacteria and yeast to mice and men. *Nat Rev Mol Cell Biol* **2008,** *9* (3), 206-218.

(11) Gao, L.; Cueto, M. A.; Asselbergs, F.; Atadja, P., Cloning and Functional Characterization of HDAC11, a Novel Member of the Human Histone Deacetylase Family. *Journal of Biological Chemistry* **2002,** *277* (28), 25748-25755.

(12) Bieliauskas, A. V.; Pflum, M. K. H., Isoform-selective histone deacetylase inhibitors. *Chem. Soc. Rev.* **2008,** *37* (7), 1402-1413.

(13) Miyake, Y.; Keusch, J. J.; Wang, L.; Saito, M.; Hess, D.; Wang, X.; Melancon, B. J.; Helquist, P.; Gut, H.; Matthias, P., Structural insights into HDAC6 tubulin deacetylation and its selective inhibition. *Nat Chem Biol* **2016,** *12* (9), 748-754.

(14) Hai, Y.; Christianson, D. W., Histone deacetylase 6 structure and molecular basis of catalysis and inhibition. *Nat. Chem. Biol.* **2016,** *12* (9), 741-747.

(15) Somoza, J. R.; Skene, R. J.; Katz, B. A.; Mol, C.; Ho, J. D.; Jennings, A. J.; Luong, C.; Arvai, A.; Buggy, J. J.; Chi, E.; Tang, J.; Sang, B.-C.; Verner, E.; Wynands, R.; Leahy, E. M.; Dougan, D. R.; Snell, G.; Navre, M.; Knuth, M. W.; Swanson, R. V.; McRee, D. E.; Tari, L. W., Structural Snapshots of Human HDAC8 Provide Insights into the Class I Histone Deacetylases. *Structure* **2004,** *12*, 1324-1334.

(16) Vannini, A.; Volpari, C.; Filocamo, G.; Casavola, E. C.; Brunetti, M.; Renzoni, D.; Chakravarty, P.; Paolini, C.; Francesco, R. D.; Gallinari, P.; Steinkuhler, C.; Marco, S. D., Crystal structure of a eukaryotic zinc-dependent histone deacetylase, human HDAC8, complexed with a hydroxamic acid inhibitor. *Proc Natl Acad Sci U S A* **2004,** *101* (42), 15064-15069.

(17) Millard, C. J.; Watson, P. J.; Celardo, I.; Gordiyenko, Y.; Cowley, S. M.; Robinson, C. V.; Fairall, L.; Schwabe, J. W. R., Class I HDACs Share a Common Mechanism of Regulation by Inositol Phosphates. *Mol. Cell* **2013,** *51* (1), 57-67.

(18) Watson, P. J.; Fairall, L.; Santos, G. M.; Schwabe, J. W., Structure of HDAC3 bound to co-repressor and inositol tetraphosphate. *Nature* **2012,** *481* (7381), 335-40.

(19) Bressi, J. C.; Jennings, A. J.; Skene, R.; Wu, Y.; Melkus, R.; Jong, R. D.; O'Connell, S.; Grimshaw, C. E.; Navre, M.; Gangloff, A. R., Exploration of the HDAC2 foot pocket: synthesis and SAR of substituted N-(2-aminophenyl)benzamides. *Bioorg. Med. Chem. Lett.* **2010,** *20* (10), 3142-3145.

(20) Bottomley, M. J.; Lo Surdo, P.; Di Giovine, P.; Cirillo, A.; Scarpelli, R.; Ferrigno, F.; Jones, P.; Neddermann, P.; De Francesco, R.; Steinkuhler, C.; Gallinari, P.; Carfi, A., Structural and Functional Analysis of the Human HDAC4 Catalytic Domain Reveals a Regulatory Structural Zinc-binding Domain. *The Journal of biological chemistry* **2008,** *283* (39), 26694-26704.

(21) Schuetz, A.; Min, J.; Allali-Hassani, A.; Schapira, M.; Shuen, M.; Loppnau, P.; Mazitschek, R.; Kwiatkowski, N. P.; Lewis, T. A.; Maglathin, R. L.; McLean, T. H.; Bochkarev, A.; Plotnikov, A. N.; Vedadi, M.; Arrowsmith, C. H., Human HDAC7 Harbors a Class IIa Histone Deacetylase-specific Zinc Binding Motif and Cryptic Deacetylase Activity. *The Journal of biological chemistry* **2008,** *283* (17), 11355-11363.

(22) Estiu, G.; Greenberg, E.; Harrison, C. B.; Kwiatkowski, N. P.; Mazitschek, R.; Bradner, J. E.; Wiest, O., Structural origin of selectivity in class II-selective histone deacetylase inhibitors. *J. Med. Chem.* **2008,** *51* (10), 2898-2906.

(23) Wang, D. F.; Helquist, P.; Wiech, N. L.; Wiest, O., Toward Selective Histone Deacetylase Inhibitor Design: Homology Modeling, Docking Studies, and Molecular Dynamics Simulations of Human Class I Histone Deacetylases. *J. Med. Chem.* **2005,** *48* (22), 6936-6947.

(24) Gantt, S. M.; Decroos, C.; Lee, M. S.; Gullett, L. E.; Bowman, C. M.; Christianson, D. W.; Fierke, C. A., General Base-General Acid Catalysis in Human Histone Deacetylase 8. *Biochemistry* **2016,** *55* (5), 820-32.

(25) Finnin, M. S.; Donigian, J. R.; Cohen, A.; Richon, V. M.; Rifkind, R. A.; Marks, P. A.; Pavletich, N. P., Structure of a histone deacetylase homologue bound to trichostatin A. *Nature* **1999,** *401*, 188-193.

(26) Fischle, W.; Dequiedt, F.; Hendzel, M. J.; Guenther, M. G.; Lazar, M. A.; Voelter, W.; Verdin, E., Enzymatic Activity Associated with Class II HDACs Is Dependent on a Multiprotein Complex Containing HDAC3 and SMRT/N-CoR. *Molecular cell* **2002,** *9* (1), 45-57.

(27) Chuang, C.; Pan, J.; Hawke, D. H.; Lin, S. H.; Yu-Lee, L. Y., NudC deacetylation regulates mitotic progression. *PLoS One* **2013,** *8* (9), e73841.

(28) Glozak, M. A.; Seto, E., Histone deacetylases and cancer. *Oncogene* **2007,** *26* (37), 5420-32.

(29) Walsh, C. T.; Garneau-Tsodikova, S.; Gatto, G. J., Protein posttranslational modifications: the chemistry of proteome diversifications. *Angew. Chem., Int. Ed.* **2005,** *44* (45), 7342-7372.

(30) Hebbes, T. R.; Thorne, A. W.; Crane-Robinson, C., A direct link between core histone acetylation and transcriptionally active chromatin. *EMBO J.* **1988,** *7* (5), 1395-1402.

(31) Krämer, O. H.; Göttlicher, M.; Heinzel, T., Histone deacetylase as a therapeutic target. *Trends Endocrinol. Metab.* **2001,** *12*, 294-300.

(32) Hu, E.; Chen, Z.; Fredrickson, T.; Zhu, Y.; Kirkpatrick, R.; Zhang, G.-F.; Johanson, K.; Sung, C.-M.; Liu, R.; Winkler, J., Cloning and characterization of a novel class I histone deacetylase that functions as a transcription repressor. *J. Biol. Chem.* **2000,** *275*, 15254-15264.

(33) Roche, J.; Bertrand, P., Inside HDACs with more selective HDAC inhibitors. *European Journal of Medicinal Chemistry* **2016,** *121*, 451-483.

(34) Bartling, B.; Hofmann, H. S.; Boettger, T.; Hansen, G.; Burdach, S.; Silber, R. E.; Simm, A., Comparative application of antibody and gene array for expression profiling in human squamous cell lung carcinoma. *Lung Cancer* **2005,** *49* (2), 145-154.

(35) Khabele, D.; Son, D.-S.; Parl, A. K.; Goldberg, G. L.; Augenlicht, L. H.; Mariadason, J. M.; Rice, V. M., Drug-Induced Inactivation or Gene Silencing of Class I Histone Deacetylases Suppresses Ovarian Cancer Cell Growth: Implications for Therapy. *Cancer biology & therapy* **2007,** *6* (5), 785-791.

(36) Choi, J. H.; Kwon, H. J.; Yoon, B. I.; Kim, J. H.; Han, S. U.; Joo, H. J.; Kim, D. Y., Expression profile of histone deacetylase 1 in gastric cancer tissues. *Japanese Journal of Cancer Research* **2001,** *92* (12), 1300-1304.

(37) Halkidou, K.; Gaughan, L.; Cook, S.; Leung, H. Y.; Neal, D. E.; Robson, C. N., Upregulation and nuclear recruitment of HDAC1s in hormone refractory prostate cancer. *Prostate* **2004,** *59* (2), 177-189.

(38) Zhang, Z.; Yamashita, H.; Toyama, T.; Sugiura, H.; Ando, Y.; Mita, K.; Hamaguchi, M.; Hara, Y.; Kobayashi, S.; Iwase, H., Quantitation of HDAC1 mRNA expression in invasive carcinoma of the breast*. *Breast cancer research and treatment* **2005,** *94* (1), 11-6.

(39) Wilson, A. J.; Byun, D.-S.; Popova, N.; Murray, L. B.; L'Italien, K.; Sowa, Y.; Arango, D.; Velcich, A.; Augenlicht, L. H.; Mariadason, J. M., Histone deacetylase 3 (HDAC3) and other Class I HDACs regulate colon cell maturation and p21 expression and are deregulated in human colon cancer. *J. Biol. Chem.* **2006,** *281* (19), 13548-13558.

(40) Huang, B. H.; Laban, M.; Leung, C. H.-W.; Lee, L.; Lee, C. K.; Salto-Tellez, M.; Raju, G. C.; Hooi, S. C., Inhibition of histone deacetylase 2 increases apoptosis and p21Cip1/WAF1 expression, independent of histone deacetylase 1. *Cell Death Differ.* **2005,** *12* (4), 395-404.

(41) Oehme, I.; Deubzer, H. E.; Wegener, D.; Pickert, D.; Linke, J.-P.; Hero, B.; Kopp-Schneider, A.; Westermann, F.; Ulrich, S. M.; von Deimling, A.; Fischer, M.; Witt, O., Histone deacetylase 8 in neuroblastoma tumorigenesis. *Clin. Cancer Res.* **2009,** *15* (1), 91-99.

(42) Oehme, I.; Deubzer, H. E.; Lodrini, M.; Milde, T.; Witt, O., Targeting of HDAC8 and investigational inhibitors in neuroblastoma. *Expert Opin. Invest. Drugs* **2009,** *18* (11), 1605-1617.

(43) Sakuma, T.; Uzawa, K.; Onda, T.; Shiiba, M.; Yokoe, H.; Shibahara, T.; Tanzawa, H., Aberrant expression of histone deacetylase 6 in oral squamous cell carcinoma. *Int. J. Oncol.* **2006,** *29* (1), 117-24.

(44) Bazzaro, M.; Lin, Z.; Santillan, A.; Lee, M. K.; Wang, M.-C.; Chan, K. C.; Bristow, R. E.; Mazitschek, R.; Bradner, J.; Roden, R. B. S., Ubiquitin Proteasome System Stress Underlies Synergistic Killing of Ovarian Cancer Cells by Bortezomib and a Novel HDAC6 Inhibitor. *Clinical Cancer Research* **2008,** *14* (22), 7340-7347.

(45) Aldana-Masangkay, G. I.; Sakamoto, K. M., The role of HDAC6 in cancer. *J. Biomed. Biotechnol.* **2011,** *2011*, 875824.

(46) Boyault, C.; Zhang, Y.; Fritah, S.; Caron, C.; Gilquin, B.; Kwon, S. H.; Garrido, C.; Yao, T. P.; Vourc'h, C.; Matthias, P.; Khochbin, S., HDAC6 controls major cell response pathways to cytotoxic accumulation of protein aggregates. *Genes Dev.* **2007,** *21* (17), 2172-81.

(47) Park, S. Y.; Jun, J. A.; Jeong, K. J.; Heo, H. J.; Sohn, J. S.; Lee, H. Y.; Park, C. G.; Kang, J., Histone deacetylases 1, 6 and 8 are critical for invasion in breast cancer. *Oncol. Rep.* **2011,** *25* (6), 1677-81.

(48) Prince, H. M.; Dickinson, M., Romidepsin for cutaneous T-cell lymphoma. *Clinical cancer research : an official journal of the American Association for Cancer Research* **2012,** *18* (13), 3509-15.

(49) Grant, S.; Easley, C.; Kirkpatrick, P., Vorinostat. *Nat. Rev. Drug Discovery* **2007,** *6* (1), 21-22.

(50) Warrell, R. P., Jr.; He, L. Z.; Richon, V.; Calleja, E.; Pandolfi, P. P., Therapeutic targeting of transcription in acute promyelocytic leukemia by use of an inhibitor of histone deacetylase. *J. Natl. Cancer Inst.* **1998,** *90* (21), 1621-1625.

(51) Plumb, J. A.; Finn, P. W.; Williams, R. J.; Bandara, M. J.; Romero, M. R.; Watkins, C. J.; La Thangue, N. B.; Brown, R., Pharmacodynamic response and inhibition of growth of human tumor xenografts by the novel histone deacetylase inhibitor PXD101. *Mol. Cancer Ther.* **2003,** *2* (8), 721-728.

(52) Laubach, J. P.; Moreau, P.; San-Miguel, J. F.; Richardson, P. G., Panobinostat for the treatment of multiple myeloma. *Clin. Cancer Res.* **2015,** *21* (21), 4767-4773.

(53) Lin, R. J.; Nagy, L.; Inoue, S.; Shao, W.; Miller, W. H.; Evans, R. M., Role of the histone deacetylase complex in acute promyelocytic leukaemia. *Nature* **1998,** *391*, 811-814.

(54) Grignani, F.; De Matteis, S.; Nervi, C.; Tomassoni, L.; Gelmetti, V.; Cioce, M.; Fanelli, M.; Ruthardt, M.; Ferrara, F. F.; Zamir, I.; Seiser, C.; Grignani, F.; Lazar, M. A.; Minucci, S.; Pelicci, P. G., Fusion proteins of the retinoic acid receptor-α recruit histone deacetylase in promyelocytic leukaemia. *Nature* **1998,** *391*, 815-818.

(55) Johnstone, R. W., Histone-deacetylase inhibitors: novel drugs for the treatment of cancer. *Nat Rev Drug Discov* **2002,** *1* (4), 287-299.

(56) West, A. C.; Johnstone, R. W., New and emerging HDAC inhibitors for cancer treatment. *J. Clin. Invest.* **2014,** *124* (1), 30-39.

(57) Marks, P.; Rifkind, R. A.; Richon, V. M.; Breslow, R.; Miller, T.; Kelly, W. K., Histone deacetylases and cancer: causes and therapies. *Nat Rev Cancer* **2001,** *1* (3), 194-202.

(58) Weidle, U. H.; Grossmann, A., Inhibition of histone deacetylases: a new strategy to target epigenetic modifications for anticancer treatment. *Anticancer research* **2000,** *20* (3A), 1471-85.

(59) Marks, P. A.; Richon, V. M.; Rifkind, R. A., Histone deacetylase inhibitors: inducers of differentiation or apoptosis of transformed cells. *J Natl Cancer Inst* **2000,** *92* (15), 1210-6.

(60) Kramer, O. H.; Gottlicher, M.; Heinzel, T., Histone deacetylase as a therapeutic target. *Trends Endocrinol. Metab.* **2001,** *12* (7), 294-300.

(61) Qiu, L.; Burgess, A.; Fairlie, D. P.; Leonard, H.; Parsons, P. G.; Gabrielli, B. G., Histone deacetylase inhibitors trigger a G2 checkpoint in normal cells that is defective in tumor cells. *Molecular biology of the cell* **2000,** *11* (6), 2069-83.

(62) Saygin, C.; Carraway, H. E., Emerging therapies for acute myeloid leukemia. *Journal of Hematology & Oncology* **2017,** *10* (1), 93.

(63) Ruefli, A. A.; Ausserlechner, M. J.; Bernhard, D.; Sutton, V. R.; Tainton, K. M.; Kofler, R.; Smyth, M. J.; Johnstone, R. W., The histone deacetylase inhibitor and chemotherapeutic agent suberoylanilide hydroxamic acid (SAHA) induces a cell-death pathway characterized by cleavage of Bid and production of reactive oxygen species. *Proc Natl Acad Sci U S A* **2001,** *98* (19), 10833-10838.

(64) Vrana, J. A.; Decker, R. H.; Johnson, C. R.; Wang, Z.; Jarvis, W. D.; Richon, V. M.; Ehinger, M.; Fisher, P. B.; Grant, S., Induction of apoptosis in U937 human leukemia cells by suberoylanilide hydroxamic acid (SAHA) proceeds through pathways that are regulated by Bcl-2/Bcl-XL, c-Jun, and p21CIP1, but independent of p53. *Oncogene* **1999,** *18* (50), 7016-25.

(65) Kwon, S. H.; Ahn, S. H.; Kim, Y. K.; Bae, G. U.; Yoon, J. W.; Hong, S.; Lee, H. Y.; Lee, Y. W.; Lee, H. W.; Han, J. W., Apicidin, a histone deacetylase inhibitor, induces apoptosis and Fas/Fas ligand expression in human acute promyelocytic leukemia cells. *The Journal of biological chemistry* **2002,** *277* (3), 2073-80.

(66) Glick, R. D.; Swendeman, S. L.; Coffey, D. C.; Rifkind, R. A.; Marks, P. A.; Richon, V. M.; La Quaglia, M. P., Hybrid polar histone deacetylase inhibitor induces apoptosis and CD95/CD95 ligand expression in human neuroblastoma. *Cancer research* **1999,** *59* (17), 4392-9.

(67) Maeda, T.; Towatari, M.; Kosugi, H.; Saito, H., Up-regulation of costimulatory/adhesion molecules by histone deacetylase inhibitors in acute myeloid leukemia cells. *Blood* **2000,** *96* (12), 3847-56.

(68) Magner, W. J.; Kazim, A. L.; Stewart, C.; Romano, M. A.; Catalano, G.; Grande, C.; Keiser, N.; Santaniello, F.; Tomasi, T. B., Activation of MHC class I, II, and CD40 gene expression by histone deacetylase inhibitors. *Journal of immunology* **2000,** *165* (12), 7017-24.

(69) Mishra, N.; Brown, D. R.; Olorenshaw, I. M.; Kammer, G. M., Trichostatin A reverses skewed expression of CD154, interleukin-10, and interferon-gamma gene and protein expression in lupus T cells. *Proc Natl Acad Sci U S A* **2001,** *98* (5), 2628-33.

(70) Shestakova, E.; Bandu, M. T.; Doly, J.; Bonnefoy, E., Inhibition of histone deacetylation induces constitutive derepression of the beta interferon promoter and confers antiviral activity. *Journal of virology* **2001,** *75* (7), 3444-52.

(71) Duvic, M.; Talpur, R.; Ni, X.; Zhang, C.; Hazarika, P.; Kelly, C.; Chiao, J. H.; Reilly, J. F.; Ricker, J. L.; Richon, V. M.; Frankel, S. R., Phase 2 trial of oral vorinostat (suberoylanilide hydroxamic acid, SAHA) for refractory cutaneous T-cell lymphoma (CTCL). *Blood* **2007,** *109* (1), 31-39.

(72) Duvic, M.; Vu, J., Vorinostat: a new oral histone deacetylase inhibitor approved for cutaneous T-cell lymphoma. *Expert opinion on investigational drugs* **2007,** *16* (7), 1111-20.

(73) Grant, C.; Rahman, F.; Piekarz, R.; Peer, C.; Frye, R.; Robey, R. W.; Gardner, E. R.; Figg, W. D.; Bates, S. E., Romidepsin: a new therapy for cutaneous T-cell lymphoma and a potential therapy for solid tumors. *Expert Rev Anticancer Ther* **2010,** *10* (7), 997-1008.

(74) Poole, R. M., Belinostat: first global approval. *Drugs* **2014,** *74* (13), 1543-54.

(75) Fenichel, M. P., FDA approves new agent for multiple myeloma. *J Natl Cancer Inst* **2015,** *107* (6), djv165.

(76) Mottamal, M.; Zheng, S.; Huang, T. L.; Wang, G., Histone deacetylase inhibitors in clinical studies as templates for new anticancer agents. *Molecules* **2015,** *20* (3), 3898-941.

(77) Wagner, J. M.; Hackanson, B.; Lubbert, M.; Jung, M., Histone deacetylase (HDAC) inhibitors in recent clinical trials for cancer therapy. *Clinical epigenetics* **2010,** *1* (3-4), 117-136.

(78) Khan, N.; Jeffers, M.; Kumar, S.; Hackett, C.; Boldog, F.; Khramtsov, N.; Qian, X.; Mills, E.; Berghs, S. C.; Carey, N.; Finn, P. W.; Collins, L. S.; Tumber, A.; Ritchie, J. W.; Jensen, P. B.; Lichenstein, H. S.; Sehested, M., Determination of the class

and isoform selectivity of small-molecule histone deacetylase inhibitors. *Biochem. J.* **2008,** *409* (2), 581-589.

(79) Kelly, W. K.; O'Connor, O. A.; Krug, L. M.; Chiao, J. H.; Heaney, M.; Curley, T.; MacGregore-Cortelli, B.; Tong, W.; Secrist, J. P.; Schwartz, L.; Richardson, S.; Chu, E.; Olgac, S.; Marks, P. A.; Scher, H.; Richon, V. M., Phase I Study of an Oral Histone Deacetylase Inhibitor, Suberoylanilide Hydroxamic Acid, in Patients With Advanced Cancer. *Journal of Clinical Oncology* **2005,** *23* (17), 3923-3931.

(80) Sandor, V.; Bakke, S.; Robey, R. W.; Kang, M. H.; Blagosklonny, M. V.; Bender, J.; Brooks, R.; Piekarz, R. L.; Tucker, E.; Figg, W. D.; Chan, K. K.; Goldspiel, B.; Fojo, A. T.; Balcerzak, S. P.; Bates, S. E., Phase I trial of the histone deacetylase inhibitor, Depsipeptide (FR901228, NSC 630176), in patients with refractory neoplasms. *Clin. Cancer Res.* **2002,** *8*, 718-728.

(81) Duan, W.; Li, J.; Inks, E. S.; Chou, C. J.; Jia, Y.; Chu, X.; Li, X.; Xu, W.; Zhang, Y., Design, Synthesis, and Antitumor Evaluation of Novel Histone Deacetylase Inhibitors Equipped with a Phenylsulfonylfuroxan Module as a Nitric Oxide Donor. *Journal of medicinal chemistry* **2015,** *58* (10), 4325-4338.

(82) Hutt, D. M.; Olsen, C. A.; Vickers, C. J.; Herman, D.; Chalfant, M. A.; Montero, A.; Leman, L. J.; Burkle, R.; Maryanoff, B. E.; Balch, W. E.; Ghadiri, M. R., Potential Agents for Treating Cystic Fibrosis: Cyclic Tetrapeptides That Restore Trafficking and Activity of ΔF508-CFTR. *ACS Medicinal Chemistry Letters* **2011,** *2* (9), 703-707.

(83) Furumai, R.; Matsuyama, A.; Kobashi, N.; Lee, K.-H.; Nishiyama, M.; Nakajima, H.; Tanaka, A.; Komatsu, Y.; Nishino, N.; Yoshida, M.; Horinouchi, S., FK228

(Depsipeptide) as a Natural Prodrug That Inhibits Class I Histone Deacetylases. *Cancer research* **2002,** *62* (17), 4916-4921.

(84) Methot, J. L.; Chakravarty, P. K.; Chenard, M.; Close, J.; Cruz, J. C.; Dahlberg, W. K.; Fleming, J.; Hamblett, C. L.; Hamill, J. E.; Harrington, P.; Harsch, A.; Heidebrecht, R.; Hughes, B.; Jung, J.; Kenific, C. M.; Kral, A. M.; Meinke, P. T.; Middleton, R. E.; Ozerova, N.; Sloman, D. L.; Stanton, M. G.; Szewczak, A. A.; Tyagarajan, S.; Witter, D. J.; Paul Secrist, J.; Miller, T. A., Exploration of the internal cavity of histone deacetylase (HDAC) with selective HDAC1/HDAC2 inhibitors (SHI-1:2). *Bioorg Med Chem Lett* **2008,** *18* (3), 973-978.

(85) Malvaez, M.; McQuown, S. C.; Rogge, G. A.; Astarabadi, M.; Jacques, V.; Carreiro, S.; Rusche, J. R.; Wood, M. A., HDAC3-selective inhibitor enhances extinction of cocaine-seeking behavior in a persistent manner. *Proc. Natl. Acad. Sci. U. S. A.* **2013,** *110* (7), 2647-2652.

(86) Butler, K. V.; Kalin, J.; Brochier, C.; Vistoli, G.; Langley, B.; Kozikowski, A. P., Rational design and simple chemistry yield a superior, neuroprotective HDAC6 inhibitor, tubastatin A. *J. Am. Chem. Soc.* **2010,** *132* (31), 10842-10846.

(87) Balasubramanian, S.; Ramos, J.; Luo, W.; Sirisawad, M.; Verner, E.; Buggy, J. J., A novel histone deacetylase 8 (HDAC8)-specific inhibitor PCI-34051 induces apoptosis in T-cell lymphomas. *Leukemia* **2008,** *22*, 1026-1034.

(88) Fass, D. M.; Shah, R.; Ghosh, B.; Hennig, K.; Norton, S.; Zhao, W.-N.; Reis, S. A.; Klein, P. S.; Mazitschek, R.; Maglathlin, R. L.; Lewis, T. A.; Haggarty, S. J., Short-chain HDAC inhibitors differentially affect vertebrate development and neuronal chromatin. *ACS Med. Chem. Lett.* **2011,** *2* (1), 39-42.

(89) Olson, D. E.; Wagner, F. F.; Kaya, T.; Gale, J. P.; Aidoud, N.; Davoine, E. L.; Lazzaro, F.; Weiwer, M.; Zhang, Y. L.; Holson, E. B., Discovery of the first histone deacetylase 6/8 dual inhibitors. *J. Med. Chem.* **2013,** *56* (11), 4816-4820.

(90) Tang, G.; Wong, J. C.; Zhang, W.; Wang, Z.; Zhang, N.; Peng, Z.; Zhang, Z.; Rong, Y.; Li, S.; Zhang, M.; Yu, L.; Feng, T.; Zhang, X.; Wu, X.; Wu, J. Z.; Chen, L., Identification of a Novel Aminotetralin Class of HDAC6 and HDAC8 Selective Inhibitors. *Journal of medicinal chemistry* **2014,** *57* (19), 8026-8034.

(91) Rodrigues, D. A.; Ferreira-Silva, G. À.; Ferreira, A. C. S.; Fernandes, R. A.; Kwee, J. K.; Sant'Anna, C. M. R.; Ionta, M.; Fraga, C. A. M., Design, Synthesis, and Pharmacological Evaluation of Novel N-Acylhydrazone Derivatives as Potent Histone Deacetylase 6/8 Dual Inhibitors. *Journal of medicinal chemistry* **2016,** *59* (2), 655-670.

(92) Witter, D. J.; Harrington, P.; Wilson, K. J.; Chenard, M.; Fleming, J. C.; Haines, B.; Kral, A. M.; Secrist, J. P.; Miller, T. A., Optimization of biaryl Selective HDAC1&2 Inhibitors (SHI-1:2). *Bioorg Med Chem Lett* **2008,** *18* (2), 726-731.

(93) Padige, G.; Negmeldin, A. T.; Pflum, M. K. H., Development of an ELISA-based HDAC activity assay for characterization of isoform-selective inhibitors. *J. Biomol. Screening* **2015,** *20* (10), 1277-1285.

(94) Garcia-Manero, G.; Assouline, S.; Cortes, J.; Estrov, Z.; Kantarjian, H.; Yang, H.; Newsome, W. M.; Miller, W. H., Jr.; Rousseau, C.; Kalita, A.; Bonfils, C.; Dubay, M.; Patterson, T. A.; Li, Z.; Besterman, J. M.; Reid, G.; Laille, E.; Martell, R. E.; Minden, M., Phase 1 study of the oral isotype specific histone deacetylase inhibitor MGCD0103 in leukemia. *Blood* **2008,** *112* (4), 981-9.

(95) Gojo, I.; Jiemjit, A.; Trepel, J. B.; Sparreboom, A.; Figg, W. D.; Rollins, S.; Tidwell, M. L.; Greer, J.; Chung, E. J.; Lee, M.-J.; Gore, S. D.; Sausville, E. A.; Zwiebel, J.; Karp, J. E., Phase 1 and pharmacological study of MS-275, a histone deacetylase inhibitor, in adults with refractory and relapsed acute leukemias. *Blood* **2007,** *109* (7), 2781-2790.

(96) Kelly, W. K.; O'Connor, O. A.; Krug, L. M.; Chiao, J. H.; Heaney, M.; Curley, T.; MacGregore-Cortelli, B.; Tong, W.; Secrist, J. P.; Schwartz, L.; Richardson, S.; Chu, E.; Olgac, S.; Marks, P. A.; Scher, H.; Richon, V. M., Phase I study of an oral histone deacetylase inhibitor, suberoylanilide hydroxamic acid, in patients with advanced cancer. *J. Clin. Oncol.* **2005,** *23* (17), 3923-3931.

(97) McKinsey, T. A., Isoform-selective HDAC inhibitors: closing in on translational medicine for the heart. *Journal of molecular and cellular cardiology* **2011,** *51* (4), 491-496.

(98) Wambua, M. K.; Nalawansha, D. A.; Negmeldin, A. T.; Pflum, M. K., Mutagenesis studies of the 14 Å internal cavity of histone deacetylase 1: Insights towards the acetate escape hypothesis and selective inhibitor design. *J. Med. Chem.* **2014,** *57* (3), 642-650.

(99) Millard, Christopher J.; Watson, Peter J.; Celardo, I.; Gordiyenko, Y.; Cowley, Shaun M.; Robinson, Carol V.; Fairall, L.; Schwabe, John W. R., Class I HDACs Share a Common Mechanism of Regulation by Inositol Phosphates. *Molecular cell* **2013,** *51* (1), 57-67.

(100) Watson, P. J.; Fairall, L.; Santos, G. M.; Schwabe, J. W. R., Structure of HDAC3 bound to co-repressor and inositol tetraphosphate. *Nature* **2012,** *481* (7381), 335-340.

(101) Hai, Y.; Christianson, D. W., Histone deacetylase 6 structure and molecular basis of catalysis and inhibition. *Nat Chem Biol* **2016,** *12* (9), 741-747.

(102) Bieliauskas, A. V.; Weerasinghe, S. V. W.; Negmeldin, A. T.; Pflum, M. K. H., Structural requirements of histone deacetylase inhibitors: SAHA analogs modified on the hydroxamic acid. *Arch. Pharm. (Weinheim, Ger.)* **2016,** *349*, 373-382.

(103) Bieliauskas, A.; Weerasinghe, S.; Pflum, M. H., Structural requirements of HDAC inhibitors: SAHA analogs functionalized adjacent to the hydroxamic acid. *Bioorg. Med. Chem. Lett.* **2007,** *17* (8), 2216-2219.

(104) Choi, S. E.; Weerasinghe, S. V.; Pflum, M. K., The structural requirements of histone deacetylase inhibitors: Suberoylanilide hydroxamic acid analogs modified at the C3 position display isoform selectivity. *Bioorg. Med. Chem. Lett.* **2011,** *21* (20), 6139-6142.

(105) Choi, S. E.; Pflum, M. K. H., The structural requirements of histone deacetylase inhibitors: Suberoylanilide hydroxamic acid analogs modified at the C6 position. *Bioorg. Med. Chem. Lett.* **2012,** *22* (23), 7084-7086.

(106) Choi, S. E. THE STRUCTURAL REQUIREMENTS OF HISTONE DEACETYLASE (HDAC) INHIBITORS: SUBEROLYANILIDE HYDROXAMIC ACID (SAHA) ANALOGUES MODIFIED AT C3, C6, AND C7 POSITIONS ENHANCE SELECTIVITY. Wayne State University, 2012.

(107) Park, S. Y.; Jun, J. A.; Jeong, K. J.; Heo, H. J.; Sohn, J. S.; Lee, H. Y.; Park, C. G.; Kang, J., Histone deacetylases 1, 6 and 8 are critical for invasion in breast cancer. *Oncology reports* **2011,** *25* (6), 1677-81.

(108) Padige, G. Development Of Elisa-Based Hdac Activity Assay For Identification Of Isoform Selective Hdac Inhibitors. PhD dissertation, Wayne State University, 2014.

(109) Shinji, C.; Maeda, S.; Imai, K.; Yoshida, M.; Hashimoto, Y.; Miyachi, H., Design, synthesis, and evaluation of cyclic amide/imide-bearing hydroxamic acid derivatives as class-selective histone deacetylase (HDAC) inhibitors. *Bioorg Med Chem* **2006,** *14* (22), 7625-7651.

(110) Jones, P.; Altamura, S.; De Francesco, R.; Gallinari, P.; Lahm, A.; Neddermann, P.; Rowley, M.; Serafini, S.; Steinkuhler, C., Probing the elusive catalytic activity of vertebrate class IIa histone deacetylases. *Bioorg Med Chem Lett* **2008,** *18* (6), 1814-1819.

(111) Halley, F.; Reinshagen, J.; Ellinger, B.; Wolf, M.; Niles, A. L.; Evans, N. J.; Kirkland, T. A.; Wagner, J. M.; Jung, M.; Gribbon, P.; Gul, S., A Bioluminogenic HDAC Activity Assay: Validation and Screening. *Journal of biomolecular screening* **2011,** *16* (10), 1227-1235.

(112) Negmeldin, A. T.; Padige, G.; Bieliauskas, A. V.; Pflum, M. K. H., Structural Requirements of HDAC Inhibitors: SAHA Analogues Modified at the C2 Position Display HDAC6/8 Selectivity. *ACS Medicinal Chemistry Letters* **2017,** *8* (3), 281-286.

(113) Bradner, J. E.; West, N.; Grachan, M. L.; Greenberg, E. F.; Haggarty, S. J.; Warnow, T.; Mazitschek, R., Chemical phylogenetics of histone deacetylases. *Nat. Chem. Biol.* **2010,** *6* (3), 238-243.

(114) Hackanson, B.; Rimmele, L.; Benkißer, M.; Abdelkarim, M.; Fliegauf, M.; Jung, M.; Lübbert, M., HDAC6 as a target for antileukemic drugs in acute myeloid leukemia. *Leuk. Res.* **2012,** *36* (8), 1055-1062.

(115) Vickers, C. J.; Olsen, C. A.; Leman, L. J.; Ghadiri, M. R., Discovery of HDAC inhibitors that lack an active site Zn2+-binding functional group. *ACS Med. Chem. Lett.* **2012,** *3* (6), 505-508.

(116) Sodji, Q. H.; Patil, V.; Kornacki, J. R.; Mrksich, M.; Oyelere, A. K., Synthesis and structure–activity relationship of 3-hydroxypyridine-2-thione-based histone deacetylase inhibitors. *J. Med. Chem.* **2013,** *56* (24), 9969-9981.

(117) Li, X.; Inks, E. S.; Li, X.; Hou, J.; Chou, C. J.; Zhang, J.; Jiang, Y.; Zhang, Y.; Xu, W., Discovery of the first N-hydroxycinnamamide-based histone deacetylase 1/3 dual inhibitors with potent oral antitumor activity. *J. Med. Chem.* **2014,** *57* (8), 3324-3341.

(118) Chatterjee, A. K.; Choi, T.-L.; Sanders, D. P.; Grubbs, R. H., A General Model for Selectivity in Olefin Cross Metathesis. *J. Am. Chem. Soc.* **2003,** *125* (37), 11360-11370.

(119) Morris, G. M.; Huey, R.; Lindstrom, W.; Sanner, M. F.; Belew, R. K.; Goodsell, D. S.; Olson, A. J., AutoDock4 and AutoDockTools4: automated docking with selective receptor flexibility. *J. Comput. Chem.* **2009,** *30* (16), 2785-2791.

(120) Weerasinghe, S. V. W.; Estiu, G.; Wiest, O.; Pflum, M. K. H., Residues in the 11Å channel of histone deacetylase 1 promote catalytic activity: Implications for designing isoform-selective histone deacetylase inhibitors. *J. Med. Chem.* **2008,** *51* (18), 5542-5551.

(121) Schäfer, S.; Saunders, L.; Eliseeva, E.; Velena, A.; Jung, M.; Schwienhorst, A.; Strasser, A.; Dickmanns, A.; Ficner, R.; Schlimme, S.; Sippl, W.; Verdin, E.; Jung, M., Phenylalanine-containing hydroxamic acids as selective inhibitors of class IIb histone deacetylases (HDACs). *Bioorg. Med. Chem. Lett.* **2008,** *16* (4), 2011-2033.

(122) Kozikowski, A. P.; Chen, Y.; Gaysin, A. M.; Savoy, D. N.; Billadeau, D. D.; Kim, K. H., Chemistry, biology, and QSAR studies of substituted biaryl hydroxamates and mercaptoacetamides as HDAC inhibitors-nanomolar-potency inhibitors of pancreatic cancer cell growth. *ChemMedChem* **2008,** *3* (3), 487-501.

(123) Wagner, F. F.; Olson, D. E.; Gale, J. P.; Kaya, T.; Weiwer, M.; Aidoud, N.; Thomas, M.; Davoine, E. L.; Lemercier, B. C.; Zhang, Y. L.; Holson, E. B., Potent and selective inhibition of histone deacetylase 6 (HDAC6) does not require a surface-binding motif. *J. Med. Chem.* **2013,** *56* (4), 1772-1776.

(124) Gottlieb, H. E.; Kotlyar, V.; Nudelman, A., NMR Chemical Shifts of Common Laboratory Solvents as Trace Impurities. *The Journal of organic chemistry* **1997,** *62* (21), 7512-7515.

(125) Bonnett, S. A.; Papireddy, K.; Higgins, S.; del Cardayre, S.; Reynolds, K. A., Functional Characterization of an NADPH Dependent 2-Alkyl-3-ketoalkanoic Acid

Reductase Involved in Olefin Biosynthesis in Stenotrophomonas maltophilia. *Biochemistry* **2011,** *50* (44), 9633-9640.

(126) Green, M. R.; Sambrook, J., *Molecular Cloning: A Laboratory Manual*. Cold Spring Harbor Laboratory Press, 2012.

(127) Sanner, M. F., Python: a programming language for software integration and development. *Journal of molecular graphics & modelling* **1999,** *17* (1), 57-61.

(128) Bressi, J. C.; Jennings, A. J.; Skene, R.; Wu, Y.; Melkus, R.; De Jong, R.; O'Connell, S.; Grimshaw, C. E.; Navre, M.; Gangloff, A. R., Exploration of the HDAC2 foot pocket: Synthesis and SAR of substituted N-(2-aminophenyl)benzamides. *Bioorganic & medicinal chemistry letters* **2010,** *20* (10), 3142-5.

(129) Bergman, J. A.; Woan, K.; Perez-Villarroel, P.; Villagra, A.; Sotomayor, E. M.; Kozikowski, A. P., Selective Histone Deacetylase 6 Inhibitors Bearing Substituted Urea Linkers Inhibit Melanoma Cell Growth. *Journal of medicinal chemistry* **2012,** *55* (22), 9891-9899.

(130) Senger, J.; Melesina, J.; Marek, M.; Romier, C.; Oehme, I.; Witt, O.; Sippl, W.; Jung, M., Synthesis and Biological Investigation of Oxazole Hydroxamates as Highly Selective Histone Deacetylase 6 (HDAC6) Inhibitors. *J. Med. Chem.* **2016,** *59* (4), 1545-1555.

(131) Evans, D. A.; Ennis, M. D.; Mathre, D. J., Asymmetric alkylation reactions of chiral imide enolates. A practical approach to the enantioselective synthesis of .alpha.-substituted carboxylic acid derivatives. *Journal of the American Chemical Society* **1982,** *104* (6), 1737-1739.

(132) Dale, J. A.; Dull, D. L.; Mosher, H. S., .alpha.-Methoxy-.alpha.-trifluoromethylphenylacetic acid, a versatile reagent for the determination of enantiomeric composition of alcohols and amines. *The Journal of organic chemistry* **1969,** *34* (9), 2543-2549.

(133) Altendorfer, M.; Raja, A.; Sasse, F.; Irschikc, H.; Menche, D., Modular synthesis of polyene side chain analogues of the potent macrolide antibiotic etnangien by aflexible coupling strategy based on hetero-bis-metallated alkenes. *Org. Biomol. Chem.* **2013,** *11*, 2116.

(134) Miller, J. F.; Chong, P. Y.; Shotwell, J. B.; Catalano, J. G.; Tai, V. W. F.; Fang, J.; Banka, A. L.; Roberts, C. D.; Youngman, M.; Zhang, H.; Xiong, Z.; Mathis, A.; Pouliot, J. J.; Hamatake, R. K.; Price, D. J.; Seal, J. W.; Stroup, L. L.; Creech, K. L.; Carballo, L. H.; Todd, D.; Spaltenstein, A.; Furst, S.; Hong, Z.; Peat, A. J., Hepatitis C Replication Inhibitors That Target the Viral NS4B Protein. *Journal of medicinal chemistry* **2014,** *57* (5), 2107-2120.

(135) Kim, D. H.; Chung, S., Stereochemistry in enzyme inhibition: synthesis and evaluation of enantiomerically pure 2-benzyl-3-formylpropanoic acids as inhibitors of carboxypeptidase A. *Tetrahedron: Asymmetry* **1999,** *10* (19), 3769-3776.

(136) Tredwell, M.; Luft, J. A. R.; Schuler, M.; Tenza, K.; Houk, K. N.; Gouverneur, V., Fluorine-Directed Diastereoselective Iodocyclizations. *Angewandte Chemie* **2008,** *120* (2), 363-366.

(137) Hutchison, P. C.; Heightman, T. D.; Procter, D. J., Application of a Recyclable Pseudoephedrine Resin in Asymmetric Alkylations on Solid Phase. *The Journal of organic chemistry* **2004,** *69* (3), 790-801.

(138) Afewerki, S.; Ibrahem, I.; Rydfjord, J.; Breistein, P.; Córdova, A., Direct Regiospecific and Highly Enantioselective Intermolecular α-Allylic Alkylation of Aldehydes by a Combination of Transition-Metal and Chiral Amine Catalysts. *Chemistry – A European Journal* **2012,** *18* (10), 2972-2977.

(139) Jöst, C.; Nitsche, C.; Scholz, T.; Roux, L.; Klein, C. D., Promiscuity and Selectivity in Covalent Enzyme Inhibition: A Systematic Study of Electrophilic Fragments. *Journal of medicinal chemistry* **2014,** *57* (18), 7590-7599.

(140) Negmeldin, A. T.; Pflum, M. K. H., The structural requirements of histone deacetylase Inhibitors: SAHA analogs modified at the C5 Position Display dual HDAC6/8 Selectivity. *Bioorganic & medicinal chemistry letters* **2017**.

(141) Miller, D. C.; Choi, G. J.; Orbe, H. S.; Knowles, R. R., Catalytic Olefin Hydroamidation Enabled by Proton-Coupled Electron Transfer. *Journal of the American Chemical Society* **2015,** *137* (42), 13492-13495.

(142) Wang, D. F.; Wiest, O.; Helquist, P.; Lan-Hargest, H. Y.; Wiech, N. L., On the Function of the 14 Å Long Internal Cavity of Histone Deacetylase-Like Protein: Implications for the Design of Histone Deacetylase Inhibitors. *J. Med. Chem.* **2004,** *47* (13), 3409-3417.

(143) Haider, S.; Joseph, C. G.; Neidle, S.; Fierke, C. A.; Fuchter, M. J., On the function of the internal cavity of histone deacetylase protein 8: R37 is a crucial residue for catalysis. *Bioorg Med Chem Lett* **2011,** *21* (7), 2129-32.

(144) Moradei, O. M.; Mallais, T. C.; Frechette, S.; Paquin, I.; Tessier, P. E.; Leit, S. M.; Fournel, M.; Bonfils, C.; Trachy-Bourget, M. C.; Liu, J. H.; Yan, T. P.; Lu, A. H.; Rahil, J.; Wang, J.; Lefebvre, S.; Li, Z. M.; Vaisburg, A. F.; Besterinan, J. M., Novel

aminophenyl benzamide-type histone deacetylase inhibitors with enhanced potency and selectivity. *J. Med. Chem.* **2007,** *50* (23), 5543-5546.

(145) Di Micco, S.; Chini, M. G.; Terracciano, S.; Bruno, I.; Riccio, R.; Bifulco, G., Structural basis for the design and synthesis of selective HDAC inhibitors. *Bioorg Med Chem* **2013,** *21* (13), 3795-807.

(146) Giannini, G.; Marzi, M.; Marzo, M. D.; Battistuzzi, G.; Pezzi, R.; Brunetti, T.; Cabri, W.; Vesci, L.; Pisano, C., Exploring bis-(indolyl)methane moiety as an alternative and innovative CAP group in the design of histone deacetylase (HDAC) inhibitors. *Bioorg Med Chem Lett* **2009,** *19* (10), 2840-3.

(147) Lamblin, M.; Dabbas, B.; Spingarn, R.; Mendoza-Sanchez, R.; Wang, T. T.; An, B. S.; Huang, D. C.; Kremer, R.; White, J. H.; Gleason, J. L., Vitamin D receptor agonist/histone deacetylase inhibitor molecular hybrids. *Bioorg Med Chem* **2010,** *18* (11), 4119-37.

(148) Jadhav, S. V. V.; Bandyopadhyay, A.; Benke, S. N.; Malia, S. M.; Gopi, H. N., A facile synthesis and crystallographic analysis of N-protected β-amino alcohols and short peptaibols. *Organic & biomolecular chemistry* **2011,** *9* (11), 4182-4187.

(149) Zhang, Y.; Yang, P.; Chou, C. J.; Liu, C.; Wang, X.; Xu, W., Development of N-Hydroxycinnamamide-Based Histone Deacetylase Inhibitors with an Indole-Containing Cap Group. *ACS Medicinal Chemistry Letters* **2013,** *4* (2), 235-238.

(150) Junek, R.; Kverka, M.; Jandera, A.; Panajotová, V.; Šatinský, D.; Macháček, M.; Kuchař, M., Antileukotrienic phenethylamido derivatives of arylalkanoic acids in the treatment of ulcerative colitis. *European Journal of Medicinal Chemistry* **2009,** *44* (1), 332-344.

(151) Zhai, L.; Zhang, Y.-L.; Kang, J. S.; Oelschlaeger, P.; Xiao, L.; Nie, S.-S.; Yang, K.-W., Triazolylthioacetamide: A Valid Scaffold for the Development of New Delhi Metallo-β-Lactmase-1 (NDM-1) Inhibitors. *ACS Medicinal Chemistry Letters* **2016,** *7* (4), 413-417.

(152) Stolfa, D. A.; Stefanachi, A.; Gajer, J. M.; Nebbioso, A.; Altucci, L.; Cellamare, S.; Jung, M.; Carotti, A., Design, Synthesis, and Biological Evaluation of 2-Aminobenzanilide Derivatives as Potent and Selective HDAC Inhibitors. *ChemMedChem* **2012,** *7* (7), 1256-1266.

ABSTRACT

DESIGN, SYNTHESIS AND BIOLOGICAL EVALUATION OF HISTONE DEACETYLASE (HDAC) INHIBITORS: SAHA (VORINOSTAT) ANALOGS AND BIARYL INDOLYL BENZAMIDE INHIBITORS DISPLAY ISOFORM SELECTIVITY

by

AHMED THABET NEGMELDIN

August 2017

Advisor: Dr. Mary Kay H. Pflum

Major: Chemistry (Organic)

Degree: Doctor of Philosophy

HDAC proteins have emerged as interesting targets for anti-cancer drugs due to their involvement in cancers, as well as several other diseases. Several HDAC inhibitors have been approved by the FDA as anti-cancer drugs, including SAHA (suberoylanilide hydroxamic acid, Vorinostat). Unfortunately, SAHA inhibits most HDAC isoforms, which limit its use as a pharmacological tool and may lead to side effects in the clinic. In this work we were interested in developing isoform selective HDAC inhibitors, which may decrease or eliminate the side effects associated with non-selective inhibitors treatment. In addition, isoform selective HDAC inhibitors can be used as biological tools to help understand the HDAC-related cancer biology. Our strategy was based on synthesis and screening of several derivatives of the non-selective FDA approved drug SAHA substituted at different positions of the linker region. Several SAHA analogs modified at the C4 and C5 positions of the linker were synthesized. The new C4- and C5-modified SAHA libraries, along with the previously synthesized C2-modified SAHA analogs were screened *in vitro* and *in*

cellulo for HDAC isoform selectivity. Interestingly, several analogs exhibited dual HDAC6/HDAC8 selectivity. Enantioselective syntheses of the pure enantiomers of some of the interesting analogs were performed and the enantiomers were screened *in vitro*. Among the most interesting analogs, (*R*)-C4-benzyl SAHA displayed 520- to 1300-fold selectivity for HDAC6 and HDAC8 over HDAC1, 2, and 3, with IC_{50} values of 48 and 27 nM with HDAC6 and 8, respectively. Docking studies were performed to provide structural rationale for the observed selectivity of the new analogs. In addition, rational design, synthesis, and screening of several other biaryl indolyl benzamide HDAC inhibitors is discussed, and some showed modest HDAC1 selectivity. The new biaryl indolyl benzamides can be useful to further develop HDAC1 selective inhibitors. The dual HDAC6/8 selective inhibitors can be used as lead compounds and as a chemical tool to study HDAC related cancer biology. The observed enhancement of selectivity upon modifying the linker region of the non-selective inhibitor SAHA shows that modifying current drugs, like SAHA, could lead to substantial improvement in its pharmacodynamic properties.

AUTOBIOGRAPHICAL STATEMENT

AHMED THABET NEGMELDIN

Educational background

Ph.D. in Chemistry, 2017 (Organic Chemistry)
Wayne State University, Detroit, MI, 48202, USA

M.Sc. in Pharmaceutical Sciences, 2011 (Pharmaceutical Organic Chemistry)
Faculty of Pharmacy, Cairo University, Cairo, Egypt

B.Sc. in Pharmacy and Pharmaceutical Sciences, 2006
Faculty of Pharmacy, Cairo University, Cairo, Egypt

Fellowships, Scholarships and Awards

- **2017**: Willard R. Lenz, Jr. Endowed Memorial Scholarship, Wayne State University.
- **2017**: Graduate school symposium award for 2nd place in the best poster presentation competition.
- **2017**: Wayne State University graduate school micro-credentials for demonstrating best practices in oral presentation, and for best practices in academic poster design.
- **2016-2017**: Thomas C. Rumble University Graduate Fellowship, Wayne State University.
- **2016**: Dr. Cal Stevens memorial scholarship (travel award for outstanding record in research), Wayne State University.
- **2016**: Clifford G. Drouillard Annual Chemistry Award for outstanding record in departmental service and/or research, Wayne State University.
- **2016**: James C. French Graduate award for outstanding academic and research record, Wayne State University.
- **2016**: Graduate Student Professional Travel Award (GSPTA), Wayne State University.
- **2015**: Graduate School honor citation for excellence in teaching award, Wayne State University.
- **2014**: Norman A. LeBel Endowed Graduate Award in Organic Chemistry, Wayne State University.
- **2014**: Departmental honor citation for excellence in teaching award, Wayne State University.
- **2012-2016**: Graduate Teaching Assistant Award and scholarship, Wayne State University.
- **2006**: Honors, Faculty of Pharmacy, Cairo University, Cairo, Egypt.

Publications

- **Ahmed T. Negmeldin** and Mary Kay H. Pflum, "The structural requirements of histone deacetylase inhibitors: C4-modified SAHA analogs display dual HDAC6/HDAC8 selectivity" (***Eur. J. Med. Chem.***, *Submitted*).
- **Ahmed T. Negmeldin** and Mary Kay H. Pflum, "The structural requirements of histone deacetylase inhibitors: SAHA analogs modified at the C5 position display dual HDAC6/8 selectivity" (***Bioorg. Med. Chem. Lett.***, **2017**, *Accepted*).
- **Ahmed T. Negmeldin**, Geetha Padige, Anton V. Bieliauskas, and Mary Kay H. Pflum, "Structural requirements of HDAC inhibitors: SAHA analogues modified at the C2 position display HDAC6/8 selectivity", ***ACS Med. Chem. Lett.***, **2017**, *8* (3), 281-286.
- Jehad Almaliti, Ayad A. Al-Hamashi, **Ahmed T. Negmeldin**, Christin L. Hanigan, Lalith Perera, Mary Kay H Pflum, Robert A. Casero, Jr., and L. M. Viranga Tillekeratne, "Largazole Analogues Embodying Radical Changes in the Depsipeptide Ring: Development of a More Selective and Highly Potent Analogue", ***J. Med. Chem.*****, 2016**, *59* (23), 10642-10660.
- Anton V. Bieliauskas, Sujith V.W. Weerasinghe, **Ahmed T. Negmeldin**, and Mary Kay H. Pflum, "The structural requirements of histone deacetylase inhibitors: SAHA analogs modified on the hydroxamic acid", ***Arch. Pharm. (Weinheim, Ger.)***, **2016**, *349* (5), 373-382.
- Geetha Padige, **Ahmed T. Negmeldin**, and Mary Kay H. Pflum, "Development of an ELISA-Based HDAC Activity Assay for Characterization of Isoform-Selective Inhibitors", ***J. Biomol. Screen.***, **2015**, *20* (10), 1277-1285.
- Magdalene K. Wambua, Dhanusha A. Nalawansha, **Ahmed T. Negmeldin**, and Mary Kay H. Pflum, "Mutagenesis Studies of the 14 Å Internal Cavity of Histone Deacetylase 1: Insights toward the Acetate-Escape Hypothesis and Selective Inhibitor Design", ***J. Med. Chem.*****, 2014**, *57* (3), 642-650.
- Manal M. Kandeel, Lamia W. Mohamed, Mohamed K. Abd El-hamid, **Ahmed T. Negmeldin**, "Design, Synthesis, and Antitumor Evaluation of Novel Pyrazolo[3,4-d]pyrimidine Derivatives", ***Sci. Pharm.*****, 2012**, *80* (3), 531-545.
- Manal M. Kandeel, Lamia W. Mohamed, Mohamed K. Abd El-hamid, **Ahmed T. Negmeldin**, "Synthesis of novel arylsubstituted pyrazolo[3,4-d]pyrimidines and their evaluation as cytotoxic agents", ***Int. J. Chem. Sci. Tech.*****, 2011**, *1* (4), 126-140.